ADVANCES IN UNDERSTANDING NEUROHIV ASSOCIATED CHANGES IN NEUROIMMUNE COMMUNICATION IN THE COMBINED ANTI-RETROVIRAL THERAPY (cART) ERA

EDITED BY: Peter J. Gaskill, Jerel Adam Fields, Dianne T. Langford, Kelly Stauch and Dionna W. Williams

PUBLISHED IN: Frontiers in Neurology and Frontiers in Immunology

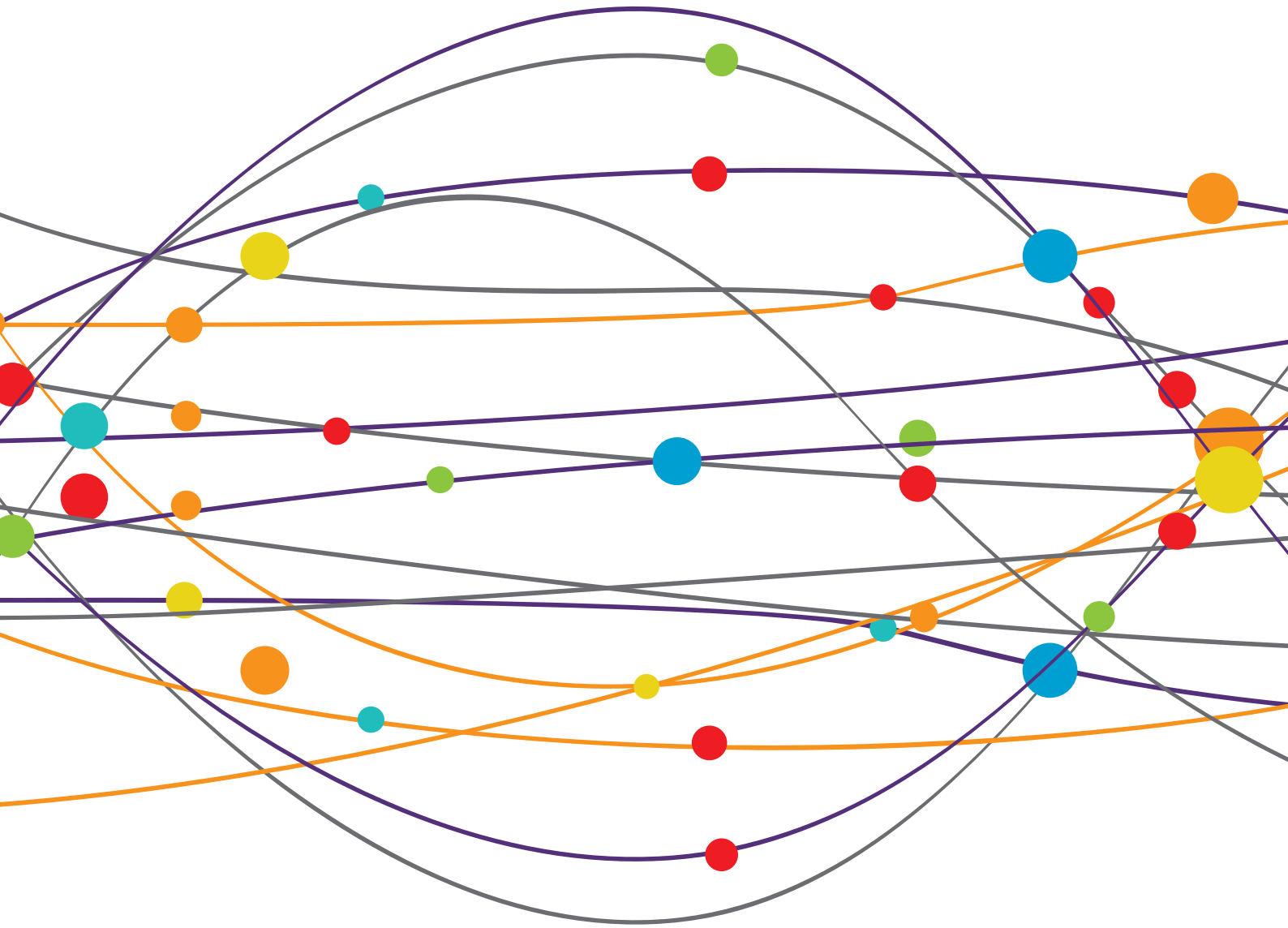

frontiers Research Topics

frontiers

ISSN 1664-8714
ISBN 978-2-88971-711-8
DOI 10.3389/978-2-88971-711-8

About Frontiers

Frontiers is more than just an open-access publisher of scholarly articles: it is a pioneering approach to the world of academia, radically improving the way scholarly research is managed. The grand vision of Frontiers is a world where all people have an equal opportunity to seek, share and generate knowledge. Frontiers provides immediate and permanent online open access to all its publications, but this alone is not enough to realize our grand goals.

Frontiers Journal Series

The Frontiers Journal Series is a multi-tier and interdisciplinary set of open-access, online journals, promising a paradigm shift from the current review, selection and dissemination processes in academic publishing. All Frontiers journals are driven by researchers for researchers; therefore, they constitute a service to the scholarly community. At the same time, the Frontiers Journal Series operates on a revolutionary invention, the tiered publishing system, initially addressing specific communities of scholars, and gradually climbing up to broader public understanding, thus serving the interests of the lay society, too.

Dedication to Quality

Each Frontiers article is a landmark of the highest quality, thanks to genuinely collaborative interactions between authors and review editors, who include some of the world's best academicians. Research must be certified by peers before entering a stream of knowledge that may eventually reach the public - and shape society; therefore, Frontiers only applies the most rigorous and unbiased reviews.
Frontiers revolutionizes research publishing by freely delivering the most outstanding research, evaluated with no bias from both the academic and social point of view. By applying the most advanced information technologies, Frontiers is catapulting scholarly publishing into a new generation.

What are Frontiers Research Topics?

Frontiers Research Topics are very popular trademarks of the Frontiers Journals Series: they are collections of at least ten articles, all centered on a particular subject. With their unique mix of varied contributions from Original Research to Review Articles, Frontiers Research Topics unify the most influential researchers, the latest key findings and historical advances in a hot research area! Find out more on how to host your own Frontiers Research Topic or contribute to one as an author by contacting the Frontiers Editorial Office: frontiersin.org/about/contact

ADVANCES IN UNDERSTANDING NEUROHIV ASSOCIATED CHANGES IN NEUROIMMUNE COMMUNICATION IN THE COMBINED ANTI-RETROVIRAL THERAPY (cART) ERA

Topic Editors:
Peter J. Gaskill, Drexel University, United States
Jerel Adam Fields, University of California, San Diego, United States
Dianne T. Langford, Temple University, United States
Kelly Stauch, University of Nebraska Medical Center, United States
Dionna W. Williams, Johns Hopkins Medicine, United States

Citation: Gaskill, P. J., Fields, J. A., Langford, D. T., Stauch, K., Williams, D. W., eds. (2021). Advances in Understanding NeuroHIV Associated Changes in Neuroimmune Communication in the Combined Anti-retroviral Therapy (cART) Era. Lausanne: Frontiers Media SA. doi: 10.3389/978-2-88971-711-8

Table of Contents

frontiers in Neurology

EDITORIAL
published: 05 October 2021
doi: 10.3389/fneur.2021.763448

Editorial: Advances in Understanding NeuroHIV Associated Changes in Neuroimmune Communication in the Combined Anti-retroviral Therapy (cART) Era

Peter J. Gaskill[1]*, *Jerel Adam Fields*[2], *Dianne T. Langford*[3], *Kelly L. Stauch*[4] and *Dionna W. Williams*[5]

[1] Department of Pharmacology and Physiology, Drexel University College of Medicine, Philadelphia, PA, United States, [2] Department of Psychiatry, University of California San Diego, La Jolla, CA, United States, [3] Department of Neuroscience, Lewis Katz School of Medicine, Philadelphia, PA, United States, [4] Department of Neurological Sciences, University of Nebraska Medical Center, Omaha, NE, United States, [5] Department of Molecular and Comparative Pathobiology, School of Medicine, Johns Hopkins University, Baltimore, MD, United States

Keywords: neuroAIDS, neuroimmunity, neuropathogenesis, neurotransmission, CART, neuroHIV

Editorial on the Research Topic

Advances in Understanding NeuroHIV Associated Changes in Neuroimmune Communication in the Combined Anti-retroviral Therapy (cART) Era

OPEN ACCESS

Edited and reviewed by:
Hans-Peter Hartung, Heinrich Heine University of Düsseldorf, Germany

***Correspondence:**
Peter J. Gaskill
pjg63@drexel.edu

Specialty section:
This article was submitted to Multiple Sclerosis and Neuroimmunology, a section of the journal Frontiers in Neurology

Received: *23 August 2021*
Accepted: *08 September 2021*
Published: *05 October 2021*

Citation:
Gaskill PJ, Fields JA, Langford DT, Stauch KL and Williams DW (2021) Editorial: Advances in Understanding NeuroHIV Associated Changes in Neuroimmune Communication in the Combined Anti-retroviral Therapy (cART) Era. Front. Neurol. 12:763448. doi: 10.3389/fneur.2021.763448

It has been almost 40 years since the first cases of AIDS were reported in Morbidity and Mortality Weekly in the fall of 1981 (1). During that time, almost 80 million people have been infected and more than 36 million people have died from HIV, with 1.5 million new infections and 680,000 deaths occurring in 2020. Despite these alarming numbers, there has been significant progress in controlling this pandemic as HIV infections and deaths have decreased 50–60% from their peaks in 1997 and 2004, respectively. This is largely due to the development and implementation of antiretroviral therapy (ART). In 2020, around two thirds of people living with HIV (PLWH) were treated with ART to suppress viral replication (2–6). Widespread access to ART has brought us to an inflection point in the pandemic, transforming HIV from a terminal diagnosis to a chronic condition.

Unfortunately, chronic infection and ART treatment have led to a variety of new health challenges, including long-term neurological dysfunction. In the absence of ART, PLWH showed rampant neuroinflammation and significant neuronal death associated with high rates of dementia. With ART, the neuropathology associated with HIV infection has become both more subtle and more complex. Importantly, even with suppression of viral replication to below the level of detection, neuropathological changes, minor neurocognitive dysfunction, depression, and other neuropsychiatric adverse events (NPAE) remain prevalent (5, 7–15), suggesting that the etiology of these conditions is not solely derived from viral replication. As Spagnolo-Allende and Gutierrez discuss in their review of cerebrovascular complications in neuroHIV, HIV proteins and associated neuroinflammation can initiate and/or exacerbate multiple types of vascular complications. Distinct phenotypes of vascular insults are associated with the presence or absence of ART in PLWH, so further study in this area is important given the growing incidence of cerebrovascular disease in PLWH on ART, particularly older individuals.

Neuronal health and function are maintained by complex, bidirectional interactions among neurons, astrocytes, microglia, and central nervous system (CNS) macrophages (16–18). Data suggest that neuroHIV stems, at least partially, from disruption of this communication, impairing neurotransmission, synapse formation/dissolution and neuroimmune communication. Some studies suggest that antiretroviral (ARV) drugs themselves may contribute to these changes in neuroimmune communication and neurological dysfunction (19–22). The data from Tripathi et al. support this possibility, showing that in both isolated rodent microglia and in HIV-1 transgenic rats, exposure to ART mediates microglial activation through oxidative stress-mediated lysosomal dysfunction. George et al., also demonstrate that antiretroviral drugs dolutegravir, emtricitabine, and efavirenz induce cell-type specific changes in ATP generation and mitochondrial respiration in epithelial and microglial cell lines, suggesting metabolic changes may contribute ARV toxicity in specific cell types. Dastgheyb et al. compared neurocognitive function between 929 virally suppressed women living with HIV and 717 HIV-uninfected women, identifying distinct neuropsychological profiles associated with both demographic and clinical variables, including the use of specific ARVs. Together, these data indicate more in-depth analyses of specific impacts of distinct ARVs both *in vitro* in discrete cell types and in humans in conjunction with analyses of a larger combination of variables could help to identify and/or predict neuropathological and neurocognitive response patterns to specific ART regimens.

Currently, the spread of HIV is increasingly driven by marginalized populations, including transgender women, sex workers, men who have sex with men and individuals using injection drugs. In each of these groups, the risk of HIV infection is 25 to 35 times higher than that in the general population (3). These populations have a high prevalence of substance use disorders (23–28) and hepatitis C (HCV) (29–32), so it is critical to evaluate their impact on neuroimmune communication, neuropathogenesis and neurological function. Paul et al. analyzed the neurocognitive response to ART in PLWH with co-occurring HCV infection, showing that both mono-HIV infected, and co-HIV/HCV infected individuals had significant neurocognitive improvement in response to ART. Notably, a subgroup of co-infected individuals with higher HIV plasma viral load and lower plasma $CD4^+$ T cell count at baseline showed persistent motor deficits. In contrast, Matt et al. show that exposure to dopamine concentrations induced by the use of addictive drugs (33, 34) alters the efficacy of the CCR5 antagonist Maraviroc by increasing CCR5 expression on the macrophage surface. Cisneros et al., show that methamphetamine mediated activation of trace amino acid receptor 1 (TAAR1) triggers multiple signaling pathways in human astrocytes, regulating the expression of the glutamate receptor EAAT-2 through activation of CAMKII and Ca^{2+} release, and phosphorylating CREB via both the Ca^{2+} release and cAMP pathways. These data support substantial research indicating that both dopamine and substances of abuse can potentially exacerbate HIV infection and dysregulate associated cellular processes in the CNS.

While the above studies suggest that substances of abuse could exacerbate neuroHIV, other studies on abused substances suggest novel therapeutic activity for different drugs or neurotransmitter systems. In primary rodent neurons, League et al., show that blocking the activity of monoacylglycerol lipase (MAGL) reduces the neurotoxic effects of Tat. As MAGL drives metabolism of the cannabinoid receptor (CB_1R) agonist, 2-arachidonoylglycerol, these data support the idea of using the endocannabinoid system as a target for neurotherapeutic adjuvants in ART-treated PLWH. Lin et al. show that the benzodiazepine, alprazolam (Xanax), alters the activity of the transcription factor RUNX1 and STAT5. Recent data show that benzodiazepines are overprescribed to PLWH and are associated with neurocognitive deficits, so these data suggest alprazolam may influence neuroinflammation and provide a mechanism underlying prior studies showing alprazolam can reactivate latent HIV. Han et al. use the iTat rodent model to show that Tat expression increases functional and structural indices of motor and sensory neuropathy, dysregulating the expression of proteins in the electron transport chain and the mitochondria. These effects were blocked by treatment with the muscarinic receptor 1 antagonist pirenzepine, which promotes mitochondrial biogenesis, suggesting the involvement of the muscarinic system in HIV distal sensory polyneuropathy. In another study using the iTat model, Joshi et al., compare acute vs. prolonged Tat induction and show prolonged Tat induction reduced locomotor activity and caused a small but significant increase in the ratio of MMP to TIMP1, while the acute induction of Tat reduced IL-6 mRNA expression.

The studies from this special collection reinforce that the development of neuroHIV is multi-factorial, driven by altered interactions among distinct types of CNS cells and interconnecting neurotransmitter, signaling and metabolic pathways. These data also collectively show that neuroHIV can be exacerbated by a variety of comorbidities and other factors including ART. Future studies should continue to evaluate the discrete impacts of ART and comorbidities, like substance abuse and HCV, as well as the combined effects of these conditions and their capacity to drive the growing number of complications associated with neuroHIV.

AUTHOR CONTRIBUTIONS

PJG, JAF, DTL, KLS, and DWW wrote the editorial and invited authors to participate in the collection. All authors contributed to the article and approved the submitted version.

FUNDING

This work was supported by grants from the National Institutes of Drug Abuse (DA039005 and DA049227 to PJG, DA037830 to DTL, DA044838 and DA052859 to DWW), National Institutes of Mental Health (MH115819 to JAF, MH107340 to DTL, MH062261 pilot funding to KLS), National Institutes of Aging (AG066215 to JAF) and the W.W. Smith Charitable Trust (A2003 to PJG).

REFERENCES

1. CDC. Pneumocystis pneumonia — Los Angeles. *MMWR*. (1981) 30:250–2.
2. UNAIDS. *Fact Sheet 2021* (2021).
3. UNAIDS. *CONFRONTING INEQUALITIES Lessons for pandemic responses from 40 years of AIDS*. Joint United Nations Programme on HIV/AIDS, Geneva (2021).
4. Cihlar T, Fordyce M. Current status and prospects of HIV treatment. *Curr Opin Virol.* (2016) 18:50–6. doi: 10.1016/j.coviro.2016.03.004
5. Saylor D, Dickens AM, Sacktor N, Haughey N, Slusher B, Pletnikov M, et al. HIV-associated neurocognitive disorder–pathogenesis and prospects for treatment. *Nat Rev Neurol.* (2016) 12:234–48. doi: 10.1038/nrneurol.2016.27
6. Boender TS, Smit C, van Sighem A, Bezemer D, Ester CJ, Zaheri S, et al. AIDS therapy evaluation in the Netherlands (ATHENA) national observational HIV cohort: cohort profile. *BMJ Open.* (2018) 8:e022516. doi: 10.1136/bmjopen-2018-022516
7. Eggers C, Arendt G, Hahn K, Husstedt IW, Maschke M, Neuen-Jacob E, et al. HIV-1-associated neurocognitive disorder: epidemiology, pathogenesis, diagnosis, and treatment. *J Neurol.* (2017) 264:1715–27. doi: 10.1007/s00415-017-8503-2
8. Bell JE. An update on the neuropathology of HIV in the HAART era. *Histopathology*. (2004) 45:549–59. doi: 10.1111/j.1365-2559.2004.02004.x
9. Everall IP, Hansen LA, Masliah E. The shifting patterns of HIV encephalitis neuropathology. *Neurotoxicity Res.* (2005) 8:51–61. doi: 10.1007/BF03033819
10. Saylor D, Dickens AM, Sacktor N, Haughey N, Slusher B, Pletnikov M, et al. HIV-associated neurocognitive disorder - pathogenesis and prospects for treatment. *Nat Rev Neurol.* (2016) 12:309. doi: 10.1038/nrneurol.2016.53
11. Becker JT, Sanders J, Madsen SK, Ragin A, Kingsley L, Maruca V, et al. Subcortical brain atrophy persists even in HAART-regulated HIV disease. *Brain Imaging Behav.* (2011) 5:77–85. doi: 10.1007/s11682-011-9113-8
12. Ipser JC, Brown GG, Bischoff-Grethe A, Connolly CG, Ellis RJ, Heaton RK, et al. HIV infection is associated with attenuated frontostriatal intrinsic connectivity: a preliminary study. *J Int Neuropsychol Soc.* (2015) 21:203–13. doi: 10.1017/S1355617715000156
13. Ortega M, Brier MR, Ances BM. Effects of HIV and combination antiretroviral therapy on cortico-striatal functional connectivity. *AIDS.* (2015) 29:703–12. doi: 10.1097/QAD.0000000000000611
14. Alakkas A, Ellis RJ, Watson CW, Umlauf A, Heaton RK, Letendre S, et al. White matter damage, neuroinflammation, neuronal integrity in HAND. *J Neurovirol.* (2019) 25:32–41. doi: 10.1007/s13365-018-0682-9
15. Valcour V, Sithinamsuwan P, Letendre S, Ances B. Pathogenesis of HIV in the central nervous system. *Curr HIV/AIDS Rep.* (2011) 8:54–61. doi: 10.1007/s11904-010-0070-4
16. Dantzer R, Kelley KW. Psychoneuroimmune phenomena: neuroimmune interactions. In: Pfaff DW, Volkow ND, editors. *Neuroscience n the 21st Century*. New York, NY: Springer (2016). p. 643–71.
17. Herz J, Filiano AJ, Smith A, Yogev N, Kipnis J. Myeloid cells in the central nervous system. *Immunity.* (2017) 46:943–56. doi: 10.1016/j.immuni.2017.06.007
18. Liddelow SA, Marsh SE, Stevens B. Microglia and astrocytes in disease: dynamic duo or partners in crime? *Trends Immunol.* (2020) 41:820–35. doi: 10.1016/j.it.2020.07.006
19. Lagathu C, Eustace B, Prot M, Frantz D, Gu Y, Bastard JP, et al. Some HIV antiretrovirals increase oxidative stress and alter chemokine, cytokine or adiponectin production in human adipocytes and macrophages. *Antivir Ther.* (2007) 12:489–500. doi: 10.1177/125965350701200407
20. Chen L, Al-Harthi L, Hu XT. Triumeq increases excitability of pyramidal neurons in the medial prefrontal cortex by facilitating voltage-gated Ca(2+) channel function. *Front Pharmacol.* (2020) 11:617149. doi: 10.3389/fphar.2020.617149
21. Shah A, Gangwani MR, Chaudhari NS, Glazyrin A, Bhat HK, Kumar A. Neurotoxicity in the post-HAART era: caution for the antiretroviral therapeutics. *Neurotox Res.* (2016) 30:677–97. doi: 10.1007/s12640-016-9646-0
22. Yuan NY, Kaul M. Beneficial and adverse effects of cART affect neurocognitive function in HIV-1 infection: balancing viral suppression against neuronal stress and injury. *J Neuroimmune Pharmacol.* (2021) 16:90–112. doi: 10.1007/s11481-019-09868-9
23. Bourne A, Weatherburn P. Substance use among men who have sex with men: patterns, motivations, impacts and intervention development need. *Sex Transm Infect.* (2017) 93:342–6. doi: 10.1136/sextrans-2016-052674
24. Rosińska M, Gios L, Nöstlinger C, Berghe WV, Marcus U, Schink S, et al. Prevalence of drug use during sex amongst MSM in Europe: results from a multi-site bio-behavioural survey. *Int J Drug Policy.* (2018) 55:231–41. doi: 10.1016/j.drugpo.2018.01.002
25. Connolly D, Gilchrist G. Prevalence and correlates of substance use among transgender adults: a systematic review. *Addict Behav.* (2020) 111:106544. doi: 10.1016/j.addbeh.2020.106544
26. Strathdee SA, West BS, Reed E, Moazan B, Azim T, Dolan K, et al. Substance use and HIV among female sex workers and female prisoners: risk environments and implications for prevention, treatment, and policies. *J Acquir Immune Defic Syndr.* (2015) 69(Suppl. 2):S110–17. doi: 10.1097/QAI.0000000000000624
27. Reback CJ, Fletcher JB. HIV prevalence, substance use, and sexual risk behaviors among transgender women recruited through outreach. *AIDS Behav*. (2014) 18:1359–67. doi: 10.1007/s10461-013-0657-z
28. Roxburgh A, Degenhardt L, Larance B, Copeland J. *Mental Health, Drug Use and Risk Among Female Street-Based Sex Workers in Greater Syndney*. Sydney, NSW: National Drug and Alcohol Research Centre (2005).
29. Midgard H, Weir A, Palmateer N, Re III VL, Pineda JA, Macías J, et al. HCV epidemiology in high-risk groups and the risk of reinfection. *J Hepatol.* (2016) 65:S33–45. doi: 10.1016/j.jhep.2016.07.012
30. Goldenberg SM, Montaner J, Braschel M, Socias E, Guillemi S, Shannon K, et al. Dual sexual and drug-related predictors of hepatitis C incidence among sex workers in a Canadian setting: gaps and opportunities for scale-up of hepatitis C virus prevention, treatment, and care. *Int J Infect Dis.* (2017) 55:31–7. doi: 10.1016/j.ijid.2016.12.019
31. Hernandez CJ, Trujillo D, Sicro S, Meza J, Bella M, Daza E, et al. High hepatitis C virus seropositivity, viremia, and associated risk factors among trans women living in San Francisco, California. *PLoS ONE.* (2021) 16:e0249219. doi: 10.1371/journal.pone.0249219
32. Karimi SE, Bayani A, Higgs P, Bayat AH, Hemmat M, Ahounbar E, et al. Prevalence and high risk behaviours associated with HCV testing among people who inject drugs: a systematic review and Meta-analysis. *Subst Abuse Treat Prev Policy.* (2020) 15:64. doi: 10.1186/s13011-020-00306-1
33. Matt SM, Gaskill PJ. Where is dopamine and how do immune cells see it?: Dopamine-mediated immune cell function in health and disease. *J Neuroimmune Pharmacol.* (2020) 15:114–64. doi: 10.1007/s11481-019-09851-4
34. Di Chiara G, Imperato A. Drugs abused by humans preferentially increase synaptic dopamine concentrations in the mesolimbic system of freely moving rats. *Proc Natl Acad Sci USA.* (1988) 85:5274–8. doi: 10.1073/pnas.85.14.5274

Conflict of Interest: The authors declare that the research was conducted in the absence of any commercial or financial relationships that could be construed as a potential conflict of interest.

frontiers in Neurology

ORIGINAL RESEARCH
published: 04 September 2020
doi: 10.3389/fneur.2020.00840

N-Acetylcysteine Reverses Antiretroviral-Mediated Microglial Activation by Attenuating Autophagy-Lysosomal Dysfunction

Ashutosh Tripathi, Annadurai Thangaraj, Ernest T. Chivero, Palsamy Periyasamy, Maria E. Burkovetskaya, Fang Niu, Ming-Lei Guo and Shilpa Buch**

Department of Pharmacology and Experimental Neuroscience, University of Nebraska Medical Center, Omaha, NE, United States

Successful suppression of viral replication by combined antiretroviral therapy (cART) in HIV-1 infected individuals is paradoxically also accompanied by an increased prevalence of HIV-associated neurocognitive disorders (HAND) in these individuals. HAND is characterized by a state of chronic oxidative stress and inflammation. Microglia are extremely sensitive to a plethora of stimuli, including viral proteins and cART. The current study aimed to assess the effects of cART-mediated oxidative stress on the induction of inflammatory responses in microglia. In the present study, we chose a combination of three commonly used antiretroviral drugs—tenofovir disoproxil fumarate, emtricitabine, and dolutegravir. We demonstrated that exposure of microglia to the chosen cART cocktail induced generation of reactive oxygen species, subsequently leading to lysosomal dysfunction and dysregulated autophagy, ultimately resulting in the activation of microglia. Intriguingly, the potent antioxidant, N-acetylcysteine, reversed the damaging effects of cART. These *in vitro* findings were further corroborated *in vivo* wherein cART-treated HIV transgenic (Tg) rats demonstrated increased microglial activation, exaggerated lysosome impairment, and dysregulated autophagy in the prefrontal cortices compared with HIV Tg rats not exposed to cART. Similar to *in vitro* findings, the treatment of HIV Tg rats with N-acetylcysteine also mitigated the deleterious effects of cART. Taken together, our findings suggest that oxidative stress-mediated lysosomal dysfunction plays a critical role in the pathogenesis of HAND in drug-treated HIV-infected individuals and that antioxidant-mediated mitigation of oxidative stress could thus be considered as an adjunctive therapeutic strategy for ameliorating/dampening some of the neurological complications of HAND.

Keywords: combined antiretroviral therapy, N-acetylcysteine, lysosome, autophagy, microglial activation, neuroinflammation

OPEN ACCESS

Edited by:
Dianne T. Langford, Temple University, United States

Reviewed by:
Cagla Akay-Espinoza, University of Pennsylvania, United States
Tory P. Johnson, Johns Hopkins University, United States

****Correspondence:***
Ming-Lei Guo
minglei.guo@unmc.edu
Shilpa Buch
sbuch@unmc.edu

Specialty section:
This article was submitted to Neuroinfectious Diseases, a section of the journal Frontiers in Neurology

Received: *27 March 2020*
Accepted: *06 July 2020*
Published: *04 September 2020*

Citation:
Tripathi A, Thangaraj A, Chivero ET, Periyasamy P, Burkovetskaya ME, Niu F, Guo M-L and Buch S (2020) N-Acetylcysteine Reverses Antiretroviral-Mediated Microglial Activation by Attenuating Autophagy-Lysosomal Dysfunction. Front. Neurol. 11:840. doi: 10.3389/fneur.2020.00840

INTRODUCTION

With the advent of combined antiretroviral therapy (cART), HIV infection has transformed from a death sentence to a more chronic and manageable disease (1–3). Almost 50% of the infected individuals develop HIV-associated neurocognitive disorders (HANDs), with symptoms ranging from asymptomatic to mild cognitive–motor disorders. This, in turn, severely impacts the quality

of life of those afflicted with the disease (3). Although the mechanism(s) underlying pathogenesis of HAND is not clearly understood, associated oxidative stress, immune activation, and inflammation have been implicated in the process (4, 5).

Microglia are the predominant brain-resident macrophages that maintain central nervous system (CNS) homeostasis under basal conditions and also during moderate activation. Prolonged microglial activation, on the other hand, impairs the ability of microglia to maintain cellular homeostasis and leads to significant neuronal dysfunction and cognitive impairment, with exacerbated neuroinflammation in the CNS (6, 7). Exacerbated microglial activation and neuroinflammation are hallmark features of HAND pathogenesis in HIV-infected individuals on cART (8–10). Prolonged exposure to cART has been reported to activate microglia (11–13). Impaired lysosomal functioning has been shown to underlie microglial activation and increased neuroinflammation (14, 15). In fact, findings from our group have identified the role of lysosomal dysfunction in cART-mediated dysregulation of autophagy (13).

Lysosomes are specialized membrane-enclosed cellular organelles that receive and degrade macromolecules from phagocytosis, endocytosis, or autophagy pathways (16). Lysosomes are extremely sensitive to oxidative stress, which causes lysosomal dysfunction (17). The role of oxidative stress, caused by an imbalance between the production and elimination of reactive oxygen species (ROS), has been well-documented in the onset of chronic inflammatory diseases (18, 19). Along these lines, redox imbalance has been reported in the serum and cerebrospinal fluid of HIV-1 patients treated with cART (20, 21). In fact, there is also a report on the involvement of oxidative stress in antiretroviral drugs-mediated neuronal damage in the CNS (22). Oxidative stress could thus play a key role in the pathogenesis of HAND. Strategies aimed at reducing or preventing the generation of oxidative stress (23) could thus be a plausible mechanism to mitigate cART-mediated induction of microglial activation and neuroinflammation.

In the current study, induction of oxidative stress was examined by assessing the levels of ROS in microglial cells exposed to cART. Furthermore, it was also shown that the treatment of microglia with potent antioxidant N-acetylcysteine (NAC) abrogated cART-mediated activation of microglia. We acknowledge that there are several other combinations of antiretroviral drugs, and the most common first-line cART regimens include two nucleoside reverse transcriptase inhibitors (NRTIs) plus a boosted protease inhibitor or an integrase inhibitor (24, 25). In the present study, we chose to study a combination of two NRTIs, tenofovir disoproxil fumarate (TDF) and emtricitabine (FTC), and an integrase inhibitor, dolutegravir (DTG). This combination has been effectively used in the simian immunodeficiency virus (SIV)/macaque model (26, 27), and these drugs are also common in the clinical setting (25, 28–30). Our *in vitro* findings were further corroborated by *in vivo* studies, wherein HIV Tg rats (expressing seven of the nine HIV proteins) that were treated with cART exhibited exaggerated neuroinflammation and lysosomal damage compared with HIV Tg rats not treated with cART. Consistently, the treatment of HIV Tg rats with NAC resulted in the failure of cART to mediate microglial activation, and this was also accompanied by the restoration of impaired lysosomal and autophagy processes. Our findings thus suggest that oxidative stress-mediated lysosomal dysfunction likely plays a critical role in the pathogenesis of HAND in cART-treated HIV-infected individuals and that antioxidant-mediated mitigation of oxidative stress could be considered as an adjunctive therapeutic strategy for ameliorating/dampening some of the neurological complications of HAND.

Abbreviations: ACTB, actin, beta; AIF1, allograft inflammatory factor 1; BECN1, beclin 1, autophagy related; cART, combined antiretroviral therapy; CASP3, caspase 3; CNS, central nervous system; CTSD, cathepsin D; DAPI, 4,6-diamidino-2-phenylindole; DMEM, Dulbecco modified Eagle medium; DTG, dolutegravir; FBS, fetal bovine serum; FTC, emtricitabine; GAPDH, glyceraldehyde-3-phosphate dehydrogenase; HAND, HIV-1-associated neurocognitive disorders; HIV-1 Tat, human immunodeficiency virus-1 transactivator of transcription; *Il1β*, interleukin 1, beta; *Il6*, interleukin 6; ITGAM, integrin subunit alpha M; LAMP2, lysosome-associated membrane protein 2; GAL3, galectin 3; LMP, lysosomal membrane permeabilization; MAP1LC3B, microtubule-associated protein 1 light chain 3 beta; mitoTEMPO, (2-(2,2,6,6-Tetramethylpiperidin-1-oxyl-4-ylamino)-2-oxoethyl)triphenylphosphonium chloride; NAC, N-acetylcysteine; NRTIs, nucleoside reverse transcriptase inhibitors; PBS, phosphate-buffered saline; ROS, reactive oxygen species; rPMs, rat primary microglial cells; SQSTM1, sequestosome 1; TBHP, tert-butyl hydroperoxide; TDF, tenofovir disoproxil fumarate; TEMPOL, 4-hydroxy-2,2,6,6-tetramethylpiperidin-1-oxyl; *Tnf*, tumor necrosis factor.

MATERIALS AND METHODS

Reagents

Antiretroviral drugs TDF, FTC (Gilead Sciences, Foster City, CA, USA), and DTG (ViiV Healthcare, Research Triangle Park, NC, USA) were used. NAC (A7250) and (2-(2,2,6,6-Tetramethylpiperidin-1-oxyl-4-ylamino)-2-oxoethyl)triphenylphosphonium chloride (mitoTEMPO; SML0737) were purchased from Sigma-Aldrich, St. Louis, MO, USA, and 4-hydroxy-2,2,6,6-tetramethylpiperidin-1-oxyl (TEMPOL; sc-200825) was purchased from Santa Cruz Biotechnology, Dallas, TX, USA. Antibody resources: beclin 1 (BECN1; sc-11427) was purchased from Santa Cruz Biotechnology, Dallas, TX, USA. Lysosome associated membrane protein 2 (LAMP2; NB300-591), microtubule-associated protein 1 light chain 3 beta (MAP1LC3B; NB100-2220), and integrin subunit alpha M (ITGAM; NB110-89474) were purchased from Novus Biological Company, Centennial, CO, USA. Cathepsin D (CTSD; ab75852) and caspase 3 (CASP3; ab13585) were purchased from Abcam, Cambridge, MA, USA. Galectin 3 (GAL3) (A3A12) was purchased from Invitrogen. Sequestosome 1 (SQSTM1; PM045) was purchased from MBL International, Woburn, MA, USA, and allograft inflammatory factor 1 (AIF1; 019-19741) was purchased from Wako Pure Chemicals Industries, Chuo-ku, Osaka, Japan. Goat anti-rabbit (sc-2004) and goat anti-mouse (sc-2005) were purchased from Santa Cruz Biotechnology, Dallas, TX, USA.

Animals

Male Sprague–Dawley (8–9 months old) HIV-1 transgenic rats (HIV-1, F344) were housed in a 12-h light and 12-h dark cycle

under conditions of constant temperature and humidity. Food and water were available *ad libitum*. All animal procedures were performed according to the protocols approved by the Institutional Animal Care and Use Committee of the University of Nebraska Medical Center and the National Institutes of Health.

Rat Primary Microglial Cell Isolation

Primary microglial cells were obtained from the cerebral cortices of 1–3-days-old newborn Sprague–Dawley pups. Briefly, cerebral cortices from the pups were dissected, and meninges were removed. Mixed glial cultures were prepared by form-dissected brain cortices after digestion and dissociation in Hank's buffered salt solution (HBSS, Thermo Fisher Scientific Waltham, MA, USA, 14025076) supplemented with 0.25% trypsin (Thermo Fisher Scientific, Waltham, MA, USA, 25300-054), followed by triturating and passing through a 40-μm nylon mesh. Cells were centrifuged and resuspended in Dulbecco modified Eagle medium (DMEM, Thermo Fisher Scientific, Waltham, MA, USA, 11995-065) supplemented with 10% heated inactivated fetal bovine serum (FBS, Thermo Fisher Scientific Waltham, MA, USA, 16000-044), 100-U/ml penicillin—0.1-mg/ml streptomycin, and 0.25-ng/ml macrophage colony-stimulating factor (Thermo Fisher Scientific Waltham, MA, USA, PHC9504). Cells were plated at 20×10^6 cells/flask density onto 75-cm^2 cell culture flasks. The cell culture medium was changed every third day. When confluent (around 8–10 days), mixed glial cultures were shaken at 37°C at 220 g for 2 h, to detach microglia from the flasks. Detached microglia were plated and cultured for an additional 24 h for further experimental use. Microglial purity was evaluated by immune-histochemical staining using the antibody specific for AIF1 (Wako Pure Chemical Industries Chuo-ku, Osaka, Japan, 019-19741) and was >95% pure.

Antiretroviral Drugs

For *in vitro* experiments, antiretroviral stock solutions were prepared by dissolving the drugs (TDF, FTC, and DTG) in dimethyl sulfoxide (DMSO). Final concentrations of each antiretroviral drugs (TDF, FTC, and DTG) in the cART cocktail were 5 μM. DMSO was <0.01% (v/v) in the cART-treated and control groups.

Western Blotting

Treated rat primary microglial cells (rPMs) and brain tissues were lysed using radioimmunoprecipitation assay buffer supplemented with a cocktail of protease inhibitor (Thermo Fisher Scientific Waltham, MA, USA, 78429) and phosphatase inhibitor (Thermo Fisher Scientific Waltham, MA, USA, 78426) using Fisherbrand™ Q125 Sonicator. Cell and tissue lysates were centrifuged at 12,000 g for 15 min at 4°C to remove the debris. The concentration of protein was determined by a bicinchoninic acid assay (Thermo Fisher Scientific Waltham, MA, USA, 23227) according to the manufacturer's guidelines. Proteins were electrophoresed in equal concentration in a sodium dodecyl sulfate-polyacrylamide gel under reducing conditions and then transferred to polyvinylidene difluoride membranes (Sigma-Aldrich, St. Louis, MO, USA, IPVH00010). Then, the polyvinylidene difluoride membranes were blocked with 5% non-fat dry milk in 1× Tween–Tris-buffered saline (1.21-g Tris [Fisher Scientific, Hampton, NH, USA, BP152-5], 8.77-g sodium chloride [Fisher Scientific, Hampton, NH, USA, BP358-212], 500-μl Tween-20 [Fisher Scientific, Hampton, NH, USA, BP337-500], pH 7.6 for 1 L). After, blocking blots were then probed with primary antibodies overnight at 4°C. Actin beta (ACTB; Sigma-Aldrich, St. Louis, MO, USA, A5441) was used to normalize the protein. The horseradish peroxidase-conjugated secondary antibodies to goat anti-mouse/rabbit IgG were probed for 1 h followed by detection of immunoreactive bands using Super Signal West Pico Chemiluminescent Substrate (Thermo Fisher Scientific Waltham, MA, USA, 34078).

Immunocytochemistry

After the treatment, rPMs were fixed with 4% paraformaldehyde at room temperature for 15 min, then permeabilized with 0.3% Triton X-100 (Fisher Scientific, Hampton, NH, USA, BP151-500) in phosphate-buffered saline (PBS, Fisher Scientific, Hampton, NH, USA, SH3025801). Cells were then blocked with 10% normal goat serum in PBS for 1 h at room temperature. Then, primary antibodies were added and incubated overnight at 4°C. Following this, the secondary antibodies were added for 2 h. Cells were then washed in PBS (three times) and mounted with Prolong gold antifade reagent with 4,6-diamidino-2-phenylindole (Thermo Fisher Scientific, Waltham, MA, USA, P36935). Images of fluorescent cells were taken with a Zeiss Observer using a Z1 inverted microscope (Carl Zeiss, Thornwood, NY, USA), and analysis of the images was done using the AxioVs 40 Version 4.8.0.0 software (Carl Zeiss, Thornwood, NY, USA).

Quantification of Microtubule-Associated Protein 1 Light Chain 3 Beta and Lysosome Associated Membrane Protein 2 Puncta

Fluorescence images were acquired with Zeiss Observer using a Z1-inverted microscope (Carl Zeiss, Thornwood, NY, USA). Images thus acquired were analyzed using Image J software. Firstly, the region of interest in the cells to be analyzed was selected using the polygon selection tool. Fluorescence was converted to black pixels over a white background. The regions of interest were then analyzed by Measure Particle algorithm to record puncta number, area, and size (13).

Reactive Oxygen Species Detection

Detection of ROS was performed according to the manufacturer's (Life technologies, D-339) recommended protocol using Image-iT™ LIVE Green ROS Detection Kit (Thermo Fisher Scientific, Waltham, MA, USA, 136007). Briefly, cells were seeded in 96 wells a day before the experiment. Cells were washed with HBSS (Thermo Fisher Scientific Waltham, MA, USA, 14025076), supplemented with a 25-μM carboxy-H_2DCFDA working solution, and incubated for 30 min at 37°C. In addition to carboxy-H_2DCFDA, the kit provides the common inducer of ROS production tert-butyl hydroperoxide (TBHP) as a positive control. The changes in fluorescence were measured using a spectrofluorometer set at 485-nm excitation and 530-nm emission.

Real-Time Quantitative PCR

Total RNA was extracted using Quick-RNA™ Miniprep Kit (Zymo Research, Irvine, CA, USA, R1055). Column purified, total RNA was reverse transcribed to complementary DNA using a Verso complementary DNA Synthesis Kit (Thermo Fisher Scientific, Waltham, MA, USA, AB-1453/B). Reverse-transcribed RNA was analyzed by Applied Biosystems™ 7500 Real-Time PCR (Thermo Fisher Scientific, Waltham, MA, USA) using the real-time PCR that was performed using the TaqMan-Master mix and TaqMan gene expression assays with FAM-labeled probes using standard amplification protocol (Applied Biosystems). Rat primers for tumor necrosis factor (*Tnf; Rn01525859_g1),* interleukin 6 (*Il6*; Rn01410330_m1), interleukin 1 beta (*Il1β*; Rn00580432_m1), and *Gapdh* (Rn01775763_g1) were purchased from Thermo Fisher Scientific, Waltham, MA, USA. *Gapdh* was used as an internal control for normalization. Experiments were carried out in triplicate. The fold change in expression was then obtained by the $2^{-\Delta\Delta CT}$ method.

Immunohistochemistry

Animals were perfused, and immunohistochemical procedures were performed as described later. Rapidly frozen sections with 20 μM were co-incubated with primary anti-AIF1 antibody (Wako Pure Chemical Industries, Chuo-ku, Osaka, Japan, 019-19741) and anti-LAMP2 antibody (Santa Cruz Biotechnology, Dallas, TX, USA, sc-19991) overnight at 4°C. Secondary AlexaFluor 488 goat anti-rabbit IgG (A-11008) or AlexaFluor 594 goat anti-mouse (A-11032) from Thermo Fisher Scientific Waltham, MA, USA, was added for 2 h to detect Iba1 and LAMP2, followed by mounting of sections with prolong gold antifade reagent with 4,6-diamidino-2-phenylindole (Thermo Fisher Scientific, Waltham, MA, USA, P36935). Fluorescent images were acquired on a Zeiss Observer. AxioVs 40 4.8.0.0 software (Carl Zeiss, Thornwood, NY, USA) was used to process the images.

Cathepsin D Activity

CTSD Activity Assay Kit (Fluorometric; ab65302) from Abcam, Cambridge, MA, USA, was used to study CTSD activity. The cell lysates were incubated with reaction buffer for 1 h at 37°C. CTSD activity was determined by comparing the relative fluorescence units (Ex/Em = 328/460 nm) against the levels of the controls.

Lysosomal Membrane Permeability Assay

Acridine orange is a versatile fluorescence dye that easily crosses the cell membrane and reversibly accumulates into acidified membrane-bound compartments, such as lysosomes. Acridine orange gives fluorescence emission in a concentration-dependent manner, which is red at high concentrations (e.g., in lysosomes) to green at low concentrations (e.g., in the cytosol), with yellow as intermediate (e.g., upon trapping in nucleoli). The ratio of red-to-green emission in comparison with controls may thus either monitor lysosomal leakage or change in lysosomal pH. rPMs were grown in 96-well culture plates. rPMs were first exposed with acridine orange (5 μg/ml) at 37°C for 15 min, which were rinsed, then incubated in HBSS with or without cART and NAC for the indicated times. Cells were examined at 1 h intervals using a Synergy™ Mx Monochromator-Based Multi-Mode Microplate Reader (BioTek Instruments, Inc. Winooski, VT, USA) with excitation wavelength at 485 nm and emission recorded at 530 and 620 nm. To further confirm cART-mediated lysosomal membrane permeabilization (LMP), cells were stained with GAL3 and LAMP2.

Plasmid Transfection

To study the autophagosome formation and maturation, rPMs were transfected with tandem fluorescent-tagged MAP1LC3B plasmid (ptfLC3; a gift from Tamotsu Yoshimori; Addgene, 21074) (31). Briefly, cells were grown in 10% FBS-DMEM overnight until 70% confluence. Then, the culture medium was replaced with 250 μl of Opti-MEM® I Reduced Serum Medium. Cells were then transfected with the GFP-MAP1LC3B plasmid using Lipofectamine® 3000 Reagent, according to the manufacturer's protocol, for 12 h. After that, the culture medium was replaced with the 10% heat-inactivated FBS-DMEM for 24 h. Cells were then treated with various reagents for the indicated time and processed for further analysis.

Combined Antiretroviral Therapy Injection in HIV Tg Rats

HIV-1 Tg rats (8–9 months old) were randomly separated into four groups ($n = 3$): (1) saline, (2) cART, (3) cART + NAC, and (4) NAC. For the usage of cART, the preformulated cocktail contained two reverse transcriptase inhibitors, 10-mg/kg TDF, and 25-mg/kg FTC plus 1.25 mg/kg of the integrase inhibitor DTG in a solvent containing 25% (v/v) polyethylene glycol 400 (PEG-400, Sigma-Aldrich, St. Louis, MO, USA, PX1286B-2), 15% (w/v) captisol, and 0.075-N sodium hydroxide (Sigma-Aldrich, St. Louis, MO, USA, S8045) in water. We do acknowledge that there are several combinations of antiretroviral drugs and that the common first-line cART regimen includes two NRTIs and a boosted protease inhibitor or an integrase inhibitor (24, 25). In the present study, we sought to assess the effect of a combination of two NRTIs, TDF and FTC, and an integrase inhibitor, DTG, on microglial activation. The rationale for using the antiretroviral cocktail in this study is based on the fact that this regimen is not only shown to be effective in inhibiting virus replication in the clinical setting (25, 28–30) but also have been efficacious in the SIV–macaque model (26, 27), as well as the humanized mouse model of HIV-1 infection (32). According to the US Food and Drug Administration, due to the increased metabolic rates exhibited by rats, the recommended equivalent drug dose should be ∼6 times higher than the human dose (33, 34). We have followed guidelines for maximum injection volume by species and site location (33). The antiretroviral regimen (TDF, FTC, and DTG) and NAC (200 mg/kg) were injected (intraperitoneal) for 3 weeks. Rats were killed 1 h after the last injection. Rats were perfused with 0.1-M cold PBS for brain removal. The prefrontal cortex was used for total RNA and protein extraction along with the brain section preparation.

Statistical Analysis

The results are presented as mean ± SEM and were evaluated using a one-way analysis of variance followed by a Bonferroni

(Dunn) comparison of multiple experimental groups. The Student *t*-test was used for comparing two groups. All the statistical analyses were assessed using the GraphPad Prism software (Version 6.01). Values were considered statistically significant when $P < 0.05$.

RESULTS

Combined Antiretroviral Therapy-Mediated Generation of Reactive Oxygen Species in Rat Primary Microglial Cells

Our recent findings have shown that cART-mediated lysosomal dysfunction causes dysregulated autophagy leading, in turn, to microglial activation (13). In the present study, we sought to explore the upstream mediators underlying these processes. Induction of oxidative stress has been well-documented in the setting of HIV-1 infection and the context of antiretroviral therapy (20, 21, 35). For example, increased levels of oxidants and a concomitant decrease in antioxidant levels have been documented in the serum of HIV-1 infected individuals receiving antiretroviral therapy (21). We thus next sought to determine the possible involvement of ROS in cART-mediated lysosomal dysfunction and autophagy dysregulation. rPMs were exposed to cART (TDF, FTC, and DTG), each at 5 μM for various time points (0–24 h), and assessed for a generation of ROS using the DCFH-DA assay. The rationale for choosing the combination and concentrations of drugs is based on several published reports (36–38). In our previous published study (13), we have studied the effects of individual and the combinations of TDF, FTC, and DTG on lysosomal function. Our data showed a combination of three antiretroviral drugs that significantly

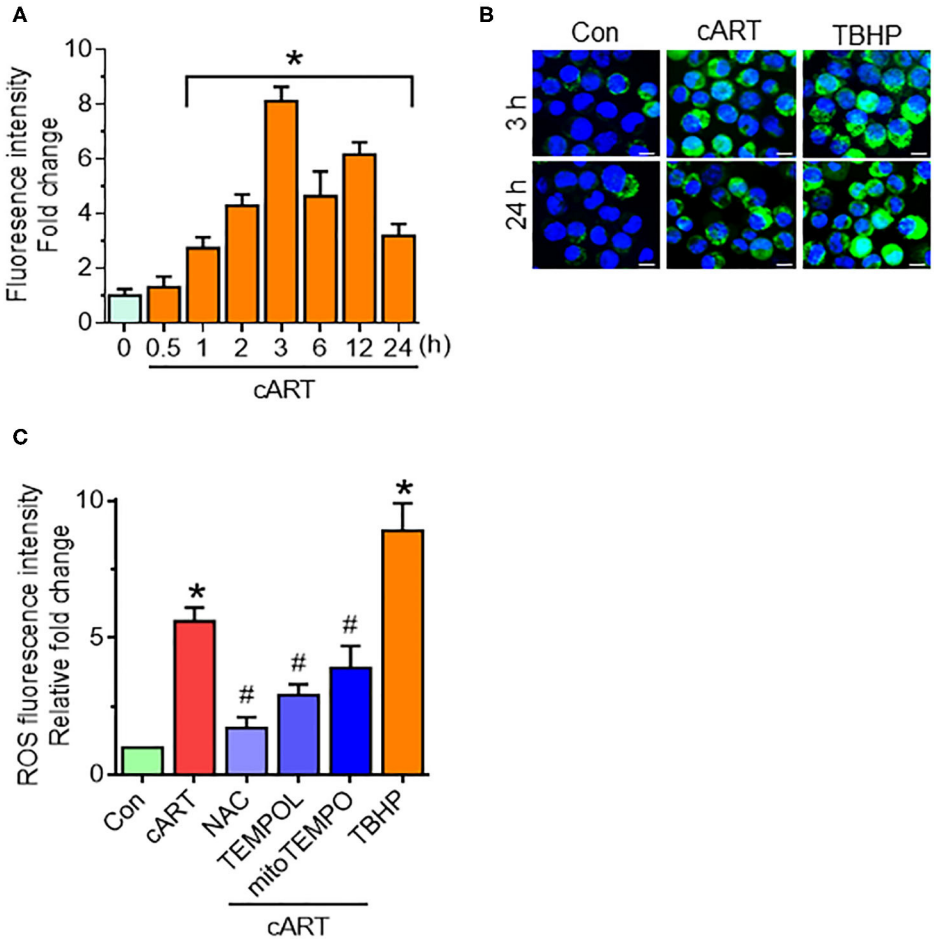

FIGURE 1 | Combined antiretroviral therapy (cART)-mediated reactive oxygen species (ROS) generation in rat primary microglial cells (rPMs). **(A)** Representative graph showing increased generation of ROS in rPMs exposed to cART at varying time points. **(B)** Representative fluorescent-microscopic image showing cART-mediated ROS generation at 3 and 24 h (Scale bar: 10 μm). **(C)** Representative graph showing effect of ROS scavengers N-acetylcysteine (NAC), 4-hydroxy-2,2,6,6-tetramethylpiperidin-1-oxyl (TEMPOL) or (2-(2,2,6,6-Tetramethylpiperidin-1-oxyl-4-ylamino)-2-oxoethyl)triphenylphosphonium chloride (mitoTEMPO) on cART-mediated upregulation of ROS. rPMS was treated with ROS scavengers for 1 h, followed by exposure of cells to cART for an additional 24 h. Tert-butyl hydroperoxide (TBHP) was used as a positive control for ROS generation. Data are from three independent experiments and are represented as means ± SEM using a one-way analysis of variance followed by a Bonferroni (Dunn) comparison of groups. $^{*}P < 0.05$ vs. control; $^{\#}P < 0.05$ vs. cART.

affected lysosomal function, which is often recommended as first-line therapy for HIV-1 infection (24). Thus, cART (TDF, FTC, and DTG; each at 5 μM) was chosen for the subsequent experiments. Firstly, the toxicity of the cART cocktail was checked by analyzing cell survival. As shown in **Figure S1A**, there was no significant difference in the cell survival of the cART-treated and non-treated rPMs. Next, as shown in **Figure 1A**, exposure of rPMs to cART resulted in significant induction of ROS within 60 min, with a peak induction at 3 h (∼8-fold; representative ROS staining is shown in **Figure 1B**), followed by a gradual decline, however, maintained ∼4-fold higher as compared with control rPMs. Next, we inhibited the generation of ROS by treating the rPMs with ROS scavengers, such as NAC (5 mM; a thiol-containing ROS scavenger), TEMPOL (20 μM; a non-thiol-containing ROS scavenger), or mitoTEMPO (10 μM; a mitochondria-specific ROS scavenger), for 1 h followed by exposure of cells to cART for an additional 24 h. TBHP was used as a positive control for ROS generation. As shown in **Figure 1C**, treatment of the cells with either NAC, TEMPOL, or mitoTEMPO significantly abrogated cART-mediated induction of ROS. Among the three ROS scavengers, NAC showed a maximum ROS scavenging effect in the rPMs treated with cART. NAC is a potent antioxidant that is well-known for its ability to mitigate oxidative stress and its downstream adverse effects (39). NAC exhibits both direct as well as indirect antioxidant properties. Its direct effect is due to a free thiol group interacting with and scavenging ROS. Its indirect antioxidant effect, on the other hand, is related to its role as glutathione (GSH) precursor, leading to increased intracellular GSH concentrations (40). There are reports suggesting replenishment of whole-blood GSH and T-cell GSH levels in HIV-infected individuals after NAC treatment (41).

N-Acetylcysteine-Reversed Combined Antiretroviral Therapy-Mediated Lysosomal Dysfunction in Rat Primary Microglial Cells

Our previous findings showed cART-mediated lysosomal dysfunction (13). Our data showed significant downregulation of LAMP2 expression starting at 6 h, with a continued trend of downregulation up to 24 h in the rPMs exposed to cART. In the present study, we sought to determine whether cART-mediated ROS induction played a role in lysosomal dysfunction. To validate this, rPMs were treated with cART cocktail with or without NAC (5 mM) for 24 h, after which the expression of LAMP2 and mature (m)CTSD proteins was assessed by Western blotting. LAMP2 is a lysosome membrane protein whose downregulation affects lysosomal membrane permeability. mCTSD is the mature form of pro-cathepsin (pCTSD). The maturation of cathepsins and their activity is dependent on the acidity of the lysosomes (low pH) (42–44). Interestingly, rPMs treated with NAC abrogated cART-mediated downregulation of LAMP2 (**Figure 2A**) and mCTSD (**Figure 2B**). Additionally, we also performed a lysosomal functional analysis in rPMs treated with cART cocktail with or without NAC for 24 h. Treatment of rPMs with NAC significantly abrogated cART-mediated upregulation of LMP (**Figure 2C**). Furthermore, NAC abrogated cART-mediated downregulation of CTSD activity (**Figure 2D**). Next, we thus sought to determine the role of NAC in maintaining lysosomal pH in the rPMs treated with cART. As shown in **Figure 2E**, the treatment of rPMs with NAC inhibited a cART-mediated increase in lysosomal pH in rPMs.

To further assess the role of cART on LMP, we analyzed the translocation of GAL3 into the damaged lysosomes. GAL3 staining is one of the best approaches for determining LMP, a process by which leaky lysosomes are detected because of abundant and rapid translocation of GAL3 into the leaky lysosomes. Under normal conditions, GAL3 is uniformly distributed in the cells, and any change in LMP results in the translocation of GAL3 into the leaky lysosomes, thereby forming the puncta (45). As shown in **Figures 2F,G**, exposure of rPMs to cART (24 h) significantly increased the colocalization of LAMP2 with GAL3, and this effect was significantly abrogated in cells that were treated with NAC, followed by exposure to cART. Furthermore, acridine orange staining was performed in rPMs exposed to cART to validate further the findings observed with LMP. Acridine orange is a fluorescent dye that easily traverses the cell membrane. Acridine orange, which is a weak base, reversibly accumulates into the acidified membrane-bound compartments, such as the lysosomes. The fluorescent emission of acridine orange is concentration-dependent, being red at high concentrations (e.g., in lysosomes) and green at low concentrations (e.g., in the cytosol), with yellow as intermediate (e.g., upon trapping in nucleoli). Thus, lysosomal leakage or lysosomal pH change can be easily assessed by determining the shifts from red-to-green emission ratio in comparison with the respective control cells. As shown in **Figures S1B,C**, rPMs exposed to cART exhibited increased green emission that was significantly abrogated in cells treated with NAC followed by exposure to cART. Furthermore, as the cART stock solutions were prepared in DMSO, the effect of untreated and DMSO (vehicle, 0.01% [v/v]) treatment was checked on rPMs. As shown in **Figure S3**, there was no significant difference in the ROS, CD11b, and LAMP2 levels in the untreated and DMSO (vehicle)-treated rPMs.

N-Acetylcysteine-Reversed Combined Antiretroviral Therapy-Mediated Autophagy Dysregulation in Rat Primary Microglial Cells

In our previous published study, we have shown cART-mediated autophagy dysregulation (13). Autophagy is regulated by autophagy-associated proteins, such as BECN1, an autophagosome initiation marker, and microtubule-associated protein 1 light chain 3 beta (MAP1LC3B/LC3B), an autophagosome formation marker, and SQSTM1/p62, an autophagy degradation marker. Defective or impaired autophagy, on the other hand, is shown to be associated with the accumulation of the protein p62 (46, 47). Data from our previous study showed no significant difference in the accumulation of MAP1LC3B and SQSTM1 in the rPMs exposed to cART

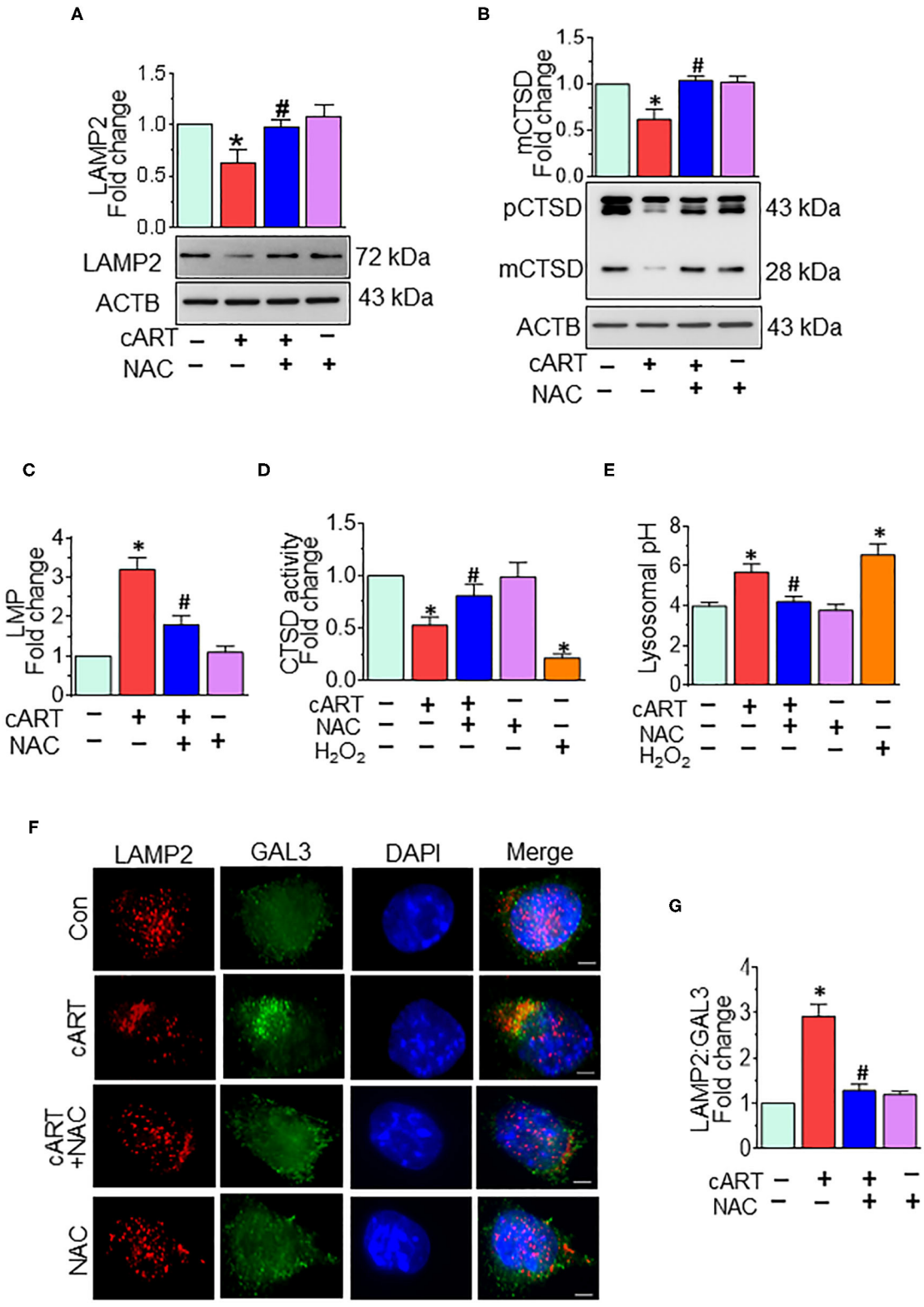

FIGURE 2 | N-acetylcysteine (NAC) reverses combined antiretroviral therapy (cART)-mediated lysosomal dysfunction in rat primary microglial cells (rPMs). rPMs were seeded into six-well plates and subject to various treatments for 24 h. Protein homogenates were prepared for the detection of indicated molecules.

(Continued)

FIGURE 2 | (A,B) Representative Western blots showing treatment of microglia with NAC-reversed cART-mediated downregulation of lysosomal-associated membrane protein 2 (LAMP2) **(A)** and mature cathepsin D (mCTSD) expression levels **(B)**. mCTSD is the mature form of pro-cathepsin (pCTSD). Maturation of cathepsins and their activity is dependent on the acidity of the lysosomes (low pH). **(C–E)** Representative bar graph showing NAC-mediated protection of lysosomal membrane permeabilization (LMP) **(C)**, CTSD activity **(D)**, and lysosomal pH **(E)** in the presence of cART. **(F)** Representative fluorescent-microscopic image showing the cART-mediated increase in LAMP2 and galectin 3 (GAL3) colocalization (Scale bar: 5 μm). **(G)** Representative bar graph showing quantitative values of LAMP2 and GAL3 colocalization. A minimum of 50 randomly chosen cells for each experimental group were analyzed. For all Western blots, ACTB served as a protein loading control. Data are from three independent experiments and are represented as means ± SEM and were analyzed using one-way ANOVA. $^{*}P < 0.05$ vs. control; $^{\#}P < 0.05$ vs. cART.

in the presence/absence of Bafilomycin A1, which confirmed the accumulation of autophagosomes in the cART-treated rPMs. In the present study, we sought to determine the role of cART-mediated ROS induction in dysregulation of autophagy. To validate this, rPMs were treated with cART cocktail with or without NAC for 24 h, after which the expression of autophagy markers MAP1LC3B and SQSTM1 was assessed by Western blotting. As expected, and as shown in **Figures 3A,B**, the treatment of rPMs with NAC markedly blocked the cART-mediated upregulation of MAP1LC3B along with SQSTM1, thereby implying increased autophagosome–lysosome fusion. To further validate these findings and to decipher the ability of cART to regulate the autophagosome–lysosome fusion efficiency, rPMs were transfected with a tandem fluorescent-tagged MAP1LC3B reporter plasmid followed by treatment of cells with cART with or without NAC. This reporter plasmid is an indicator of the extent of autophagic flux, as evidenced by the fluorescent color (yellow or red) (31). Under basal conditions, there is an even distribution of the red and the green signals. Autophagosome formation is represented by yellow puncta, owing to the colocalization of red and green fluorescence. Additionally, the maturation stage is represented by the red puncta, as green fluorescence is quenched in the autolysosomes, owing to the acidic environment. As shown in **Figures 3C,D**, rPMs treated with cART exhibited a significant increase in the yellow puncta and decreased in the red puncta, thereby indicating incomplete autophagosome maturation. On the other hand, rPMs treated with NAC followed by cART exposure (for 24 h) demonstrated a significant increase in the red puncta with a moderate level of yellow puncta compared with rPMs exposed to cART alone.

N-Acetylcysteine-Reversed Combined Antiretroviral Therapy-Mediated Activation of Rat Primary Microglial Cells

Our previous findings demonstrated that in rPMs, cART treatment resulted in increased expression of pro-inflammatory cytokine messenger RNAs (mRNAs) (*Il1β*, *Il6*, and *Tnf* at 6- and 12-h post-treatment (13). Next, we sought to examine the role of NAC in abrogating cART-mediated activation of microglia. To validate this, rPMs were treated with the cART cocktail (TDV, FTC, DTG, each at 5 μM) with or without NAC (5 mM) for 12 h, after which, the expression of pro-inflammatory cytokine mRNAs was assessed by real-time quantitative PCR. Treatment of rPMs with NAC significantly blocked the cART-mediated upregulation of pro-inflammatory cytokine (*Il1β*, *Il6*, and *Tnf*) mRNAs (**Figure 4**).

N-Acetylcysteine-Reversed Combined Antiretroviral Therapy-Mediated Lysosome Impairment and Autophagy Dysregulation *in vivo*

Having demonstrated the protective effects of NAC on cART-mediated lysosomal damage and microglial activation *in vitro*, the next step was to explore *in vivo* the effects of cART on lysosomes and microglia. It must be noted that despite low viremia, viral proteins, such as transactivator of transcription (Tat) and the envelope gp120 do persist in the brains of cART-treated infected individuals (48). Therefore, to understand the efficacy of NAC in the context of cART, we resorted to using the well-established HIV Tg rat model. These rats express seven of nine HIV proteins with no active HIV replication *in vivo,* thereby best-mimicking a scenario of HIV-infected individuals on cART regimen, wherein the viral replication is often below the threshold of detection, although viral proteins continue to persist (49–52). Groups of HIV Tg rats were saline, cART, cART with NAC, and NAC-alone group, daily administration (intraperitoneal) for 3 weeks. Animals were then killed and brains removed for assessment of lysosomal markers and functioning and microglial status. Specifically, the prefrontal cortex region that is intricately linked with movement and cognitive decline in HAND patients was chosen for this study. Interestingly, similar to cell culture findings, HIV Tg rats exposed to cART also demonstrated the decreased expression of brain LAMP2, as well as mCTSD, and NAC treatment blocked these effects of cART (**Figures 5A,B**). The protective role of NAC against cART was also observed in lysosomal functioning, as evidenced by increased CTSD activity (**Figure 5C**) in the prefrontal cortex of NAC-treated rats compared with that in the cART-alone group.

We next sought to explore the effects of NAC treatment on cART-mediated dysregulation of autophagy in HIV Tg rats. Autophagy is regulated by autophagy-specific proteins, such as BECN1, MAP1LC3B/LC3B, and SQSTM1/p62. BECN1 acts during the initiation stage of autophagy by forming the isolation membrane, a double-membrane structure that engulfs cytoplasmic material to form the autophagosome. MAP1LC3B/LC3B is an autophagosome formation marker, and SQSTM1/p62 is an autophagy degradation marker. Defective or impaired autophagy is associated with the accumulation of p62 (46, 47). As shown in **Figures 5D–F**, and as expected,

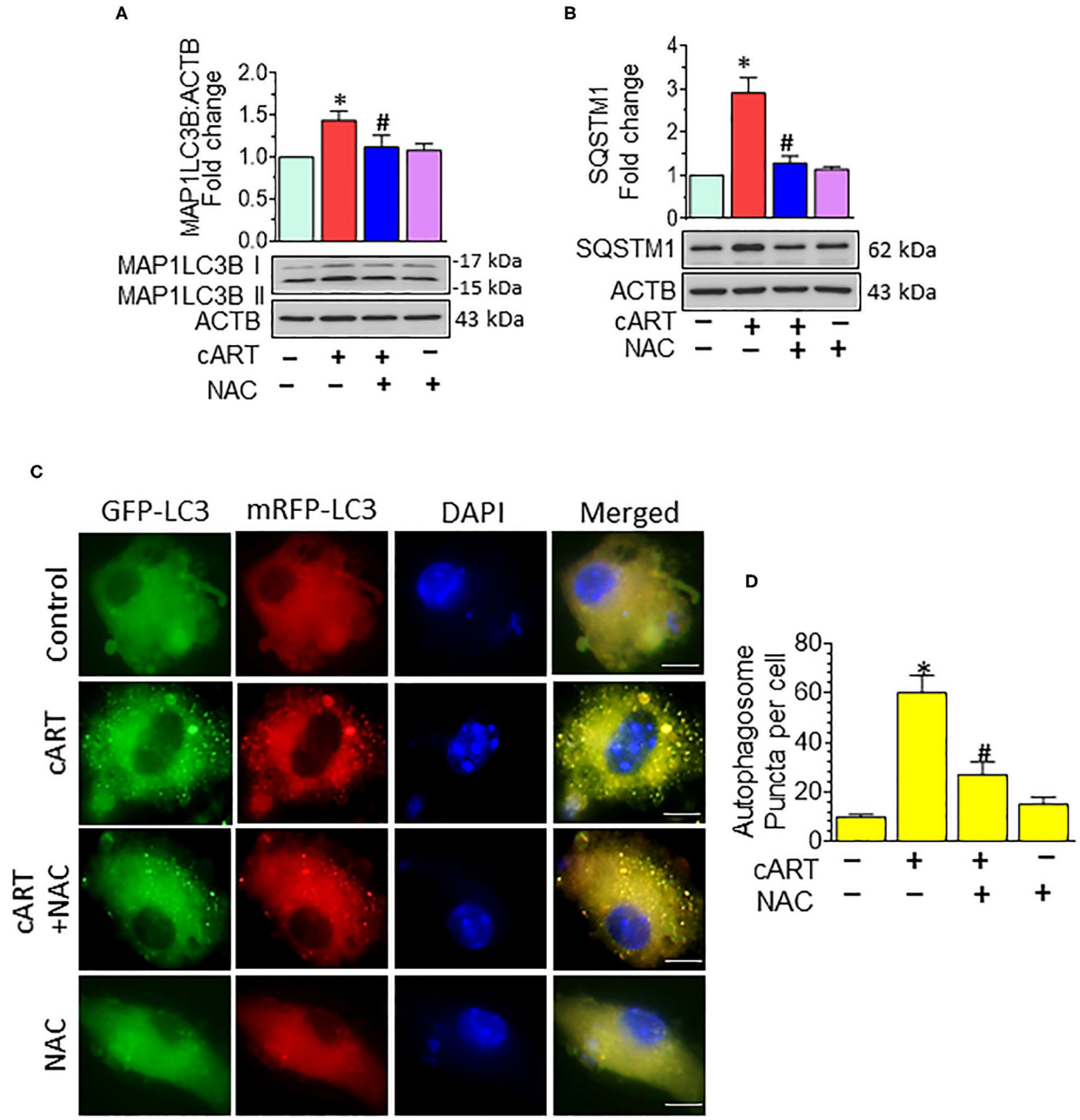

FIGURE 3 | N-acetylcysteine (NAC) reverses combined antiretroviral therapy (cART)-mediated autophagy dysregulation in rat primary microglial cells (rPMs). **(A,B)** Representative Western blots showing treatment of NAC-reversed cART-mediated upregulation of autophagy markers microtubule-associated protein 1 light chain 3 beta (MAP1LC3B) **(A)** and sequestosome 1 (SQSTM1) **(B)**. **(C,D)** rPMs were seeded into 12-well plates followed by transfection of cells with the tandem fluorescent-tagged MAP1LC3B plasmid. Cells were then exposed to various treatments for an additional 24 h and fluorescent intensity assessed by confocal microscopy (Scale bar: 5 μm). A minimum of 50 randomly chosen cells for each experimental group were analyzed. For all Western blots, ACTB served as a protein loading control. Data are from three independent experiments and are expressed as means ± SEM and were analyzed using a one-way analysis of variance followed by a Bonferroni (Dunn) comparison of groups. $^{*}P < 0.05$ vs. control; $^{\#}P < 0.05$ vs. cART.

cART treatment significantly increased the expression of BECN1 (**Figure 5D**), MAP1LC3B (**Figure 5E**), and SQSTM1 (**Figure 5F**) in the prefrontal cortices of HIV Tg rats compared with rats not exposed to cART. Interestingly, NAC treatment blocked cART-mediated dysregulation of autophagy in the prefrontal cortices of HIV Tg rats.

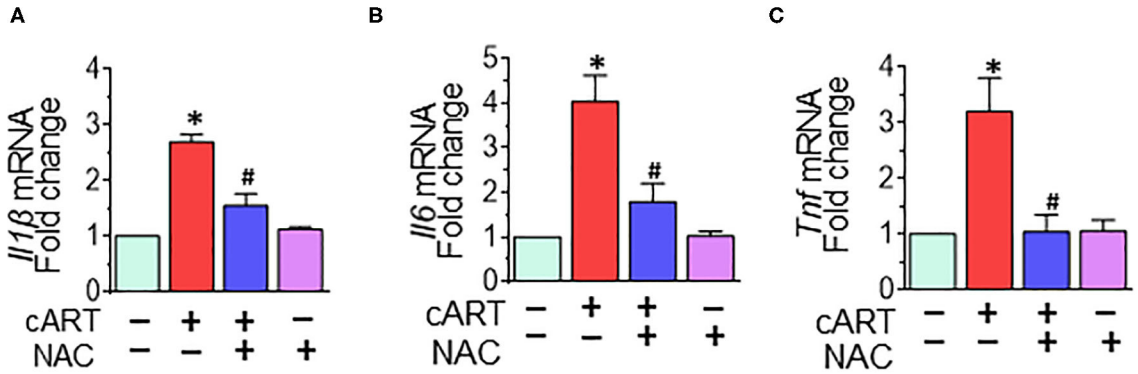

FIGURE 4 | N-acetylcysteine (NAC) reverses combined antiretroviral therapy (cART)-mediated activation of rat primary microglial cells (rPMs). rPMs were seeded into six-well plates and subject to various treatments for 12 h. **(A–C)** Representative bar graph demonstrating NAC-mediated abrogation of cART-induced messenger RNA expression of pro-inflammatory cytokines: interleukin 1 beta (*Il1β*), interleukin 6 (*Il6*), and tumor necrosis factor (*Tnf*). Data are from three independent experiments and are represented as means ± SEM and were analyzed using one-way ANOVA. $^{*}P < 0.05$ vs. control; $^{\#}P < 0.05$ vs. cART.

N-Acetylcysteine-Reversed Combined Antiretroviral Therapy-Mediated Microglial Activation *in vivo*

As shown in **Figures 6A,B**, cART administration resulted in significantly increased expression of microglial marker—ITGAM—in the prefrontal cortex, and these effects were abrogated in rats treated with NAC. To further validate lysosomal alterations in microglia *in vivo*, we next performed double immunostaining on sections of the prefrontal cortex from HIV Tg rats exposed to NAC/saline and cART. Exposure of cART to HIV Tg rats resulted in increased expression of microglial activation marker—AIF1 (**Figure S5**) with a concomitant decrease in the length of microglial processes (**Figures 6C,D**). HIV Tg rats exposed to cART also exhibited decreased LAMP2 expression and decreased colocalization of LAMP2 with AIF1 (**Figures 6E,F**) in the prefrontal cortices. As expected, NAC treatment abrogated cART-mediated impairment of lysosomes and microglial activation. The protective role of NAC was also observed in neuroinflammatory responses, as evidenced by decreased Il1β protein levels (**Figure 6G**) in the prefrontal cortices of HIV Tg rats treated with cART with NAC compared with the cART-alone group. Furthermore, we have checked the neuronal marker microtubule-associated protein 2 (MAP2) in the prefrontal cortex of HIV Tg rats treated with cART with or without NAC. **Figure S4** shows decreased MAP2 staining in the prefrontal cortex of the HIV Tg rats treated with cART, which was reversed by NAC treatment. MAP2 stabilizes neuronal shape by promoting microtubule synthesis and cross-linking with other components of the cytoskeleton and regulating microtubule networks in the axons and dendrites of neurons (53). Studies have reported that prolonged LMP activates lysosomal-dependent cell death. To exclude cell death-induced activation of microglia, we have also examined the expression of the apoptotic marker, CASP3, in the brains of HIV Tg rats treated with cART. As shown in **Figure S2**, there was no significant change in cleaved CASP3 expression in HIV Tg rats in the presence or absence of cART.

DISCUSSION

Increased neuroinflammation and microglia activation are hallmark features of HIV-infected individuals on cART (2, 6, 7). Mechanism(s) underlying these processes, although extensively studied, remains less understood. It has been well-documented that despite the effectiveness of cART in suppressing viremia, the long-term use of cART could result in severe adverse effects, including oxidative stress, mitochondrial damage, disruption of phagocytosis, and amyloid-β production in various cells (54–59). Induction of oxidative stress has been widely reported in the setting of HIV-1 infection and antiretroviral therapy (20, 21, 35). An oxidative imbalance has been demonstrated in the serum of HIV-1-infected individuals receiving antiretroviral therapy (21). There are several combinations of antiretrovirals that are clinically used to treat HIV infection (60). In the present study, we demonstrated that exposure of microglia to the three commonly used antiretrovirals (TDF, FTC, and DTG) induced the generation of ROS, which, in turn, impaired lysosomal functioning and blocked autophagosome–lysosome fusion, ultimately resulting in microglial activation.

Lysosomes are specialized cellular organelles critical for the degradation of macromolecules/damaged organelles. Lysosomal dysfunction is shown to correlate with inflammation (14, 15). Various studies have demonstrated the role of HIV-1 Tat protein (61) as well as antiretrovirals (38) in mediating endolysosomal dysfunction. Findings from our earlier *in vitro* study demonstrated that cART-mediated activation of microglia involved impaired lysosomal functioning and dysregulated autophagy (13). Herein, we sought to determine the involvement of oxidative stress as an upstream event of cART-mediated lysosomal dysfunction, leading

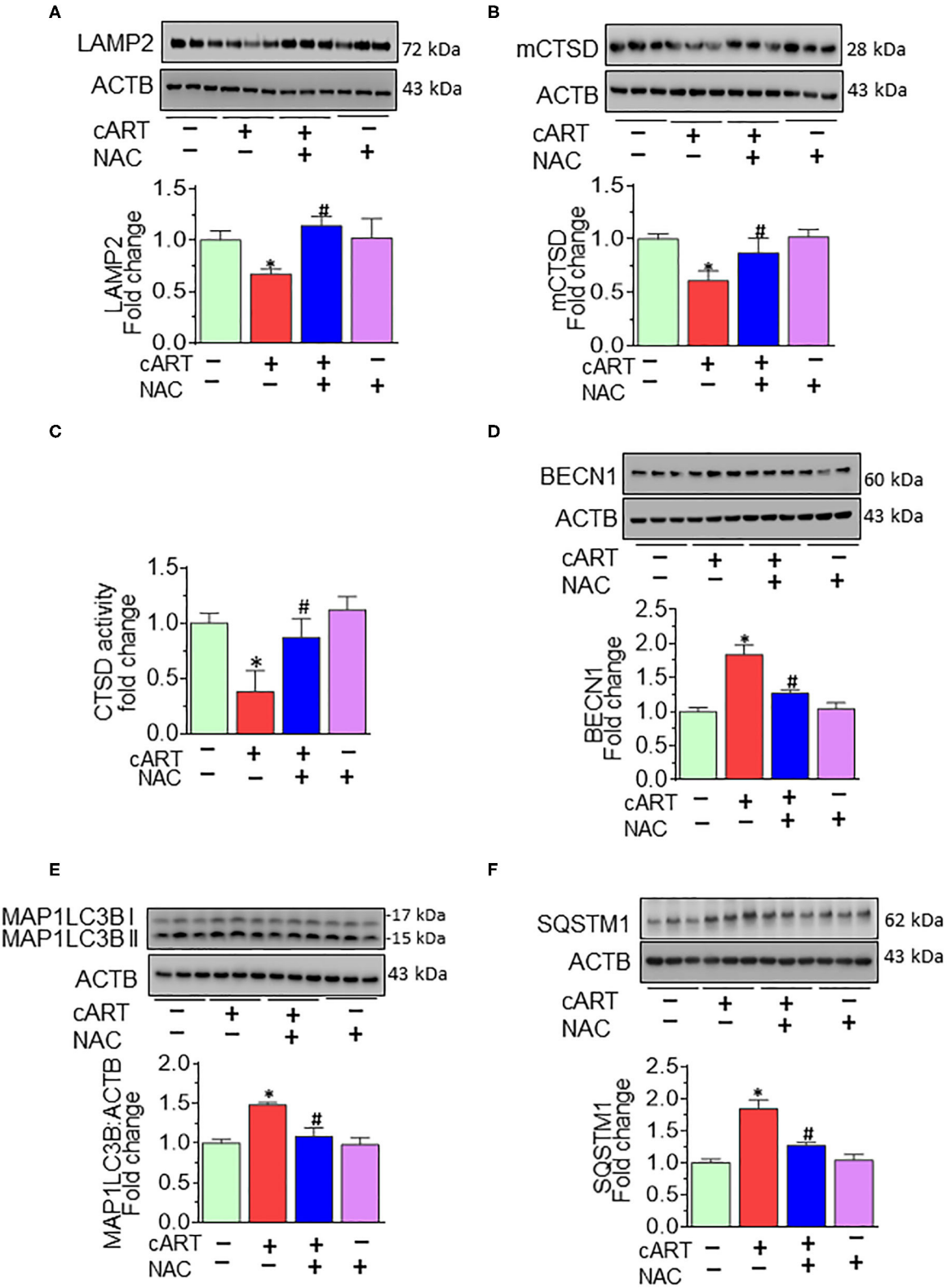

FIGURE 5 | N-acetylcysteine (NAC) reverses combined antiretroviral therapy (cART)-mediated lysosome impairment and autophagy dysregulation *in vivo*. HIV Tg rats received cART injection with or without NAC (200 mg/kg) treatment (n = 3/group, intraperitoneal, 3 weeks). Saline-injected HIV Tg rats were used as controls. Protein

(Continued)

FIGURE 5 | homogenates of prefrontal cortices were prepared to detect the levels of indicated molecules. **(A,B)** Representative Western blots showing treatment of NAC-reversed cART-mediated downregulation of both LAMP2 **(A)** and mCTSD **(B)** in the prefrontal cortices. **(C)** Representative bar graph showing NAC-reversed cART-mediated downregulation of CTSD activity. **(D–F)** Representative Western blots showing treatment of NAC-reversed cART-mediated upregulation of beclin 1 (BECN1) **(D)**, microtubule-associated protein 1 light chain 3 beta (MAP1LC3B) **(E)**, and sequestosome 1 (SQSTM1) **(F)** in the prefrontal cortices of HIV Tg rats. For all Western blots, ACTB served as a protein loading control. Data are from three independent experiments and are represented as means ± SEM and were analyzed using one-way ANOVA. $^{*}P < 0.05$ vs. control; $^{\#}P < 0.05$ vs. cART.

to microglial activation. We also examined the role of NAC in mitigating cART-mediated defects in microglia. Furthermore, our *in vitro* findings were also corroborated by *in vivo* studies, wherein we examined the protective effects of NAC against cART-mediated microglial activation in HIV Tg rats.

In the present study, we demonstrated that exposure of rPMs to cART resulted in the induction of ROS and that the ROS scavenger, NAC, significantly abrogated cART-mediated induction of ROS. NAC not only scavenges ROS but also increases the concentration of intracellular GSH to reduce oxidative stress (40). Studies have shown GSH deficiency in HIV-infected individuals, which was replenished by NAC treatment (41). Another study showed oxidative stress-mediated blood–brain barrier damage in mice exposed to HIV proteins (gp120 and Tat) and methamphetamine, which was protected by N-acetylcysteine amide, a modified form of NAC (62). NAC is an inexpensive generic supplemental drug and one of the 40 essential medicines in the list laid out by the World Health Organization (40). NAC is used as an adjunctive therapeutics for several neurological and neuropsychiatric disorders (63, 64).

Our previously published report has demonstrated cART-mediated lysosomal dysfunction in rPMs (13). Herein, we sought to examine the protective effects of NAC treatment on cART-mediated lysosomal dysfunction. Our findings demonstrated that exposure of rPMs to cART resulted in impaired lysosomes, as shown by downregulated expression of LAMP2 and mCTSD, and this effect was abrogated by treatment of cells with NAC. Next, we also sought to determine the effects of NAC treatment on cART-mediated defects in lysosomal functions. For this, we examined LMP, CTSD activity, and lysosomal pH. Treatment of NAC protected rPMs against cART-mediated increased LMP and decreased CTSD activity. NAC also maintained lysosomal pH in rPMs exposed to cART. LMP is the major cause of proton leakage through a destabilized membrane, resulting in loss of the pH gradient (65, 66). Changes in LMP were further confirmed by assessing the GAL3 translocation into the damaged lysosomes. Normally, GAL3 is uniformly distributed in the cells. Upon insult and after LMP, GAL3 translocates into the leaky lysosomes, resulting in the formation of puncta (45). In keeping with this, our studies demonstrated significant colocalization of LAGLS3 with the lysosomal LAMP2 in cART-exposed microglial cells. Intriguingly, NAC treatment abrogated translocation of GAL3 into the damaged lysosomes. These data further confirmed NAC-mediated protection of lysosomes in cART-exposed rPMs.

Lysosomes are critical for the maturation of autophagy, as the fusion of autophagosomes and lysosomes form the autolysosome, which is necessary for protein degradation (67, 68). The autophagy–lysosome pathway has been implicated in many disease conditions (69–72). Dysregulated autophagy is a hallmark feature of many types of cancers (67, 73) and multiple neurodegenerative diseases, including Parkinson's (74, 75), Alzheimer's diseases (76, 77), and HIV neuropathogenesis (78, 79).

Our findings also suggested cART-mediated dysregulation of autophagy as assessed by increased expression of autophagy mediators MAP1LC3B and SQSTM1 in rPMS exposed to cART. cART-mediated blockage of autophagy was assessed using tandem fluorescent-tagged MAP1LC3B plasmid *in vitro*. Intriguingly, ROS scavenger and lysosome protecting agent NAC ameliorated cART-mediated dysregulation of autophagy in microglia. Autophagy dysregulation and neuroinflammation are closely linked in the development of neurodegeneration (80). CNS Inflammation is a common feature in HIV-infected patients on cART (81). Our findings demonstrated cART-mediated upregulation of pro-inflammatory mediators, such as *Il6*, *Il1β,* and *Tnf*. Furthermore, the treatment of NAC inhibited cART-mediated upregulation of pro-inflammatory mediators in rPMs. Intriguingly, NAC ameliorated cART-mediated lysosomal dysfunction, autophagy dysregulation, and microglial activation, implying thereby that cART-mediated induction of ROS is upstream of lysosomal damage, dysregulated autophagy, and microglial activation. These results thus underscore the fact that strategies aimed at curbing ROS and protecting lysosomes could dampen cART-mediated neuroinflammation in treated HIV-infected individuals. NAC can thus be envisioned as an ideal candidate for scavenging cellular ROS and protecting the lysosomal membrane (66, 82). Although various studies have underscored the role of NAC as an adjunctive treatment in diseases involving ROS, the failure in clinical trials to prove the beneficial effects of antioxidant therapies remains a great disappointment in the field. For example, clinical trials with high doses of NAC did not improve respiratory health in patients with COPD and chronic bronchitis (83). Furthermore, in a large randomized trial, NAC did not reduce the risk of acute kidney injury or other clinically relevant outcomes in patients undergoing coronary and peripheral vascular angiography (84, 85). However, the major reason for the clinical trial failure was premature suspension or termination of the studies (40). Moreover, adjunctive therapy using antioxidants is one of the best approaches to harness their beneficial effects as well as to diminish the likelihood of disease exacerbation. Unraveling the mechanisms of action, optimization of concentration, and delivery at appropriate physiological sites could aid in improving the treatment efficacy of antioxidants, thus making them as efficacious

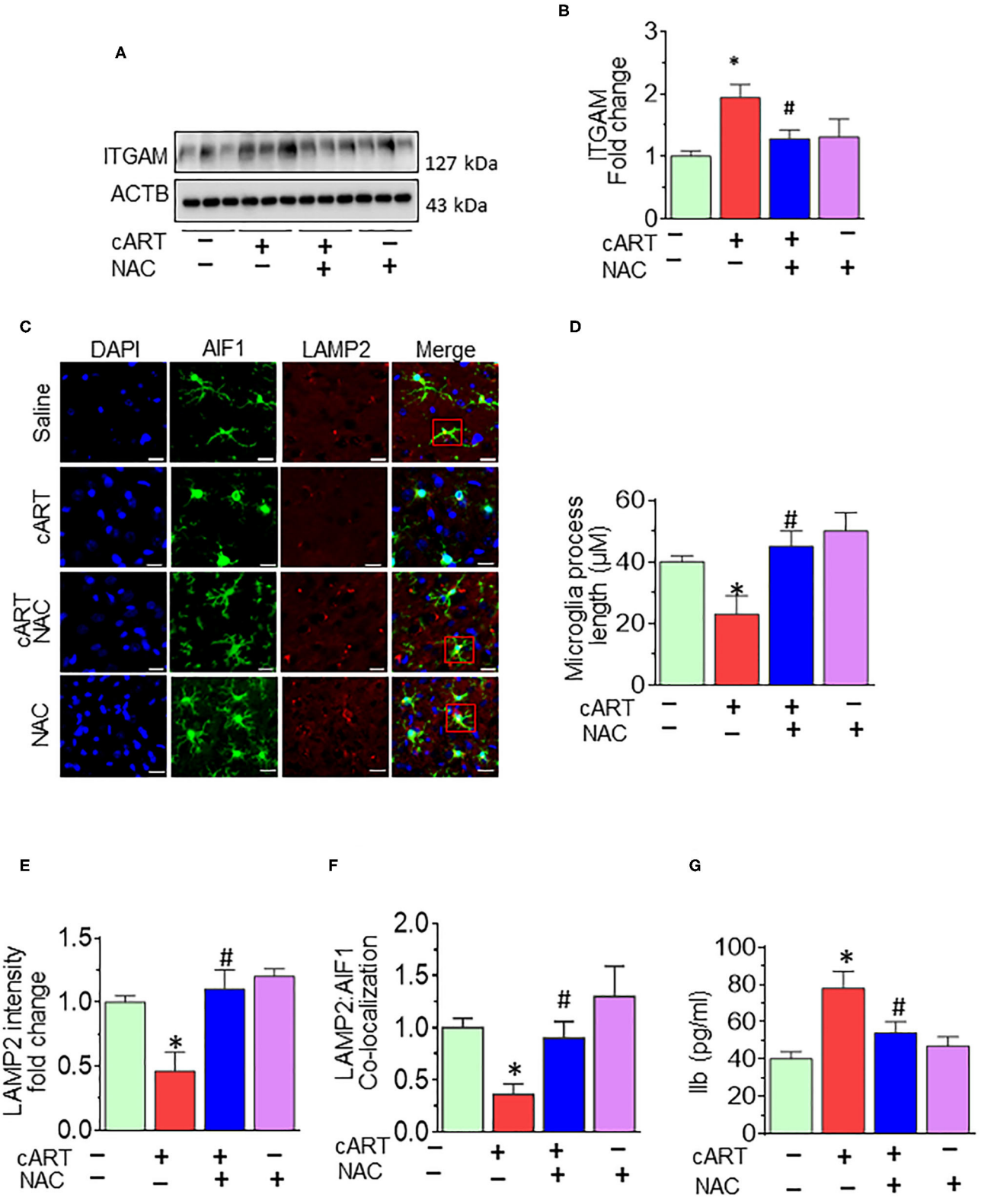

FIGURE 6 | N-acetylcysteine (NAC) reverses combined antiretroviral therapy (cART)-mediated microglial activation *in vivo*. **(A,B)** Representative Western blot and bar graph showing treatment of NAC-reversed cART-mediated upregulation of integrin subunit alpha M (ITGAM) in the prefrontal cortices of HIV Tg rats.

(Continued)

FIGURE 6 | (C) Representative fluorescent-microscopic image showing the fluorescent intensity of allograft inflammatory factor 1 (AIF1) and lysosome-associated membrane protein 2 (LAMP2) in the prefrontal cortices of HIV Tg rats receiving various treatments (Scale bar: 20 μm). A minimum of 50 randomly chosen cells for each experimental group were analyzed. Red boxes in control, NAC + cART, and NAC-alone groups represent the microglial cells with ramified cellular processes with LAMP2 colocalization, which is absent in the cART group. **(D)** Representative bar graph showing treatment of NAC-reversed cART-mediated downregulation of microglial process length. **(E,F)** Representative bar graphs showing treatment of NAC-reversed cART-mediated downregulation of LAMP2 staining and decreases colocalization of LAMP2 and AIF1 in microglia in the prefrontal cortex region. **(G)** Representative bar graph showing treatment of NAC-reversed cART-mediated upregulation of Il1β protein levels in the prefrontal cortex. Data are from three independent experiments and are represented as means ± SEM and were analyzed using one-way ANOVA. $^{*}P < 0.05$ vs. control; $^{\#}P < 0.05$ vs. cART.

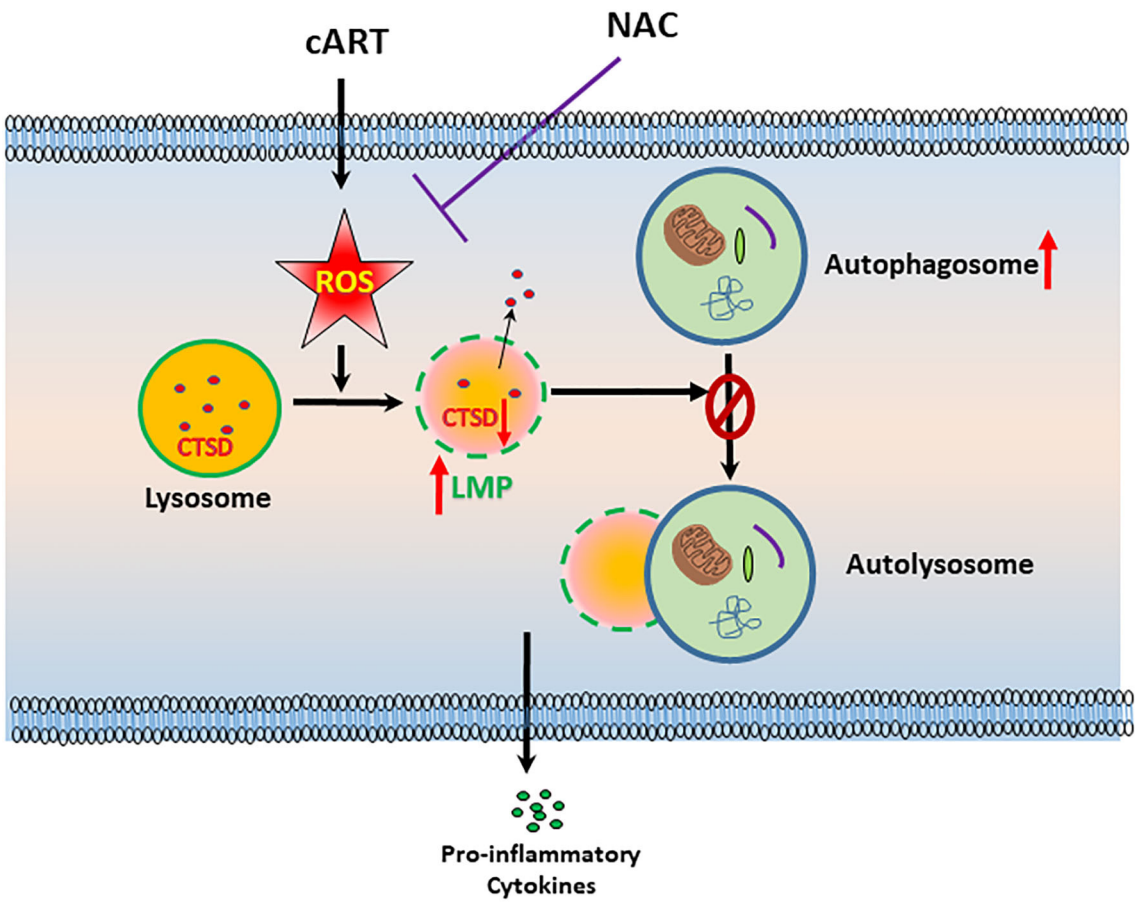

FIGURE 7 | Schematic depicting the involvement of reactive oxygen species (ROS) in combined antiretroviral therapy (cART)-mediated autophagy–lysosomal dysfunction in microglia. Exposure of microglia to cART increases ROS generation, leading, in turn, lysosomal dysfunction and autophagy dysregulation, which ultimately led to microglial activation and increased expression of pro-inflammatory cytokines. ROS scavenger N-acetylcysteine (NAC) reversed these deleterious effects of cART.

and successful therapeutic options. More clinical trials are underway that could underpin the role of NAC as an antioxidant (40, 86).

Current studies were done in isolated rat primary microglia, and we do acknowledge that data from *in vitro* microglial experiments should be interpreted with utmost care while extrapolating data in the context of the whole brain. Microglia activation status is continually affected by external cues. In cell culture, microglia are devoid of any inhibitory signals owing to lack of cell–cell interactions between microglia and other CNS cells, which are essential for maintaining microglia in quiescence (87). Furthermore, *in vitro* microglia are cultured in serum-containing medium, which is not the case under *in vivo* conditions. Serum is a poorly defined cell culture component with batch-to-batch variability that can contribute negatively to rigor and reproducibility (88, 89). Another challenge of working with microglial cultures is their species variability. Differential responses have been exhibited by rat and mouse microglial cells to the external stimuli (90). It has also been reported that human and mouse microglia age differently

(91). Overall, it is a major challenge to work with dissociated microglia with the optimal mix of environmental cues that they receive *in vivo*. In the absence of other types of CNS cells, the phenotype of microglia in cultures begins to significantly diverge from that of microglia *in vivo,* leading, in turn, to a major limitation in their predictive ability for *in vivo* biology (92).

In the present study, we resorted to validating our cell culture findings in a rodent model that recapitulates some aspects of HAND—the HIV Tg rats. HIV Tg rat mimics many of the metabolic disturbances seen in HIV-1-infected humans and is a useful tool to study the relationship between the accumulation of HIV-1 protein in the brain and the manifested clinical neurological processes (49–52). Our findings demonstrated that similar to cell culture findings, exposure of HIV Tg rats to cART also resulted in increased activation of microglia, as evidenced by increased AIF1 density and decreased length of the microglial processes in the prefrontal cortices. Our findings also demonstrated lysosomal dysfunction and autophagy dysregulation in the prefrontal cortices of HIV Tg rats exposed to cART. Some reports show dysregulated autophagy in the prefrontal cortex of post-mortem brains of persons with HIV-1-associated encephalitis (93). There is also a report that products of SIV-infected microglia inhibit neuronal autophagy (94). Based on the premise that dysregulated autophagy and inflammation are implicated as the driving force underlying pathogenesis of HAND, our results underscore the role of cART as a contributor to the progression of HAND.

In summary, our findings demonstrate that ROS-mediated autophagy–lysosomal dysfunction is central in cART-mediated microglial activation and that the potent ROS scavenger—NAC—reverses cART-mediated effects both *in vitro* and *in vivo* (**Figure 7**). Antioxidant-mediated mitigation of oxidative stress could be considered as an adjunctive therapeutic strategy for ameliorating/dampening some of the neurological complications of HAND.

DATA AVAILABILITY STATEMENT

The original contributions presented in the study are included in the article/**Supplementary Material**, further inquiries can be directed to the corresponding author/s.

ETHICS STATEMENT

All animal procedures were performed according to the protocols approved by the Institutional Animal Care and Use Committee of the University of Nebraska Medical Center and the National Institutes of Health.

AUTHOR CONTRIBUTIONS

SB, ATr, and M-LG designed the experiments. ATr, ATh, EC, PP, MB, and FN performed the experiments. SB, ATr, and M-LG analyzed the data and wrote the manuscript. All authors contributed to the article and approved the submitted version.

FUNDING

This work was supported by National Institutes of Health grants: DA047156, DA043138, DA036157 (SB and M-LG), and R25MH080661 (ATr). The support by Chronic HIV Infection and Aging in NeuroAIDS Center grant (P30MH062261; SB and Howard Fox) and the Nebraska Center for Substance Abuse Research was highly acknowledged.

ACKNOWLEDGMENTS

We thank Siddappa Byrareddy for his help in the procurement of cART.

SUPPLEMENTARY MATERIAL

The Supplementary Material for this article can be found online at: https://www.frontiersin.org/articles/10.3389/fneur.2020.00840/full#supplementary-material

REFERENCES

1. Saloner R, Cysique LA. HIV-associated neurocognitive disorders: a global perspective. *J Int Neuropsychol Soc.* (2017) 23:860–9. doi: 10.1017/S1355617717001102
2. Farhadian S, Patel P, Spudich S. Neurological complications of HIV infection. *Curr Infect Dis Rep.* (2017) 19:50. doi: 10.1007/s11908-017-0606-5
3. Ru W, Tang SJ. HIV-associated synaptic degeneration. *Mol Brain.* (2017) 10:40. doi: 10.1186/s13041-017-0321-z
4. Saylor D, Dickens AM, Sacktor N, Haughey N, Slusher B, Pletnikov M, et al. HIV-associated neurocognitive disorder–pathogenesis and prospects for treatment. *Nat Rev Neurol.* (2016) 12:234–48. doi: 10.1038/nrneurol.2016.27
5. Clifford DB, Ances BM. HIV-associated neurocognitive disorder. *Lancet Infect Dis.* (2013) 13:976–86. doi: 10.1016/S1473-3099(13)70269-X
6. Mecca C, Giambanco I, Donato R, Arcuri C. Microglia and aging: the role of the TREM2-DAP12 and CX3CL1-CX3CR1 axes. *Int J Mol Sci.* (2018) 19:318. doi: 10.3390/ijms19010318
7. Kabba JA, Xu Y, Christian H, Ruan W, Chenai K, Xiang Y, et al. Microglia: housekeeper of the central nervous system. *Cell Mol Neurobiol.* (2018) 38:53–71. doi: 10.1007/s10571-017-0504-2
8. Rubin LH, Sacktor N, Creighton J, Du Y, Endres CJ, Pomper MG, et al. Microglial activation is inversely associated with cognition in individuals living with HIV on effective anti-retroviral therapy. *AIDS.* (2018) 32:1661–7. doi: 10.1097/QAD.0000000000001858
9. Garvey LJ, Pavese N, Politis M, Ramlackhansingh A, Brooks DJ, Taylor-Robinson SD, et al. Increased microglia activation in neurologically asymptomatic HIV-infected patients receiving effective ART. *AIDS.* (2014) 28:67–72. doi: 10.1097/01.aids.0000432467.54003.f7
10. Eden A, Price RW, Spudich S, Fuchs D, Hagberg L, Gisslen M. Immune activation of the central nervous system is still present after >4 years of effective highly active anti-retroviral therapy. *J Infect Dis.* (2007) 196:1779–83. doi: 10.1086/523648
11. Lisi L, Tramutola A, Navarra P, Dello Russo C. Antiretroviral agents increase NO production in gp120/IFNgamma-stimulated cultures of rat microglia via an arginase-dependent mechanism. *J Neuroimmunol.* (2014) 266:24–32. doi: 10.1016/j.jneuroim.2013.10.013

12. Lisi L, Laudati E, Miscioscia TF, Dello Russo C, Topai A, Navarra P. Antiretrovirals inhibit arginase in human microglia. *J Neurochem.* (2016) 136:363–72. doi: 10.1111/jnc.13393
13. Tripathi A, Thangaraj A, Chivero ET, Periyasamy P, Callen S, Burkovetskaya ME, et al. Antiretroviral-mediated microglial activation involves dysregulated autophagy and lysosomal dysfunction. *Cells.* (2019) 8:1168. doi: 10.3390/cells8101168
14. Bosch ME, Kielian T. Neuroinflammatory paradigms in lysosomal storage diseases. *Front Neurosci.* (2015) 9:417. doi: 10.3389/fnins.2015.00417
15. Fiorenza MT, Moro E, Erickson RP. The pathogenesis of lysosomal storage disorders: beyond the engorgement of lysosomes to abnormal development and neuroinflammation. *Hum Mol Genet.* (2018) 27:R119–29. doi: 10.1093/hmg/ddy155
16. Platt FM, Boland B, van der Spoel AC. The cell biology of disease: lysosomal storage disorders: the cellular impact of lysosomal dysfunction. *J Cell Biol.* (2012) 199:723–34. doi: 10.1083/jcb.201208152
17. Pascua-Maestro R, Diez-Hermano S, Lillo C, Ganfornina MD, Sanchez D. Protecting cells by protecting their vulnerable lysosomes: Identification of a new mechanism for preserving lysosomal functional integrity upon oxidative stress. *PLoS Genet.* (2017) 13:e1006603. doi: 10.1371/journal.pgen.1006603
18. Hussain T, Tan B, Yin Y, Blachier F, Tossou MC, Rahu N. Oxidative stress and inflammation: what polyphenols can do for us? *Oxid Med Cell Longev.* (2016) 2016:7432797. doi: 10.1155/2016/7432797
19. Zuo L, Zhou T, Pannell BK, Ziegler AC, Best TM. Biological and physiological role of reactive oxygen species–the good, the bad and the ugly. *Acta Physiol (Oxf).* (2015) 214:329–48. doi: 10.1111/apha.12515
20. Sharma B. Oxidative stress in HIV patients receiving anti-retroviral therapy. *Curr HIV Res.* (2014) 12:13–21. doi: 10.2174/1570162x12666140402100959
21. Mandas A, Iorio EL, Congiu MG, Balestrieri C, Mereu A, Cau D, et al. Oxidative imbalance in HIV-1 infected patients treated with anti-retroviral therapy. *J Biomed Biotechnol.* (2009) 2009:749575. doi: 10.1155/2009/749575
22. Akay C, Cooper M, Odeleye A, Jensen BK, White MG, Vassoler F, et al. Anti-retroviral drugs induce oxidative stress and neuronal damage in the central nervous system. *J Neurovirol.* (2014) 20:39–53. doi: 10.1007/s13365-013-0227-1
23. Poljsak B. Strategies for reducing or preventing the generation of oxidative stress. *Oxid Med Cell Longev.* (2011) 2011:194586. doi: 10.1155/2011/194586
24. *Antiretroviral Therapy for HIV Infection: Overview, FDA-Approved Antivirals and Regimens*. Medscape (2018). Available online at: https://emedicine.medscape.com/article/1533218-overview#showall (accessed February 15, 2020).
25. Saag MS, Benson CA, Gandhi RT, Hoy JF, Landovitz RJ, Mugavero MJ, et al. Antiretroviral drugs for treatment and prevention of HIV infection in adults: 2018 recommendations of the International Antiviral Society-USA panel. *JAMA.* (2018) 320:379–96. doi: 10.1001/jama.2018.8431
26. Okoye AA, Hansen SG, Vaidya M, Fukazawa Y, Park H, Duell DM, et al. Early anti-retroviral therapy limits SIV reservoir establishment to delay or prevent post-treatment viral rebound. *Nat Med.* (2018) 24:1430–40. doi: 10.1038/s41591-018-0130-7
27. Del Prete GQ, Smedley J, Macallister R, Jones GS, Li B, Hattersley J, et al. Short communication: comparative evaluation of coformulated injectable combination antiretroviral therapy regimens in simian immunodeficiency virus-infected rhesus macaques. *AIDS Res Hum Retroviruses.* (2016) 32:163–8. doi: 10.1089/AID.2015.0130
28. Baldin G, Ciccullo A, Capetti A, Rusconi S, Sterrantino G, Cossu MV, et al. Efficacy and safety of switching to dolutegravir plus emtricitabine/tenofovir disoproxil fumarate (TDF) or elvitegravir/cobicistat/emtricitabine/TDF in virologically suppressed HIV-infected patients in clinical practice: results from a multicentre, observational study. *HIV Med.* (2019) 20:164–8. doi: 10.1111/hiv.12688
29. Stellbrink HJ, Arribas JR, Stephens JL, Albrecht H, Sax PE, Maggiolo F, et al. Co-formulated bictegravir, emtricitabine, and tenofovir alafenamide versus dolutegravir with emtricitabine and tenofovir alafenamide for initial treatment of HIV-1 infection: week 96 results from a randomised, double-blind, multicentre, phase 3, non-inferiority trial. *Lancet HIV.* (2019) 6:e364–72. doi: 10.1016/S2352-3018(19)30080-3
30. Cahn P, Madero JS, Arribas JR, Antinori A, Ortiz R, Clarke AE, et al. Dolutegravir plus lamivudine versus dolutegravir plus tenofovir disoproxil fumarate and emtricitabine in antiretroviral-naive adults with HIV-1 infection (GEMINI-1 and GEMINI-2): week 48 results from two multicentre, double-blind, randomised, non-inferiority, phase 3 trials. *Lancet.* (2019) 393:143–55. doi: 10.1016/S0140-6736(18)32462-0
31. Kimura S, Noda T, Yoshimori T. Dissection of the autophagosome maturation process by a novel reporter protein, tandem fluorescent-tagged LC3. *Autophagy.* (2007) 3:452–60. doi: 10.4161/auto.4451
32. Medina-Moreno S, Zapata JC, Cottrell ML, Le NM, Tao S, Bryant J, et al. Disparate effects of cytotoxic chemotherapy on the antiviral activity of anti-retroviral therapy: implications for treatments of HIV-infected cancer patients. *Antivir Ther.* (2019) 24:177–86. doi: 10.3851/IMP3285
33. Nair AB, Jacob S. A simple practice guide for dose conversion between animals and human. *J Basic Clin Pharm.* (2016) 7:27–31. doi: 10.4103/0976-0105.177703
34. Everson F, Genis A, Ogundipe T, De Boever P, Goswami N, Lochner A, et al. Treatment with a fixed dose combination anti-retroviral therapy drug containing tenofovir, emtricitabine and efavirenz is associated with cardioprotection in high calorie diet-induced obese rats. *PLoS ONE.* (2018) 13:e0208537. doi: 10.1371/journal.pone.0208537
35. Popoola TD, Awodele O. Interplay between anti-retroviral therapy and oxidative stress in HIV seropositive patients. *Afr J Med Med Sci.* (2016) 45:5–21.
36. Calcagno A, Di Perri G, Bonora S. Pharmacokinetics and pharmacodynamics of anti-retrovirals in the central nervous system. *Clin Pharmacokinet.* (2014) 53:891–906. doi: 10.1007/s40262-014-0171-0
37. Patel SH, Ismaiel OA, Mylott WR Jr, Yuan M, McClay JL, Paris JJ, et al. Cell-type specific differences in anti-retroviral penetration and the effects of HIV-1 Tat and morphine among primary human brain endothelial cells, astrocytes, pericytes, and microglia. *Neurosci Lett.* (2019) 712:134475. doi: 10.1016/j.neulet.2019.134475
38. Hui L, Ye Y, Soliman ML, Lakpa KL, Miller NM, Afghah Z, et al. Antiretroviral drugs promote amyloidogenesis by de-acidifying endolysosomes. *J Neuroimmune Pharmacol.* (2019). doi: 10.1007/s11481-019-09862-1. [ahead of print].
39. Kerksick C, Willoughby D. The antioxidant role of glutathione and N-acetyl-cysteine supplements and exercise-induced oxidative stress. *J Int Soc Sports Nutr.* (2005) 2:38–44. doi: 10.1186/1550-2783-2-2-38
40. Salamon S, Kramar B, Marolt TP, Poljsak B, Milisav I. Medical and dietary uses of N-acetylcysteine. *Antioxidants (Basel).* (2019) 8:111. doi: 10.3390/antiox8050111
41. De Rosa SC, Zaretsky MD, Dubs JG, Roederer M, Anderson M, Green A, et al. N-acetylcysteine replenishes glutathione in HIV infection. *Eur J Clin Invest.* (2000) 30:915–29. doi: 10.1046/j.1365-2362.2000.00736.x
42. Turk V, Stoka V, Vasiljeva O, Renko M, Sun T, Turk B, et al. Cysteine cathepsins: from structure, function and regulation to new frontiers. *Biochim Biophys Acta.* (2012) 1824:68–88. doi: 10.1016/j.bbapap.2011.10.002
43. Ishidoh K, Kominami E. Processing and activation of lysosomal proteinases. *Biol Chem.* (2002) 383:1827–31. doi: 10.1515/BC.2002.206
44. Erickson AH. Biosynthesis of lysosomal endopeptidases. *J Cell Biochem.* (1989) 40:31–41. doi: 10.1002/jcb.240400104
45. Aits S, Kricker J, Liu B, Ellegaard AM, Hamalisto S, Tvingsholm S, et al. Sensitive detection of lysosomal membrane permeabilization by lysosomal galectin puncta assay. *Autophagy.* (2015) 11:1408–24. doi: 10.1080/15548627.2015.1063871
46. Park JM, Huang S, Wu TT, Foster NR, Sinicrope FA. Prognostic impact of Beclin 1, p62/sequestosome 1 and LC3 protein expression in colon carcinomas from patients receiving 5-fluorouracil as adjuvant chemotherapy. *Cancer Biol Ther.* (2013) 14:100–7. doi: 10.4161/cbt.22954
47. Mathew R, Karp CM, Beaudoin B, Vuong N, Chen G, Chen HY, et al. Autophagy suppresses tumorigenesis through elimination of p62. *Cell.* (2009) 137:1062–75. doi: 10.1016/j.cell.2009.03.048
48. Nath A. Eradication of human immunodeficiency virus from brain reservoirs. *J Neurovirol.* (2015) 21:227–34. doi: 10.1007/s13365-014-0291-1
49. Reid W, Sadowska M, Denaro F, Rao S, Foulke J Jr, Hayes N, et al. An HIV-1 transgenic rat that develops HIV-related pathology and immunologic dysfunction. *Proc Natl Acad Sci USA.* (2001) 98:9271–6. doi: 10.1073/pnas.161290298

50. Peng J, Vigorito M, Liu X, Zhou D, Wu X, Chang SL. The HIV-1 transgenic rat as a model for HIV-1 infected individuals on HAART. *J Neuroimmunol.* (2010) 218:94–101. doi: 10.1016/j.jneuroim.2009.09.014
51. Royal W III, Zhang L, Guo M, Jones O, Davis H, Bryant JL. Immune activation, viral gene product expression and neurotoxicity in the HIV-1 transgenic rat. *J Neuroimmunol.* (2012) 247:16–24. doi: 10.1016/j.jneuroim.2012.03.015
52. Vigorito M, Connaghan KP, Chang SL. The HIV-1 transgenic rat model of neuroHIV. *Brain Behav Immun.* (2015) 48:336–49. doi: 10.1016/j.bbi.2015.02.020
53. Dehmelt L, Halpain S. The MAP2/Tau family of microtubule-associated proteins. *Genome Biol.* (2005) 6:204. doi: 10.1186/gb-2004-6-1-204
54. Manda KR, Banerjee A, Banks WA, Ercal N. Highly active anti-retroviral therapy drug combination induces oxidative stress and mitochondrial dysfunction in immortalized human blood-brain barrier endothelial cells. *Free Radic Biol Med.* (2011) 50:801–10. doi: 10.1016/j.freeradbiomed.2010.12.029
55. Apostolova N, Gomez-Sucerquia LJ, Gortat A, Blas-Garcia A, Esplugues JV. Compromising mitochondrial function with the anti-retroviral drug efavirenz induces cell survival-promoting autophagy. *Hepatology.* (2011) 54:1009–19. doi: 10.1002/hep.24459
56. Brinkman K, Smeitink JA, Romijn JA, Reiss P. Mitochondrial toxicity induced by nucleoside-analogue reverse-transcriptase inhibitors is a key factor in the pathogenesis of antiretroviral-therapy-related lipodystrophy. *Lancet.* (1999) 354:1112–5. doi: 10.1016/S0140-6736(99)06102-4
57. Blas-Garcia A, Apostolova N, Ballesteros D, Monleon D, Morales JM, Rocha M, et al. Inhibition of mitochondrial function by efavirenz increases lipid content in hepatic cells. *Hepatology.* (2010) 52:115–25. doi: 10.1002/hep.23647
58. Apostolova N, Gomez-Sucerquia LJ, Alegre F, Funes HA, Victor VM, Barrachina MD, et al. ER stress in human hepatic cells treated with Efavirenz: mitochondria again. *J Hepatol.* (2013) 59:780–9. doi: 10.1016/j.jhep.2013.06.005
59. Bollmann FM. Telomerase inhibition may contribute to accelerated mitochondrial aging induced by anti-retroviral HIV treatment. *Med Hypotheses.* (2013) 81:285–7. doi: 10.1016/j.mehy.2013.04.028
60. Adolescents USDoHaHSPOAGfAa. *Recommendation on Integrase Inhibitor Use in Antiretroviral Treatment-Naive HIV-Infected Individuals.* (2013). Available online at: https://aidsinfo.nih.gov/news/1392/recommendation-on-integrase-inhibitor-use-in-antiretroviral-treatment-naive-hiv-infected-individuals-from-the-hhs-panel-on-antiretroviral-guidelines-for-adults-and-adolescents
61. Hui L, Chen X, Haughey NJ, Geiger JD. Role of endolysosomes in HIV-1 Tat-induced neurotoxicity. *ASN Neuro.* (2012) 4:243–52. doi: 10.1042/AN20120017
62. Banerjee A, Zhang X, Manda KR, Banks WA, Ercal N. HIV proteins (gp120 and Tat) and methamphetamine in oxidative stress-induced damage in the brain: potential role of the thiol antioxidant N-acetylcysteine amide. *Free Radic Biol Med.* (2010) 48:1388–98. doi: 10.1016/j.freeradbiomed.2010.02.023
63. Bavarsad Shahripour R, Harrigan MR, Alexandrov AV. N-acetylcysteine (NAC) in neurological disorders: mechanisms of action and therapeutic opportunities. *Brain Behav.* (2014) 4:108–22. doi: 10.1002/brb3.208
64. Deepmala, Slattery J, Kumar N, Delhey L, Berk M, Dean O, et al. Clinical trials of N-acetylcysteine in psychiatry and neurology: a systematic review. *Neurosci Biobehav Rev.* (2015) 55:294–21. doi: 10.1016/j.neubiorev.2015.04.015
65. Repnik U, Cesen MH, Turk B. The use of lysosomotropic dyes to exclude lysosomal membrane permeabilization. *Cold Spring Harb Protoc.* (2016) 2016:447–50. doi: 10.1101/pdb.prot087106
66. Wang F, Gomez-Sintes R, Boya P. Lysosomal membrane permeabilization and cell death. *Traffic.* (2018) 19:918–31. doi: 10.1111/tra.12613
67. Zhong Z, Sanchez-Lopez E, Karin M. Autophagy, inflammation, and immunity: a troika governing cancer and its treatment. *Cell.* (2016) 166:288–98. doi: 10.1016/j.cell.2016.05.051
68. Green DR, Levine B. To be or not to be? How selective autophagy and cell death govern cell fate. *Cell.* (2014) 157:65–75. doi: 10.1016/j.cell.2014.02.049
69. Malicdan MC, Noguchi S, Nishino I. Autophagy in a mouse model of distal myopathy with rimmed vacuoles or hereditary inclusion body myopathy. *Autophagy.* (2007) 3:396–8. doi: 10.4161/auto.4270
70. Pan T, Kondo S, Le W, Jankovic J. The role of autophagy-lysosome pathway in neurodegeneration associated with Parkinson's disease. *Brain.* (2008) 131:1969–78. doi: 10.1093/brain/awm318
71. Yu C, Huang X, Xu Y, Li H, Su J, Zhong J, et al. Lysosome dysfunction enhances oxidative stress-induced apoptosis through ubiquitinated protein accumulation in Hela cells. *Anat Rec (Hoboken).* (2013) 296:31–9. doi: 10.1002/ar.22612
72. Liu WJ, Shen TT, Chen RH, Wu HL, Wang YJ, Deng JK, et al. Autophagy-lysosome pathway in renal tubular epithelial cells is disrupted by advanced glycation end products in diabetic nephropathy. *J Biol Chem.* (2015) 290:20499–510. doi: 10.1074/jbc.M115.666354
73. Moscat J, Karin M, Diaz-Meco MT. p62 in cancer: signaling adaptor beyond autophagy. *Cell.* (2016) 167:606–9. doi: 10.1016/j.cell.2016.09.030
74. Zeng XS, Geng WS, Jia JJ, Chen L, Zhang PP. Cellular and molecular basis of neurodegeneration in Parkinson disease. *Front Aging Neurosci.* (2018) 10:109. doi: 10.3389/fnagi.2018.00109
75. Cerri S, Blandini F. Role of autophagy in Parkinson's disease. *Curr Med Chem.* (2019) 26:3702–18. doi: 10.2174/0929867325666180226094351
76. Colacurcio DJ, Pensalfini A, Jiang Y, Nixon RA. Dysfunction of autophagy and endosomal-lysosomal pathways: roles in pathogenesis of Down syndrome and Alzheimer's Disease. *Free Radic Biol Med.* (2018) 114:40–51. doi: 10.1016/j.freeradbiomed.2017.10.001
77. Moloudizargari M, Asghari MH, Ghobadi E, Fallah M, Rasouli S, Abdollahi M. Autophagy, its mechanisms and regulation: implications in neurodegenerative diseases. *Ageing Res Rev.* (2017) 40:64–74. doi: 10.1016/j.arr.2017.09.005
78. Leymarie O, Lepont L, Berlioz-Torrent C. Canonical and non-canonical autophagy in HIV-1 replication cycle. *Viruses.* (2017) 9:270. doi: 10.3390/v9100270
79. Liu Z, Xiao Y, Torresilla C, Rassart E, Barbeau B. Implication of different HIV-1 genes in the modulation of autophagy. *Viruses.* (2017) 9:389. doi: 10.3390/v9120389
80. Jin MM, Wang F, Qi D, Liu WW, Gu C, Mao CJ, et al. A critical role of autophagy in regulating microglia polarization in neurodegeneration. *Front Aging Neurosci.* (2018) 10:378. doi: 10.3389/fnagi.2018.00378
81. Tavazzi E, Morrison D, Sullivan P, Morgello S, Fischer T. Brain inflammation is a common feature of HIV-infected patients without HIV encephalitis or productive brain infection. *Curr HIV Res.* (2014) 12:97–110. doi: 10.2174/1570162x12666140526114956
82. De Milito A, Iessi E, Logozzi M, Lozupone F, Spada M, Marino ML, et al. Proton pump inhibitors induce apoptosis of human B-cell tumors through a caspase-independent mechanism involving reactive oxygen species. *Cancer Res.* (2007) 67:5408–17. doi: 10.1158/0008-5472.CAN-06-4095
83. Johnson K, McEvoy CE, Naqvi S, Wendt C, Reilkoff RA, Kunisaki KM, et al. High-dose oral N-acetylcysteine fails to improve respiratory health status in patients with chronic obstructive pulmonary disease and chronic bronchitis: a randomized, placebo-controlled trial. *Int J Chron Obstruct Pulmon Dis.* (2016) 11:799–807. doi: 10.2147/COPD.S102375
84. ACT Investigators. Acetylcysteine for prevention of renal outcomes in patients undergoing coronary and peripheral vascular angiography: main results from the randomized Acetylcysteine for Contrast-induced nephropathy Trial (ACT). *Circulation.* (2011) 124:1250–9. doi: 10.1161/CIRCULATIONAHA.111.038943
85. Weisbord SD, Gallagher M, Jneid H, Garcia S, Cass A, Thwin SS, et al. Outcomes after angiography with sodium bicarbonate and acetylcysteine. *N Engl J Med.* (2018) 378:603–14. doi: 10.1056/NEJMoa1710933
86. Steinhubl SR. Why have antioxidants failed in clinical trials? *Am J Cardiol.* (2008) 101:14D−9D. doi: 10.1016/j.amjcard.2008.02.003
87. Bajramovic JJ. Regulation of innate immune responses in the central nervous system. *CNS Neurol Disord Drug Targets.* (2011) 10:4–24. doi: 10.2174/187152711794488610
88. Bohlen CJ, Bennett FC, Tucker AF, Collins HY, Mulinyawe SB, Barres BA. Diverse requirements for microglial survival, specification, and function revealed by defined-medium cultures. *Neuron.* (2017) 94:759–73 e758. doi: 10.1016/j.neuron.2017.04.043
89. Timmerman R, Burm SM, Bajramovic JJ. An overview of *in vitro* methods to study microglia. *Front Cell Neurosci.* (2018) 12:242. doi: 10.3389/fncel.2018.00242

90. Lam D, Lively S, Schlichter LC. Responses of rat and mouse primary microglia to pro- and anti-inflammatory stimuli: molecular profiles, K(+) channels and migration. *J Neuroinflammation.* (2017) 14:166. doi: 10.1186/s12974-017-0941-3
91. Galatro TF, Holtman IR, Lerario AM, Vainchtein ID, Brouwer N, Sola PR, et al. Transcriptomic analysis of purified human cortical microglia reveals age-associated changes. *Nat Neurosci.* (2017) 20:1162–71. doi: 10.1038/nn.4597
92. Carson MJ, Crane J, Xie AX. Modeling CNS microglia: the quest to identify predictive models. *Drug Discov Today Dis Models.* (2008) 5:19–25. doi: 10.1016/j.ddmod.2008.07.006
93. Zhou D, Masliah E, Spector SA. Autophagy is increased in postmortem brains of persons with HIV-1-associated encephalitis. *J Infect Dis.* (2011) 203:1647–57. doi: 10.1093/infdis/jir163
94. Alirezaei M, Kiosses WB, Flynn CT, Brady NR, Fox HS. Disruption of neuronal autophagy by infected microglia results in neurodegeneration. *PLoS ONE.* (2008) 3:e2906. doi: 10.1371/journal.pone.0002906

Conflict of Interest: The authors declare that the research was conducted in the absence of any commercial or financial relationships that could be construed as a potential conflict of interest.

frontiers in Neurology

ORIGINAL RESEARCH
published: 25 November 2020
doi: 10.3389/fneur.2020.593146

OPEN ACCESS

Edited by:
Jerel Adam Fields, University of California, San Diego, United States

Reviewed by:
Maria Cecilia G. Marcondes, San Diego Biomedical Research Institute, United States
Thangavel Samikkannu, Texas A&M University Kingsville, United States

***Correspondence:**
Irma E. Cisneros
ircisner@utmb.edu

†Present address:
Irma E. Cisneros, Department of Pathology, Center for Addiction Research, Institute for Human Infections and Immunity, University of Texas Medical Branch, Galveston, TX, United States
Anuja Ghorpade, Albany College of Pharmacy and Health Sciences, Albany, NY, United States; Medical Innovation Collaborative of North Texas, Dallas, TX, United States
Kathleen Borgmann, Department of Pharmacology and Neuroscience, University of North Texas Health Science Center, Fort Worth, TX, United States

Specialty section:
This article was submitted to Multiple Sclerosis and Neuroimmunology, a section of the journal Frontiers in Neurology

Received: *09 August 2020*
Accepted: *28 October 2020*
Published: *25 November 2020*

Citation:
Cisneros IE, Ghorpade A and Borgmann K (2020) Methamphetamine Activates Trace Amine Associated Receptor 1 to Regulate Astrocyte Excitatory Amino Acid Transporter-2 via Differential CREB Phosphorylation During HIV-Associated Neurocognitive Disorders. Front. Neurol. 11:593146. doi: 10.3389/fneur.2020.593146

Methamphetamine Activates Trace Amine Associated Receptor 1 to Regulate Astrocyte Excitatory Amino Acid Transporter-2 via Differential CREB Phosphorylation During HIV-Associated Neurocognitive Disorders

Irma E. Cisneros†, Anuja Ghorpade† and Kathleen Borgmann†*

Department of Microbiology, Immunology, and Genetics, University of North Texas Health Science Center, Fort Worth, TX, United States

Methamphetamine (METH) use, referred to as methamphetamine use disorder (MUD), results in neurocognitive decline, a characteristic shared with HIV-associated neurocognitive disorders (HAND). MUD exacerbates HAND partly through glutamate dysregulation. Astrocyte excitatory amino acid transporter (EAAT)-2 is responsible for >90% of glutamate uptake from the synaptic environment and is significantly decreased with METH and HIV-1. Our previous work demonstrated astrocyte trace amine associated receptor (TAAR) 1 to be involved in EAAT-2 regulation. Astrocyte EAAT-2 is regulated at the transcriptional level by cAMP responsive element binding (CREB) protein and NF-κB, transcription factors activated by cAMP, calcium and IL-1β. Second messengers, cAMP and calcium, are triggered by TAAR1 activation, which is upregulated by IL-1β METH-mediated increases in these second messengers and signal transduction pathways have not been shown to directly decrease astrocyte EAAT-2. We propose CREB activation serves as a master regulator of EAAT-2 transcription, downstream of METH-induced TAAR1 activation. To investigate the temporal order of events culminating in CREB activation, genetically encoded calcium indicators, GCaMP6s, were used to visualize METH-induced calcium signaling in primary human astrocytes. RNA interference and pharmacological inhibitors targeting or blocking cAMP-dependent protein kinase A and calcium/calmodulin kinase II confirmed METH-induced regulation of EAAT-2 and resultant glutamate clearance. Furthermore, we investigated METH-mediated CREB phosphorylation at both serine 133 and 142, the co-activator and co-repressor forms, respectively. Overall, this work revealed METH-induced differential CREB phosphorylation is a critical regulator for EAAT-2 function and may thus serve as a mechanistic target for the attenuation of METH-induced excitotoxicity in the context of HAND.

Keywords: calcium, cyclic AMP, excitotoxicity, glutamate, inflammation, kinase activation

INTRODUCTION

Methamphetamine use disorder (MUD) is correlated to heightened transmission of human immunodeficiency virus (HIV) (1–3) and increases the severity and onset of HIV-associated neurocognitive disorders (HAND) (4, 5). Cognitive decline observed in the HIV+, methamphetamine (METH) using population is partly attributed to glutamate dysregulation (2, 6, 7). As a major excitatory neurotransmitter in the CNS, optimal glutamate concentrations are vital for learning, memory, problem solving and comprehension. Glutamate imbalances are linked to mental disorders including autism, schizophrenia and depression (8, 9). Glutamate homeostasis and uptake from the synaptic cleft is primarily mediated via excitatory amino acid transporters (EAATs) [as reviewed in (10, 11)]. Of the five human glutamate transporters, EAAT-2 is predominantly expressed by astrocytes and is responsible for >90% of total glutamate uptake in the brain (10, 12, 13). *In vitro*, HIV-1 results in EAAT-2 downregulation and reduced glutamate uptake in astrocytes (14–16). Glutamate, partially mediates the toxic outcomes of METH, inducing excitotoxicity (17–19). However, direct mechanisms of METH-induced EAAT-2 downregulation in astrocytes remain unclear. We previously demonstrated decreased astrocyte EAAT-2 and impaired glutamate uptake following METH and HIV-1 exposure (7). Furthermore, we identified astrocyte trace amine associated receptor (TAAR) 1 is activated by METH, leading to increased intracellular cAMP and regulation of astrocyte EAAT-2 (7). Here, we investigate signal transduction cascades, downstream of TAAR1 regulation and activation, to elucidate the mechanisms of astrocyte EAAT-2 downregulation.

We have previously shown METH-induced EAAT-2 downregulation may be partially due to the activation of astrocyte TAAR1 (7). Of the six functional human TAAR genes, TAAR1 is reported in multiple organs and within several CNS regions, including the prefrontal cortex (20). TAAR1 functions in the neuromodulation of biogenic amines and regulates subcortical monoaminergic transmission and NMDA receptor-mediated glutamate transmission. Thus, TAAR1 plays a critical role in cognitive processing (21–23). TAAR1 activation leads to increased secondary messenger, cAMP, and activation of protein kinase A and C (PKA/C) (24–26). Although the direct mechanism of PKC activation remains vague, PKC becomes activated by increased levels of intracellular calcium [$(Ca^{+2})_i$], which is documented to occur following METH exposure (27, 28).

Analysis of the EAAT-2 promoter revealed a cAMP responsive element binding protein (CREB) at −310 and nuclear factor kappa light chain enhancer of activated B cells (NF-κB) elements at −583, −334, −272, and −251 (29, 30), elements associated with immune activation. Dibutyryl cAMP significantly increases EAAT-2 transcription (12), presumably via CREB. For instance, cAMP is well-established to activate transcription of genes containing conserved cAMP responsive elements (CRE)s through the ability to phosphorylate CREB at serine 133 ($pCREB^{Ser133}$). CREB phosphorylation at serine 133 increases dimerization affinity of the CREB binding protein (CBP) and induces transcription. METH increases intracellular cAMP *via* TAAR1 activation in astrocytes (7). NF-κB promoter elements traditionally control transcription of genes involved in the regulation of host immune responses, synaptic plasticity, and memory (31, 32). Previous studies reveal that HIV-1 proteins, including negative regulatory factor (Nef), transactivator of transcription (tat), and glycoprotein 120 (gp120), activate NF-κB signaling pathways in astrocytes (33, 34). Despite METH-induced cAMP increases and HIV-1-mediated NF-κB activation, EAAT-2 expression is reduced by both METH and HIV-1, alone and in combined conditions. While EAAT-2 can be positively or negatively regulated by NF-κB and YY1 (14, 35), the mechanisms dictating CREB-mediated EAAT-2 regulation remains to be investigated. Interestingly, CREB phosphorylation at serine 142, downstream of increased intracellular calcium and calcium/calmodulin kinase (CaMK)II activation, overrides $pCREB^{Ser133}$ transcriptional activation (36, 37).

Glutamate dysregulation is a significant contributing factor to the neurotoxicity associated with METH abuse and HAND. Our previous data demonstrating METH increases intracellular cAMP *via* TAAR1 activation in astrocytes and subsequently regulates EAAT-2 and glutamate clearance levels, sets a strong basis for further investigations of METH-induced TAAR1 signaling in the transcriptional regulation of astrocyte EAAT-2. Therefore, in this study, we investigated the dichotomous outcomes of TAAR1-mediated activation of cAMP/PKA/$pCREB^{Ser133}$ and $[Ca^{+2}]_i$/CaMKII/$pCREB^{Ser142}$. Our data revealed that differential CREB phosphorylation results in EAAT-2 regulation, indicating that tipping the balance of METH-induced signaling to favor cAMP/PKA/$pCREB^{Ser133}$ serves as a promising countermeasure in reversing METH-induced EAAT-2 downregulation.

Abbreviations: $[Ca^{+2}]_I$, intracellular calcium concentrations; CaMKII, calcium/calmodulin kinase II; cAMP, cyclic adenosine monophosphate; CBP, CREB binding protein; CNS, central nervous system; CREB, cAMP responsive element binding protein; EAAT-2, excitatory amino acid transporter-2; EPPTB, benzamide N-(3-ethoxyphenyl)-4-(1-pyrrdidinyl)-3-(trifluoromethyl); GAPDH, glyceraldehyde 3-phosphate dehydrogenase; GCaMP6s, pGP-CMV-GCaMP6s plasmid; GFAP, glial fibrillary acidic protein; HAND, HIV-associated neurocognitive disorders; HIV-1, human immunodeficiency virus-1; IL-1β, interleukin 1 beta; METH, methamphetamine; NF-κB, nuclear factor kappa light chain enhancer of activated B cells; NMDA, N-methyl-D-aspartate receptor; $pCREB^{Ser133}$, CREB phosphorylated at serine 133; $pCREB^{Ser142}$, CREB phosphorylated at serine 142; PKA, protein kinase A; TAAR1, trace amine associated receptor 1.

EXPERIMENTAL PROCEDURES

Isolation, Cultivation, and Activation of Primary Human Astrocytes

Human astrocytes were isolated from first and early second trimester electively aborted specimens as previously described (38, 39). Tissues were procured in full compliance with the ethical guidelines of the National Institutes of Health, Universities of Washington and North Texas Health Science Center. Cell suspensions were centrifuged, washed, suspended in media, and plated at a density of 20×10^6 cells/150 cm^2. Adherent astrocytes were treated with trypsin and cultured to enhance the

purity of replicating astroglial cells. These astrocyte preparations were >99% pure as measured by immunocytochemistry staining for GFAP. Astrocytes were treated with METH [100 or 500 μM, National Institute on Drug abuse (NIDA) Drug Supply Program, Research Resources Identifiers (RRID):SCR_013300], HIV-1_{JRFL} (p24, 10 ng/mL), IL-1β (20 ng/mL, R&D Systems, Minneapolis, MN), N-(3-Ethoxy-phenyl)-4-pyrrolidin-1-yl-23-trifluoromethyl-benzamide (EPPTB, 20 μM, Cat# 4518 Tocris-BioTechne, Minneapolis, MN) (40–43), a cell permeable inhibitor for TAAR1, cAMP-dependent PKA inhibitor, PKI (20 μM, Cat# 476485 Sigma-Aldrich, St. Louis, MO, and Cat# V5681, Promega, Madison, WI) (44–46) and/or CaMKII inhibitor, KN62 (20 μM, Cat# 422706 and I2142, Sigma-Aldrich) (47, 48) at 37°C and 5% CO_2. HIV-1_{JRFL} was obtained through the NIH AIDS Reagent Program, Division of AIDS, NIAID, NIH: HIV-1 JR-FL Virus from Dr. Irvin Chen (49–51). Normal peripheral blood mononuclear cells (Nebraska Medicine, Apheresis Center, Omaha NE) were isolated and infected with HIV-1_{JRFL} as previously described (52). Culture supernatants were clarified by centrifugation at 10,000 g for 20 min and stored at −80°C. The concentration of HIV-1 JRFL was determined by HIV-1 p24 ELISA (Cat#: XB-1000, Xpress Bio International). Viral stocks were diluted in ASM prior to primary human astrocytes treatment. Astrocytes are not actively infected with HIV-1. Untreated astrocytes were maintained in parallel as control.

RNA Extraction and Gene Expression Analyses

Astrocyte RNA was isolated 8 h post-treatment, as previously described (53), and mRNA levels were assayed by real-time polymerase chain reaction (PCR). TaqMan 5′ nuclease real-time PCR was performed using StepOnePlus detection system (Thermo Fisher Scientific, Carlsbad, CA). Commercially available TaqMan® Gene Expression Assays were used to measure EAAT-2 (Cat# Hs00188189_m1), TAAR1 (Cat# Hs00373229_s1), PKA (Cat# Hs00427274_m1), CaMKII (Cat# Hs00947041_m1), and glyceraldehyde 3-phosphate dehydrogenase (GAPDH) (Thermo Fisher Scientific; Cat# 4310884E) mRNA levels. GAPDH, a ubiquitously expressed housekeeping gene, was used as an internal normalizing control. The 25 μl reactions were carried out at 48°C for 30 min, 95°C for 10 min, followed by 40 cycles of 95°C for 15 s and 60°C for 1 min in 96-well-optical, real-time PCR plates. Transcripts were quantified by the comparative ΔΔCT method and represented as fold-changes to respective controls.

Glutamate Clearance Assay

Primary human astrocytes were plated in 48-well-tissue culture plates at a density of 0.15×10^6 cells/well and allowed to recover for 24 h prior to treatment. Following 24 h of treatment, glutamate (400 μM), dissolved in phenol-free astrocyte medium was added into each well, and glutamate clearance was assayed at 10 h post-glutamate addition. The assay was performed and analyzed according to manufacturer's guidelines (Amplex Red Glutamic Acid/Glutamate Oxidase Assay Kit, Cat# A12221, Thermo Fisher Scientific, Carlsbad, CA). Following collection of glutamate supernatants, a colorimetric assay for measurement of metabolic activity was performed using 3-(4,5-dimethylthiazol-2-yl)-2,5-diphenyltetrazolium bromide (MTT, Cat# M2128, Sigma-Aldrich) (54). Briefly, five percent MTT reagent was added to astrocytes and incubated for 20–45 min at 37°C. The MTT solution was removed, and crystals were dissolved in DMSO for 15 min with gentle agitation. Absorbance was assayed at 490 nm in a Spectromax M5 microplate reader (Molecular Devices, Sunnyvale, CA).

cAMP Assay

Intracellular cAMP levels in astrocytes were measured using a commercially available homogenous, bioluminescence cAMP-Glo™ Assay (Cat# V1502, Promega). Adherent monolayers of astrocytes cultured in 96-well-plates (50,000 cells/well) were stimulated with forskolin (Cat# F686, Sigma-Aldrich) and METH (NIDA Drug Supply Program, RRID:SCR_013300). Cells were activated and lysed in the tissue culture plate. Lysates were diluted to a final cell concentration of ∼1,000 cells/μL in lysis buffer supplemented with cAMP specific phosphodiesterase inhibitors [500 μM 3-isobutyl-1-methylxanthine (IBMX, Cat# I7018, Sigma-Aldrich) and 100 μM Ro 20-1724 (Cat# B8279, Sigma-Aldrich)] and transferred to white opaque flat bottom 96-well-assay plates at approximately 5,000 cells/reaction. Intracellular cAMP levels were assayed using GloMax 96 Microplate Luminometer with dual injectors (Promega).

Kinase Assays

Intracellular PKA and CaMKII levels in astrocytes were measured using a commercially available homogenous, high-throughput screening method for measuring kinase activity, Kinase-Glo® Max Luminescent Assay, (Cat# V6073, Promega) and commercially available PKA Kinase Enzyme System (Cat# V4246, Promega) and CaMKIIα Kinase Enzyme System (Cat# V4018, Promega). cAMP-dependent PKA catalytic subunit α is a 40 kDa bovine recombinant enzyme expressed and purified from *E. coli* (Accession number NM_174584.2). PKA purity was 90% as defined from Promega quality control assays. Human recombinant CaMKIIα was expressed by baculovirus in sf9 insect cells using N-terminal GST tag (Accession number NM_171825, a Ser/Thr protein kinase and a member of the Ca^{+2}/calmodulin dependent protein kinase family). The specific activity of CaMKIIα was determined to be 960 nmol/min/mg as per assay protocol. Briefly, adherent monolayers of astrocytes cultured in 96-well-plates (50,000 cells/well) were treated (+/− METH, 500 μM) in PKA or CaMKIIα reaction buffer for 5, 15, or 30 min. Cells were directly activated in the tissue culture plate. Lysates were diluted to a final cell concentration of approximately 1,000 cells/μL in lysis buffer and transferred to a white opaque flat bottom 384-well-assay plate at approximately 3,000 cells/reaction. Intracellular PKA and CaMKIIα levels were assayed using GloMax 384 Microplate Luminometer with dual injectors (Promega).

Immunofluorescent Cytochemical Analyses

Cultured human astrocytes were fixed with 1:1 acetone: methanol (V/V) solution following 24 h of treatment with METH, IL-1β or HIV-1. Astrocytes were fixed for 20 min at −20°C and blocked with blocking buffer (2% BSA in 1X PBS containing 0.1% Triton X-100) for 1 h. Cells were then incubated with primary antibodies specific to TAAR1 (1:700, rabbit pAb, Abcam, Cambridge, MA, Cat# ab65633, RRID:AB_1143252, lot GR30601-3), CREB (1:500, rabbit mAb, Cell Signaling Technology Cat# 9197, RRID:AB_331277, lot #16), pCREB^{Ser133} (1:500, rabbit mAb, Cell Signaling Technology Cat# 9198, RRID:AB_2561044, lot #10), pCREB^{Ser142} (1:200, rabbit pAb, Signalway Antibody, College Park, MD, Cat# 11300-2, RRID:AB_1263514, lot #3520) and GFAP (1:400 chicken pAb, Covance, Princeton, NJ, Cat# PCK-591P-100, RRID:AB_291542, lot # D15KF02159) in blocking buffer overnight at 4°C, washed and incubated with Alexa Fluor® secondary antibodies (1:100), anti-rabbit (488 nm, green, Thermo Fisher Scientific Cat# A-11034, RRID:AB_2576217) and anti-chicken (594 nm, red, Thermo Fisher Scientific Cat# A-11042, RRID:AB_2534099). Nuclei were visualized with DAPI (1:800, Cat# D3571, Thermo Fisher Scientific). Micrographs were obtained on an ECLIPSE Ti-4 using the NLS-Elements BR. 3.0 software at room temperature.

Western Blot Analyses

Non-transfected or transfected astrocytes were cultured as adherent monolayers in 75 cm^2 flasks at a density of 8×10^6 cells/flask and allowed to recover for 24 or 48 h. Following recovery, cells were treated for 24 h with varying stimuli, and whole cell extracts were isolated using mammalian protein extraction reagent (Cat# 78501, Thermo Fisher Scientific). Cells were collected by scraping in sterile ice-cold PBS to avoid alteration of protein expression on surface of cell membranes. Protein extracts (40 μg) were boiled with 4X NuPAGE lithium dodecyl sulfate loading sample buffer (Cat# NP0007, Thermo Fisher Scientific) at 100°C for 5–10 min, resolved by Bolt 4–12% Bis-Tris gel and subsequently transferred to nitrocellulose membranes using iBlot (Thermo Fisher Scientific). The membranes were incubated with antibodies against PKA [1:700, rabbit pAb, (Cell Signaling Technology Cat# 4782, RRID:AB_2170170, lot #3], pPKA (1:700, rabbit mAb, Cell Signaling Technology Cat# 5661, RRID:AB_10707163, lot # 3), CREB (1:700, rabbit mAb, Cell Signaling Technology Cat# 9197, RRID:AB_331277, lot #16), pCREB^{Ser133} (1:700, rabbit mAb, Cell Signaling Technology Cat# 9198, RRID:AB_2561044, lot #10), CaMKII (1:500, rabbit pAb, Santa Cruz Biotechnology Cat# sc-9035, RRID:AB_634551, lot #E1313), pCaMKII (1:500, mouse mAb, Santa Cruz Biotechnology Cat# sc-32289, RRID:AB_626786, lot #J2913), or pCREB^{Ser142} (1:200, rabbit, Signalway Cat# 11300-2, RRID:AB_1263514, lot #3520) overnight at 4°C, washed and then incubated with anti-rabbit goat antibody IgG conjugated to horseradish peroxidase (1:10,000, Bio-Rad, Hercules, CA, Cat# 170-5046, RRID:AB_11125757) or anti-mouse goat antibody IgG conjugated to horseradish peroxidase (1:10,000, Bio-Rad Cat# 170-5047, RRID:AB_11125753) for 2 h at room temperature. The membranes were then developed with SuperSignal West Femto substrate (Cat# 34095, Thermo Fisher Scientific) and imaged in a Fluorochem HD2 Imager (Protein Simple, Santa Clara, CA). GAPDH (mouse, 1:1000, Santa Cruz Biotechnology Cat# sc-32233, RRID:AB_627679) was used as a loading control.

Transfection of Astrocytes

Cultured human astrocytes were transfected with On-Target plus® small interfering RNA (siRNA, Dharmacon, Lafayette, CO) pools specific to PKAαβ (siPKAα Cat# L-004649 & siPKAβ, Cat# L−004650), CaMKII (siCaMKII, Cat# L-004942), non-targeting control siRNA pools (siCON, Cat# D-001810), and without siRNA (MOCK) or with pGP-CMV-GCaMP6s, deposited by Douglas Kim (RRID:Addgene_40753) using the Amaxa™ P3 primary cell 96-well-Nucleofector kit and shuttle attachment (Lonza, Walkersville, MD) according to the manufacturer's instructions. Briefly, 1.6×10^6 astrocytes were suspended in 20 μl nucleofector solution containing siCON, siPKAαβ, siCaMKII, (100 nM) or GCaMP6s (0.5 μg/1.6×10^6 cells) and transfected using shuttle protocol CL133. GCaMP6s transfection efficiency averaged approximately 80%. Multiple chambers from the same biological donors were assayed in a minimum of triplicate determinations. Areas were randomly chosen for confocal imaging from each chamber. Baseline green fluorescence suggested successful transfection. Background fluorescence was subtracted from the standardization well for each individual biological donor, to prevent saturation of fluorescence. Transfected cells were supplemented with astrocyte media and incubated for 30 min at 37°C prior to plating. Cells were allowed to recover for 48 h prior to experimental use.

Confocal Analysis

MOCK- and GCaMP6s-transfected astrocytes were cultured on tissue culture treated μ-slides with a channel height of 0.4 mm (Cat# 86060, Ibidi, Madison, WI) at a density of 1×10^5 cells/chamber in astrocyte media. Prior to live cell imaging, astrocytes were briefly washed with PBS and supplemented with HBSS at 37°C. Time lapse images were obtained every 500 ms, from astrocytes treated with METH (500 μM) or ionomycin (10 μM). Micrographs were obtained on a Carl Zeiss LSM (Jena, Germany). Objective used was 20× Plan-Apochromat, 0.8NA, 0.55 mmWD. PMT photo detection was used with an excitation of 450–490 nm and emission of 593–668 nm. Histogram analysis were performed using ImageJ software; Version: 2.0.0-rc-41/1.5d (Fiji ImageJ Software, the National Institutes of Health, Bethesda, MD) (55). Histogram was generated from fluorescence units obtained at selected time points.

Ratiometric Calcium Imaging

Primary human astrocytes were seeded at approximately 0.1×10^6 cells on poly-D-lysine coated 22 × 22 × 1 mm coverslips, placed in 6 well-tissue culture dishes and allowed to reach confluency for 24 h. Protocol was modified as previously described (56, 57). Astrocytes were preincubated for 1 h in Krebs–Ringer buffer solution (155 mM NaCl, 2.5 mM $CaCl_2$, 1.2 mM $MgCl_2$, 24 mM $NaHCO_3$, 5 mM KCl, 25 mM HEPES and

5 mM glucose, pH 7.4) containing 3 mM Fura-2-AM (Prokine, Cat# PK-CA707-50033, Heidelberg, Germany) at 37°C prior to METH treatment (500 μM). Coverslips were mounted on laminar-flow perfusion chambers (Warner Instrument, Hamden, CT) mounted on an inverted microscope (Olympus IX81, Olympus, Melville, NY) and attached to a gravity-driven flow-controlled perfusion system (Warner Instrument). Cells were perfused continuously with Krebs-Ringer buffer +/− METH. $[Ca^{+2}]_i$ was calculated using a Fura-2 calcium calibration standard curve (Thermo Fisher Scientific, Cat# F6774). Basal $[Ca^{+2}]_i$ measurements were taken following stabilization period of 5 min prior to METH administration, and peak $[Ca^{+2}]_i$ were measured following METH treatment. Ratiometric data were collected from cells that were alternately illuminated with 340- and 380-nm wavelengths using xenon light source (Lumen200PRO, Prior Scientific, Rockland, MD). The emitted light was captured at 520 nm wavelength using a CCD camera (Hamamatsu camera controller C10600, Hamamatsu Photonics KK, Hamamatsu, Japan). Pixel data were binned (2x2), and images were captured every 3 s. Data were collected and analyzed using commercially available software (Slidebook 5.0, Intelligent Imaging Innovations, Denver, CO).

Statistical Analyses

Statistical analyses were performed using GraphPad Prism (Version 8.4.0, RRID:SCR_002798) with one-way analysis of variance (ANOVA) and Tukey's *post-test* for multiple comparisons. Linear regression and correlation analysis were performed using Prism with a two-tailed, Pearson correlation coefficient set at 95% confidence interval. $P \leq 0.05$ were considered statistically significant, and data represent means ± standard error of the mean (SEM).

RESULTS

HIV-1 and IL-1β Differentially Regulate Astrocyte TAAR1 and EAAT-2 Levels and Activity

We have previously demonstrated astrocyte TAAR1 overexpression resulted in a significant decrease in astrocyte EAAT-2 and glutamate clearance (7). Astrocyte TAAR1 knockdown prevented METH-induced EAAT-2 downregulation and increased glutamate clearance (7). Since METH abuse during CNS inflammation and HIV-1 poses greater threat due to their potential to increase TAAR1 levels/activity and crosstalk, we investigated whether IL-1β and HIV-1 downregulated EAAT-2 and affected TAAR1 levels and function (**Figure 1**). TAAR1 mRNA levels increased significantly with IL-1β (15-fold, $^{***}p < 0.001$) and HIV-1 (2.5-fold, $^{**}p < 0.01$) alone or in combined treatments (7.5-fold $^{***}p < 0.001$; **Figure 1A**). TAAR1 levels were significantly lower in combined treatments compared to IL-1β but significantly higher compared to HIV-1 (**Figure 1A**, $^{***}p < 0.001$). After IL-1β +/− HIV-1 pretreatment, baseline cAMP levels were unchanged (**Figure 1B**). Forskolin, a commonly used tool to increase intracellular cAMP levels, significantly increased astrocyte cAMP by ∼35-fold, regardless of pretreatments with IL-1β +/− HIV-1 (**Figure 1B**, $^{***}p < 0.001$). METH significantly increased intracellular cAMP in all IL-1β, HIV-1, and IL-1β + HIV-1 pretreated astrocytes (**Figure 1B**, $^{***}p < 0.001$, $^{**}p < 0.01$, $^{***}p < 0.001$, respectively). However, only IL-1β pretreatment resulted in a significantly increased cAMP response to METH, compared to METH-mediated increases in astrocytes without pretreatment (**Figure 1B**, $^{**}p < 0.01$). As IL-1β and/or HIV-1 increased TAAR1 levels, they also significantly decreased astrocyte EAAT-2 levels in parallel (**Figure 1C**). IL-1β and HIV-1, alone or in combination, significantly decreased EAAT-2 mRNA levels by 50% ($^{***}p < 0.001$), 25% ($^{**}p < 0.01$), and 55% ($^{***}p < 0.001$), respectively (**Figure 1C**). Comparisons between treatments showed that IL-1β + HIV-1 was significantly lower compared to HIV-1 alone (**Figure 1C**, $^{***}p < 0.001$). Glutamate clearance, taken as a ratio to MTT activity and converted to a fold change from control, mirrored EAAT-2 mRNA levels (**Figure 1D**). TAAR1 protein levels increased with IL-1β pre-treatment in astrocytes fixed and immunostained for TAAR1 (green), GFAP (red) and DAPI (blue) (**Figures 1E–H**). IL-1β mediated a reactive phenotype and increased TAAR1 levels when compared to control astrocytes (**Figures 1F,H**). Merged images represent TAAR1, GFAP and DAPI overlay (**Figures 1G,H**). Thus, these data demonstrated that astrocyte TAAR1 expression and intracellular cAMP are elevated in the presence of proinflammatory cytokine, IL-1β, and negatively correlated to astrocyte EAAT-2 ($^{***}p < 0.001$, $R^2 = 0.92$, data not shown).

METH Activates PKA, Phosphorylating CREB at Serine 133

METH increases intracellular cAMP in primary human astrocytes (7). cAMP, as a secondary messenger, mediates canonical signal transduction pathways that activate PKA and lead to downstream phosphorylation of substrates, including CREB, at serine 133 (58). Therefore, we next investigated PKA activity in primary human astrocytes following METH treatment, represented as fold changes +/− SEM (**Figure 2A**). PKA activity did not change in control astrocytes over time; however, METH significantly increased PKA activity at 15 min that continued to significantly increase at 30 min (**Figure 2A**, $^{***}p < 0.001$). PKA mRNA levels significantly decreased in astrocytes transfected with siPKA compared to siCON-transfected astrocytes, with/out METH treatment (**Figure 2B**, $^{***}p < 0.001$). In parallel, total PKA levels decreased 50% in siPKA-transfected astrocytes compared to siCON-transfected astrocytes (**Figure 2C**). METH induced a significant increase in PKA activity in siCON-transfected astrocytes ($^{**}p < 0.01$) that was significantly reduced with PKA RNAi (**Figure 2D**, $^{***}p < 0.001$). Furthermore, baseline PKA activity was lower in siPKA-transfected astrocytes reflecting decreases in baseline PKA (**Figure 2D**, $^{*}p < 0.05$). Western blots confirmed METH-induced phosphorylation of CREB at serine 133 ($pCREB^{Ser133}$) (**Figure 2E**). Densitometry analyses, from four independent biological donors, showed METH to significantly induce $pCREB^{Ser133}$ in 15 min (**Figure 2E**, $^{*}p < 0.05$) that remained elevated at 30 min (**Figure 2E**, $^{**}p < 0.01$). METH-mediated phosphorylation of CREB at

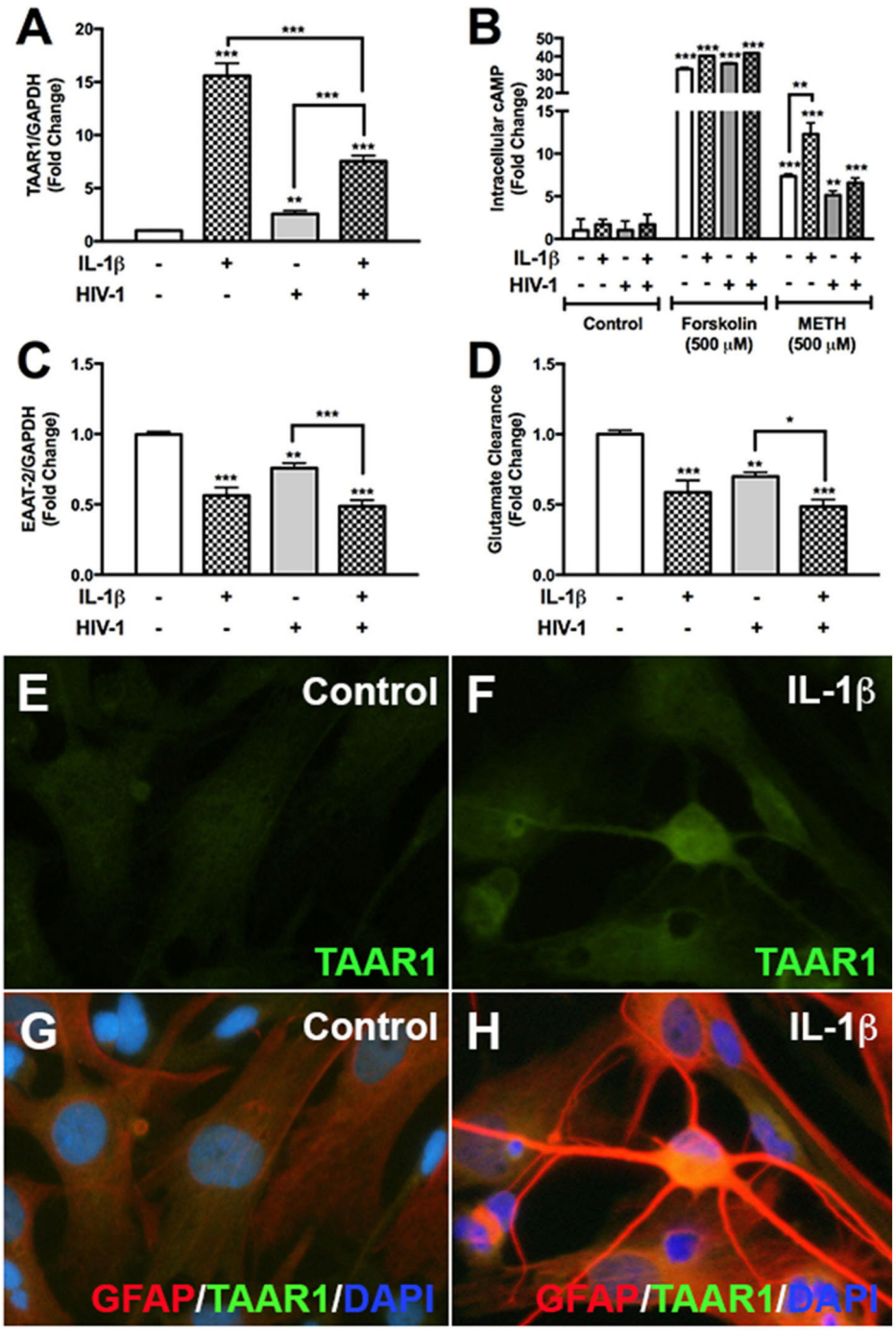

FIGURE 1 | HIV-1 and IL-1β regulate astrocyte TAAR1 & EAAT-2 mRNA levels and function. Primary human astrocytes were treated with HIV-1 (p24 10 ng/mL, gray bars) and IL-1β (20 ng/mL, hatched bars) alone or in combination, and untreated astrocytes were maintained in parallel. TAAR1 mRNA levels were analyzed following treatment with IL-1β ± HIV-1 **(A)**. Intracellular cAMP was quantified to evaluate TAAR1 signaling subsequent to IL-1β ± HIV-1 pretreatment and following 15 min of forskolin or METH stimulation and represented as fold change to control **(B)**. EAAT-2 mRNA levels were evaluated following IL-1β ± HIV-1 treatment **(C)**. Glutamate clearance was measured at 10 h post-glutamate addition **(D)**. Control and IL-1β pretreated cells were fixed and immunostained for glial fibrillary acidic protein (GFAP, red), TAAR1 (green) and DAPI (blue) **(E–H)**. Statistical analyses were performed using GraphPad Prism V6.0 with One-way ANOVA and Tukey's *post-test* for multiple comparisons. $P \leq 0.05$ were considered statistically significant and data represent means ± SEM. Representative donors were chosen from a minimum of three astrocyte donors each tested and analyzed in a minimum of triplicate determinations (*$p < 0.05$, **$p < 0.01$, ***$p < 0.001$).

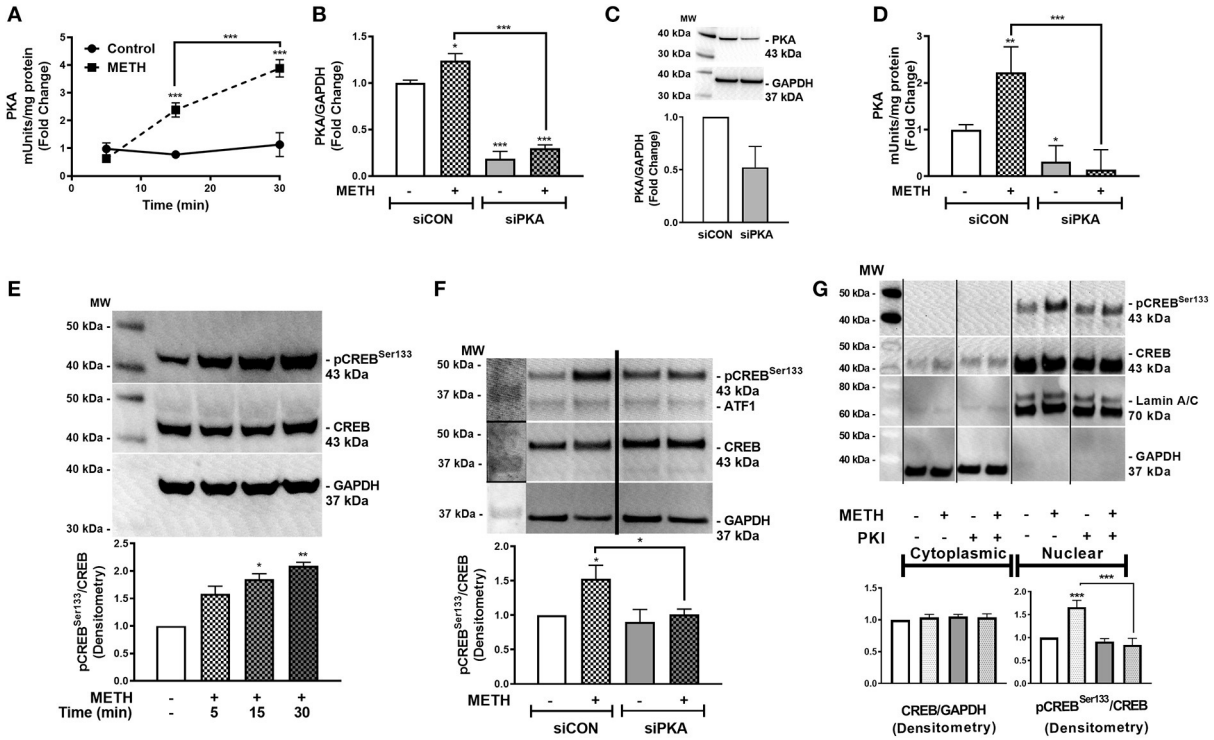

FIGURE 2 | METH activates PKA and phosphorylates CREB at serine 133 ($pCREB^{Ser133}$). PKA enzyme activity in equivalent total cell lysates was quantified at select times post-METH treatment (500 μM, square and hatched lines) and represented as fold changes of PKA mUnits/mg total protein **(A)**. PKA levels and activity were quantified in siCON- and siPKA-transfected astrocytes (clear and gray bars, respectively, as shown by fold changes in PKA/GAPDH mRNA **(B)**, protein **(C)** and PKA activity (mUnits/mg total protein) **(D)**. Immunoblotting for METH induction of $pCREB^{Ser133}$ to total CREB over time was assayed by western blot with detected bands at 43 kDa **(E)**. To determine METH-induced $pCREB^{Ser133}$ via PKA, total cell lysates were collected at 30 min post-METH treatment in siCON- and siPKA-transfected astrocytes and immunoblotted for $pCREB^{Ser133}$ and total CREB. Bands are detected at 43 kDa for $pCREB^{Ser133}$ and total CREB **(F)**. Cytoplasmic and nuclear protein extracts were collected from astrocytes treated with PKI (gray bars) +/– METH (hatched bars) and immunoblotted for $pCREB^{Ser133}$ **(G)**. The same blot is represented in panel F & G from different sections; dividing lines represent cut sections. Representative western blots are shown in **(E–G)**. Densitometry analyses were performed to quantify band intensities of phospho-proteins to total proteins on multiple immunoblots and represented as fold changes to control ± SEM, in respective panels [**(E–G)**, $n = 3$]. **(A–D)** is a representative donor chosen from multiple individual biological astrocyte donors that were tested; each was analyzed in a minimum of triplicate determinations. Molecular weight markers are identified on each western blot (MW) ($^{*}p < 0.05$, $^{**}p < 0.01$, $^{***}p < 0.001$).

serine 133 increased in siCON-transfected astrocytes at 30 min (**Figure 2F**, $^{*}p < 0.05$) that was significantly lower in siPKA-transfected astrocytes (**Figure 2F**, $^{*}p < 0.05$). Constitutively phosphorylated CREB at serine 133 is localized in the nucleus, and nuclear $pCREB^{Ser133}$ is significantly increased following METH treatment at 30 min (**Figure 2G**, $^{***}p < 0.001$). METH-mediated $pCREB^{Ser133}$ was prevented by cAMP-dependent PKA inhibitor, PKI, by ∼60% (**Figure 2G**, $^{***}p < 0.001$) implying $pCREB^{Ser133}$ is *via* METH-induced PKA activation.

METH Transiently Increases Intracellular Calcium in GCaMP6s-Transfected Astrocytes

Reports suggest that METH results in increased $[Ca^{+2}]_i$ in neurons (27, 59). To determine METH-induced activation of $[Ca^{+2}]_i$ stores, primary human astrocytes were transfected with a GCaMP6s plasmid (60). Baseline fluorescence was measured in the absence of external stimuli and plotted as 0 FLU (**Figures 3A,D**), demonstrating undetectable $[Ca^{+2}]_i$, i.e., no fluorescence (**Figure 3A**). There was an approximate 80% transfection efficiency for GCaMP6s transfection in primary human astrocytes. Although low fluorescence was detectable following 12 s of METH treatment (**Figure 3B**), a robust increase in fluorescence was visualized at 100 s (**Figure 3C**). FLU represents fluorescence from imaged astrocyte over time (**Figure 3D**). These data support the innovative use of GCaMP6s-transfected astrocytes in visualizing METH-induced increases of intracellular calcium via live cell imaging. To further support METH-mediated increases of $[Ca^{+2}]_i$, astrocytes were treated with Fura-2-AM and stimulated with METH, and subsequent calcium levels were quantified (**Figures 3E,F**). Baseline measurements were taken for 5 min prior to METH stimulation. METH (500 μM) raised intracellular calcium concentrations by ∼750 nM, reaching 1,000–1.250 nM $[Ca^{+2}]_i$ (**Figure 3E**, representative donor). Averages from 15 individual astrocytes show basal $[Ca^{+2}]_i$ to be ∼500 nM with significant increases of $[Ca^{+2}]_i$ mediated by METH (**Figure 3F**, $^{***}p <$

0.001). These data confirm that increases of $[Ca^{+2}]_i$ are sufficient to activate downstream signaling cascades and phosphorylation of substrates.

METH Activates CaMKII, Phosphorylating CREB at Serine 142

Activation of CaMKII is sensitive to increases in $[Ca^{+2}]_i$ (47). We showed METH increases $[Ca^{+2}]_i$ in primary human astrocytes (**Figure 3**). Thus, we investigated CaMKII activity in primary human astrocytes following METH treatment (**Figure 4A**). CaMKII activity did not change in control astrocytes over time. METH significantly reduced CaMKII activity as early as 5 min (**Figure 4A**, $^{**}p < 0.01$) that increased at 15 min and was significantly higher than control at 30 min (**Figure 4A**, $^{***}p < 0.001$). CaMKII mRNA levels significantly decreased in siCaMKII-transfected astrocytes by approximately 50% +/- METH treatment (**Figure 4B**, $^{***}p < 0.001$, $^{**}p < 0.01$). METH treatment alone significantly reduced CaMKII levels in siCON-transfected astrocytes (**Figure 4B**, $^{**}p < 0.01$). METH significantly increased CaMKII activity in siCON- transfected astrocytes (**Figure 4C**, $^{***}p < 0.001$). However, CaMKII activity was ∼2-fold lower in siCaMKII-transfected astrocytes as compared to siCON-transfected astrocytes (**Figure 4C**, $^{***}p < 0.001$). Immunoblotting confirmed METH-induced phosphorylation of CaMKII over time, detected as pCaMKII at 54 kDa (**Figure 4D**). Densitometry analyses from three independent biological donors confirmed METH induced significant increases in pCaMKII at 20 and 30 min (**Figure 4D**, $^{***}p < 0.001$). METH treatment over time mediated $pCREB^{Ser142}$ that was significantly increased at 30 min (**Figure 4E**, $^{**}p < 0.01$). METH significantly increased $pCREB^{Ser142}$ in siCON-transfected astrocytes (**Figure 4F**, $^{*}p < 0.05$). CaMKII RNA interference abrogated METH-induced $pCREB^{Ser142}$ compared to siCON (**Figure 4F**, $^{**}p < 0.01$) implying $pCREB^{Ser142}$ is via METH-induced CaMKII activation. Taken together, METH mediates CREB phosphorylation at serine 142 via CaMKII activation.

TAAR1 Selective Antagonist, EPPTB, Blocks METH-Induced Signaling in Astrocytes

EPPTB is a selective high affinity antagonist for TAAR1 in neurons, potently antagonizing TAAR1-induced cAMP accumulation in HEK293 cells (40). There are no studies describing EPPTB antagonism of astrocyte TAAR1 activity and/or regulation of astrocyte EAAT-2. Therefore, we evaluated EPPTB effects on astrocyte EAAT-2 (**Figure 5A**). There were no changes in astrocyte EAAT-2 with EPPTB alone. As previously observed, METH significantly reduced astrocyte EAAT-2 mRNA that significantly increased with EPPTB pretreatment (**Figure 5A**, $^{**}p < 0.01$, $^{***}p < 0.001$, respectively). The effects of EPPTB on METH-mediated TAAR1 activation were quantified by measuring intracellular cAMP (**Figure 5B**). EPPTB pretreatment did not significantly affect forskolin-induced intracellular cAMP ($^{***}p < 0.001$). On the other hand, increased cAMP, mediated by METH, was significantly reduced with EPPTB pretreatment (**Figure 5B**, $^{***}p < 0.001$). Additionally, TAAR1 antagonism with EPPTB prevented METH-mediated increases of $[Ca^{+2}]_i$ (**Figure 5C**). Together, these data suggest that successful antagonism of TAAR1 with EPPTB prevented METH-induced TAAR1 activation and prevented METH-mediated EAAT-2 downregulation. To investigate METH-induced CREB phosphorylation *via* TAAR1, astrocytes pretreated with EPPTB, and activated with METH (500 μM), were fixed and immunostained for CREB (green), $pCREB^{Ser133}$ (green), $pCREB^{Ser142}$ (green), GFAP (red), and DAPI (blue) (**Figures 5D–J**). In control astrocytes, total CREB was primarily within the nucleus (**Figure 5D**). CREB phosphorylated at serine 133 in control astrocytes was low (**Figure 5E**). CREB phosphorylated at serine 142 showed to be primarily localized perinuclear in the absence of stimulation (**Figure 5F**). Upon METH treatment, $pCREB^{Ser133/142}$ appeared more robust in astrocyte nucleus, as seen localized with DAPI (**Figures 5G,H**). EPPTB pretreatment blocked METH-induced nuclear localization of both $pCREB^{Ser133}$ and $pCREB^{Ser142}$ (**Figures 5I,J**). Thus, these data demonstrate that EPPTB successfully antagonizes astrocyte TAAR1 preventing METH-induced activation and CREB phosphorylation at serine 133 and 142, ultimately preventing EAAT-2 regulation.

IL-1β and HIV-1 Activate CREB

Although METH phosphorylated the co-activating form of CREB, astrocyte EAAT-2 remains downregulated. Likewise, IL-1β and HIV-1 resulted in EAAT-2 downregulation regardless of four NF-κB elements in the EAAT-2 promoter. To address this conundrum and determine if IL-1β and HIV-1 signal similarly to activate the dominant repressor form of CREB, $pCREB^{Ser142}$, we measured $[Ca^{+2}]_i$ changes following IL-1β treatments. IL-1β led to increased $[Ca^{+2}]_i$ in GCaMP6s-transfected astrocytes (**Figures 6A–D**). Fluorescence increased as early as 100 s of IL-1β treatment and began quenching at 150 s (**Figures 6B,D**). The change in FLU is plotted as a histogram in (**Figure 6D**). Furthermore, IL-1β significantly increased CaMKII activity at 30 min by 2.5-fold (**Figure 6E**, $^{***}p < 0.001$). Western blots showed IL-1β and HIV-1 induced CREB phosphorylation at serine 133 and 142 (**Figures 6F,G**). Densitometry analyses, from three independent donors, confirmed IL-1β and HIV-1 alone, and in combination, significantly induced $pCREB^{Ser133}$ at 30 min (**Figure 6F**, $^{**}p < 0.01$, $^{*}p < 0.05$, $^{***}p < 0.001$, respectively). Likewise, IL-1β and HIV-1 alone and in combination significantly induced $pCREB^{Ser142}$ at 30 min (**Figure 6G**, $^{*}p < 0.05$, $^{***}p < 0.001$, $^{**}p < 0.01$, respectively). Taken together, these data demonstrate IL-1β and HIV-1 induced both the co-activating and co-repressor forms of CREB.

Astrocyte EAAT-2 Is Regulated by METH-Mediated Activation of CaMKII, Not PKA

We have demonstrated METH activates PKA/$pCREB^{Ser133}$ and CaMKII/$pCREB^{Ser142}$ signal transduction pathways in primary human astrocytes. To further evaluate the impact of PKA/$CREB^{Ser133}$ and CaMKII/$CREB^{Ser142}$ on EAAT-2 regulation we transfected astrocytes with siRNAs targeting PKA and

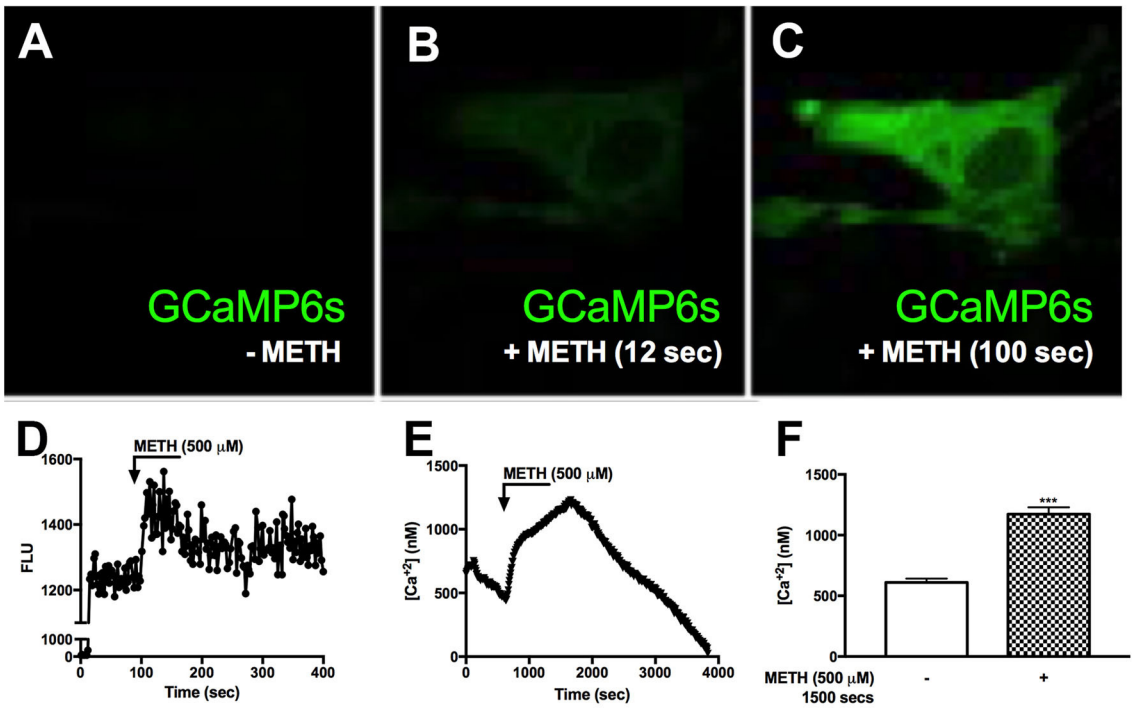

FIGURE 3 | METH induces intracellular calcium signaling in GCaMP6s-transfected astrocytes. Primary human astrocytes were transfected with GCaMP6s, a plasmid expressing an ultrasensitive protein calcium sensor, and allowed to recover overnight. MOCK-transfected astrocytes were maintained as controls in parallel. Transfected cells were treated with METH (500 μM, hatched bars) and ionomycin (10 μM) as a positive control [images not shown, **(A–C)**]. Fluorescence was visualized by confocal microscopy, and images were captured every 500 msec. **(A–C)** depict images taken from one specific cell prior to METH addition **(A)**, and post-METH addition at 12 and 100 s, respectively **(B,C)**. The histogram shows cumulative data of the pictured astrocyte captured over the entire imaging period **(D)**. $[Ca^{+2}]_i$ were quantified with a Fura-2 standard curve, representing changes in emission at 340 and 380 nm at an excitation of 510 nm (image not shown). Absolute $[Ca^{+2}]_i$ are represented in **(E,F)**. **((A–E))** is a single astrocyte traced over time representing average changes **(E)**. Several astrocytes ($n = 15$) are represented as a bar graph **(F)**. **(A–E)** are a single cell representing average change of multiple astrocyte donors that were tested; each was analyzed in a minimum of triplicate determinations. $^{***}p < 0.001$.

CaMKII or pretreated astrocytes with PKA or CaMKII inhibitors prior to METH treatment; as they are the downstream substrate targets for secondary messengers, cAMP and $[Ca^{+2}]_i$. METH mediated EAAT-2 downregulation and decreased glutamate clearance activity in siCON-and siPKA-transfected astrocytes (**Figures 7A,B**, $^{***}p < 0.001$). CaMKII downregulation did not change EAAT-2 levels but significantly increased glutamate clearance alone (**Figures 7A,B**, $^{**}p < 0.01$). METH significantly increased EAAT-2 levels in siCaMKII-transfected astrocytes compared to siCON + METH and siPKA + METH (**Figure 7A**, $^{\#\#\#}p < 0.001$) or to siCaMKII transfection alone (**Figure 7A**, $^{**}p < 0.01$). Likewise, glutamate clearance was significantly higher following METH treatment in siCaMKII-transfected astrocytes compared to that in siCON- and siPKA-transfected astrocytes (**Figure 7B**, $^{\#\#\#}p < 0.001$). PKI significantly reduced EAAT-2 mRNA levels alone or with METH (**Figure 7C**, $^{**}p < 0.01$), but did not change astrocyte glutamate clearance regardless of METH treatment (**Figure 7D**). CaMKII inhibitor, KN62, prevented METH-mediated EAAT-2 downregulation (**Figure 7C**) and significantly increased astrocyte glutamate clearance following METH treatment (**Figure 7D**, $^{*}p<0.05$). Astrocytes pretreated with PKI or KN62, with or without METH, were fixed and immunostained for EAAT-2 (green), GFAP (red), and DAPI (blue) (**Figures 7E–J**). Astrocyte EAAT-2 protein levels did not robustly change with PKI or KN62 alone compared to control astrocytes (**Figures 7E–G**). METH reduced EAAT-2 protein expression alone or in combination with PKI (**Figures 7H,I**). However, pretreatment with KN62 inhibited EAAT-2 downregulation by METH (**Figure 7J**). Taken together, our data show compelling evidence that $[Ca^{+2}]_i$/CaMKII/pCREB^{Ser142} is the predominate pathway resulting in METH-induced EAAT-2 downregulation.

DISCUSSION

This study uncovers critical signaling pathways in astrocytes mediated via METH-induced TAAR1 activation. Importantly, we identify CREB as a master regulator of astrocyte EAAT-2 following METH treatment. We demonstrate METH activates canonical cAMP/PKA/pCREB^{Ser133} and $[Ca^{+2}]_i$/CaMKII/pCREB^{Ser142} signaling in primary human astrocytes, downstream of TAAR1. TAAR1 is established to trigger an accumulation of intracellular cAMP (24), regulating expression, localization and function of monoamine

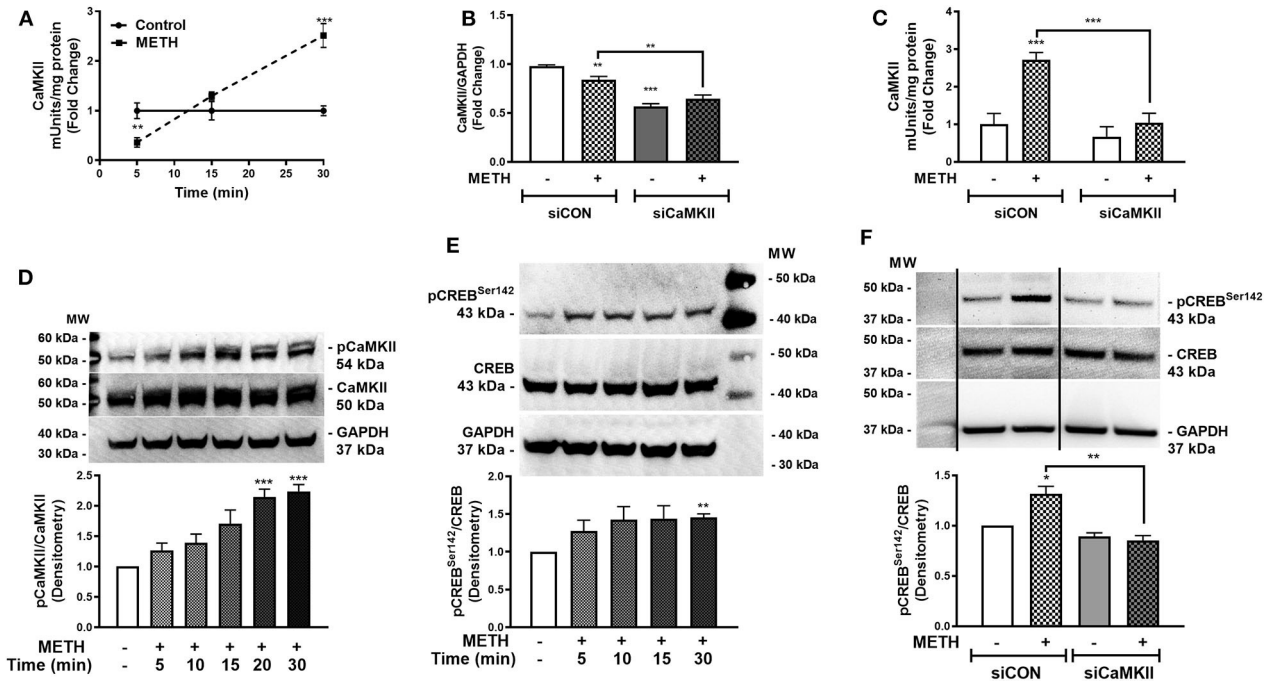

FIGURE 4 | METH activates CaMKII and phosphorylates CREB at serine 142 (pCREB^{Ser142}). CaMKII enzyme activity was quantified at 5, 15, and 30 min post-METH treatment (500 μM, squares and hatched bars) in equal amounts of cell lysates and represented as fold changes of CaMKII mUnits/mg total protein **(A)**. CaMKII levels and activity were quantified in siCON- and siCaMKII-transfected astrocytes (clear and gray bars, respectively), and represented as CaMKII/GAPDH fold changes and fold changes of CaMKII mUnits/mg total protein **(B,C)**. To evaluate METH-induced phosphorylation of CaMKII, immunoblotting for pCaMKII total CaMKII and GAPDH was detected at 54, 50, and 37 kDa, respectively in astrocytes treated with METH (500 μM) at different time points **(D)**. Immunoblotting for pCREB^{Ser142} to total CREB over time was assayed by western blot with detected bands at 43 kDa **(E)**. To determine METH-induced pCREB^{Ser142} via CaMKII, total cell lysates were collected at 30 min post-METH treatment in siCON- and siCaMKII-transfected astrocytes and immunoblotted for pCREB^{Ser142} and total CREB **(F)**. The same blot is represented in **(F)** from different sections, dividing line represents a cut section. Representative donors are shown in all panels from multiple astrocyte donors that were tested; each was analyzed in a minimum of triplicate determinations. Densitometry analyses of ratio for phospho-proteins to total proteins was performed to quantify band intensities on multiple immunoblots and represented as fold changes to control ± SEM [**(D–F)**, $n = 3$]. Molecular weight markers are identified on each western blot (MW) (*$p < 0.05$, **$p < 0.01$, ***$p < 0.001$).

transporters *via* phosphorylation of PKA and PKC (61–64). Activation of kinases such as PKA, results in phosphorylation of substrates including CREB. CREB phosphorylation traditionally involves transcriptional activation of CREB binding genes (65). Recruitment of CREB to the EAAT-2 promoter suggests increased promoter activity and EAAT-2 upregulation (29, 66). This study identifies that METH phosphorylates CREB at serine 133; however, EAAT-2 transcription decreases, indicating a differential role for CREB in EAAT-2 regulation, downstream of TAAR1. We tested the hypothesis that TAAR1-mediated signaling, following METH stimulation, dually triggers the activating and dominant repressing forms of CREB, thus dictating EAAT-2 downregulation. We demonstrate astrocyte TAAR1 levels increase following IL-1β and HIV-1 treatment, suggesting a broader role for astrocyte TAAR1 during neuroinflammation. Taken together, our studies reveal a delicate balance between METH-induced activation of cAMP/PKA/pCREB^{Ser133} and $[Ca^{+2}]_i$/CaMKII/pCREB^{Ser142} signaling in the regulation of astrocyte EAAT-2, which tips the downstream balance of EAAT-2 function from glutamate uptake to excitotoxicity.

In this study we confirm that following METH treatments, intracellular cAMP increases, activating PKA, and phosphorylating CREB at serine 133, yet results in astrocyte EAAT-2 downregulation. Kim et al. showed that exogenous application of dibutyl cAMP increases EAAT-2 transcription supporting our hypothesis that selectively activating cAMP/PKA/pCREB^{Ser133} pathway is enough to prevent METH-mediated EAAT-2 downregulation (66). Decreases in astrocyte EAAT-2, subsequent to METH treatment, is not prevented with PKA downregulation, indicating METH responses in astrocytes are likely activating transcriptional repressors. Alternatively, the abundance and distribution of cAMP-regulated guanine nucleotide exchange factors (Epac/cAMP-GEF) warrants further studies, since activation of this exchange protein may converge synergistically with PKA, or mediate increases of $[Ca^{+2}]_i$ to regulate other biological functions [reviewed in (67)]. Nonetheless, we demonstrate TAAR1 activation increases $[Ca^{+2}]_i$ in primary human astrocytes in parallel to cAMP. Several lines of evidence suggest CaMKs, downstream of increased $[Ca^{+2}]_i$, activate CREB, and result in transcriptional activation and/or repression

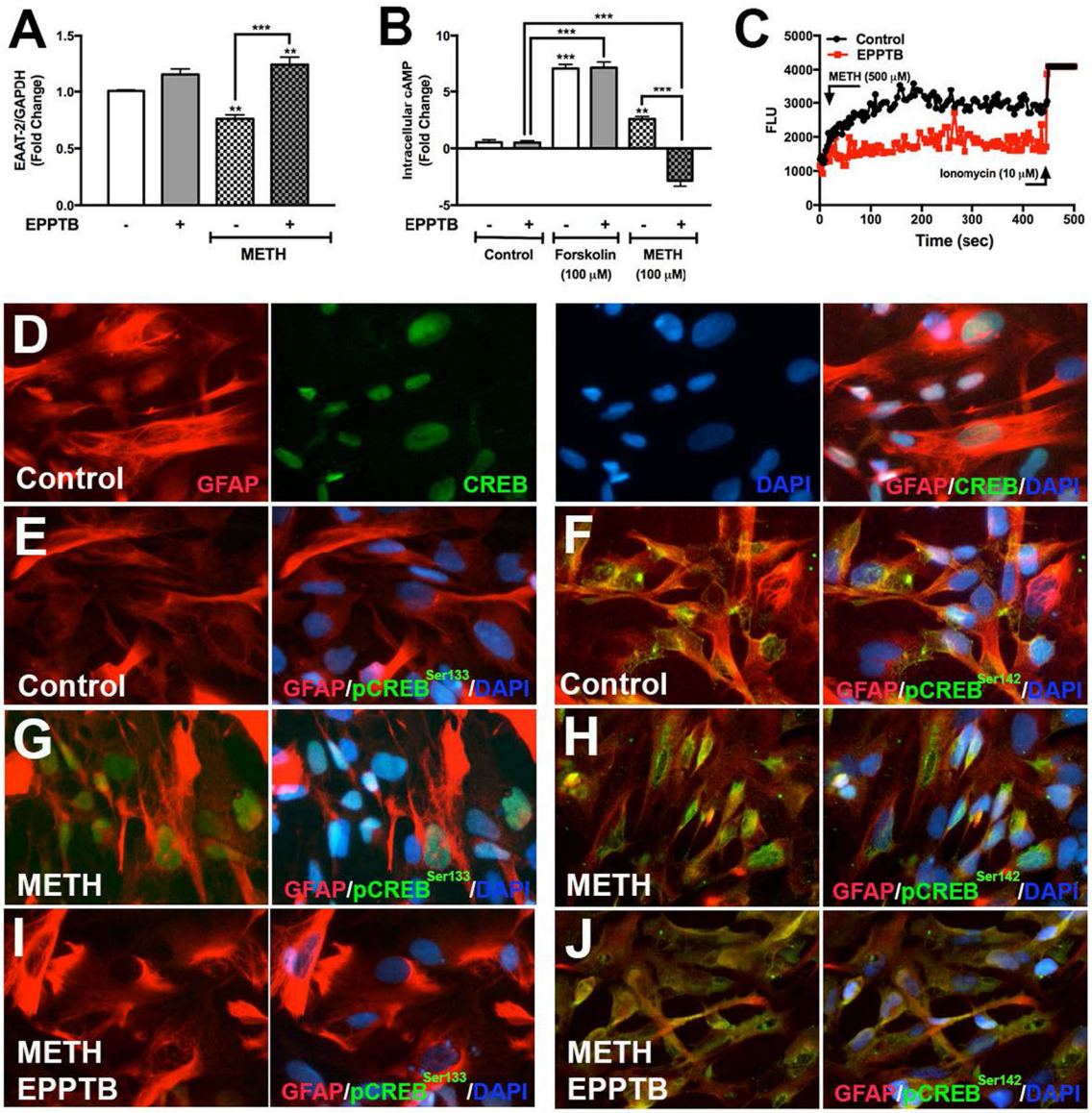

FIGURE 5 | TAAR1 selective antagonist, EPPTB, blocks METH-induced signaling in astrocytes. EAAT-2 mRNA levels were assayed in RNA isolated at 8 h post METH (hatched bars) +/– EPPTB (20 μM, gray bars), a TAAR1 selective antagonist **(A)**. Changes in cAMP levels were quantified in astrocytes treated with EPPTB for 1 h prior to METH treatment (100 μM) or forskolin treatment (100 μM) and represented as fold changes ± SEM **(B)**. GCaMP6s-transfected astrocytes were pretreated with EPPTB (red) for 1 h prior to METH stimulation in parallel to untreated astrocytes. Increases in $[Ca^{+2}]_i$ were visualized by confocal microscopy and represented as a histogram over time **(C)**. Astrocytes treated with METH, +/– EPPTB pretreatment, were fixed and immunostained with antibodies specific for total CREB [green, **(D)**], $pCREB^{Ser133}$ [green, **(E,G,I)**] or $pCREB^{Ser142}$ [green, **(F,H,J)**], GFAP (red) and DAPI [blue, **(D–J)**]. Statistical analyses were performed using GraphPad Prism V6.0 with One-way ANOVA and Tukey's *post-test* for multiple comparisons. $P \leq 0.05$ were considered statistically significant, and data represent ± SEM. Representative donors chosen from multiple astrocyte donors were tested; each was analyzed in a minimum of triplicate determinations (*$p < 0.01$, ***$p < 0.001$).

(68). This balance is mediated via phosphorylation of serine 133 and 142 (36, 37). Phosphorylation of CREB at serine 142 acts as a dominant negative regulator of $pCREB^{Ser133}$-induced transcriptional activation, despite significantly higher amounts of pCREB at serine 133 vs. serine 142 (37, 68). Efficient binding of $pCREB^{Ser133}$ to promoter elements continues; however, $pCREB^{Ser142}$ prevents CBP dimerization, thus inhibiting CREB-supported transcription (68). We hypothesize that the absence of the dominant repressor, $pCREB^{Ser142}$, would permit transcriptional activation of EAAT-2. Consistent with increased EAAT-2 transcription following dibutyl cAMP application that selectively activates PKA/$pCREB^{Ser133}$, we propose that forfeiting CaMKII/$pCREB^{Ser142}$-induced transcriptional repression, while

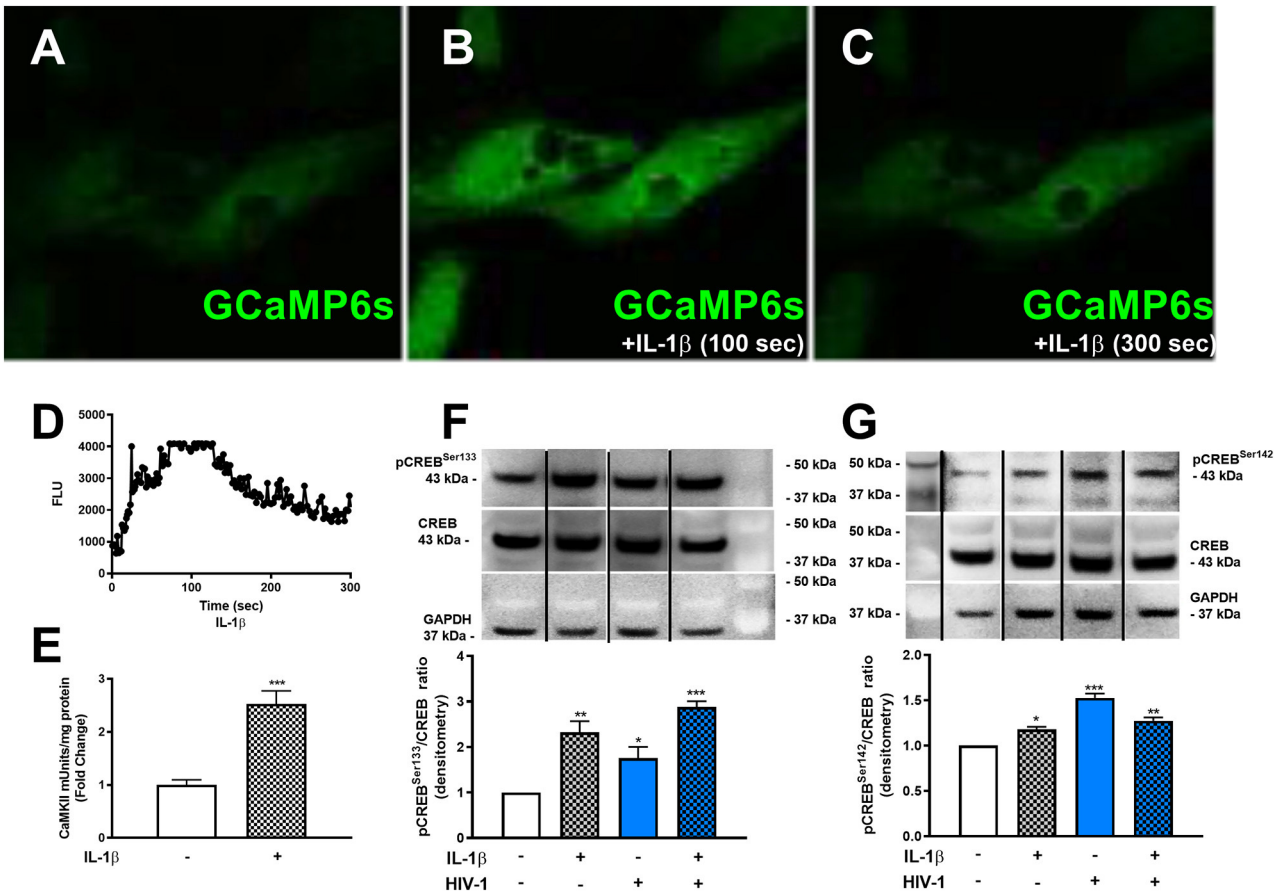

FIGURE 6 | HAND-relevant stimuli increase $[Ca^{+2}]_i$, CaMKII activity and phosphorylation of CREB at serine 133 & 142. Primary human astrocytes were transfected with GCaMP6s. MOCK-transfected astrocytes were maintained as controls in parallel. Transfected cells were treated with IL-1β (20 ng/mL, **A–C**) or ionomycin (10 μM) as a positive control (images not shown). Fluorescence was visualized by confocal microscopy, and images were captured every 500 ms for 5 min. **(A–C)** depict astrocytes treated with IL-1 at selected time points. The histogram shows cumulative data, captured over 5 min **(D)**. CaMKII activity was measured in astrocytes stimulated with IL-1β (20 ng/mL, hatched bars) for 30 min **(E)**. Primary human astrocytes were treated with IL-1β and HIV-1 (blue bars), alone and in combination. Protein lysates were collected 30 min post-treatment and immunoblotted for total CREB, $pCREB^{Ser133}$, $pCREB^{Ser142}$, and GAPDH **(F,G)**. Dividing lines on blots represented in **(F,G)** represent cut sections from the same blot. Representative western blots are shown in **(F,G)**. Densitometry analyses were performed to quantify band intensities on multiple immunoblots and represented as fold changes to control ± SEM, in [**(F,G)**, $n = 3$]. Statistical analyses were performed using GraphPad Prism V6.0 with one-way ANOVA and Tukey's *post-test* for multiple comparisons. $P \leq 0.05$ were considered statistically significant, and data represent means ± SEM. This figure depicts representative donors chosen from multiple astrocyte donors that were tested; each was analyzed in a minimum of triplicate determinations. Data are shown as cumulative fold changes. *n* represents individual biological replicates. Molecular weight markers are identified on each western blot (MW) (*$p < 0.05$, **$p < 0.01$, ***$p < 0.001$).

activating PKA/$pCREB^{Ser133}$ is a mechanistic strategy for increasing EAAT-2.

Recently Kumar et al. demonstrated that METH exposure decreased pCaMKII levels in several brain regions of HIV tat transgenic mice (69). These changes correlated with decreased working and spatial memory, neurotrophin levels, and decreased synaptodendritic integrity. Autophosphorylation of CaMKII at threonine 286 is required for kinase activity (70). Both HIV and METH have been shown to reduce pCaMKII in rodents and SIV in rhesus macaques (71, 72). These changes have been associated with neuronal responses and have not been evaluated in astrocytes. Here we show that METH significantly reduced CaMKII activity at 5 min and increased activity by 30 min in human astrocytes. Further, METH, HIV-1, and IL-1β increased $pCREB^{Ser142}$ phosphorylation, which was associated with total CaMKII levels and activity. Together, this suggests that CaMKII activity may be regulated differently in neurons and astrocytes by METH and HIV.

Antagonizing astrocyte TAAR1 with EPPTB, blocked METH-mediated increases in cAMP and $[Ca^{+2}]_i$, prevented METH-induced phosphorylation of CREB at serine 133/142 and averted METH-mediated EAAT-2 decreases. In fact, in EPPTB pretreated astrocytes, METH significantly reduced cAMP levels below baseline, reflecting decreased ATP levels, and potential dysregulation of cellular energy. Inhibiting and/or antagonizing

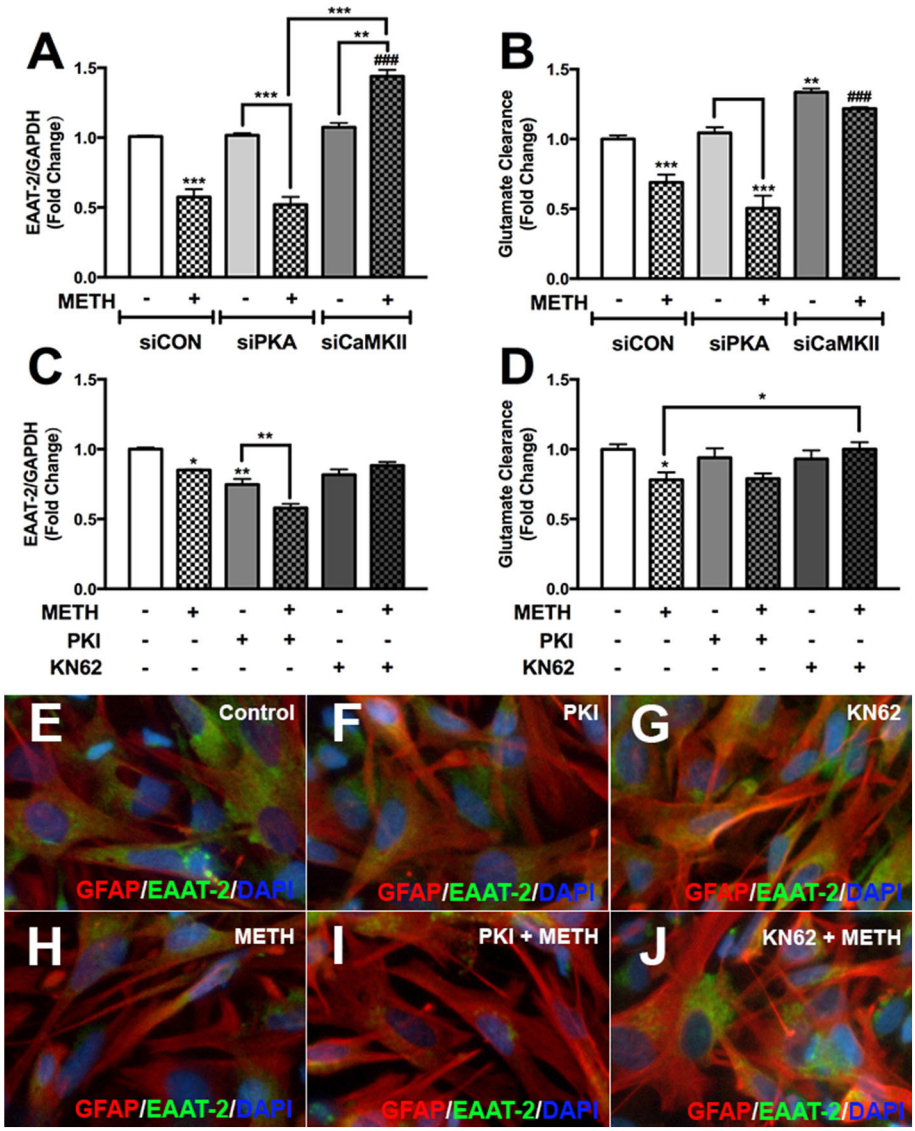

FIGURE 7 | METH-induced activation of PKA and CaMKII differentially regulates astrocyte EAAT-2. Cultured human astrocyte transfected with siCON (clear bars), siPKA (light gray bars), and siCaMKII (dark gray bars) were treated with METH (500 μM, hatched bars). Alternatively, astrocytes were pretreated with cAMP-dependent PKA inhibitor, PKI (light gray bars), or CaMKII inhibitor, KN62 (dark gray bars), for 1 h prior to METH treatment (hatched bars). RNA was collected from transfected and pretreated astrocytes, and EAAT-2 mRNA levels were analyzed 8 h post-METH treatment **(A,C)**. Glutamate clearance was quantified at 10 h post-glutamate addition **(B,D)**. Astrocytes pretreated with PKA and CaMKII inhibitor +/– METH treatment were immunostained for GFAP (red), EAAT-2 (green), or DAPI [blue, **(E–J)**]. Statistical analyses were performed using GraphPad Prism V6.0 with one-way ANOVA and Tukey's *post-test* for multiple comparisons. $P \leq 0.05$ were considered statistically significant, and data represent means ± SEM. This figure depicts representative donors chosen from multiple astrocyte donors that were tested; each was analyzed in a minimum of triplicate determinations. Data are shown as cumulative fold changes (*$p < 0.05$, **$p < 0.01$, ***$p < 0.001$, ###$p < 0.001$).

TAAR1, with EPPTB, may be enough to prevent METH-induced EAAT-2 downregulation; yet, METH abuse during CNS inflammation and HIV-1 poses greater threat due to their potential to increase TAAR1 levels/activity and crosstalk between PKA, CaMKII and NF-κB. For instance, the rate of NF-κB translocation into the nucleus is regulated by PKA-induced phosphorylation of NF-κB/Rel complexes, downstream of cAMP (73). Interestingly, NF-κB activation of target genes is optimized by interaction of the RelA subunit with CREB co-activators, CBP and p300 (74, 75). Furthermore, the region of pCREB^{Ser133} that interacts with CBP also interacts with RelA, thereby inhibiting NF-κB activity (76). This serves as compelling evidence for CREB and NF-κB mechanistic crosstalk, ultimately influencing how they regulate transcription of target genes in astrocytes. IL-1β and HIV-1 initiate similar signaling mechanisms in astrocytes as METH, independent of TAAR1 activation. The additive effects of IL-1β and HIV-1 on pCREB^{Ser133} vs. inhibitory effects on pCREB^{Ser142} need to be further investigated and may be

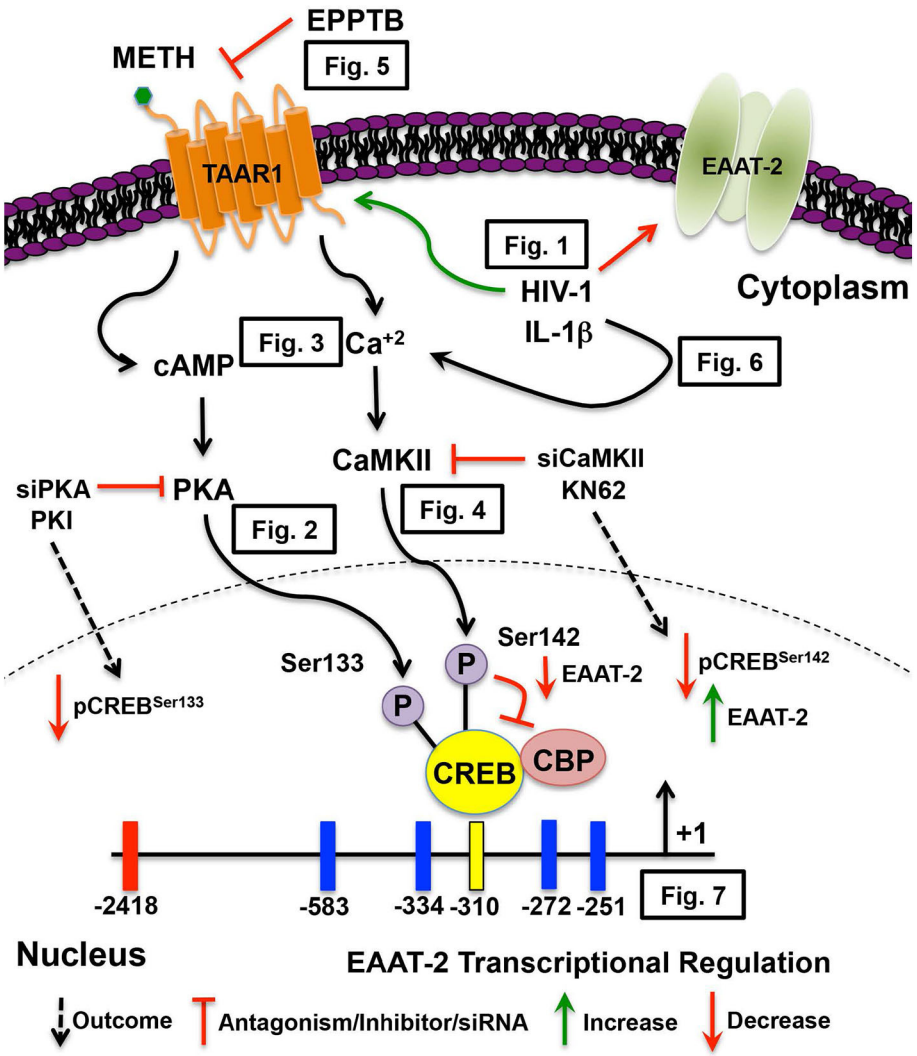

FIGURE 8 | METH-induced TAAR1 signaling regulates astrocyte EAAT-2. METH likely activates different signaling pathways in astrocytes that are exacerbated by HIV relevant inflammatory cytokine, IL-1β and/or HIV-1. Intracellular signal transduction pathways lead to CREB phosphorylation, thereby differentially regulating EAAT-2. We have previously demonstrated METH-induced activation of astrocyte TAAR1 increases intracellular cAMP and regulates EAAT-2. In this manuscript, TAAR1 upregulation and increased activity negatively correlate to astrocyte EAAT-2 and impair glutamate clearance capabilities as demonstrated by (**Figure 1**). Investigation of signal transduction pathways revealed METH-induced TAAR1 activation leads to cAMP/PKA/pCREB^{Ser133} **(Figure 2)** and $[Ca^{+2}]_i$/CaMKII/pCREB^{Ser142} (**Figures 3**, **4**). As METH activates TAAR1, antagonism with TAAR1 selective antagonist, EPPTB, prevents METH-induced increases of intracellular cAMP and $[Ca^{+2}]_i$, blocking METH-induced phosphorylation of CREB at both serine 133 and 142 (**Figure 5**). Additionally, exogenous treatment of IL-1β and HIV-1 dually activate cAMP/PKA/pCREB^{Ser133} and $[Ca^{+2}]_i$/CaMKII/pCREB^{Ser142} suggesting similar mechanisms mediating EAAT-2 downregulation (**Figure 6**). Extrinsic regulation of signaling factors including PKA and CaMKII not only reduce activation of subsequent signaling but also regulate METH-mediated decreases in astrocyte EAAT-2 (**Figure 7**). Together, our data suggest that pCREB^{Ser142} acts as a dominant repressor of CREB transcriptional activation. Therefore, therapeutically targeting and inhibiting the $[Ca^{+2}]_i$/CaMKII/pCREB^{Ser142} signal transduction pathways have broader implications in the context of METH abuse and neuroinflammation.

a promising mechanistic intervention to prevent glutamate excitotoxicity during neuroinflammatory disorders. Targeting downstream of CaMKII, to prevent pCREB^{Ser142,} has larger implications for all genes with CREB promoter elements in astrocytes including inflammatory mediators, oxidative stress genes and growth factors (77–81).

Non-functional mutations in mouse TAAR1 affect METH intake, hypothermia and conditioned taste aversion (82, 83). Humans possess many TAAR1 variants with sensitivity to ligands (84–87). However, the effects of TAAR1 variants on signaling cascades and risk for MUD, HAND, and neuropsychological disease will need to be evaluated. Additionally, there is an apparent dichotomy for TAAR1-associated regulation in neurons vs. astrocytes. TAAR1 function appears to be critical for proper neuronal function (20–22, 88), while increased activity in astrocytes may be detrimental to brain health (27, 41, 89). Targeting TAAR1 in the CNS in a cell specific manner may be difficult; however, these findings

open the door for personalized medical interventions for these disorders.

In this study we investigated the duality of METH-induced signaling pathways leading to EAAT-2 transcriptional repression, thereby exacerbating HIV-1-induced decreases in EAAT-2. **Figure 8** illustrates signal transduction pathways mediated via TAAR1, METH, HIV-1, and IL-1β in astrocyte EAAT-2 downregulation. We propose that triggering the preferential activation of cAMP/PKA/pCREB^{Ser133} while inhibiting $[Ca^{+2}]_i$/CaMKII/pCREB^{Ser142} signaling would alleviate excitotoxic insult via upregulation of astrocyte EAAT-2 transcription. Additionally, counteracting IL-1β and HIV-1 induced upregulation of TAAR1 would reduce METH effects in astrocytes. Transcriptional regulation of astrocyte TAAR1 via NF-κB warrants further investigation. In addition, mutation of the four NF-κB sites within the EAAT-2 promoter will elucidate on the correlation identified between TAAR1 and EAAT-2 levels and function following IL-1β treatment. Altogether, our studies shed light on tripartite signaling of PKA, CaMKII, and NF-κB involved in TAAR1 and EAAT-2 regulation, METH abuse, and HAND.

Taken together, we have identified crucial mechanistic pathways involved in METH-induced astrocyte neurotoxicity in the context of HAND. Our data provide strong evidence to support the notion that manipulation of signal transduction pathways to favor cAMP/PKA/pCREB^{Ser133} and to abolish $[Ca^{+2}]_i$/CaMKII/pCREB^{Ser142} is a promising strategy for restoring astrocyte EAAT-2 function in the context of METH abuse and HAND.

DATA AVAILABILITY STATEMENT

The datasets presented in this study can be found in online repositories. The names of the repository/repositories and accession number(s) can be found in the article/supplementary material.

ETHICS STATEMENT

The studies involving human participants were reviewed and approved by North Texas Regional IRB. Written informed consent for participation was not required for this study in accordance with the national legislation and the institutional requirements.

AUTHOR CONTRIBUTIONS

AG, IC, and KB conceived, designed and coordinated the study, and wrote the manuscript. All authors reviewed the results and approved the final version of the manuscript.

FUNDING

This work was supported by R01DA039789 from NIDA to AG and then Dr. Michael Mathis, and F31DA037832 from NIDA to IC. We appreciate the assistance of the Laboratory of Developmental Biology for providing us with human brain tissues, which is supported by NIH Award Number 5R24HD0008836 from the Eunice Kennedy Shriver National Institute of Child Health & Human Development.

ACKNOWLEDGMENTS

We acknowledge the National Institute of Drug Abuse Drug Supply Program for the methamphetamine supplied in these studies. Ms. Lenore Price and Ms. Satomi Stacy assisted with editing of the manuscript. Ms. Lin Tang provided consistent primary human astrocyte cultures. Dr. Thomas Cunningham and his lab group graciously assisted in the acquisition of calcium imaging and quantification of intracellular calcium concentrations. Ms. I-Fen Chang provided technical assistance for all confocal imaging.

REFERENCES

1. Blackstone K, Iudicello JE, Morgan EE, Weber E, Moore DJ, Franklin DR, et al. Human immunodeficiency virus infection heightens concurrent risk of functional dependence in persons with long-term methamphetamine use. *J Addict Med*. (2013) 7:255–63. doi: 10.1097/ADM.0b013e318293653d
2. Cisneros IE, Ghorpade A. HIV-1, methamphetamine and astrocyte glutamate regulation: combined excitotoxic implications for neuro-AIDS. *Curr HIV Res*. (2012) 10:392–406. doi: 10.2174/157016212802138832
3. Reback CJ, Fletcher JB. Elevated HIV and STI prevalence and incidence among methamphetamine-using men who have sex with men in Los Angeles county. *AIDS Educ Prev*. (2018) 30:350–6. doi: 10.1521/aeap.2018.30.4.350
4. Mediouni S, Marcondes MC, Miller C, McLaughlin JP, Valente ST. The cross-talk of HIV-1 tat and methamphetamine in HIV-associated neurocognitive disorders. *Front Microbiol*. (2015) 6:1164. doi: 10.3389/fmicb.2015.01164
5. Paolillo EW, Saloner R, Montoya JL, Campbell LM, Pasipanodya EC, Iudicello JE, et al. Frailty in comorbid HIV and lifetime methamphetamine use disorder: associations with neurocognitive and everyday functioning. *AIDS Res Hum Retroviruses*. (2019) 35:1044–53. doi: 10.1089/aid.2019.0062
6. Castellano P, Nwagbo C, Martinez LR, Eugenin EA. Methamphetamine compromises gap junctional communication in astrocytes and neurons. *J Neurochem*. (2016) 137:561–75. doi: 10.1111/jnc.13603
7. Cisneros IE, Ghorpade A. Methamphetamine and HIV-1-induced neurotoxicity: role of trace amine associated receptor 1 cAMP signaling in astrocytes. *Neuropharmacology*. (2014) 85:499–507. doi: 10.1016/j.neuropharm.2014.06.011
8. Marquez J, Campos-Sandoval JA, Penalver A, Mates JM, Segura JA, Blanco E, et al. Glutamate and brain glutaminases in drug addiction. *Neurochem Res*. (2017) 42:846–57. doi: 10.1007/s11064-016-2137-0
9. Merritt K, McGuire P, Egerton A. Relationship between glutamate dysfunction and symptoms and cognitive function in psychosis. *Front Psychiatry*. (2013) 4:151. doi: 10.3389/fpsyt.2013.00151
10. Anderson CM, Swanson RA. Astrocyte glutamate transport: review of properties, regulation, and physiological functions. *Glia*. (2000) 32:1–14. doi: 10.1002/1098-1136(200010)32:1<1::AID-GLIA10>3.0.CO;2-W
11. Fontana AC. Current approaches to enhance glutamate transporter function and expression. *J Neurochem*. (2015) 134:982–1007. doi: 10.1111/jnc.13200
12. Rothstein JD, Dykes-Hoberg M, Pardo CA, Bristol LA, Jin L, Kuncl RW, et al. Knockout of glutamate transporters reveals a major role for astroglial

transport in excitotoxicity and clearance of glutamate. *Neuron*. (1996) 16:675–86. doi: 10.1016/S0896-6273(00)80086-0
13. Sharma A, Kazim SF, Larson CS, Ramakrishnan A, Gray JD, McEwen BS, et al. Divergent roles of astrocytic versus neuronal EAAT2 deficiency on cognition and overlap with aging and Alzheimer's molecular signatures. *Proc Natl Acad Sci USA*. (2019) 116:21800–11. doi: 10.1073/pnas.1903566116
14. Vartak-Sharma N, Gelman BB, Joshi C, Borgamann K, Ghorpade A. Astrocyte elevated gene-1 is a novel modulator of HIV-1-associated neuroinflammation via regulation of nuclear factor-kappaB signaling and excitatory amino acid transporter-2 repression. *J Biol Chem*. (2014) 289:19599–612. doi: 10.1074/jbc.M114.567644
15. Wang Z, Pekarskaya O, Bencheikh M, Chao W, Gelbard HA, Ghorpade A, et al. Reduced expression of glutamate transporter EAAT2 and impaired glutamate transport in human primary astrocytes exposed to HIV-1 or gp120. *Virology*. (2003) 312:60–73. doi: 10.1016/S0042-6822(03)00181-8
16. Xing HQ, Zhang Y, Izumo K, Arishima S, Kubota R, Ye X, et al. Decrease of aquaporin-4 and excitatory amino acid transporter-2 indicate astrocyte dysfunction for pathogenesis of cortical degeneration in HIV-associated neurocognitive disorders. *Neuropathology*. (2017) 37:25–34. doi: 10.1111/neup.12321
17. Blaker AL, Moore ER, Yamamoto BK. Serial exposure to ethanol drinking and methamphetamine enhances glutamate excitotoxicity. *J Neurochem*. (2019) 151:749–63. doi: 10.1111/jnc.14861
18. Stephans SE, Yamamoto BK. Methamphetamine-induced neurotoxicity: roles for glutamate and dopamine efflux. *Synapse*. (1994) 17:203–9. doi: 10.1002/syn.890170310
19. Tata DA, Yamamoto BK. Chronic stress enhances methamphetamine-induced extracellular glutamate and excitotoxicity in the rat striatum. *Synapse*. (2008) 62:325–36. doi: 10.1002/syn.20497
20. Rutigliano G, Accorroni A, Zucchi R. The Case for TAAR1 as a Modulator of Central Nervous System Function. *Front Pharmacol*. (2017) 8:987. doi: 10.3389/fphar.2017.00987
21. Espinoza S, Lignani G, Caffino L, Maggi S, Sukhanov I, Leo D, et al. TAAR1 Modulates Cortical Glutamate NMDA Receptor Function. *Neuropsychopharmacology*. (2015) 40:2217–27. doi: 10.1038/npp.2015.65
22. Revel FG, Moreau JL, Gainetdinov RR, Bradaia A, Sotnikova TD, Mory R, et al. TAAR1 activation modulates monoaminergic neurotransmission, preventing hyperdopaminergic and hypoglutamatergic activity. *Proc Natl Acad Sci USA*. (2011) 108:8485–90. doi: 10.1073/pnas.1103029108
23. Revel FG, Moreau JL, Pouzet B, Mory R, Bradaia A, Buchy D, et al. A new perspective for schizophrenia: TAAR1 agonists reveal antipsychotic- and antidepressant-like activity, improve cognition and control body weight. *Mol Psychiatry*. (2013) 18:543–56. doi: 10.1038/mp.2012.57
24. Barak LS, Salahpour A, Zhang X, Masri B, Sotnikova TD, Ramsey AJ, et al. Pharmacological characterization of membrane-expressed human trace amine-associated receptor 1 (TAAR1) by a bioluminescence resonance energy transfer cAMP biosensor. *Mol Pharmacol*. (2008) 74:585–94. doi: 10.1124/mol.108.048884
25. Pei Y, Asif-Malik A, Canales JJ. Trace Amines and the Trace Amine-Associated Receptor 1: Pharmacology, Neurochemistry, and Clinical Implications. *Front Neurosci*. (2016) 10:148. doi: 10.3389/fnins.2016.00148
26. Underhill SM, Hullihen PD, Chen J, Fenollar-Ferrer C, Rizzo MA, Ingram SL, et al. Amphetamines signal through intracellular TAAR1 receptors coupled to Galpha13 and GalphaS in discrete subcellular domains. *Mol Psychiatry*. (2019). doi: 10.1038/s41380-019-0469-2. [Epub ahead of print].
27. Chen X, Xing J, Jiang L, Qian W, Wang Y, Sun H, et al. Involvement of calcium/calmodulin-dependent protein kinase II in methamphetamine-induced neural damage. *J Appl Toxicol*. (2016) 36:1460–7. doi: 10.1002/jat.3301
28. Yorgason JT, Hedges DM, Obray JD, Jang EY, Bills KB, Woodbury M, et al. Methamphetamine increases dopamine release in the nucleus accumbens through calcium-dependent processes. *Psychopharmacology*. (2020) 237:1317–30. doi: 10.1007/s00213-020-05459-2
29. Lee SG, Su ZZ, Emdad L, Gupta P, Sarkar D, Borjabad A, et al. Mechanism of ceftriaxone induction of excitatory amino acid transporter-2 expression and glutamate uptake in primary human astrocytes. *J Biol Chem*. (2008) 283:13116–23. doi: 10.1074/jbc.M707697200
30. Schlag BD, Vondrasek JR, Munir M, Kalandadze A, Zelenaia OA, Rothstein JD, et al. Regulation of the glial Na+-dependent glutamate transporters by cyclic AMP analogs and neurons. *Mol Pharmacol*. (1998) 53:355–69. doi: 10.1124/mol.53.3.355
31. Meffert MK, Chang JM, Wiltgen BJ, Fanselow MS, Baltimore D. NF-kappa B functions in synaptic signaling and behavior. *Nat Neurosci*. (2003) 6:1072–8. doi: 10.1038/nn1110
32. Memet S. NF-kappaB functions in the nervous system: from development to disease. *Biochem Pharmacol*. (2006) 72:1180–95. doi: 10.1016/j.bcp.2006.09.003
33. Liu X, Shah A, Gangwani MR, Silverstein PS, Fu M, Kumar A. HIV-1 Nef induces CCL5 production in astrocytes through p38-MAPK and PI3K/Akt pathway and utilizes NF-kB, CEBP and AP-1 transcription factors. *Sci Rep*. (2014) 4:4450. doi: 10.1038/srep04450
34. Nookala AR, Shah A, Noel RJ, Kumar A. HIV-1 Tat-mediated induction of CCL5 in astrocytes involves NF-kappaB, AP-1, C/EBPalpha and C/EBPgamma transcription factors and JAK, PI3K/Akt and p38 MAPK signaling pathways. *PLoS ONE*. (2013) 8:e78855. doi: 10.1371/journal.pone.0078855
35. Hou X, Li Y, Huang Y, Zhao H, Gui L. Adenosine receptor A1-A2a heteromers regulate EAAT2 expression and glutamate uptake via YY1-induced repression of PPARgamma transcription. *PPAR Res*. (2020) 2020:2410264. doi: 10.1155/2020/2410264
36. Kornhauser JM, Cowan CW, Shaywitz AJ, Dolmetsch RE, Griffith EC, Hu LS, et al. CREB transcriptional activity in neurons is regulated by multiple, calcium-specific phosphorylation events. *Neuron*. (2002) 34:221–33. doi: 10.1016/S0896-6273(02)00655-4
37. Sun P, Enslen H, Myung PS, Maurer RA. Differential activation of CREB by Ca2+/calmodulin-dependent protein kinases type II and type IV involves phosphorylation of a site that negatively regulates activity. *Genes Dev*. (1994) 8:2527–39. doi: 10.1101/gad.8.21.2527
38. Gardner J, Borgmann K, Deshpande MS, Dhar A, Wu L, Persidsky R, et al. Potential mechanisms for astrocyte-TIMP-1 downregulation in chronic inflammatory diseases. *J Neurosci Res*. (2006) 83:1281–92. doi: 10.1002/jnr.20823
39. You Y, Borgmann K, Edara VV, Stacy S, Ghorpade A, Ikezu T. Activated human astrocyte-derived extracellular vesicles modulate neuronal uptake, differentiation and firing. *J Extracell Vesicles*. (2020) 9:1706801. doi: 10.1080/20013078.2019.1706801
40. Bradaia A, Trube G, Stalder H, Norcross RD, Ozmen L, Wettstein JG, et al. The selective antagonist EPPTB reveals TAAR1-mediated regulatory mechanisms in dopaminergic neurons of the mesolimbic system. *Proc Natl Acad Sci USA*. (2009) 106:20081–6. doi: 10.1073/pnas.0906522106
41. Dave S, Chen L, Yu C, Seaton M, Khodr CE, Al-Harthi L, et al. Methamphetamine decreases K(+) channel function in human fetal astrocytes by activating the trace amine-associated receptor type-1. *J Neurochem*. (2019) 148:29–45. doi: 10.1111/jnc.14606
42. Kleinau G, Pratzka J, Nurnberg D, Gruters A, Fuhrer-Sakel D, Krude H, et al. Differential modulation of Beta-adrenergic receptor signaling by trace amine-associated receptor 1 agonists. *PLoS ONE*. (2011) 6:e27073. doi: 10.1371/journal.pone.0027073
43. Stalder H, Hoener MC, Norcross RD. Selective antagonists of mouse trace amine-associated receptor 1 (mTAAR1): discovery of EPPTB (RO5212773). *Bioorg Med Chem Lett*. (2011) 21:1227–31. doi: 10.1016/j.bmcl.2010.12.075
44. Fetalvero KM, Shyu M, Nomikos AP, Chiu YF, Wagner RJ, Powell RJ, et al. The prostacyclin receptor induces human vascular smooth muscle cell differentiation via the protein kinase A pathway. *Am J Physiol Heart Circ Physiol*. (2006) 290:H1337–46. doi: 10.1152/ajpheart.00936.2005
45. Iino Y, Sawada T, Yamaguchi K, Tajiri M, Ishii S, Kasai H, et al. Dopamine D2 receptors in discrimination learning and spine enlargement. *Nature*. (2020) 579:555–60. doi: 10.1038/s41586-020-2115-1
46. Zhang B, Zhang Y, Shacter E. Rac1 inhibits apoptosis in human lymphoma cells by stimulating bad phosphorylation on Ser-75. *Mol Cell Biol*. (2004) 24:6205–14. doi: 10.1128/MCB.24.14.6205-6214.2004
47. Wu CY, Hsieh HL, Sun CC, Yang CM. IL-1beta induces MMP-9 expression via a Ca2+-dependent CaMKII/JNK/c-JUN cascade in rat brain astrocytes. *Glia*. (2009) 57:1775–89. doi: 10.1002/glia.20890

48. Yan X, Liu J, Ye Z, Huang J, He F, Xiao W, et al. CaMKII-mediated CREB phosphorylation is involved in Ca2+-induced BDNF mRNA transcription and neurite outgrowth promoted by electrical stimulation. *PLoS ONE*. (2016) 11:e0162784. doi: 10.1371/journal.pone.0162784
49. Koyanagi Y, Miles S, Mitsuyasu RT, Merrill JE, Vinters HV, Chen IS. Dual infection of the central nervous system by AIDS viruses with distinct cellular tropisms. *Science*. (1987) 236:819–22. doi: 10.1126/science.3646751
50. Koyanagi Y, O'Brien WA, Zhao JQ, Golde DW, Gasson JC, Chen IS. Cytokines alter production of HIV-1 from primary mononuclear phagocytes. *Science*. (1988) 241:1673–5. doi: 10.1126/science.3047875
51. O'Brien WA, Koyanagi Y, Namazie A, Zhao JQ, Diagne A, Idler K, et al. HIV-1 tropism for mononuclear phagocytes can be determined by regions of gp120 outside the CD4-binding domain. *Nature*. (1990) 348:69–73. doi: 10.1038/348069a0
52. Gorantla S, Che M, Gendelman HE. Isolation, propagation, and HIV-1 infection of monocyte-derived macrophages and recovery of virus from brain and cerebrospinal fluid. *Methods Mol Biol*. (2005) 304:35–48. doi: 10.1385/1-59259-907-9:035
53. Chadderton T, Wilson C, Bewick M, Gluck S. Evaluation of three rapid RNA extraction reagents: relevance for use in RT-PCR's and measurement of low level gene expression in clinical samples. *Cell Mol Biol*. (1997) 43:1227–34.
54. Manthrope M, Fagnani R, Skaper SD, Varon S. An automated colorimetric microassay for neurotrophic factors. *Dev Brain Res*. (1986) 25:191–8. doi: 10.1016/0165-3806(86)90208-7
55. Schneider CA, Rasband WS, Eliceiri KW. NIH Image to ImageJ: 25 years of image analysis. *Nat Methods*. (2012) 9:671–5. doi: 10.1038/nmeth.2089
56. Park YH, Mueller BH II, McGrady NR, Ma HY, Yorio T. AMPA receptor desensitization is the determinant of AMPA receptor mediated excitotoxicity in purified retinal ganglion cells. *Exp Eye Res*. (2015) 132:136–50. doi: 10.1016/j.exer.2015.01.026
57. Saxena A, Bachelor M, Park YH, Carreno FR, Nedungadi TP, Cunningham JT. Angiotensin II induces membrane trafficking of natively expressed transient receptor potential vanilloid type 4 channels in hypothalamic 4B cells. *Am J Physiol Regul Integr Comp Physiol*. (2014) 307:R945–955. doi: 10.1152/ajpregu.00224.2014
58. Edwards HV, Christian F, Baillie GS. cAMP: novel concepts in compartmentalised signalling. *Semin Cell Dev Biol*. (2012) 23:181–90. doi: 10.1016/j.semcdb.2011.09.005
59. Yu SJ, Wu KJ, Bae EK, Hsu MJ, Richie CT, Harvey BK, et al. Methamphetamine induces a rapid increase of intracellular Ca levels in neurons overexpressing GCaMP5. *Addict Biol*. (2014) 21:255–66. doi: 10.1111/adb.12193
60. Li H, Wang X, Zhang N, Gottipati MK, Parpura V, Ding S. Imaging of mitochondrial Ca2+ dynamics in astrocytes using cell-specific mitochondria-targeted GCaMP5G/6s: mitochondrial Ca2+ uptake and cytosolic Ca2+ availability via the endoplasmic reticulum store. *Cell Calcium*. (2014) 56:457–66. doi: 10.1016/j.ceca.2014.09.008
61. Casado M, Bendahan A, Zafra F, Danbolt NC, Aragon C, Gimenez C, et al. Phosphorylation and modulation of brain glutamate transporters by protein kinase C. *J Biol Chem*. (1993) 268:27313–7.
62. Guillet BA, Velly LJ, Canolle B, Masmejean FM, Nieoullon AL, Pisano P. Differential regulation by protein kinases of activity and cell surface expression of glutamate transporters in neuron-enriched cultures. *Neurochem Int*. (2005) 46:337–46. doi: 10.1016/j.neuint.2004.10.006
63. Kalandadze A, Wu Y, Robinson MB. Protein kinase C activation decreases cell surface expression of the GLT-1 subtype of glutamate transporter. Requirement of a carboxyl-terminal domain and partial dependence on serine 486. *J Biol Chem*. (2002) 277:45741–50. doi: 10.1074/jbc.M203771200
64. Tan ES, Naylor JC, Groban ES, Bunzow JR, Jacobson MP, Grandy DK, et al. The molecular basis of species-specific ligand activation of trace amine-associated receptor 1 (TAAR(1)). *ACS Chem Biol*. (2009) 4:209–20. doi: 10.1021/cb800304d
65. Longatti A. The dual role of exosomes in hepatitis A and C virus transmission and viral immune activation. *Viruses*. (2015) 7:6707–15. doi: 10.3390/v7122967
66. Kim K, Lee SG, Kegelman TP, Su ZZ, Das SK, Dash R, et al. Role of excitatory amino acid transporter-2 (EAAT2) and glutamate in neurodegeneration: opportunities for developing novel therapeutics. *J Cell Physiol*. (2011) 226:2484–93. doi: 10.1002/jcp.22609
67. Robichaux WG III, Cheng X. Intracellular cAMP sensor EPAC: physiology, pathophysiology, and therapeutics development. *Physiol Rev*. (2018) 98:919–1053. doi: 10.1152/physrev.00025.2017
68. Wu X, McMurray CT. Calmodulin kinase II attenuation of gene transcription by preventing cAMP response element-binding protein (CREB) dimerization and binding of the CREB-binding protein. *J Biol Chem*. (2001) 276:1735–41. doi: 10.1074/jbc.M006727200
69. Nookala AR, Schwartz DC, Chaudhari NS, Glazyrin A, Stephens EB, Berman NEJ, et al. Methamphetamine augment HIV-1 Tat mediated memory deficits by altering the expression of synaptic proteins and neurotrophic factors. *Brain Behav Immun*. (2018) 71:37–51. doi: 10.1016/j.bbi.2018.04.018
70. Yang E, Schulman H. Structural examination of autoregulation of multifunctional calcium/calmodulin-dependent protein kinase II. *J Biol Chem*. (1999) 274:26199–208. doi: 10.1074/jbc.274.37.26199
71. Akiyama K, Suemaru J. Effect of acute and chronic administration of methamphetamine on calcium-calmodulin dependent protein kinase II activity in the rat brain. *Ann N Y Acad Sci*. (2000) 914:263–74. doi: 10.1111/j.1749-6632.2000.tb05201.x
72. Gupta RG, Kelly KM, Helke KL, Queen SE, Karper JM, Dorsey JL, et al. HIV and SIV induce alterations in CNS CaMKII expression and activation: a potential mechanism for cognitive impairment. *Am J Pathol*. (2010) 176:2776–84. doi: 10.2353/ajpath.2010.090809
73. King CC, Sastri M, Chang P, Pennypacker J, Taylor SS. The rate of NF-kappaB nuclear translocation is regulated by PKA and A kinase interacting protein 1. *PLoS ONE*. (2011) 6:e18713. doi: 10.1371/journal.pone.0018713
74. Ghosh S, Hayden MS. New regulators of NF-kappaB in inflammation. *Nat Rev Immunol*. (2008) 8:837–48. doi: 10.1038/nri2423
75. Medzhitov R, Horng T. Transcriptional control of the inflammatory response. *Nat Rev Immunol*. (2009) 9:692–703. doi: 10.1038/nri2634
76. Ollivier V, Parry GC, Cobb RR, de Prost D, Mackman N. Elevated cyclic AMP inhibits NF-kappaB-mediated transcription in human monocytic cells and endothelial cells. *J Biol Chem*. (1996) 271:20828–35. doi: 10.1074/jbc.271.34.20828
77. Kim KH, Jeong JY, Surh YJ, Kim KW. Expression of stress-response ATF3 is mediated by Nrf2 in astrocytes. *Nucleic Acids Res*. (2010) 38:48–59. doi: 10.1093/nar/gkp865
78. Krasnova IN, Justinova Z, Cadet JL. Methamphetamine addiction: involvement of CREB and neuroinflammatory signaling pathways. *Psychopharmacology*. (2016) 233:1945–62. doi: 10.1007/s00213-016-4235-8
79. Lee B, Butcher GQ, Hoyt KR, Impey S, Obrietan K. Activity-dependent neuroprotection and cAMP response element-binding protein (CREB): kinase coupling, stimulus intensity, and temporal regulation of CREB phosphorylation at serine 133. *J Neurosci*. (2005) 25:1137–48. doi: 10.1523/JNEUROSCI.4288-04.2005
80. Spooren A, Kooijman R, Lintermans B, Van Craenenbroeck K, Vermeulen L, Haegeman G, et al. Cooperation of NFkappaB and CREB to induce synergistic IL-6 expression in astrocytes. *Cell Signal*. (2010) 22:871–81. doi: 10.1016/j.cellsig.2010.01.018
81. Wang B, Chen T, Wang J, Jia Y, Ren H, Wu F, et al. Methamphetamine modulates the production of interleukin-6 and tumor necrosis factor-alpha via the cAMP/PKA/CREB signaling pathway in lipopolysaccharide-activated microglia. *Int Immunopharmacol*. (2018) 56:168–78. doi: 10.1016/j.intimp.2018.01.024
82. Reed C, Baba H, Zhu Z, Erk J, Mootz JR, Varra NM, et al. A spontaneous mutation in Taar1 impacts methamphetamine-related traits exclusively in DBA/2 mice from a single vendor. *Front Pharmacol*. (2017) 8:993. doi: 10.3389/fphar.2017.00993
83. Stafford AM, Reed C, Baba H, Walter NA, Mootz JR, Williams RW, et al. Taar1 gene variants have a causal role in methamphetamine intake and response and interact with Oprm1. *Elife*. (2019) 8:e46472. doi: 10.7554/eLife.46472.022
84. Loftis JM, Lasarev M, Shi X, Lapidus J, Janowsky A, Hoffman WF, et al. Trace amine-associated receptor gene polymorphism increases drug craving in individuals with methamphetamine dependence. *PLoS ONE*. (2019) 14:e0220270. doi: 10.1371/journal.pone.0220270
85. Rutigliano G, Braunig J, Del Grande C, Carnicelli V, Masci I, Merlino S, et al. Non-functional trace amine-associated receptor 1 variants in patients with mental disorders. *Front Pharmacol*. (2019) 10:1027. doi: 10.3389/fphar.2019.01027

86. Rutigliano G, Zucchi R. Molecular variants in human trace amine-associated receptors and their implications in mental and metabolic disorders. *Cell Mol Neurobiol*. (2020) 40:239–55. doi: 10.1007/s10571-019-00743-y
87. Shi X, Walter NA, Harkness JH, Neve KA, Williams RW, Lu L, et al. Genetic polymorphisms affect mouse and human trace amine-associated receptor 1 function. *PLoS ONE*. (2016) 11:e0152581. doi: 10.1371/journal.pone.0152581
88. Lindemann L, Meyer CA, Jeanneau K, Bradaia A, Ozmen L, Bluethmann H, et al. Trace amine-associated receptor 1 modulates dopaminergic activity. *J Pharmacol Exp Ther*. (2008) 324:948–56. doi: 10.1124/jpet.107.132647
89. Fleischer LM, Somaiya RD, Miller GM. Review and meta-analyses of TAAR1 expression in the immune system and cancers. *Front Pharmacol*. (2018) 9:683. doi: 10.3389/fphar.2018.00683

Conflict of Interest: The authors declare that the research was conducted in the absence of any commercial or financial relationships that could be construed as a potential conflict of interest.

frontiers in Neurology

ORIGINAL RESEARCH
published: 15 December 2020
doi: 10.3389/fneur.2020.593188

OPEN ACCESS

Edited by:
Dianne T. Langford,
Temple University, United States

Reviewed by:
Eliseo A. Eugenin,
University of Texas Medical Branch at Galveston, United States
Tory P. Johnson,
Johns Hopkins University, United States
Sylvia Fitting,
University of North Carolina at Chapel Hill, United States
Ian Jacobs,
University of North Carolina, Chapel Hill, United States, in collaboration with reviewer SF

***Correspondence:**
Kathleen Borgmann
kathleen.borgmann@unthsc.edu

†Present address:
Chaitanya R. Joshi,
Department of Neurology and Neurotherapeutics, UT Southwestern Medical Center, Dallas, TX, United States
Anuja Ghorpade,
Albany College of Pharmacy and Health Sciences, Albany, NY, United States;
Medical Innovation Collaborative of North Texas,
Dallas, TX, United States

Specialty section:
This article was submitted to Neuroinfectious Diseases, a section of the journal Frontiers in Neurology

Received: *10 August 2020*
Accepted: *12 November 2020*
Published: *15 December 2020*

Citation:
Joshi CR, Stacy S, Sumien N, Ghorpade A and Borgmann K (2020) Astrocyte HIV-1 Tat Differentially Modulates Behavior and Brain MMP/TIMP Balance During Short and Prolonged Induction in Transgenic Mice. Front. Neurol. 11:593188. doi: 10.3389/fneur.2020.593188

Astrocyte HIV-1 Tat Differentially Modulates Behavior and Brain MMP/TIMP Balance During Short and Prolonged Induction in Transgenic Mice

***Chaitanya R. Joshi*[1†], *Satomi Stacy*[2], *Nathalie Sumien*[2], *Anuja Ghorpade*[1†] *and Kathleen Borgmann*[2*]**

[1] *Department of Microbiology, Immunology, and Genetics, University of North Texas Health Science Center, Fort Worth, TX, United States,* [2] *Department of Pharmacology and Neuroscience, University of North Texas Health Science Center, Fort Worth, TX, United States*

Despite effective antiretroviral therapy (ART), mild forms of HIV-associated neurocognitive disorders (HAND) continue to afflict approximately half of all people living with HIV (PLWH). As PLWH age, HIV-associated inflammation perturbs the balance between brain matrix metalloproteinases (MMPs) and their tissue inhibitors of metalloproteinases (TIMPs), likely contributing to neuropathogenesis. The MMP/TIMP balance is associated with cognition, learning, and memory, with TIMPs eliciting neuroprotective effects. Dysregulation of the MMP/TIMP balance was evident in the brains of PLWH where levels of TIMP-1, the inducible family member, were significantly lower than non-infected controls, and MMPs were elevated. Here, we evaluated the MMP/TIMP levels in the doxycycline (DOX)-induced glial fibrillary acidic protein promoter-driven HIV-1 transactivator of transcription (Tat) transgenic mouse model. The HIV-1 protein Tat is constitutively expressed by most infected cells, even during ART suppression of viral replication. Many studies have demonstrated indirect and direct mechanisms of short-term Tat-associated neurodegeneration, including gliosis, blood-brain barrier disruption, elevated inflammatory mediators and neurotoxicity. However, the effects of acute vs. prolonged exposure on Tat-induced dysregulation remain to be seen. This is especially relevant for TIMP-1 as expression was previously shown to be differentially regulated in human astrocytes during acute vs. chronic inflammation. In this context, acute Tat expression was induced with DOX intraperitoneal injections over 3 weeks, while DOX-containing diet was used to achieve long-term Tat expression over 6 months. First, a series of behavior tests evaluating arousal, ambulation, anxiety, and cognition was performed to examine impairments analogous to those observed in HAND. Next, gene expression of components of the MMP/TIMP axis and known HAND-relevant inflammatory mediators were assessed. Altered anxiety-like, motor and/or cognitive behaviors were observed in Tat-induced (iTat) mice. Gene expression of MMPs and TIMPs was altered depending on the duration of Tat expression, which was independent

of the HIV-associated neuroinflammation typically implicated in MMP/TIMP regulation. Collectively, we infer that HIV-1 Tat-mediated dysregulation of MMP/TIMP axis and behavioral changes are dependent on duration of exposure. Further, prolonged Tat expression demonstrates a phenotype comparable to asymptomatic to mild HAND manifestation in patients.

Keywords: HIV-associated neurocognitive disorders (HAND), neuroinflammation, TIMP1, iTat mice, anxiety, locomotor activity, tissue inhibitor of metalloproteinases 1

INTRODUCTION

During the antiretroviral therapy (ART) era, the brain remains a viral reservoir for HIV (1–3), and milder forms of HIV-associated neurocognitive disorders (HAND) affect nearly 18 million HIV-infected individuals lowering the quality of life (4–7). Patients suffering from these milder forms of HAND exhibit difficulty with working memory, executive functioning, and speed of information processing (6). Despite a mild or asymptomatic phenotype, complex underlying mechanisms are implicated in HAND pathogenesis. These mechanisms include secretion of proinflammatory mediators from infected and affected cells, blood-brain barrier (BBB) compromise, reactive astrogliosis, excitotoxicity, and imbalance of matrix metalloproteinases (MMPs) – tissue inhibitor of metalloproteinases (TIMPs) axis (8–10).

Imbalance of MMPs and TIMPs has been an important indicator of altered central nervous system (CNS) homeostasis. Increased MMPs disrupt the BBB *via* breakdown of tight junction proteins, recruit immune cells into the CNS, and cause direct neuronal damage potentially contributing to HAND pathology (11–13). On the other hand, MMP-independent neurotropic effects of TIMPs are well-documented (14–16), including our previous work on TIMP-1-mediated neuroprotection in primary human neurons in response to HAND-relevant stimuli (17). Four MMP and TIMP family proteins are the most investigated in the CNS due to their critical role(s) in modulating brain MMP/TIMP balance during multiple CNS diseases and disorders (18–20). These include both constitutively expressed (MMP-2 and TIMP-2) and inducible (MMP-9, TIMP-1) proteins following injury or inflammation.

In the context of HAND, levels of MMP-2 and/or MMP-9 were elevated in primary brain cell cultures treated with HIV or HIV-relevant stimuli (11, 21, 22) as well as in cerebrospinal fluid (CSF) specimens (23) and postmortem brain tissues of infected patients (24). Concurrently, reduced TIMP-1 levels were also observed in CSF and brain tissues of HIV-infected patients indicative of chronic inflammation (24). Our previous *in vitro* work in primary human astrocytes demonstrated that TIMP-1 increased or decreased with acute or prolonged HIV-relevant inflammatory stimuli, respectively (24, 25). It remains to be seen if such biphasic changes in TIMP-1 expression in response to acute vs. chronic inflammatory stimuli are observed *in vivo*, and it may provide insights on using TIMP-1 as a therapeutic option as its neurotropic effects are established.

To address this "knowledge gap," we employed a doxycycline (DOX)-inducible, glial fibrillary acidic protein (GFAP) promoter-driven HIV-1 transactivator of transcription (Tat)-expressing transgenic (iTat) mouse model (26, 27). HIV-1 Tat is a key protein involved in neuronal dysfunction (28, 29), BBB disruption (22), oxidative stress (30, 31), elevating MMPs (32, 33), and possesses chemokine-like abilities that promote immune infiltration into the brain (26, 34). Several investigations using HIV-1 Tat based transgenic models elucidated effects of acute Tat expression, i.e., a few days after Tat induction (35–41), while the effects of prolonged Tat expression were seldom tested until recently (42, 43). It is imperative to test how duration of Tat expression alters its direct and indirect neurotoxic effects since Tat is known to be produced by infected cells during early as well as late stages, even in the presence of ART. More importantly, it would elucidate if TIMP-1 and subsequently MMP/TIMP axis could be modeled during acute versus prolonged HAND-relevant stimuli *in vivo*.

To evaluate if Tat-mediated effects on MMP/TIMP axis are similar or biphasic in the context of duration of Tat expression, two DOX administration paradigms were compared to induce acute vs. prolonged Tat expression in the iTat mouse model (**Figure 1A**). First, a series of behavioral tests investigating anxiety, arousal, ambulation, learning, and memory was conducted to validate functional changes characteristic of HAND in these mice. Following behavior testing, brain gene expressions of MMPs, TIMPs and associated proinflammatory mediators were measured.

MATERIALS AND METHODS

Animals

All animal experiments were conducted in strict accordance with the recommendations in the Guide for the Care and Use of Laboratory Animals of the National Institutes of Health. The study and associated protocols were approved by the University of North Texas Health Science Center Institutional Animal Care and Use Committee in Fort Worth, TX prior to initiation of the study. The iTat mice generated as previously described (26) were provided by Dr. Johnny He. iTat mice were rederived by Jackson Laboratory and expressed both transgenes i.e., *hiv tat* and reverse tetracycline-controlled transactivator (rtTA) as confirmed by genotyping. Breeder C57BL6/J wild-type (WT) mice (6 weeks old) were purchased from Jackson Laboratory. All experimental mice were bred in house under the same conditions. The mice were housed in groups of three to five in polycarbonate

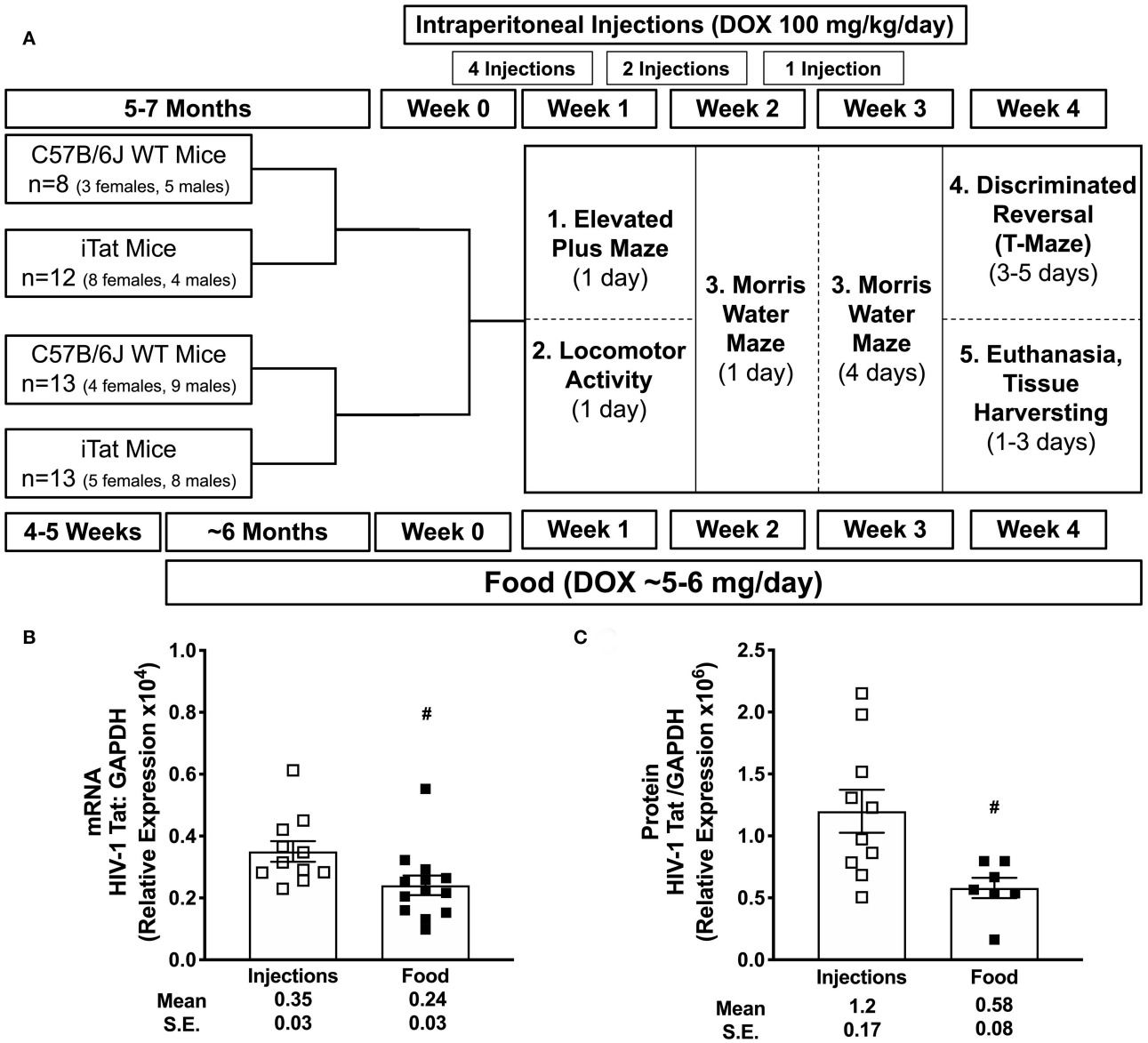

FIGURE 1 | Experimental schematic and acute vs. prolonged *Tat* expression. C57BL/6 wild-type (WT) and iTat mice of both sexes were administered doxycycline (DOX) *via* intraperitoneal (*i.p.*) injections (100 mg/kg/day) or DOX-containing food *ad libitum* (about 5–6 mg DOX/day). **(A)** A total of seven *i.p.* injections were given to 5–7 month old mice over 3 weeks prior to and during behavior testing. In parallel, mice were fed DOX food for about 7 months (6 months prior to and 1 month during the behavior testing) starting at 4 to 5 weeks of age. Therefore, these groups were age-matched at the initiation of behavior testing, which was carried out over 4 weeks. After behavior testing, mice were euthanized, and brain tissues were harvested for gene expression and/or protein analyses. **(B)** Tat mRNA expression was measured in iTat mice using one-step real-time PCR. GAPDH was used as an internal housekeeping control. The iTat mice received acute Tat induction by DOX *i.p.* injections ($n = 11$, open squares) and prolonged Tat induction *via* DOX food ($n = 13$, solid squares). Each bar represents the mean ± SEM. $^{\#}p < 0.050$ by unpaired *T*-test. **(C)** Tat protein expression was measured in WT and iTat mice using simple western (WES, protein simple). GAPDH was used as an internal housekeeping control. The WT and iTat mice received acute Tat induction by DOX *i.p.* injections ($n = 10$, open squares) and prolonged Tat induction *via* DOX food ($n = 7$, solid squares). Each bar represents the mean ± SEM. $^{\#}p < 0.050$ by unpaired *T*-test.

cages with corncob bedding, fed *ad libitum*, and maintained at an ambient temperature (23 ± 1°C), under a 12 h light/dark cycle.

Treatments

Wild-type and iTat mice were administered DOX by two different methods, intraperitoneal (*i.p.*) injections or food in order to delineate effects of acute vs. prolonged Tat expression, respectively. We hypothesized that high concentration DOX *via i.p.* injections compared to food (100 mg/kg/day vs. ∼5–6 mg/day) would lead to higher and acute Tat expression, whereas low dose DOX *via* food would mimic the low level, mild Tat expression, analogous to chronic phenotype. Age- and sex-matched WT mice were used to evaluate off-target DOX effects. The schematic representation of the experimental

timeline is presented in **Figure 1A**. Additional mice with varied frequencies of DOX injections and food were used in preliminary and/or validation experiments (**Supplementary Figure 1A**).

Acute Tat Induction

Previous studies reported that Tat expression increased significantly after three DOX (100 mg/kg) *i.p.* injections and returned to baseline in 2 weeks after last injection in a similar GFAP promoter-driven HIV-1 Tat expression mouse model (38). To evaluate an optimal injection paradigm in iTat mice, we performed studies with different DOX concentrations, frequency of *i.p.* injections and time course to determine an optimal method to model acute Tat expression. Our initial experimental design included 10 injections over 4 weeks to maintain a high Tat expression over 4 weeks of behavior testing. However, an attrition rate of 35% was observed in iTat mice and 30% in WT mice, potentially due to highly acidic pH of doxycycline hyclate (data not shown). Thus, based on preliminary data and previous reports, seven *i.p.* injections of 100 mg/kg DOX (Cat no. D9891, Sigma-Aldrich, St. Louis, MO) were administered over 3 weeks for an acute Tat induction. Specifically, 5–7 month old mice were injected four times in the week prior to, two times during the 1st week, and once in the 2nd week of behavior testing to maintain Tat expression above baseline during behavioral testing and at the time of brain tissue harvesting.

Prolonged Tat Induction

Mice were fed with chow containing DOX (1,250 mg/kg, Cat no. TD.160353, +maltodextrin, green, Harlan Laboratories, Indianapolis, IN) starting at 4 to 5 weeks of age for a total of 6 months prior to and during the 4 weeks of behavior studies to mimic prolonged Tat expression responses. DOX food intake was consistent for 2 months prior to and during behavior studies.

Behavioral Assessments

At 6 to 7 months, experimental animals were characterized for behavior reflecting anxiety, arousal, spatial learning and memory, and cognitive flexibility. All mice were euthanized within a week after completing behavioral tests. Mice were weighed weekly during behavior studies (**Supplementary Figure 2**).

Elevated Plus Maze (EPM)

To measure anxiety (38), a plus-shaped maze elevated three feet was placed in a dimly lit test room (60 Watts). The maze consisted of two arms opened to the room and two arms enclosed such that the floor and the rest of the room were not visible. An automated tracking system monitored the position of each mouse in the maze (Any-maze, Stoelting Co., Wood Dale, IL). Mice were acclimated to the testing room for a minimum of 10 min prior to testing. Each mouse was placed in the center of the maze facing an open arm and was given 5 min to explore the maze. Percent time spent in the open arms and total distance covered were recorded.

Locomotor Activity (LMA)

Spontaneous locomotor activity was measured as described previously (44). In this test, each mouse was placed in a clear acrylic box (40.5 × 40.5 × 30.5 cm), surrounded by a photocells-lined metal frame. The test cage was then placed in a dimly lit chamber equipped with a fan that provided background noise (80 dB). The test was conducted for 16 min, in which movements in the horizontal plane and vertical plane (7.6 cm above the floor of the box) were detected by the photocells and processed by a software program (Digiscan apparatus, Omnitech Electronics, model RXYZCM-16, Columbus, OH) to yield different measures including distance covered, vertical activity, and spatial components of spontaneous activity in the box.

Morris Water Maze (MWM)

Spatial learning and memory were measured using a MWM test. Testing was carried out as described previously (45). Mice were acclimated to the testing room for a minimum of 10 min prior to testing each day. During each trial, the mouse was put in a tank filled with opacified water (using non-toxic acrylic white paint) to swim and was able to escape the water by finding and climbing on a platform hidden 1.5 cm below the water surface. The water temperature was maintained at 24 ± 1°C. An automated tracking system recorded various measures such as latency, path length and swimming speed for each trial (Any-maze, Stoelting Co.). The test consisted of two phases. [1] Pre-training phase: during this phase, the tank was covered with a black curtain to hide surrounding visual cues. Each mouse was trained over a single session of five trials with 5 min inter-trial intervals. During each trial, the mouse was allowed to swim until it climbed on the platform or for a maximum of 60 s, whichever was earlier. This pre-training was done so that the mice could learn the motor components of the task such as swimming and climbing onto a platform, and to reduce the bias of anxiety to a new environment during the subsequent phases [2] Acquisition phase: mice were then tested for their ability to locate a hidden platform using spatial cues around the room over four sessions (one session/day). Each session consisted of five trials, at 2-min intervals. For each trial, the mouse was placed at one of four different starting points at the edge of tank and had to swim to the platform, which remained at the same location. The mouse was allowed to swim until it reached the platform or for a maximum of 90 s. Path length (distance taken to reach the platform) over all sessions was used as the primary measure of performance. The swim speed was calculated by dividing path length by the latency (to reach the platform) for each trial.

Discrimination Reversal

The discrimination reversal testing assessed memory with a T-maze as described previously (45). Briefly, the T-maze was constructed of acrylic with black sides to hide spatial cues for the mouse and clear tops for the tester to observe the mouse. The maze consisted of three compartments: a start box (10 × 6.3 × 6 cm), which extended into the stem (17.5 × 6.3 × 6 cm), and two arms (14.5 × 6.3 × 6 cm), each separated by acrylic flaps manually operated by the tester. The maze rested on a metal grid wired to deliver 0.69 mA scrambled shock to the feet. Mice were acclimated to the testing room for a minimum of 10 min prior to testing. Each mouse was tested in three sessions separated by 1 h. At the beginning of each trial, the mouse was placed in the start box, and the start flap was removed for the mouse to enter

the stem. During the first trial of the first session, the mouse received a mild shock (0.69 mA) on entering an arm (preferred arm) and was allowed to avoid it by running to the other arm, which then became the correct arm for the remainder of first session. For subsequent trials, shock was initiated 5 s after the opening of the start flap if the mouse had not entered the correct arm or immediately upon entry into the incorrect arm. The shock continued until the correct arm was entered or for a maximum of 60 s. Once the mouse entered the correct arm, the flap was closed to prevent escape, and the mouse was moved after 10 s, by detaching the arm, into a holding cage for 1 min before beginning the next trial. This trial paradigm continued until the mouse fulfilled the correct avoidance criterion, i.e., running directly to the correct arm within 5 s, in four of the five consecutive training trials including the last two. In the second and third sessions, there was a reversal in correct arm such that the mouse was required to run to the other arm compared to the one it was trained for in the previous session. The ability of the mice to learn is inversely proportional to number of trials required to fulfill the avoidance criteria.

Cardiac Perfusion, Euthanasia, and Tissue Harvesting

Mice were euthanized by *i.p.* injections of 100 mg/kg ketamine hydrochloride (100 mg/ml, Putney, Inc, Portland, ME) and 10 mg/kg xylazine (20 mg/ml, Akorn, Inc, Lake Forest, IL) followed by cardiac perfusion using 1X phosphate buffer saline. For animals that underwent behavior testing, each harvested brain was cut in three parts. Posterior half of one hemisphere was used for RNA isolation and subsequent gene expression testing. The posterior half of the other hemisphere was snap frozen prior to protein isolation as described below. The frontal lobe sections were fixed in 4% PFA for future use. Brain tissues of additional mice that received either DOX injections or food at the similar frequencies or duration, respectively, as the mice in the behavior studies were used to elucidate if gene expression patterns observed in different parts of the brain were comparable, namely right hemisphere (RH), left anterior (LA) and left posterior (LP) (**Supplementary Figures 1, 3**).

RNA Isolation, cDNA Synthesis, and Real-Time PCR

Tissue was homogenized with Trizol (Sigma Aldrich). The homogenates (1 mL Trizol/∼100 mg tissue weight) were centrifuged to remove debris, and viscous supernatants were used for RNA isolation. Total RNA was isolated using phenol-chloroform extraction method, treated with DNAse (Thermo Fisher, Waltham, MA) as per manufacturer's instructions to digest genomic DNA, and then reverse transcribed into cDNA template for real-time PCR. TaqMan™ Fast Advanced Master Mix (Cat no. 4444557, Applied Biosystems, Foster City, CA) and Applied Biosystems TaqMan gene expression assays for TIMP-1 (Cat no. Mm01341361), TIMP-2 (Cat no. Mm00441825), MMP-2 (Cat no. Mm00439498), MMP-9 (Cat no. Mm00442991), interleukin (IL)-1β (Cat no. Mm00434228), tumor necrosis factor (TNF)-α (Cat no. Mm00443258), CCL2 (Cat no. Mm00441242), IL-6 (Cat no. Mm00446190), IL-17 (Cat no. Mm00439618), GFAP (Cat no. Mm01253033), glyceraldehyde 3-phosphate dehydrogenase (GAPDH) (Cat no. 4352339E), beta-actin (Cat no. Mm01205647_g1) and phosphoglycerate kinase (PGK)-1 (Cat no. Mm00435617) were used for gene expression analysis by real-time PCR. Each 20 μL PCR reaction consisted of 100 ng of cDNA, 1X TaqMan™ Fast Advanced Master Mix, 1X probes for both experimental and housekeeping gene targets. The samples were incubated at 95°C for 5 min for polymerase activation, followed by 40 cycles of denaturation and annealing-extension at 95°C for 1 s and 60°C for 20 s. Each sample was measured in triplicates. The threshold cycle (C_T) values were converted into $\Delta\Delta C_T$ to obtain fold-change in expression as compared to treatment WT controls (behavior injection WT $n = 7$, behavior food WT $n = 13$, gross brain region injection WT $n = 3$, gross brain region food WT $n = 5$). We noted a difference in basal GAPDH expression, a commonly used housekeeping control, between both strains (**Supplementary Table 1**). Subsequently, we tested two other housekeeping genes, *i.e.,* β-actin and PGK-1. PGK-1 was selected to be used as a housekeeping control for gene expression comparisons between strains, based on least difference between the two strains.

For Tat mRNA measurements, mRNA was isolated from total RNA using Dynabeads mRNA direct purification kit (Cat no. 61012, Thermo Fisher). Primers used for Tat detection were 5′ ggaagcatccaggaagtcag 3′ and 5′ ggaggtgggttgctttgata 3′ with 5′ cctcctcaaggcagtcagac 3′ used as probe. Tat mRNA expression was evaluated using TaqMan™ Fast Virus 1-Step Mastermix (Cat no. 4444432, Applied Biosystems). GAPDH was used as an internal housekeeping control. Each 20 μL PCR reaction consisted of 20 ng of mRNA, 1X Fast Virus 1-Step Mastermix, 1X probes for Tat and GAPDH gene targets. The samples were incubated at 50°C for 5 min, 95°C for 20 s, followed by 40 cycles of denaturation and annealing-extension at 95°C for 3 s and 60°C for 30 s. Each sample was measured in triplicates. The ratios of threshold cycle (C_T) values of Tat and GAPDH were used for quantitative assessments.

Protein Isolation and Simple Western

Tissue was homogenized in 2 μL RIPA buffer (Thermo Fisher) per mg tissue using a red bead lysis kit with a mix of zirconium beads (Cat no. REDE5, Next Advance, Troy, NY) and the Bead Mill 4 (Fisher) at speed 4 for 3 min. Several WT and iTat brain sections from the food group were homogenized using at 5 μl RIPA/ 1 mg tissue using the PRO200 homogenizer (PRO Scientific, Oxford, CT). However, some of these lysates were too dilute for further analysis. The homogenates were centrifuged for 10 min at 10,000 g to remove the beads and debris. Protein concentrations of the clarified lysates were determined by the BCA protein assay microplate method (Thermo Fisher) according to manufacturer's instructions. Brain lysates were diluted to 2 mg/ml and assayed by simple western (Protein Simple, San Jose, CA) according to their standard protocol. HIV-1 Tat was detected with a rabbit polycolonal antibody (Cat no. ab43014, lot no. GR3264810-9, abcam, Cambridge, MA) at a 1:10 dilution using the 2-40 kDa separation and anti-rabbit

detection modules. HIV-1 IIIB Tat recombinant protein was obtained through the NIH AIDS Reagent Program, Division of AIDS, NIAID, NIH and used as a positive control and standard across WES assays. GAPDH was detected using a monocolonal mouse antibody 6C5 (Cat no. sc32233, lot no. K0315, Santa Cruz Biotechnology, Dallas, TX) at a 1:5000 dilution using the 12-230 kDa separation and anti- mouse detection modules. Brain HIV Tat levels were normalized to the HIV-1 Tat positive control column before normalization to GAPDH.

Statistical Analysis

All data are presented as mean ± SEM. Differences between mean values were determined using analyses of variance (ANOVA) or *T*-test. Tat mRNA and protein levels in iTat mice between two induction paradigms were analyzed using a two-sided *T*-test. All behavior and gene expression data were subjected to two-way ANOVA, with Treatment Time (acute vs. prolonged) and Strain (WT vs. iTat) as between group factors. Additionally, Water maze and body weight data were subjected to three-way ANOVA, with Treatment Time and Strain as between-group factors, and duration or session as within group factors. Planned individual comparisons between groups were made using the single degree-of-freedom F tests. The alpha level was set at 0.05 for all analyses. Statistical analyses for behavioral tests and gene expression post behavior testing were performed using Systat 13 (**Figures 2**–**7**). Gene expression data for Tat mRNA, protein and brain region-specific gene expression in additional mice were analyzed using Prism 8.0 (**Figure 1**, **Supplementary Figures 1, 3**).

RESULTS

Evaluating Tat Transgene Expression

Acute Tat expression was induced using DOX injection method, similar to previous studies investigating Tat-mediated behavioral changes in iTat mice (36, 38, 39). Additionally, prolonged Tat expression was induced *via* food, which was also used in this model previously (43). Tat gene expression was quantified in mRNA isolated from iTat mouse brain tissues using one-step PCR. Preliminary assessments for acute induction model indicated that, Tat expression increased significantly with increased number of DOX injections increased from six injections to ten injections and reduced sharply after a week while remaining at detectable levels (**Supplementary Figure 1B**). Further, Tat expression was higher in the left posterior (LP) brain region ($p = 0.013$ and $p = 0.023$, respectively), compared to right hemisphere (RH) and left anterior (LA) with the *i.p.* induction method, while prolonged food-based method did not show changes in Tat expression in different gross brain regions (**Supplementary Figure 1C**). In the mice that underwent behavior studies, relative *tat* gene expression was evaluated in brain harvested at the end of the study. Tat mRMA levels were higher in acute iTat brains (injection) compared to prolonged iTat brains (**Figure 1B**) ($^{\#}p = 0.026$). Tat gene expression was undetectable in WT brain tissues (data not shown). Similar to mRNA levels, Tat protein levels were significantly higher than DOX-injected iTat mice compared to DOX-fed mice ($^{*}p = 0.013$) (**Figure 1C**).

Elevated Plus Maze (EPM)

Anxiety was measured using the percent time spent in the open arms of the EPM (**Figure 2A**). In the injected group, the iTat mice spent less time than their WT controls in the open arms ($p < 0.05$), while in the food group, there was no significant difference between the iTat mice and their WT controls. Overall, the DOX fed mice spent less time in the open arms than the DOX injected mice, and the iTat mice, regardless of treatment, spent less time in the open arms than the WT. These observations were supported by an ANOVA, which revealed significant main effects of Treatment Time ($p = 0.002$) and Strain ($p = 0.014$) on the percent time spent in the open arms; however, there was no significant interaction between the two factors ($p = 0.170$).

Distance traveled by the mice in the maze was measured to determine if activity affected the time spent in the arms (**Figure 2B**). There was no difference between any of the groups, which was supported by a lack of significant main effects of Treatment Time ($p = 0.342$), Strain ($p = 0.339$), or their interaction ($p = 0.586$).

Locomotor Activity (LMA)

The effects of Treatment Time and Strain on the horizontal, vertical, and spatial components of spontaneous activity are presented in **Figure 3**. In the injected group, there was no difference between the iTat and the WT, while in the food group, the iTat traveled less distance than the WT ($p < 0.050$) (**Figure 3A**). The two-way ANOVA revealed a significant main effect of Treatment Time ($p = 0.034$), but no effect of Strain ($p = 0.202$) or an interaction between Strain and Treatment Time ($p = 0.071$).

The number of rearing counts served as a measure for vertical activity and is presented in **Figure 3B**. In the injection group, the iTat mice had higher rearing counts compared to their WT ($p < 0.050$), while in the food group, there was no difference between iTat and WT. This finding was supported by a significant interaction of Treatment Time and Strain ($p = 0.040$). The two-way ANOVA also yielded a significant main effect of Treatment Time ($p = 0.030$) but no effect of Strain ($p = 0.180$).

In **Figure 3C**, the amount of time spent in the center of the apparatus is presented. In both injected and food groups, the time spent in the center was comparable between WT and iTat. Overall, there was no difference between the WT and iTat mice; however, the injected mice spent more time in the center than the food mice. These observations are supported by a two-way ANOVA yielding a main effect of Treatment Time ($p = 0.029$), and no effect of Strain ($p = 0.516$) or interaction of the two factors ($p = 0.322$).

Given the differences observed in acute vs. prolonged iTat mice, we further evaluated if these were driven by Sex as a secondary analysis. However, in a three-way ANOVA using on all measures of LMA there was no significant interaction of Sex with Strain or Treatment. We also looked at averages for each and similar trends were seen in both sexes supporting the lack of interaction reported by the analyses.

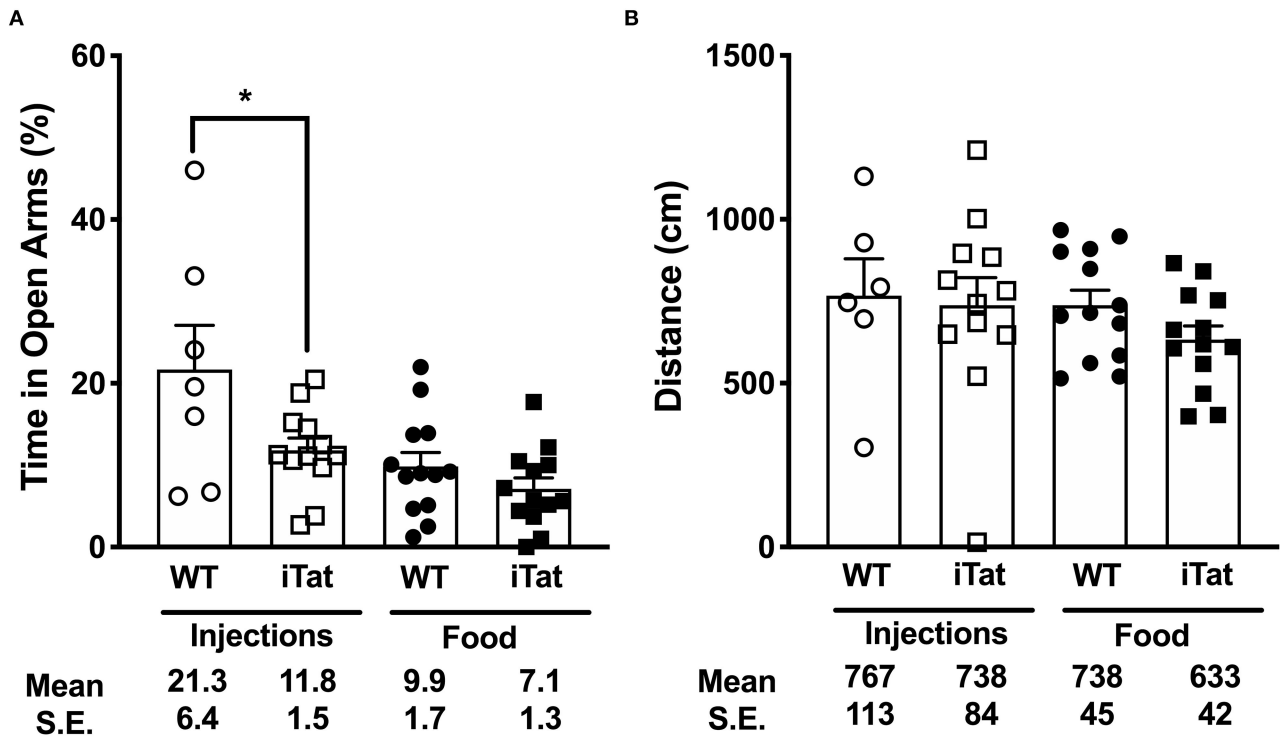

FIGURE 2 | Higher anxiety levels were observed in iTat mice compared to Treatment Time WT controls in elevated plus maze testing. Anxiety levels were measured by **(A)** the percent time spent in the open arms and **(B)** total distance covered on the maze in iTat and WT mice. The WT mice ($n = 6$, open circles) and the iTat mice ($n = 12$, open squares) received acute induction by DOX *i.p.* injections, while the WT mice ($n = 13$, solid circles) and the iTat mice ($n = 13$, solid squares) received prolonged induction *via* DOX food. Each bar represents the mean ± SEM. $^{*}p < 0.050$ for same Treatment Time comparisons between Strains by two-way ANOVA using Treatment Time and Strain as variables.

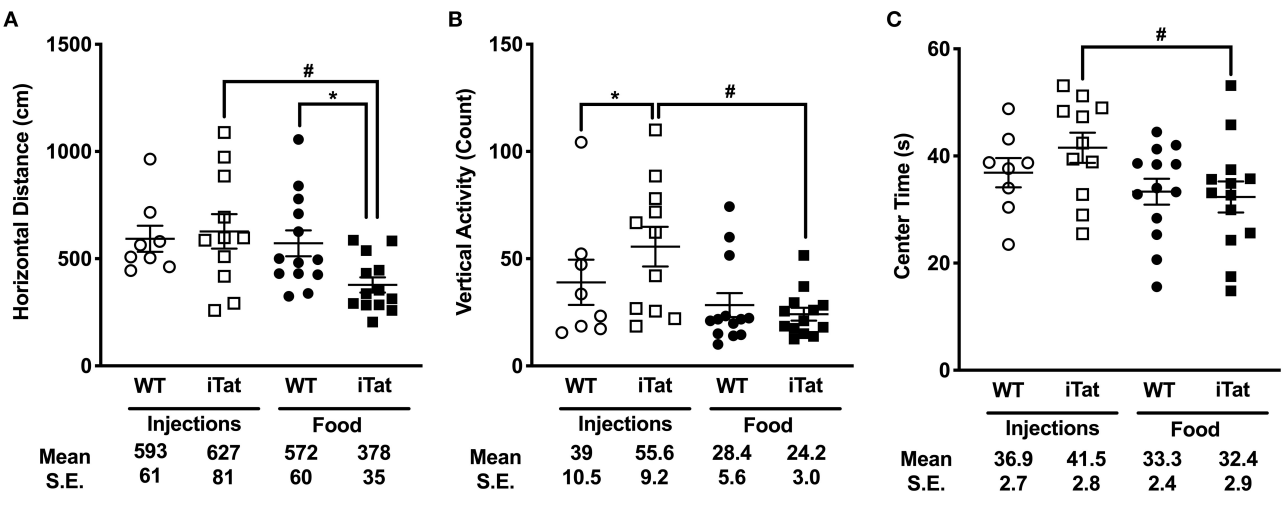

FIGURE 3 | Prolonged HIV-1 Tat expression led to slower ambulation, reduced vertical activity, and reduced center time compared to acute Tat expression in iTat mice. **(A)** Horizontal Distance, **(B)** Vertical Activity, and **(C)** Center Time in iTat and WT mice were measured. Average per minute values for each parameter were plotted. The WT mice ($n = 7$–8, open circles) and the iTat mice ($n = 10$–11, open squares) received acute induction by DOX *i.p.* injections, while the WT mice ($n = 13$, solid circles) and the iTat mice ($n = 13$, solid squares) received prolonged induction *via* DOX food. Each bar represents the mean ± SEM. $^{*}p < 0.050$ for same Treatment Time comparisons between Strains, $^{\#}p < 0.050$ for same Strain comparisons across Treatment Time by two-way ANOVA using Treatment Time and Strain as variables.

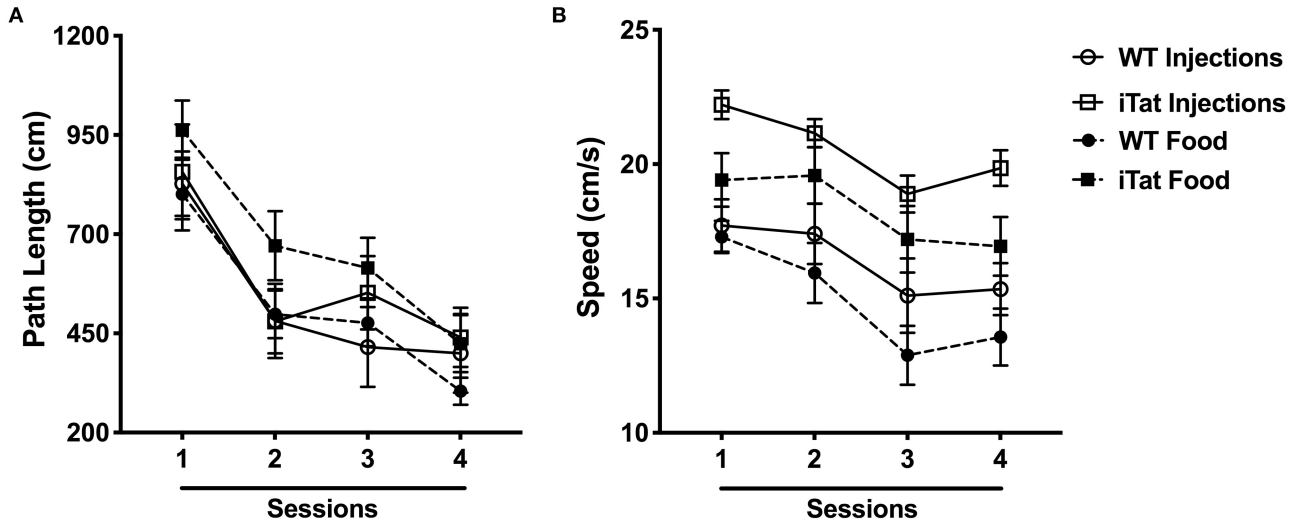

FIGURE 4 | Morris water maze performance indicated faster swim speeds in iTat mice during acute vs. prolonged HIV-1 Tat expression. **(A)** Path length and **(B)** swimming speed were assessed in iTat and WT mice over four sessions. Each data point represents the mean ± SEM from an average of four trials per session. One session is equivalent to 1 day. The WT mice ($n = 7$, solid line with open circles) and the iTat mice ($n = 11$, solid line with open squares) received acute induction by DOX *i.p.* injections, while the WT mice ($n = 13$, dashed line with solid circles) and the iTat mice ($n = 13$, dashed line with solid squares) received prolonged induction *via* DOX food.

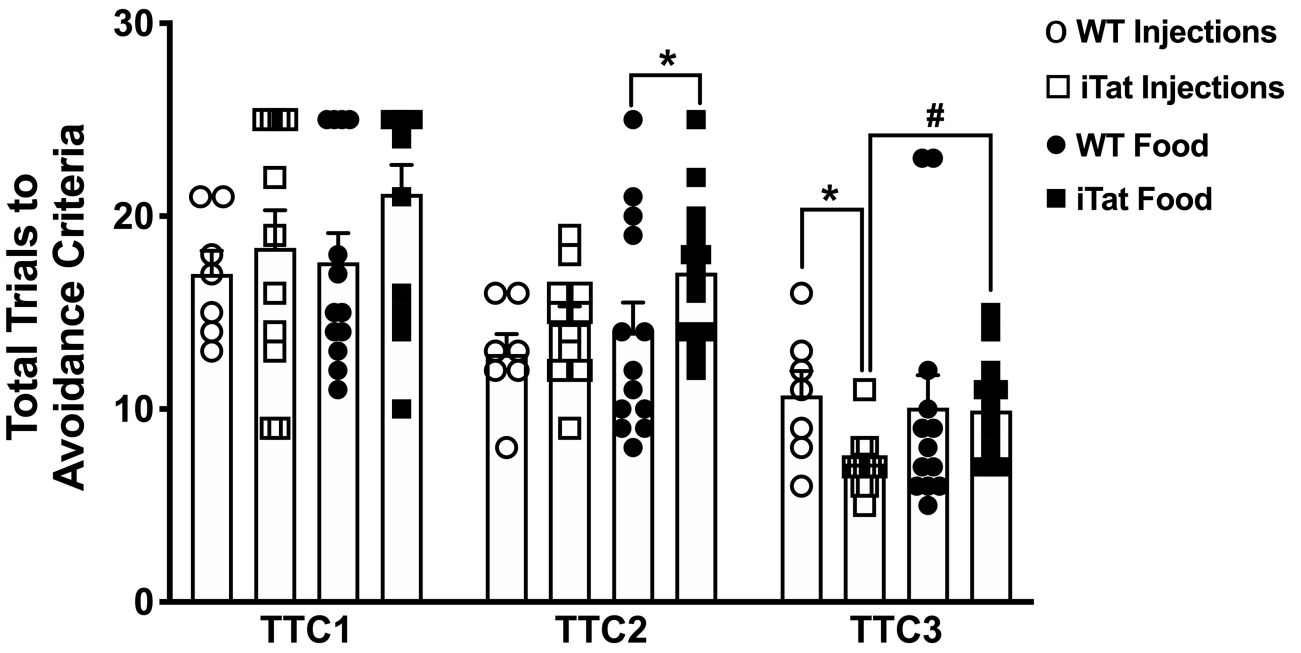

FIGURE 5 | Prolonged HIV-1 Tat expression increased trials to reach avoidance criteria in iTat mice in discrimination reversal test. The T-maze test measured the number of total trials taken by iTat and WT mice to reach discriminated avoidance criteria during three sessions. The WT mice ($n = 7$, open circles) and the iTat mice ($n = 11$, open squares) received acute induction by DOX *i.p.* injections, while the WT mice ($n = 12$, solid circles) and the iTat mice ($n = 13$, solid squares) received prolonged induction *via* DOX food. Each bar represents the mean ± SEM, TTC: total trials to criteria, TTC1: Acquisition session, TTC2, TTC3: Reversal session, $^{*}p < 0.050$ for same Treatment Time comparisons between Strains, $^{\#}p < 0.050$ for same Strain comparisons across Treatment Time by two-way ANOVA using Treatment Time and Strain as variables.

Morris Water Maze (MWM)

Spatial memory was assessed measuring path length and swim speed of mice to locate a hidden platform under the water surface (**Figure 4A**). All mice learned to locate the platform across sessions, and a similar pattern of learning efficiency was observed across the groups. This was supported by a significant effect of Session ($p < 0.05$) and a lack of interaction between Session and any other factors (all

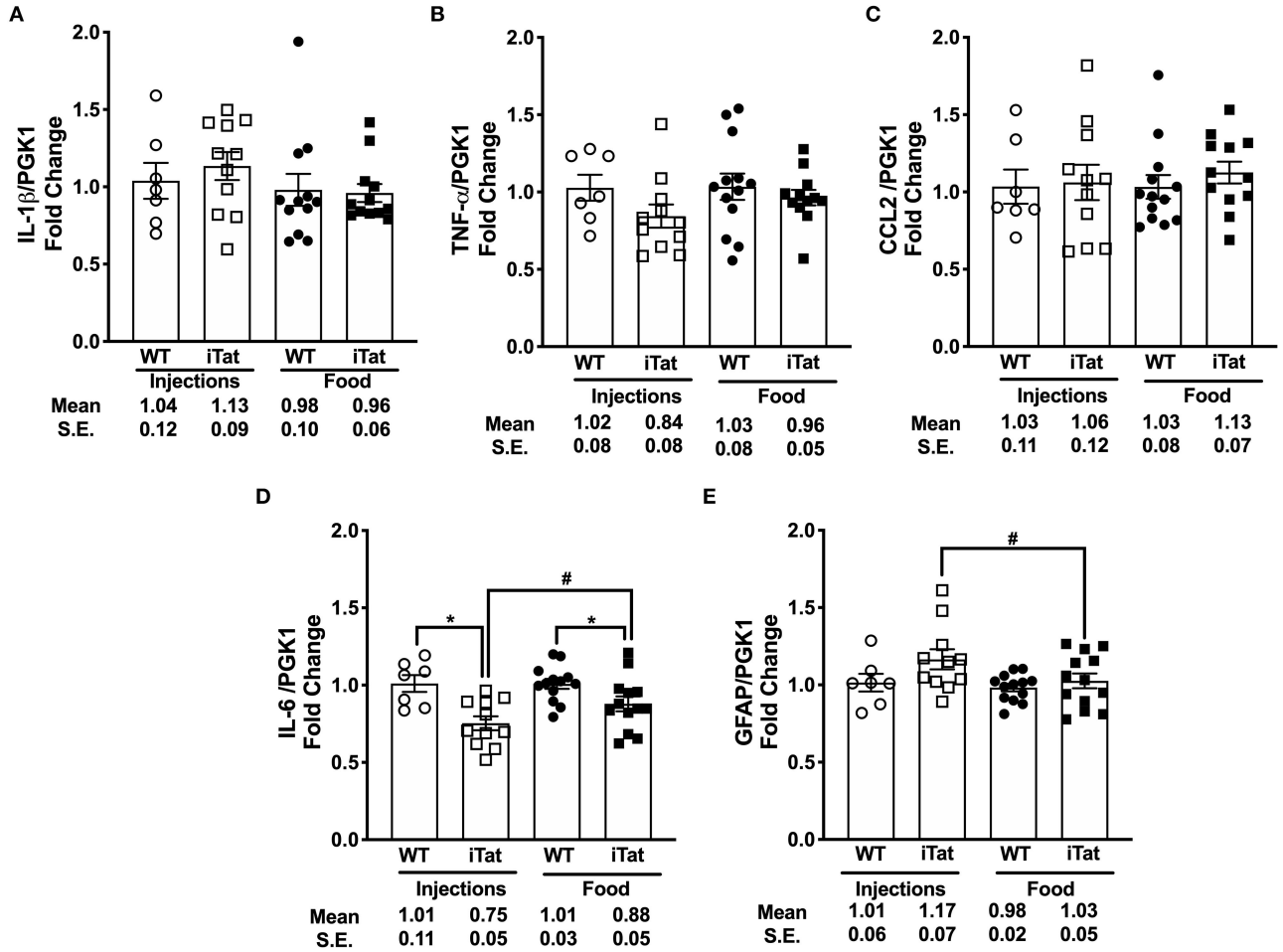

FIGURE 6 | Key pro-inflammatory biomarkers gene expression remained comparable with acute and prolonged HIV-1 Tat induction in iTat mice. **(A)** IL-1β **(B)** TNF-α **(C)** CCL2, **(D)** IL-6, and **(E)** GFAP mRNA levels were measured in iTat and WT mouse brain tissues by real-time PCR. The WT mice ($n = 7$, open circles) and the iTat mice ($n = 11$, open squares) received acute induction by DOX *i.p.* injections, while the WT mice ($n = 12$–13, solid circles) and the iTat mice ($n = 12$–13, solid squares) received prolonged induction *via* DOX food. Each bar represents the mean ± SEM, $^{*}p < 0.050$ for same Treatment Time comparisons between Strains, $^{\#}p < 0.050$ for same Strain comparisons across Treatment Time by two-way ANOVA using Treatment Time and Strain as variables.

$p > 0.400$) following a repeated measure ANOVA. In the injected group, there was no difference between iTat and WT, while in the food group, the iTat took longer path length at every session than the WT. This observation was not supported by a main effect of Strain ($p = 0.089$) or Treatment Time ($p = 0.516$), or an interaction between the two factors ($p = 0.399$).

Swim speed was analyzed and is presented in **Figure 4B.** The swim speed of the mice varied across sessions ($p < 0.010$), but the other factors did not have an effect across sessions (all $p > 0.2$). Overall, the iTat mice swam faster than the WT mice in both paradigms, and the injected mice seemed to swim faster than the food mice, but it was mostly due to the injected iTat mice. These observations were supported by a main effect of Strain ($p < 0.001$), a main effect of Treatment Time ($p = 0.049$), and no interaction between two factors ($p = 0.676$).

Discrimination Reversal (T-Maze)

Data from the first session of the discriminated avoidance task (TTC1) represent a measure of learning/acquisition and the subsequent two sessions represent a measure of cognitive flexibility (TTC2, TTC3) (**Figure 5**). During the acquisition session, even though the food iTat mice seem to take more trials to reach criterion it did not reach significance. Neither strain nor treatment time seem to affect the performance of the mice during acquisition, which is supported by lack of main effects or interaction following a two-way ANOVA (all $p > 0.132$) (**Figure 5**). During the first reversal session (TTC2), there was no difference between the two genotypes in the injected group. However, in the food group, the iTat mice took more trials to reach criterion compared to the WT ($p < 0.05$). A two-way ANOVA yielded a main effect of Strain ($p = 0.021$) which was mostly due to the effect in the food group, and there was no main effect of Treatment

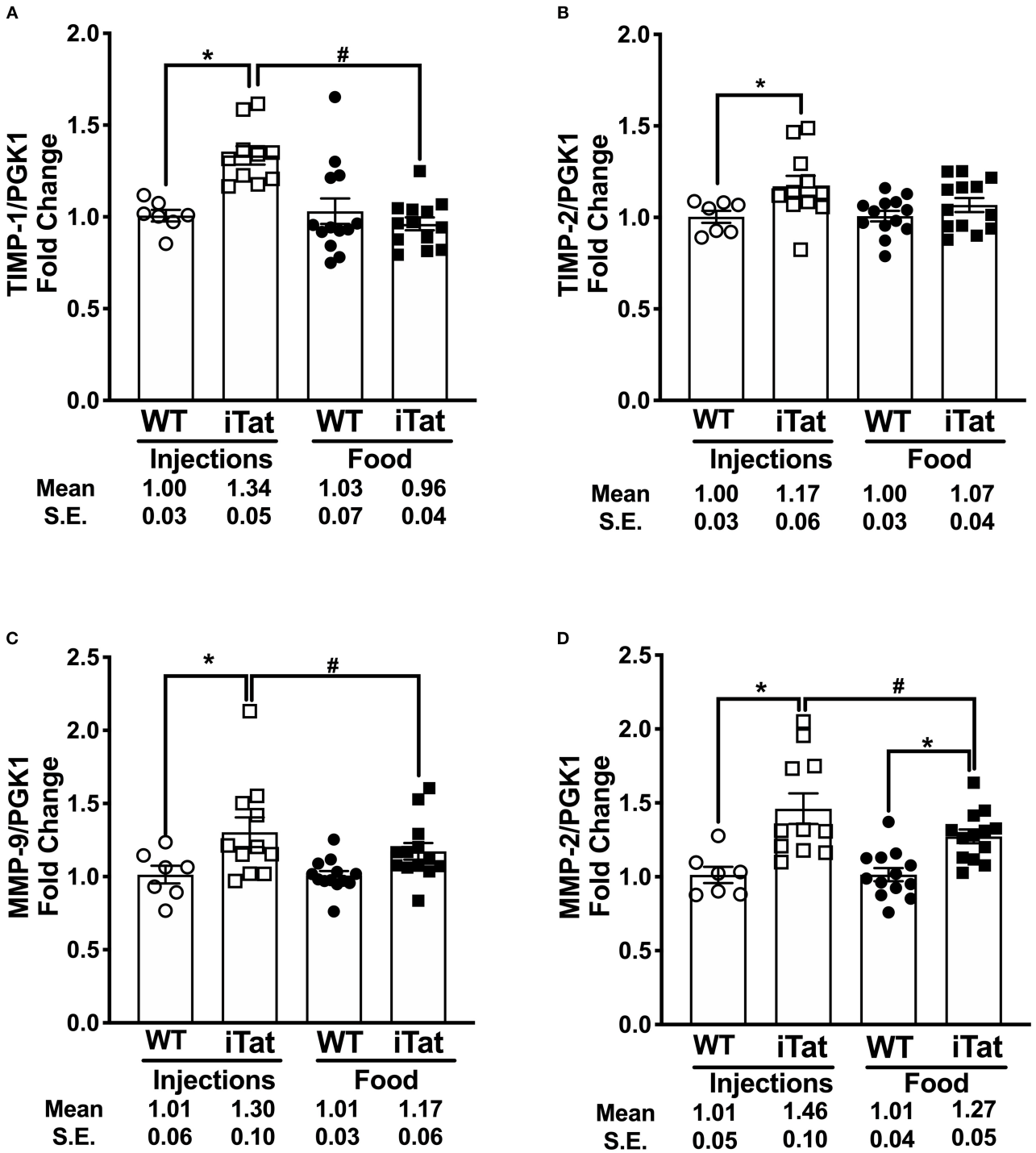

FIGURE 7 | Acute vs. prolonged HIV-1 Tat induction dysregulated MMP/TIMP balance in iTat mice. **(A)** TIMP-1, **(B)** TIMP-2, **(C)** MMP-9, **(D)** and MMP-2 gene expression was measured in iTat and WT mice. The WT mice ($n = 7$, open circles) and the iTat mice ($n = 11$, open squares) received acute induction by DOX *i.p.* injections, while the WT mice ($n = 12$–13, solid circles) and the iTat mice ($n = 12$ – 13, solid squares) received prolonged induction *via* DOX food. Each bar represents the mean ± SEM, $^{*}p < 0.050$ same Treatment Time comparisons between Strains, $^{\#}p < 0.050$ for the same Strain comparisons across the treatments by two-way ANOVA using Treatment Time and Strain as variables.

Time or an interaction (all $p > 0.226$). In the last reversal session (TTC3), the injected iTat mice took less trials than the WT, while the food iTat mice took more trials than the WT to reach criterion. This observation was supported by a significant interaction between Strain and Treatment Time ($p = 0.041$).

Evaluating Expression of Proinflammatory Cytokines and Gliosis

The mRNA levels of a number of proinflammatory cytokines including IL-1β, TNF-α, and CCL2 were comparable among all treatment groups (**Figures 6A–C**). Subsequently, a two-way ANOVA failed to show main effects of Treatment Time and Strain or their interaction on their gene expression (all $p > 0.305$). The gene expression of IL-6 was significantly reduced in iTat mice compared to Treatment Time WT controls, respectively (both $p < 0.050$) (**Figure 6D**). Further, the IL-6 expression was significantly higher in DOX-fed iTat mice ($p = 0.044$) compared to DOX-injected iTat mice. A two-way ANOVA indicated a main effect of Strain ($p < 0.001$), but there was no effect of Treatment Time or interaction of the two-factors. Gene expression of another known inflammatory cytokine IL-17 was undetectable in both WT and iTat mice (data not shown). As the Tat transgene expression is driven by the GFAP promoter and elevated GFAP expression is a marker of astrogliosis, we measured if there were transcriptional changes in GFAP expression. While GFAP mRNA expression in acute and prolonged Tat expressing mice was comparable to their respective WT controls, acute Tat expressing mice showed significantly higher GFAP mRNA expression when compared to prolonged Tat-expressing mice ($p < 0.05$) (**Figure 6E**). This was also reflected in a main effect of Strain approaching significance ($p = 0.062$); however, there was no effect of Treatment Time ($p = 0.097$) and its interaction with Strain ($p = 0.298$) on GFAP gene expression.

Gene Expression of MMP/TIMP Balance Components

Simultaneously, we evaluated the MMP/TIMP balance in iTat mice, by measuring TIMP-1, TIMP-2, MMP-9, and MMP-2 gene expression profiles (**Figure 7**). Among inducible proteins regulating the MMP/TIMP axis, TIMP-1 mRNA levels increased significantly in acute Tat-expressing mice compared to their WT controls, while prolonged Tat expressing iTat mice showed comparable expression to their respective WT mice (**Figure 7A**). More importantly, TIMP-1 expression was significantly lower in prolonged Tat-expressing iTat mice compared to their acute Tat-expressing counterparts. These trends were reflected in the two-way ANOVA, which showed main effects of Treatment Time ($p = 0.015$) and Strain ($p = 0.043$) as well as their interaction on TIMP-1 gene expression ($p = 0.009$). Acute Tat-expressing iTat mice had higher TIMP-2 mRNA expression compared to their WT control (**Figure 7B**). The levels of MMP-9 and MMP-2 were higher in iTat mice compared to their WT (**Figures 7C,D**). A two-way ANOVA indicated a main effect of Strain (all $p < 0.011$) on TIMP-2, MMP-9, and MMP-2 levels; however, there were no effects of Treatment Time and its interaction with Strain (all $p > 0.134$). The changes in mRNA expression were also analyzed as MMP/TIMP ratios for iTat mice (**Table 1**). Both MMP-2 and MMP-9 ratios to TIMP-1 were higher in the prolonged Tat-induction paradigm compared to acute Tat-expressing iTat mice. On the other hand, MMP-2 ratio to TIMP-2 was comparable across Treatment Time for iTat mice. Our preliminary studies also established that relative changes in the mRNA expression of MMP/TIMP components remained consistent in different parts of the brain (**Supplementary Figure 3**) and changes observed following behavior studies were consistent in mice that did not undergo behavior, highlighting that there was no effect of behavior studies and/or gross brain regions on the changes reported here.

TABLE 1 | MMP/TIMP ratios in acute and prolonged DOX-treated iTat mice injected and fed with DOX, respectively.

Ratio	iTat Inj $n = 11$	iTat Food $n = 13$
MMP-9/TIMP-1	0.95 (0.38)	1.24 (0.3)$^{\#}$
MMP-2/TIMP-2	1.26 (0.28)	1.20 (0.2)
MMP-2/TIMP-1	1.05 (0.38)	1.34 (0.25)$^{\#}$
MMP-9/TIMP-2	1.13 (0.32)	1.11 (0.21)

*TIMP-1, TIMP-2, MMP-9, and MMP-2 mRNA fold change values presented in **Figure 7** were used to obtain the above ratios in iTat mice. The ratios were calculated from the mean of relative fold change calculated for iTat mice, relative to their treatment time matched WT controls. Each row represents the mean ± Standard Deviation $^{\#}p < 0.05$ for same Strain comparisons across Treatment Time by one-way ANOVA.*

DISCUSSION

The iTat mice used in this study (26, 46) and a similar inducible HIV-1 Tat model (35, 47) have been used to evaluate behavior (36, 38, 43, 48) and/or gene expression (49, 50) following either DOX *i.p.* injections or food. In this study, both DOX-administration methods, *i.e., i.p.* injections and food, were used simultaneously to mimic acute vs. prolonged Tat induction, respectively. A previous study concurrently evaluated acute and prolonged effects of Tat in Sprague-Dawley rats; however, resulting changes from both methods were not directly compared (31). Further, induction methods consisted of direct Tat injection in the brain for acute effects, while chronic expression was achieved *via* injection of SV40-derived vector expressing Tat (31). Thus, to the best of our knowledge, this is the first report directly comparing two different HIV-1 Tat induction methods to evaluate changes in behavior and gene expression in a rodent model.

We showed that Tat induction in iTat mice led to mild behavioral deficits when compared to WT controls including one or more of the following trends [1] higher anxiety levels depicted by reduced time spent in the open arms of EPM [2] altered ambulation during LMA [3] higher swim speeds in MWM [4] altered learning in T-maze. Simultaneously, we also depicted that gene expressions of [1] select inflammatory cytokines were unchanged, [2] MMPs were elevated, [3] TIMPs were altered depending on the duration of Tat exposure, subsequently impacting the brain MMP/TIMP balance. Lastly, when Treatment Time was considered as a variable, DOX-injected iTat mice were distinctly different as compared to DOX-fed iTat mice in terms of behavior and gene expression.

Psychiatric conditions including anxiety disorders are frequently observed in PLWH (51). HIV-1 proteins including Tat and glycoprotein120 (gp120) are implicated in direct or indirect mechanisms that manifest into anxiety-like symptoms (52).

Indeed, several previous reports investigated Tat-induced anxiety and/or stress, including sex-specific differences, in transgenic HIV-1 Tat rodent models (42, 43, 48, 53). Since our investigations did not focus on sex-specific changes, we did not test for sex as a confounding variable for anxiety. Paris et al. reported a DOX *i.p.* dose- and duration-dependent increase in anxiety using open field and marble burying tests in iTat mice (38). The data from our studies is consistent in part with these findings, as we observed increased anxiety in EPM in DOX-injected iTat mice compared to their WT counterparts. However, such difference in anxiety was not observed in DOX-fed iTat mice, despite a much longer duration of Tat expression. Reduced ambulation is also among metrics for increased anxiety (54). Additionally, increased swim speed in MWM was associated with higher stress in mice (55) as well as rats (56). Thus, data from this study for DOX-injected vs. DOX-fed iTat mice, as compared to their Treatment Time WT controls, collectively present two overlapping, yet distinct behavioral phenotypes; related to higher anxiety and stress. The DOX-injected mice spent less time in the open arms of the EPM and swam faster in MWM but showed no differences in spontaneous locomotor activity. On the other hand, DOX-fed mice displayed lower ambulation in LMA and swam faster in MWM; yet, showed no differences in EPM. In turn, these findings indicate that there are multiple underlying mechanisms that modulate the anxiety-like behaviors, which are potentially regulated by varied Tat concentrations and/or exposure durations.

Impaired motor skills, characterized by slowed movements and incoordination, were among the symptoms of the mild cognitive motor disorder (MCMD) as per the 1991 American Academy of Neurology criteria (57). In the revised HAND classification system, commonly known as Frascati criteria, motor skills testing was included in the cognitive neuropsychological assessments (4). Further, motor symptoms such as leg weakness and unsteady gait were observed in mild forms of HAND (4). In this context, the lowered ambulation observed in DOX-fed mice was consistent with previous reports measuring ambulation using same test and model (43) as well as a different HIV-1 Tat model, which measured ambulation using open field test (48). In parallel, the DOX-injected iTat mice showed similar ambulation, center time, and higher vertical activity as compared to their Treatment Time controls. Thus, we observed Treatment Time-specific difference in iTat mice for all three measures of LMA. It might be argued that these differences were impacted by body weight since the DOX-fed mice had an average 33% higher body weight. However, such distinction was not observed in DOX-injected and -fed WT mice, despite exhibiting a similar weight difference. Thus, it can be inferred that the differential Tat exposure led to distinct locomotor changes in iTat mice.

Lastly, we used MWM and T-maze to study spatial learning and memory, and cognitive flexibility. We did not observe robust changes between iTat and WT mice by either induction paradigm, except the DOX-fed iTat mice demonstrated poorer learning during the second reversal trial in T-maze. These data were in contrast to previous literature that found distinct memory and cognitive impairments (36, 43, 58, 59). It is possible that differences observed in behavioral trends in this study compared to previous reports could be attributed to different readouts in a test, such as MWM conducted over 4 days in this study vs. 18 days in a previous study (43), or due to differences in two strains of Tat mice, which differ in Tat copy number (42). Additionally, two induction paradigms present different handling requirements and it is not known if additional handling of mice during injection may change their response to behavior.

Our approach to mimic acute Tat expression using *i.p.* injections was based previous reports that depicted dynamic dose- and frequency-dependent changes in Tat expression (36, 38). In contrast, studies employing DOX-containing chow ranging from 3 weeks to 1 year have emphasized on the paradigm mimicking a chronic, low level inflammation, and leading to detrimental effects including reduced brain volume, increased ventricular volume, gliosis, inflammatory cytokine expression, and neuronal damage (42, 43, 48, 50). In this regard, our study provides a first direct comparison of Tat expression by two DOX administration methods. As stated earlier, the objective for evaluating behavior prior to studying MMP/TIMP axis in these mice was to evaluate if the behavioral changes are consistent in both induction paradigms and if the observed phenotype would be analogous to symptoms observed in HAND patients. Both paradigms resulted in changes including increased anxiety, motor and/or learning deficits. However, higher Tat levels resulting from DOX *i.p.* injections did not translate into relatively increased deficits when compared to mildly elevated Tat expression *via* DOX-containing chow. Further, the high expression obtained with DOX-injections reduced rapidly and there was a high attrition rate observed. Alternately, the food-based induction provided a mild, yet sustained expression over a longer time with minimal to no attrition. These observations highlight that Tat induction method should be selected carefully depending on the goals of the study.

Previous reports documented that Tat-induced behavioral impairments were sex dependent and males were more vulnerable than female mice (48, 60). Further, direct intervention with progesterone reduced anxiety-like effects in ovariectomized female iTat mice indicating direct effect of sex hormones in modulating Tat-induced behavioral impairments (53). In this context, we performed a preliminary analysis of our data to evaluate sex-based differences in behavior. It was observed that characteristic behavioral deficit phenotype may be more prominent in male mice compared to female mice. However, further testing with more mice and thorough analysis will be required to evaluate these trends further.

Despite milder symptoms observed in PLWH during the ART era, underlying neuropathogenesis remains persistent and complex involving multiple underlying processes such as gliosis, elevated inflammatory factors, and neurotoxicity (6). Alterations in the tightly regulated brain MMP/TIMP balance is among the phenomena associated with neuroinflammation and intensively studied in multiple neurological conditions (8, 61). The principal MMP-driven mechanisms contributing to HAND pathogenesis include blood-brain barrier (BBB) breakdown, inducing neuronal dysfunction, and myelin degradation (11). The effects of MMPs are inhibited by TIMPs, mainly TIMP-1

and TIMP-2. TIMP-1 is produced in response to injury by multiple cell types including reactive astrocytes (62) and reactive astrogliosis is one of the hallmarks of chronic neuroinflammation characteristic of HAND (63). Therefore, it is essential to understand brain TIMP-1 regulation in the HAND-relevant iTat model.

It must be noted that the iTat mouse model produces only one viral protein, *i.e.,* HIV-1 Tat, in a specific cell type, *i.e.,* astrocytes. Astrocytes are highly relevant in HAND pathology, as they are infected by HIV, possess an ability to harbor virus, and remain a latent viral reservoir in the brain (64–66). Astrocytes are also capable of producing viral proteins such as Nef and Tat (67, 68). Transcriptomic analysis in an *in vitro* model of latently infected human astrocytes found upregulated neuroinflammatory pathways including interferon signaling, death receptor signaling, and activation of pattern recognition receptors (69). Another recent study demonstrated that astrocyte-derived HIV trafficked out of CNS and was found in peripheral organs in a transgenic mouse model (3). Thus, while it is not possible to mimic HAND in its entirety in iTat mice, it remains a clinically relevant model to understand impact of astrocytes on neuroinflammation in HAND.

We and several others depicted inflammatory biomarkers TNF-α- or IL-1β-mediated MMP and/or TIMP expression regulation *in vitro* or *in vivo*, particularly in astrocytes (24, 70–72). Further, Tat-mediated upregulation of TNF-α was linked to MMP regulation and subsequent neurotoxicity (33, 73). In a study that found altered MMPs and TIMPs levels in the CSF and blood of HAND patients, TNF-α and CCL2 were among top three altered proinflammatory cytokines (23). A recent study in a similar Tat-transgenic model demonstrated increase in TNF-α, IL-1β, CCL2, IL-6, and IL-17 gene expression in the cortex with prolonged Tat expression (50). Contrary to these findings, the basal levels of IL-1β, TNF-α, CCL2 were comparable to respective WT controls in our studies. In parallel, IL-6 mRNA expression was reduced in iTat mice compared to WT mice and IL-17 was not detected in the brains of both WT and iTat mice. Our results suggest that Tat expression may not directly upregulate these select inflammatory cytokines transcriptionally in this model. It remains to be seen if the baseline expression levels of these cytokines regulate MMPs and TIMPs transcriptionally in addition to Tat-driven mechanisms. Simultaneously, it is also possible that using PGK-1 as a housekeeping gene instead of commonly used GAPDH may alter the gene expression results and the presented data must be interpreted accordingly.

Lastly, we observed marginal increases in GFAP transcription in iTat mice that were not significant compared to WT controls. However, GFAP gene expression in DOX-injected iTat mice was higher than DOX-fed mice. Dr. He and colleagues demonstrated a Tat-induced GFAP protein elevation in iTat mice in several reports (46, 49). Our data corroborate this on a transcriptional level since changes in GFAP in acute vs. prolonged Tat expression correspond with relative Tat levels in both paradigms.

All four tested MMPs and TIMPs were elevated in DOX-injected iTat mice, which showed a higher Tat expression. In parallel, DOX-fed iTat mice, with lower Tat expression, indicated comparable levels of inducible proteins TIMP-1, MMP-9, as well as, TIMP-2. These results suggest that Tat-induced transcriptional changes in MMP/TIMP axis might be driven by reversible, negative feedback mechanisms. This hypothesis is also supported by the results observed in our preliminary experiments. In the preliminary experiments, mice euthanized 1 day after six DOX injections showed robust changes in MMP and TIMP gene expression. In comparison, increases in gene expression of MMPs and TIMPs were not as robust in DOX-injected mice that underwent behavior and were harvested 2 weeks after the last DOX injection. Further, both TIMP-1 and TIMP-2 have known neurotropic and neuroprotective effects (74, 75), and their return normal levels during prolonged inflammation tipped the scale toward MMPs.

These results validated our hypotheses that TIMP-1 is a key regulator in maintaining the brain MMP/TIMP balance and it is differentially regulated during acute vs. prolonged inflammatory stimuli. It was documented that TIMP-1 and TIMP-2 preferentially inhibit MMP-9 and MMP-2, respectively (74). In this context, the MMP-9/TIMP-1 ratio was investigated extensively in multiple neurological conditions such as multiple sclerosis (76, 77), stroke/ischemia (78, 79), and Alzheimer's disease (80). Our data confirms that both of these ratios are relevant in the context of HAND as MMP-2/TIMP-2 ratio remains higher in iTat mice compared to WT mice irrespective of the duration of Tat exposure whereas elevated MMP-9/TIMP-1 may be used to predict prolonged inflammation in this model. There are a couple of potential caveats that should be considered in the context of presented data. First, previous reports documented DOX induced transcriptional inhibition of MMPs (81) and hence using a DOX-inducible transgenic model for studying gene expression of MMP/TIMP axis may not be appropriate. However, we used appropriate WT controls that were either injected or fed with DOX, potentially eliminating DOX-specific effects from interpretation. Further, despite high amounts of DOX administration, significant changes were observed in MMPs. Second, our study does not indicate a direct Tat-mediated regulation of MMP/TIMP balance and further investigations will be required to delineate specific underlying mechanisms. Overall, our data emphasizes the potential role of MMP/TIMP axis during Tat-mediated neurotoxicity.

A previous report documented that CSF MMP-9 and MMP-2 had deleterious effects on verbal fluency and motor speed parameters, respectively (82). More recently, we reported that plasma levels of TIMP-1 correlated significantly with neurocognitive performance measures including complex attention, cognitive flexibility, psychomotor speed, and executive function in HIV+ cohort. In this regard, it is logical to speculate the impact of MMP/TIMP axis on behavioral changes observed in iTat mice. This hypothesis is supported by previous studies, which found impact of MMP/TIMP axis components on rodent behavior. In particular, TIMP-1 was shown to impact memory and cognition in mice in an olfactory maze test (83, 84) and MMP-9 knockout mice

exhibited lower anxiety in EPM and higher vertical activity in an open field test (85). The MMP-9/TIMP-1 balance was also associated with altered neuronal plasticity and memory in rodent models (86, 87). Further, increased MMP levels are also linked to long-term memory (85, 87) as well as learning impairments (83, 84), and altered synaptic plasticity (86). Since the link between dysregulated intracellular mechanisms and behavioral phenotypes in HAND is not yet well-established, we infer that our data provides a potential novel direction for HAND investigations.

CONCLUSION

As per recent reports, neurological complications in PLWH have become less severe with impairments related to working memory, executive functioning, and speed of information processing (88). The mild behavioral impairments observed in our studies provide a relevant model for future tests on the effects of treatment and/or mitigating interventions. The gene expression established that prolonged Tat expression tipped the MMP/TIMP axis toward MMPs in iTat mice. Consistent with our previous work, TIMP-1 expression increased with acute Tat expression and was reduced in comparison during prolonged Tat expression (24, 25). Considering the MMP-independent neuroprotective functions of TIMP-1 (14, 15, 17, 89), these findings support our hypothesis of TIMP-1 restoration as a therapeutic strategy to treat or prevent neurological deficits in HAND. Astrocytes are the primary producers of TIMP-1 in the brain following injury or inflammatory stimuli. Thus, a tested, efficient, astrocyte-targeted gene therapy approach (90, 91) to modulate TIMP-1 would be the most logical next step. These future studies could have broader implications not just for HAND, but other neurodegenerative conditions as well.

DATA AVAILABILITY STATEMENT

The raw data supporting the conclusions of this article will be made available by the authors, without undue reservation.

ETHICS STATEMENT

The study and associated protocols were approved by the University of North Texas Health Science Center Institutional Animal Care and Use Committee in Fort Worth, TX prior to initiation of the study.

AUTHOR CONTRIBUTIONS

CJ performed the behavior experiments, processed the experimental data, performed the analysis, drafted the manuscript, and designed the figures. CJ, KB, and SS performed preliminary induction experiments. CJ and SS performed gene expression analyses. NS, AG, and KB were involved in planning, supervised the work, aided in interpreting the results, and worked on the manuscript. All authors discussed the results and commented on the manuscript.

FUNDING

This work was supported by the National Institute of Neurological Disorders and Stroke award R01 NS048837 to AG and KB.

ACKNOWLEDGMENTS

We sincerely thank Dr. Johnny He for providing the iTat transgenic breeders and his valuable inputs on the experimental design of the study. We appreciate the assistance of members of Dr. Sumien Lab in conducting rodent behavioral studies. The authors also acknowledge the help of Drs. Ghorpade and Borgmann Lab members for their help with proofreading and critical reading of the manuscript.

SUPPLEMENTARY MATERIAL

The Supplementary Material for this article can be found online at: https://www.frontiersin.org/articles/10.3389/fneur.2020.593188/full#supplementary-material

REFERENCES

1. Cenker JJ, Stultz RD, Mcdonald D. Brain microglial cells are highly susceptible to HIV-1 infection and spread. *AIDS Res Hum Retrovirus.* (2017) 33:1155–65. doi: 10.1089/aid.2017.0004
2. Lee CA, Beasley E, Sundar K, Smelkinson M, Vinton C, Deleage C, et al. Simian immunodeficiency virus-infected memory $CD4^+$ T cells infiltrate to the site of infected macrophages in the neuroparenchyma of a chronic macaque model of neurological complications of AIDS. *mBio.* (2020) 11:mbio00602. doi: 10.1128/mBio.00602-20
3. Lutgen V, Narasipura SD, Barbian HJ, Richards M, Wallace J, Razmpour R, et al. HIV infects astrocytes *in vivo* and egresses from the brain to the periphery. *PLoS Pathog.* (2020) 16:e1008381. doi: 10.1371/journal.ppat.1008381
4. Sanmarti M, Ibáñez L, Huertas S, Badenes D, Dalmau D, Slevin M, et al. HIV-associated neurocognitive disorders. *J Mol Psychiatr.* (2013) 13:976–86. doi: 10.1186/2049-9256-2-2
5. Eggers C, Arendt G, Hahn K, Husstedt IW, Maschke M, Neuen-Jacob E, et al. HIV-1-associated neurocognitive disorder: epidemiology, pathogenesis, diagnosis, and treatment. *J Neurol.* (2017) 264:1715–27. doi: 10.1007/s00415-017-8503-2
6. Sacktor N. Changing clinical phenotypes of HIV-associated neurocognitive disorders. *J Neurovirol.* (2018) 24:141–5. doi: 10.1007/s13365-017-0556-6
7. Paul R. Neurocognitive phenotyping of HIV in the Era of antiretroviral therapy. *Curr HIV AIDS Rep.* (2019) 16:230–5. doi: 10.1007/s11904-019-00426-9
8. Gardner J, Ghorpade A. Tissue inhibitor of metalloproteinase (TIMP)-1: the TIMPed balance of matrix metalloproteinases in the central nervous system. *J Neurosci Res.* (2003) 74:801–6. doi: 10.1002/jnr.10835
9. Kaul M, Lipton SA. Mechanisms of neuronal injury and death in HIV-1 associated dementia. *Curr HIV Res.* (2006) 4:307–18. doi: 10.2174/157016206777709384

10. Saylor D, Dickens AM, Sacktor N, Haughey N, Slusher B, Pletnikov M, et al. HIV-associated neurocognitive disorder–pathogenesis and prospects for treatment. *Nat Rev Neurol.* (2016) 12:234–48. doi: 10.1038/nrneurol.2016.27
11. Rumbaugh J, Turchan-Cholewo J, Galey D, St Hillaire C, Anderson C, Conant K, et al. Interaction of HIV Tat and matrix metalloproteinase in HIV neuropathogenesis: a new host defense mechanism. *FASEB J.* (2006) 20:1736. doi: 10.1096/fj.05-5619fje
12. Louboutin J, Reyes B, Agrawal L, Van Bockstaele E, Strayer D. HIV-1 gp120 upregulates matrix metalloproteinases and their inhibitors in a rat model of HIV encephalopathy. *Eur J Neurosci.* (2011) 34:2015. doi: 10.1111/j.1460-9568.2011.07908.x
13. Xu R, Feng X, Xie X, Zhang J, Wu D, Xu L. HIV-1 Tat protein increases the permeability of brain endothelial cells by both inhibiting occludin expression and cleaving occludin via matrix metalloproteinase-9. *Brain Res.* (2012) 1436:13. doi: 10.1016/j.brainres.2011.11.052
14. Magnoni S, Baker A, Thomson S, Jordan G, George SJ, Mccoll BW, et al. Neuroprotective effect of adenoviral-mediated gene transfer of TIMP-1 and−2 in ischemic brain injury. *Gene Ther.* (2007) 14:621–5. doi: 10.1038/sj.gt.3302894
15. Tejima E, Guo S, Murata Y, Arai K, Lok J, Van Leyen K, et al. Neuroprotective effects of overexpressing tissue inhibitor of metalloproteinase TIMP-1. *J Neurotrauma.* (2009) 26:1935–41. doi: 10.1089/neu.2009.0959
16. Saha P, Sarkar S, Paidi RK, Biswas SC. TIMP-1: a key cytokine released from activated astrocytes protects neurons and ameliorates cognitive behaviours in a rodent model of Alzheimer's disease. *Brain Behav Immun.* (2020) 87:804–19. doi: 10.1016/j.bbi.2020.03.014
17. Ashutosh CC, Borgmann K, Brew K, Ghorpade A. Tissue inhibitor of metalloproteinases-1 protects human neurons from staurosporine and HIV-1-induced apoptosis: mechanisms and relevance to HIV-1-associated dementia. *Cell Death Dis.* (2012) 3:e332. doi: 10.1038/cddis.2012.54
18. Dzwonek J, Rylski M, Kaczmarek L. Matrix metalloproteinases and their endogenous inhibitors in neuronal physiology of the adult brain. *FEBS Lett.* (2004) 567:129–35. doi: 10.1016/j.febslet.2004.03.070
19. Nazdik MK, Taheri M, Sajjadi E, Arsang-Jang S, Koohpar ZK, Inoko H, et al. Increased expression ratio of matrix metalloproteinase-9 (MMP9) and tissue inhibitor of matrix metalloproteinase (TIMP-1) RNA levels in Iranian multiple sclerosis patients. *Hum Antibodies.* (2016) 24:65–70. doi: 10.3233/HAB-160296
20. Boziki M, Grigoriadis N. An update on the role of matrix metalloproteinases in the pathogenesis of multiple sclerosis. *Med Chem.* (2018) 14:155–69. doi: 10.2174/1573406413666170906122803
21. Zhang K, Mcquibban G, Silva C, Butler G, Johnston J, Holden J, et al. HIV-induced metalloproteinase processing of the chemokine stromal cell derived factor-1 causes neurodegeneration. *Nat Neurosci.* (2003) 6:1064. doi: 10.1038/nn1127
22. Eugenin EA, Osiecki K, Lopez L, Goldstein H, Calderon TM, Berman JW. CCL2/monocyte chemoattractant protein-1 mediates enhanced transmigration of human immunodeficiency virus (HIV)-infected leukocytes across the blood-brain barrier: a potential mechanism of HIV-CNS invasion and NeuroAIDS. *J Neurosci.* (2006) 26:1098–106. doi: 10.1523/JNEUROSCI.3863-05.2006
23. Xing Y, Shepherd N, Lan J, Li W, Rane S, Gupta SK, et al. MMPs/TIMPs imbalances in the peripheral blood and cerebrospinal fluid are associated with the pathogenesis of HIV-1-associated neurocognitive disorders. *Brain Behav Immun.* (2017) 65:161–72. doi: 10.1016/j.bbi.2017.04.024
24. Suryadevara R, Holter S, Borgmann K, Persidsky R, Labenz-Zink C, Persidsky Y, et al. Regulation of tissue inhibitor of metalloproteinase-1 by astrocytes: Links to HIV-1 dementia. *Glia.* (2003) 44:47–56. doi: 10.1002/glia.10266
25. Gardner J, Borgmann K, Deshpande MS, Dhar A, Wu L, Persidsky R, et al. Potential mechanisms for astrocyte-TIMP-1 downregulation in chronic inflammatory diseases. *J Neurosci Res.* (2006) 83:1281–92. doi: 10.1002/jnr.20823
26. Kim BO, Liu Y, Ruan Y, Xu ZC, Schantz L, He JJ. Neuropathologies in transgenic mice expressing human immunodeficiency virus type 1 Tat protein under the regulation of the astrocyte-specific glial fibrillary acidic protein promoter and doxycycline. *Am J Pathol.* (2003) 162:1693–707. doi: 10.1016/S0002-9440(10)64304-0
27. Langford D, Oh Kim B, Zou W, Fan Y, Rahimain P, Liu Y, et al. Doxycycline-inducible and astrocyte-specific HIV-1 Tat transgenic mice (iTat) as an HIV/neuroAIDS model. *J Neurovirol.* (2018) 24:168–79. doi: 10.1007/s13365-017-0598-9
28. Maggirwar SB, Tong N, Ramirez S, Gelbard HA, Dewhurst S. HIV-1 Tat-mediated activation of glycogen synthase kinase-3β contributes to tat-mediated neurotoxicity. *J Neurochem.* (1999) 73:578–86. doi: 10.1046/j.1471-4159.1999.0730578.x
29. Haughey NJ, Mattson MP. Calcium dysregulation and neuronal apoptosis by the HIV-1 proteins Tat and gp120. *J Acquir Immune Defic Syndr.* (2002) 31(Suppl 2):S55–61. doi: 10.1097/00126334-200210012-00005
30. Kruman Ii, Nath A, Mattson MP. HIV-1 protein Tat induces apoptosis of hippocampal neurons by a mechanism involving caspase activation, calcium overload, and oxidative stress. *Exp Neurol.* (1998) 154:276–88. doi: 10.1006/exnr.1998.6958
31. Agrawal L, Louboutin J-P, Reyes BA, Van Bockstaele EJ, Strayer DS. HIV-1 Tat neurotoxicity: a model of acute and chronic exposure, and neuroprotection by gene delivery of antioxidant enzymes. *Neurobiol Dis.* (2012) 45:657–70. doi: 10.1016/j.nbd.2011.10.005
32. Theodore S, Cass WA, Maragos WF. Involvement of cytokines in human immunodeficiency virus-1 protein Tat and methamphetamine interactions in the striatum. *Exp Neurol.* (2006) 199:490–8. doi: 10.1016/j.expneurol.2006.01.009
33. Ju SM, Song HY, Lee JA, Lee SJ, Choi SY, Park J. Extracellular HIV-1 Tat up-regulates expression of matrix metalloproteinase-9 via a MAPK-NF-kappaB dependent pathway in human astrocytes. *Exp Mol Med.* (2009) 41:86–93. doi: 10.3858/emm.2009.41.2.011
34. Conant K, Garzino-Demo A, Nath A, Mcarthur J, Halliday W, Power C, et al. Induction of monocyte chemoattractant protein-1 in HIV-1 Tat-stimulated astrocytes and elevation in AIDS dementia. *Proc Natl Acad Sci USA.* (1998) 95:3117–21. doi: 10.1073/pnas.95.6.3117
35. Fitting S, Xu R, Bull C, Buch SK, El-Hage N, Nath A, et al. Interactive comorbidity between opioid drug abuse and HIV-1 Tat: chronic exposure augments spine loss and sublethal dendritic pathology in striatal neurons. *Am J Pathol.* (2010) 177:1397–410. doi: 10.2353/ajpath.2010.090945
36. Carey AN, Sypek EI, Singh HD, Kaufman MJ, Mclaughlin JP. Expression of HIV-Tat protein is associated with learning and memory deficits in the mouse. *Behav Brain Res.* (2012) 229:48–56. doi: 10.1016/j.bbr.2011.12.019
37. Fitting S, Scoggins KL, Xu R, Dever SM, Knapp PE, Dewey WL, et al. Morphine efficacy is altered in conditional HIV-1 Tat transgenic mice. *Eur J Pharmacol.* (2012) 689:96–103. doi: 10.1016/j.ejphar.2012.05.029
38. Paris JJ, Singh HD, Ganno ML, Jackson P, Mclaughlin JP. Anxiety-like behavior of mice produced by conditional central expression of the HIV-1 regulatory protein, Tat. *Psychopharmacology.* (2014) 231:2349–60. doi: 10.1007/s00213-013-3385-1
39. Mclaughlin JP, Eans S, Medina J, Hymel K, Rock A, Mintzopoulos D, et al. HIV-1 Tat-protein elevates forebrain glutathione levels and increases morphine drug-seeking and depression-like behaviors in mice. *Drug Alcohol Depend.* (2017). 171:e139. doi: 10.1016/j.drugalcdep.2016.08.386
40. Kesby JP, Chang A, Najera JA, Marcondes MCG, Semenova S. Brain reward function after chronic and binge methamphetamine regimens in mice expressing the HIV-1 TAT protein. *Curr HIV Res.* (2019) 17:126–33. doi: 10.2174/1570162X17666190703165408
41. Strauss M, O'donovan B, Ma Y, Xiao Z, Lin S, Bardo MT, et al. [^{3}H]Dopamine uptake through the dopamine and norepinephrine transporters is decreased in the prefrontal cortex of transgenic mice expressing HIV-1 transactivator of transcription protein. *J Pharmacol Exp Ther.* (2020) 374:241–251. doi: 10.1124/jpet.120.266023
42. Nass S, Hahn Y, Mclane V, Varshneya N, Damaj M, Knapp P, et al. Chronic HIV-1 Tat exposure alters anterior cingulate cortico-basal ganglia-thalamocortical synaptic circuitry, associated behavioral control, and immune regulation in male mice. *Brain Behav Immun Health.* (2020) 5:77. doi: 10.1016/j.bbih.2020.100077
43. Zhao X, Fan Y, Vann PH, Wong JM, Sumien N, He JJ. Long-term HIV-1 tat expression in the brain led to neurobehavioral, pathological, and epigenetic changes reminiscent of accelerated aging. *Aging Dis.* (2020) 11:93–107. doi: 10.14336/AD.2019.0323

44. Shetty RA, Forster MJ, Sumien N. Coenzyme Q(10) supplementation reverses age-related impairments in spatial learning and lowers protein oxidation. *Age.* (2013) 35:1821–34. doi: 10.1007/s11357-012-9484-9
45. Chaudhari K, Wong JM, Vann PH, Sumien N. Exercise training and antioxidant supplementation independently improve cognitive function in adult male and female GFAP-APOE mice. *J Sport Health Sci.* (2014) 3:196–205. doi: 10.1016/j.jshs.2014.04.004
46. Zhou BY, Liu Y, Kim B, Xiao Y, He JJ. Astrocyte activation and dysfunction and neuron death by HIV-1 Tat expression in astrocytes. *Mol Cell Neurosci.* (2004) 27:296–305. doi: 10.1016/j.mcn.2004.07.003
47. Bruce-Keller AJ, Turchan-Cholewo J, Smart EJ, Geurin T, Chauhan A, Reid R, et al. Morphine causes rapid increases in Glial activation and neuronal injury in the striatum of inducible HIV-1 tat transgenic mice. *Glia.* (2008) 56:1414. doi: 10.1002/glia.20708
48. Hahn YK, Podhaizer EM, Farris SP, Miles MF, Hauser KF, Knapp PE. Effects of chronic HIV-1 Tat exposure in the CNS: heightened vulnerability of males versus females to changes in cell numbers, synaptic integrity, and behavior. *Brain Struc Func.* (2015) 220:605. doi: 10.1007/s00429-013-0676-6
49. Fan Y, He JJ. HIV-1 Tat induces unfolded protein response and endoplasmic reticulum stress in astrocytes and causes neurotoxicity through glial fibrillary acidic protein (GFAP) activation and aggregation. *J Biol Chem.* (2016) 291:22819–29. doi: 10.1074/jbc.M116.731828
50. Dickens AM, Yoo SW, Chin AC, Xu J, Johnson TP, Trout AL, et al. Chronic low-level expression of HIV-1 Tat promotes a neurodegenerative phenotype with aging. *Sci Rep.* (2017) 7:7748. doi: 10.1038/s41598-017-07570-5
51. Fellows RP, Byrd DA, Morgello S, Manhattan HIVBB. Major depressive disorder, cognitive symptoms, and neuropsychological performance among ethnically diverse HIV+ men and women. *J Int Neuropsychol Soc.* (2013) 19:216–25. doi: 10.1017/S1355617712001245
52. Rivera-Rivera Y, Vazquez-Santiago FJ, Albino E, Sanchez MD, Rivera-Amill V. Impact of depression and inflammation on the progression of HIV disease. *J Clin Cell Immunol.* (2016) 7:423. doi: 10.4172/2155-9899.1000423
53. Paris JJ, Fenwick J, Mclaughlin JP. Progesterone protects normative anxiety-like responding among ovariectomized female mice that conditionally express the HIV-1 regulatory protein, Tat, in the CNS. *Horm Behav.* (2014) 65:445–53. doi: 10.1016/j.yhbeh.2014.04.001
54. Crawley JN. Exploratory behavior models of anxiety in mice. *Neurosci Biobehav Rev.* (1985) 9:37–44. doi: 10.1016/0149-7634(85)90030-2
55. Buchanan JB, Sparkman NL, Chen J, Johnson RW. Cognitive and neuroinflammatory consequences of mild repeated stress are exacerbated in aged mice. *Psychoneuroendocrinology.* (2008) 33:755–65. doi: 10.1016/j.psyneuen.2008.02.013
56. Gehring TV, Luksys G, Sandi C, Vasilaki E. Detailed classification of swimming paths in the morris water maze: multiple strategies within one trial. *Sci Rep.* (2015) 5:14562. doi: 10.1038/srep14562
57. Cherner M, Cysique L, Heaton RK, Marcotte TD, Ellis RJ, Masliah E, et al. Neuropathologic confirmation of definitional criteria for human immunodeficiency virus-associated neurocognitive disorders. *J Neurovirol.* (2007) 13:23–8. doi: 10.1080/13550280601089175
58. Fitting S, Ignatowska-Jankowska BM, Bull C, Skoff RP, Lichtman AH, Wise LE, et al. Synaptic dysfunction in the hippocampus accompanies learning and memory deficits in human immunodeficiency virus type-1 Tat transgenic mice. *Biol Psychiatr.* (2013) 73:443–53. doi: 10.1016/j.biopsych.2012.09.026
59. Nookala AR, Schwartz DC, Chaudhari NS, Glazyrin A, Stephens EB, Berman NEJ, et al. Methamphetamine augment HIV-1 Tat mediated memory deficits by altering the expression of synaptic proteins and neurotrophic factors. *Brain Behav Immun.* (2018) 71:37–51. doi: 10.1016/j.bbi.2018.04.018
60. Hahn YK, Paris JJ, Lichtman AH, Hauser KF, Sim-Selley LJ, Selley DE, et al. Central HIV-1 Tat exposure elevates anxiety and fear conditioned responses of male mice concurrent with altered mu-opioid receptor-mediated G-protein activation and β-arrestin 2 activity in the forebrain. *Neurobiology of disease.* (2016) 92:124. doi: 10.1016/j.nbd.2016.01.014
61. Rivera S, Garcia-Gonzalez L, Khrestchatisky M, Baranger K. Metalloproteinases and their tissue inhibitors in Alzheimer's disease and other neurodegenerative disorders. *Cell Mol Life Sci.* (2019) 76:3167–91. doi: 10.1007/s00018-019-03178-2
62. Jaworski DM. Differential regulation of tissue inhibitor of metalloproteinase mRNA expression in response to intracranial injury. *Glia.* (2000) 30:199–208. doi: 10.1002/(SICI)1098-1136(200004)30:2<199::AID-GLIA9>3.0.CO;2-#
63. Borgmann K, Ghorpade A. HIV-1, methamphetamine and astrocytes at neuroinflammatory Crossroads. *Front Microbiol.* (2015) 6:1143. doi: 10.3389/fmicb.2015.01143
64. Atwood WJ, Tornatore CS, Meyers K, Major EO. HIV-1 mRNA transcripts from persistently infected human fetal astrocytes. *Ann N Y Acad Sci.* (1993) 693:324–5. doi: 10.1111/j.1749-6632.1993.tb26298.x
65. Thompson KA, Mcarthur JC, Wesselingh SL. Correlation between neurological progression and astrocyte apoptosis in HIV-associated dementia. *Ann Neurol.* (2001) 49:745–52. doi: 10.1002/ana.1011
66. Churchill MJ, Wesselingh SL, Cowley D, Pardo CA, Mcarthur JC, Brew BJ, et al. Extensive astrocyte infection is prominent in human immunodeficiency virus-associated dementia. *Ann Neurol.* (2009) 66:253–8. doi: 10.1002/ana.21697
67. Saito Y, Sharer LR, Epstein LG, Michaels J, Mintz M, Louder M, et al. Overexpression of nef as a marker for restricted HIV-1 infection of astrocytes in postmortem pediatric central nervous tissues. *Neurology.* (1994) 44:474–81. doi: 10.1212/WNL.44.3_Part_1.474
68. Chauhan A, Turchan J, Pocernich C, Bruce-Keller A, Roth S, Butterfield DA, et al. Intracellular human immunodeficiency virus Tat expression in astrocytes promotes astrocyte survival but induces potent neurotoxicity at distant sites via axonal transport. *J Biol Chem.* (2003) 278:13512–9. doi: 10.1074/jbc.M209381200
69. Edara VV, Ghorpade A, Borgmann K. Insights into the gene expression profiles of active and restricted Red/Green-HIV^{+} human astrocytes: implications for shock or lock therapies in the brain. *J Virol.* (2020) e01563–19. doi: 10.1128/JVI.01563-19
70. Nath A, Conant K, Chen P, Scott C, Major EO. Transient exposure to HIV-1 Tat protein results in cytokine production in macrophages and astrocytes. A hit and run phenomenon. *J Biol Chem.* (1999) 274:17098–102. doi: 10.1074/jbc.274.24.17098
71. Leveque T, Le Pavec G, Boutet A, Tardieu M, Dormont D, Gras G. Differential regulation of gelatinase A and B and TIMP-1 and−2 by TNFalpha and HIV virions in astrocytes. *Microbes Infect.* (2004) 6:157–63. doi: 10.1016/j.micinf.2003.11.006
72. Dhar A, Gardner J, Borgmann K, Wu L, Ghorpade A. Novel role of TGF-beta in differential astrocyte-TIMP-1 regulation: implications for HIV-1-dementia and neuroinflammation. *J Neurosci Res.* (2006) 83:1271–80. doi: 10.1002/jnr.20787
73. Buscemi L, Ramonet D, Geiger JD. Human immunodeficiency virus type-1 protein tat induces tumor necrosis factor-α-mediated neurotoxicity. *Neurobiol Dis.* (2007) 26:661. doi: 10.1016/j.nbd.2007.03.004
74. Brew K, Dinakarpandian D, Nagase H. Tissue inhibitors of metalloproteinases: evolution, structure and function. *Biochim Biophys Acta.* (2000) 1477:267–83. doi: 10.1016/S0167-4838(99)00279-4
75. Visse R, Nagase H. Matrix metalloproteinases and tissue inhibitors of metalloproteinases: structure, function, and biochemistry. *Circ Res.* (2003) 92:827. doi: 10.1161/01.RES.0000070112.80711.3D
76. Waubant E, Goodkin DE, Gee L, Bacchetti P, Sloan R, Stewart T, et al. Serum MMP-9 and TIMP-1 levels are related to MRI activity in relapsing multiple sclerosis. *Neurology.* (1999) 53:1397–401. doi: 10.1212/WNL.53.7.1397
77. Waubant E, Goodkin D, Bostrom A, Bacchetti P, Hietpas J, Lindberg R, et al. IFNbeta lowers MMP-9/TIMP-1 ratio, which predicts new enhancing lesions in patients with SPMS. *Neurology.* (2003) 60:52–7. doi: 10.1212/WNL.60.1.52
78. Kurzepa J, Szczepanska-Szerej A, Stryjecka-Zimmer M, Malecka-Massalska T, Stelmasiak Z. Simvastatin could prevent increase of the serum MMP-9/TIMP-1 ratio in acute ischaemic stroke. *Folia Biol.* (2006) 52:181−3. Available online at: https://fb.cuni.cz/Data/files/folia_biologica/volume_52_2006_6/FB2006A0023.pdf
79. Li DD, Song JN, Huang H, Guo XY, An JY, Zhang M, et al. The roles of MMP-9/TIMP-1 in cerebral edema following experimental acute cerebral infarction in rats. *Neurosci Lett.* (2013) 550:168–72. doi: 10.1016/j.neulet.2013.06.034

80. Ridnour LA, Dhanapal S, Hoos M, Wilson J, Lee J, Cheng RY, et al. Nitric oxide-mediated regulation of beta-amyloid clearance via alterations of MMP-9/TIMP-1. *J Neurochem.* (2012) 123:736–49. doi: 10.1111/jnc.12028
81. Burggraf D, Trinkl A, Dichgans M, Hamann G. Doxycycline inhibits MMPs via modulation of plasminogen activators in focal cerebral ischemia. *Neurobiol Dis.* (2007) 25:506. doi: 10.1016/j.nbd.2006.10.013
82. Li S, Wu Y, Keating SM, Du H, Sammet CL, Zadikoff C, et al. Matrix metalloproteinase levels in early HIV infection and relation to *in vivo* brain status. *J Neurovirol.* (2013) 452–60. doi: 10.1007/s13365-013-0197-3
83. Jourquin J, Tremblay E, Bernard A, Charton G, Chaillan FA, Marchetti E, et al. Tissue inhibitor of metalloproteinases-1 (TIMP-1) modulates neuronal death, axonal plasticity, and learning and memory. *Eur J Neurosci.* (2005) 22:2569–78. doi: 10.1111/j.1460-9568.2005.04426.x
84. Chaillan FA, Rivera S, Marchetti E, Jourquin J, Werb Z, Soloway PD, et al. Involvement of tissue inhibition of metalloproteinases-1 in learning and memory in mice. *Behav Brain Res.* (2006) 173:191–8. doi: 10.1016/j.bbr.2006.06.020
85. Mizoguchi H, Ibi D, Takuma K, Toth E, Sato J, Itohara S, et al. Alterations of emotional and cognitive behaviors in matrix metalloproteinase-2 and-9-deficient mice. *Open Behav Sci J.* (2010) 4:19–25. doi: 10.2174/1874230001004010019
86. Nagy V, Bozdagi O, Huntley GW. The extracellular protease matrix metalloproteinase-9 is activated by inhibitory avoidance learning and required for long-term memory. *Learn Memory.* (2007) 14:655. doi: 10.1101/lm.678307
87. Okulski P, Jay T, Jaworski J, Duniec K, Dzwonek J, Konopacki F, et al. TIMP-1 abolishes MMP-9-dependent long-lasting long-term potentiation in the prefrontal cortex. *Biol Psychiatr.* (2007) 62:359. doi: 10.1016/j.biopsych.2006.09.012
88. Sacktor N, Skolasky RL, Seaberg E, Munro C, Becker JT, Martin E, et al. Prevalence of HIV-associated neurocognitive disorders in the multicenter AIDS cohort study. *Neurology.* (2016) 86:334–40. doi: 10.1212/WNL.0000000000002277
89. Atluri VSR, Jayant RD, Pilakka-Kanthikeel S, Garcia G, Samikkannu T, Yndart A, et al. Development of TIMP1 magnetic nanoformulation for regulation of synaptic plasticity in HIV-1 infection. *Int J Nanomed.* (2016) 11:4287. doi: 10.2147/IJN.S108329
90. Joshi CR, Raghavan V, Vijayaraghavalu S, Gao Y, Saraswathy M, Labhasetwar V, et al. Reaching for the stars in the brain: polymer-mediated gene delivery to human astrocytes. *Mol Ther Nucleic Acids.* (2018) 12:645–57. doi: 10.1016/j.omtn.2018.06.009
91. Proulx J, Joshi C, Vijayaraghavalu S, Saraswathy M, Labhasetwar V, Ghorpade A, et al. Arginine-modified polymers facilitate poly (lactide-co-glycolide)-based nanoparticle gene delivery to primary human astrocytes. *Int J Nanomed.* (2020) 15:3639–47. doi: 10.2147/IJN.S250865

Conflict of Interest: The authors declare that the research was conducted in the absence of any commercial or financial relationships that could be construed as a potential conflict of interest.

frontiers in Neurology

ORIGINAL RESEARCH
published: 11 February 2021
doi: 10.3389/fneur.2021.604984

Patterns and Predictors of Cognitive Function Among Virally Suppressed Women With HIV

*Raha M. Dastgheyb[1], Alison S. Buchholz[2], Kathryn C. Fitzgerald[1], Yanxun Xu[3,4], Dionna W. Williams[5,6], Gayle Springer[7], Kathryn Anastos[8], Deborah R. Gustafson[9], Amanda B. Spence[10], Adaora A. Adimora[11], Drenna Waldrop[12], David E. Vance[13], Joel Milam[14], Hector Bolivar[15], Kathleen M. Weber[16], Norman J. Haughey[1,2], Pauline M. Maki[17] and Leah H. Rubin[1,2,7]**

[1] Department of Neurology, Johns Hopkins University School of Medicine, Baltimore, MD, United States, [2] Department of Psychiatry, Johns Hopkins University School of Medicine, Baltimore, MD, United States, [3] Department of Applied Mathematics and Statistics, Johns Hopkins University, Baltimore, MD, United States, [4] Division of Biostatistics and Bioinformatics, The Sidney Kimmel Comprehensive Cancer Center, Johns Hopkins University School of Medicine, Baltimore, MD, United States, [5] Department of Molecular and Comparative Pathobiology, Johns Hopkins University School of Medicine, Baltimore, MD, United States, [6] Division of Clinical Pharmacology, Johns Hopkins University School of Medicine, Baltimore, MD, United States, [7] Department of Epidemiology, Johns Hopkins Bloomberg School of Public Health, Baltimore, MD, United States, [8] Montefiore Medical Center, Albert Einstein College of Medicine, Bronx, NY, United States, [9] Department of Neurology, State University of New York Downstate Health Sciences University, Brooklyn, NY, United States, [10] Division of Infectious Disease and Travel Medicine, Department of Medicine, Georgetown University, Washington, DC, United States, [11] Division of Infectious Diseases, Department of Medicine, University of North Carolina at Chapel Hill, Chapel Hill, NC, United States, [12] Nell Hodgson Woodruff School of Nursing, Emory University, Atlanta, GA, United States, [13] School of Nursing, University of Alabama at Birmingham, Birmingham, AL, United States, [14] Institute for Health Promotion & Disease Prevention Research, University of Southern California, Los Angeles, CA, United States, [15] Department of Psychiatry & Behavioral Science, University of Miami Miller School of Medicine, Miami, FL, United States, [16] CORE Center, Cook County Health, Hektoen Institute of Medicine, Chicago, IL, United States, [17] Department of Psychiatry and Psychology, University of Illinois at Chicago, Chicago, IL, United States

OPEN ACCESS

Edited by:
Pankaj Seth, National Brain Research Centre (NBRC), India

Reviewed by:
Robert Paul, University of Missouri–St. Louis, United States
Walter Royal III, Morehouse School of Medicine, United States

***Correspondence:**
Leah H. Rubin
lrubin@jhu.edu

Specialty section:
This article was submitted to Neuroinfectious Diseases, a section of the journal Frontiers in Neurology

Received: *10 September 2020*
Accepted: *18 January 2021*
Published: *11 February 2021*

Citation:
Dastgheyb RM, Buchholz AS, Fitzgerald KC, Xu Y, Williams DW, Springer G, Anastos K, Gustafson DR, Spence AB, Adimora AA, Waldrop D, Vance DE, Milam J, Bolivar H, Weber KM, Haughey NJ, Maki PM and Rubin LH (2021) Patterns and Predictors of Cognitive Function Among Virally Suppressed Women With HIV. Front. Neurol. 12:604984. doi: 10.3389/fneur.2021.604984

Cognitive impairment remains frequent and heterogeneous in presentation and severity among virally suppressed (VS) women with HIV (WWH). We identified cognitive profiles among 929 VS-WWH and 717 HIV-uninfected women from 11 Women's Interagency HIV Study sites at their first neuropsychological (NP) test battery completion comprised of: Hopkins Verbal Learning Test-Revised, Trail Making, Symbol Digit Modalities, Grooved Pegboard, Stroop, Letter/Animal Fluency, and Letter-Number Sequencing. Using 17 NP performance metrics (T-scores), we used Kohonen self-organizing maps to identify patterns of high-dimensional data by mapping participants to similar nodes based on T-scores and clustering those nodes. Among VS-WWH, nine clusters were identified (entropy = 0.990) with four having average T-scores ≥45 for all metrics and thus combined into an "unimpaired" profile (n = 311). Impaired profiles consisted of weaknesses in: (1) sequencing (*Profile-1*; n = 129), (2) speed (*Profile-2*; n = 144), (3) learning + recognition (*Profile-3*; n = 137), (4) learning + memory (*Profile-4*; n = 86), and (5) learning + processing speed + attention + executive function (*Profile-5*; n = 122). Sociodemographic, behavioral, and clinical variables differentiated profile membership using Random Forest models. The top 10 variables distinguishing the combined impaired vs. unimpaired profiles were: clinic site, age, education, race, illicit substance use, current and nadir CD4 count, duration of effective antiretrovirals, and protease inhibitor use. Additional variables differentiating each impaired from unimpaired profile included:

depression, stress-symptoms, income (*Profile-1*); depression, employment (*Profile 2*); depression, integrase inhibitor (INSTI) use (*Profile-3*); employment, INSTI use, income, atazanavir use, non-ART medications with anticholinergic properties (*Profile-4*); and marijuana use (*Profile-5*). Findings highlight consideration of NP profile heterogeneity and potential modifiable factors contributing to impaired profiles.

Keywords: HIV, cognition, women, heterogeneity, phenotypes, random forest, machine learning

INTRODUCTION

Early in the HIV epidemic, people with HIV (PWH) frequently exhibited distinct clinical features including cognitive, behavioral, and motor dysfunction characteristic of a subcortical dementia (1, 2). The clinical syndrome was progressive, severe and included slow mental processing, memory impairment, gait disturbance, tremors, apathy, and depressive symptoms. Since the advent of effective and accessible antiretroviral therapy (ART), PWH are living longer and may be more likely to develop comorbidities that include hypertension, diabetes, cardiovascular disease, chronic liver and renal disease, and malignancies (3, 4). Although it remains unclear as to whether these comorbidities accelerate and/or potentiate CNS dysfunction, different combinations of comorbidities are likely to result in diverse patterns of cognitive function. Thus, in PWH there is a need to understand cognitive profiles and their correlates, including sociodemographic, clinical, and behavioral factors in the context of viral suppression. Cognitive phenotyping in NeuroHIV research may facilitate a better understanding of the underlying pathophysiological mechanisms of each specific cognitive profile.

Several studies using different methodological approaches focus on patterns and predictors of cognitive function in PWH (5–7). Cognitive patterns in PWH were first investigated by Lojek and Bornstein (5), who identified four patterns in 162 predominately White (93%), young (mean age = 34 years), and educated (mean years of education = 14) men at various stages of HIV infection. Using dimension reduction (factor analysis) of seven neuropsychological (NP) outcome metrics from 16 tests followed by k-means clustering, the four profiles consisted of (1) a generally unimpaired group; and weaknesses or impairments in (2) only psychomotor speed, (3) only memory and learning, and (4) most domains. A recent cross-sectional study identified three profiles using five cognitive domain T-scores in a latent profile analysis in almost 3,000 predominately White (69%), educated (mean years of education = 15) men with HIV (MWH; 53%) and without HIV from the Multicenter AIDS Cohort Study (MACS; mean age = 40 years) (7). The three profiles included an unimpaired profile, a profile below average on learning and memory, and a profile below average on all domains. Similarly, three profiles were identified using 10 NP outcome metrics in a latent profile analysis in 361 PWH who were predominately men (88%), actively receiving ART (94%) at the Southern Alberta Clinic (6). Again, an unimpaired profile was identified along with a profile with specific weaknesses in executive function and memory and one with more global NP impairment. Notably, each of these studies focused on all or predominately White, educated MWH and included mixed samples of virological suppressed (VS) and non-suppressed (NVS) individuals. Findings in MWH cannot necessarily be generalized to women with HIV (WWH). WWH may be at greater risk for cognitive impairment due, in part, to a disproportionate burden of poverty, low literacy levels, substance abuse, poor mental health, barriers to health care services, and environmental exposures prevalent in predominantly minority urban communities in which they reside (8, 9). Biological factors, such as sex steroid hormones and female-specific factors (e.g., pregnancy, menopause), may also contribute to the pattern and magnitude of cognitive impairment in PWH (9). Combining samples of NVS and VS individuals introduces heterogeneity in cognitive function and findings from combined samples may not be generalizable to VS-PWH, a population that is expanding with the introduction of increasingly tolerable and available medication options.

As the pattern and predictors of cognitive function are likely not the same in (1) MWH and WWH as well as in (2) VS vs. NVS individuals (9), we examined heterogeneity in NP performance in the largest sample to date of VS-WWH and HIV-uninfected women. We accomplished this by applying novel machine learning methods to identify subgroups who demonstrated similar NP profiles. This approach may help guide our understanding of profiles that are associated with patterns of NP weakness. We also identified factors associated with each profile from a constellation of sociodemographic, behavioral, and clinical factors that have been found to be import distinguishing factors in prior studies (5–7), with the addition of female-specific factors (e.g., pregnancy, menopausal stage) that could not be examined in mixed-sex studies.

MATERIALS AND METHODS

Participants

The Women's Interagency HIV Study (WIHS) is a multi-center, longitudinal, study of WWH and HIV-uninfected women. The first three waves of study enrollment occurred between October 1994 and November 1995, October 2001 and September 2002, and January 2011 and January 2013 from six sites (Brooklyn, Bronx, Chicago, DC, Los Angeles, and San Francisco). A more recent wave of enrollment occurred at sites in the southern US (Chapel Hill, Atlanta, Miami, Birmingham, and Jackson) between October 2013 and September 2015. Study methodology including recruitment procedures and eligibility criteria, training, and

quality assurance procedures were previously published (10–12). This analysis was restricted to all participants completing the first NP test battery. NP data for the initial six sites were collected between 2009 and 2011, while NP data from the southern sites were collected between 2013 and 2015.

Neuropsychological (NP) Test Battery and Outcomes

The NP test battery included the Hopkins Verbal Learning Test-Revised (HVLT-R; outcomes: trial 1 learning, total learning, delayed free recall, percent retention, recognition), Letter-Number Sequencing (LNS; outcomes: total correct on the working memory and attention conditions), Trail Making Test (TMT; outcomes: time to complete Parts A and B), Stroop (outcome: time to complete Trials 1 [color reading], 2 [color naming], and 3 [color-word]), Symbol Digit Modalities Test (SDMT; outcome: total correct), Letter-guided verbal fluency (Controlled Oral Word Associations Test (COWAT; outcome: total correct words generated across three trials [F, A, S]), Animal fluency (outcome: total correct animals generated), and Grooved Pegboard (GPEG; outcomes: time to completion, dominant, and non-dominant hand). Timed outcomes were log transformed to normalize distributions and reverse scored so higher equated to better performance. Demographically-adjusted T-scores were calculated for each outcome (13, 14). T-scores are normalized to have an average of 50 and a standard deviation of 10. Mean T-scores >55 were considered high performing, between 45 and 55 were considered within the normal range, <45 were considered as weaknesses, and those <40 were considered impaired.

Factors Associated With NP Profiles

Factors of interest were based on prior NP WIHS studies (13, 14) and included: clinic site; enrollment wave; sociodemographic, mental health, behavioral, clinical, and female-specific factors; and common non-ART medications with known neurocognitive adverse effects (NCAEs) (15, 16). Sociodemographic factors included age, education, WRAT-III reading subscale score, race/ethnicity, employment status, average annual household income ($\leq$\$12,000), and health insurance status. Mental health factors included depressive symptoms (Center for Epidemiological Studies Depression scale [CES-D] $\leq$16]), perceived stress (perceived stress scale [PSS]-10 top tertile cutoff), and post-traumatic stress symptoms (PTSD Checklist—Civilian Scale) (17). Behavioral factors included current smoking status, recent alcohol intake, marijuana, and crack, cocaine, and heroin use. General clinical, metabolic, and cardiovascular factors included Hepatitis C antibody positive, body mass index (BMI), non-ART medication use [e.g., NCAEs, statins, NCAE medications with a higher anticholinergic burden (16)], and history of stroke, hypertension, and diabetes mellitus. Female-specific factors included ever pregnant, history of hysterectomy and/or bilateral oophorectomy, hormonal contraceptive use, hormone therapy use, and menopausal stage [defined using the Study of Women's Health Across the Nation [SWAN] criteria (18) which is also used in previous WIHS studies (19)]. HIV-related clinical factors included HIV RNA, nadir and current $CD4^+$ T lymphocyte count, ART use and adherence, duration of ART use, and previous AIDS diagnosis.

Statistical Analyses

All 17 NP measures were used to find groups of similar cognitive profiles within each participant subset (VS-WWH, HIV-uninfected) utilizing Kohonen self-organizing maps (SOM) followed by clustering with MClust. SOM is an unsupervised machine learning technique used to identify patterns in high dimensional data by producing a two-dimensional grid representation consisting of multiple nodes which have a fixed position in the SOM grid along with associated participants who are mapped to that node. The coordinates of the node represent the similarity to other nodes (i.e., nodes that are closer together in the grid have similar patterns than nodes that are further away) and one node can represent multiple participants. Following the identification of the nodes, the nodes were clustered using the MClust package. Once the clustering of the nodes was completed, cluster profiles were assigned to the participants associated to that node. Profiles where the mean T-Score on all cognitive outcomes was $\geq$45 were combined into an "unimpaired" profile. By using SOM and MClust in sequence, we were able to achieve fine-tuned clustering based on patterns of NP performance.

Factors associated with profile membership between each impaired profile and the unimpaired profile within each group (VS-WWH, HIV-uninfected) were explored by creating Random Forest (RF) models and then extracting variable importance. The datasets were randomly separated into training (70%) and testing (30%) sets. RF models were created on the training sets using internal validation via a 10-fold resampling method repeated five times. Prior to model creation, the Synthetic Minority Over-sampling Technique (SMOTE) was used to control for bias due to any imbalance in the number of cases. Variables were removed from the model if they had low variance or if they had $>30\%$ missing data. Any missing data in the remaining variables was imputed before model creation using RF imputations and ridge regression (α size of 0.0001 for a compromise between stability and lack of bias). For comparison to previous studies we also created RF models for each group comparing the combined unimpaired and impaired profiles. Models were also validated on the testing set to confirm that they still had predictive power balanced between classes and that success of the trained models was not due to overfitting. All variables were plotted by relative variable importance based on the training set models, and attention was given to the top 10 variables in each profile.

All analysis was done using R analysis packages. SOM was achieved using the Kohonen package in R (20) and clustering was done using the MClust package (21). MClust is an R Software package used for model-based clustering using finite normal mixture modeling that provides functions for parameter estimation via the Expectation-Maximization algorithm with an assortment of covariance structures. This program identifies the best model for 10 parameterized covariance structures and chooses the best one based on the lowest Bayesian Information Criterion (BIC). The covariance structures consist of varying distributions (spherical, diagonal, or ellipsoidal), volumes (equal or variable), shapes (equal of variable), and orientation (equal or

variable, only for ellipsoidal distribution). Random Forest model creation was achieved using the Caret (22) package in R. SMOTE resampling was done using the DMwR (23) package. Imputation of missing data was done using the Multivariate Imputation by Chained Equations (24) (MICE) package in R. ROC confidence intervals were calculated using the pROC package in R with 2,000 stratified bootstrap replicates (95%CI).

RESULTS

Participants

Participants included 929 VS-WWH and 717 HIV-uninfected women at their first study visit with complete NP testing (**Supplementary Table 1**). On average, participants were 45.1 ± 9.3 years of age with 12.7 years of education. Thirty percent were from the southern WIHS sites, 69% were non-Hispanic Black, and 15% identified as Hispanic. Only 41% were employed and 48% reported having an average annual household income <$12,000/year, while 87% were currently insured. Thirty percent had depressive symptoms while 35% were identified as having higher perceived stress levels. Nineteen percent had recently used marijuana, 7% were currently using crack, cocaine, and/or heroin, and 40% were current smokers. Ninety percent reported ever having been pregnant and 41% were post-menopausal. The average T-score for all NP tests in VS-WWH and HIV- women was in the normal range between 45 and 55 (**Supplementary Table 2**).

Cognitive Profiles in VS-WWH and HIV-Uninfected Women

For both VS-WWH and HIV-uninfected women, clusters of participants with similar patterns of relative performance on all 17 NP were profiled using a sequence of SOM and MClust. VS-WWH and HIV-uninfected women had good fits

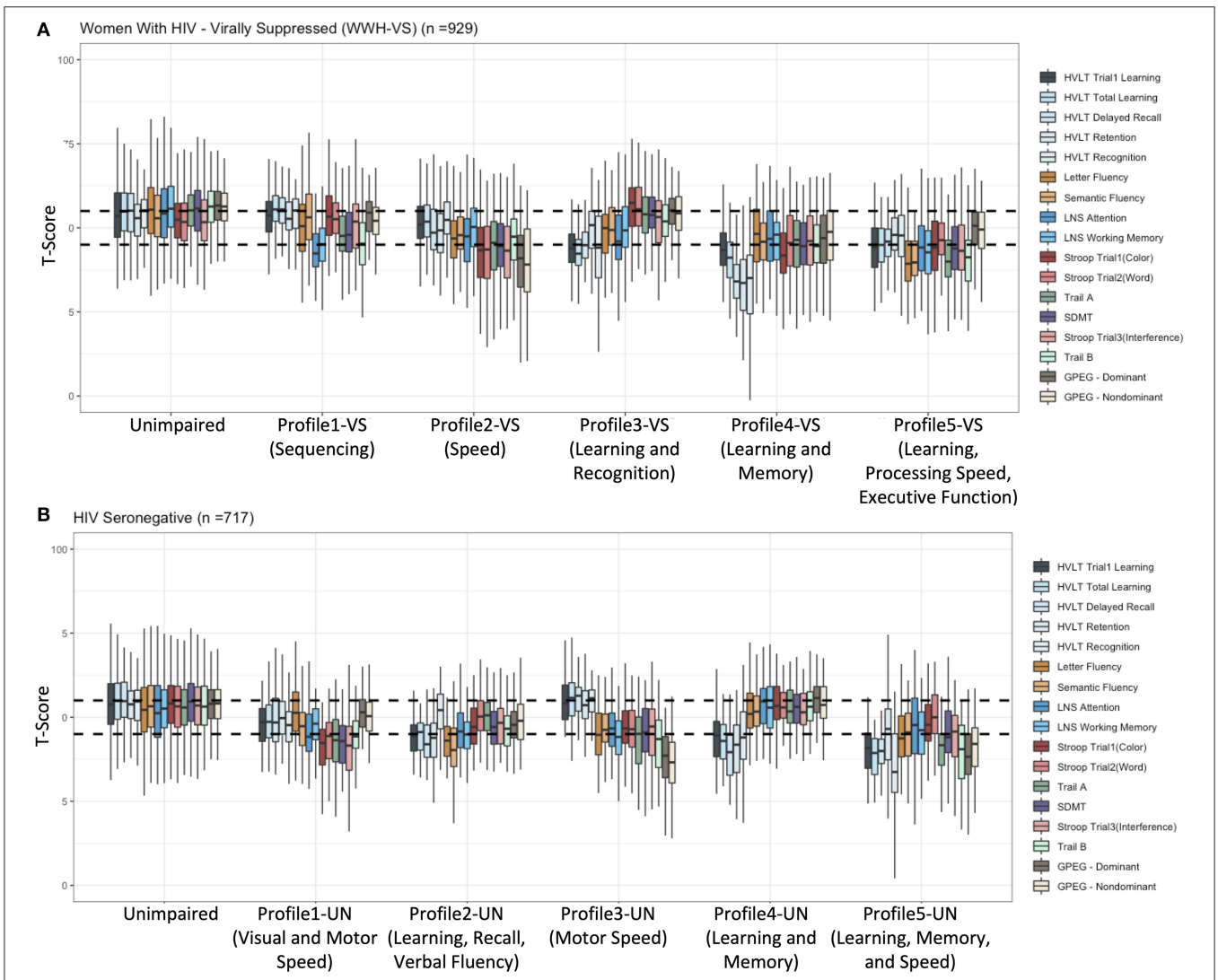

FIGURE 1 | Neuropsychological profiles in **(A)** virally suppressed women with HIV(VS-WWH) and **(B)** HIV-uninfected women. HVLT-R, Hopkins Verbal Learning Test-Revised; LNS, Letter-Number Sequencing; GPEG, Grooved Pegboard.

(entropy = 0.99) and were then assigned names based on their relative patterns of weaknesses after consultation with a clinical neuropsychologist. The profiles are visualized in **Figure 1** and univariate differences between the test scores, as well as univariate differences in predictor variables, are given in **Tables 1**, **2** (**Supplementary Tables 3, 4**).

Profile Results in VS-WWH

Profiling of the 929 VS-WWH resulted in nine total clusters using an ellipsoidal multivariate mixture model with equal orientation (VVE) with an entropy of 0.99. Of these clusters, four were combined into a large "unimpaired" cluster consisting of 311 women (**Figure 1A**; **Table 1**). Of the remaining clusters:

Profiling of the 1,666 PWH resulted in three total groups from a using an ellipsoidal multivariate mixture model with equal orientation with an entropy of 0.982 (**Figure 1A**).

- ***Profile 1-VS* (*n* = 129): *sequencing*** indicated by weaknesses on tests of sequencing (LNS, TMT-Part B). Learning, memory, verbal fluency, processing speed, inhibition, and manual speed were preserved.
- ***Profile 2-VS* (*n* = 144): *speed*** indicated by weaknesses or impairments on most tests of speed (weak: Stroop, TMT, SDMT, GPEG-dominant hand; impaired: GPEG non-dominant hand). Verbal fluency, attention, working memory, learning, and memory were preserved.
- ***Profile 3-VS* (*n* = 137): *learning and recognition*** indicated by weak learning (HVLT-R trial 1 and total learning) and recognition (HVLT-R recognition). Retention, verbal fluency, attention, working memory, processing speed, executive functioning, and manual speed were preserved.
- ***Profile 4-VS* (*n* = 86): *learning and memory*** indicated primarily by impaired memory (HVLT-R delayed recall, recognition, retention) and weak learning (HVLT-R trial 1 and total learning), with mild weaknesses on select speeded measures (Stroop-trial 1, TMT, SDMT). Verbal fluency, attention, working memory, executive functioning, and manual speed were relatively preserved.
- ***Profile 5-VS* (*n* = 122): *learning, processing speed, attention, and executive functioning*** indicated by impaired and/or weak learning, processing speed, attention, and executive functioning (impaired: COWAT, TMT-Part A; weak: HVLT-R trial 1 and total learning, animal fluency, LNS, SDMT, Stroop-trial 3, TMT-Part B). Manual speed and memory were preserved.

Profile Results in HIV-Uninfected Women

Profiling of the 717 HIV-uninfected women also resulted in nine total clusters (**Figure 1B**; **Table 2**) from an ellipsoidal multivariate model with equal volume and orientation (EVE) with an entropy of 0.99. Of these clusters, four did not have mean T-scores that were <45 on any test and were therefore combined into a large "unimpaired" cluster consisting of 400 women. Of the remaining clusters:

- ***Profile 1-UN* (*n* = 68): *visual and motor speed*** indicated by weaknesses on tests of visual and motor speed (Stroop, TMT, SDMT). Learning, memory, verbal fluency, attention, working memory, and manual speed were preserved.
- ***Profile 2-UN* (*n* = 58): *learning, recall, and verbal fluency*** indicated primarily by weak learning, recall, and verbal fluency (HVLT-R trial 1, total learning, delayed recall, retention, COWAT, animal fluency). Recognition, processing speed, executive functioning, and manual speed were relatively preserved.
- ***Profile 3-UN* (*n* = 72): *manual speed*** indicated primarily by impaired manual speed (GPEG) and weak TMT. Learning and memory were spared and all other domains remained relatively preserved.
- ***Profile* 4-*UN* (*n* = 75): *learning and memory*** indicated by impaired recall (HVLT-R delayed recall and retention) and weak learning and recognition (HVLT-R trial 1, total learning, and recognition). All other domains were spared.
- ***Profile 5-UN* (*n* = 44): *learning, memory, speed*** indicated primarily by impaired learning and memory (HVLT-R total learning, delayed recall, and recognition) with impairments or weaknesses on select speeded tests (TMT, GPEG, Stroop-trial 3). Verbal fluency, attention, working memory, and visuo-verbal processing speed (Stroop Trials 1 and 2) were relatively preserved.

Predictors of Cognitive Profiles

For each group of women, a RF model was created to help identify variables contributing in a non-linear fashion to distinguishing between each impaired and the unimpaired profile. An additional model was created to distinguish between all combined impairment profiles and the unimpaired profile in order to compare the differences in variables. For each model, variable importance was calculated and those that ranked as the top 10 were identified.

Predictors of Cognitive Profiles in VS-WWH

In RF models (**Figure 2**), the top 10 variables distinguishing women in the impaired from unimpaired profiles (ROC = 0.91) included clinic site, sociodemographic factors (age, race, education), behavioral (crack, cocaine, and/or heroin use), and clinical factors (BMI, protease inhibitor [PI]-based regimen, current and nadir CD4 count, and years of cART use). Specifically, women in the impaired vs. unimpaired profiles had: a higher minority and southern site representation (non-Hispanic Black, 76 vs. 66%; southern clinics, 36 vs. 32%), less education (12.6 vs. 12.8 years), PI use(70 vs. 60%), healthy BMI of 18.5–24.9 kg/m^2 (19 vs. 24%), and ever use of crack, cocaine, and/or heroin (49 vs. 40%). Many of these variables were also important contributors to the individual impairment profiles, although some additional variables were found to be important distinguishers. Compared to the unimpaired profile:

- ***Profile 1-VS* (*n* = 129): *sequencing*** (ROC = 0.89, Testing Accuracy = 0.89, Testing Sensitivity = 0.84, Testing Specificity = 1.0) were more likely to have a lower annual household income (48 vs. 40%), depressive symptoms (30 vs. 21%), and higher perceived (40 vs. 26%) and post-traumatic stress (25 vs. 13%).

TABLE 1 | Sociodemographic, clinical, and behavioral factors by subgroup of virally suppressed [VS] women with HIV [WWH].

	Unimpaired *n* (%)	Profile1-VS: executive function and sequencing *n* (%)	Profile2-VS: processing speed, executive function, and manual speed *n* (%)	Profile3-VS: learning and recall *n* (%)	Profile4-VS: learning, memory, and speed *n* (%)	Profile5-VS: global weakness, processing speed *n* (%)	*p*-value
Sample size	311	129	144	137	86	122	
Enrollment wave							0.32
1994–1995	126 (41)	39 (30)	55 (38)	48 (35)	32 (37)	49 (40)	
2001–2002	59 (19)	29 (23)	29 (20)	17 (12)	13 (15)	26 (21)	
2011–2013	32 (10)	16 (12)	10 (7)	14 (10)	10 (12)	7 (6)	
2013–2015	94 (30)	45 (35)	50 (35)	58 (42)	31 (36)	40 (33)	
Clinic site locations							0.42
Chicago, DC, LA, NY, SF	212 (69)	84 (65)	95 (66)	79 (58)	54 (63)	81 (66)	
Atlanta, Birmingham, Chapel Hill, Jackson	99 (32)	45 (35)	49 (34)	58 (42)	32 (37)	41 (34)	
Sociodemographic							
Age, M (SD)	46.7 (8.1)	45.8 (8.6)	47.3 (8.9)	46.8 (8.5)	47.4 (8.1)	44.6 (9.3)	0.10
Years of Education, M (SD)	12.8 (3.3)	13.0 (2.9)	12.5 (3.0)	12.4 (2.7)	12.1 (2.9)	12.9 (2.9)	0.19
Race							0.05
Black non-Hispanic	202 (65)	103 (80)	104 (72)	94 (69)	65 (76)	89 (73)	
Hispanic	45 (15)	7 (5)	15 (10)	18 (13)	12 (14)	16 (13)	
Other	8 (3)	5 (4)	8 (6)	3 (2)	2 (2)	6 (5)	
White	56 (18)	14 (11)	17 (12)	22 (16)	7 (8)	11 (9)	
Annual income <$12,000 per year	126 (41)	62 (48)	80 (56)	65 (47)	60 (70)	64 (53)	<0.001
Employed	152 (49)	47 (36)	41 (29)	58 (42)	23 (27)	43 (35)	<0.001
Insured	294 (95)	125 (97)	140 (97)	135 (99)	85 (99)	115 (94)	0.16
Mental health and substance use							
Depressive symptoms	66 (21)	39 (30)	51 (35)	46 (34)	39 (45)	43 (35)	<0.001
Higher perceived stress	81 (26)	52 (40)	50 (35)	44 (32)	42 (49)	45 (37)	0.001
Post-traumatic stress	39 (13)	32 (25)	24 (17)	27 (20)	26 (31)	19 (16)	<0.001
Crack/Cocaine/Heroine							<0.001
Recent	16 (5)	4 (3)	9 (6)	8 (6)	6 (7)	5 (4.1)	
Former	170 (55)	58 (45)	79 (55)	66 (48)	46 (54)	35 (29)	
Never	125 (40)	67 (52)	56 (39)	63 (46)	34 (40)	82 (67)	
Marijuana use							0.002
Recent	63 (20)	23 (18)	22 (15)	25 (18)	13 (15)	9 (7)	
Former	170 (55)	63 (49)	77 (54)	68 (50)	49 (57)	54 (44)	
Never	78 (25)	43 (33)	45 (31)	44 (32)	24 (28)	59 (48)	
Smoking							0.01
Current	106 (34)	41 (32)	60 (42)	62 (45)	34 (40)	36 (30)	
Former	105 (34)	36 (28)	41 (29)	29 (21)	24 (28)	28 (23)	
Never	100 (32)	52 (40)	43 (30)	46 (34)	28 (33)	58 (48)	
Heavy drinker	20 (6)	8 (6)	8 (6)	5 (4)	5 (6)	4 (3)	0.71
Female-specific factors							
Ever pregnant	277 (89)	117 (91)	131 (91)	124 (91)	77 (90)	114 (93)	0.84
History of oophorectomy	54 (18)	20 (17)	20 (15)	30 (23)	25 (30)	16 (14)	0.04
Ever use oral contraceptives	260 (84)	101 (78)	119 (83)	106 (77)	70 (81)	86 (71)	0.05
Ever use hormone therapy	65 (21)	25 (19)	38 (26)	27 (29)	11 (13)	24 (20)	0.26
Menopause stage							0.19
Pre-	109 (36)	45 (36)	48 (34)	41 (30)	25 (29)	58 (48)	
Peri-	57 (19)	27 (22)	28 (20)	26 (19)	13 (15)	19 (16)	
Post-	140 (46)	52 (42)	65 (46)	68 (50)	47 (55)	45 (37)	

(Continued)

TABLE 1 | Continued

	Unimpaired *n* (%)	Profile1-VS: executive function and sequencing *n* (%)	Profile2-VS: processing speed, executive function, and manual speed *n* (%)	Profile3-VS: learning and recall *n* (%)	Profile4-VS: learning, memory, and speed *n* (%)	Profile5-VS: global weakness, processing speed *n* (%)	*p*-value
HIV-related clinical characteristics							
Nadir CD4 (cells/mL)	306 (236)	310 (237)	306 (229)	311 (218)	322 (214)	304 (206)	0.99
Current CD4 (cells/mL)	677 (343)	660 (317)	705 (312)	682 (311)	629 (287)	664 (288)	0.63
Years of effective ART	7.93 (4.75)	7.59 (4.59)	8.33 (4.29)	7.77 (4.59)	8.02 (4.49)	8.47 (4.45)	0.62
Viral Load (log)	3.45 (0.44)	3.40 (0.44)	3.41 (0.44)	3.33 (0.43)	3.35 (0.43)	3.41 (0.44)	0.14
ART adherence (≥95%)	270 (87)	119 (92)	129 (90)	120 (88)	76 (88)	109 (89)	0.70
Non-ART use							
NCAE	60 (19)	23 (18)	35 (24)	23 (17)	23 (27)	19 (16)	0.22
Meds with anticholinergic properties	34 (11)	14 (11)	25 (17)	16 (12)	19 (22)	11 (9.0)	0.03
Anticonvulsants	9 (3)	5 (4)	5 (4)	3 (2)	2 (2)	5 (4.1)	0.93
Statins	19 (6)	6 (5)	13 (9)	9 (7)	4 (5)	7 (5.7)	0.71
Anticholinergics	4 (1)	3 (2)	4 (3)	1 (1)	3 (4)	0 (0.0)	0.27
Antipsychotics	11 (4)	5 (4)	11 (8)	5 (4)	11 (13)	1 (0.8)	< 0.001
Amphetamines	2 (1)	1 (1)	0 (0)	0 (0)	0 (0)	0 (0.0)	0.64
Opioids	24 (8)	7 (5)	5 (4)	7 (5)	5 (6)	4 (3.3)	0.39
Beta blockers	7 (2)	3 (2)	6 (4)	2 (2)	2 (2)	1 (0.8)	0.56
Gastrointestinal agents	4 (1)	2 (2)	6 (4)	2 (2)	5 (6)	2 (1.6)	0.09
Antihistamines	15 (5)	6 (5)	6 (4)	5 (4)	5 (6)	4 (3.3)	0.95
Muscle relaxants	8 (3)	1 (1)	4 (3)	2 (2)	0 (0)	1 (0.8)	0.40
Antidepressants	34 (11)	12 (9)	20 (14)	13 (10)	16 (19)	16 (13.1)	0.28

ART, antiretrovirals; M, mean; NCAE, medications with adverse neurocognitive effects; SD, standard deviation.

- ***Profile 2-VS* (*n* = 144): *speed*** (ROC = 0.90, Testing Accuracy = 0.90, Testing Sensitivity = 0.85, Testing Specificity = 1.0) were more likely to be unemployed (71 vs. 51%) and have depressive symptoms (35 vs. 21%).
- ***Profile 3-VS* (*n* = 137): *learning and recognition*** (ROC = 0.90, Testing Accuracy = 0.88, Testing Sensitivity = 0.83, Testing Specificity = 1.0) were more likely to have depressive symptoms (34 vs. 21%) and be on an integrase inhibitor (INSTI)-based regimen (27 vs. 19%).
- ***Profile 4-VS* (*n* = 86): *learning and memory*** (ROC = 0.88, Testing Accuracy = 0.89, Testing Sensitivity = 0.87, Testing Specificity = 0.96) were more likely to be unemployed (73 vs. 51%, $P<0.001$), have a lower annual household income (70 vs. 40%), be on INSTI-based regimen (28 vs. 19%), atazanavir (ATZ, 24 vs. 15%), and non-ART medications with higher anticholinergic burden (22 vs. 11%).
- ***Profile 5-VS* (*n* = 122): *learning, processing speed, and executive function*** (ROC = 0.91, Testing Accuracy = 0.86, Testing Sensitivity = 0.81, Testing Specificity = 1.0) were less likely to currently use marijuana (15 vs. 20%).

Predictors of Cognitive Profiles in HIV-Uninfected Women

In RF models (**Figure 3**), the top 10 variables distinguishing the impaired profiles from unimpaired profiles (ROC = 0.93) included: clinic site, cohort wave, sociodemographic factors (age, education, race, employment status), behavioral (smoking, marijuana, crack, cocaine, and/or heroin use), and clinical factors (BMI). Many of these factors were also important contributors to the individual impairment profiles, with some differences. Compared to women in the unimpaired profile:

- ***Profile 1-UN* (*n* = 68): *visual and motor speed*** (ROC = 0.83, Testing Accuracy = 0.67, Testing Sensitivity = 0.90, Testing Specificity = 0.63) were more likely to have diabetes (22 vs. 16%), depressive symptoms (44 vs. 25%), high perceived stress (43 vs. 34%), use antidepressants (9 vs. 7%), and more non-ART drugs with anticholinergic properties (3 vs. 1%).
- ***Profile 2-UN* (*n* = 58): *learning, recall, and verbal fluency*** (ROC = 0.72, Testing Accuracy = 0.71, Testing Sensitivity = 1.0, Testing Specificity = 0.67) were more likely to have a lower annual household income (47 vs. 41%), have had an oophorectomy (17 vs. 13%), depressive symptoms (33 vs. 25%), high perceived stress (45 vs. 34%), diabetes (21 vs. 16%), and hypertension (36 vs. 38%).
- ***Profile 3-UN* (*n* = 72): *motor speed*** (ROC = 0.85, Testing Accuracy = 0.75, Testing Sensitivity = 1.0, Testing Specificity = 0.71) were more likely to have depressive symptoms (47 vs. 25%), perceived stress (47 vs. 34%) and post-traumatic symptoms (28 vs. 19%), HCV (18 vs. 10%), and less likely to have had an oophorectomy (9 vs. 13%).
- ***Profile* 4-*UN* (*n* = 75): *learning and memory*** (ROC = 0.79, Testing Accuracy = 0.76, Testing Sensitivity = 0.95, Testing Specificity = 0.73) were less likely to have ever been pregnant (88 vs. 91%).

TABLE 2 | Sociodemographic, clinical, and behavioral factors by subgroup of HIV-uninfected (UN) women.

	Unimpaired *n* (%)	Profile1-UN: visual and motor speed *n* (%)	Profile2-UN: learning, recall, and verbal fluency *n* (%)	Profile3-UN: motor speed *n* (%)	Profile4-UN: learning and memory *n* (%)	Profile5-UN: learning, memory, and speed *n* (%)	*p*-value
Sample size	400	68	58	72	75	44	
Enrollment wave							0.24
1994–1995	111 (28)	19 (28)	20 (35)	25 (35)	28 (37)	17 (38.6)	
2001–2001	161 (40)	33 (49)	16 (28)	25 (35)	20 (27)	12 (27.3)	
2011–2013	44 (11)	5 (7)	5 (9)	4 (6)	7 (9)	5 (11.4)	
2013–2015	84 (21)	11 (16)	17 (29)	18 (25)	20 (27)	10 (22.7)	
Clinic site locations							0.40
Chicago, DC, LA, NY, SF	312 (78)	56 (82)	41 (71)	54 (75)	52 (69)	34 (77.3)	
Atlanta, Birmingham, Chapel Hill, Jackson	88 (22)	12 (18)	17 (29)	18 (25)	23 (31)	10 (23)	
Sociodemographic							
Age	43.3 (9.7)	42.4 (9.7)	42.6 (10.9)	43.4 (10.9)	44.5 (9.0)	44.3 (11.1)	0.78
Years of education	12.7 (3.2)	13.0 (2.9)	12.7 (2.9)	12.9 (2.6)	12.4 (2.5)	12.9 (3.7)	0.89
Race							0.45
Black non-Hispanic	266 (66)	47 (69)	40 (69.0)	48 (67)	45 (60)	33 (75)	
Hispanic	84 (21)	12 (18)	10 (17)	12 (17)	12 (16)	7 (16)	
Other	15 (4)	5 (7)	2 (3)	3 (4)	7 (9)	3 (7)	
White, non-Hispanic	35 (9)	4 (6)	6 (10)	9 (13)	11 (15)	1 (2)	
Annual income <$12,000 per year	165 (41)	31 (45.6)	27 (46.6)	38 (53)	40 (53)	25 (57)	0.13
Employed	201 (50)	22 (32.4)	24 (41.4)	22 (31)	31 (42)	17 (39)	0.006
Insured	302 (76)	55 (81)	43 (74)	61 (85)	48 (64)	35 (80)	0.07
Mental health and substance use							
Depressive symptoms	99 (25)	30 (44.)	19 (33)	34 (47)	17 (23)	14 (32)	<0.001
Higher perceived stress	135 (34)	29 (43)	26 (45)	34 (47)	20 (27)	15 (34)	0.05
Post-traumatic stress	77 (19)	21 (31)	12 (21)	20 (28)	13 (17)	9 (20)	0.19
Crack/Cocaine/Heroine							0.77
Recent	33 (8)	7 (10)	8 (14)	8 (11)	7 (9)	2 (5)	
Former	200 (50)	30 (44)	27 (47)	35 (49)	41 (55)	19 (43)	
Never	167 (42)	31 (46)	23 (40)	29 (40)	27 (36)	23 (52)	
Marijuana use							0.01
Recent	85 (21)	21 (31)	18 (31)	9 (13)	19 (25)	13 (30)	
Former	226 (57)	28 (41)	24 (41)	49 (68)	48 (64)	21 (48)	
Never	89 (22)	19 (28)	16 (28)	14 (19)	8 (11)	10 (23)	
Heavy drinker	59 (16)	10 (16)	5 (10)	9 (13)	9 (13)	3 (7)	0.57
Smoking							0.91
Recent	172 (43)	34 (50)	27 (47)	31 (43)	37 (49)	21 (48)	
Former	114 (29)	18 (27)	15 (26)	21 (29)	24 (32)	13 (30)	
Never	114 (29)	16 (24)	16 (28)	20 (28)	14 (19)	10 (23)	
Female-specific factors							
Ever pregnant	366 (92)	62 (91)	53 (91)	63 (88)	66 (88)	42 (96)	0.69
History of oopherectomy	48 (13)	7 (10)	9 (17)	6 (9)	12 (17)	5 (12)	0.68
Ever use oral contraceptives	340 (85)	51 (75)	46 (79)	61 (85)	60 (80)	35 (80)	0.34
Ever use hormone therapy	63 (16)	11 (16)	11 (19)	11 (15)	11 (15)	6 (14)	0.98
Menopause stage							0.75
Peri-	74 (19)	7 (11)	12 (22)	16 (23)	12 (16)	7 (16)	
Post-	134 (34)	20 (31)	19 (35)	25 (35)	26 (36)	18 (41)	
Pre-	182 (47)	38 (59)	24 (44)	30 (42)	35 (48)	19 (43)	

(Continued)

TABLE 2 | Continued

	Unimpaired *n* (%)	Profile1-UN: visual and motor speed *n* (%)	Profile2-UN: learning, recall, and verbal fluency *n* (%)	Profile3-UN: motor speed *n* (%)	Profile4-UN: learning and memory *n* (%)	Profile5-UN: learning, memory, and speed *n* (%)	*p*-value
Non-ART use							
NCAE	53 (13)	12 (18)	8 (14)	12 (17)	8 (11)	5 (11)	0.81
Meds with anticholinergic properties	41 (10)	10 (15)	5 (9)	9 (13)	6 (8)	3 (7)	0.70
Anticonvulsants	11 (3)	0 (0)	3 (5)	3 (4)	2 (3)	0 (0)	0.40
Statins	13 (3)	4 (6)	2 (4)	2 (3)	5 (7)	2 (5)	0.70
Anticholinergics	4 (1)	2 (3)	1 (2)	2 (3)	1 (1)	0 (0)	0.65
Antipsychotics	13 (3)	4 (6)	3 (5)	1 (1)	5 (7)	1 (2)	0.47
Amphetamines	1 (0)	1 (2)	0 (0)	0 (0)	0 (0)	0 (0)	0.52
Opioids	16 (4)	4 (6)	3 (5)	6 (8)	3 (4)	2 (5)	0.72
Beta blockers	3 (1)	1 (2)	1 (2)	2 (3)	2 (3)	0 (0)	0.54
Gastrointestinal agents	5 (1)	0 (0)	1 (2)	2 (3)	1 (1)	0 (0)	0.72
Antihistamines	17 (4)	2 (3)	2 (3)	1 (1)	1 (1)	0 (0)	0.48
Muscle relaxants	7 (2)	2 (3)	1 (2)	2 (3)	1 (1)	1 (2)	0.97
Antidepressants	29 (7)	6 (9)	6 (10)	7 (10)	5 (7)	3 (7)	0.93

ART, antiretrovirals; M, mean; NCAE, medications with adverse neurocognitive effects; SD, standard deviation.

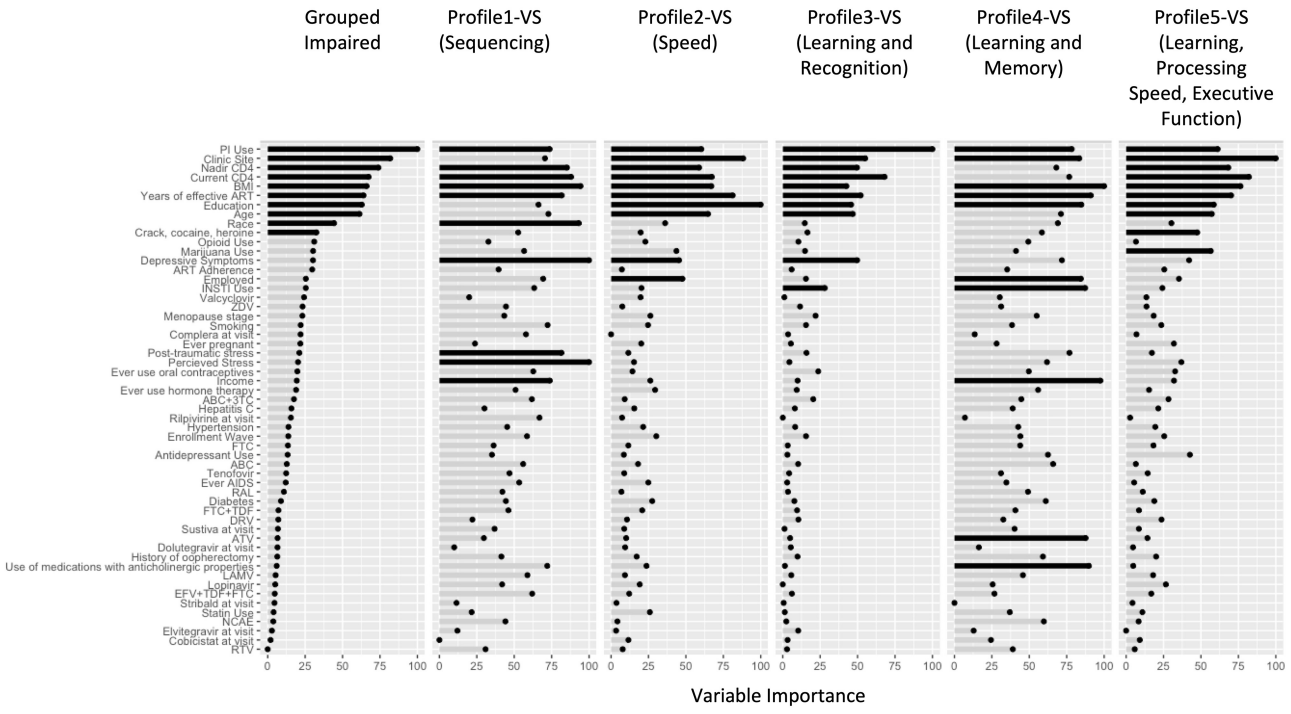

FIGURE 2 | Variable Importance results from the Random Forest Models in virally suppressed women with HIV (VS-WWH). The length of the bars indicates the relative importance of the variable in that model. The top 10 variables in each model have been highlighted in black. 3TC, lamivudine; ABC, abacavir; ART, antiretroviral therapy; ATV, atazanavir; BMI, body mass index; COBI, cobicistat; DRV, darunavir; DTG, dolutegravir; EFV, efavirenz; EVG, elvitegravir; FTC, emtricitabine; INSTI, integrase inhibitor; PI, protease inhibitor; RAL, raltegravir; RPV, rilpivirine; RTV, ritonavir; TDF, tenofovir disoproxil fumarate; ZDV, Zidovudine; NCAE, non-ART medications with neurocognitive adverse effects.

- ***Profile 5-UN* (*n* = 44): *learning, memory, and speed*** (ROC = 0.76, Testing Accuracy = 0.73, Testing Sensitivity = 1.0, Testing Specificity = 0.70) were more likely to have diabetes (32 vs. 16%) and hypertension (53 vs. 38%).

DISCUSSION

We used machine learning models to identify distinct homogenous subgroups (profiles) in the largest dataset to

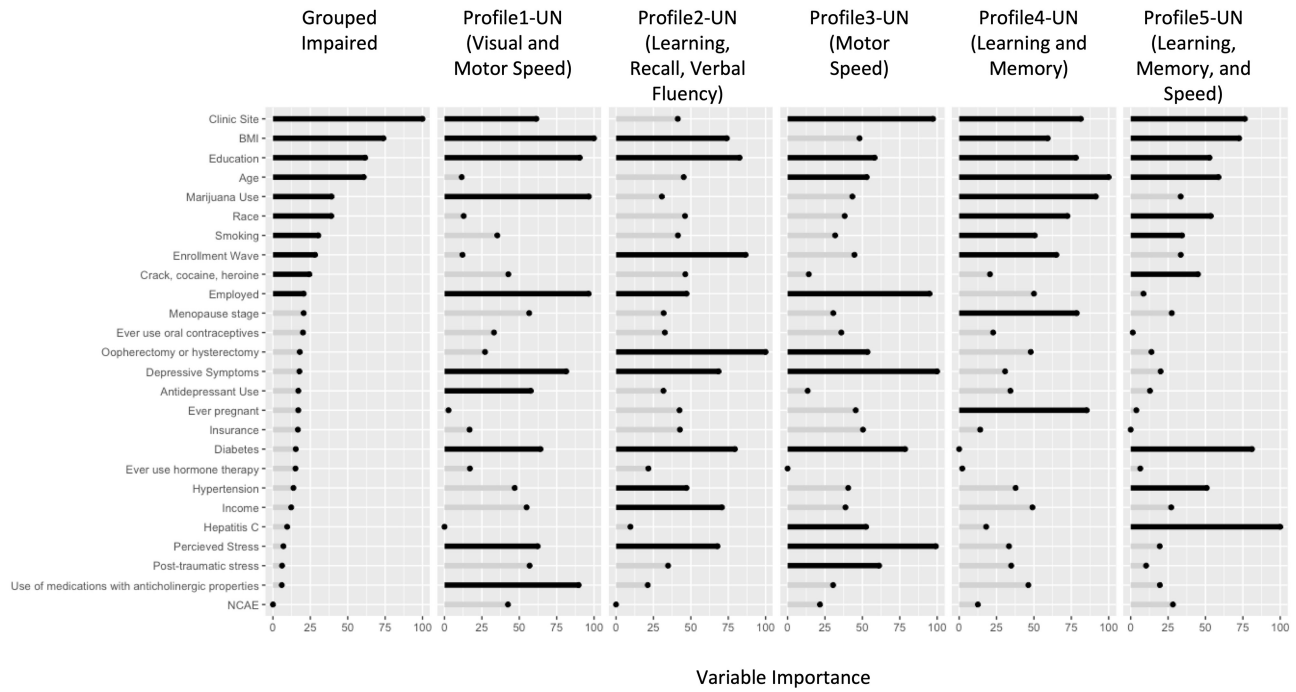

FIGURE 3 | Variable Importance results from the Random Forest Models in HIV-uninfected (UN) women. The length of the bars indicates the relative importance of the variable in that model. The top 10 variables in each model have been highlighted in black. BMI, body mass index; NCAE, non-ART medications with neurocognitive adverse effects; OOPH, oopherectomy.

date in VS-WWH and HIV-uninfected women. Separate patterns of cognitive performance, as well as associated factors of those patterns among each subgroup of women, were identified. The factors identified allow for screening and intervention, including potentially changing non-ART medications, as well as mental health and substance use screening and intervention.

In the context of viral suppression, we identified several profiles with distinct patterns of performance across 17 NP outcomes. While these profiles are statistically-derived, some of the profiles found here parallel commonly identified patterns in other neurological conditions or processes. Among the virally suppressed group, Profile 1-VS revealed a unique pattern reflecting exclusive weaknesses in cognitive sequencing (LNS Attention and Working Memory) and motor set-shifting (TMT-Part B). While to our knowledge, this combination of isolated deficits in cognitive sequencing and motor set-shifting has not been appreciated in other disease populations, specific deficits in cognitive sequencing/verbal working memory have been observed in individuals with schizophrenia and their first-degree relatives (25). Additionally, McDonald et al. (26) identified specific problems with motor set-shifting (TMT-Part B) in individuals with frontal lobe epilepsy. In contrast to the very specific weaknesses identified in Profile 1-VS, Profile 2-VS reflects general slowing, which is most often associated with typical (i.e., "healthy") aging (27). Profile 3-VS, characterized by poor encoding and recognition with intact retention, is more of a typical HIV-associated profile (28) compared to mild cognitive impairment due to Alzheimer's disease (AD) (29). Profile 4-VS showed a mostly amnestic profile with some evidence of cognitive slowing, as can be observed in AD or in AD with vascular contributions (30). This profile is similar to Profile 4-UN, which reflected an amnestic profile that is often observed in typical AD (31). Profile 5-VS, showing intact memory storage and manual speed/dexterity, but weak or impaired attention, processing speed, learning, and executive functioning is similar to what is observed in individuals with diffuse frontal-subcortical small vessel disease (32). Interestingly, a profile did not emerge among VS-WWH reflecting specific motor slowing which has been linked to HIV infection. This is consistent with prior cross-sectional WIHS analyses, where motor slowing was not a prominent feature among WWH but rather verbal learning and memory (13).

Among the seronegative group, Profile1-UN was more likely to have diabetes, raising the possibility that their specific visual and motor deficits could be related to physical complications of diabetes, including diabetic retinopathy and neuropathy (33, 34). Profile2-UN reflects unique impairments on the most verbally mediated tasks (i.e., verbal learning and recall, and verbal fluencies). While we are unaware of any specific disease process or syndrome that shows the same pattern, this group of individuals has clear weakness in verbal skills, which could be due to many factors, including learning differences or damage to brain regions associated with verbally mediated tasks. Profile 3-UN, reflecting specific motor slowing, is commonly observed in individuals with basal ganglia dysfunction, such as Parkinson's

disease (35). Profile 5-UN, revealing rather generalized cognitive weaknesses or impairments, but relatively preserved attention and visual processing, does not reflect any specific disease process or syndrome to our knowledge.

Even though the HIV group was virally suppressed, the dominant profiles did not fully align with the HIV-uninfected women, suggesting that HIV affects cognitive function even in the era of effective ART. There is a wealth of literature postulating neuronal damage as a result of ART agents (36), a viral reservoir that persists possibly due to poor CNS penetration of ART (37), or even legacy effects of damage occurring earlier during infection (38). Indeed, in the VS-WWH RF model where all impaired groups were grouped together, nadir CD4 was a top predictor of group membership. This also points to how existing studies that consider impairment to be a unidimensional construct may only be able to detect differences in these variables and miss those associated more strongly with some profiles than others.

Despite different cognitive profiles among VS-WWH, the most discriminative factors between each impaired profile vs. the unimpaired profile were similar and included a number of well-established sociodemographic cognitive correlates, such as years of education, age, and race/ethnicity (39). Clinic site location also emerged, a factor that we have also seen using more standard statistical approaches in the WIHS (13, 14). The factors underlying this rather robust association is unknown but may involve neighborhood factors, such as violence and food insecurity. Additionally, common behavioral correlates of cognition emerged including illicit substance use (40, 41), which in the case of marijuana was more likely to be used in the unimpaired profile compared to the impaired profile demonstrating weaknesses in learning, processing speed, and executive function (Profile 5-VS). This finding is consistent with some studies demonstrating the protective effects of marijuana use on cognition in PWH (42). We also found common clinical correlates of cognition that distinguished cognitive profiles among VS-WWH including BMI (43, 44) and PI use (45). Likely proxies of HIV disease burden, including nadir CD4 count and years of ART use, were also discriminators (38, 46, 47). In contrast, sociodemographic and medical variables were unable to distinguish cognitive profiles based on seven major cognitive domains (48).

Mental health factors also emerged as important profile discriminators among VS-WWH, including depressive and stress-related symptoms. Depressive symptoms differentiated a number of impaired profiles (4 of 5 profiles) compared to the unimpaired profile, whereas stress-related symptoms only emerged for two profiles including Profile 1-VS (sequencing) and Profile 4-VS (learning and memory). These findings align with our WIHS studies demonstrating numerous cognitive correlates of depressive symptoms (19, 49, 50), whereas stress-related symptoms related most strongly to learning and memory in the context of HIV (49, 51). Importantly, mental health factors are an unmet medical need and are modifiable targets to improve cognition in WWH (52).

INSTI use discriminated both Profile3-VS (learning and recognition) and Profile 4-VS (learning and memory) from the unimpaired profile. This finding is consistent with a number of recently published studies indicating INSTI use as a contributor to NP function. One study demonstrated an association between INSTI use and poorer learning and memory but not any other cognitive domains (53). A second study also demonstrated that switching or starting an INSTI was primarily associated with poorer learning among WWH (54). A third study demonstrated that long-term INSTI exposure distinguished two impaired profiles from an unimpaired profile (55).

Our study also allows us to investigate female-specific factors that are often ignored and identify the importance of oophorectomy and/or hysterectomy (Profile2-UN[Learning, Recall, Verbal Fluency], and Profile3-UN[Motor Speed]) and menopause status (Profile4-UN[Learning and Memory]). Interestingly, these female-specific factors only emerged as important profile discriminators among HIV-uninfected women. As the proportion of menopause-inducing and non-inducing oophorectomy and/or hysterectomy was similar across VS-WWH and HIV-uninfected women, one possible explanation is that the virus itself and clinical factors, such as ART may explain more of the variance in cognitive function in VS-WWH. However, in the absence of HIV, negative effects of oophorectomy and/or hysterectomy on cognition may become more apparent. Overall, these female-specific factors are potential contributions that are missed in other studies, which are predominately male. Future studies of women should evaluate these variables in a similar stratified form to identify potential mechanistic contributions.

The existence of distinctive patterns of cognitive performance, as well as distinct factors associated with those patterns, also adds to existing evidence of differing neuropathological mechanisms. The dominant profiles often contained patterns of weaknesses that were subclinical, yet still lower than the unimpaired profiles. In many cases, the associated factors are intervenable and should be followed up with mechanistic and longitudinal studies.

Differences between the profiles identified here and previous efforts to identify cognitive patterns can be attributed to both the methods used and the study population. To identify meaningful cognitive patterns, we used a combination of SOM and MClust, which is a slight deviation from tradition k-means clustering. The nature of k-means is that it yields clusters where the most dramatic differences are shown, which may ignore subtle differences in patterns. Even Molsberry et al. (7) and Amusan et al. (55) who used latent profile analysis using domain T-scores had their fit dominated by a high-performing and a low-performing group. Using SOM for dimension reduction on the T-scores for individual tests prevented us from following pre-conceived notions about the latent structures of cognitive domains, which have been shown to be different in HIV (56). Another reason that we may have found different profiles than prior studies is that we focused on a diverse sample of underserved lower-income, African-American and Hispanic WWH where social correlates of health are common (e.g., low educational attainment, poverty, food insecurity, etc.) (8, 57) and may lead to more heterogeneous patterns of cognitive function. Of importance, this demographic is a more accurate reflection of the HIV epidemic

as opposed to the predominantly White populations evaluated in other cohorts.

The addition of machine learning models to traditional univariate statistics to identify dominating predictor variables is another distinguishing aspect of the current study. It is important to point out that RF modeling is a non-linear model, and that the variable importance measure does not take into account directionality. Therefore, it is possible to have a top predictor variable from RF that does not have $P < 0.05$ using a t-test. RF models are also multivariate; instead of, the predictive capabilities of variables are always observed within the context of other variables. This is important considering that none of these factors exist in isolation. This makes the model more powerful, but one limitation of this statistical approach is that it becomes more difficult to interpret and should be used as a springboard for more mechanistic studies and interventions, which is why machine learning models are often thought of as "hypothesis-generating" models.

In conclusion, in the largest sample of women to date in the United States, we have used a novel pipeline of machine learning methods to identify subgroups of patterns in NP performance and created predictive models to identify the factors that distinguish each pattern from an overall "unimpaired" group. We identified distinct patterns of cognitive weaknesses in VS-WWH that differed from the distinct patterns in HIV-uninfected women. We also identified factors that may contribute to these specific profiles as a springboard for mechanistic or interventional studies. Future studies should also investigate the stability of these profiles over time, and identify the ones, if any, that are prone to future decline.

DATA AVAILABILITY STATEMENT

Data from our study are available upon request to the MACS/WIHS Combined Cohort Study (MWCCS; https://statepi.jhsph.edu/mwccs/). This committee may be contacted via email at https://statepi.jhsph.edu/mwccs/contact-us/.

ETHICS STATEMENT

The studies involving human participants were reviewed and approved by Institutional Review Board. The patients/participants provided their written informed consent to participate in this study.

AUTHOR CONTRIBUTIONS

LR has primary responsibility for final content and conceived the study idea. RD conducted the statistical analyses. RD, AB, and LR wrote the paper. All authors contributed to manuscript editing and statistical review, read, and approved the final manuscript.

FUNDING

This work was supported by the Johns Hopkins University NIMH Center for novel therapeutics for HIV-associated cognitive disorders (P30MH075773) 2018 pilot award to LR and Johns Hopkins University Center for AIDS Research (CFAR) Scholar Award (P30AI094189 and R03MH123290-02). Data in this manuscript were collected by the Women's Interagency HIV Study, now the MACS/WIHS Combined Cohort Study (MWCCS). The contents of this publication are solely the responsibility of the authors and do not represent the official views of the National Institutes of Health (NIH). MWCCS (Principal Investigators): Atlanta CRS (Ighovwerha Ofotokun, Anandi Sheth, and Gina Wingood), U01-HL146241; Baltimore CRS (Todd Brown and Joseph Margolick), U01-HL146201; Bronx CRS (KA and Anjali Sharma), U01-HL146204; Brooklyn CRS (DG and Tracey Wilson), U01-HL146202; Data Analysis and Coordination Center (Gypsyamber D'Souza, Stephen Gange, and Elizabeth Golub), U01-HL146193; Chicago-Cook County CRS (Mardge Cohen and Audrey French), U01-HL146245; Chicago-Northwestern CRS (Steven Wolinsky), U01-HL146240; Connie Wofsy Women's HIV Study, Northern California CRS (Bradley Aouizerat and Phyllis Tien), U01-HL146242; Los Angeles CRS (Roger Detels), U01-HL146333; Metropolitan Washington CRS (Seble Kassaye and Daniel Merenstein), U01-HL146205; Miami CRS (Maria Alcaide, Margaret Fischl, and Deborah Jones), U01-HL146203; Pittsburgh CRS (Jeremy Martinson and Charles Rinaldo), U01-HL146208; UAB-MS CRS (Mirjam-Colette Kempf and Deborah Konkle-Parker), U01-HL146192; UNC CRS (AA), U01-HL146194. The MWCCS was funded primarily by the National Heart, Lung, and Blood Institute (NHLBI), with additional co-funding from the Eunice Kennedy Shriver National Institute of Child Health & Human Development (NICHD), National Human Genome Research Institute (NHGRI), National Institute on Aging (NIA), National Institute of Dental & Craniofacial Research (NIDCR), National Institute of Allergy and Infectious Diseases (NIAID), National Institute of Neurological Disorders and Stroke (NINDS), National Institute of Mental Health (NIMH), National Institute on Drug Abuse (NIDA), National Institute of Nursing Research (NINR), National Cancer Institute (NCI), National Institute on Alcohol Abuse and Alcoholism (NIAAA), National Institute on Deafness and Other Communication Disorders (NIDCD), National Institute of Diabetes and Digestive and Kidney Diseases (NIDDK). MWCCS data collection was also supported by UL1-TR000004 (UCSF CTSA), P30-AI-050409 (Atlanta CFAR), P30-AI-050410 (UNC CFAR), and P30-AI-027767.

ACKNOWLEDGMENTS

We would also like to thank Kendra Radtke, Pharm.D. and Bani Tamraz, Pharm.D., Ph.D. for their work in coding all of the non-ART medications and to the study participants, for without them this work would not be possible.

SUPPLEMENTARY MATERIAL

The Supplementary Material for this article can be found online at: https://www.frontiersin.org/articles/10.3389/fneur.2021.604984/full#supplementary-material

REFERENCES

1. Navia BA, Jordan BD, Price RW. The AIDS dementia complex: I. Clinical features. *Ann Neurol.* (1986) 19:517–24. doi: 10.1002/ana.410190602
2. McArthur JC, Brew BJ, Nath A. Neurological complications of HIV infection. *Lancet Neurol.* (2005) 4:543–55. doi: 10.1016/S1474-4422(05)70165-4
3. Vance DE, Fazeli PL, Dodson JE, Ackerman M, Talley M, Appel SJ. The synergistic effects of HIV, diabetes, and aging on cognition: implications for practice and research. *J Neurosci Nurs.* (2014) 46:292–305. doi: 10.1097/JNN.0000000000000074
4. Stoff DM, Goodkin K, Jeste D, Marquine M. Redefining aging in HIV infection using phenotypes. *Curr HIV/AIDS Rep.* (2017) 14:184–99. doi: 10.1007/s11904-017-0364-x
5. Lojek E, Bornstein RA. The stability of neurocognitive patterns in HIV infected men: classification considerations. *J Clin Exp Neuropsychol.* (2005) 27:665–82. doi: 10.1081/13803390490918426
6. Gomez D, Power C, Gill MJ, Koenig N, Vega R, Fujiwara E. Empiric neurocognitive performance profile discovery and interpretation in HIV infection. *J Neurovirol.* (2018) 25:72–84. doi: 10.1007/s13365-018-0685-6
7. Molsberry SA, Cheng Y, Kingsley L, Jacobson L, Levine AJ, Martin E, et al. Neuropsychological phenotypes among men with and without HIV disease in the multicenter AIDS cohort study. *AIDS.* (2018) 32:1679–88. doi: 10.1097/QAD.0000000000001865
8. Maki PM, Martin-Thormeyer E. HIV, cognition and women. *Neuropsychol Rev.* (2009) 19:204–14. doi: 10.1007/s11065-009-9093-2
9. Rubin LH, Neigh GN, Sundermann EE, Xu Y, Scully EP, Maki PM. Sex differences in neurocognitive function in adults with HIV: patterns, predictors, and mechanisms. *Curr Psychiatry Rep.* (2019) 21:94. doi: 10.1007/s11920-019-1089-x
10. Barkan SE, Melnick SL, Preston-Martin S, Weber K, Kalish LA, Miotti P, et al. The Women's Interagency HIV Study. WIHS Collaborative Study Group. *Epidemiology.* (1998) 9:117–25. doi: 10.1097/00001648-199803000-00004
11. Bacon MC, Von Wyl V, Alden C, Sharp G, Robison E, Hessol N, et al. The Women's Interagency HIV Study: an observational cohort brings clinical sciences to the bench. *Clin Diagn Lab Immunol.* (2005) 12:1013–9. doi: 10.1128/CDLI.12.9.1013-1019.2005
12. Adimora AA, Ramirez C, Benning L, Greenblatt RM, Kempf MC, Tien PC, et al. Cohort profile: the Women's Interagency HIV Study (WIHS). *Int J Epidemiol.* (2018) 47:393–394i. doi: 10.1093/ije/dyy021
13. Maki PM, Rubin LH, Valcour V, Martin E, Crystal H, Young M, et al. Cognitive function in women with HIV: findings from the Women's Interagency HIV Study. *Neurology.* (2015) 84:231–40. doi: 10.1212/WNL.0000000000001151
14. Rubin LH, Maki PM, Springer G, Benning L, Anastos K, Gustafson D, et al. Cognitive trajectories over 4 years among HIV-infected women with optimal viral suppression. *Neurology.* (2017) 89:1594–603. doi: 10.1212/WNL.0000000000004491
15. Radtke KK, Bacchetti P, Anastos K, Merenstein D, Crystal H, Karim R, et al. Use of nonantiretroviral medications that may impact neurocognition: patterns and predictors in a large, long-term HIV cohort study. *J Acquir Immune Defic Syndr.* (2018) 78:202–8. doi: 10.1097/QAI.0000000000001658
16. Rubin LH, Radtke KK, Eum S, Tamraz B, Kumanan KN, Springer G, et al. Cognitive burden of common non-antiretroviral medications in HIV-infected women. *J Acquir Immune Defic Syndr.* (2018) 79:83–91. doi: 10.1097/QAI.0000000000001755
17. Rubin LH, Cook JA, Springer G, Weber KM, Cohen MH, Martin EM, et al. Perceived and post-traumatic stress are associated with decreased learning, memory, and fluency in HIV-infected women. *AIDS.* (2017) 31:2393–1401. doi: 10.1097/QAD.0000000000001625
18. Greendale GA, Wight RG, Huang MH, Avis N, Gold EB, Joffe H, et al. Menopause-associated symptoms and cognitive performance: results from the study of women's health across the nation. *Am J Epidemiol.* (2010) 171:1214–24. doi: 10.1093/aje/kwq067
19. Rubin LH, Sundermann EE, Cook JA, Martin EM, Golub ET, Weber KM, et al. Investigation of menopausal stage and symptoms on cognition in human immunodeficiency virus-infected women. *Menopause.* (2014) 21:997–1006. doi: 10.1097/GME.0000000000000203
20. Wehrens R, Buydens LMC. Self- and super-organizing maps in R: the Kohonen package. *J. Stat. Softw.* (2007) 21:1–19. doi: 10.18637/jss.v021.i05
21. Fraley C, Raftery A, Scrucca L. *mclust: Normal Mixture Modeling for Model-Based Clustering, Classification, and Density Estimation* (2014).
22. Kuhn M. Building predictive models in R using the caret package. *J. Stat. Softw.* (2008) 28:1–26. doi: 10.18637/jss.v028.i05
23. Torgo L, Torgo M. *Package 'DMwR'*. Comprehensive R Archive Network (2013).
24. Van Buuren S, Groothuis-Oudshoorn K. mice: Multivariate imputation by chained equations in R. *J. Stat. Softw.* (2011) 45:1–67. doi: 10.18637/jss.v045.i03
25. Horan WP, Braff DL, Nuechterlein KH, Sugar CA, Cadenhead KS, Calkins ME, et al. Verbal working memory impairments in individuals with schizophrenia and their first-degree relatives: findings from the Consortium on the Genetics of Schizophrenia. *Schizophr Res.* (2008) 103:218–28. doi: 10.1016/j.schres.2008.02.014
26. McDonald CR, Delis DC, Norman MA, Wetter SR, Tecoma ES, Iragui VJ. Response inhibition and set shifting in patients with frontal lobe epilepsy or temporal lobe epilepsy. *Epilepsy Behav.* (2005) 7:438–46. doi: 10.1016/j.yebeh.2005.05.005
27. Salthouse TA. The processing-speed theory of adult age differences in cognition. *Psychol Rev.* (1996) 103:403–28. doi: 10.1037/0033-295X.103.3.403
28. Scott JC, Woods SP, Carey CL, Weber E, Bondi MW, Grant I, et al. Neurocognitive consequences of HIV infection in older adults: an evaluation of the "cortical" hypothesis. *AIDS Behav.* (2011) 15:1187–96. doi: 10.1007/s10461-010-9815-8
29. Milanini B, Allen I, Javandel S, Joanna H, Paul R, Valcour V. Discriminant analysis of neuropsychological testing differentiates HIV-associated neurocogntive disorder from mild cognitive impairment due to Alzheimer's disease. *Int. Soc. Neurovirol.* (2016) 22:55.
30. Snyder HM, Corriveau RA, Craft S, Faber JE, Greenberg SM, Knopman D, et al. Vascular contributions to cognitive impairment and dementia including Alzheimer's disease. *Alzheimers Dement.* (2015) 11:710–7. doi: 10.1016/j.jalz.2014.10.008
31. Rubin LH, Sundermann EE, Moore DJ. The current understanding of overlap between characteristics of HIV-associated neurocognitive disorders and Alzheimer's disease. *J Neurovirol.* (2019) 25:661–72. doi: 10.1007/s13365-018-0702-9
32. Wallin A, Roman GC, Esiri M, Kettunen P, Svensson J, Paraskevas GP, et al. Update on vascular cognitive impairment associated with subcortical small-vessel disease. *J Alzheimers Dis.* (2018) 62:1417–41. doi: 10.3233/JAD-170803
33. Brands AM, Biessels GJ, De Haan EH, Kappelle LJ, Kessels RP. The effects of type 1 diabetes on cognitive performance: a meta-analysis. *Diabetes Care.* (2005) 28:726–35. doi: 10.2337/diacare.28.3.726
34. Allen RS, Feola A, Motz CT, Ottensmeyer AL, Chesler KC, Dunn R, et al. Retinal deficits precede cognitive and motor deficits in a rat model of type II diabetes. *Invest Ophthalmol Vis Sci.* (2019) 60:123–33. doi: 10.1167/iovs.18-25110
35. Magrinelli F, Picelli A, Tocco P, Federico A, Roncari L, Smania N, et al. Pathophysiology of motor dysfunction in Parkinson's disease as the rationale for drug treatment and rehabilitation. *Parkinsons Dis.* (2016) 2016:9832839. doi: 10.1155/2016/9832839
36. Robertson K, Liner J, Meeker RB. Antiretroviral neurotoxicity. *J Neurovirol.* (2012) 18:388–99. doi: 10.1007/s13365-012-0120-3
37. Letendre S, Marquie-Beck J, Capparelli E, Best B, Clifford D, Collier AC, et al. Validation of the CNS penetration-effectiveness rank for quantifying antiretroviral penetration into the central nervous system. *Arch Neurol.* (2008) 65:65–70. doi: 10.1001/archneurol.2007.31
38. Ellis RJ, Badiee J, Vaida F, Letendre S, Heaton RK, Clifford D, et al. CD4 nadir is a predictor of HIV neurocognitive impairment in the era of combination antiretroviral therapy. *AIDS.* (2011) 25:1747–51. doi: 10.1097/QAD.0b013e32834a40cd
39. Manly JJ, Smith C, Crystal HA, Richardson J, Golub ET, Greenblatt R, et al. Relationship of ethnicity, age, education, and reading level to speed and executive function among HIV+ and HIV– women: the Women's Interagency HIV Study (WIHS) neurocognitive substudy. *J Clin Exp Neuropsychol.* (2011) 33:853–63. doi: 10.1080/13803395.2010.547662
40. Meyer VJ, Rubin LH, Martin E, Weber KM, Cohen MH, Golub ET, et al. HIV and recent illicit drug use interact to affect verbal memory in women. *J Acquir Immune Defic Syndr.* (2013) 63:67–76. doi: 10.1097/QAI.0b013e318289565c

41. Meyer VJ, Little DM, Fitzgerald DA, Sundermann EE, Rubin LH, Martin EM, et al. Crack cocaine use impairs anterior cingulate and prefrontal cortex function in women with HIV infection. *J Neurovirol.* (2014) 20:352–61. doi: 10.1007/s13365-014-0250-x
42. Saloner R, Campbell LM, Serrano V, Montoya JL, Pasipanodya E, Paolillo EW, et al. Neurocognitive superaging in older adults living with HIV: demographic, neuromedical and everyday functioning correlates. *J Int Neuropsychol Soc.* (2019) 25:507–19. doi: 10.1017/S1355617719000018
43. Gustafson DR, Mielke MM, Tien PC, Valcour V, Cohen M, Anastos K, et al. Anthropometric measures and cognition in middle-aged HIV-infected and uninfected women. The Women's Interagency HIV Study. *J Neurovirol.* (2013) 19:574–85. doi: 10.1007/s13365-013-0219-1
44. Rubin LH, Gustafson D, Hawkins KL, Zhang L, Jacobson LP, Becker JT, et al. Midlife adiposity predicts cognitive decline in the prospective Multicenter AIDS Cohort Study. *Neurology.* (2019) 93:e261–71. doi: 10.1212/WNL.0000000000007779
45. Rubin LH, Li Y, Fitzgerald KC, Dastgheyb R, Spence AB, Maki PM, et al. Associations between antiretrovirals and cognitive function in women with HIV. *J Neuroimmune Pharmacol.* (2020). doi: 10.1007/s11481-020-09910-1. [Epub ahead of print].
46. Stankoff B, Calvez V, Suarez S, Bossi P, Rosenblum O, Conquy L, et al. Plasma and cerebrospinal fluid human immunodeficiency virus type-1 (HIV-1) RNA levels in HIV-related cognitive impairment. *Eur J Neurol.* (1999) 6:669–75. doi: 10.1046/j.1468-1331.1999.660669.x
47. Valcour V, Yee P, Williams AE, Shiramizu B, Watters M, Selnes O, et al. Lowest ever CD4 lymphocyte count (CD4 nadir) as a predictor of current cognitive and neurological status in human immunodeficiency virus type 1 infection–the Hawaii aging with HIV cohort. *J Neurovirol.* (2006) 12:387–91. doi: 10.1080/13550280600915339
48. Dawes S, Suarez P, Casey CY, Cherner M, Marcotte TD, Letendre S, et al. Variable patterns of neuropsychological performance in HIV-1 infection. *J Clin Exp Neuropsychol.* (2008) 30:613–26. doi: 10.1080/13803390701565225
49. Rubin LH, Pyra M, Cook JA, Weber KM, Cohen MH, Martin E, et al. Post-traumatic stress is associated with verbal learning, memory, and psychomotor speed in HIV-infected and HIV-uninfected women. *J Neurovirol.* (2016) 22:159–69. doi: 10.1007/s13365-015-0380-9
50. Rubin LH, Springer G, Martin EM, Seaberg EC, Sacktor NC, Levine A, et al. Elevated depressive symptoms are a stronger predictor of executive dysfunction in HIV-infected women than men. *J Acquir Immune Defic Syndr.* (2019) 81:274–83. doi: 10.1097/QAI.0000000000002029
51. Rubin LH, Cook JA, Weber KM, Cohen MH, Martin E, Valcour V, et al. The association of perceived stress and verbal memory is greater in HIV-infected versus HIV-uninfected women. *J Neurovirol.* (2015) 21:422–32. doi: 10.1007/s13365-015-0331-5
52. Pence BW, O'Donnell JK, Gaynes BN. Falling through the cracks: the gaps between depression prevalence, diagnosis, treatment, and response in HIV care. *AIDS.* (2012) 26:656–8. doi: 10.1097/QAD.0b013e3283519aae
53. O'Halloran JA, Cooley SA, Strain JF, Boerwinkle A, Paul R, Presti RM, et al. Altered neuropsychological performance and reduced brain volumetrics in people living with HIV on integrase strand transfer inhibitors. *AIDS.* (2019) 33:1477–83. doi: 10.1097/QAD.0000000000002236
54. O'Halloran JA, Wang K, Williams DW, Dastgheyb R, Fitzgerald K, Kamkwalala A, et al. Integrase inhibitor start or switch impacts learning in women with HIV. In: *Conference on Retroviruses and Opportunistic Infections*. Boston, MA (2020).
55. Amusan P, Power C, Gill MJ, Gomez D, Johnson E, Rubin LH, et al. Lifetime antiretroviral exposures and neurocognitive impairment in HIV. *J Neurovirol.* (2020) 26:743–53. doi: 10.1007/s13365-020-00870-z
56. May PE, Heithoff AJ, Wichman CS, Phatak VS, Moore DJ, Heaton RK, et al. Assessing cognitive functioning in people living with HIV (PLWH): factor analytic results from CHARTER and NNTC cohorts. *J Acquir Immune Defic Syndr.* (2020) 83:251–9. doi: 10.1097/QAI.0000000000002252
57. Rubin LH, Maki PM. Neurocognitive complications of HIV infection in women: insights from the WIHS cohort. *Curr Top Behav Neurosci.* (2019). doi: 10.1007/7854_2019_101

Conflict of Interest: The authors declare that the research was conducted in the absence of any commercial or financial relationships that could be construed as a potential conflict of interest.

frontiers in Neurology

ORIGINAL RESEARCH
published: 12 March 2021
doi: 10.3389/fneur.2021.602263

Neurocognitive Trajectories After 72 Weeks of First-Line Anti-retroviral Therapy in Vietnamese Adults With HIV-HCV Co-infection

Robert H. Paul[1], Cecilia M. Shikuma[2], Nguyen Van Vinh Chau[3], Lishomwa C. Ndhlovu[2,4], Nguyen Tat Thanh[5], Andrew C. Belden[1], Dominic C. Chow[2], Glen M. Chew[2], Thomas A. Premeaux[2,4], Vo Trieu Ly[3,6], Joseph A. D. McBride[1], Jacob D. Bolzenius[1] and Thuy Le[5,7]*

[1] University of Missouri–St. Louis, St. Louis, MO, United States, [2] Hawai'i Center for AIDS, University of Hawai'i at Manoa, Honolulu, HI, United States, [3] Hospital for Tropical Diseases, Ho Chi Minh City, Vietnam, [4] Cornell University School of Medicine, New York City, NY, United States, [5] Oxford University Clinical Research Unit, Ho Chi Minh City, Vietnam, [6] University of Medicine and Pharmacy at Ho Chi Minh City, Vietnam, [7] Duke University School of Medicine, Durham, NC, United States

OPEN ACCESS

Edited by:
Jerel Adam Fields, University of California, San Diego, United States

Reviewed by:
Dianne T. Langford, Temple University, United States
Leah Helane Rubin, Johns Hopkins University, United States

***Correspondence:**
Robert H. Paul
paulro@umsl.edu

Specialty section:
This article was submitted to Neuroinfectious Diseases, a section of the journal Frontiers in Neurology

Received: *23 September 2020*
Accepted: *08 February 2021*
Published: *12 March 2021*

Citation:
Paul RH, Shikuma CM, Chau NVV, Ndhlovu LC, Thanh NT, Belden AC, Chow DC, Chew GM, Premeaux TA, Ly VT, McBride JAD, Bolzenius JD and Le T (2021) Neurocognitive Trajectories After 72 Weeks of First-Line Anti-retroviral Therapy in Vietnamese Adults With HIV-HCV Co-infection. Front. Neurol. 12:602263. doi: 10.3389/fneur.2021.602263

Background: Long-term neurocognitive outcomes following first-line suppressive anti-retroviral therapy (ART) remain uncertain for individuals with HIV and hepatitis C (HCV) co-infection. The study examined neurocognitive performance before and after 72 weeks of ART using repeated multivariate analyses and latent trajectory models.

Methods: One hundred and sixty adults with chronic, untreated HIV infection ($n = 80$ with HCV co-infection and $n = 80$ HIV mono-infected) and 80 demographically similar healthy controls were recruited from the Hospital for Tropical Diseases in Ho Chi Minh City and the surrounding community, respectively. Neurocognitive measures (adapted for use in Vietnam) and liver enzyme tests were compared across groups at baseline. Repeated multivariate and group-based trajectory analyses (GBTA) examined neurocognitive subgroup profiles of the co-infected individuals after 72 weeks of *de novo* efavirenz- ($n = 41$) or raltegravir-based ($n = 39$) ART.

Results: Baseline analyses revealed worse motor function in HIV-HCV co-infected individuals compared to both comparison groups. Longitudinal analyses revealed improved neurocognitive performance by week 48 for most participants regardless of treatment arm. GBTA identified a subgroup (35% of HIV-HCV sample) with persistent motor impairment despite otherwise successful ART. Higher HIV viral load and lower $CD4^+$ T cell count at baseline predicted persistent motor dysfunction. Liver indices and ART regimen did not predict neurocognitive outcomes in HIV-HCV co-infected individuals.

Conclusions: Most HIV-HCV co-infected individuals achieve normative neurocognitive performance after 48 weeks of de novo suppressive ART. However, individuals with more severe HIV disease prior to ART exhibited motor impairment at baseline and 72 weeks

after otherwise successful treatment. Interventions aimed at improving motor symptoms at the time of HIV treatment onset may improve long-term clinical outcomes in HIV-HCV co-infected adults.

Keywords: human immunodeficiency virus, HCV (hepatitis C), co-infection, neurocognition, treatment

INTRODUCTION

As of 2016, 2.3 million cases of HIV-HCV co-infection were reported globally (1). HIV-HCV co-infection disproportionately affects individuals residing in resource-limited settings, where access to direct acting anti-viral treatment for HCV is less readily available (2–5). Recent studies report a high rate of HCV infection among PLWH in Vietnam, with a prevalence of nearly 90% in high-risk subgroups (6, 7). The individual and societal burden of co-occurring HIV and HCV infection is significant. Despite long-term use of anti-retroviral therapy (ART) HIV-HCV co-infected adults report increased use of medical services and level of disability, as well as a greater burden of chronic health complications compared to individuals with HIV mono-infection (8, 9).

HIV-HCV co-infection significantly increases risk for chronic neurocognitive difficulties. Additive or synergistic effects of co-infection have been observed most consistently in the domains of motor, executive function, and learning, with less involvement of core language (e.g., comprehension, reception, repetition), and memory retention abilities (10–14). While mechanisms underlying more neurocognitive difficulties remain unclear, preliminary evidence points toward HCV-associated liver dysfunction as an important contributing factor, particularly in the context of poorly controlled HIV (13, 14). Clifford et al. (11) reported no difference in neurocognitive profiles of HIV-HCV co-infected compared to HIV mono-infected individuals with stable HIV suppression. However, other studies report higher levels of activated $CD4^+$ and $CD8^+$ T cells (15), immune activation (16), and T cell exhaustion (15, 17) in co-infected individuals on stable ART. Additionally, Fabiani et al. (18) reported a significant association between global neurocognitive status and plasma levels of HCV-RNA in co-infected individuals who were receiving suppressive ART. These results suggest that HIV treatment alone does not prevent the development of neurocognitive complications, but longitudinal studies are needed to tease apart neurocognitive profiles of HIV presenting with or without comorbid HCV.

Few studies have examined neurocognitive profiles of co-infected individuals before and after the initiation of suppressive ART. To date, most studies have been cross-sectional in nature and comprised of participants with variable degrees of ART adherence and HIV viral suppression. Additionally, prior work has relied on traditional analytic methods that assume similar rates of neurocognitive sequelae across all co-infected individuals, rather than specific risk subgroups. Analytic methods such as group-based trajectory analysis [GBTA (19)] are sensitive to latent risk phenotypes that differ according to specific underlying mechanisms and have potential to inform novel therapeutic strategies to manage neurocognitive symptoms in this population.

In this study we used multivariate analysis of variance (MANOVA) tests to examine baseline differences on neurocognitive performance (per domain) between the three groups (HIV-HCV, HIV+, and HIV–) at their baseline assessment. Next, we conducted a repeated measures analysis of variance (RM-ANOVA) using data from weeks 0, 24, 48, and 72 within the HIV-HCV group to examine differences in neurocognitive testing performance over time and as a function of treatment arm (i.e., raltegravir vs. efavirenz). Finally, we conducted an exploratory group-based trajectory analysis within the HIV co-infected group to test for latent class groups of individuals following similar neurocognitive trajectories over time and agnostic to treatment arm. We then examined whether belonging to specific neurocognitive latent class trajectories differed in relation to treatment arm, liver function, or HIV disease indices. We hypothesized that viral, immune, and liver indices would predict neurocognitive performance at baseline (pre-ART) and differentiate individual neurocognitive trajectories from baseline through week 72 post-ART.

MATERIALS AND METHODS

Statement of Ethics

The study was approved by the ethics committees of the Vietnam Ministry of Health, the Hospital for Tropical Diseases (HTD) in Ho Chi Minh City (HCMC), University of Hawaii at Manoa in the U.S., and the Oxford University Tropical Research Ethics Committee in the U.K.

Study Participants

160 PLWH (80 with HIV-HCV co-infection) were recruited from the Hospital for Tropical Diseases in Ho Chi Minh City. All participants with HIV reported no history of ART. The HIV-HCV co-infected participants were enrolled in a phase IV randomized, controlled trial comparing raltegravir- vs. efavirenz-based ART on clinical outcomes over 72 weeks (ClinicalTrials.gov Identifier: NCT01147107). Inclusion criteria included: (1) age 18–65; (2) education level $>$ 6 years; (3) able and willing to provide written informed consent; (4) laboratory confirmed HIV; (5) no prior use of ART; and (6) eligible to initiate ART based on guidelines from the Vietnam Ministry of Health during study enrollment from 2014 to 2016 (i.e., $CD4^+$ T cell count $<$350 and/or WHO stage III or IV).

Additional inclusion criteria for HIV-HCV co-infected participants included detectable serum HCV RNA, serum aspartate aminotransferase (AST), alanine aminotransferase (ALT) $\leq$80 U/L, and creatinine clearance $\geq$60 mL/min. Exclusion criteria included: (1) history of anti-viral treatment for HIV or

HCV; (2) positive hepatitis B surface antigen; (3) clinical evidence of de-compensated cirrhosis (e.g., ascites, encephalopathy, esophageal bleeding); (4) history of AIDS-defining illness within the preceding 2 weeks from study entry; and/or (5) possible pregnancy or intent to breastfeed during the study period.

Demographically similar healthy controls ($n = 80$) were recruited from the surrounding community. Inclusion and exclusion criteria were similar between the control group and the two HIV-infected groups, with the exception of HIV and HCV seronegative status. Study participants provided written informed consent following a thorough explanation of study procedures.

HIV Treatment

Following the baseline evaluation, HIV-HCV co-infected participants were randomized to initiate *de novo* ART comprised of emtricitabine and tenofovir combined with either raltegravir ($n = 39$) or efavirenz ($n = 41$). The primary endpoint for the clinical trial was the frequency of AST or ALT toxicities grade >2. The secondary endpoints were HIV RNA <150 copies/mL, change in $CD4^+$ counts, time to AIDS or death, and neurocognitive function. Preliminary analyses over 72 weeks revealed higher rates of hepatotoxicity and a higher number of total adverse events in the efavirenz arm compared to raltegravir arm, but HIV viral suppression was similar in both groups (20).

Neurocognitive Assessment

Neurocognitive evaluations were completed at baseline for all three groups and at follow-up for the HIV-HCV co-infected participants. The test battery was selected based on sensitivity to both HIV and HCV mono-infection as described in prior studies (10, 14, 21), Prior to enrollment, the neurocognitive tests were reviewed for cultural relevance by a consensus panel comprised of local stakeholders in Vietnam (e.g., hospital staff and study personnel) and US investigators. The panel recommended modifications to the verbal learning and memory test and lexical fluency. Modifications to the verbal learning and memory test included replacement of English words with Vietnamese words matched on content meaning, level of familiarity among the target population, degree of abstraction/concreteness, and phonological complexity. Lexical fluency was modified by replacing fluency for English letters (F, A, S) with fluency for first names.

The test battery included the following cognitive domains (see **Supplementary Table 1**): *Psychomotor Speed:* Color Trails 1 (22), and Digit-Symbol (23); *Executive Function:* Digit Span Backward, Color Trails 2 (22), Action Fluency (24), and fluency for first names (25); *Learning and Memory:* total recall on the learning and delayed trials of the Hopkins Verbal Learning Test-Revised [HVLT-R (26)], and Brief Visuospatial Memory Test-Revised [BVMT-R (27)]; *Motor:* Grooved Pegboard dominant and non-dominant hand (28) and gait measured vis-à-vis time to complete a 10-meter midline cross-over walk (29), averaged across three trials.

Alternate test forms were utilized when applicable. Performances on the neurocognitive tests were converted to standardized scores using regression-based norms developed from the uninfected group. Raw scores were utilized as dependent variables in the baseline multivariate analyses, and regression-based standardized scores were utilized to determine the frequency of clinically relevant impairment, defined as z below −1.0.

Mood Assessment

Participants completed the Beck Depression Scale-II [BDI-II (30)], which had been translated into Vietnamese in prior work (31). Total score served as the dependent variable.

Viral and Immunological Indices

$CD4^+$ T cell count, HIV viral load, and HCV viral load (co-infected participants) were performed in real time at the HTD for the HIV-HCV subgroup.

Liver Function

Liver function testing was conducted for HIV-HCV co-infected participants. Dependent variables included serum levels of ALT, AST, alpha-fetoprotein (AFP), and transient liver elastography using FibroScan® (Fibrometer).

Statistical Analysis

Data were analyzed using IBM SPSS 26.0 (Armonk, New York), STATA 14.2 (College Station, Texas), and STATA plugin for estimating group-based trajectory models (32). Preliminary analyses examined missingness, presence of outliers, and non-normal distributions. Age, number of years of education, distribution of sex, and self-reported depression on the BDI-II were compared between the three groups to identify covariates for inclusion in the baseline analyses. Results revealed higher BDI-II scores among co-infected and HIV mono-infected participants compared to healthy controls and higher education among the control group compared to the HIV-infected participants. BDI-II scores were included as a covariate in all multivariate analyses. Education was included in the regression-based standardized scores.

Baseline neurocognitive performances were compared using a series of MANOVAs and MANCOVAs with group (HIV-HCV co-infected, HIV mono-infected, uninfected healthy controls) serving as the independent variable, neurocognitive performance on tests that were grouped by domain (see **Table 1**) as the dependent variables, and BDI-II total score as the covariate. ANOVA tests were used for univariate *post-hoc* comparisons, and False Discovery Rate [FDR (33)] was applied to adjust for multiple comparisons. The percentages of individuals in each group with neurocognitive test performance worse than −1.0 (z score) were compared using Chi Square test. All p-values were considered significant at 0.05 (two sided).

Neurocognitive performances from weeks 0, 24, 48, and 72 were examined for the co-infected group using RM-ANOVA tests. Treatment arm served as the independent variable and z-scored neurocognitive test scores served as the dependent variable. GBTA (19) was used to explore the possibility of latent classes existing within the HIV-HCV subgroup who followed distinct neurocognitive trajectories across the 72-week observation period. The best fit trajectory

TABLE 1 | Baseline demographic and clinical characteristics.

	HIV-HCV ($n = 80$)	HIV($n = 80$)	Controls ($n = 80$)	p-value
Sex (male)	68 (87%)	69 (86%)	62 (78%)	0.191
Age (years)	32 (31–36)	32 (27–37)	31 (24–44)	0.945
Plasma CD4 (cells/μL)	118 (27–280)	–	–	–
Plasma HIV viral load (log10 copies/mL)	5.2 (4.9–5.5)	–	–	
Plasma HCV viral load (log10 copies/mL)	6.6 (5.7–7.2)	–	–	–
Beck Depression Inventory-II	16 (14)	14.50 (12)	7.00 (10)	**<0.0001**
Education				0.437
Secondary school	63 (80.8%)	68 (85.0%)	64 (80.0%)	
High school	8 (10.3%)	7 (8.8%)	13 (16.3%)	
College and above	7 (9.0%)	5 (6.3%)	3 (3.8%)	

Summary statistic is absolute count (%) for categorical variables and median (IQR) for continuous data. Bold values represent statistically significant differences between groups.

group number and shape were determined using Bayesian Information Criterion (34). Posterior probabilities and odds ratios were used to assess overall model fit parameters (35) and are reported in **Supplementary Materials.** Group homogeneity was determined by minimum fit requirements of group average posterior probability >0.7 and odds of correct classification >4.0 (36). Individuals were assigned to the group for which posterior probability of membership was highest. Baseline disease variables, immune indices, ART regimen, liver function test results, demographic variables, and psychosocial factors were tested as possible predictors of latent class trajectory subgroups using multiple linear and logistic regressions.

RESULTS

Sample Characteristics

Demographic characteristics are provided in **Table 1**. Analyses of baseline demographic data revealed no differences in age or the proportion of males to females. As noted above, the HIV-infected groups reported a lower average number of years of education than the uninfected group (∼1-year difference between groups). Significant differences were also observed on the BDI-II, with higher scores reported by co-infected and HIV mono-infected individuals compared to uninfected controls. As expected, co-infected individuals randomized to the raltegravir-based vs. efavirenz-based treatment arms did not differ on baseline levels of plasma HCV RNA, HIV RNA, $CD4^+$ T cell count, AFP, ALT, AST, or Fibroscan (ps > 0.14, effect sizes < 0.02), but did differ on hepatotoxicity (see **Supplementary Tables 2, 3**).

Baseline Neurocognitive Comparisons

Neurocognitive test performances are summarized in **Table 2**. Results from the MANCOVA revealed a significant multivariate effect of group status for the motor domain (Wilks' Lambda = 0.92, F (6, 446) = 2.99, $p < 0.01$). Follow-up univariate analyses revealed a main effect on timed gait ($p = 0.004$), with significantly lower performance among the HIV-HCV co-infected ($p = 0.006$) and HIV mono-infected ($p = 0.03$) group compared to the uninfected controls. No other multivariate comparisons were statistically significant. Follow-up univariate analyses revealed a significant effect of group status on HVLT-R delay ($p < 0.05$). *Post-hoc* analyses using Tukey's test indicated that the HIV-HCV co-infected group performed more poorly than the uninfected controls ($p = 0.03$). Additionally, a main effect of group status was observed on Action Fluency ($p < 0.01$), with the HIV-HCV co-infected group achieving lower scores than the HIV mono-infected ($p = 0.004$) and the uninfected control group ($p = 0.05$). **Supplementary Figures 1–4** provide boxplots of neurocognitive test raw scores by group.

At baseline, the rates of neurocognitive impairment in each domain (see **Table 3**) were as follows: *Psychomotor:* co-infected (9%), HIV mono-infected (8%), and uninfected controls (16%). Low performance on Color Trails 1 accounted for the higher rate of impairment among the healthy controls, but the maximum difference between these groups did not exceed one-half standard deviation. *Executive Function*: co-infected (20%), HIV mono-infected (16%), and uninfected controls (17%). Performance on Action Fluency differed most significantly by group (co-infected, mono-infected, controls: 30%, 10%, 16%, respectively). *Learning and Memory:* co-infected (19%), HIV mono-infected (21%), and uninfected controls (16%). *Motor:* co-infected (24%), HIV mono-infected (20%), and uninfected controls (10%).

Longitudinal Analyses

All HIV-HCV participants achieved undetectable HIV status by week 48. Viral suppression was maintained from week 48 to week 72 with no treatment failures by treatment arm. As reported previously, individuals randomized to efavirenz-based ART exhibited a higher degree of hepatotoxicity and number of adverse events compared to individuals randomized to raltegravir-based ART, but virological suppression did not differ by treatment regimen (20). Results indicated that HCV RNA viral load values did not differ significantly over time between treatment arms (**Supplementary Table 3**). As seen in **Supplementary Table 2**, analyses revealed that liver functioning as measured by Fibroscan, AFP, and AST did not differ significantly over time as a function of treatment arm (RAL vs. EFV). In contrast, ALT values differed significantly over time as a function of treatment arm ($p < 0.01$, $eta^2 = 0.12$). Specifically, participants in the RAL treatment group had lower (healthier)

TABLE 2 | Baseline neurocognitive performance.

Domain/test	HIV-HCV mean (SD)	HIV mean (SD)	Controls mean (SD)	*F*	*p*-Value	Eta^2
Psychomotor				1.02	0.39	0.009
Digit Symbol	45 (15)	46 (16)	42 (16)	1.31	0.27	0.01
Color Trails 1	45 (15)	45 (14)	49 (16)	1.73	0.18	0.02
Executive function				*1.92*	*0.06*	*0.03*
Digits backward	7 (2)	8 (3)	7 (2)	1.67	0.19	0.01
Color trails 2	94 (30)	91 (31)	96 (28)	0.52	0.60	0.005
Action fluency	**10 (4)**	**12 (5)**	**11 (4)**	**5.52**	**0.005**	**0.05**
First name fluency	20 (5)	21 (5)	21 (4)	2.33	0.10	0.02
Learning and memory				1.70	0.10	0.02
HVLT-R learning	*22 (5)*	*24 (6)*	*24 (5)*	*2.97*	*0.05*	*0.03*
HVLT-R delay	**8 (2)**	**8 (3)**	**9 (2)**	**3.09**	**0.04**	**0.03**
BVMT-R learning	22 (7)	24 (7)	23 (7)	1.31	0.27	0.01
BVMT-R delay	9 (3)	9 (3)	9 (2)	0.77	0.57	0.005
Motor				**2.96**	**0.007**	**0.04**
Pegboard dom	66 (10)	64 (12)	64 (14)	1.08	0.34	0.009
Pegboard nondom	73 (15)	70 (14)	73 (16)	1.69	0.19	0.02
Timed gait	**16 (4)**	**16 (4)**	**14 (3)**	**5.60**	**0.004**	**0.05**

Bold values indicate statistically significant differences between groups on that outcome variable. Italics indicate trend level significant difference between HIV groups on a given variable. HVLT-R, Hopkins Verbal Learning Test-Revised; BVMT-R, Brief Visuospatial Memory Test- Revised.

TABLE 3 | Baseline percentages of neurocognitive impairment by group.

	Psychomotor speed	Executive function	Learning and memory	Motor
HIV-HCV	9%	20%	19%	24%
HIV	8%	16%	21%	20%
Controls	16%	17%	16%	10%

Impairment was defined by scoring ≤1.00 standard deviation below the mean.

AST values over time compared to the EFV group. Additional analyses using RM-ANOVA with FDR showed no significant difference between treatment arm over time on depression scores or CD4$^+$ T cell count.

Neurocognitive performances improved on all measures except Color Trails 1 ($p = 0.06$) and Digit Span Backwards ($p = 0.77$). The largest gain in performance occurred between weeks 0 and 48. Repeated measures analyses revealed no significant effect of treatment arm and no interaction between treatment arm and time on any of the neurocognitive measures (**Table 4**). The frequency of neurocognitive impairment at week 72 was significantly lower than the frequency of impairment at baseline. Rates of impairment at week 72 were as follows for the HIV-HCV co-infected group: *Psychomotor* (7%), *Executive Function* (8%), *Learning and Memory* (3%), and *Motor* (9%). The rate of impairment at week 72 did not differ between treatment arms.

GBTA modeled from enrollment to week 72 revealed that the best fitting models for all neurocognitive tests were obtained when using two latent trajectory groups for modeling (see **Supplementary Tables 4–7**). The 2-group latent class trajectories represent HIV-HCV participant clusters defined by higher vs. lower neurocognitive performance over time (minimum threshold requirement for group assignment ≥0.7 for posterior probability and/or ≥4.0 for odds ratio). Closer examination of the trajectories for each neurocognitive test revealed that, in general, both subgroups demonstrated improved performances over time (**Figures 1–4**). However, the low performing trajectory group remained impaired on the timed gait task at week 72 (**Figure 4C**). Results indicated that treatment status predicted latent class trajectories for a single neurocognitive test, Action Fluency. Participants in the RAL treatment arm were approximately four times as likely as participants in the EFV treatment arm to be in the low scoring latent trajectory, OR = 3.82, CI:1.3–11.4 (**Figure 2C**). Baseline demographic variables (i.e., age, sex, or education) were unrelated to trajectory subgroups on any of the individual neurocognitive tests. Regression analyses revealed that baseline lower plasma CD4$^+$ T cell count and plasma viral load predicted membership in the low trajectory group on the timed gait task (variables examined included those listed in **Table 1**).

DISCUSSION

Our study is the first prospective, multi-dimensional investigation of neurocognitive outcomes among PLWH with co-occurring HCV infection before and after *de novo* ART. Consistent with prior studies (37–39), HIV-HCV co-infected

TABLE 4 | Change in neurocognitive performance among HIV-HCV participants.

Domain/tests	*F*	*p*-Value	Effect size Eta^2
Psychomotor			
Digit symbol			
Treatment arm	1.78	0.19	0.03
Time	11.51	**<0.01**	0.35
Interaction	0.29	0.83	0.01
Color trails 1			
Treatment arm	3.03	0.09	0.05
Time	2.84	0.06	0.12
Interaction	0.27	0.85	0.01
Executive function			
Digits backward			
Treatment arm	0.001	0.97	0.001
Time	0.37	0.77	0.02
Interaction	0.86	0.47	0.04
Color trails 2			
Treatment arm	3.35	*0.07*	0.05
Time	19.41	**<0.01**	0.48
Interaction	0.88	0.46	0.04
Action fluency			
Treatment arm	0.70	0.41	0.01
Weeks	9.60	**<0.001**	0.31
Interaction	2.63	0.06	0.11
First Name fluency			
Treatment arm	0.01	0.91	0.001
Weeks	5.63	**0.002**	0.21
Interaction	0.48	0.70	0.02
Learning and Memory			
HVLT-R learning			
Treatment arm	0.14	0.71	0.002
Time	29.10	**<0.01**	0.58
Interaction	0.13	0.94	0.002
HVLT-R delay			
Treatment arm	0.71	0.40	0.01
Time		**<0.01**	0.54
Interaction	24.200.36	0.78	0.02
BVMT-R learning			
Treatment arm	0.81	0.37	0.01
Time	16.46	**<0.01**	0.44
Interaction	0.40	0.75	0.02
BVMT-R delay			
Treatment arm	0.81	0.37	0.01
Time	8.14	**<0.01**	0.28
Interaction	0.14	0.93	0.007
Motor			
Pegboard dominant			
Treatment arm	3.22	*0.07*	0.05
Time	31.38	**<0.001**	0.60
Interaction	0.82	0.49	0.04
Pegboard nondominant			
Treatment arm	3.15	0.08	0.05
Time	5.25	**0.003**	0.20
Interaction	1.19	0.32	0.05
Timed gait			
Treatment arm	0.07	0.80	0.001
Time	7.68	**<0.001**	0.27
Interaction	2.10	0.11	0.09

Significant effects are in bold. Trend level effects p < 0.07 are indicated in italics.

individuals exhibited worse neurocognitive performance at baseline compared to HIV mono-infected individuals and healthy uninfected controls. Additionally, a larger proportion of co-infected individuals met clinical criteria for neurocognitive impairment prior to ART use. Neurocognitive performance improved within 48 weeks of ART onset, but latent trajectory analyses identified a subgroup of HIV-HCV co-infected individuals who demonstrated persistent impairment in the motor domain. Results of this study emphasize the need to investigate variability that exists within groups as a path toward discovery of driving mechanisms. In this study, we utilized group-based trajectory modeling to identify latent phenotypes of higher vs. lower neurocognitive performance. This approach revealed clusters of individuals that were predicted at baseline by differences in $CD4^+$ T cell count and HIV viral load.

Cross-sectional studies report increased severity of neurocognitive complications among PLWH with co-occurring HCV infection. Our study results align with previously reported outcomes in that significant neurocognitive sequelae are prevalent with HIV-HCV co-infection. HCV may potentiate viral-host mechanisms (e.g., monocyte/macrophage activation) of HIV before and after ART initiation. The increased impact of HIV co-infection on brain systems may explain the prevalence of chronic health complications (e.g., frailty) reported in HCV co-infected PLWH receiving ART despite achieving sustained HIV viral suppression (40, 41). Baseline comparisons revealed more severe and clinically relevant neurocognitive symptoms among individuals with co-infection. After controlling for depressive symptoms, PLWH with co-occurring HCV infection exhibited worse performance on measures of motor function and select measures of executive function.

Longitudinal analyses revealed significant gains in neurocognitive performance over 72 weeks of effective ART, with the largest gains observed in the first 48 weeks. The magnitude of change exceeded chance and the slope of improvement exceeded the window in which practice effects from repeat testing are most pronounced. Critically, the magnitude of change in neurocognitive performance was clinically meaningful, as the rate of neurocognitive impairment at week 72 was <10% for each neurocognitive domain. These results confirm hypotheses from prior cross-sectional work (11) suggesting that brain dysfunction associated with co-infection is manifest in the setting of uncontrolled HIV viremia.

Latent models identified distinct neurocognitive phenotypes (higher vs. lower cognitive performance subgroups) that followed and maintained separate trajectories throughout the course of this study. To our knowledge, this is the first study application of latent trajectory modeling to identify subgroups of HIV-HCV co-infection. Results from the GBTA revealed three important findings. First, while the subgroups differed on the degree of neurocognitive complications, both clusters followed a positive trajectory after ART, consistent with improved performance in most domains. Second, baseline neurocognitive status was predictive of trajectory subgroup designation. That is, the low trajectory group demonstrated worse baseline neurocognitive performance. Similar results have been described in prior studies of HIV mono-infection before and after the start of suppressive

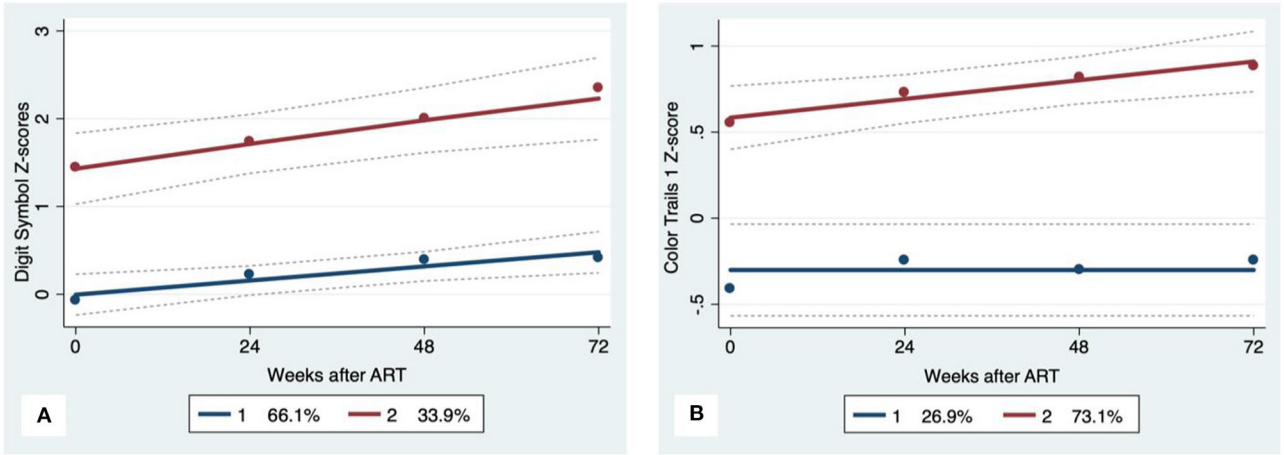

FIGURE 1 | Psychomotor trajectory groups. Solid lines represent estimated trajectories, dot symbols are observed group means at each assessment wave, and dashed lines are 95% pointwise confidence intervals on the estimated trajectories. **(A)** WAIS-III Digit Symbol and **(B)** Color Trails 1.

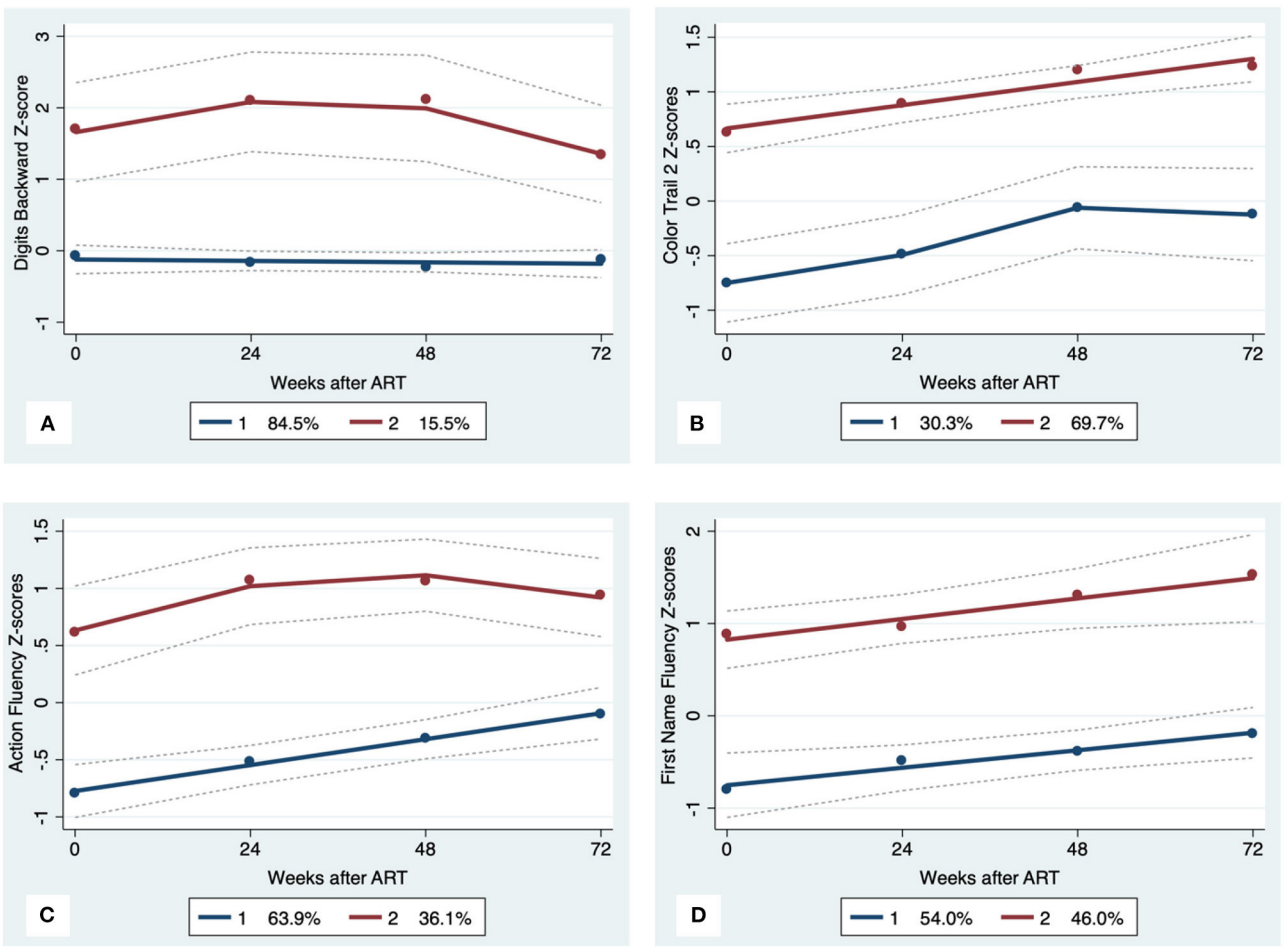

FIGURE 2 | Executive Function trajectory subgroups, Solid lines represent estimated trajectories, dot symbols are observed group means at each assessment wave, and dashed lines are 95% pointwise confidence intervals on the estimated trajectories. **(A)** WAIS-III Digits Backward; **(B)** Color Trails 2; **(C)** Action Fluency; and **(D)** First Name Fluency.

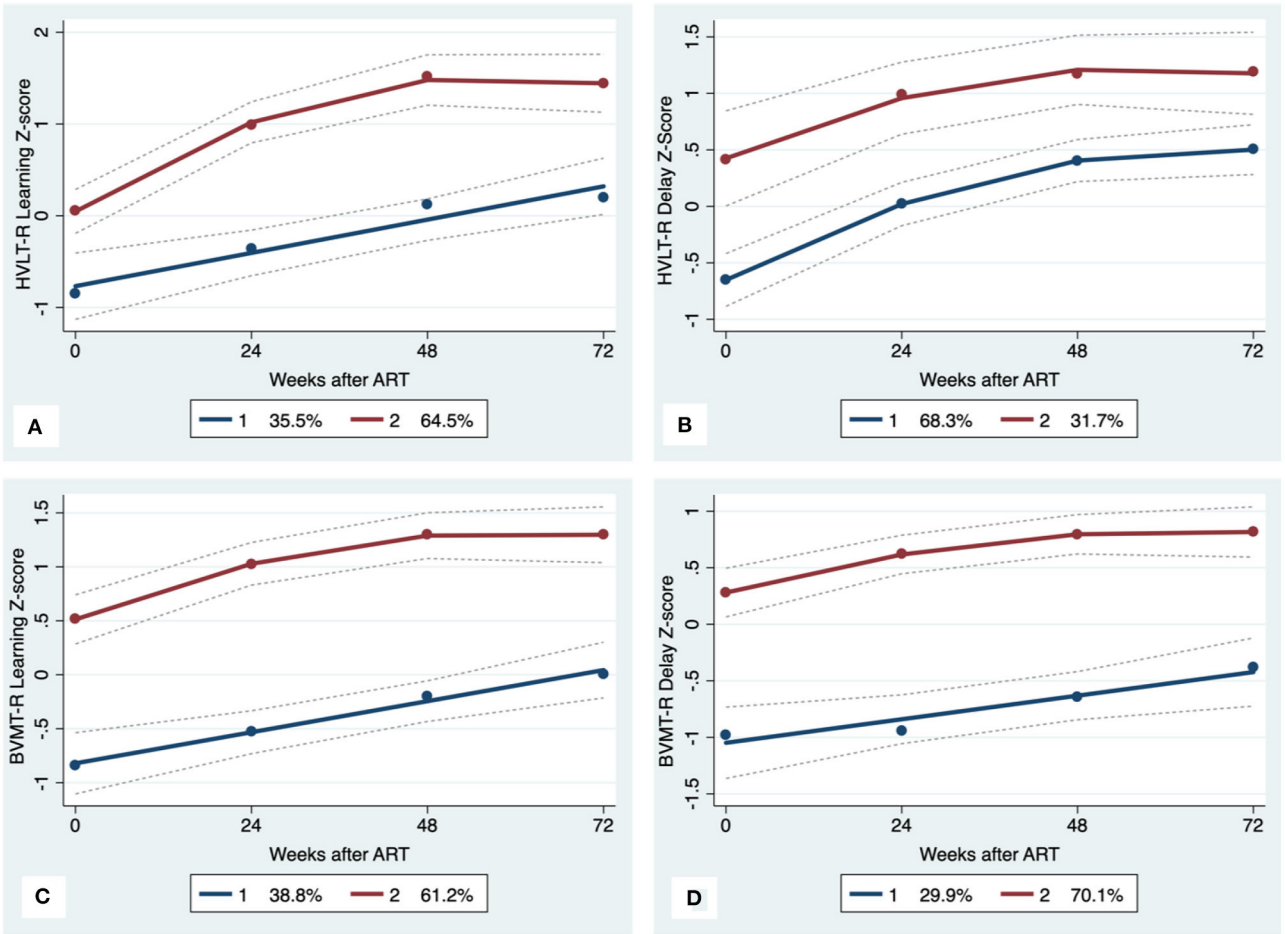

FIGURE 3 | Learning and memory trajectory groups. Solid lines represent estimated trajectories, dot symbols are observed group means at each assessment wave, and dashed lines are 95% pointwise confidence intervals on the estimated trajectories. **(A)** HVLT-R Learning; **(B)** HVLT-R Delay; **(C)** BVMT-R Learning; and **(D)** BVMT-R Delay.

ART (42). Finally, more than one-third of the co-infected group exhibited persistent impairment in motor function despite otherwise successful ART.

The impaired motor performance among individuals with higher HIV viral load and lower plasma $CD4^+$ T cell count at baseline may reflect an early signature of chronic brain dysfunction in co-infected individuals. HCV co-infection is a known predictor of frailty in PLWH receiving suppressive ART (10, 40, 42, 43). Our recent work using machine learning and multi-modal neuroimaging identified evidence of visuomotor dysfunction among PLWH who met clinical criteria for frailty (44). Additional work is needed to define putative causal pathways between HCV co-infection, motor impairment, and frailty in PLWH. Additionally, interventions aimed at supporting motor function at the time of HIV treatment onset may improve long-term clinical outcomes in HIV-HCV co-infected adults.

Results reported in this study represent the first prospective investigation of neurocognitive performance before and after *de novo* ART in a large sample of HIV-HCV co-infected individuals. Additional strengths of the current study include the use of data driven algorithms to examine neurocognitive performance adjusted for demographic variables relevant to the local population. This approach overcomes the limitations of traditional methods that require large samples to stratify data based on assumptions as to how specific factors (e.g., sex, age) impact neurocognitive status. Regression-based norms utilize a quantitative approach to adjust neurocognitive performances for psychosocial factors, which provides a more accurate estimate of brain structure and function. Additional strengths include the comprehensive approach to neurocognitive assessment and use of latent trajectory modeling. Limitations include the absence of comparison groups for longitudinal analysis and the absence of neuroimaging. Additionally, our sample was predominately male, and therefore we did not have sufficient power to examine sex-related differences in outcomes. Longitudinal studies of HIV mono-infected, HCV mono-infected, and uninfected controls are needed, including investigations that incorporate multi-modal neuroimaging. Latent analytic models are encouraged to confirm the relevance of early and persistent motor dysfunction in adults with HIV-HCV co-infection.

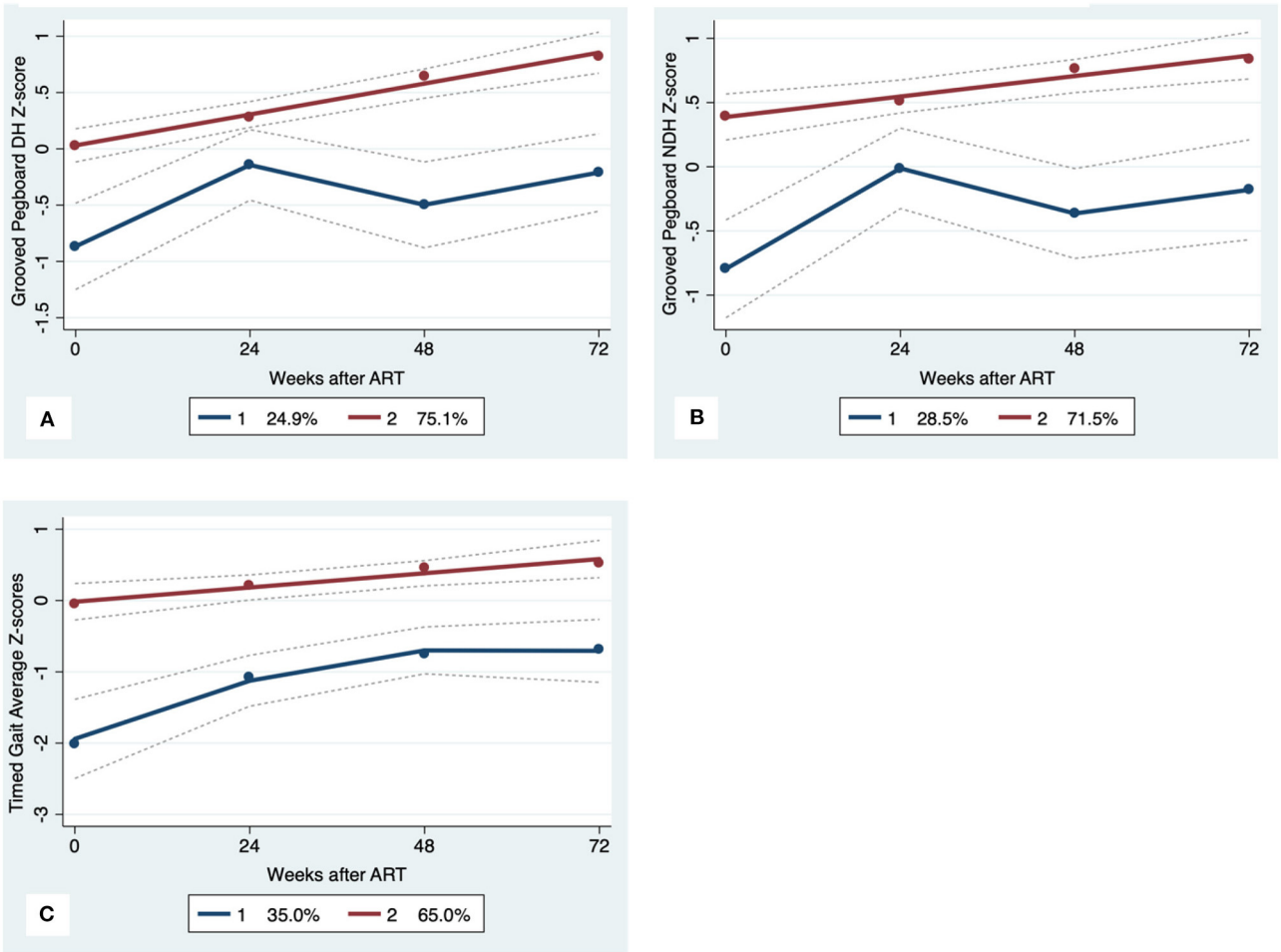

FIGURE 4 | Motor Trajectory subgroups, Solid lines represent estimated trajectories, dot symbols are observed group means at each assessment wave, and dashed lines are 95% pointwise confidence intervals on the estimated trajectories. **(A)** Grooved Pegboard Dominant Hand, **(B)** Grooved Pegboard Non-Dominant Hand; and **(C)** Timed Gait.

DATA AVAILABILITY STATEMENT

The raw data supporting the conclusions of this article will be made available by the authors, without undue reservation.

ETHICS STATEMENT

The studies involving human participants were reviewed and approved by Vietnam Ministry of Health Hospital for Tropical Diseases (HTD) in Ho Chi Minh City (HCMC), University of Hawaii at Manoa in the U.S., and Oxford University Tropical Research Ethics Committee in the U.K. The patients/participants provided their written informed consent to participate in this study.

AUTHOR CONTRIBUTIONS

RP, CS, LN, DC, GC, TP, and VL contributed to conception and design of the study. NC, NT, and VL were responsible for study data collection and interpretation. AB and JB completed data analysis for the proposed manuscript. RP, CS, LN, AB, DC, GC, TP, JM, JB, and TL contributed to drafting the manuscript. TL contributed to conception and design of the study. All authors contributed to manuscript revision and read and approved the submitted version.

FUNDING

The authors declare that this study received funding from Merck and Co. and Gilead Sciences, Inc. The funder was not involved in the study design, collection, analysis, interpretation of data, the writing of this article or the decision to submit it for publication.

ACKNOWLEDGMENTS

We thank the patients who participated in this study. We thank Prof. Nguyen Tran Chinh and Dr. Ngo Thi Kim Cuc from the Hospital for Tropical Diseases in Ho Chi Minh City for providing a dedicated research room and for their overall support of this study. We thank Prof. Guy Thwaites, Prof. Jeremy Day, and the Clinical Trials Unit at the Oxford University Clinical Research

Unit in Vietnam for the outstanding clinical trial support. We thank nurse Hoang Suong Nguyet Anh for her primary role in study enrollment, performing the neurocognitive tests, and participant follow up. We thank Dr. Vu Phuong Thao for providing the data management.

SUPPLEMENTARY MATERIAL

The Supplementary Material for this article can be found online at: https://www.frontiersin.org/articles/10.3389/fneur.2021.602263/full#supplementary-material

REFERENCES

1. Dolan K, Wirtz AL, Moazen B, Ndeffo-Mbah M, Galvani A, Kinner SA, et al. Global burden of HIV, viral hepatitis, and tuberculosis in prisoners and detainees. *Lancet.* (2016) 388:1089–102. doi: 10.1016/S0140-6736(16)30466-4
2. Paris R, Sirisopana N, Benenson M, Amphaiphis R, Tuntichaivanich C, Myint KS, et al. The association between hepatitis C virus and HIV-1 in preparatory cohorts for HIV vaccine trials in Thailand. *AIDS.* (2003) 17:1363–7. doi: 10.1097/00002030-200306130-00010
3. Ruan YH, Hong KX, Liu SZ, He YX, Zhou F, Qin GM, et al. Community-based survey of HCV and HIV coinfection in injection drug abusers in Sichuan Province of China. *World J Gastroenterol.* (2004) 10:1589–93. doi: 10.3748/wjg.v10.i11.1589
4. Strader DB. Coinfection with HIV and hepatitis C virus in injection drug users and minority populations. *Clin Infect Dis.* (2005) 41(Suppl. 1):S7–13. doi: 10.1086/429489
5. Murdock RM, Brizzi MB, Perez O, Badowski ME. Public health considerations among people who inject drugs with HIV/HCV co-infection: a review. *Infect Dis Ther.* (2019) 8:23–32. doi: 10.1007/s40121-018-0228-8
6. Quan VM, Go VF, Nam le V, Bergenstrom A, Thuoc NP, Zenilman J, et al. Risks for HIV, HBV, and HCV infections among male injection drug users in northern Vietnam: a case-control study. *AIDS Care.* (2009) 21:7–16. doi: 10.1080/09540120802017610
7. Nguyen Truong T, Laureillard D, Lacombe K, Duong Thi H, Pham Thi Hanh P, Truong Thi Xuan L, et al. High proportion of HIV-HCV coinfected patients with advanced liver fibrosis requiring hepatitis C treatment in Haiphong, Northern Vietnam (ANRS 12262). *PLoS ONE.* (2016) 11:e0153744. doi: 10.1371/journal.pone.0153744
8. Linas B, Wang B, Smurzynski M, Losina E, Bosch R, Schackman B, et al. The impact of HIV/HCV co-infection on health care utilization and disability: results of the ACTG Longitudinal Linked Randomized Trials (ALLRT) Cohort. *J Viral Hepat.* (2011) 18:506–12. doi: 10.1111/j.1365-2893.2010.01325.x
9. Mattingly TJ, Pandit NS, Onukwugha E. Burden of co-infection: a cost analysis of human immunodeficiency virus in a commercially insured hepatitis C virus population. *Infect Dis Ther.* (2019) 8:219–28. doi: 10.1007/s40121-019-0240-7
10. Paul R, Letendre S, Dearborn J. Impact of hepatitis C coinfection on cognitive outcomes in HIV-infected individuals. *Current Hepatitis Reports.* (2007) 6:145–52. doi: 10.1007/s11901-007-0017-4
11. Clifford DB, Smurzynski M, Park LS, Yeh TM, Zhao Y, Blair L, et al. Effects of active HCV replication on neurologic status in HIV RNA virally suppressed patients. *Neurology.* (2009) 73:309–14. doi: 10.1212/WNL.0b013e3181af7a10
12. Sun B, Abadjian L, Rempel H, Monto A, Pulliam L. Differential cognitive impairment in HCV coinfected men with controlled HIV compared to HCV monoinfection. *J Acquir Immune Defic Syndr.* (2013) 62:190. doi: 10.1097/QAI.0b013e31827b61f1
13. Valcour VG, Rubin LH, Obasi MU, Maki PM, Peters MG, Levin S, et al. Liver fibrosis linked to cognitive performance in HIV and hepatitis C. *J Acquir Immune Defic Syndr.* (2016) 72:266–73. doi: 10.1097/qai.0000000000000957
14. de Almeida SM, de Pereira AP, Pedroso MLA, Ribeiro CE, Rotta I, Tang B, et al. Neurocognitive impairment with hepatitis C and HIV co-infection in Southern Brazil. *J Neurovirol.* (2018) 24:339–49. doi: 10.1007/s13365-018-0617-5
15. Feuth T, Arends JE, Fransen JH, Nanlohy NM, van Erpecum KJ, Siersema PD, et al. Complementary role of HCV and HIV in T-cell activation and exhaustion in HIV/HCV coinfection. *PLoS ONE.* (2013) 8:e59302. doi: 10.1371/journal.pone.0059302
16. Rempel H, Sun B, Calosing C, Abadjian L, Monto A, Pulliam L. Monocyte activation in HIV/HCV coinfection correlates with cognitive impairment. *PLoS ONE.* (2013) 8:e55776. doi: 10.1371/journal.pone.0055776
17. Rallón N, García M, García-Samaniego J, Cabello A, Álvarez B, Restrepo C, et al. Expression of PD-1 and Tim-3 markers of T-cell exhaustion is associated with CD4 dynamics during the course of untreated and treated HIV infection. *PLoS ONE.* (2018) 13:e0193829. doi: 10.1371/journal.pone.0193829
18. Fabiani S, Fallahi P, Ferrari SM, Miccoli M, Antonelli A. Hepatitis C virus infection and development of type 2 diabetes mellitus: systematic review and meta-analysis of the literature. *Rev Endocr Metab Disord.* (2018) 19:405–20. doi: 10.1007/s11154-017-9440-1
19. Nagin DS. *Group-Based Modeling of Development*. Cambridge, MA: Harvard University Press (2005).
20. Le T, Chau NV, Thao VP, Ly VT, Thanh NT, Thu NT, et al. A randomized controlled trial of raltegravir vs. efavirenz-based ART in HIV-HCV coinfection. In: Poster presented at CROI. Boston, MA (2020).
21. Kuhn T, Sayegh P, Jones JD, Smith J, Sarma MK, Ragin A, et al. Improvements in brain and behavior following eradication of hepatitis C. *J Neurovirol.* (2017) 23:593–602. doi: 10.1007/s13365-017-0533-0
22. D'Elia LF, Satz P, Uchiyama CL, White T. *Color Trails Test*. Odessa, FL: Psychological Assessment Resources (1996).
23. Tulsky D, Zhu J, Ledbetter M. *WAIS-III and WMS-III Technical Manual*. San Antonio, TX: The Psychological Corporation (1997).
24. Piatt AL, Fields JA, Paolo AM, Tröster AI. Action (verb naming) fluency as an executive function measure: convergent and divergent evidence of validity. *Neuropsychologia.* (1999) 37:1499–503. doi: 10.1016/s0028-3932(99)00066-4
25. Rosen WG. Verbal fluency in aging and dementia. *J Clin Neuropsychol.* (1980) 2:135–46. doi: 10.1080/01688638008403788
26. Brandt J, Benedict RH. *Hopkins Verbal Learning Test—Revised: Professional Manual*. Odessa, FL: Psychological Assessment Resources (2001).
27. Benedict RH. *Brief Visuospatial Memory Test-Revised.* Odessa, FL: Psychological Assessment Resources (1997).
28. Matthews C, Klove H. *Instruction Manual for the Adult Neuropsychology Test Battery.* Madison, WI: University of Wisconsin Medical School (1964).
29. Chomiak T, Meyer N, Cihal A, Johnson J, Crofts C, Hu B. Correlation between midline gait function performance and verbal fluency in patients with Parkinson's disease. *Aging Clin Exp Res.* (2016) 28:469–73. doi: 10.1007/s40520-015-0426-0
30. Beck AT, Steer RA, Ball R, Ranieri W. Comparison of beck depression inventories-IA and -II in psychiatric outpatients. *J Pers Assess.* (1996) 67:588–97. doi: 10.1207/s15327752jpa6703_13
31. Lin LH, Hung CH. Vietnamese women immigrants' life adaptation, social support, and depression. *J Nurs Res.* (2007) 15:243–54. doi: 10.1097/01.jnr.0000387621.95306.98
32. Jones BL, Nagin DS. A note on a Stata plugin for estimating group-based trajectory models. *Sociol Methods Res.* (2013) 42:608–13. doi: 10.1177/0049124113503141
33. Benjamini Y, Drai D, Elmer G, Kafkafi N, Golani I. Controlling the false discovery rate in behavior genetics research. *Behav Brain Res.* (2001) 125:279–84. doi: 10.1016/s0166-4328(01)00297-2
34. Raftery AE. Bayesian model selection in social research. *Sociol Methodol.* (1995) 25:111–63. doi: 10.2307/271063
35. Van De Schoot R, Sijbrandij M, Winter SD, Depaoli S, Vermunt JK. The GRoLTS-checklist: guidelines for reporting on latent trajectory studies. *Struct Equ Model.* (2017) 24:451–67. doi: 10.1080/10705511.2016.1247646

36. Klijn SL, Weijenberg MP, Lemmens P, van den Brandt PA, Lima Passos V. Introducing the fit-criteria assessment plot—a visualisation tool to assist class enumeration in group-based trajectory modelling. *Stat Methods Med Res.* (2017) 26:2424–36. doi: 10.1177/0962280215598665
37. Hinkin CH, Castellon SA, Levine AJ, Barclay TR, Singer EJ. Neurocognition in individuals co-infected with HIV and hepatitis C. *J Addict Dis.* (2008) 27:11–7. doi: 10.1300/J069v27n02_02
38. Ciccarelli N, Fabbiani M, Grima P, Falasca K, Tana M, Baldonero E, et al. Comparison of cognitive performance in HIV or HCV mono-infected and HIV-HCV co-infected patients. *Infection.* (2013) 41:1103–9. doi: 10.1007/s15010-013-0503-2
39. Miller TR, Weiss JJ, Bräu N, Dieterich DT, Stivala A, Rivera-Mindt M. Greater decline in memory and global neurocognitive function in HIV/hepatitis C co-infected than in hepatitis C mono-infected patients treated with pegylated interferon and ribavirin. *J Neurovirol.* (2017) 23:260–72. doi: 10.1007/s13365-016-0494-8
40. Paul RH, Cooley SA, Garcia-Egan PM, Ances BM. Cognitive performance and frailty in older HIV-positive adults. *J Acquir Immune Defic Syndr.* (2018) 79:375–80. doi: 10.1097/qai.0000000000001790
41. Morgello S, Gensler G, Sherman S, Ellis RJ, Gelman BB, Kolson DL, et al. Frailty in medically complex individuals with chronic HIV. *AIDS.* (2019) 33:1603–11. doi: 10.1097/qad.0000000000002250
42. Cysique LA, Brew BJ. Neuropsychological functioning and antiretroviral treatment in HIV/AIDS: a review. *Neuropsychol Rev.* (2009) 19:169–85. doi: 10.1007/s11065-009-9092-3
43. Cysique LA, Vaida F, Letendre S, Gibson S, Cherner M, Woods SP, et al. Dynamics of cognitive change in impaired HIV-positive patients initiating antiretroviral therapy. *Neurology.* (2009) 73:342–8. doi: 10.1212/WNL.0b013e3181ab2b3b
44. Paul RH, Cho KS, Luckett PM, Strain JF, Belden AC, Bolzenius JD, et al. Machine learning analysis reveals novel neuroimaging and clinical signatures of frailty in HIV. *J Acquir Immune Defic Syndr.* (2020) 84:414–21. doi: 10.1097/QAI.0000000000002360

Conflict of Interest: The authors declare that the research was conducted in the absence of any commercial or financial relationships that could be construed as a potential conflict of interest.

frontiers in Immunology

ORIGINAL RESEARCH
published: 19 May 2021
doi: 10.3389/fimmu.2021.663061

Dopamine Levels Induced by Substance Abuse Alter Efficacy of Maraviroc and Expression of CCR5 Conformations on Myeloid Cells: Implications for NeuroHIV

Stephanie M. Matt[1], *Emily A. Nickoloff-Bybel*[1], *Yi Rong*[1], *Kaitlyn Runner*[1], *Hannah Johnson*[1], *Margaret H. O'Connor*[2,3], *Elias K. Haddad*[2,3] *and Peter J. Gaskill*[1]*

[1] Department of Pharmacology and Physiology, Drexel University College of Medicine, Philadelphia, PA, United States,
[2] Division of Infectious Diseases and HIV Medicine, Drexel University College of Medicine, Philadelphia, PA, United States,
[3] Department of Medicine, Drexel University College of Medicine, Philadelphia, PA, United States

OPEN ACCESS

Edited by:
Serge Nataf,
Université Claude Bernard Lyon 1, France

Reviewed by:
Tobias Zrzavy,
Medical University of Vienna, Austria
Isabella Wimmer,
Medical University of Vienna, Austria

***Correspondence:**
Peter J. Gaskill
pjg63@drexel.edu

Specialty section:
This article was submitted to Multiple Sclerosis and Neuroimmunology, a section of the journal Frontiers in Immunology

Received: 02 February 2021
Accepted: 26 April 2021
Published: 19 May 2021

Citation:
Matt SM, Nickoloff-Bybel EA, Rong Y, Runner K, Johnson H, O'Connor MH, Haddad EK and Gaskill PJ (2021) Dopamine Levels Induced by Substance Abuse Alter Efficacy of Maraviroc and Expression of CCR5 Conformations on Myeloid Cells: Implications for NeuroHIV. Front. Immunol. 12:663061. doi: 10.3389/fimmu.2021.663061

Despite widespread use of antiretroviral therapy (ART), HIV remains a major public health issue. Even with effective ART many infected individuals still suffer from the constellation of neurological symptoms now known as neuroHIV. These symptoms can be exacerbated by substance abuse, a common comorbidity among HIV-infected individuals. The mechanism(s) by which different types of drugs impact neuroHIV remains unclear, but all drugs of abuse increase central nervous system (CNS) dopamine and elevated dopamine increases HIV infection and inflammation in human myeloid cells including macrophages and microglia, the primary targets for HIV in the brain. Thus, drug-induced increases in CNS dopamine may be a common mechanism by which distinct addictive substances alter neuroHIV. Myeloid cells are generally infected by HIV strains that use the chemokine receptor CCR5 as a co-receptor, and our data indicate that in a subset of individuals, drug-induced levels of dopamine could interfere with the effectiveness of the CCR5 inhibitor Maraviroc. CCR5 can adopt distinct conformations that differentially regulate the efficiency of HIV entry and subsequent replication and using qPCR, flow cytometry, Western blotting and high content fluorescent imaging, we show that dopamine alters the expression of specific CCR5 conformations of CCR5 on the surface of human macrophages. These changes are not affected by association with lipid rafts, but do correlate with dopamine receptor gene expression levels, specifically higher levels of D1-like dopamine receptors. These data also demonstrate that dopamine increases HIV replication and alters CCR5 conformations in human microglia similarly to macrophages. These data support the importance of dopamine in the development of neuroHIV and indicate that dopamine signaling pathways should be examined as a target in antiretroviral therapies specifically tailored to HIV-infected drug abusers. Further, these studies show the potential immunomodulatory role of dopamine, suggesting changes in this neurotransmitter may also affect the progression of other diseases.

Keywords: neuroHIV, macrophage, microglia, dopamine, drug abuse, CCR5, maraviroc

INTRODUCTION

While antiretroviral therapy (ART) has been broadly successful, HIV infection remains a global health crisis and HIV-infected individuals are still vulnerable to a wide array of comorbid diseases. Among these are a collection of neurological sequelae, collectively known as neuroHIV, which remain prevalent in infected individuals (1–4). NeuroHIV can be altered and exacerbated by substance abuse (5–8), one of the most common comorbidities in the HIV-infected population (8–15). Substance abuse is associated with altered neuropathology, increased neuroinflammation, cognitive decline and increased neuropsychiatric comorbidities, even with effective ART (16–26). However, the mechanism(s) by which distinct substances of abuse exacerbate these symptoms are unclear. Therefore, delineating these mechanisms is critical to the development of therapies that ameliorate the impact of substance abuse on neuroHIV and other comorbid neuropathologies (27, 28).

Abused substances can dysregulate immune function and increase HIV replication in myeloid cells such as macrophages and microglia (17, 18, 29–31), the primary central nervous system (CNS) targets for HIV infection (32–35). Abused substances can influence CNS myeloid cells by acting directly through surface receptors such as TLR4 (36, 37), or by altering the release of neurotransmitters, immunomodulatory and cytotoxic factors to which myeloid cells could be exposed (38, 39). These effects are prominent in dopaminergic brain regions (40, 41), and in HIV-infected individuals, neuropathology, neuroinflammation and levels of viral replication are elevated in dopamine-rich regions relative to non-dopaminergic areas (35, 42, 43). Different classes of drugs have distinct mechanisms of action, but the use of all addictive substances induces the production of the neurotransmitter dopamine in the mesocorticolimbic system (44, 45). Commonly studied as a central component of the reward or motor pathways, increasing evidence indicates that dopamine also regulates immune function (46–51). Immune cells in the CNS and periphery express all five subtypes of dopamine receptors (DRD1, 2, 3, 4, 5) and other dopamine-related proteins, enabling dopamine to regulate a variety of immune functions in both homeostatic and pathological conditions (52, 53). Exposure to dopamine concentrations induced by substance abuse increases HIV replication by increasing the number of infected macrophages (54–56). Further, dopamine has been shown to alter a variety of other functions that differ by cell type but include modulation of cytokine and chemokine secretion, changes in phagocytic activity, proliferation and chemotaxis (50, 57–60).

Drug abuse is also associated with delayed viral suppression after ART initiation and increased frequency of drug resistance mutations in HIV-infected individuals (61–64). HIV-infected individuals with methamphetamine in their system show increased plasma virus loads only if they were receiving ART, suggesting that recent drug use and ART can interact (65). The mechanistic connection between substance abuse and the HIV progression is not clear, but one connection could be through changes in the HIV co-receptor CCR5. This chemokine receptor generally mediates the entry of HIV virions into myeloid cells such as macrophages or microglia (66, 67), and our prior data show that the impact of dopamine on HIV infection requires CCR5 (55). In addition, both methamphetamine and cocaine increase CCR5 expression in non-human primate (68, 69) and rodent models of substance abuse (70). Cocaine also produces place preference and locomotor activation that are reduced by the ART drug maraviroc (MVC), a CCR5 inhibitor (70). The promoter region of CCR5 has binding sites specific to dopamine-responsive transcription factors (71) and CCR5 deficiency in mice induces both a loss of dopaminergic neurons and microglial activation (72). These and other data indicate that CCR5 expression and function could be altered in HIV-infected substance abusers and suggest a bidirectional interaction between dopamine and CCR5 in the formation of drug-associated behaviors.

The CCR5 receptor exists in several durable, antigenically distinct subpopulations within the plasma membrane (73–75), each representing different physical conformations of CCR5. Changes in conformation regulate the accessibility or binding affinity of certain CCR5 regions to different ligands, altering processes such as receptor endocytosis, G-protein signaling and HIV entry (73, 74). Most of these conformational changes alter binding affinities for either the 2nd extracellular loop (ECL2) or N-terminal (NT) regions of the receptor. These domains are central to receptor interactions with both endogenous ligands (76) and the HIV envelope protein gp120 (77). The distinct conformational subpopulations of CCR5 differentially colocalize to lipid raft regions of the plasma membrane (75), which are important to receptor function (78). Critically, even small changes in CCR5 surface expression mediate distinct biological effects (79–82), so factors that alter the relative proportions of distinct CCR5 conformations could have an outsized biological impact. However, the stimuli mediating conformational shifts in CCR5 are not well understood. Our previous studies indicate that dopamine does not change the surface expression of the CCR5 conformation exposing the ECL2 region (ECL2 CCR5) (55), but in human THP-1 myeloid cells dopamine increases the surface expression of CCR5 exposing the NT region (NT CCR5) (83). This suggests drug-induced increases in dopamine could alter the expression, conformation and/or localization of CCR5 on myeloid cells, altering both the spread of HIV infection and therapeutics that specifically target the viral entry process.

To address this, we examined the impact of drug-induced dopamine levels on HIV infection and CCR5 expression and conformation in both human macrophages and microglia. Our data show that dopamine has bimodal effects on the CCR5 inhibitor Maraviroc on HIV infection in human monocyte-derived macrophages (hMDM), reducing its effectiveness in hMDM from some individuals and enhancing its effectiveness in others. Genetic analyses show that dopamine receptor expression significantly correlates with CCR5 expression in hMDM. Analysis of specific CCR5 conformations on the hMDM surface demonstrate that short term dopamine significantly increases the expression of the CCR5

conformation exposing the NT CCR5 region, and that more long term exposure to dopamine increases both NT and ECL2 CCR5. High-content imaging across hMDM populations indicates that dopamine can increase the number of individual cells expressing higher amounts of NT and ECL2 CCR5. Additionally, dopamine-mediated increases in both HIV infection and NT CCR5 expression were seen in iPSC-derived microglia and a human microglial cell line. These data demonstrate that dopamine levels induced by substance abuse increase HIV infection and can alter effectiveness of ART targeting CCR5, potentially through changes in the surface expression of different CCR5 conformations in multiple types of myeloid cells.

METHODS

Reagents

RPMI-1640 and DMEM media, sodium pyruvate, trypsin, penicillin/streptomycin (P/S) and TrypLE were from Invitrogen (ThermoFisher, Carlsbad, CA, USA). Bovine serum albumin (BSA) and glycine were from Fisher Scientific (Waltham, MA, USA). Tween, dimethyl sulfoxide (DMSO), and hydroxyethyl piperazineethanesulfonic acid (HEPES) were obtained from Sigma-Aldrich (St. Louis, MO, USA). Fetal calf serum (FBS) was from Corning (cat # MT35010CV) and human AB serum was from Gemini Bio-Products (cat # 100-512). Paraformaldehyde (16%) was from Electron Microscopy Sciences (cat # 50980488). Macrophage colony stimulating factor (M- CSF), IL-34, TGF-β1, and IL-10 were from Peprotech (Rocky Hill, NJ, USA). The CCR5 inhibitor, Maraviroc (cat #11580) was obtained through the NIH AIDS Reagent Program, Division of AIDS, NIAID, NIH. Maraviroc was diluted to a stock concentration of 10 mM in DMSO and stored at -80°C prior to use. Dopamine hydrochloride (DA), from Sigma-Aldrich, was resuspended in diH_2O as a 10 mM stock and stored at -20°C prior to use. All dopamine treatments were performed in the dark using 10^{-6}M dopamine, unless otherwise noted, as this is the concentration of dopamine to which CNS myeloid populations could be exposed to during the abuse of substances such as cocaine and methamphetamine (52). Dopamine can oxidize and form reactive oxygen species *in vitro* (84, 85), but our previous data show that the impact of dopamine on HIV infection of macrophages is not affected by dopamine oxidation (54).

Generation of Primary Macrophages From Human Donors

Human peripheral blood mononuclear cells (PBMC) were separated from blood obtained from de-identified healthy donors (New York Blood Center, Long Island City, NY, USA or the University of Pennsylvania Human Immunology Core, Philadelphia, PA, USA) by Ficoll-Paque (GE Healthcare, Piscataway, NJ, USA) gradient centrifugation. PBMC were isolated and matured into monocyte-derived macrophages (hMDM) using adherence isolation. Cells were cultured for 6-7 days in macrophage media (RPMI-1640 with 10% FBS, 5% human AB serum, 10 mM HEPES, 1% P/S, and 10 ng/mL M-CSF). Limited, de-identified demographic information obtained from the New York Blood Center and Penn for each donor, including age, gender, ethnicity, blood type and CMV status are found in **Table 1**. All data categories were not available for each donor, and medication, history of surgery, alcohol use and drug use status were not available. The entire data set of 88 donors was used to determine the relative expression of dopamine receptors, but not all demographic information was disclosed for every donor so not every donor was used for every correlation. Dopamine receptor expression from subsets of these donors have been previously published (50, 56) and this study examines all donors combined from previous studies as well as new donors used in this study. Our previous studies using hMDM indicated that a large data set was needed to examine correlations with dopamine receptors due to the variability inherent in primary human macrophages (50).

Differentiation and Culture of Human iPSC-Derived Microglia

The inducible pluripotent stem-derived microglia (iMicroglia) were generated from common myeloid progenitors obtained from the Human Pluripotent Stem Cell Core at the Children's Hospital of Philadelphia (CHOP). This process used a defined 11-day differentiation protocol that produces ramified cells that are susceptible to HIV infection and express the microglial markers CX_3CR_1, IBA1, TMEM119, and P2RY12, with very similar gene expression to human microglia (86). The cells used in this study were derived from the WT6 iPSC cell line. These cells were differentiated and maintained in 24 or 96 well Cellbind plates (Fisher Scientific) in RPMI-1640 supplemented with 1% FBS, 0.1% P/S, and the cytokines IL-34 (100 ng/mL), M-CSF (25 ng/mL), and TGF-β1 (50 ng/mL) at 37°C in a humidified incubator under 5% CO_2. Cytokines were added

TABLE 1 | Demographic characteristics of donors (N=88).

Variable	Statistic
Age (years)[ab]	39.7 (16) [16-71]
Ethnicity	
Caucasian	33%
African-American	13.6%
Hispanic/Latino	12.5%
Asian	6.8%
Multi-Race	1.1%
Not disclosed	33%
Gender (% men)[b]	51.9%
Blood Type	
O+	39.8%
A+	20.5%
O-	10.2%
B+	10.2%
A-	1.1%
B-	1.1%
Not disclosed	17%
CMV status (% +)[c]	50.7 %

[a]*Mean (standard deviation) [range].*
[b]*Statistic based on 79/88 donors.*
[c]*Statistic based on 73/88 donors.*

fresh with each media change. The C06 human microglial cells (87) were a generous gift from David Alvarez-Carbonell and Jonathan Karn (Case Western University). These cells were maintained in 150-cm^2 tissue culture flasks (Falcon) in DMEM supplemented with 5% FBS, 10 mM HEPES, 1% P/S, and 1% sodium pyruvate at 37°C in a humidified incubator under 5% CO_2.

Viral Stocks

Viral stocks of HIV_{ADA} were generated by infecting CEM-SS cells with HIV_{ADA}, a blood-derived, R5-tropic strain of HIV (88). Cell-free supernatants were collected daily from 18 to 41 days post-infection, centrifuged to remove cell debris then aliquoted and stored at -80°C for use as viral stocks. Stock concentration was determined by quantifying the amount of HIV capsid protein p24Gag (p24) per mL using an HIV p24 (high sensitivity) AlphaLISA Detection kit (Perkin-Elmer, Waltham, MA).

Replication Assay

Human monocyte-derived macrophages (hMDM) cultured in Nunc™ MicroWell™ 96-well optical-bottom plates (Thermo Fisher Scientific, Waltham, MA) at 24,000 cells per well were inoculated in triplicate with 0.5 ng/ml HIV_{ADA} for 24 hours at 37°C. Inoculations were performed concurrently with treatment with either vehicle (DMSO), maraviroc, and/or dopamine (10^{-6}M). After 24 hours, hMDM were washed and replaced with fresh macrophage media. Supernatants were collected from each well at 3 days post-inoculation. The iPSC-derived Microglia (iMicroglia) were cultured in black walled, 96-well Cellbind plates (Fisher Scientific, 0720196) at 50,000 cells per well. iMicroglia were inoculated in triplicate with 1 ng/ml HIV_{ADA} for 24 hours, concurrent with treatment with either vehicle (diH_2O) or dopamine (10^{-6}M). After 24 hours, cells were washed and cultured for 10 days, collecting supernatant and acquiring brightfield images at 10x with a Nikon Inverted Microscope Eclipse Ts2. The C06 microglial cells were cultured in 24-well plates (Fisher Scientific, 087721) at 2,500 cells per well. These cells were inoculated with 2.5 ng/ml HIV_{ADA} in triplicate concurrent with vehicle (diH_2O) or dopamine (10^{-6}M) treatment. Media was changed 48 hours post inoculation, and a fraction of the starting media was collected from each well every 24 hours starting at 48 hours post-inoculation. Viral replication in all cultures was determined by quantifying the concentration of p24 in the supernatant by AlphaLISA (Perkin-Elmer), as supernatant p24 directly corresponds to production of HIV virions.

Quantitative RT-PCR

Total RNA was extracted from cultured cells using Trizol (Invitrogen) or the RNeasy Mini Plus™ kit (Qiagen), and RNA quantity and purity were determined using a NanoDropOne spectrophotometer (Nanodrop Technologies). cDNA synthesis was performed on RNA (1 µg) using the high-capacity reverse transcriptase cDNA synthesis kit (Abcam). All dopamine receptor subtypes, CCR5, and 18s (housekeeping gene) were amplified from cDNA by quantitative PCR (qPCR) on a QuantStudio 7 using gene-specific primers. TaqMan Fast Universal Master Mix, and PCR assay probes for CCR5 (Hs99999149_s1), DRD1-5 (Hs00265245_s1, Hs00241436_m1, Hs00364455_m1, Hs00609526_m1, Hs00361234_s1), and 18s (4319413E) genes were purchased from Applied Biosystems (ThermoFisher, Waltham, MA, USA).

Flow Cytometry

Human monocyte-derived macrophages (hMDM) cultured in 6-well plates at 950,000 cells per well were treated for 1 hour or 48 hours with vehicle (diH_2O), dopamine (10^{-6} M) or IL-10 (50 ng/mL) as a positive control (79). Following incubation, hMDM were gently detached from culture dishes using TrypLE Express (1X) for 30 minutes at 37°C and washed with FACS buffer (PBS supplemented with 1% BSA). Cells were incubated at room temperature for 10 min in F_c Block, then with live/dead stain (ThermoFisher, cat # L34957) for an additional 15 min at 4°C in the dark. Following incubation, cells were washed and stained with either 2D7 anti-human CCR5-PE (20 µL, BDB555993), 3A9 anti-human CCR5-PE (20 µL, BDB556042) or the isotype-matched control IgG2a-PE (20 µL, BD Biosciences, cat # 556653). These antibodies were titrated to determine optimal concentration for hMDM and have been used to study dopamine-mediated changes in surface CCR5 in myeloid cells (55, 83) and to compare ECL2 CCR5 with NT CCR5 (89). Staining was performed for 30 min in the dark at 4°C in a volume of 100 µL. After 30 min, cells were washed with FACS buffer, fixed with 500 µL 2% paraformaldehyde, filtered using BD FACS tubes with cell strainer caps (35 µm pores) and stored at 4°C protected from light. During data acquisition, doublets were excluded using forward scatter height (FSC-H) *vs.* forward scatter area (FSC-A) gating. Forward versus side scatter (FSC *vs.* SSC) was used to identify cells of interest based on size and granularity. Live-dead staining was used to exclude cell debris. Isotype controls defined background caused by nonspecific antibody binding, and percentage of CCR5 positive cells was based off of this background removal. Flow cytometric analysis of C06 cells at 1 hour was performed identically to hMDM, except that these cells were seeded in 6-well plates at 500,000 cells per well and experiments were performed 24 hours after plating. All samples were acquired on a BD LSRFortessa (BD Biosciences, Franklin Lakes, NJ). All data was analyzed using FlowJo Version 10.

Western Blot

Human monocyte-derived macrophages (hMDM) were cultured in 6-well plates at 950,000 cells per well and C06 cells were cultured in 6-well plates at 500,000 cells per well. All hMDM used in these experiments demonstrated IL-10-mediated increases in CCR5 surface expression by flow cytometry. Both hMDM and C06 cells were incubated with vehicle (H_2O) or dopamine (10^{-6} M) for 1 hour, washed (1X PBS) and lysed with mammalian protein extraction reagent (M-PER, Thermo Fisher Scientific, Waltham, MA), containing 1% Halt Protease and Phosphatase Inhibitor cocktail and 1% EDTA (Thermo Fisher Scientific, Waltham, MA). Lysates were sonicated with a Q125 sonicator (Qsonica, Newtown, CT) at 25% power for 5 seconds and spun down at 13,000 RPM for 10 minutes at 4°C. Lysates

were stored at 4°C for 1 – 7 days, then protein concentrations were quantified using a Bicinchoninic acid assay (BCA) using the Pierce BCA Protein Assay Kit (Thermo Fisher Scientific). Lysates were diluted to a concentration of 1 – 3 μg/μL and stored at -80°C until analyzed by Western blot.

Protein lysates were separated by gel electrophoresis on Bolt Bis-Tris Plus 10% precast gels in MOPS/SDS running buffer in a Mini gel tank (Life Technologies, Carlsbad CA). Separation was performed for 120 minutes at 150V, then protein was transferred to an Immobilon PVDF membrane (EMD Millipore, Temecula, CA) at 25V for 60 minutes. To generate an internal loading control, membrane was imaged after treatment with Revert Total Protein Stain (LI-COR Biosciences, Lincoln, NE) according to the manufacturer's instructions. Total protein stain was then removed, membranes were blocked (5% BSA at room temperature for 1 hour) then incubated overnight at 4°C in anti-CCR5 antibody (AB1889, 1:1000 in 5% BSA, EMD Millipore). Following primary antibody incubation, blots were washed (TBS with 0.1% Tween), stained with anti-rabbit IgG HRP linked antibody (CST 7074, 1:3000 in 5% milk) and incubated at room temperature for 1 hour. After secondary incubation, blots were washed and incubated in Supersignal West Pico PLUS plus Chemiluminescent Substrate (2 mL, 30 sec, ThermoFisher, 34580). Blots were imaged using an Odyssey Fc Imaging System and analyzed using Image Studio Lite (Licor Biosciences, Lincoln, NE). Target bands were normalized to total protein stain, and then each condition was compared to the vehicle control to determine fold-change in expression.

Immunofluorescent Analysis of CCR5

Human monocyte-derived macrophages (hMDM) were cultured in Nunc™ MicroWell™ 96-well optical-bottom plates (Thermo Fisher Scientific, Waltham, MA) at 24,000 cells per well. All cells were treated with vehicle (H_2O), IL-10, or 10^{-6}M dopamine in triplicate for 1 hour. Following treatment, cells were fixed (4% PFA at room temperature for 10 minutes, 50980488, Fisher Scientific), then incubated with wheat germ agglutinin (10 μg/mL, 10 min, W32466, Thermo Fisher). The hMDM were incubated with blocking buffer (1% BSA, 0.1% Tween 20, and 22.52 mg/mL glycine in 1XPBS) for 30 minutes at room temperature. For analysis of CCR5 surface expression, cells were incubated with primary antibodies overnight at 4°C, using either 2D7 (ECL2) CCR5 antibody (BDB555991, Fisher Scientific) or primary 3A9 (NT) CCR5 antibody (BDB556041, Fisher Scientific) made in blocking buffer. Following primary incubation, hMDM were incubated with either Alexa Fluor 488 secondary antibody (A-11001, Fisher Scientific) or Alexa Fluor 546 secondary antibody (A-11003, Fisher Scientific) made in blocking buffer for 1 hour at room temperature. All cells were then stained with DAPI (D1306, Fisher Scientific) for 10 minutes. Images were acquired on the CellInsight CX7 High Content Screening Platform (CX7), an automated 7-channel confocal microscope. Ten fields per well were imaged using a 10x objective, and images were analyzed using HCS software.

For analysis of CCR5 colocalization with lipid rafts, hMDM were treated with vehicle (H_2O) or 10^{-6}M dopamine in triplicate for 1 hour, fixed and incubated with blocking buffer as just described, and then incubated with primary 2D7 (ECL2) CCR5 antibody or primary 3A9 (NT) CCR5 antibody, primary CD71 antibody (sc-32272, Santa Cruz Biotechnology Santa Cruz, CA), and anti-Flotillin-1 antibody (BDB610820, Fisher Scientific BDB610820). All primary antibody incubations were performed in blocking buffer overnight at 4°C. Following primary incubation, hMDM were washed and incubated for 1 hour at room temperature in either Alexa Fluor 568 secondary antibody (A-11004, Fisher Scientific A-11004), Alexa Fluor 488 secondary antibody, or Alexa Fluor 647 secondary antibody (A-21235, Fisher Scientific), made in blocking buffer. Cells were then stained with DAPI and imaged on the CX7. For each well, 100 field images were taken using a 40X objective at an exposure time of 0.1 seconds, and images were analyzed using HCS software. More detailed methodology for High Content imaging and analyses is included in the **Supplemental Materials**.

Statistical Analysis

To determine the appropriate statistical tests, all data sets were evaluated by analysis of skewness and evaluation of normality to determine the distribution of the data. Extreme data points presumed to be technical outliers were identified *via* ROUT test (Q = 0.1%) and removed from analysis. *Post-hoc* analyses were performed when appropriate. In studies analyzing gene expression, all statistical tests were performed on data normalized to $2^{-\delta C_T}$ to preserve variance. In all experiments using a positive control, changes in the positive control were not analyzed alongside the experimental condition. Therefore, while the effects mediated by the positive control IL-10 are shown on the same graph as dopamine-mediated changes, since the effects of IL-10 were analyzed separately, they are shown by the @ sign, rather than the * used to show significance in the analyses of dopamine-mediated changes. All data analysis was performed using GraphPad Prism 9.0 (Graphpad, La Jolla, CA). $p < 0.05$ was considered significant.

RESULTS

Dopamine Alters Effectiveness of Maraviroc in HIV-Infected hMDM

Substances of abuse can decrease the effectiveness of antiretroviral drugs (65), including maraviroc (90), the only FDA approved antiretroviral drug that targets CCR5. To determine whether dopamine was associated with this effect, hMDM from 12 donors were inoculated with HIV_{ADA} (0.5 ng/mL) for 24 hours in the presence of vehicle (diH_2O or DMSO), dopamine (10^{-6}M), maraviroc (MVC) or MVC + dopamine (10^{-6}M). MVC was used at 0.1 or 1 μM, based on approximate blood molarity from c_{max} plasma values resulting from commonly prescribed doses of MVC (150 or 300 mg/day) (91, 92). Supernatant from each infection was collected on day 3 and examined for the presence of p24 as a measure of viral replication. As expected, analysis showed variations in infection between individuals (93, 94), but also showed dopamine significantly increased HIV infection alone relative

to the mean of vehicle-treated, HIV-infected cells, similar to our prior data (54–56) (**Figure 1A**). Individual donors are designated with a specific color throughout **Figure 1**, showing dopamine increased p24 levels in hMDM from 10 of the 12 donors examined. We also examined whether MVC successfully suppressed viral replication, and at both 0.1 μM (**Figure 1B**) and 1μM (**Supplementary Figure 1A**), MVC significantly decreased p24 levels relative to the mean of vehicle-treated, HIV-infected cells.

To examine dopamine-mediated changes in the efficacy of MVC, we compared the mean day 3 p24 levels in HIV-infected hMDM treated with MVC to the p24 levels in HIV-infected hMDM treated with MVC and dopamine. Donors were defined as having a diminished or enhanced response to MVC if the addition of dopamine resulted in a greater than 10% change from the p24 level in the HIV+MVC condition. This analysis showed a bimodal response to dopamine in hMDM treated with 0.1 μM MVC (**Figure 1C**). hMDM from 5/12 (46.7%) donors showed a diminished response to MVC, with significantly higher levels of p24 in cultures treated with dopamine. Similarly, 5/12 (46.7%) showed an enhanced response to MVC, with relatively lower p24 levels in cultures treated with dopamine. In 2/12 donors (16.6%) dopamine did not alter the efficacy of MVC. Although not significant, similar results were obtained in the 1 μM MVC experiments (**Supplementary Figure 1B**). These data suggest that individual variations in the response to dopamine could alter the effectiveness of MVC, changing the efficacy of antiretroviral therapy in HIV-infected substance abusers.

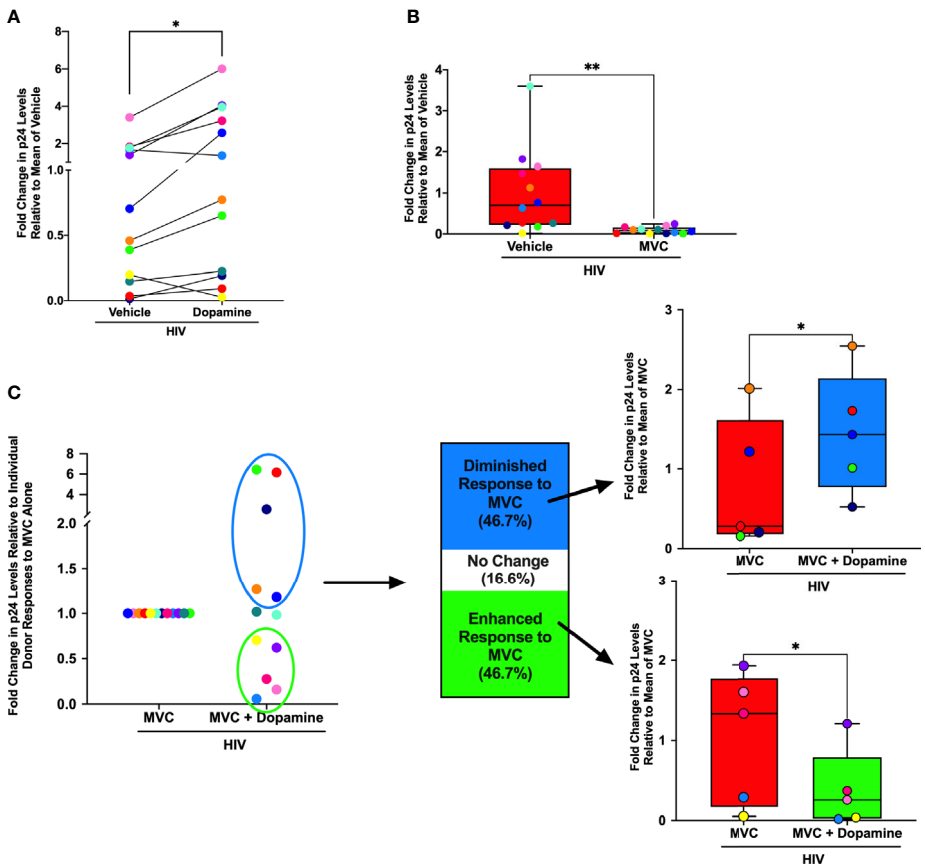

FIGURE 1 | Dopamine Alters Effectiveness of Maraviroc in HIV-infected hMDM. Primary human monocyte-derived macrophages (hMDM) from twelve donors were inoculated with HIV_{ADA} (0.5 ng/mL) for 24 hours in the presence of vehicle (diH_2O or DMSO), a dopamine (10^{-6}M) condition maraviroc (MVC) (0.1 μM) or MVC + dopamine (10^{-6}M). Infections were maintained in culture for 3 days, at which point supernatants were collected and examined for levels of HIV replication (p24). Responses from each donor are designated with a specific color throughout. **(A)** When examining fold change in p24 levels relative to the mean of vehicle treatment, dopamine significantly increased HIV infection alone (Paired t-test, n = 12, *p = 0.0162, t=2.835, df=11). **(B)** When examining fold change in p24 levels relative to the mean of vehicle treatment, MVC also successfully suppressed viral replication at 0.1μM, in that MVC significantly decreased p24 levels relative to HIV alone (Paired t-test, n = 12, **p = 0.008, t=3.229, df=11). **(C)** When examining fold change in p24 levels relative to individual donor responses to MVC treatment alone, there was a bimodal response to dopamine in hMDM treated with 0.1 μM MVC. Compared to the p24 levels relative to the mean of MVC alone, five out of twelve donors (46.7%) showed a dopamine-mediated diminished response to MVC (Paired t-test, n = 5, *p = 0.0391, t=3.021, df=4), and five out of twelve donors (46.7%) showed a dopamine-mediated enhanced response to MVC (Paired t-test, n = 5, *p = 0.049, t=2.796, df=4). Two of the twelve donors (16.6%) showed no response to dopamine in respect to the efficacy of MVC.

As differences in dopamine receptor levels can contribute to donor-specific responses to dopamine (50), the donor responses to MVC and/or dopamine were compared to expression of all five subtypes of dopamine receptors (D1-like, DRD1 and DRD5; and D2-like, DRD2, 3, 4). These correlations were performed using expression of dopamine receptor transcripts by qPCR due to the lack of effective antibodies against human dopamine receptors and the inability of existing antibodies to differentiate between DRD1 and DRD5. These analyses showed no significant correlations between dopamine receptor expression and response to MVC. As age has also been shown to affect ART efficacy (95), the fold change response to dopamine and MVC was also compared to age. Although not statistically significant, the average age for the group that had a diminished response to MVC was 50.2, and the oldest donor (red dots) had the largest fold change increase in p24 levels relative to the MVC only condition. In the group that had an enhanced response to MVC, the average age was 42.8, and in this group the oldest donor had the smallest fold change decrease in p24 levels relative to the MVC only condition (yellow dots).

Expression of CCR5 Correlates With Dopamine Receptor Expression in hMDM

Both dopamine receptors and associated proteins play a role in regulating CCR5 expression in multiple cell types (83, 96). To more precisely define the connection between the effects of dopamine and maraviroc efficacy, we examined the relationship between dopamine receptors and CCR5, using the expression levels of CCR5 and all five subtypes of dopamine receptors on uninfected hMDM from a large group of donors (N = 88) with the available demographic details shown in **Table 1**. Not all demographic details were available for every donor, so the specific numbers of donors used for each analysis are noted in the table. Gene expression analysis confirmed our previous findings showing that hMDM can express mRNA for all five subtypes of dopamine receptors, with wide variation in expression levels between donors. DRD5 is the only receptor expressed on every donor, and was significantly greater than expression of DRD1 and D2-like receptors across all donors (**Figure 2A**).

In the subset of donors for whom CCR5 expression data was available (N = 65), analyses showed a positive trend between CCR5 and age (**Supplementary Figure 2A**), corroborating other studies (97). The data also showed that females have greater CCR5 expression than males (**Supplementary Figure 2B**), which could be due to the modulation of CCR5 by sex hormones such as progesterone and estrogen (98, 99). And infection with cytomegalovirus (CMV), which is common in the adult population, can increase CCR5 expression (100), and the donors who were CMV+ had greater CCR5 expression compared to the donors that were CMV- (**Supplementary Figure 2C**).

This cohort was then used to generate a correlation matrix comparing expression between individual dopamine receptors and CCR5. There was a significant positive correlation between CCR5 and both DRD1 and DRD5 (**Figure 2B**), as well as a weaker, but still significant, negative correlation with CCR5 and DRD3 (**Figure 2B**). There were no correlations between expression of DRD2 or DRD4 and CCR5. To account for the lack of DRD3 and DRD4 expression in a number of donors, data were reanalyzed for correlations between CCR5 and either the D1-like (DRD1 and DRD5) or D2-like (DRD2, 3, 4) dopamine receptors. These analyses showed a positive correlation between CCR5 and D1-like receptors (**Figure 2C**) but no correlation between CCR5 and D2-like receptors (**Supplementary Figure 2D**).

These correlations were strengthened by examination of CCR5 expression in hMDM that did or did not express DRD1. hMDM without DRD1 showed significantly lower levels of CCR5 mRNA than those expressing DRD1 (**Figure 2D**). For D2-like dopamine receptors, there was no change in CCR5 expression in groups with or without DRD2 expression (**Supplementary Figure 2E**). Interestingly, hMDM not expressing either DRD3 or DRD4 had higher levels of CCR5 mRNA than those expressing either dopamine receptor (**Supplementary Figures 2F, G**). These analyses could not be performed for DRD5 because all donors expressed this receptor. These data suggest that both D1-like and D2-like receptors influence CCR5 expression, so CCR5 levels were correlated with a D1-like receptor/D2-like receptor ratio (D1/D2 ratio), generated by pooling the values for D1-like receptor expression and dividing them by the pooled values for D2-like expression from each donor, as has been done previously (101). Analysis showed a significant, positive correlation between the D1/D2 ratio and CCR5 expression (**Figure 2E**). Overall, these data indicate that CCR5 expression is significantly correlated with the expression of dopamine receptors, primarily D1-like receptors, on primary human macrophages.

Dopamine Alters the Proportion of CCR5 Conformations in hMDM

To determine whether activation of dopamine receptors influences CCR5 expression, hMDM were treated with vehicle (diH_2O), dopamine (10^{-6} M), or IL-10 (50 ng/mL) for 1 hour and 48 hours. The 1 hour time point has previously been used to assess dopamine-mediated changes in CCR5 surface expression (83), and focuses on the HIV entry process, as we have previously published that dopamine increases entry at an early timepoint (55, 56). As the maraviroc experiments showed that dopamine also influences HIV replication after 3 days in hMDM, changes in CCR5 were also examined at 48 hours. Treatment with IL-10 (50 ng/mL) was used as a positive control, as this cytokine increases CCR5 expression in human monocytes, macrophages, and microglia (79, 102, 103). This use of a positive control in hMDM is similar to what we and others have published (50, 60, 104), as there is considerable variation in the hMDM inflammatory response to environmental stimuli (105–107). Therefore, donors in which IL-10 did not increase CCR5 at 1 hour were excluded from the analysis. After 1 hour or 48 hours, cells were examined by flow cytometry for changes in expression of different surface CCR5 conformations, ECL2 CCR5 or NT CCR5 (**Figure 3A**).

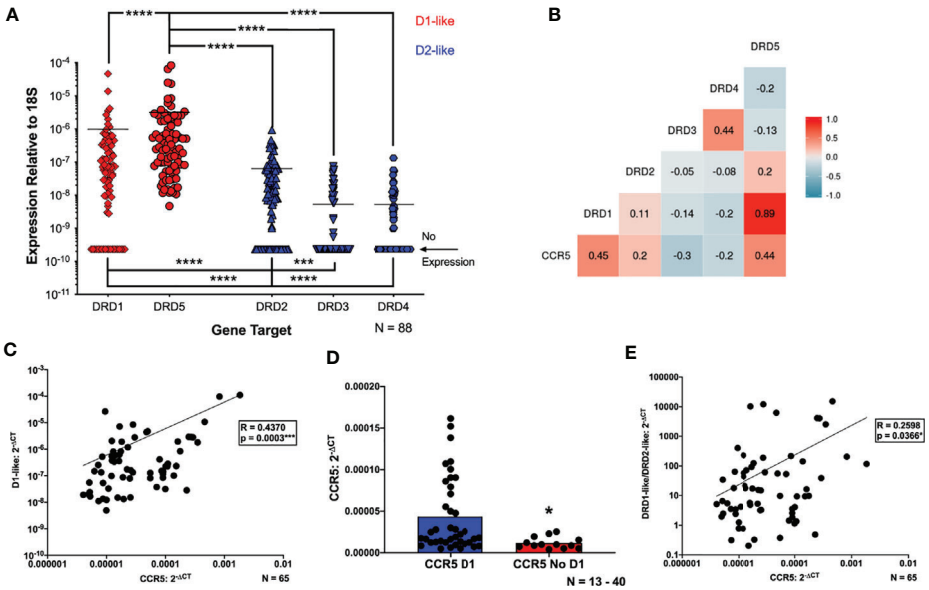

FIGURE 2 | Expression of CCR5 correlates with dopamine receptor expression in hMDM. **(A)** Quantitative RT-PCR detected mRNA for all subtypes of dopamine receptors (D1R, D2R, D3R, D4R and D5R) in primary human monocyte-derived macrophages (hMDM) (N=88). Expression of all receptors was normalized to 18s for each donor. The D1-like receptors (red dots) were expressed at significantly higher levels than the D2-like receptors (blue dots) (Friedman test, n=88, Friedman statistic 233, ****p < 0.0001; *Post-hoc* with Dunn's multiple comparisons, DRD5 *vs.* DRD1, DRD2, DRD3, or DRD4 ****p < 0.0001, DRD1 *vs.* DRD3 or DRD4, ****p < 0.0001, DRD2 *vs.* DRD3, ***p = 0.0003, and DRD2 *vs.* DRD4, ****p < 0.0001). Correlational analyses were then performed to look at correlations between each dopamine receptor and CCR5 mRNA expression (N=65). A matrix to visualize these correlations is shown in **(B)**, and we found that increased expression of CCR5 is associated with greater expression of the D1-like receptors (CCR5 vs D1, n = 65, Spearman r = 0.4454, ***p = 0.0002, CCR5 *vs* D5, n = 65, Spearman r = 0.4448, ***p = 0.0002). Increased expression of CCR5 is also associated with decreased DRD3 expression (CCR5 *vs* D3, n = 65, Spearman r = -0.3007, *p = 0.0149), and no association was found between the other D2-like receptors and CCR5. A number of donors lacked expression of one or more dopamine receptors, so the data were reanalyzed for correlations between CCR5 and the **(C)** D1-like (DRD1 and DRD5) dopamine receptors. These analyses showed a positive correlation between CCR5 and D1-like receptors (CCR5 vs D1-like dopamine receptors, n = 65, Spearman r = 0.4370, ***p = 0.0003). The connection between D1-like receptors and CCR5 was strengthened by analysis of CCR5 levels in hMDM that did or did not express DRD1. These analyses showed hMDM without DRD1 had significantly lower levels of CCR5 mRNA than those expressing DRD1 (Mann-Whitney test, n = 17 - 48, *p = 0.0218, sum of (D1, No D1) ranks 1737, 408, U=255) **(D)**. This was not done for DRD5 because all donors expressed this receptor. CCR5 levels were also correlated with a D1-like receptor/D2-like receptor ratio (D1/D2 ratio) **(E)**, and we showed a significant, positive correlation between the D1/D2 ratio and CCR5 expression (CCR5 *vs* D1/D2-like dopamine receptors, n = 65, Spearman r = 0.2598, *p = 0.0366).

Flow cytometric analysis of the pooled CCR5 expression in dopamine-treated cells after 1 hour showed a small but significant (8.71%) increase in the percentage of surface NT CCR5, almost identical to that seen in response to IL-10 (8.63%). There was no significant increase in the expression of ECL2 CCR5 after 1 hour (**Figure 3B**). A representative dot plot for the 1 hour time point is shown in **Figure 3C**. In contrast to the effect observed at 1 hour, flow cytometric analysis demonstrated that dopamine significantly increased the percentage of both surface ECL2 (12%) and NT CCR5 (16%) at 48 hours (**Figure 3D**). Notably, when there was high baseline expression, neither dopamine nor the positive control showed robust increases in CCR5 (1-5% increase), while increases in NT CCR5 were much greater when baseline NT CCR5 expression was lower (**Figure 3B**). This indicates a potential ceiling effect for this assay, suggesting the effect could be greater than reported as the potential signal saturation limited the increase in some donors. These data demonstrate that dopamine increases surface CCR5 expression and may be a part of the mechanism by which dopamine increases early viral replication and interferes with the efficacy of maraviroc.

These data were corroborated by Western blotting using a different antibody that targets the entire N-terminal region and not just a specific N-terminal epitope. In these studies, hMDM from 7 donors were treated with vehicle (diH_2O) or dopamine (10^{-6} M) for 1 hour and then examined for CCR5. Analyzing the pooled data from all donors showed a significant, 32% increase in CCR5 expression in cells treated with dopamine relative to vehicle (**Figure 3E**). Representative blots for two donors, normalized to total protein stain (TPS) are shown (**Figure 3F**, full blots in **Supplementary Figure 3**).

While these data indicate that dopamine increases the percentage of hMDM expressing CCR5 across a population, they do not define whether individual hMDM also express more surface CCR5. To examine this, hMDM from two donors were treated with vehicle or dopamine for 1 hour, with IL-10 again used as a positive control. After 1 hour, hMDM were fixed and stained for cell nuclei (DAPI), cell membranes [wheat germ

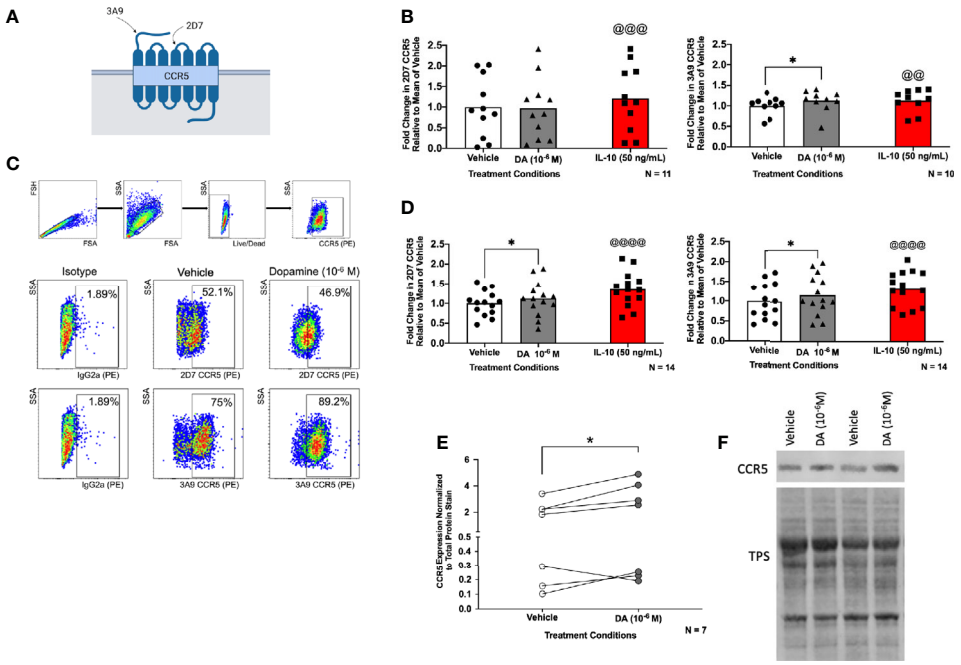

FIGURE 3 | Dopamine alters the proportion of CCR5 conformations in hMDM. Surface expression of 2D7 (ECL2) and 3A9 (NT) CCR5 as depicted in **(A)** (created with BioRender.com) was analyzed by flow cytometry after hMDM were treated with vehicle (diH_2O), dopamine (10^{-6} M), or IL-10 (50 ng/mL) as a positive control (N= 10-11, donors are not the same for each analysis) for 1 hour **(B)**. The separate statistical tests performed on the IL-10-treated samples are denoted by the use of the @ sign, rather than the * used to show significance in the analyses of dopamine-mediated changes. Fold change in CCR5 is relative to the mean of the vehicle. We found a significant increase in NT CCR5 but not ECL2 CCR5 following dopamine exposure (ECL2 CCR5, Paired t-tests, n = 11, Dopamine, p = 0.8776, t=0.1579, df=10; IL-10, $^{@@@}$p = 0.0009, t=4.684, df=10; NT CCR5, Wilcoxon tests, n = 10, Dopamine, *p = 0.0273, sum of (+,-) ranks 49, -6, IL-10, $^{@@}$p = 0.002, sum of (+,-) ranks 55, 0). **(C)** Gating strategy of hMDM by flow cytometry, and dot plot data from one representative donor, in that dopamine increases the percentage of surface NT CCR5 but not ECL2CCR5. **(D)** hMDM were also treated with vehicle (diH_2O), dopamine (10^{-6} M), or IL-10 (50 ng/mL) as a positive control (N= 14, donors are not the same for each analysis) for 48 hours. We found a significant increase in ECL2 and NT CCR5 following dopamine exposure (ECL2 CCR5, Paired t-tests, n = 14, Dopamine, *p = 0.0296, t=2.444, df=13; IL-10, $^{@@@@}$p < 0.0001, t=5.936, df=13; NT CCR5, Paired t-tests, n = 14, Dopamine, *p = 0.0491 t=2.170, df=13; IL-10, $^{@@@@}$p < 0.0001, t=7.227, df=13). To determine whether dopamine affects N-terminal CCR5 in general, hMDM were treated with dopamine (10^{-6} M) for 1 hour and probed for CCR5. Pooled data showing fold change in hMDM from 7 donors relative to the vehicle condition is shown with CCR5 normalized to total protein stain, and dopamine significantly increased the expression of N-terminal CCR5 **(E)** (Paired t-test, n = 7, Dopamine, *p = 0.048, t=2.477, df=6). A representative blot is show in **(F)**.

agglutinin (WGA)] and either ECL2 or NT CCR5, then imaged using the CX7. Representative images are shown in **Figure 4A** and data from high-content immunofluorescent imaging were used to generate a frequency distribution, segregating the data from each cell into bins based on intensity, with a bin size of 100,000. To increase accessibility, these data were graphed as a histogram, representing the number of cells contained in each bin from each experimental condition (**Figures 4B, C**). To analyze these data, we determined the 95% confidence intervals for the total population in each set of conditions (either dopamine or IL-10). Then the number of individual cells above the 95% confidence interval - representing higher levels of surface CCR5 - were enumerated for each condition and compared using a chi-squared test. For the donor in 4B, IL-10 significantly increased the population of cells with higher levels of both ECL2 and NT CCR5, while dopamine only increased the number of cells with higher levels of NT CCR5. For the donor in 4C, IL-10 significantly increased the population of cells with higher levels of both ECL2 and NT CCR5, while surprisingly dopamine also increased the number of cells with high levels of ECL2 and NT CCR5. These data demonstrate that dopamine not only altered the total number of cells with different CCR5 conformations on the cell surface, but that dopamine specifically increased the amount of CCR5 on the cells expressing a particular conformation. These findings corroborate our flow cytometry and Western blot analyses and indicate that exposure to dopamine for 1 hour could significantly change the responses mediated by CCR5 across myeloid populations.

Dopamine Does Not Alter the Localization of Specific CCR5 Conformations Within the Plasma Membrane

Specific conformations of CCR5 preferentially localize to cholesterol-rich lipid raft microdomains within the plasma membrane (75), and in macrophages, lipid rafts are important for CCR5-mediated HIV viral entry, maintaining the conformational integrity and ligand binding activity of CCR5, and disruption of raft regions interferes with macrophage

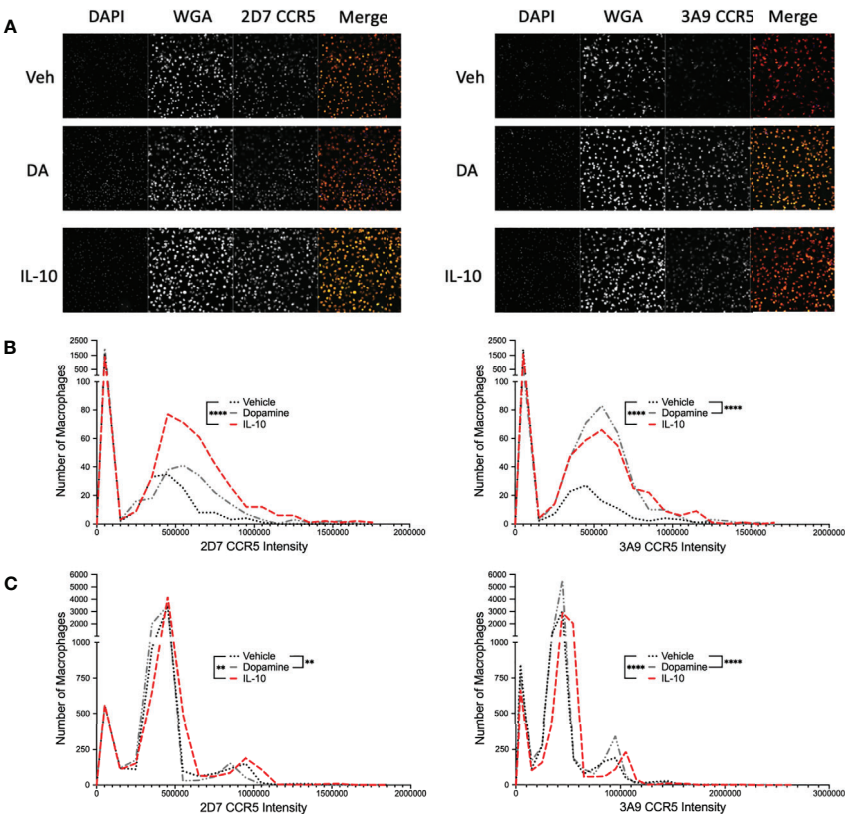

FIGURE 4 | Dopamine increases the proportion of hMDM with N-Terminal CCR5. **(A)** Representative images of immunocytochemical staining of hMDM with DAPI (blue), wheat germ agglutinin (WGA) (far red) and ECL2 or NT CCR5 (red). Images were acquired on the Cell Insight CX7 automated 7-channel confocal microscope, imaging ten fields per well using a 10x objective in a 96 well plate. CX7 data from two donors were then used to generate a frequency distribution, segregating the data from each cell into bins based on intensity, with a bin size of 100,000, and graphed as a histogram, representing the number of cells contained in each bin from each experimental condition **(B)** IL-10 significantly increased the population of cells with higher levels of both 2D7 and 3A9 CCR5, while dopamine only increased the number of cells with higher levels of 3A9 CCR5 (IL-10, 2D7, ****$p < 0.0001$, Chi-square = 114.6, df = 1, z = 10.71, 3A9, ****$p < 0.0001$, Chi-square = 128.5, df = 1, z = 11.34; Dopamine, 3A9, ****$p < 0.0001$, Chi-square = 373.1, df = 1, z = 19.31). **(C)** IL-10 significantly increased the population of cells with higher levels of both 2D7 and 3A9 CCR5, while surprisingly dopamine also increased the number of cells with high levels of 2D7 and 3A9 CCR5 (IL-10, 2D7, **$p < 0.01$, Chi-square = 9.128, df = 1, z = 3.021, 3A9, ****$p < 0.0001$, Chi-square = 49.83, df = 1, z = 7.059; Dopamine, 2D7, **$p < 0.01$, Chi-square = 8.535, df = 1, z = 2.921, 3A9, ****$p < 0.0001$, Chi-square = 108.6, df = 1, z = 10.42).

infection (108, 109). Substances of abuse can alter the translocation of receptors into lipid raft domains (110, 111) and lipid raft proteins, such as caveolin-1, can alter the function of the D1 dopamine receptor (112, 113). Therefore, high content imaging was used to assess the impact of dopamine on the localization of specific CCR5 conformations within lipid rafts in the hMDM plasma membrane.

hMDM were treated with either vehicle (diH_2O) or dopamine (10^{-6}M) for 1 hour, then fixed and stained for cell nuclei (DAPI), flotillin-1, CD71, and either ECL2 CCR5 or NT CCR5. Representative images of each stain are found in **Figures 5A, B**. Flotillin-1 and CD71 are expressed in lipid raft (114) or non-raft areas (115), respectively, and were used to differentiate lipid raft regions from non-raft regions. Changes in the colocalization of each CCR5 conformation with Flotillin-1 and CD71 were defined using Pearson's correlation coefficient (PCC). Using PCC, correlation values above 0.3 indicate varying degrees of colocalization, while those below 0.3 indicate no colocalization. Colocalization between Flotillin-1 and CD71 was used as a positive control for accurate staining, as lipid raft and non-lipid raft should be detected as distinct regions within the macrophage membrane. To ensure the accuracy of these analyses, control studies were performed to show that dopamine treatment did not alter the expression of either CD71 or Flotillin-1, or the colocalization of these markers (**Supplementary Figures 4A, B**). In addition, PCC between Flotillin-1 and CD71 did not change with dopamine treatment, indicating no dopamine-mediated change in colocalization between these markers (**Supplementary Figure 4C**). Image analysis of CCR5 and lipid raft of non-raft PCC showed colocalization of both ECL2 CCR5 and NT CCR5 with Flotillin-1, indicating that both conformations of CCR5 are found in lipid rafts. Dopamine did not change the PCC of either NT CCR5 or ECL2 CCR5 relative to vehicle, and there was no difference between NT CCR5/Flotillin-1 colocalization and

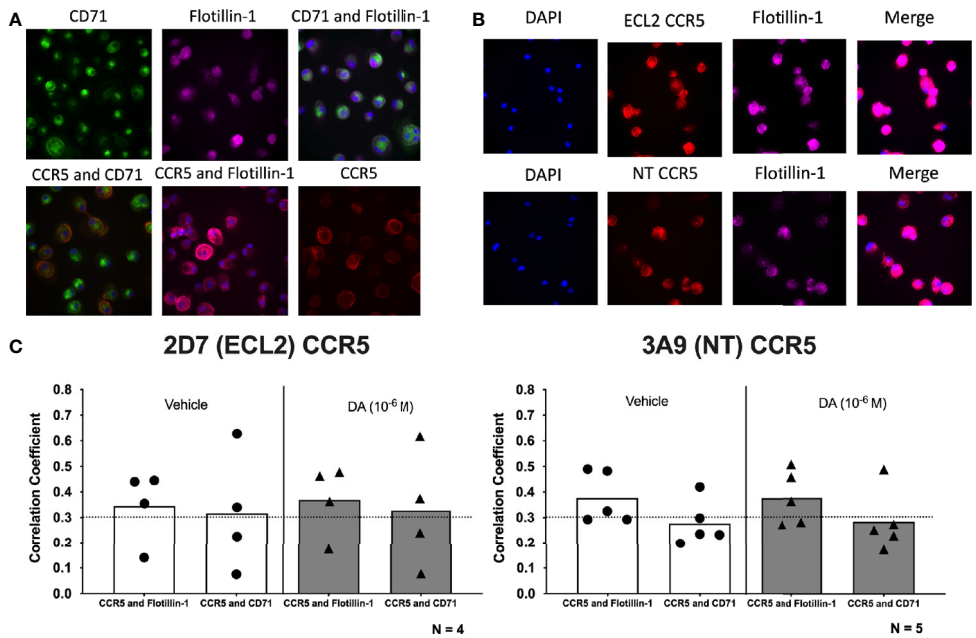

FIGURE 5 | Dopamine does not alter the localization of specific CCR5 conformations within the plasma membrane. **(A)** Representative images of immunocytochemical staining of hMDM with CCR5 (red), the non-lipid raft marker CD71 (green), and the lipid raft marker flotillin-1 (purple), as well as overlay images of CCR5 and CD71 (orange), CCR5 and flotillin-1 (pink), and CD71 and flotillin-1 (blue). Images were acquired on the Cell Insight CX7 automated 7-channel confocal microscope, imaging 100 fields per well using a 40x objective in a 96-well plate. **(B)** Representative images of immunocytochemical staining of hMDM with DAPI (blue), 2D7 or 3A9 CCR5 (red), flotillin-1 (purple), and merged. **(C)** Quantitative analysis using Pearson's correlation coefficient shows a positive correlation for 2D7 CCR5 and flotillin-1 as well as 2D7 CCR5 and CD71 in both vehicle-treated and dopamine-treated cultures ECL2 CCR5: Flotillin-1, vehicle PCC = 0.345, dopamine PCC = 0.369; ECL2 CCR5:CD71, vehicle PCC = 0.317, dopamine PCC = 0.328. In contrast, colocalization of NT CCR5 was only shown between NT CCR5 and Flotillin-1, with NT CCR5 showing no colocalization with CD71 (NT CCR5: Flotillin-1, vehicle PCC = 0.377, dopamine PCC = 0.376; NT CCR5:CD71, vehicle PCC = 0.277, dopamine PCC = 0.283).

ECL2 CCR5/Flotillin-1 colocalization in either condition (**Figure 5C**). In contrast, PCC did not show colocalization between NT CCR5 and CD71, although this was shown for ECL2 CCR5. Dopamine also had no effect on colocalization (or not) with CD71 (**Figure 5C**). This corroborates prior studies showing distinct CCR5 conformations differentially concentrate in lipid rafts (75). Overall, these data indicate that distinct conformations of CCR5 segregate differently within the plasma membrane, but that dopamine does not appear to have any impact on this process at the time point examined.

Dopamine Increases HIV Replication and NT CCR5 in Human Microglia

The concentrations of dopamine induced by substance abuse are greatest in the CNS, where the major myeloid populations include microglia as well as several distinct types of macrophages (116, 117). Microglia express dopamine receptors and can respond to dopamine (118–120), therefore we examined whether dopamine affects HIV infection in microglia similarly to macrophages. To do this, we used iPSC-derived microglia (iMicroglia) with very similar gene expression to primary human microglia (86). iMicroglia were inoculated in triplicate with vehicle or HIV_{ADA} (1 ng/mL) treated concurrently with vehicle (diH_2O) or dopamine (10^{-6}M) for 24 hours, then washed and cultured until 10 days post-inoculation. Representative brightfield images show uninfected or HIV-infected iMicroglia at 7 days post infection, showing high levels of cell fusion in infected cultures relative to healthy ramified microglia in mock-infected cultures (**Figure 6A**). Analysis of supernatant p24 levels in iMicroglia indicates increasing viral replication over time. Levels of p24 in dopamine-treated cultures were significantly higher than those in vehicle-infected cultures at every time point examined, indicating that dopamine does increase HIV infection in microglia (**Figure 6B**). Analysis of dopamine receptor expression in this line of iMicroglia showed that these cells express the D1-like dopamine receptors, DRD1 and DRD5, but not D2-like receptors (**Figure 6C**).

To examine whether dopamine-mediated changes in CCR5 in microglia are similar to macrophages, we chose to use a more tractable system, the C06 microglial cell line. These cells exhibit microglia-like morphology and express key microglial surface markers including CD11b, TGFβR, and P2RY12 (87). Gene expression analysis demonstrates that these cells also express dopamine receptors; DRD1, DRD5, and DRD2, and there is significantly higher expression of DRD2 compared to DRD1 and DRD5 (**Figure 7A**). Unlike hMDM and iMicroglia, C06 cells actively replicate, so they were infected with a range of concentrations of HIV_{ADA} (0.5, 1, 2.5, and 5 ng/ml) to define the optimal conditions for HIV infection in these cells. Cultures show an initial burst of replication followed by a steady level of

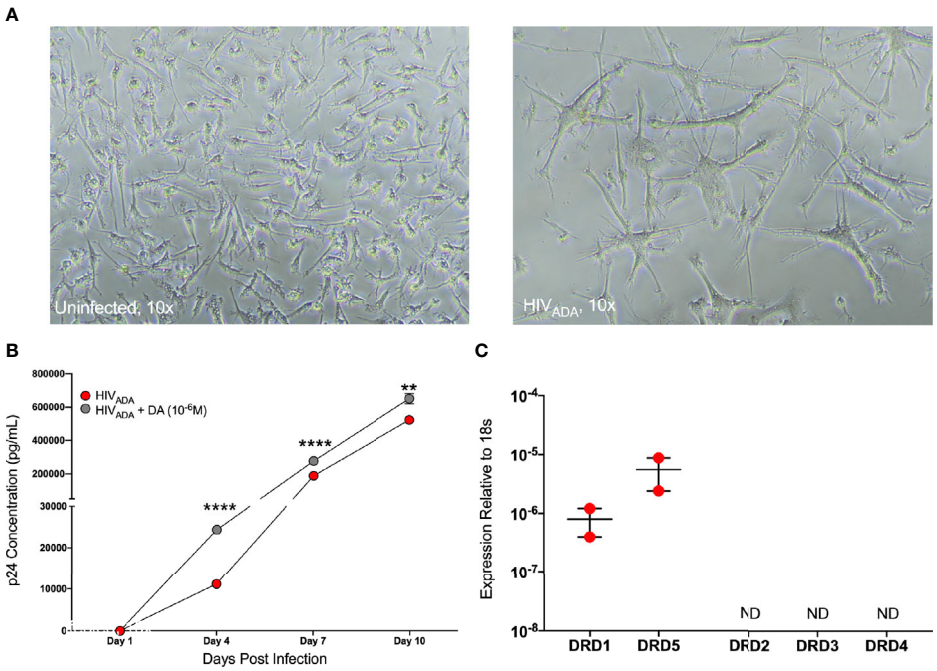

FIGURE 6 | iMicroglia are infectable with HIV and dopamine increases HIV replication. iMicroglia were inoculated with 1 ng/mL of HIV_{ADA} or vehicle and concurrently treated with vehicle (diH_2O) or dopamine (10^{-6}M). **(A)** Representative brightfield images show uninfected or HIV-infected iMicroglia at 7 days post infection, showing high levels of cell fusion and giant cell formation in infected cultures relative to healthy ramified microglia in mock-infected cultures. **(B)** Analysis of supernatant p24 levels over 10 days post-infection in one iMicroglia line (WT6) shows increasing viral replication over time. The p24 levels in dopamine-treated cultures were significantly higher than those in HIV-infected cultures treated with vehicle at every time point examined, indicating that dopamine does increase HIV infection in microglia (multiple t-tests corrected for multiple comparisons using the Holm-Sidak method, Day 4, ****$p < 0.0001$, t=53.35, df=4, HIV SEM=241.73, HIV+DA SEM=51.5; Day 7, ****$p < 0.0001$, t=27.52, df=4, HIV SEM=287.37, HIV+DA SEM=3189.41; Day 10, **$p = 0.002$, t=7.07, df=4, HIV SEM=2294.24, HIV+DA SEM=17989.88). **(C)** Quantitative RT-PCR analysis of dopamine receptor expression in this line of iMicroglia (WT6) showed that these cells express the D1-like dopamine receptors, DRD1 and DRD5, but not D2-like receptors.

replication over time, with significantly different levels of p24 production in response to different infection levels (**Figure 7B**). Differences in infection dynamics relative to hMDM and iMicroglia are likely due to the fact that these cells divide. Infection with 2.5 ng/ml HIV_{ADA} showed the widest assay window, so the C06 cells were inoculated with this concentration of HIV and concurrently treated with vehicle (diH_2O) or dopamine (10^{-6}M). Analysis of p24 concentrations in infections of 5 distinct passages of C06 cells shows that dopamine increased the amount of HIV infection in C06 microglia at two to five days post-infection compared to vehicle treatment, with 3 representative infections shown in **Figure 7C**. Analysis of different concentrations of dopamine (10^{-6}M - 10^{-9}M), show that only dopamine at 10^{-6}M increases p24 levels (**Supplementary Figure 5**), unlike studies in hMDM showing an effect of dopamine at 10^{-8}M and above (55).

After demonstrating that dopamine increased HIV infection in C06 cells, we examined whether dopamine could alter CCR5 conformations, similar to hMDM. Pooled data from flow cytometric analyses of 5 passages of dopamine-treated microglia showed that dopamine significantly increased the percentage of surface NT CCR5 but not ECL2 CCR5 at 1 hour (**Figure 8A**). Similar data were seen by Western blot analysis using an antibody that targets the entire N-terminal region (**Figure 8B**, full blot in **Supplementary Figure 3**). Analysis of the pooled Western data show that dopamine increased NT CCR5 in 3 out of 4 passages, but this did not reach significance (**Figure 8C**). These data indicate that dopamine also increased HIV infection in microglia and that these effects may also be mediated by dopamine-induced changes in the surface conformation of CCR5.

DISCUSSION

Substance abuse is a major comorbidity in HIV infection, and rates of HIV infection among substance abusers are up to twenty-two times higher than in the general public (8–15). Greater disparities are seen among older adults, a significant portion of the infected population (121, 122). Substance abuse is a significant issue during HIV infection, as it substantively worsens clinical outcomes and accelerates systemic disease even in infected individuals on suppressive ART (17, 83, 123–132). This is also true in the CNS, where substance abuse can still promote neuroinflammation, altering the progression of neuropathology and increasing the risk of neuropsychiatric comorbidities and cognitive decline (16–26). Substance abuse

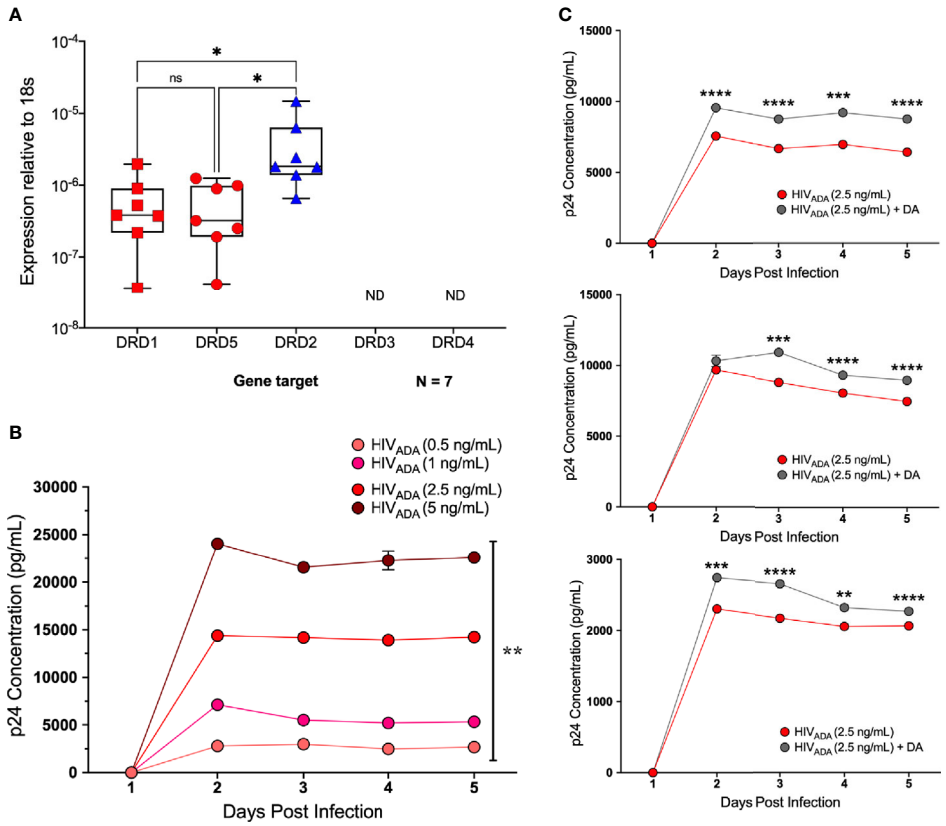

FIGURE 7 | C06 human microglia are infectable with HIV and dopamine increases HIV replication. **(A)** Quantitative RT-PCR detected mRNA for DRD1, DRD2, and DRD5 in C06 cells (N=7), and DRD2 expression is higher compared to DRD1 and DRD5 (Kruskal-Wallis test, n = 7, **p = 0.0048, Dunn's multiple comparisons test, DRD1 *vs.* DRD2, *p = 0.0331, DRD5 *vs* DRD2, *p=0.0175). **(B)** C06 cells were infected with a range of concentrations of HIV$_{ADA}$ (0.5, 1, 2.5, and 5 ng/ml) for 5 days, and analysis of p24 levels shows significant changes in response to different infection levels at each day post-infection (rmANOVA, Day 2, ****p<0.0001, F (1.208, 2.417) = 2992, HIV 0.5 SEM=16.05, HIV 1 SEM=49.75, HIV 2.5 SEM=199.2 HIV 5 SEM=223.17; Day 3, ****p<0.0001, F (1.270, 2.539) = 2429, HIV 0.5 SEM=23.36, HIV 1 SEM=125.7, HIV 2.5 SEM= 241.63, HIV 5 SEM=171.17; Day 4, **p= 0.0031, F (1.024, 2.047) = 292, HIV 0.5 SEM=122.89, HIV 1 SEM=60.18, HIV 2.5 SEM=147.54, HIV 5 SEM=983.1; Day 5, ***p= 0.0004, F (1.052, 2.104) = 1825, HIV 0.5 SEM=42.66, HIV 1 SEM=52.72, HIV 2.5 SEM=31.0, HIV 5 SEM=417.7). **(C)** Representative p24 analysis in 3 C06 passages demonstrating increased HIV replication in dopamine-treated (10^{-6} M), HIV infected (HIV$_{ADA}$ 2.5 ng/ml) cells compared to cells only infected with HIV (multiple t-tests corrected for multiple comparisons using the Holm-Sidak method, top infection: Day 2, ****p < 0.0001, t=13.47, df=4, HIV SEM=132.0, HIV + DA SEM=67.31; Day 3, ****p < 0.0001, t=26.19, df=4, HIV SEM=47.06, HIV + DA SEM=63.88; Day 4, ***p = 0.0018, t=7.355, df=4, HIV SEM=294.12, HIV + DA SEM=84.26; Day 5, ****p < 0.0001, t=18.51, df=4, HIV SEM=114.5, HIV + DA SEM=53.27; middle infection: Day 2, p > 0.05, HIV SEM=63.46, HIV + DA SEM=414.56; Day 3, ***p =0.0002, t=12.96, df=4, HIV SEM=89.97, HIV + DA SEM=137.34; Day 4, ****p < 0.0001, t=18.84, df=4, HIV SEM=17.89, HIV + DA SEM=64.83; Day 5, ****p < 0.0001, t=28.65, df=4, HIV SEM=37.37, HIV + DA SEM=36.39; bottom infection: Day 2, ***p=0.0002, t=12.95, df=4, HIV SEM=27.99, HIV + DA SEM=19.09; Day 3, ****p < 0.0001, t=26.98, df=4, HIV SEM=3.3, HIV + DA SEM=17.64; Day 4, **p = 0.009, t=4.743, df=4, HIV SEM=26.47, HIV + DA SEM=49.53; Day 5, ****p < 0.0001, t=18.35, df=4, HIV SEM=4.94, HIV + DA SEM=9.99). ns, not significant.

likely mediates these effects by dysregulating immune function and increasing HIV replication in CNS myeloid cells such as macrophages and microglia (17, 18, 29–31, 133), which are primary drivers of HIV neuropathogenesis (32–35). Previous data from our lab shows that dopamine, which is increased by the use of all addictive substances, enhances both HIV infection and inflammatory cytokine production in primary human macrophages (50, 54–56, 60).

Infection of myeloid cells requires the chemokine receptor CCR5, and this receptor is also required for dopamine-mediated increases in HIV entry into these cells (55, 83). The interaction of HIV with CCR5 is mediated by the envelope protein, gp120, which generally binds to sites in the N-terminal (NT) and second extracellular loop (ECL2) regions of the receptor. Both gp120 and endogenous CCR5 ligands have different affinities for each region, meaning that binding affinity varies depending on the region(s) exposed and available for binding (134, 135). Binding site availability depends on receptor conformation, which is heterogeneous across the plasma membrane. This is why some antibodies to CCR5 more effectively inhibit chemokine binding and function (136), while others more successfully inhibit HIV infection (75). The associations between drug-related behaviors, dopamine and CCR5 (70) suggest dopamine-mediated shifts in the expression of distinct CCR5 conformations could alter the functions of this receptor. Thus, dopamine levels induced by substance abuse could, at least in part, promote the development

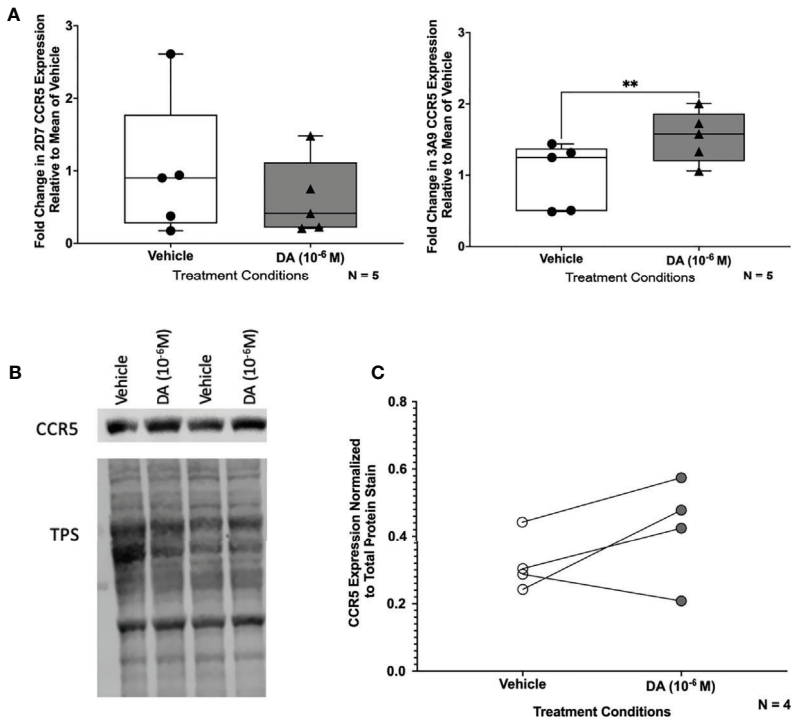

FIGURE 8 | Dopamine increases NT CCR5 in C06 human microglia. **(A)** Change in CCR5 expression relative to the mean of vehicle-treated (diH_2O) C06 cells demonstrates that dopamine increases NT but not ECL2 CCR5, similar to what we found in hMDM (N=5) (ECL2 CCR5, Paired t-test, n=5, Dopamine, p=0.1818, t=1.614, df=4; NT CCR5, Paired t-test, n=5, Dopamine, **p=0.0043, t=5.837, df=4). C06 cells were also treated with dopamine (10^{-6} M) for 1 hour and probed for pan NT CCR5. A representative blot is shown in **(B). (C)** Pooled data showing fold change in C06 cells from 4 passages relative to the vehicle condition is shown with CCR5 normalized to total protein stain. Although this did not reach significance (Paired t-test, n=4, Dopamine, p=0.2182, t=1.553, df=3), three out of four passages show an increase in NT CCR5 with dopamine relative to vehicle.

of neuroHIV by increasing HIV entry and also by interfering with CCR5-targeted antiretroviral therapies such as the CCR5 inhibitor, maraviroc.

Maraviroc acts by blocking the interaction between CCR5 and gp120 through allosteric inhibition, stabilizing a CCR5 conformation inducing inefficient ligand binding at the ECL2 binding site (137). This allosteric inhibition is less effective at blocking binding activity that primarily targets the N-terminal region (138), resulting in diminished effectiveness of maraviroc against strains of HIV that have stronger interactions with the CCR5 N-terminus (139–141). This suggests that dopamine induced shifts in the expression of NT CCR5 would reduce maraviroc efficacy. Our data support this hypothesis, confirming that dopamine increases HIV infection in myeloid cells and alters the effectiveness of this inhibitor. Dopamine had multi-modal effects on maraviroc in hMDM from 12 donors, enhancing (5/12 donors), inhibiting (5/12 donors), or having no effect (2/12 donors) on maraviroc efficacy in these studies. When comparing the effect of dopamine on maraviroc efficacy to the effect of dopamine on infection, the hMDM in which dopamine reduced the efficacy of maraviroc showed an average of a 4.67-fold increase in p24 concentrations in response to dopamine alone. In contrast, the hMDM in which dopamine enhanced the efficacy of maraviroc only showed an average of a 1.48-fold increase in response to dopamine. The hMDM from donors in which dopamine did not increase p24 levels also showed that dopamine enhanced maraviroc efficacy. Thus, hMDM in which dopamine inhibited the effectiveness of maraviroc also had a much greater dopamine-mediated increase in HIV infection, suggesting that the mechanism by which dopamine increases HIV entry is connected to the impact of dopamine on maraviroc. This also suggests that dopamine responsiveness varies between donors, and that individuals with the greatest responsiveness to dopamine would also see the most detrimental effects of dopamine on maraviroc- mediated inhibition of HIV infection.

HIV entry and replication increase with CCR5 density (142), and CCR5 is necessary for dopamine to increase HIV entry (55), suggesting that dopamine-mediated changes in CCR5 are at least a part of the mechanism by which dopamine increases HIV infection. R5-tropic strains of HIV originating in the brain have increased affinity for CCR5 (143, 144), potentially due to increases in CCR5 binding efficiency mediated by additional atomic contacts at the gp120-NT CCR5 interface (145, 146). Thus, across a population, an increase in the number of hMDM expressing CCR5 would enhance viral spread. This hypothesis correlates well with our previous studies showing that dopamine increases the amount of HIV entry and replication by increasing the number of HIV-infected cells (54, 55). The data in this study

further support this hypothesis, showing that populations of hMDM and microglia exposed to drug-induced dopamine levels have an increased number of cells expressing greater levels of CCR5 on the cell surface. An initial increase is observed in NT CCR5 and not ECL2 CCR5, corroborating previous findings (55, 83). In addition, dopamine treatment significantly increased expression of both conformations of CCR5 at 48 hours, with a greater increase in expression than observed at the 1 hour timepoint. This indicates that dopamine has a greater effect on multiple CCR5 populations over a longer period of time, potentially explaining the dopamine-mediated changes in HIV replication seen at 3 days.

It is important to note that changes in both NT and ECL2 CCR5 were observed at 1 hour using immunofluorescence assays and high throughput imaging, suggesting that the flow cytometry assays used were not sensitive enough to detect changes in ECL2 CCR5 at 1 hour. This could be due to the effects of dopamine affecting ECL2 CCR5 levels on a smaller number of macrophages. An additional consideration highlighted by the flow cytometry assays is that the effects of dopamine on CCR5 were not uniform across the population, increasing expression of NT CCR5 from 3 to 90% in hMDM derived from different individuals. On average, the significant increases in CCR5 were relatively modest, approximately 9% (NT CCR5) at 1 hour, and approximately 12% (ECL2 CCR5) and 16% (NT CCR5) at 48 hours. However, even small increases in surface CCR5 have been shown to have a robust functional impact. Both *in vitro* and *in vivo* studies show progression of HIV infection is heavily dependent on CCR5 expression, with increases in both CCR5 expression and the percentage of CCR5-expressing cells correlating with immune cell activation, plasma viremia, and disease progression (81, 82, 147). In HIV infection of human macrophages and microglia *in vitro*, 50 – 60% increases in surface CCR5 increased HIV entry by 588 – 985% (79), while increasing CCR5 expression approximately 300%, from 7 x 10^2 to 2 x 10^3 CCR5 molecules in a HeLa indicator cell line increased HIV infectivity titers more than three orders of magnitude (80). Similarly, decreasing surface CCR5 by approximately 20% reduces viral fusion and p24 production by 50 – 80% in primary human macrophages (148). These data and our previous studies have shown that the effect of dopamine varies widely between donors, but that on average, dopamine increases HIV entry and replication by between 100 – 200% (54–56) which is in line with the smaller increases in CCR5 observed in response to dopamine in these studies. Overall, this suggests that a) dopamine-mediated changes in CCR5 could be the mechanism by which dopamine increases HIV infection and b) if the variation in the impact of dopamine on myeloid susceptibility to HIV infection is connected to the dopaminergic impact on CCR5, it is likely to vary between individuals, similarly to the dopamine-mediated influence on maraviroc efficacy.

Our correlations suggest the dopamine-mediated changes in CCR5 are associated with expression of multiple types of dopamine receptors. The data show a positive correlation between D1-like receptors and CCR5 expression, and increased expression of CCR5 transcripts in hMDM with detectable DRD1 expression. There is also a negative correlation between CCR5 and expression of DRD3, and hMDM with no DRD3 or DRD4 show high levels of CCR5. This suggests that both the activity of D1-like receptors and the lack of activity of DRD3/DRD4 influence CCR5 expression and conformational rearrangements. This is supported by the larger increase in NT CCR5 expression in the C06 microglial cell line, which expresses DRD1 but no DRD3 or DRD4. This is also supported by studies indicating that D1-like dopamine receptors are the most prevalent subtype on macrophages, and that these receptors are likely the primary mediators of dopamine signaling in this cell type (56). In contrast to this hypothesis, others have shown that D1-like agonists reduce CCR5 expression in THP-1 cells, but these differences may be due to the distinct expression levels of dopamine receptors in this cell type, as they express high levels of DRD4 while hMDM and other myeloid cells do not (83). While many types of immune cells express dopamine receptors (52), the nature and the relative proportions of distinct CCR5 populations may vary in other cell types, meaning that the dopamine-mediated effects on HIV infection could be unique to myeloid cells (75, 149).

The specific mechanisms by which dopamine could induce changes in CCR5 conformation are not clear, but distinct CCR5 conformations preferentially localize to lipid rafts and are dependent on cholesterol in order to facilitate productive HIV infection (75, 150). Further, substances of abuse can increase the localization of GPCRs to lipid rafts (110, 151), suggesting dopamine might induce changes in the localization of specific CCR5 conformations. However, the data show that while NT CCR5 is preferentially localized to lipid rafts, this effect is not dependent on dopamine levels. Dopamine could also alter CCR5 conformation by mediating post-translational modifications, such as glycosylation, phosphorylation, or palmitoylation, as these have been shown to alter the HIV entry process and influence CCR5 binding to both chemokines (152–154). Dopamine also regulates the internalization and recycling of G-protein coupled receptors other than dopamine receptors (155), and different CCR5 conformations exhibit distinct sensitivities to endocytosis inhibition (74). Thus, dopamine could potentially promote changes in CCR5 internalization that alter the expression of CCR5 populations on the cell surface. Similarly, dopamine-mediated changes in CCR5 conformations could alter the proportion of cells coupling to different signaling pathways activated by this receptor, as there is select sensitivity of CCR5 conformations to different G proteins (156, 157). Our previous data show that D1-like dopamine receptors in macrophages act primarily through calcium release mediated by $G_{q/11}$ (56), which is also a major signaling mechanism for CCR5. Thus, crosstalk between D1-like receptors and CCR5 signaling is another possible mechanism for interaction between these receptor systems. This is important as CCR5 inhibitors, such as TAK-779 and maraviroc, have different affinities for CCR5 that depend on G protein coupling. Thus, dopamine-mediated changes in CCR5 that lead to differential G protein association could affect the potency and efficiency of these inhibitors in blocking gp120 binding (158).

There are a number of limitations that should be considered in regard to these data, many of which are associated with the inherent variability among primary immune cells from different donors (106, 107, 159). While this variability is expected, it often interferes with standard statistical analysis and necessitates larger n to properly evaluate results. The variance is likely due to genetic factors, as differences in infection levels (93, 160) and the response to dopamine are very high between donors, and in these studies maraviroc showed variable effectiveness across donors. It is possible that these differences could create experimental artifacts in some donors due to a smaller assay window. For example, in the flow cytometry data, donors with high baseline CCR5 showed less impact of dopamine or the positive control (IL-10) on CCR5 expression. Similarly, the effects of dopamine on maraviroc may have been more observable in donors with higher baseline infection due to the larger potential range of changes to infection, an artifact of the culture system in which there are only a limited number of cells to infect. Another caveat is that the hMDM in these studies only have a small amount of epidemiologic data associated with them, precluding analysis of a number of factors that differ between donors that may influence HIV infection or hMDM function. In particular, ongoing substance abuse or dopaminergic medications may influence dopamine levels in the periphery (161–163), potentially influencing expression or sensitivity of hMDM dopamine receptors. Thus, some of the inter-donor variability, as well as the lack of correlation in some analyses, may be attributed to changes in dopamine-responsiveness due to exogenous drugs or therapeutics.

Despite these caveats, we have previously published a consistent effect of dopamine on HIV infection of primary human macrophages derived from these sources (54–56). Further, the dopamine-mediated increases in HIV infection were also seen in the iPSC-derived microglia and C06 microglial cell line, and the C06 cells also showed the dopamine-mediated changes to CCR5. Taken with the need for a relatively large n, this suggests that while the effects we are observing are consistent, the magnitude is modest and can therefore be obscured due to donor variability and the detection limits of the assays. A final caveat regarding the use of primary cells is that many of the studies occurred sequentially using human blood that is de-identified and of limited supply, so it was not possible to perform all of the experiments in each donor. Future analyses based on these studies will be designed to better accommodate running all assays for a particular study in cells from each donor. Another technical caveat to consider is the capacity for CCR5 antibodies to detect different CCR5 conformations. Our data show a differential average surface expression of ~40% for the ECL2 CCR5 (2D7) *vs.* an ~80% average expression for the NT CCR5 (3A9). While these studies were performed using well-established antibodies validated for this type of assay, using only one CCR5 antibody might underestimate the total CCR5 cell surface expression level under certain conditions. Future studies investigating CCR5 should use multiple antibodies – although this will necessitate the generation of a large number of more effective antibodies – and should consider the existence of multiple conformations during analysis (74).

Overall, these data indicate that induction of an increased concentration of extracellular dopamine may be a common mechanism by which different classes of abused substances could drive neuroHIV. Dopamine-mediated increases in HIV entry may be driven by changes in the diversity of CCR5 populations on the surface of myeloid cells. In addition to increasing the general susceptibility to HIV infection, these changes may alter the effectiveness of the CCR5 inhibitor maraviroc. This demonstrates a critical need to better define the specific neurobiology driving neuroHIV in infected substance abusers, and to specifically evaluate the efficacy of ART drugs in this unique environment. To accommodate this, studies should consider targeting specific conformations of CCR5, or developing bivalent ligands, such as dual DR/CCR5 antagonists, that could block possible signaling pathways that promote HIV infectivity. These data also suggest novel therapeutic approaches for a variety of other pathologies, such as multiple sclerosis, atherosclerosis and several types of cancers, that may be impacted by dopamine-driven CCR5 expression. Future studies in this area will be facilitated through further examination of human primary macrophages with more detailed epidemiologic data, as well as through the use of iPSC-derived myeloid cells. These studies show for the first time that dopamine increases HIV infection in iMicroglia, and future studies using iMicroglia and iMacrophages will be extremely valuable as a more tractable platform in which to perform more complex molecular assays. Use of both macrophages and microglia is important because myeloid populations in the CNS are transcriptionally related (164), but microglia and macrophages are distinct cell types (165), and infection of both populations is central to the development of neuropathology (32–35, 166–170).

More broadly, these data further emphasize the role of dopamine as an immunomodulatory factor in a variety of pathological and homeostatic conditions. Many dopaminergic drugs are currently in use as treatment for a variety of disorders, and concentrations of dopamine induced by both substance abuse and these therapeutics have both subtle and robust effects on a wide array of immune functions. Thus, future therapeutic strategies based on development and repurposing of these drugs in order to manipulate dopaminergic immunology would likely be beneficial for not only neuroHIV but many diseases in which CCR5 plays a role. Returning to neuroHIV, these data highlight the critical need for studies that define more precisely the relationship between substance abuse and progression of neuroHIV. Further studies in this area are essential to the development of specific strategies, ART combinations and other targeted therapeutics that are efficient and effective at blocking the development of neuropathology specifically in the vulnerable population of HIV-infected substance abusers.

DATA AVAILABILITY STATEMENT

The original contributions presented in the study are included in the article/**Supplementary Material**. Further inquiries can be directed to the corresponding author.

ETHICS STATEMENT

Ethical review and approval was not required for the study on human participants due to the deidentified nature of the material, but all human material was obtained in accordance with the local legislation and institutional requirements set out by the Institutional Review Board of Drexel University. Written informed consent for participation was not required for this study in accordance with the national legislation and the institutional requirements.

AUTHOR CONTRIBUTIONS

SM, YR, and PG contributed to the design and conception of the study. SM, EN-B, YR, KR, HJ, MO'C, and PG designed and analyzed the experiments, and SM, EN-B, YR, KR, HJ, and MO'C performed the experiments. EH and PG helped supervise the project. SM and PG performed the statistical analyses and wrote the manuscript. PG was responsible for the final approval of the submitted version. All authors contributed to the article and approved the submitted version.

FUNDING

This work was supported by grants from the National Institutes of Drug Abuse, DA039005 and DA049227 (PJG), the W.W. Smith Charitable Trust Foundation Grant A2003 (PJG), the Brody Family Medical Trust Fund (SM), the Clarkston Scholarship program (HJ) and the Drug, Discovery and Development program and the Department of Pharmacology and Physiology at Drexel University College of Medicine. NIH 1RO1AI106482-01 to EKH, and EAN is a trainee of the T32 grant "Interdisciplinary and Translational Research Training in neuroAIDS" from the National Institute of Mental Health (MH079785).

ACKNOWLEDGMENTS

We would like to state our tremendous appreciation for all the individuals who donated the biological materials used in these studies. We would also like to thank all the members of the Gaskill lab as well as Dr. Vasiliki Pappa and Katelyn Reeb for their contributions to this work.

SUPPLEMENTARY MATERIAL

The Supplementary Material for this article can be found online at: https://www.frontiersin.org/articles/10.3389/fimmu.2021.663061/full#supplementary-material

REFERENCES

1. Ortega M, Brier MR, Ances BM. Effects of HIV and Combination Antiretroviral Therapy on Cortico-Striatal Functional Connectivity. *Aids* (2015) 29(6):703–12. doi: 10.1097/QAD.0000000000000611
2. Becker JT, Sanders J, Madsen SK, Ragin A, Kingsley L, Maruca V, et al. Subcortical Brain Atrophy Persists Even in HAART-regulated HIV Disease. *Brain Imaging Behav* (2011) 5(2):77–85. doi: 10.1007/s11682-011-9113-8
3. Alakkas A, Ellis RJ, Watson CW, Umlauf A, Heaton RK, Letendre S, et al. White Matter Damage, Neuroinflammation, and Neuronal Integrity in HAND. *J Neurovirol* (2019) 25(1):32–41. doi: 10.1007/s13365-018-0682-9
4. Boban J, Kozic D, Turkulov V, Ostojic J, Semnic R, Lendak D, et al. HIV-Associated Neurodegeneration and Neuroimmunity: Multivoxel MR Spectroscopy Study in Drug-Naive and Treated Patients. *Eur Radiol* (2017) 27(10):4218–36. doi: 10.1007/s00330-017-4772-5
5. Dahal S, Chitti SVP, Nair MPN, Saxena SK. Interactive Effects of Cocaine on HIV Infection: Implication in HIV-associated Neurocognitive Disorder and Neuroaids. *Front Microbiol* (2015) 6:931. doi: 10.3389/fmicb.2015.00931
6. Hauser KF, Knapp PE. Interactions of HIV and Drugs of Abuse: The Importance of Glia, Neural Progenitors, and Host Genetic Factors. *Int Rev Neurobiol* (2014) 118:231–313. doi: 10.1016/B978-0-12-801284-0.00009-9
7. Chilunda V, Calderon TM, Martinez-Aguado P, Berman JW. The Impact of Substance Abuse on HIV-mediated Neuropathogenesis in the Current ART Era. *Brain Res* (2019) 1724:146426. doi: 10.1016/j.brainres.2019.146426
8. Gamarel KE, Brown L, Kahler CW, Fernandez MI, Bruce D, Nichols S, et al. Prevalence and Correlates of Substance Use Among Youth Living With HIV in Clinical Settings. *Drug Alcohol Depend* (2016) 169:11–8. doi: 10.1016/j.drugalcdep.2016.10.002
9. UNODC. *World Drug Report*. (2019), (United Nations Publication Sales No. E.19.XI.8).
10. Lucas GM. Substance Abuse, Adherence With Antiretroviral Therapy, and Clinical Outcomes Among HIV-infected Individuals. *Life Sci* (2011) 88(21-22):948–52. doi: 10.1016/j.lfs.2010.09.025
11. Degenhardt L, Peacock A, Colledge S, Leung J, Grebely J, Vickerman P, et al. Global Prevalence of Injecting Drug Use and Sociodemographic Characteristics and Prevalence of HIV, HBV, and HCV in People Who Inject Drugs: A Multistage Systematic Review. *Lancet Glob Health* (2017) 5 (12):e1192–207. doi: 10.1016/S2214-109X(17)30375-3
12. Leung J, Peacock A, Colledge S, Grebely J, Cunningham EB, Hickman M, et al. A Global Meta-Analysis on HIV, Hepatitis C and Hepatitis B Among People Who Inject Drugs - do Gender Differences Vary by Country-Level Indicators? *J Infect Dis* (2019) 220(1):78–90. doi: 10.1093/infdis/jiz058
13. Mimiaga MJ, Reisner SL, Grasso C, Crane HM, Safren SA, Kitahata MM, et al. Substance Use Among HIV-infected Patients Engaged in Primary Care in the United States: Findings From the Centers for AIDS Research Network of Integrated Clinical Systems Cohort. *Am J Public Health* (2013) 103 (8):1457–67. doi: 10.2105/AJPH.2012.301162
14. Stockman JK, Strathdee SA. HIV Among People Who Use Drugs: A Global Perspective of Populations At Risk. *J Acquir Immune Defic Syndr* (2010) 55 Suppl 1:S17–22. doi: 10.1097/QAI.0b013e3181f9c04c
15. UNAIDS. Seizing the Moment: Tackling Entrenched Inequalities to End Epidemics. In: *Global AIDS Update*. Geneva, Switzerland: Joint United Nations Programme on HIV/AIDS (2020).
16. Cadet JL, Bisagno V, Milroy CM. Neuropathology of Substance Use Disorders. *Acta Neuropathol* (2014) 127(1):91–107. doi: 10.1007/s00401-013-1221-7
17. Dash S, Balasubramaniam M, Villalta F, Dash C, Pandhare J. Impact of Cocaine Abuse on HIV Pathogenesis. *Front Microbiol* (2015) 6:1111. doi: 10.3389/fmicb.2015.01111
18. Hauser KF, Fitting S, Dever SM, Podhaizer EM, Knapp PE. Opiate Drug Use and the Pathophysiology of Neuroaids. *Curr HIV Res* (2012) 10(5):435–52. doi: 10.2174/157016212802138779
19. Buch S, Yao H, Guo M, Mori T, Mathias-Costa B, Singh V, et al. Cocaine and HIV-1 Interplay in CNS: Cellular and Molecular Mechanisms. *Curr HIV Res* (2012) 10(5):425–8. doi: 10.2174/157016212802138823
20. Wang B, Chen T, Xue L, Wang J, Jia Y, Li G, et al. Methamphetamine Exacerbates Neuroinflammatory Response to Lipopolysaccharide by

Activating Dopamine D1-like Receptors. *Int Immunopharmacol* (2019) 73:1–9. doi: 10.1016/j.intimp.2019.04.053
21. Gosztonyi G, Schmidt V, Nickel R, Rothschild MA, Camacho S, Siegel G, et al. Neuropathologic Analysis of Postmortal Brain Samples of HIV-seropositive and -Seronegative I.V. Drug Addicts. *Forensic Sci Int* (1993) 62(1-2):101–5. doi: 10.1016/0379-0738(93)90052-C
22. Webber MP, Schoenbaum EE, Gourevitch MN, Buono D, Klein RS. A Prospective Study of HIV Disease Progression in Female and Male Drug Users. *AIDS* (1999) 13(2):257–62. doi: 10.1097/00002030-199902040-00014
23. Rippeth JD, Heaton RK, Carey CL, Marcotte TD, Moore DJ, Gonzalez R, et al. Methamphetamine Dependence Increases Risk of Neuropsychological Impairment in HIV Infected Persons. *J Int Neuropsychol Soc* (2004) 10(1):1–14. doi: 10.1017/S1355617704101021
24. Meyer VJ, Rubin LH, Martin E, Weber KM, Cohen MH, Golub ET, et al. HIV and Recent Illicit Drug Use Interact to Affect Verbal Memory in Women. *J Acquir Immune Defic Syndr* (2013) 63(1):67–76. doi: 10.1097/QAI.0b013e318289565c
25. Weber E, Morgan EE, Iudicello JE, Blackstone K, Grant I, Ellis RJ, et al. Substance Use is a Risk Factor for Neurocognitive Deficits and Neuropsychiatric Distress in Acute and Early HIV Infection. *J Neurovirol* (2013) 19(1):65–74. doi: 10.1007/s13365-012-0141-y
26. Hidalgo M, Atluri VS, Nair M. Drugs of Abuse in HIV Infection and Neurotoxicity. *Front Microbiol* (2015) 6:217. doi: 10.3389/fmicb.2015.00217
27. Gates TM, Cysique LA. The Chronicity of HIV Infection Should Drive the Research Strategy of NeuroHIV Treatment Studies: A Critical Review. *CNS Drugs* (2016) 30(1):53–69. doi: 10.1007/s40263-015-0302-7
28. Fenton MC, Keyes K, Geier T, Greenstein E, Skodol A, Krueger B, et al. Psychiatric Comorbidity and the Persistence of Drug Use Disorders in the United States. *Addiction* (2012) 107(3):599–609. doi: 10.1111/j.1360-0443.2011.03638.x
29. Dhillon NK, Williams R, Peng F, Tsai YJ, Dhillon S, Nicolay B, et al. Cocaine-Mediated Enhancement of Virus Replication in Macrophages: Implications for Human Immunodeficiency Virus-Associated Dementia. *J Neurovirol* (2007) 13(6):483–95. doi: 10.1080/13550280701528684
30. Guo CJ, Li Y, Tian S, Wang X, Douglas SD, Ho WZ. Morphine Enhances HIV Infection of Human Blood Mononuclear Phagocytes Through Modulation of Beta-Chemokines and CCR5 Receptor. *J Investig Med* (2002) 50(6):435–42. doi: 10.1136/jim-50-06-03
31. Liang H, Wang X, Chen H, Song L, Ye L, Wang SH, et al. Methamphetamine Enhances HIV Infection of Macrophages. *Am J Pathol* (2008) 172(6):1617–24. doi: 10.2353/ajpath.2008.070971
32. Avalos CR, Abreu CM, Queen SE, Li M, Price S, Shirk EN, et al. Brain Macrophages in Simian Immunodeficiency Virus-Infected, Antiretroviral-Suppressed Macaques: A Functional Latent Reservoir. *mBio* (2017) 8(4):e01186-17. doi: 10.1128/mBio.01186-17
33. Mallard J, Williams K. An SIV Macaque Model of SIV and HAND: The Need for Adjunctive Therapies in HIV That Target Activated Monocytes and Macrophages. *J Neurovirol* (2018) 24(2):213–9. doi: 10.1007/s13365-018-0616-6
34. Rappaport J, Volsky DJ. Role of the Macrophage in HIV-associated Neurocognitive Disorders and Other Comorbidities in Patients on Effective Antiretroviral Treatment. *J Neurovirol* (2015) 21(3):235–41. doi: 10.1007/s13365-015-0346-y
35. Navia BA, Cho ES, Petito CK, Price RW. The AIDS Dementia Complex: II. Neuropathology. *Ann Neurol* (1986) 19(6):525–35. doi: 10.1002/ana.410190603
36. Wang X, Loram LC, Ramos K, de Jesus AJ, Thomas J, Cheng K, et al. Morphine Activates Neuroinflammation in a Manner Parallel to Endotoxin. *Proc Natl Acad Sci United States America* (2012) 109(16):6325–30. doi: 10.1073/pnas.1200130109
37. Northcutt AL, Hutchinson MR, Wang X, Baratta MV, Hiranita T, Cochran TA, et al. DAT Isn't All That: Cocaine Reward and Reinforcement Require Toll-like Receptor 4 Signaling. *Mol Psychiatry* (2015) 20(12):1525–37. doi: 10.1038/mp.2014.177
38. Thomas DM, Walker PD, Benjamins JA, Geddes TJ, Kuhn DM. Methamphetamine Neurotoxicity in Dopamine Nerve Endings of the Striatum is Associated With Microglial Activation. *J Pharmacol Exp Ther* (2004) 311(1):1. doi: 10.1124/jpet.104.070961
39. Bachtell RK, Jones JD, Heinzerling KG, Beardsley PM, Comer SD. Glial and Neuroinflammatory Targets for Treating Substance Use Disorders. *Drug Alcohol Depend* (2017) 180:156–70. doi: 10.1016/j.drugalcdep.2017.08.003
40. Little KY, Ramssen E, Welchko R, Volberg V, Roland CJ, Cassin B. Decreased Brain Dopamine Cell Numbers in Human Cocaine Users. *Psychiatry Res* (2009) 168(3):173–80. doi: 10.1016/j.psychres.2008.10.034
41. Hutchinson MR, Lewis SS, Coats BD, Skyba DA, Crysdale NY, Berkelhammer DL, et al. Reduction of Opioid Withdrawal and Potentiation of Acute Opioid Analgesia by Systemic AV411 (Ibudilast). *Brain Behav Immun* (2009) 23(2):240–50. doi: 10.1016/j.bbi.2008.09.012
42. Kumar AM, Borodowsky I, Fernandez B, Gonzalez L, Kumar M. Human Immunodeficiency Virus Type 1 RNA Levels in Different Regions of Human Brain: Quantification Using Real-Time Reverse Transcriptase-Polymerase Chain Reaction. *J Neurovirol* (2007) 13(3):210–24. doi: 10.1080/13550280701327038
43. Wiley CA, Soontornniyomkij V, Radhakrishnan L, Masliah E, Mellors J, Hermann SA, et al. Distribution of Brain HIV Load in AIDS. *Brain Pathol* (1998) 8(2):277–84. doi: 10.1111/j.1750-3639.1998.tb00153.x
44. Di Chiara G, Imperato A. Drugs Abused by Humans Preferentially Increase Synaptic Dopamine Concentrations in the Mesolimbic System of Freely Moving Rats. *Proc Natl Acad Sci USA* (1988) 85(14):5274–8. doi: 10.1073/pnas.85.14.5274
45. Pierce RC, Kumaresan V. The Mesolimbic Dopamine System: The Final Common Pathway for the Reinforcing Effect of Drugs of Abuse? *Neurosci Biobehav Rev* (2006) 30(2):215–38. doi: 10.1016/j.neubiorev.2005.04.016
46. Pinoli M, Marino F, Cosentino M. Dopaminergic Regulation of Innate Immunity: A Review. *J Neuroimmune Pharmacol* (2017) 12(4):602–23. doi: 10.1007/s11481-017-9749-2
47. Yan Y, Jiang W, Liu L, Wang X, Ding C, Tian Z, et al. Dopamine Controls Systemic Inflammation Through Inhibition of NLRP3 Inflammasome. *Cell* (2015) 160(1):62–73. doi: 10.1016/j.cell.2014.11.047
48. Castellani G, Contarini G, Mereu M, Albanesi E, Devroye C, D'Amore C, et al. Dopamine-Mediated Immunomodulation Affects Choroid Plexus Function. *Brain Behav Immun* (2019) 81:138–50. doi: 10.1016/j.bbi.2019.06.006
49. Vidal PM, Pacheco R. The Cross-Talk Between the Dopaminergic and the Immune System Involved in Schizophrenia. *Front Pharmacol* (2020) 11:394. doi: 10.3389/fphar.2020.00394
50. Nolan RA, Muir R, Runner K, Haddad EK, Gaskill PJ. Role of Macrophage Dopamine Receptors in Mediating Cytokine Production: Implications for Neuroinflammation in the Context of HIV-Associated Neurocognitive Disorders. *J Neuroimmune Pharmacol* (2018) 14(1):134–56. doi: 10.1007/s11481-018-9825-2
51. Wang B, Chen T, Li G, Jia Y, Wang J, Xue L, et al. Dopamine Alters Lipopolysaccharide-Induced Nitric Oxide Production in Microglial Cells Via Activation of D1-Like Receptors. *Neurochem Res* (2019) 44(4):947–58. doi: 10.1007/s11064-019-02730-7
52. Matt SM, Gaskill PJ. Where Is Dopamine and How do Immune Cells See it?: Dopamine-Mediated Immune Cell Function in Health and Disease. *J Neuroimmune Pharmacol* (2019) 15(1):114–64. doi: 10.1007/s11481-019-09851-4
53. Nolan R, Gaskill PJ. The Role of Catecholamines in HIV Neuropathogenesis. *Brain Res* (2018) 1702:54–73. doi: 10.1016/j.brainres.2018.04.030
54. Gaskill PJ, Calderon TM, Luers AJ, Eugenin EA, Javitch JA, Berman JW. Human Immunodeficiency Virus (HIV) Infection of Human Macrophages is Increased by Dopamine: A Bridge Between HIV-associated Neurologic Disorders and Drug Abuse. *Am J Pathol* (2009) 175(3):1148–59. doi: 10.2353/ajpath.2009.081067
55. Gaskill PJ, Yano HH, Kalpana GV, Javitch JA, Berman JW. Dopamine Receptor Activation Increases HIV Entry Into Primary Human Macrophages. *PloS One* (2014) 9(9):e108232. doi: 10.1371/journal.pone.0108232
56. Nickoloff-Bybel EA, Mackie P, Runner K, Matt SM, Khoshbouei H, Gaskill PJ. Dopamine Increases HIV Entry Into Macrophages by Increasing Calcium Release Via an Alternative Signaling Pathway. *Brain Behav Immun* (2019) 82:239–52. doi: 10.1016/j.bbi.2019.08.191
57. Calderon TM, Williams DW, Lopez L, Eugenin EA, Cheney L, Gaskill PJ, et al. Dopamine Increases Cd14(+)Cd16(+) Monocyte Transmigration

Across the Blood Brain Barrier: Implications for Substance Abuse and HIV Neuropathogenesis. *J Neuroimmune Pharmacol* (2017) 12(2):353–70. doi: 10.1007/s11481-017-9726-9
58. Fan Y, Chen Z, Pathak JL, Carneiro AMD, Chung CY. Differential Regulation of Adhesion and Phagocytosis of Resting and Activated Microglia by Dopamine. *Front Cell Neurosci* (2018) 12:309–9. doi: 10.3389/fncel.2018.00309
59. Saha B, Mondal AC, Majumder J, Basu S, Dasgupta PS. Physiological Concentrations of Dopamine Inhibit the Proliferation and Cytotoxicity of Human CD4+ and CD8+ T Cells In Vitro: A Receptor-Mediated Mechanism. *Neuroimmunomodulation* (2001) 9(1):23–33. doi: 10.1159/000049004
60. Nolan RA, Reeb KL, Rong Y, Matt SM, Johnson HS, Runner K, et al. Dopamine Activates NF-κb and Primes the NLRP3 Inflammasome in Primary Human Macrophages. *Brain Behav Immun Health* (2020) 2:100030. doi: 10.1016/j.bbih.2019.100030
61. Colfax GN, Vittinghoff E, Grant R, Lum P, Spotts G, Hecht FM. Frequent Methamphetamine Use is Associated With Primary non-Nucleoside Reverse Transcriptase Inhibitor Resistance. *Aids* (2007) 21(2):239–41. doi: 10.1097/QAD.0b013e3280114a29
62. Arnsten JH, Demas PA, Grant RW, Gourevitch MN, Farzadegan H, Howard AA, et al. Impact of Active Drug Use on Antiretroviral Therapy Adherence and Viral Suppression in HIV-infected Drug Users. *J Gen Intern Med* (2002) 17(5):377–81. doi: 10.1007/s11606-002-0044-3
63. Kipp AM, Desruisseau AJ, Qian HZ. Non-Injection Drug Use and HIV Disease Progression in the Era of Combination Antiretroviral Therapy. *J Subst Abuse Treat* (2011) 40(4):386–96. doi: 10.1016/j.jsat.2011.01.001
64. Fairbairn N, Kerr T, Milloy MJ, Zhang R, Montaner J, Wood E. Crystal Methamphetamine Injection Predicts Slower HIV RNA Suppression Among Injection Drug Users. *Addict Behav* (2011) 36(7):762–3. doi: 10.1016/j.addbeh.2011.02.001
65. Ellis RJ, Childers ME, Cherner M, Lazzaretto D, Letendre S, Grant I. Increased Human Immunodeficiency Virus Loads in Active Methamphetamine Users are Explained by Reduced Effectiveness of Antiretroviral Therapy. *J Infect Dis* (2003) 188(12):1820–6. doi: 10.1086/379894
66. Ghorpade A, Xia MQ, Hyman BT, Persidsky Y, Nukuna A, Bock P, et al. Role of the Beta-Chemokine Receptors CCR3 and CCR5 in Human Immunodeficiency Virus Type 1 Infection of Monocytes and Microglia. *J Virol* (1998) 72(4):3351–61. doi: 10.1128/JVI.72.4.3351-3361.1998
67. Albright AV, Shieh JT, Itoh T, Lee B, Pleasure D, O'Connor MJ, et al. Microglia Express CCR5, CXCR4, and CCR3, But of These, CCR5 is the Principal Coreceptor for Human Immunodeficiency Virus Type 1 Dementia Isolates. *J Virol* (1999) 73(1):205–13. doi: 10.1128/JVI.73.1.205-213.1999
68. Marcondes MCG, Flynn C, Watry DD, Zandonatti M, Fox HS. Methamphetamine Increases Brain Viral Load and Activates Natural Killer Cells in Simian Immunodeficiency Virus-Infected Monkeys. *Am J Pathol* (2010) 177(1):355–61. doi: 10.2353/ajpath.2010.090953
69. Najera JA, Bustamante EA, Bortell N, Morsey B, Fox HS, Ravasi T, et al. Methamphetamine Abuse Affects Gene Expression in Brain-Derived Microglia of SIV-infected Macaques to Enhance Inflammation and Promote Virus Targets. *BMC Immunol* (2016) 17(1):7–7. doi: 10.1186/s12865-016-0145-0
70. Nayak SU, Cicalese S, Tallarida C, Oliver CF, Rawls SM. Chemokine CCR5 and Cocaine Interactions in the Brain: Cocaine Enhances Mesolimbic CCR5 mRNA Levels and Produces Place Preference and Locomotor Activation That are Reduced by a CCR5 Antagonist. *Brain Behav Immun* (2020) 83:288–92. doi: 10.1016/j.bbi.2019.09.017
71. Wierda RJ, Kuipers HF, van Eggermond MCJA, Benard A, van Leeuwen JC, Carluccio S, et al. Epigenetic Control of CCR5 Transcript Levels in Immune Cells and Modulation by Small Molecules Inhibitors. *J Cell Mol Med* (2012) 16(8):1866–77. doi: 10.1111/j.1582-4934.2011.01482.x
72. Choi DY, Lee MK, Hong JT. Lack of CCR5 Modifies Glial Phenotypes and Population of the Nigral Dopaminergic Neurons, But Not MPTP-induced Dopaminergic Neurodegeneration. *Neurobiol Dis* (2013) 49:159–68. doi: 10.1016/j.nbd.2012.08.001
73. Lee B, Sharron M, Blanpain C, Doranz BJ, Vakili J, Setoh P, et al. Epitope Mapping of CCR5 Reveals Multiple Conformational States and Distinct But Overlapping Structures Involved in Chemokine and Coreceptor Function. *J Biol Chem* (1999) 274(14):9617–26. doi: 10.1074/jbc.274.14.9617
74. Flegler AJ, Cianci GC, Hope TJ. CCR5 Conformations are Dynamic and Modulated by Localization, Trafficking and G Protein Association. *PloS One* (2014) 9(2):e89056. doi: 10.1371/journal.pone.0089056
75. Berro R, Klasse PJ, Lascano D, Flegler A, Nagashima KA, Sanders RW, et al. Multiple CCR5 Conformations on the Cell Surface Are Used Differentially by Human Immunodeficiency Viruses Resistant or Sensitive to CCR5 Inhibitors. *J Virol* (2011) 85(16):8227–40. doi: 10.1128/JVI.00767-11
76. Schnur E, Kessler N, Zherdev Y, Noah E, Scherf T, Ding F-X, et al. NMR Mapping of RANTES Surfaces Interacting With CCR5 Using Linked Extracellular Domains. *FEBS J* (2013) 280(9):2068–84. doi: 10.1111/febs.12230
77. Anastassopoulou CG, Ketas TJ, Klasse PJ, Moore JP. Resistance to CCR5 Inhibitors Caused by Sequence Changes in the Fusion Peptide of HIV-1 Gp41. *Proc Natl Acad Sci United States America* (2009) 106(13):5318–23. doi: 10.1073/pnas.0811713106
78. Cardaba CM, Kerr JS, Mueller A. CCR5 Internalisation and Signalling Have Different Dependence on Membrane Lipid Raft Integrity. *Cell Signal* (2008) 20(9):1687–94. doi: 10.1016/j.cellsig.2008.05.014
79. Wang J, Crawford K, Yuan M, Wang H, Gorry PR, Gabuzda D. Regulation of CC Chemokine Receptor 5 and CD4 Expression and Human Immunodeficiency Virus Type 1 Replication in Human Macrophages and Microglia by T Helper Type 2 Cytokines. *J Infect Dis* (2002) 185(7):885–97. doi: 10.1086/339522
80. Platt EJ, Wehrly K, Kuhmann SE, Chesebro B, Kabat D. Effects of CCR5 and CD4 Cell Surface Concentrations on Infections by Macrophagetropic Isolates of Human Immunodeficiency Virus Type 1. *J Virol* (1998) 72(4):2855. doi: 10.1128/JVI.72.4.2855-2864.1998
81. Ostrowski MA, Justement SJ, Catanzaro A, Hallahan CA, Ehler LA, Mizell SB, et al. Expression of Chemokine Receptors CXCR4 and CCR5 in HIV-1-infected and Uninfected Individuals. *J Immunol* (1998) 161(6):3195–201.
82. Reynes J, Portales P, Segondy M, Baillat V, Andre P, Reant B, et al. Cd4+ T Cell Surface CCR5 Density as a Determining Factor of Virus Load in Persons Infected With Human Immunodeficiency Virus Type 1. *J Infect Dis* (2000) 181(3):927–32. doi: 10.1086/315315
83. Basova L, Najera JA, Bortell N, Wang D, Moya R, Lindsey A, et al. Dopamine and its Receptors Play a Role in the Modulation of CCR5 Expression in Innate Immune Cells Following Exposure to Methamphetamine: Implications to HIV Infection. *PloS One* (2018) 13(6):e0199861. doi: 10.1371/journal.pone.0199861
84. Berman SB, Hastings TG. Dopamine Oxidation Alters Mitochondrial Respiration and Induces Permeability Transition in Brain Mitochondria: Implications for Parkinson's Disease. *J Neurochem* (1999) 73(3):1127–37. doi: 10.1046/j.1471-4159.1999.0731127.x
85. Meiser J, Weindl D, Hiller K. Complexity of Dopamine Metabolism. *Cell Communication Signaling* (2013) 11(1):34. doi: 10.1186/1478-811X-11-34
86. Ryan SK, Gonzalez MV, Garifallou JP, Bennett FC, Williams KS, Sotuyo NP, et al. Neuroinflammation and EIF2 Signaling Persist Despite Antiretroviral Treatment in an Hipsc Tri-culture Model of HIV Infection. *Stem Cell Rep* (2020) 14(4):703–16. doi: 10.1016/j.stemcr.2020.02.010
87. Garcia-Mesa Y, Jay TR, Checkley MA, Luttge B, Dobrowolski C, Valadkhan S, et al. Immortalization of Primary Microglia: A New Platform to Study HIV Regulation in the Central Nervous System. *J Neurovirol* (2017) 23(1):47–66. doi: 10.1007/s13365-016-0499-3
88. Gendelman HE, Orenstein JM, Martin MA, Ferrua C, Mitra R, Phipps T, et al. Efficient Isolation and Propagation of Human Immunodeficiency Virus on Recombinant Colony-Stimulating Factor 1-Treated Monocytes. *J Exp Med* (1988) 167(4):1428–41. doi: 10.1084/jem.167.4.1428
89. Lobritz MA, Ratcliff AN, Marozsan AJ, Dudley DM, Tilton JC, Arts EJ. Multifaceted Mechanisms of HIV Inhibition and Resistance to CCR5 Inhibitors PSC-RANTES and Maraviroc. *Antimicrob Agents Chemother* (2013) 57(6):2640–50. doi: 10.1128/AAC.02511-12
90. El-Hage N, Dever SM, Podhaizer EM, Arnatt CK, Zhang Y, Hauser KF. A Novel Bivalent HIV-1 Entry Inhibitor Reveals Fundamental Differences in CCR5-μ-Opioid Receptor Interactions Between Human Astroglia and Microglia. *AIDS (London England)* (2013) 27(14):2181–90. doi: 10.1097/QAD.0b013e3283639804
91. Abel S, Back DJ, Vourvahis M. Maraviroc: Pharmacokinetics and Drug Interactions. *Antivir Ther* (2009) 14(5):607–18. doi: 10.3851/IMP1297

92. Mora-Peris B, Croucher A, Else LJ, Vera JH, Khoo S, Scullard G, et al. Pharmacokinetic Profile and Safety of 150 Mg of Maraviroc Dosed With 800/100 Mg of Darunavir/Ritonavir All Once Daily, With and Without Nucleoside Analogues, in HIV-infected Subjects. *J Antimicrob Chemother* (2013) 68(6):1348–53. doi: 10.1093/jac/dkt006
93. Bol SM, van Remmerden Y, Sietzema JG, Kootstra NA, Schuitemaker H, van't Wout AB. Donor Variation in In Vitro HIV-1 Susceptibility of Monocyte-Derived Macrophages. *Virology* (2009) 390(2):205–11. doi: 10.1016/j.virol.2009.05.027
94. Anzinger JJ, Olinger GG, Spear GT. Donor Variability in HIV Binding to Peripheral Blood Mononuclear Cells. *Virol J* (2008) 5:95–5. doi: 10.1186/1743-422X-5-95
95. Jourjy J, Dahl K, Huesgen E. Antiretroviral Treatment Efficacy and Safety in Older Hiv-Infected Adults. *Pharmacotherapy* (2015) 35(12):1140–51. doi: 10.1002/phar.1670
96. Kuang Y-Q, Charette N, Frazer J, Holland PJ, Attwood KM, Dellaire G, et al. Dopamine Receptor-Interacting Protein 78 Acts as a Molecular Chaperone for CCR5 Chemokine Receptor Signaling Complex Organization. *PloS One* (2012) 7(7):e40522–2. doi: 10.1371/journal.pone.0040522
97. Picton ACP, Shalekoff S, Paximadis M, Tiemessen CT. Marked Differences in CCR5 Expression and Activation Levels in Two South African Populations. *Immunology* (2012) 136(4):397–407. doi: 10.1111/j.1365-2567.2012.03592.x
98. Prakash M, Patterson S, Kapembwa MS. Hormonal Upregulation of CCR5 Expression on T Lymphocytes as a Possible Mechanism for Increased HIV-1 Risk. *J Acquir Immune Defic Syndr* (2005) 38 Suppl 1:S14–6. doi: 10.1097/01.qai.0000167028.33525.f8
99. Cabrera-Munoz E, Fuentes-Romero LL, Zamora-Chavez J, Camacho-Arroyo I, Soto-Ramirez LE. Effects of Progesterone on the Content of CCR5 and CXCR4 Coreceptors in PBMCs of Seropositive and Exposed But Uninfected Mexican Women to HIV-1. *J Steroid Biochem Mol Biol* (2012) 132(1-2):66–72. doi: 10.1016/j.jsbmb.2012.02.001
100. King CA, Baillie J, Sinclair JH. Human Cytomegalovirus Modulation of CCR5 Expression on Myeloid Cells Affects Susceptibility to Human Immunodeficiency Virus Type 1 Infection. *J Gen Virol* (2006) 87(Pt 8):2171–80. doi: 10.1099/vir.0.81452-0
101. Araki KY, Sims JR, Bhide PG. Dopamine Receptor mRNA and Protein Expression in the Mouse Corpus Striatum and Cerebral Cortex During Pre- and Postnatal Development. *Brain Res 2007* (1156) p:31–45. doi: 10.1016/j.brainres.2007.04.043
102. Sozzani S, Ghezzi S, Iannolo G, Luini W, Borsatti A, Polentarutti N, et al. Interleukin 10 Increases CCR5 Expression and HIV Infection in Human Monocytes. *J Exp Med* (1998) 187(3):439–44. doi: 10.1084/jem.187.3.439
103. Houle M, Thivierge M, Le Gouill C, Stankovà J, Rola-Pleszczynski M. Il-10 Up-Regulates Ccr5 Gene Expression in Human Monocytes. *Inflammation* (1999) 23(3):241–51. doi: 10.1023/a:1020273903224
104. Periselneris J, Ercoli G, Pollard T, Chimalapati S, Camberlein E, Szylar G, et al. Relative Contributions of Extracellular and Internalized Bacteria to Early Macrophage Proinflammatory Responses to ≪Span Class=&Quot; Named-Content Genus-Species&Quot; Id=&Quot;named-content-1" <Streptococcus Pneumoniae≪/Span&Gt. *mBio* (2019) 10(5):e02144–19. doi: 10.1128/mBio.02144-19
105. Garelnabi M, Taylor-Smith LM, Bielska E, Hall RA, Stones D, May RC. Quantifying Donor-to-Donor Variation in Macrophage Responses to the Human Fungal Pathogen Cryptococcus Neoformans. *PloS One* (2018) 13(3):e0194615. doi: 10.1371/journal.pone.0194615
106. Buscher K, Ehinger E, Gupta P, Pramod AB, Wolf D, Tweet G, et al. Natural Variation of Macrophage Activation as Disease-Relevant Phenotype Predictive of Inflammation and Cancer Survival. *Nat Commun* (2017) 8:16041–1. doi: 10.1038/ncomms16041
107. Jaekal J, Abraham E, Azam T, Netea MG, Dinarello CA, Lim JS, et al. Individual LPS Responsiveness Depends on the Variation of Toll-Like Receptor (TLR) Expression Level. *J Microbiol Biotechnol* (2007) 17(11):1862–7.
108. van Wilgenburg B, Moore MD, James WS, Cowley SA. The Productive Entry Pathway of HIV-1 in Macrophages is Dependent on Endocytosis Through Lipid Rafts Containing CD4. *PloS One* (2014) 9(1):e86071. doi: 10.1371/journal.pone.0086071
109. Yi L, Fang J, Isik N, Chim J, Jin T. Hiv gp120-induced Interaction Between CD4 and CCR5 Requires Cholesterol-Rich Microenvironments Revealed by Live Cell Fluorescence Resonance Energy Transfer Imaging. *J Biol Chem* (2006) 281: (46):35446–53. doi: 10.1074/jbc.M607302200
110. Somkuwar SS, Fannon MJ, Head BP, Mandyam CD. Methamphetamine Reduces Expression of Caveolin-1 in the Dorsal Striatum: Implication for Dysregulation of Neuronal Function. *Neuroscience* (2016) 328:147–56. doi: 10.1016/j.neuroscience.2016.04.039
111. Yao H, Yang Y, Kim KJ, Bethel-Brown C, Gong N, Funa K, et al. Molecular Mechanisms Involving Sigma Receptor–Mediated Induction of MCP-1: Implication for Increased Monocyte Transmigration. *Blood* (2010) 115 (23):4951–62. doi: 10.1182/blood-2010-01-266221
112. Kong MM, Hasbi A, Mattocks M, Fan T, O'Dowd BF, George SR. Regulation of D1 Dopamine Receptor Trafficking and Signaling by Caveolin-1. *Mol Pharmacol* (2007) 72(5):1157–70. doi: 10.1124/mol.107.034769
113. Gildea JJ, Israel JA, Johnson AK, Zhang J, Jose PA, Felder RA. Caveolin-1 and Dopamine-Mediated Internalization of NaKATPase in Human Renal Proximal Tubule Cells. *Hyperten (Dallas Tex 1979)* (2009) 54(5):1070–6. doi: 10.1161/HYPERTENSIONAHA.109.134338
114. Nothdurfter C, Rammes G, Rein T, Rupprecht R. Pitfalls in Isolating Lipid Rafts. *Nat Rev Neurosci* (2007) 8: (7):567. doi: 10.1038/nrn2059-c1
115. Popik W, Alce TM. CD4 Receptor Localized to non-Raft Membrane Microdomains Supports HIV-1 Entry Identification of a Novel Raft Localization Marker in CD4. *J Biol Chem* (2004) 279: (1):704–12. doi: 10.1074/jbc.M306380200
116. Herz J, Filiano AJ, Smith A, Yogev N, Kipnis J. Myeloid Cells in the Central Nervous System. *Immunity* (2017) 46(6):943–56. doi: 10.1016/j.immuni.2017.06.007
117. Lacagnina MJ, Rivera PD, Bilbo SD. Glial and Neuroimmune Mechanisms as Critical Modulators of Drug Use and Abuse. *Neuropsychopharmacol Off Publ Am Coll Neuropsychopharmacol* (2017) 42(1):156–77. doi: 10.1038/npp.2016.121
118. Mastroeni D, Grover A, Leonard B, Joyce JN, Coleman PD, Kozik B, et al. Microglial Responses to Dopamine in a Cell Culture Model of Parkinson's Disease. *Neurobiol Aging* (2009) 30(11):1805–17. doi: 10.1016/j.neurobiolaging.2008.01.001
119. Kopec A, Smith CJ, Ayre NR, Sweat SC, Bilbo SD. Microglial dopamine receptor elimination defines sex-specific nucleus accumbens development and social behavior in adolescent rats. *Nat Commun* (2018) 9(1):3769. doi: 10.1038/s41467-018-06118-z
120. Huck JH, Freyer D, Bottcher C, Mladinov M, Muselmann-Genschow C, Thielke M, et al. De Novo Expression of Dopamine D2 Receptors on Microglia After Stroke. *J Cereb Blood Flow Metab* (2015) 35(11):1804–11. doi: 10.1038/jcbfm.2015.128
121. *Centers for Disease Control and Prevention Hiv Among People Aged 50 and Over* (2018). Available at: https://www.cdc.gov/hiv/group/age/olderamericans/index.html.
122. Deren S, Cortes T, Dickson VV, Guilamo-Ramos V, Han BH, Karpiak S, et al. Substance Use Among Older People Living With HIV: Challenges for Health Care Providers. *Front Public Health* (2019) 7:94. doi: 10.3389/fpubh.2019.00094
123. Salamanca SA, Sorrentino EE, Nosanchuk JD, Martinez LR. Impact of Methamphetamine on Infection and Immunity. *Front Neurosci* (2014) 8:445. doi: 10.3389/fnins.2014.00445
124. Durvasula R, Miller TR. Substance Abuse Treatment in Persons With HIV/AIDS: Challenges in Managing Triple Diagnosis. *Behav Med* (2014) 40 (2):43–52. doi: 10.1080/08964289.2013.866540
125. Suzuki S, Chuang AJ, Chuang LF, Doi RH, Chuang RY. Morphine Promotes Simian Acquired Immunodeficiency Syndrome Virus Replication in Monkey Peripheral Mononuclear Cells: Induction of CC Chemokine Receptor 5 Expression for Virus Entry. *J Infect Dis* (2002) 185(12):1826–9. doi: 10.1086/340816
126. Parikh N, Nonnemacher MR, Pirrone V, Block T, Mehta A, Wigdahl B. Substance Abuse, HIV-1 and Hepatitis. *Curr HIV Res* (2012) 10(7):557–71. doi: 10.2174/157016212803306023
127. Feldman MB, Thomas JA, Alexy ER, Irvine MK. Crystal Methamphetamine Use and HIV Medical Outcomes Among HIV-infected Men Who Have Sex With Men Accessing Support Services in New York. *Drug Alcohol Depend* (2015) 147:266–71. doi: 10.1016/j.drugalcdep.2014.09.780
128. Baum MK, Rafie C, Lai S, Sales S, Page B, Campa A. Crack-Cocaine Use Accelerates HIV Disease Progression in a Cohort of HIV-positive Drug

Users. *J Acquir Immune Defic Syndr* (2009) 50(1):93–9. doi: 10.1097/QAI.0b013e3181900129
129. Carrico AW. Substance Use and HIV Disease Progression in the HAART Era: Implications for the Primary Prevention of HIV. *Life Sci* (2011) 88(21-22):940–7. doi: 10.1016/j.lfs.2010.10.002
130. Gill AJ, Kolson DL. Chronic Inflammation and the Role for Cofactors (Hepatitis C, Drug Abuse, Antiretroviral Drug Toxicity, Aging) in HAND Persistence. *Curr HIV/AIDS Rep* (2014) 11(3):325–35. doi: 10.1007/s11904-014-0210-3
131. Bell JE, Arango JC, Anthony IC. Neurobiology of Multiple Insults: HIV-1-associated Brain Disorders in Those Who Use Illicit Drugs. *J Neuroimmune Pharmacol* (2006) 1(2):182–91. doi: 10.1007/s11481-006-9018-2
132. Spudich S. HIV and Neurocognitive Dysfunction. *Curr HIV/AIDS Rep* (2013) 10(3):235–43. doi: 10.1007/s11904-013-0171-y
133. Sekine Y, Ouchi Y, Sugihara G, Takei N, Yoshikawa E, Nakamura K, et al. Methamphetamine Causes Microglial Activation in the Brains of Human Abusers. *J Neurosci* (2008) 28(22):5756–61. doi: 10.1523/JNEUROSCI.1179-08.2008
134. Colin P, Zhou Z, Staropoli I, Garcia-Perez J, Gasser R, Armani-Tourret M, et al. CCR5 Structural Plasticity Shapes HIV-1 Phenotypic Properties. *PloS Pathog* (2018) 14(12):e1007432. doi: 10.1371/journal.ppat.1007432
135. Blanpain C, Vanderwinden J-M, Cihak J, Wittamer V, Le Poul E, Issafras H, et al. Multiple Active States and Oligomerization of CCR5 Revealed by Functional Properties of Monoclonal Antibodies. *Mol Biol Cell* (2002) 13 (2):723–37. doi: 10.1091/mbc.01-03-0129
136. Navenot JM, Wang ZX, Trent JO, Murray JL, Hu QX, DeLeeuw L, et al. Molecular Anatomy of CCR5 Engagement by Physiologic and Viral Chemokines and HIV-1 Envelope Glycoproteins: Differences in Primary Structural Requirements for RANTES, MIP-1 Alpha, and vMIP-II Binding. *J Mol Biol* (2001) 313(5):1181–93. doi: 10.1006/jmbi.2001.5086
137. Dragic T, Trkola A, Thompson DA, Cormier EG, Kajumo FA, Maxwell E, et al. A Binding Pocket for a Small Molecule Inhibitor of HIV-1 Entry Within the Transmembrane Helices of CCR5. *Proc Natl Acad Sci U.S.A.* (2000) 97 (10):5639–44. doi: 10.1073/pnas.090576697
138. Tan Q, Zhu Y, Li J, Chen Z, Han GW, Kufareva I, et al. Structure of the CCR5 Chemokine receptor-HIV Entry Inhibitor Maraviroc Complex. *Science* (2013) 341(6152):1387–90. doi: 10.1126/science.1241475
139. Laakso MM, Lee FH, Haggarty B, Agrawal C, Nolan KM, Biscone M, et al. V3 Loop Truncations in HIV-1 Envelope Impart Resistance to Coreceptor Inhibitors and Enhanced Sensitivity to Neutralizing Antibodies. *PloS Pathog* (2007) 3(8):e117. doi: 10.1371/journal.ppat.0030117
140. Moore JP, Kuritzkes DR. A Piece De Resistance: How HIV-1 Escapes Small Molecule CCR5 Inhibitors. *Curr Opin HIV AIDS* (2009) 4(2):118–24. doi: 10.1097/COH.0b013e3283223d46
141. Pfaff JM, Wilen CB, Harrison JE, Demarest JF, Lee B, Doms RW, et al. Hiv-1 Resistance to CCR5 Antagonists Associated With Highly Efficient Use of CCR5 and Altered Tropism on Primary CD4≪Sup<+≪/Sup< T Cells. *J Virol* (2010) 84(13):6505. doi: 10.1128/JVI.00374-10
142. Lin Y-L, Mettling C, Portales P, Reynes J, Clot J, Corbeau P. Cell Surface CCR5 Density Determines the Postentry Efficiency of R5 HIV-1 Infection. *Proc Natl Acad Sci* (2002) 99(24):15590. doi: 10.1073/pnas.242134499
143. Gorry PR, Taylor J, Holm GH, Mehle A, Morgan T, Cayabyab M, et al. Increased CCR5 Affinity and Reduced CCR5/CD4 Dependence of a Neurovirulent Primary Human Immunodeficiency Virus Type 1 Isolate. *J Virol* (2002) 76(12):6277–92. doi: 10.1128/JVI.76.12.6277-6292.2002
144. Mefford ME, Kunstman K, Wolinsky SM, Gabuzda D. Bioinformatic Analysis of Neurotropic HIV Envelope Sequences Identifies Polymorphisms in the gp120 Bridging Sheet That Increase Macrophage-Tropism Through Enhanced Interactions With CCR5. *Virology* (2015) 481:210–22. doi: 10.1016/j.virol.2015.01.032
145. Gorry PR, Francella N, Lewin SR, Collman RG. HIV-1 Envelope-Receptor Interactions Required for Macrophage Infection and Implications for Current HIV-1 Cure Strategies. *J Leukoc Biol* (2014) 95(1):71–81. doi: 10.1189/jlb.0713368
146. Salimi H, Roche M, Webb N, Gray LR, Chikere K, Sterjovski J, et al. Macrophage-Tropic HIV-1 Variants From Brain Demonstrate Alterations in the Way gp120 Engages Both CD4 and CCR5. *J Leukoc Biol* (2013) 93 (1):113–26. doi: 10.1189/jlb.0612308
147. Wu L, Paxton WA, Kassam N, Ruffing N, Rottman JB, Sullivan N, et al. CCR5 Levels and Expression Pattern Correlate With Infectability by Macrophage-Tropic HIV-1, In Vitro. *J Exp Med* (1997) 185(9):1681–91. doi: 10.1084/jem.185.9.1681
148. Boncompain G, Herit F, Tessier S, Lescure A, Del Nery E, Gestraud P, et al. Targeting CCR5 Trafficking to Inhibit HIV-1 Infection. *Sci Adv* (2019) 5(10): eaax0821. doi: 10.1126/sciadv.aax0821
149. Fox JM, Kasprowicz R, Hartley O, Signoret N. CCR5 Susceptibility to Ligand-Mediated Down-Modulation Differs Between Human T Lymphocytes and Myeloid Cells. *J Leuko Biol* (2015) 98(1):59–71. doi: 10.1189/jlb.2A0414-193RR
150. Carter GC, Bernstone L, Sangani D, Bee JW, Harder T, James W. HIV Entry in Macrophages is Dependent on Intact Lipid Rafts. *Virology* (2009) 386 (1):192–202. doi: 10.1016/j.virol.2008.12.031
151. Voulalas PJ, Schetz J, Undieh AS. Differential Subcellular Distribution of Rat Brain Dopamine Receptors and Subtype-Specific Redistribution Induced by Cocaine. *Mol Cell Neurosci* (2011) 46(3):645–54. doi: 10.1016/j.mcn.2011.01.004
152. Olbrich H, Proudfoot AEI, Oppermann M. Chemokine-Induced Phosphorylation of CC Chemokine Receptor 5 (CCR5). *J Leuko Biol* (1999) 65(3):281–5. doi: 10.1002/jlb.65.3.281
153. Bannert N, Craig S, Farzan M, Sogah D, Santo NV, Choe H, et al. Sialylated O-glycans and Sulfated Tyrosines in the NH2-terminal Domain of CC Chemokine Receptor 5 Contribute to High Affinity Binding of Chemokines. *J Exp Med* (2001) 194(11):1661–73. doi: 10.1084/jem.194.11.1661
154. Oppermann M. Chemokine Receptor CCR5: Insights Into Structure, Function, and Regulation. *Cell Signal* (2004) 16(11):1201–10. doi: 10.1016/j.cellsig.2004.04.007
155. Bhattacharyya S, Raote I, Bhattacharya A, Miledi R, Panicker MM. Activation, Internalization, and Recycling of the Serotonin 2A Receptor by Dopamine. *Proc Natl Acad Sci* (2006) 103(41):15248. doi: 10.1073/pnas.0606578103
156. Colin P, Benureau Y, Staropoli I, Wang Y, Gonzalez N, Alcami J, et al. HIV-1 Exploits CCR5 Conformational Heterogeneity to Escape Inhibition by Chemokines. *Proc Natl Acad Sci USA* (2013) 110(23):9475–80. doi: 10.1073/pnas.1222205110
157. Berro R, Yasmeen A, Abrol R, Trzaskowski B, Abi-Habib S, Grunbeck A, et al. Use of G-protein-coupled and -Uncoupled CCR5 Receptors by CCR5 Inhibitor-Resistant and -Sensitive Human Immunodeficiency Virus Type 1 Variants. *J Virol* (2013) 87(12):6569–81. doi: 10.1128/JVI.00099-13
158. Garcia-Perez J, Rueda P, Staropoli I, Kellenberger E, Alcami J, Arenzana-Seisdedos F, et al. New Insights Into the Mechanisms Whereby Low Molecular Weight CCR5 Ligands Inhibit HIV-1 Infection. *J Biol Chem* (2011) 286(7):4978–90. doi: 10.1074/jbc.M110.168955
159. Collman RG, Yi Y, Liu Q-H, Freedman BD. Chemokine Signaling and HIV-1 Fusion Mediated by Macrophage CXCR4: Implications for Target Cell Tropism. *J Leuko Biol* (2000) 68(3):318–23.
160. Joseph SB, Arrildt KT, Swanstrom AE, Schnell G, Lee B, Hoxie JA, et al. Quantification of Entry Phenotypes of Macrophage-Tropic HIV-1 Across a Wide Range of CD4 Densities. *J Virol* (2014) 88(4):1858–69. doi: 10.1128/JVI.02477-13
161. Stuerenburg HJ, Petersen K, Baumer T, Rosenkranz M, Buhmann C, Thomasius R. Plasma Concentrations of 5-HT, 5-HIAA, Norepinephrine, Epinephrine and Dopamine in Ecstasy Users. *Neuro Endocrinol Lett* (2002) 23(3):259–61.
162. Faraj BA, Camp VM, Davis DC, Kutner M, Cotsonis GA, Holloway T. Elevated Concentrations of Dopamine Sulfate in Plasma of Cocaine Abusers. *Biochem Pharmacol* (1993) 46(8):1453–7. doi: 10.1016/0006-2952(93)90111-9
163. Yeh SH, Lin MH, Kong FL, Chang CW, Hwang LC, Lin CF, et al. Evaluation of Inhibitory Effect of Recreational Drugs on Dopaminergic Terminal Neuron by PET and Whole-Body Autoradiography. *BioMed Res Int 2014* (2014) 157923. doi: 10.1155/2014/157923
164. Goldmann T, Wieghofer P, Jordao MJ, Prutek F, Hagemeyer N, Frenzel K, et al. Origin, Fate and Dynamics of Macrophages at Central Nervous System Interfaces. *Nat Immunol* (2016) 17(7):797–805. doi: 10.1038/ni.3423
165. Butovsky O, Jedrychowski MP, Moore CS, Cialic R, Lanser AJ, Gabriely G, et al. Identification of a Unique TGF-beta-dependent Molecular and Functional Signature in Microglia. *Nat Neurosci* (2014) 17(1):131–43. doi: 10.1038/nn.3599

166. Clayton KL, Garcia JV, Clements JE, Walker BD. Hiv Infection of Macrophages: Implications for Pathogenesis and Cure. *Pathog Immun* (2017) 2(2):179–92. doi: 10.20411/10.20411/pai.v2i2.204
167. Yadav A, Collman RG. CNS Inflammation and Macrophage/Microglial Biology Associated With HIV-1 Infection. *J Neuroimmune Pharmacol* (2009) 4(4):430–47. doi: 10.1007/s11481-009-9174-2
168. Minagar A, Shapshak P, Fujimura R, Ownby R, Heyes M, Eisdorfer C. The Role of Macrophage/Microglia and Astrocytes in the Pathogenesis of Three Neurologic Disorders: HIV-associated Dementia, Alzheimer Disease, and Multiple Sclerosis. *J Neurol Sci* (2002) 202(1):13–23. doi: 10.1016/S0022-510X(02)00207-1
169. Williams DW, Calderon TM, Lopez L, Carvallo-Torres L, Gaskill PJ, Eugenin EA, et al. Mechanisms of HIV Entry Into the CNS: Increased Sensitivity of HIV Infected CD14(+)CD16(+) Monocytes to CCL2 and Key Roles of CCR2, Jam-A, and ALCAM in Diapedesis. *PloS One* (2013) 8(7):e69270. doi: 10.1371/journal.pone.0069270
170. Crowe S, Zhu T, Muller WA. The Contribution of Monocyte Infection and Trafficking to Viral Persistence, and Maintenance of the Viral Reservoir in HIV Infection. *J Leukoc Biol* (2003) 74(5):635–41. doi: 10.1189/jlb.0503204

Conflict of Interest: The authors declare that the research was conducted in the absence of any commercial or financial relationships that could be construed as a potential conflict of interest.

frontiers in Immunology

ORIGINAL RESEARCH
published: 20 May 2021
doi: 10.3389/fimmu.2021.639378

Physiologically Relevant Concentrations of Dolutegravir, Emtricitabine, and Efavirenz Induce Distinct Metabolic Alterations in HeLa Epithelial and BV2 Microglial Cells

Joseph W. George, Jane E. Mattingly, Nashanthea J. Roland, Cassandra M. Small, Benjamin G. Lamberty, Howard S. Fox and Kelly L. Stauch *

Department of Neurological Sciences, University of Nebraska Medical Center, Omaha, NE, United States

OPEN ACCESS

Edited by:
Jorge Correale, Fundación Para la Lucha Contra las Enfermedades Neurológicas de la Infancia (FLENI), Argentina

Reviewed by:
Nadezda Apostolova, University of Valencia, Spain
Sylvia Fitting, University of North Carolina at Chapel Hill, United States

***Correspondence:**
Kelly L. Stauch
kelly.stauch@unmc.edu

Specialty section:
This article was submitted to Multiple Sclerosis and Neuroimmunology, a section of the journal Frontiers in Immunology

Received: *08 December 2020*
Accepted: *04 May 2021*
Published: *20 May 2021*

Citation:
George JW, Mattingly JE, Roland NJ, Small CM, Lamberty BG, Fox HS and Stauch KL (2021) Physiologically Relevant Concentrations of Dolutegravir, Emtricitabine, and Efavirenz Induce Distinct Metabolic Alterations in HeLa Epithelial and BV2 Microglial Cells. Front. Immunol. 12:639378. doi: 10.3389/fimmu.2021.639378

Microglia, the resident brain phagocytes, likely play a key role in human immunodeficiency virus (HIV) infection of the central nervous system (CNS) and subsequent neuropathogenesis; however, the nature of the infection-induced changes that yield damaging CNS effects and the stimuli that provoke microglial activation remains elusive, especially in the current era of using antiretroviral (ARV) drugs for ARV therapy (ART). Altered microglial metabolism can modulate cellular functionality and pathogenicity in neurological disease. While HIV infection itself alters brain energy metabolism, the effect of ARV drugs, particularly those currently used in treatment, on metabolism is understudied. Dolutegravir (DTG) and emtricitabine (FTC) combination, together with tenofovir (TAF or TDF), is one of the recommended first line treatments for HIV. Despite the relatively good tolerability and safety profile of FTC, a nucleoside reverse transcriptase inhibitor, and DTG, an integrase inhibitor, adverse side effects have been reported and highlight a need to understand off-target effects of these medications. We hypothesized that similar to previous ART regimen drugs, DTG and FTC side effects involve mitochondrial dysfunction. To increase detection of ARV-induced mitochondrial effects, highly glycolytic HeLa epithelial cells were forced to rely on oxidative phosphorylation by substituting galactose for glucose in the growth media. We assessed ATP levels, resazurin oxidation-reduction (REDOX), and mitochondrial membrane potential following 24-hour exposure (to approximate effects of one dose equivalent) to DTG, FTC, and efavirenz (EFV, a known mitotoxic ARV drug). Further, since microglia support productive HIV infection, act as latent HIV cellular reservoirs, and when dysfunctional likely contribute to HIV-associated neurocognitive disorders, the experiments were repeated using BV2 microglial cells. In HeLa cells, FTC decreased mitochondrial REDOX activity, while DTG, similar to EFV, impaired both mitochondrial ATP generation and REDOX activity. In contrast to HeLa cells, DTG increased cellular ATP generation and mitochondrial

REDOX activity in BV2 cells. Bioenergetic analysis revealed that DTG, FTC, and EFV elevated BV2 cell mitochondrial respiration. DTG and FTC exposure induced distinct mitochondrial functional changes in HeLa and BV2 cells. These findings suggest cell type-specific metabolic changes may contribute to the toxic side effects of these ARV drugs.

Keywords: antiretrovirals, dolutegravir, emtricitabine, glycolysis, microglia, mitochondria

INTRODUCTION

While antiretroviral therapy (ART) has led to tremendous reductions in morbidity and mortality associated with human immunodeficiency virus (HIV), antiretroviral (ARV) drugs are associated with a variety of peripheral and central adverse events (1, 2). Furthermore, as life expectancy for individuals living with HIV has increased, the long-term safety of ARV drugs has garnered increasing attention. Long-term complications continue to occur in HIV-infected individuals, despite the widespread use of ART, and can be related to the virus itself or to adverse effects of ARV drugs (3–5). The precise mechanisms of ARV toxicity are not fully understood, but in the case of efavirenz (EFV), we (6, 7), and others (8–12) have found effects on mitochondria.

Mitochondria, which produce energy for the cell *via* oxidative phosphorylation, have long been known to be affected by certain ARV drugs (13–16). In particular, the nucleoside reverse transcriptase inhibitors (NRTIs) affect mitochondrial function, and it has been proposed that NRTI mitochondrial toxicity may underlie the wide spectrum of clinical side effects caused by these agents (13). Similarly, neuro- and hepatotoxic effects of EFV are likely due to mitochondrial toxicity (6, 8, 11, 12, 17, 18). While EFV use is decreasing, it is important to understand if physiologically relevant concentrations of currently used ARV drugs affect mitochondrial functions. As dolutegravir (DTG) and emtricitabine (FTC, together with tenofovir (TAF or TDF)) combination is one of the first line treatments for HIV, these drugs were studied. While ARVs can affect many organs, the entry into the central nervous system (CNS) is frequently limited. DTG and FTC are both CNS penetrant, as is EFV, an ARV drug with known mitotoxic effects (19, 20).

Chronic neuroinflammation driven by glial activation is commonly implicated as a contributing factor to neurodegeneration and cognitive impairment in HIV-infected individuals (21, 22). Microglia, the CNS-resident macrophages, support productive HIV infection and likely play a major role in subsequent neurotoxicity (23, 24). Indeed, microglial activation during HIV infection is suggested to contribute to HIV-associated neurocognitive disorders (HAND) development. Modulation of microglial metabolism is increasingly recognized as a mechanism underlying activation of microglia in neurodegenerative diseases (24–26). HIV infection itself disturbs brain bioenergetics and metabolic disturbances in the CNS exist despite ART (27).

While all medications have potential side effects, it is important that these do not initiate or worsen any of the problems that HIV infection causes in the brain or elsewhere in the body. We hypothesized that similar to previous ART regimen drugs, DTG and FTC side effects involve mitochondrial dysfunction, and have the potential themselves to alter immunometabolism. The present study investigates changes in several metabolic parameters (ATP levels, resazurin oxidation-reduction (REDOX), mitochondrial membrane potential, and bioenergetics) in a non-CNS- and a CNS-derived cell line after treatment with DTG, FTC, or EFV. To increase detection of and ascribe the effects to ARV-induced mitochondrial toxicity, we employed the glucose-galactose assay. This assay, often utilized to preclinically screen for drug-induced mitochondrial dysfunction (28–30), involves culturing heavily glycolytic cells, such as HepG2 hepatoma and HeLa epithelial cells, in media where glucose has been replaced with galactose to force the cells to rely on mitochondrial oxidative phosphorylation for the production of ATP, increasing their sensitivity to mitotoxicants. Thus, HeLa cells were chosen for an initial screen for DTG- and FTC-induced mitochondrial changes, then upon identification of metabolic changes upon exposure to these ARV drugs additional experiments were performed in the well-used and characterized BV2 microglial cell line to uncover the relevance of these changes to immunometabolism. The ARV drugs were assessed separately to uncover the metabolic impact of each individual ARV drug, which is important as clinicians strive to use less toxic cART regimens.

MATERIALS AND METHODS

Cell Culture

HeLa and BV2 cells were cultured in DMEM (Gibco, Gaithersburg, MD) containing 10% FBS (Corning, Corning, New York), 1% PEN/STR (Gibco), and 4 mM L-glutamine (Gibco) in a humidified incubator with 5% CO_2 at 37°C. For Seahorse, cells were seeded at 15,000 cells/well in poly-D-lysine (PDL, Sigma, St. Louis, MO) coated 96-well microplates (Agilent Technologies, Santa Clara, CA). For ATP, AlamarBlue, and LDH, cells were seeded at 10,000 cells/well in PDL coated 96-well tissue culture plates. For LIVE/DEAD flow cytometry, cells were seeded at 150,000 cells/well in 12-well tissue culture plates. For JC-1 and TMRE flow cytometry, cells were seeded at 350,000 cells/well in 6-well tissue culture plates. HeLa cells were obtained from ATCC (Manassas, VA). BV2 cells were a kind gift from Dr. Shilpa Buch (University of Nebraska Medical Center), originally provided by Dr. Sanjay Maggirwar (George Washington University).

Antiretroviral Treatments

DTG was from BOC Sciences (Shirley, NY). FTC and EFV were from NIH AIDS Reagent Program, NIAID (Germantown, MD).

Stock solutions were made in DMSO (Sigma) and stored at -20°C. ARV drugs were prepared in DMEM containing 3% FBS and 4 mM L-glutamine, with glucose and without glucose, supplemented with 10 mM galactose (Sigma). 24-hours after plating, cells were treated with DTG (43 and 4300 nM), FTC (441 and 44100 nM), or EFV (44 and 4400 nM) at concentrations consistent with reported CSF levels (20, 31, 32) and a 100x higher concentration (all wells contained 0.1% DMSO). 24-hours after ARV treatments, the cells were used for experiments. For the ATP, REDOX, and Cytotoxicity experiments: media alone, vehicle alone, and 2% Triton X-100 (Fisher Scientific, Hampton, NH) containing wells were included in each experiment; all treatments were done in six (media, Triton X-100, and ARV drug treatments) to twelve (vehicle control) technical replicate wells, represent readings from six to twelve wells of the same plate that were averaged to one value, with four to five biological replicates (cells plated on different plates that were derived from different batches).

ATP Measurements

ATP levels were measured using the CellTiter-Glo Luminescent Cell Viability Assay (Promega, Madison, WI). Luminescence was measured using a Synergy HTX Multi-Mode Microplate Reader (BioTek, Winooski, VT). Percentage of vehicle control was calculated as follows: (experimental treatment – 2% Triton X-100)/(vehicle – 2% Triton X-100) x 100.

REDOX Measurements

Resazurin was used as an oxidation-reduction (REDOX) indicator (AlamarBlue Cell Viability Reagent, Invitrogen, Waltham, MA). Fluorescence at 560/15 nm and 590/20 nm was measured using a Synergy HTX Multi-Mode Microplate Reader. Percentage of vehicle control was calculated as follows: (experimental treatment – 2% Triton X-100)/(vehicle – 2% Triton X-100) x 100.

Cytotoxicity Detection

Cytotoxicity was measured using the Lactate Dehydrogenase (LDH) Cytotoxicity Detection Kit (Roche, Indianapolis, IN). Absorbance at 490 nM was measured using a Synergy HTX Multi-Mode Microplate Reader. LDH percent cytotoxicity was calculated as follows: (experimental treatment – media alone)/(2% Triton X-100 – media alone) x 100.

Cell Viability

Cell viability was determined using the LIVE/DEAD™ Fixable Blue Dead Cell Stain Kit (Invitrogen). As a positive control, cells were heat shocked (agitated at 65°C for 5 minutes). The cells were analyzed on a BD LSR Fortessa X-50 Cell Analyzer (BD Biosciences, San Jose, CA) with UV excitation using the 427/25 emission filters.

Mitochondrial Membrane Potential

Mitochondrial membrane potential was measured using the MitoProbe JC-1 Assay Kit for Flow Cytometry (Invitrogen). As a positive control, cells were treated with 20 μM CCCP (Sigma) for 30 minutes. The cells were analyzed on a BD LSR Fortessa X-50 Cell Analyzer with 405 nm excitation using 586/15BP and 525/50BP emission filters (33). Additionally, the TMRE-Mitochondrial Membrane Potential Assay Kit (Abcam) was used. As a positive control, HeLa cells were treated with 20 μM FCCP (Abcam), while BV2 cells were treated with 10, 20, and 40 μM FCCP for 30 minutes. Cells were then treated with 400 nM TMRE for 30 minutes and analyzed using a BD LSR Fortessa X-50 Cell Analyzer with 488 nm excitation using 586/15BP emission filters, per manufacturer's instruction.

Bioenergetics

Oxygen consumption rate (OCR) and extracellular acidification rate (ECAR) were measured at 37°C using the XFe96 Extracellular Flux analyzer (Agilent Technologies). 24-hours after ARV treatments, the cells were washed once with XF assay medium containing 4 mM L-glutamine and 25 mM glucose. Then XF assay medium containing ARV drugs was replaced and the cells were placed in a non-CO_2 incubator at 37°C for 1-hour prior to the assay. Three baseline measurements of OCR and ECAR were recorded prior to sequential injection of oligomycin (O, 1 μM, ATP synthase complex inhibitor), carbonyl-cyanide-4-phenylhydrazone (FCCP, F, 300 nM, ATP synthesis uncoupler), rotenone (R, 2 μM, complex I inhibitor) and antimycin A (AA, 2 μM, complex III inhibitor). After completion of the assay, total protein was isolated from individual wells and quantified using a BCA Protein Assay Kit (Pierce Biotechnology, Waltham, MA). Each well was normalized to μg of protein. All treatments were done in six technical replicate wells, represent readings from six wells of the same microplate that were averaged to one value, with five biological replicates (cells plated on different microplates that were derived from different batches).

Statistical Analysis

ATP, Alamar, and LDH data were acquired in Gen5 software (BioTek) and processed in Microsoft Excel (Microsoft Corporation, Redmond, WA). Outlier exclusion was applied to data points (single wells) for each treatment using the Grubb's test, at most one value (single well from the six to twelve technical replicates on an individual plate) was excluded for each test if identified as a significant outlier (Alpha = 0.05). Plate-median normalized data were grouped by treatment condition and exported to Prism software (version 6, GraphPad, San Diego, CA) for statistical analysis and plotting. LIVE/DEAD, JC-1, and TMRE data were acquired in BD FACSDiva software (version 8.0.2, BD Biosciences). For the JC-1 assay, fluorescence ratios of red to green were calculated using Excel, grouped by treatment condition, and exported to Prism for statistical analysis and plotting. Seahorse data were acquired in Wave software (version 2.2.0, Agilent Technologies) and exported to Excel for processing. Outlier exclusions were applied to data points for each treatment to identify within-plate (single wells) and between-plate variations using the Grubb's test, at most one value (single well from the six to twelve technical replicates on an individual plate or the averaged value from one biological replicate) was excluded if identified as a significant outlier (Alpha = 0.05). Total protein normalized data were grouped by treatment condition and exported to Prism for statistical analysis and plotting.

Data were analyzed statistically using one-way (ATP, Alamar, LDH, JC-1, TMRE, and LIVE/DEAD assays) or two-way (Seahorse XF Cell Mito Stress Test assay) analysis of variance (ANOVA) and the Dunnett's or Tukey's multiple comparisons post-hoc test using Prism software (Graph Pad Software, La Jolla, CA). Statistical significance was defined as $p < 0.05$.

RESULTS

Plasma-Relevant Concentrations of DTG and EFV Impair Mitochondrial ATP Production in HeLa Cells.

ATP was measured in HeLa cells after incubation with DTG, FTC, and EFV at CSF-relevant concentrations and a 100x higher concentration to approximate plasma-relevant concentrations for DTG and EFV (**Table 1**). Both glucose-containing and glucose-free (supplemented with galactose) media were used, the latter to ensure the highly glycolytic HeLa cells use mitochondrial oxidative phosphorylation. We found that plasma-relevant concentrations of DTG (4300 nM) and EFV (4400 nM) decreased ATP after 24-hours in glucose-free (**Figure 1A**), but not in glucose-containing (**Figure 1B**) media, suggesting that similar to EFV, DTG affects mitochondria.

Mitochondrial Membrane Potential Remains Unaltered in ARV Exposed HeLa Cells

To assess if mitochondrial ATP alterations upon exposure to DTG and EFV for 24-hours in glucose-free conditions coincide with mitochondrial membrane potential changes, the cells were incubated with the widely used cationic dye, JC-1. When mitochondria are well polarized, JC-1 aggregates in mitochondria fluorescing red. In mitochondria with low membrane potential, JC-1 remains in the monomeric form, which fluoresces green. No changes in mitochondrial membrane potential were observed (**Figure 2**). To confirm the JC-1 results, mitochondrial membrane potential was also assessed using the cell-permeant, cationic, red-orange fluorescent dye tetramethylrhodamine, ethyl ester (TMRE) that is readily sequestered by active mitochondria. Consistent with the JC-1 results, no changes in mitochondrial membrane potential were observed (**Supplementary Figure S1**).

Similar to EFV, DTG and FTC Alter Mitochondrial REDOX Activity in HeLa Cells

Upon accepting electrons from mitochondrial reductases and/or diaphorase-type enzymes or from non-mitochondrial cytosolic enzymes (34), the REDOX indicator Alamar Blue changes from the oxidized, non-fluorescent, blue state to the reduced, fluorescent, pink state. These studies were conducted in the absence (**Figure 3A**) and presence (**Figure 3B**) of glucose revealing that 24-hour treatment with CSF-relevant and 100x higher concentrations of DTG (43 and 4300 nM) and FTC (441 and 44100 nM), and plasma-relevant concentrations of EFV (4400 nM) impairs dye reduction in the absence of glucose, pointing to interruption of mitochondrial electron transport. The observed effects of DTG and FTC on ATP and REDOX in HeLa cells are not due to cell death, as no increase in LDH/cell death was uncovered; however, plasma-relevant EFV concentrations (4400 nM) did increase cell death in glucose-free media (**Supplementary Figure S2**). Cell viability, assessed by flow cytometry using LIVE/DEAD fluorescence, revealed no change in the percent of cells alive confirming the LDH results (**Supplementary Figures S3, S4**).

DTG and FTC Alter Cellular Metabolism in BV2 Cells in the Absence of Cell Death

In contrast to highly glycolytic HeLa cells, where mitochondrial alterations were uncovered in the absence of glucose, in BV2 cells, no ATP changes were uncovered in glucose-free media (**Figure 4A**). However, in glucose-containing media, plasma-relevant DTG concentrations (4300 nM) increased ATP and the 100x higher FTC concentration (44100 nM) decreased ATP (**Figure 4B**), suggesting glycolytic ATP production is altered. Interestingly, plasma-relevant DTG concentrations increased Alamar Blue fluorescence in the absence of glucose (**Figure 4C**) but not in the presence of glucose (**Figure 4D**), suggesting mitochondrial REDOX is elevated. Similar to HeLa cells, in BV2 cells the mitochondrial membrane potential remained unaltered in glucose-free (**Figure 5** and **Supplementary Figure S5**) and glucose-containing (**Figure 6** and **Supplementary Figure S6**) conditions. Of note, while the positive control (FCCP) yielded significant loss of TMRE fluorescence, characteristic of depolarization, in the HeLa cell experiments in glucose-free and in the BV2 cell experiments in glucose-containing conditions, this was not the case in the BV2 cell experiments in glucose-free conditions (despite titration of FCCP concentration). Rhodamine dye and its derivatives, such as TMRE, can be pumped out from cells by multidrug resistance proteins, and BV2 cells do express these proteins and depending on the cellular environment, retention of such dyes can be impaired in this cell line (35). Other reports of lack of spectral shifts in fluorescence of rhodamine derivatives in the presence of uncouplers have been observed (36). As such, JC-1 might be a more reliable indicator of mitochondrial membrane potential

TABLE 1 | Median ARV drug concentrations measured in the CSF and plasma of treated HIV patients.

ARV drug	CSF		Plasma		Reference
	ng/mL	nM	ng/mL	nM	
DTG	18	43	3360	8000	(20)
FTC	109	441	254	1027	(31)
EFV	13.9	44	2145	6795	(31)

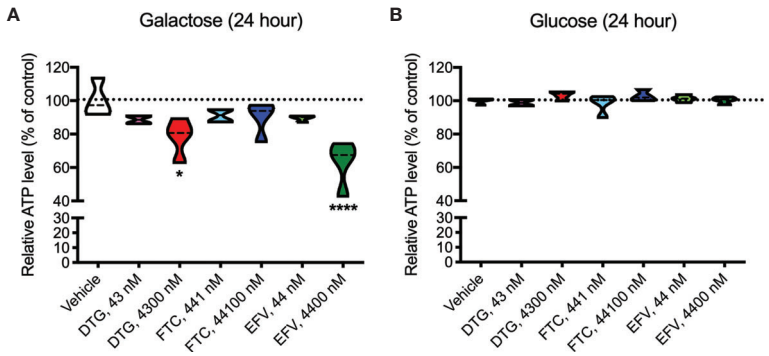

FIGURE 1 | Lower mitochondrial ATP generation in HeLa cells treated with DTG and EFV. HeLa cells were incubated for 24 hours with DTG, FTC, or EFV at the stated concentrations in the absence **(A)** or presence **(B)** of glucose. The level of ATP is given as a percentage of vehicle-treated (0.1% DMSO) cells. Statistically significant compared to vehicle ($p < 0.05$*, 0.0001****). n=4.

than TMRE for BV2 cells in glucose-free, galactose-containing conditions, similar to reports for other specific cell types and conditions (37). DTG, FTC, and EFV were not cytotoxic in BV2 cells as assessed by the LDH assay (**Supplementary Figure S7**) and flow cytometry LIVE/DEAD fluorescence (**Supplementary Figures S8, S9**).

Bioenergetic Alterations in BV2 Cells Due to ARV Drug Exposure

OCR (mitochondrial respiration) and ECAR (glycolysis) were measured after 24-hours of DTG, FTC, and EFV exposure in HeLa and BV2 cells using the Seahorse XFe96 Analyzer. Sequential additions of an ATP synthase inhibitor (O), ATP

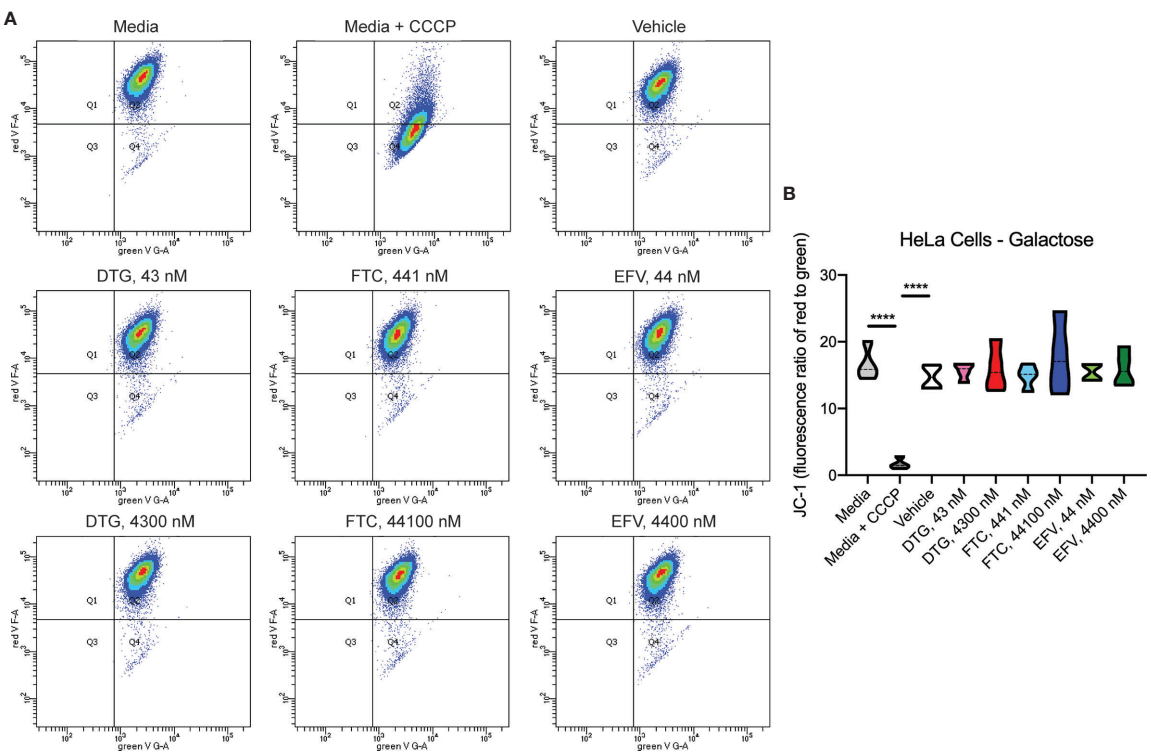

FIGURE 2 | No alteration in HeLa cell mitochondrial membrane potential due to ARV treatment. HeLa cells were incubated with JC-1 dye following incubation with DTG, FTC, or EFV at the stated concentrations for 24 hours in the absence of glucose. Treatment with 20 μM CCCP for 30 min was used as a positive control for mitochondrial depolarization. **(A)** Representative flow cytometry plot showing JC-1 staining in media, and after treatment with CCCP, vehicle, and ARV drugs. **(B)** Graph showing fluorescence ratio of red to green for JC-1 staining. Statistically significant ($p < 0.0001$****). n=4.

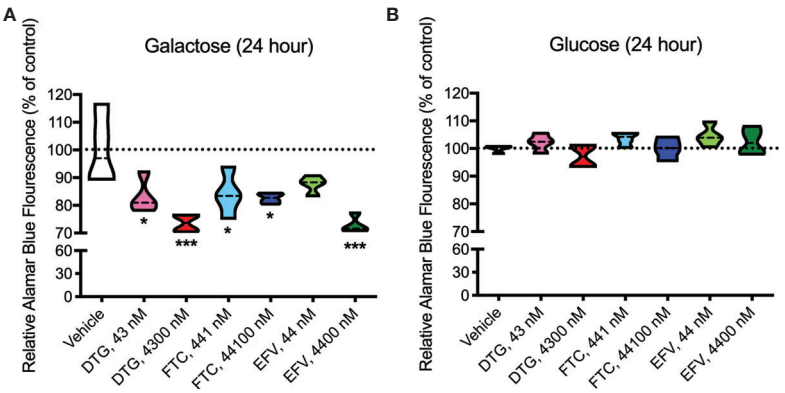

FIGURE 3 | Decreased mitochondrial REDOX in HeLa cells treated with DTG, FTC, and EFV. HeLa cells were incubated for 24 hours with DTG, FTC, or EFV at the stated concentrations in the absence **(A)** or presence **(B)** of glucose. The reduction of Alamar Blue is given as a percentage of vehicle-treated (0.1% DMSO) cells. Statistically significant compared to vehicle ($p < 0.05$*, 0.001***). n=4.

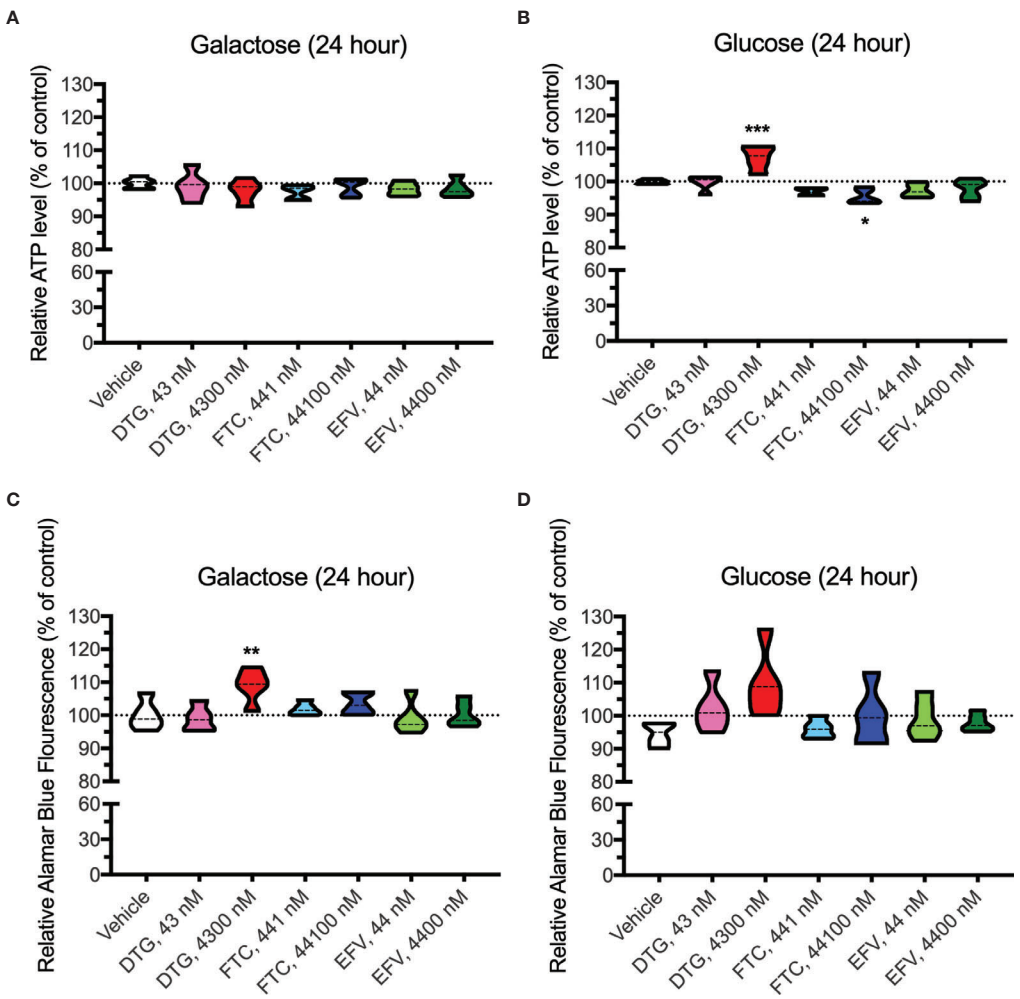

FIGURE 4 | Altered glycolytic ATP levels and mitochondrial REDOX in BV2 cells treated with DTG and FTC. BV2 cells were incubated for 24 hours with DTG, FTC, or EFV at the stated concentrations in the absence **(A, C)** or presence **(B, D)** of glucose. The level of ATP **(A, B)** and reduction of Alamar Blue **(C, D)** are given as a percentage of vehicle-treated (0.1% DMSO) cells. Statistically significant compared to vehicle ($p < 0.05$*, 0.01**, 0.001***). n=5.

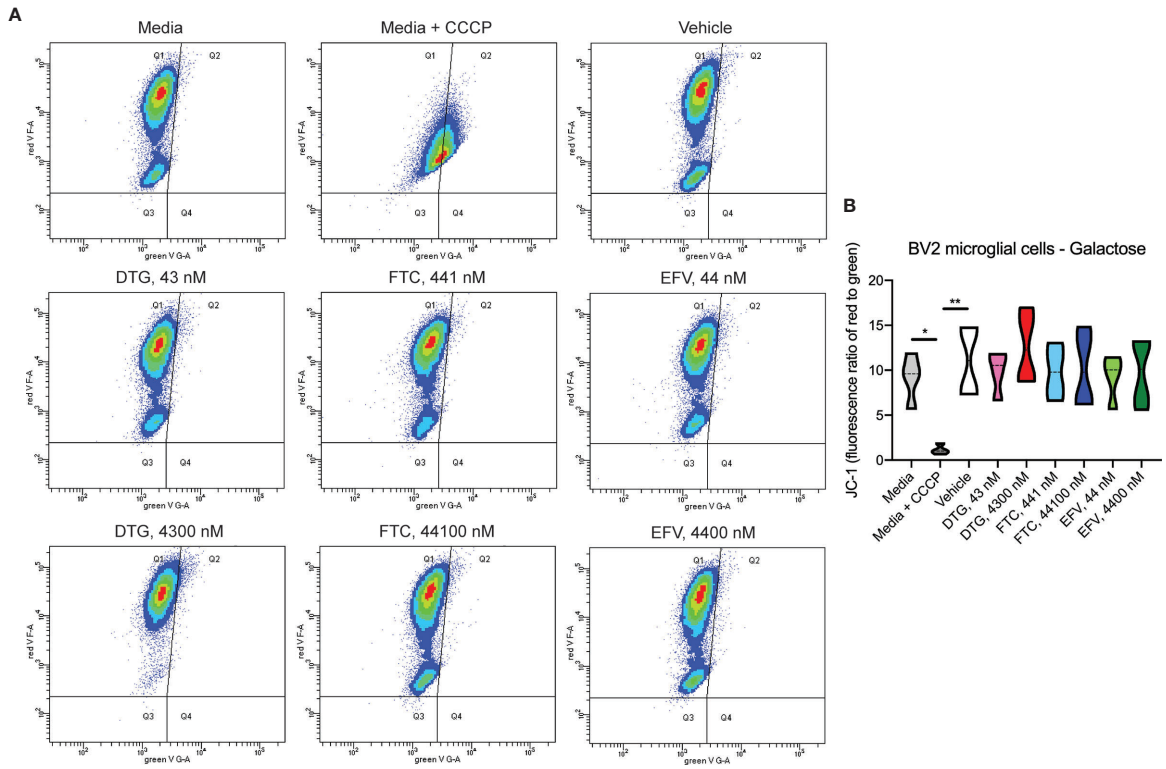

FIGURE 5 | No alteration in BV2 cell mitochondrial membrane potential due to ARV treatment in the absence of glucose. BV2 cells were incubated with JC-1 dye following incubation with DTG, FTC, or EFV at the stated concentrations for 24 hours in glucose-free media. Treatment with 20 μM CCCP for 30 min was used as a positive control for mitochondrial depolarization. **(A)** Representative flow cytometry plot showing JC-1 staining in media, and after treatment with CCCP, vehicle, and ARV drugs. **(B)** Graph showing fluorescence ratio of red to green for JC-1 staining. Statistically significant ($p < 0.05^*$, 0.01^{**}). n=4.

synthesis uncoupler (F), and mixture of complex I and III inhibitors (R/A) allowed determination of basal mitochondrial respiration, ATP production-linked rate, proton leakage, maximal mitochondrial respiration, spare respiratory capacity (SRC), and non-mitochondrial respiration. No significant alterations were uncovered in HeLa cells (**Figure 7**); however, the cells appear to shift towards becoming more glycolytic and less aerobic, particularly for both EFV and high DTG concentrations (**Figure 7E**). In contrast, in BV2 cells, maximal mitochondrial respiration was increased upon exposure to CSF-relevant DTG, FTC, and EFV, and the 100x higher FTC and EFV concentrations (**Figures 8A, B**). Further, mitochondrial SRC was elevated following exposure to the 100x higher FTC and EFV concentrations (**Figure 8B**). While no significant ECAR changes were uncovered (**Figures 8C, D**), the cells appear to become more energetic overall (more aerobic and glycolytic), particularly for both FTC and EFV concentrations (**Figure 8E**). The cell energy phenotype of HeLa and BV2 cells was determined by plotting ECAR (glycolysis) as a function of OCR (mitochondrial respiration) revealing that under baseline conditions both cell lines utilize both energy pathways; however, as compared to HeLa cells, we found that BV2 cells are less glycolytic and more aerobic (**Supplementary Figure S10**).

DISCUSSION

Neurocognitive abnormalities continue to occur in HIV-infected individuals, despite the widespread use of cART (3–5). Neuropsychiatric symptoms, including depression and anxiety disorders, mood and sleep disorders, and suicidal ideation, are common in people living with HIV and may be associated with specific ARV drugs (1, 38–40). Fifty percent of those taking EFV experience neuropsychiatric adverse effects, including vivid dreams, dizziness, balance problems, unsteadiness, light-headedness, and suicidal ideation (9). The precise mechanisms of ARV toxicity are not fully understood, but in the case of EFV, we (6, 7), and others (8–10) have found effects on neuronal mitochondria. While EFV use is decreasing, there are other CNS-penetrant ARV drugs that are currently recommended, including DTG and FTC, that we studied herein.

DTG, a second-generation integrase inhibitor, is recommended as one of the preferred options for first-line HIV treatment in European and United States treatment guidelines. Recent reports from clinical practice of neuropsychiatric adverse events with integrase inhibitors (39, 41), and DTG in particular, have highlighted a need to understand the off-target effects of these medications and

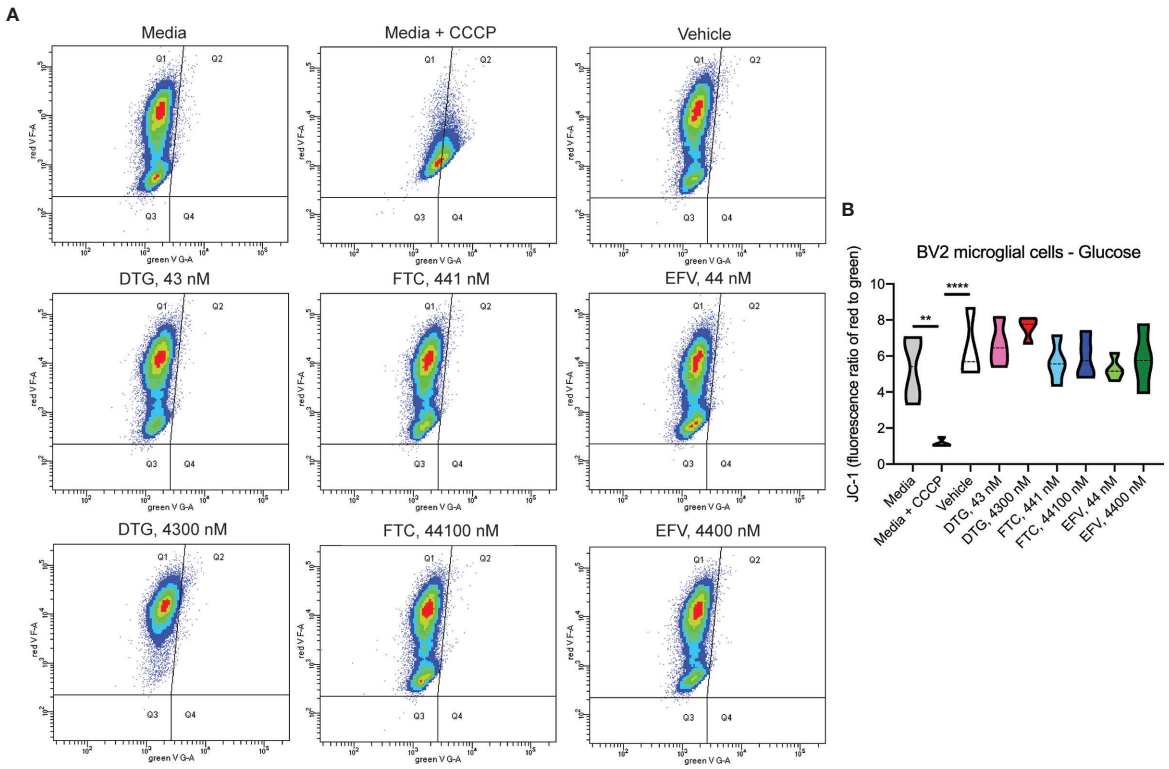

FIGURE 6 | No alteration in BV2 cell mitochondrial membrane potential due to ARV treatment in the presence of glucose. BV2 cells were incubated with JC-1 dye following incubation with DTG, FTC, or EFV at the stated concentrations for 24 hours in glucose-containing media. Treatment with 20 μM CCCP for 30 min was used as a positive control for mitochondrial depolarization. **(A)** Representative flow cytometry plot showing JC-1 staining in media, and after treatment with CCCP, vehicle, and ARV drugs. **(B)** Graph showing fluorescence ratio of red to green for JC-1 staining. Statistically significant ($p < 0.01$**, 0.0001****). n=4.

which individuals are at greatest risk, particularly as use of DTG is increased in patients. In fact, adverse CNS side effects of DTG are occurring more frequently with everyday use than clinical trials had predicted. The most frequent manifestations reported as leading to discontinuation were insomnia, dizziness, headache, anxiety, and depression (39, 41). These adverse effects are more likely to occur in women, people over 60, and those starting abacavir at the same time (41). While all medications have potential side effects, it is important that these do not initiate or worsen any of the problems that HIV infection has caused in the brain or elsewhere in the body. DTG is CNS penetrant, and known to reach effective concentrations in the CSF (20). As DTG is now a commonly used ARV option in naïve and pretreated patients, further research on its safety and neurotoxicity are needed. FTC is a NRTI with a relatively good tolerability and safety profile. However, nervous system side effects have been reported in FTC-containing cART, including headache, paresthesia, confusion, irritability, depression, and insomnia. While FTC and DTG (together with tenofovir – TDF or TAF, both non-CNS penetrant) combination is one of the recommended first line treatments for HIV, these drugs were studied individually to uncover if these drugs affect mitochondrial functions. Here, we used the glucose-galactose assay to investigate potential mitotoxic effects of DTG, FTC, and EFV in highly glycolytic HeLa cells, and upon identification of potential mitotoxicity of DTG and FTC, similar to EFV, using this screen, who chose a well-used and characterized microglial cell line, the BV2 cell line for additional experiments. We demonstrate that DTG, FTC, and EFV interfere with cellular metabolism in a cell-type specific manner, decreasing mitochondrial ATP (DTG and EFV) and mitochondrial REDOX (DTG, FTC, and EFV) in HeLa cells, but increasing glycolytic ATP (DTG) and mitochondrial REDOX (DTG) in BV2 cells. FTC was found to decrease glycolytic ATP in BV2 cells. Further, we discovered that these ARV drugs (DTG, FTC, and EFV) increased maximal mitochondrial respiration in BV2 cells.

Growing cell lines in the absence and presence of glucose in parallel to detect mitochondrial toxins is becoming more common in drug development screening activities (28–30, 42). For such glucose-galactose assays, highly glycolytic cells that are resistant to mitochondrial toxins under typical high-glucose culture conditions are typically used. Indeed, in HeLa cells, this assay uncovered reduced ATP only in glucose-free media upon ARV exposure, thus resulting from mitochondrial dysfunction. Plasma-relevant DTG concentrations caused an ~20% drop in

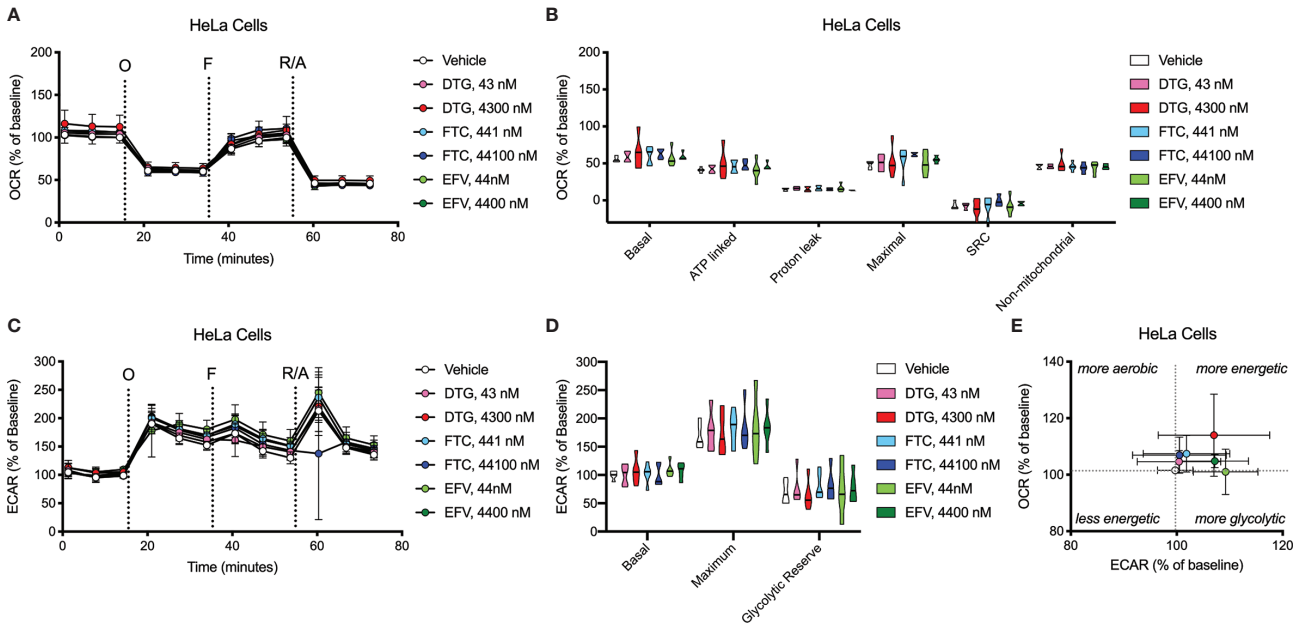

FIGURE 7 | HeLa cell bioenergetics remain intact after ARV treatment. HeLa cells were incubated for 24 hours with DTG, FTC, or EFV at the stated concentrations. **(A)** Graphical representation of the relative OCR responses over time expressed as a percent response from baseline (third measurement, before oligomycin injection); sequential additions are indicated as O (the ATP synthase inhibitor oligomycin, 1 μM), F (the ATP synthesis uncoupler FCCP, 300 nM), and R/A (a mixture of the complex I and III inhibitors rotenone and antimycin A, 2 μM each). **(B)** Mitochondrial respiratory parameters calculated from the OCR shown for basal mitochondrial respiration (baseline minus R/A), ATP linked respiration (baseline minus O), proton leak (O minus R/A), maximal mitochondrial respiration (F minus R/A), and SRC (F minus baseline). **(C)** Graphical representation of the relative ECAR responses over time. **(D)** Glycolytic rate parameters calculated from ECAR shown for basal glycolysis (baseline), maximal glycolysis (O), and glycolytic reserve (O minus baseline). **(E)** Plot of baseline ECAR and OCR levels. n=5.

mitochondrial ATP (**Figure 1**) in the absence of cell death, suggesting less essential ATP-consuming processes may be inhibited to preserve those more critical for cell survival. Studies show energy spared by reducing protein synthesis (25-30% of the cells ATP) can be allocated to more critical cell functions involved in osmotic and ionic homeostasis (43). Thus, future studies could interrogate the hierarchy of ATP-consuming processes in the context of ARV exposure to further characterize how the cellular metabolism is altered.

Despite ARV-induced decreases in mitochondrial ATP generation, mitochondrial membrane potential was unaltered (**Figure 2** and **Supplementary Figure S1**). The mitochondrial electrochemical gradient, which drives mitochondrial ATP synthesis, is comprised of the mitochondrial membrane potential and pH (proton) gradient (37). Changes in the mitochondrial membrane potential do not always mirror alterations in the mitochondrial pH, since each of these contribute independently to the proton-motive force. Here, mitochondrial membrane potential was measured using JC-1, a cationic dye that measures the charge gradient across the inner mitochondrial membrane but cannot specifically measure the mitochondrial proton gradient or be used to make direct inferences regarding respiratory status. Similarly, experiments using another cationic dye TMRE, which accumulates in active mitochondria due to their relative negative charge, shares these same limitations. Although most studies focus on mitochondrial membrane potential as it is easily measured, previous studies on HIV Tat-induced hyperpolarization of the mitochondrial membrane was not associated with increased ATP as expected, but did coincide with decreased mitochondrial pH (thus decreasing ATP generating capacity) suggesting increased cytosolic calcium, not protonic charges, were responsible for the hyperpolarization (44–46). Of note, mitochondrial membrane potential and proton gradient can be maintained *via* ATP synthase reversal, which depletes ATP (47). Thus, future experiments could interrogate the role of the mitochondrial proton gradient and/or calcium homeostasis, as well as ATP synthase reversal, in ARV-induced mitotoxicity.

Concurrent with reduced mitochondrial ATP, CSF-relevant and the 100x higher concentrations of FTC, the CSF- and plasma-relevant concentrations of DTG, and the plasma-relevant concentrations of EFV, impaired mitochondrial REDOX in HeLa cells in glucose-free conditions (**Figure 3**), attributing the loss of Alamar Blue reduction mainly to mitochondrial enzymes and electron carriers. Again, while mitochondrial membrane potential remained unaltered (**Figure 2** and **Supplementary Figure S1**), impairment of the mitochondrial membrane potential or the mitochondrial pH gradient can facilitate mitochondrial redox dysfunction. Heart studies have shown that the mitochondrial pH gradient

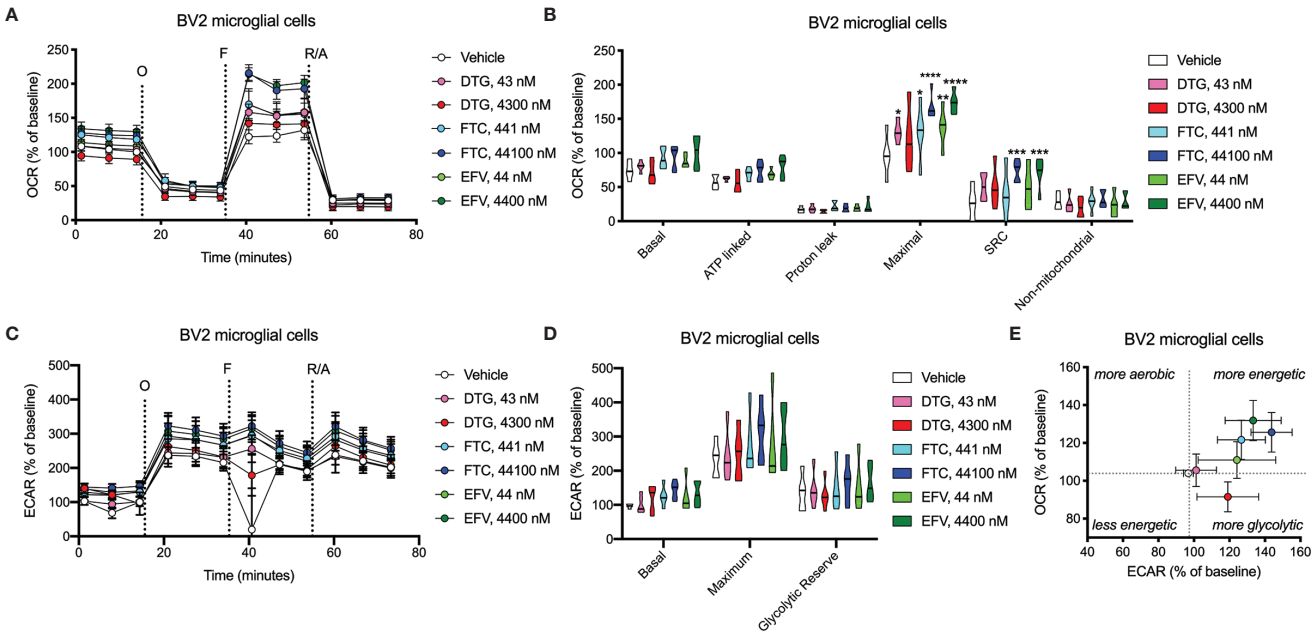

FIGURE 8 | BV2 cell bioenergetics altered after ARV treatment. BV2 cells were incubated for 24 hours with DTG, FTC, or EFV at the stated concentrations. **(A)** Graphical representation of the relative OCR responses over time expressed as a percent response from baseline (third measurement, before oligomycin injection); sequential additions are indicated as O (the ATP synthase inhibitor oligomycin, 1 μM), F (the ATP synthesis uncoupler FCCP, 300 nM), and R/A (a mixture of the complex I and III inhibitors rotenone and antimycin A, 2 μM each). **(B)** Mitochondrial respiratory parameters calculated from the OCR shown for basal mitochondrial respiration (baseline minus R/A), ATP linked respiration (baseline minus O), proton leak (O minus R/A), maximal mitochondrial respiration (F minus R/A), and SRC (F minus baseline). **(C)** Graphical representation of the relative ECAR responses over time. **(D)** Glycolytic rate parameters calculated from ECAR shown for basal glycolysis (baseline), maximal glycolysis (O), and glycolytic reserve (O minus baseline). **(E)** Plot of baseline ECAR and OCR levels. (Statistically significant compared to vehicle ($p < 0.05$*, 0.01**, 0.001***, 0.0001****). n=5.

restricts electron flow, controls superoxide generation, and results in a more reduced environment through imposed proton backpressure, while impairment of the mitochondrial pH gradient leads to a more oxidized environment (48). Thus, ARV-induced REDOX dysfunction (more oxidized Alamar Blue) may correlate with mitochondrial pH gradient impairment in the absence of mitochondrial membrane potential changes. While no changes in ECAR (glycolysis) or OCR (mitochondrial respiration) were uncovered in the HeLa cells (**Figure 7**), these experiments were performed with glucose present potentially masking the ARV-induced mitotoxic effects. Of note, the bioenergetic profile (**Figure 7E**) suggests that overall HeLa cells become more reliant on glycolysis when treated with DTG (plasma-relevant) and EFV (plasma- and CSF-relevant).

Dysfunctional microglia may contribute to HIV-associated cognitive disorder development, as well as neuropsychiatric adverse effects of ARV drugs (23, 24). While microglia rely on both glycolytic and mitochondrial metabolism depending on their activation state, microglial activation has been suggested to be associated with a metabolic switch in favor of glycolysis and decreased mitochondrial oxidative phosphorylation (25, 26). CSF-relevant DTG, FTC, and EFV concentrations did not affect ATP or REDOX in BV2 cells; however, these effects were only studied following 24-hour exposure to assess the effects of one dose equivalent (DTG, FTC, and EFV are usually taken once daily, while DTG can be taken twice daily). Patients would take these drugs daily throughout their lives, so future experiments should assess chronic exposure to CSF-relevant drug levels. Of note, CSF-relevant DTG, FTC, and EFV concentrations elevated maximal mitochondrial respiration in BV2 cells (**Figure 8**). Overall, the bioenergetic profile suggests BV2 cells become more energetic upon FTC and EFV exposure (**Figure 8E**). These findings suggest ARV exposure might metabolically reprogram the microglia towards a resting state (increased mitochondrial respiration), which could be beneficial during chronic neuroinflammation but might also inhibit acute neuroinflammatory responses.

While CSF-relevant concentrations of the ARV drugs may be applicable to studies on microglia, we note that a recent study in rhesus monkeys indicates that ARV drugs are found at concentrations ranging from 13 to 1,150-fold higher in brain tissue than in CSF (49). Thus, our higher concentrations may be quite appropriate for the brain, and the cells within the brain such as microglia. In addition, such higher concentrations are consistent with acute toxicity screens, including previous acute treatment studies on metabolic effects using relatively high ARV drug concentrations to uncover metabolic effects as discussed below. We found that these higher, plasma-relevant

concentrations of DTG increased glycolytic ATP generation, while also elevating mitochondrial reducing capacity in BV2 microglial cells (**Figure 4**). While no changes in ECAR (glycolysis) or OCR (mitochondrial respiration) were uncovered upon exposure to plasma-relevant concentrations of DTG (**Figure 8**), the bioenergetic profile suggests a switch towards a more glycolytic phenotype consistent with the ATP data. Evidence suggests metabolic reprogramming can affect microglia-derived inflammation (25), thus a shift towards a more glycolytic phenotype upon DTG exposure might induce microglial activation. The 100x higher concentrations of FTC and EFV increased both mitochondrial maximal respiration and SRC in BV2 cells (**Figure 8**). This correlates with reduced glycolytic ATP uncovered with FTC exposure (**Figure 4**), suggesting these drugs might maintain microglia in a resting state or inhibit their activation. Based on these findings, as mentioned above we anticipate that chronic exposure to CSF-relevant concentrations would alter ATP and REDOX in BV2 cells.

EFV alters the mitochondrial membrane potential in various cell-types; however, much higher EFV concentrations were used than studied here. EFV (10,000 nM, 6 hours) lowered the mitochondrial membrane potential in SH-SY5Y and U-251MG cells (18). While EFV decreased ATP in SH-SY5Y cells (25,000 nM, 24 hours), ATP levels were increased in U-251MG cells (10,000 nM, 24 hours), and these findings were confirmed in primary rat cortical neurons and astrocytes, which were more sensitive than the immortal lines (18). EFV reduced ATP in rat striatal primary neurons (12,500 nM, 2 hours) (6) and neural stem cells (5000 nM, 24 hours) (17). High EFV concentrations decrease the mitochondrial membrane potential in Hep3B cells (25,000 nM, 4 hours), and primary human hepatocytes were more sensitive than immortal lines (11). Primary mouse hepatocytes exhibit reduced ATP following EFV exposure (40,000 nM, 3 hours) (50). In CEM cells, EFV (12,700 nM, 24 hours) reduced the mitochondrial membrane potential and basal mitochondrial respiration (51). EFV (10,000 nM) acutely decreased oxygen consumption in SH-SY5Y and U-251MG (18), as well as Hep3B cells (12). Our previous studies in rat synaptosomes revealed that EFV (6250 nM, 2 hours) decreased maximal mitochondrial respiration and ATP levels (7). Although future work could study higher ARV concentrations, we believe studies using primary immune cells, including microglia, but also peripheral immune cells, may uncover more drastic metabolic effects of CSF- or plasma-relevant ARV concentrations.

Few reports of FTC and DTG metabolic effects exist, and much of this work has focused on combined treatment making it difficult to ascribe effects to a particular drug. FTC (10,000 nM) acutely reduced Hep3B cellular oxygen consumption (52). Our previous studies revealed FTC (25,000 nM, 2 hours) reduced maximal mitochondrial respiration in rat striatal synaptosomes (7). FTC (peak plasma concentration, 48 hours) did not alter mitochondrial membrane potential in CEM cells (51). $CD4^+$ T cells from HIV-negative healthy individuals were exposed to DTG (9538 nM) or FTC (4045 nM) *in vitro* for 3 days, and while FTC did not alter mitochondrial respiration, DTG decreased basal and maximal respiration, with no effect on glycolysis (53). While the DTG concentration was higher than studied here in BV2 cells (4300 nM) perhaps the effects of DTG on mitochondrial function in peripheral immune cells are different than those on CNS immune cells.

These findings reveal that physiologically relevant concentrations of DTG and FTC alter ATP metabolism, mitochondrial REDOX activity, and cellular bioenergetics in the absence of cell death in a cell-type specific manner. Thus, cellular metabolic alterations may, at least in part, explain some of the mechanisms underlying discontinuation of certain ART regimens due to peripheral and central adverse effects and likely contribute to microglial metabolic alterations in the HIV-infected brain.

DATA AVAILABILITY STATEMENT

The original contributions presented in the study are included in the article/**Supplementary Material**. Further inquiries can be directed to the corresponding author.

AUTHOR CONTRIBUTIONS

KS and JG designed the experiments. JG, NR, and BL completed the ATP, Alamar, and LDH assays. JG and CS completed the flow cytometry experiments. JM completed the bioenergetic experiments. KS and HF interpreted the data and wrote the manuscript. All authors contributed to the article and approved the submitted version.

FUNDING

This work was supported by National Institutes of Health under the award number P30 MH062261.

ACKNOWLEDGMENTS

We would like to thank the Flow Cytometry Core facility of the University of Nebraska Medical Center.

SUPPLEMENTARY MATERIAL

The Supplementary Material for this article can be found online at: https://www.frontiersin.org/articles/10.3389/fimmu.2021.639378/full#supplementary-material

Supplementary Figure 1 | No alteration in HeLa cell mitochondrial membrane potential due to ARV treatment. HeLa cells were incubated with DTG, FTC, or EFV at the stated concentrations for 24 hours in the absence of glucose followed by incubation with TMRE dye. Treatment with 20 μM FCCP for 30 min was used as a positive control for mitochondrial depolarization. Statistically significant ($p < 0.0001$****). n=4.

Supplementary Figure 2 | No HeLa cell death due to treatment with DTG and FTC. HeLa cells were incubated for 24 hours with DTG, FTC, or EFV at the stated concentrations in the absence **(A)** or presence **(B)** of glucose. Cell death measured using the LDH assay is given as a percentage of cytotoxicity. Statistically significant compared to vehicle ($p < 0.05$*). n=4.

Supplementary Figure 3 | HeLa cell viability unaffected by ARV treatment. HeLa cells were incubated for 24 hours with DTG, FTC, or EFV at the stated concentrations in glucose-free media. Cell viability was determined using the LIVE/DEAD assay for flow cytometry and reported as the percent of viable (live) cells. n=4.

Supplementary Figure 4 | HeLa cell viability unaffected by ARV treatment. HeLa cells were incubated for 24 hours with DTG, FTC, or EFV at the stated concentrations in glucose-containing media. Cell viability was determined using the LIVE/DEAD assay for flow cytometry and reported as the percent of viable (live) cells. n=4.

Supplementary Figure 5 | No alteration in BV2 cell mitochondrial membrane potential due to ARV treatment. BV2 cells were incubated with DTG, FTC, or EFV at the stated concentrations for 24 hours in the absence of glucose followed by incubation with TMRE dye. Treatment with 10, 20, and 40 μM FCCP for 30 min was used as a positive control for mitochondrial depolarization. n=4.

Supplementary Figure 6 | No alteration in BV2 cell mitochondrial membrane potential due to ARV treatment. BV2 cells were incubated with DTG, FTC, or EFV at the stated concentrations for 24 hours in the presence of glucose followed by incubation with TMRE dye. Treatment with 10 mM FCCP for 30 min was used as a positive control for mitochondrial depolarization. Statistically significant ($p <$ 0.001***, 0.0001****). n=4.

Supplementary Figure 7 | No BV2 microglial cell death due to ARV treatment. BV2 cells were incubated for 24 hours with DTG, FTC, or EFV at the stated concentrations in the absence **(A)** or presence **(B)** of glucose. Cell death measured using the LDH assay is given as a percentage of cytotoxicity. n=5.

Supplementary Figure 8 | BV2 cell viability unaltered by ARV treatment in the absence of glucose. BV2 cells were incubated for 24 hours with DTG, FTC, or EFV at the stated concentrations in glucose-free media. Cell viability was determined using the LIVE/DEAD assay for flow cytometry and reported as the percent of viable (live) cells. n=4.

Supplementary Figure 9 | BV2 cell viability unaltered by ARV treatment in the presence of glucose. BV2 cells were incubated for 24 hours with DTG, FTC, or EFV at the stated concentrations in glucose-containing media. Cell viability was determined using the LIVE/DEAD assay for flow cytometry and reported as the percent of viable (live) cells. n=4.

Supplementary Figure 10 | Cell Energy Phenotype. Plot of baseline ECAR (glycolysis) and OCR (mitochondrial respiration) levels for HeLa (white dot) and BV2 (grey dot) cells. n=5.

REFERENCES

1. Abers MS, Shandera WX, Kass JS. Neurological and Psychiatric Adverse Effects of Antiretroviral Drugs. *CNS Drugs* (2014) 28:131–45. doi: 10.1007/s40263-013-0132-4
2. Aguer C, Gambarotta D, Mailloux RJ, Moffat C, Dent R, Mcpherson R, et al. Galactose Enhances Oxidative Metabolism and Reveals Mitochondrial Dysfunction in Human Primary Muscle Cells. *PloS One* (2011) 6:e28536. doi: 10.1371/journal.pone.0028536
3. Apostolova N, Blas-Garcia A, Esplugues JV. Mitochondrial Toxicity in HAART: An Overview of In Vitro Evidence. *Curr Pharm Des* (2011) 17:2130–44. doi: 10.2174/138161211796904731
4. Apostolova N, Funes HA, Blas-Garcia A, Galindo MJ, Alvarez A, Esplugues JV. Efavirenz and the CNS: What We Already Know and Questions That Need to be Answered. *J Antimicrob Chemother* (2015) 70:2693–708. doi: 10.1093/jac/dkv183
5. Apostolova N, Gomez-Sucerquia LJ, Moran A, Alvarez A, Blas-Garcia A, Esplugues JV. Enhanced Oxidative Stress and Increased Mitochondrial Mass During Efavirenz-Induced Apoptosis in Human Hepatic Cells. *Br J Pharmacol* (2010) 160:2069–84. doi: 10.1111/j.1476-5381.2010.00866.x
6. Bellizzi MJ, Lu SM, Gelbard HA. Protecting the Synapse: Evidence for a Rational Strategy to Treat HIV-1 Associated Neurologic Disease. *J Neuroimmune Pharmacol* (2006) 1:20–31. doi: 10.1007/s11481-005-9006-y
7. Best BM, Koopmans PP, Letendre SL, Capparelli EV, Rossi SS, Clifford DB, et al. Efavirenz Concentrations in CSF Exceed IC50 for Wild-Type HIV. *J Antimicrob Chemother* (2011) 66:354–7. doi: 10.1093/jac/dkq434
8. Blas-Garcia A, Apostolova N, Ballesteros D, Monleon D, Morales JM, Rocha M, et al. Inhibition of Mitochondrial Function by Efavirenz Increases Lipid Content in Hepatic Cells. *Hepatology* (2010) 52:115–25. doi: 10.1002/hep.23647
9. Blas-Garcia A, Apostolova N, Esplugues JV. Oxidative Stress and Mitochondrial Impairment After Treatment With anti-HIV Drugs: Clinical Implications. *Curr Pharm Des* (2011) 17:4076–86. doi: 10.2174/138161211798764951
10. Blas-Garcia A, Marti-Rodrigo A, Victor VM, Polo M, Alegre F, Funes HA, et al. The Purine Analogues Abacavir and Didanosine Increase Acetaminophen-Induced Hepatotoxicity by Enhancing Mitochondrial Dysfunction. *J Antimicrob Chemother* (2016) 71:916–26. doi: 10.1093/jac/dkv424
11. Buttgereit F, Brand MD. A Hierarchy of ATP-consuming Processes in Mammalian Cells. *Biochem J* (1995) 312(Pt 1):163–7. doi: 10.1042/bj3120163
12. Chen NC, Partridge AT, Sell C, Torres C, Martin-Garcia J. Fate of Microglia During HIV-1 Infection: From Activation to Senescence? *Glia* (2017) 65:431–46. doi: 10.1002/glia.23081
13. Cotto B, Natarajanseenivasan K, Langford D. HIV-1 Infection Alters Energy Metabolism in the Brain: Contributions to HIV-associated Neurocognitive Disorders. *Prog Neurobiol* (2019) 181:101616. doi: 10.1016/j.pneurobio.2019.101616
14. De Boer MG, Van Den Berk GE, Van Holten N, Oryszcyn JE, Dorama W, Moha DA, et al. Intolerance of Dolutegravir-Containing Combination Antiretroviral Therapy Regimens in Real-Life Clinical Practice. *AIDS* (2016) 30:2831–4. doi: 10.1097/QAD.0000000000001279
15. Eakins J, Bauch C, Woodhouse H, Park B, Bevan S, Dilworth C, et al. A Combined In Vitro Approach to Improve the Prediction of Mitochondrial Toxicants. *Toxicol In Vitro* (2016) 34:161–70. doi: 10.1016/j.tiv.2016.03.016
16. Fettiplace A, Stainsby C, Winston A, Givens N, Puccini S, Vannappagari V, et al. Psychiatric Symptoms in Patients Receiving Dolutegravir. *J Acquir Immune Defic Syndr* (2017) 74:423–31. doi: 10.1097/QAI.0000000000001269
17. Funes HA, Apostolova N, Alegre F, Blas-Garcia A, Alvarez A, Marti-Cabrera M, et al. Neuronal Bioenergetics and Acute Mitochondrial Dysfunction: A Clue to Understanding the Central Nervous System Side Effects of Efavirenz. *J Infect Dis* (2014) 210:1385–95. doi: 10.1093/infdis/jiu273
18. Funes HA, Blas-Garcia A, Esplugues JV, Apostolova N. Efavirenz Alters Mitochondrial Respiratory Function in Cultured Neuron and Glial Cell Lines. *J Antimicrob Chemother* (2015) 70:2249–54. doi: 10.1093/jac/dkv098
19. Gardner K, Hall PA, Chinnery PF, Payne BA. HIV Treatment and Associated Mitochondrial Pathology: Review of 25 Years of In Vitro, Animal, and Human Studies. *Toxicol Pathol* (2014) 42:811–22. doi: 10.1177/0192623313503519
20. Ghosh S, Castillo E, Frias ES, Swanson RA. Bioenergetic Regulation of Microglia. *Glia* (2018) 66:1200–12. doi: 10.1002/glia.23271
21. Gibson CJ, Hossain MM, Richardson JR, Aleksunes LM. Inflammatory Regulation of ATP Binding Cassette Efflux Transporter Expression and Function in Microglia. *J Pharmacol Exp Ther* (2012) 343:650–60. doi: 10.1124/jpet.112.196543
22. Heaton RK, Clifford DB, Franklin DRJr., Woods SP, Ake C, Vaida F, et al. HIV-Associated Neurocognitive Disorders Persist in the Era of Potent Antiretroviral Therapy: CHARTER Study. *Neurology* (2010) 75:2087–96. doi: 10.1212/WNL.0b013e318200d727
23. Imaizumi N, Kwang Lee K, Zhang C, Boelsterli UA. Mechanisms of Cell Death Pathway Activation Following Drug-Induced Inhibition of

Mitochondrial Complex I. *Redox Biol* (2015) 4:279–88. doi: 10.1016/j.redox.2015.01.005
24. Jin J, Grimmig B, Izzo J, Brown LA, Hudson C, Smith AJ, et al. HIV non-Nucleoside Reverse Transcriptase Inhibitor Efavirenz Reduces Neural Stem Cell Proliferation In Vitro and In Vivo. *Cell Transplant* (2016) 11:1967–77. doi: 10.3727/096368916X691457
25. Kang PT, Chen CL, Lin P, Chilian WM, Chen YR. Impairment of Ph Gradient and Membrane Potential Mediates Redox Dysfunction in the Mitochondria of the Post-Ischemic Heart. *Basic Res Cardiol* (2017) 112:36. doi: 10.1007/s00395-017-0632-3
26. Kim MJ, Kim SW, Chang HH, Kim Y, Jin S, Jung H, et al. Comparison of Antiretroviral Regimens: Adverse Effects and Tolerability Failure That Cause Regimen Switching. *Infect Chemother* (2015) 47:231–8. doi: 10.3947/ic.2015.47.4.231
27. Korencak M, Byrne M, Richter E, Schultz BT, Juszczak P, Ake JA, et al. Effect of HIV Infection and Antiretroviral Therapy on Immune Cellular Functions. *JCI Insight* (2019) 4. doi: 10.1172/jci.insight.126675
28. Lauro C, Limatola C. Metabolic Reprograming of Microglia in the Regulation of the Innate Inflammatory Response. *Front Immunol* (2020) 11:493. doi: 10.3389/fimmu.2020.00493
29. Letendre S. Central Nervous System Complications in HIV Disease: HIV-associated Neurocognitive Disorder. *Top Antivir Med* (2011) 19:137–42.
30. Letendre SL, Mills AM, Tashima KT, Thomas DA, Min SS, Chen S, et al. ING116070: A Study of the Pharmacokinetics and Antiviral Activity of Dolutegravir in Cerebrospinal Fluid in HIV-1-infected, Antiretroviral Therapy-Naive Subjects. *Clin Infect Dis* (2014) 59:1032–7. doi: 10.1093/cid/ciu477
31. Li M, Sopeyin A, Paintsil E. Combination of Tenofovir and Emtricitabine With Efavirenz Does Not Moderate Inhibitory Effect of Efavirenz on Mitochondrial Function and Cholesterol Biosynthesis in Human T Lymphoblastoid Cell Line. *Antimicrob Agents Chemother* (2018) 62. doi: 10.1128/AAC.00691-18
32. Maagaard A, Kvale D. Long Term Adverse Effects Related to Nucleoside Reverse Transcriptase Inhibitors: Clinical Impact of Mitochondrial Toxicity. *Scand J Infect Dis* (2009) 41:808–17. doi: 10.3109/00365540903186181
33. Norman JP, Perry SW, Kasischke KA, Volsky DJ, Gelbard HA. HIV-1 Trans Activator of Transcription Protein Elicits Mitochondrial Hyperpolarization and Respiratory Deficit, With Dysregulation of Complex IV and Nicotinamide Adenine Dinucleotide Homeostasis in Cortical Neurons. *J Immunol* (2007) 178:869–76. doi: 10.4049/jimmunol.178.2.869
34. Norman JP, Perry SW, Reynolds HM, Kiebala M, De Mesy Bentley KL, Trejo M, et al. Hiv-1 Tat Activates Neuronal Ryanodine Receptors With Rapid Induction of the Unfolded Protein Response and Mitochondrial Hyperpolarization. *PloS One* (2008) 3:e3731. doi: 10.1371/journal.pone.0003731
35. Penafiel J, De Lazzari E, Padilla M, Rojas J, Gonzalez-Cordon A, Blanco JL, et al. Tolerability of Integrase Inhibitors in a Real-Life Setting. *J Antimicrob Chemother* (2017) 72:1752–9. doi: 10.1093/jac/dkx053
36. Perelman A, Wachtel C, Cohen M, Haupt S, Shapiro H, Tzur A. Jc-1: Alternative Excitation Wavelengths Facilitate Mitochondrial Membrane Potential Cytometry. *Cell Death Dis* (2012) 3:e430. doi: 10.1038/cddis.2012.171
37. Perry SW, Norman JP, Barbieri J, Brown EB, Gelbard HA. Mitochondrial Membrane Potential Probes and the Proton Gradient: A Practical Usage Guide. *Biotechniques* (2011) 50:98–115. doi: 10.2144/000113610
38. Perry SW, Norman JP, Litzburg A, Zhang D, Dewhurst S, Gelbard HA. HIV-1 Transactivator of Transcription Protein Induces Mitochondrial Hyperpolarization and Synaptic Stress Leading to Apoptosis. *J Immunol* (2005) 174:4333–44. doi: 10.4049/jimmunol.174.7.4333
39. Purnell PR, Fox HS. Efavirenz Induces Neuronal Autophagy and Mitochondrial Alterations. *J Pharmacol Exp Ther* (2014) 351:250–8. doi: 10.1124/jpet.114.217869
40. Rampersad SN. Multiple Applications of Alamar Blue as an Indicator of Metabolic Function and Cellular Health in Cell Viability Bioassays. *Sensors (Basel)* (2012) 12:12347–60. doi: 10.3390/s120912347
41. Robertson KR, Smurzynski M, Parsons TD, Wu K, Bosch RJ, Wu J, et al. The Prevalence and Incidence of Neurocognitive Impairment in the HAART Era. *AIDS* (2007) 21:1915–21. doi: 10.1097/QAD.0b013e32828e4e27
42. Sanuki Y, Araki T, Nakazono O, Tsurui K. A Rapid Mitochondrial Toxicity Assay Utilizing Rapidly Changing Cell Energy Metabolism. *J Toxicol Sci* (2017) 42:349–58. doi: 10.2131/jts.42.349
43. Scaduto RC Jr, Grotyohann LW. Measurement of Mitochondrial Membrane Potential Using Fluorescent Rhodamine Derivatives. *Biophys J* (1999) 76:469–77. doi: 10.1016/S0006-3495(99)77214-0
44. Simioni S, Cavassini M, Annoni JM, Rimbault Abraham A, Bourquin I, Schiffer V, et al. Cognitive Dysfunction in HIV Patients Despite Long-Standing Suppression of Viremia. *AIDS* (2010) 24:1243–50. doi: 10.1097/QAD.0b013e3283354a7b
45. Srinivas N, Rosen EP, Gilliland WMJr., Kovarova M, Remling-Mulder L, De La Cruz G, et al. Antiretroviral Concentrations and Surrogate Measures of Efficacy in the Brain Tissue and CSF of Preclinical Species. *Xenobiotica* (2019) 49:1192–201. doi: 10.1080/00498254.2018.1539278
46. Stauch KL, Emanuel K, Lamberty BG, Morsey B, Fox HS. Central Nervous System-Penetrating Antiretrovirals Impair Energetic Reserve in Striatal Nerve Terminals. *J Neurovirol* (2017) 6:795–807. doi: 10.1007/s13365-017-0573-5
47. Tovar-Y-Romo LB, Bumpus NN, Pomerantz D, Avery LB, Sacktor N, Mcarthur JC, et al. Dendritic Spine Injury Induced by the 8-Hydroxy Metabolite of Efavirenz. *J Pharmacol Exp Ther* (2012) 343:696–703. doi: 10.1124/jpet.112.195701
48. Treisman GJ, Soudry O. Neuropsychiatric Effects of HIV Antiviral Medications. *Drug Saf* (2016) 39:945–57. doi: 10.1007/s40264-016-0440-y
49. Wallet C, De Rovere M, Van Assche J, Daouad F, De Wit S, Gautier V, et al. Microglial Cells: The Main Hiv-1 Reservoir in the Brain. *Front Cell Infect Microbiol* (2019) 9:362. doi: 10.3389/fcimb.2019.00362
50. Will Y, Dykens J. Mitochondrial Toxicity Assessment in Industry–a Decade of Technology Development and Insight. *Expert Opin Drug Metab Toxicol* (2014) 10:1061–7. doi: 10.1517/17425255.2014.939628
51. Yilmaz A, Price RW, Gisslen M. Antiretroviral Drug Treatment of CNS HIV-1 Infection. *J Antimicrob Chemother* (2012) 67:299–311. doi: 10.1093/jac/dkr492
52. Zayyad Z, Spudich S. Neuropathogenesis of HIV: From Initial Neuroinvasion to HIV-associated Neurocognitive Disorder (HAND). *Curr HIV/AIDS Rep* (2015) 12:16–24. doi: 10.1007/s11904-014-0255-3
53. Zhdanov AV, Andreev DE, Baranov PV, Papkovsky DB. Low Energy Costs of F1Fo ATP Synthase Reversal in Colon Carcinoma Cells Deficient in Mitochondrial Complex IV. *Free Radic Biol Med* (2017) 106:184–95. doi: 10.1016/j.freeradbiomed.2017.02.025

Conflict of Interest: The authors declare that the research was conducted in the absence of any commercial or financial relationships that could be construed as a potential conflict of interest.

frontiers in Neurology

ORIGINAL RESEARCH
published: 15 June 2021
doi: 10.3389/fneur.2021.663373

Prevention of HIV-1 TAT Protein-Induced Peripheral Neuropathy and Mitochondrial Disruption by the Antimuscarinic Pirenzepine

May Madi Han[1], *Katie E. Frizzi*[1], *Ronald J. Ellis*[2,3], *Nigel A. Calcutt*[1] *and Jerel Adam Fields*[3]*

[1] Department of Pathology, University of California, San Diego, La Jolla, CA, United States, [2] Department of Neuroscience, University of California, San Diego, La Jolla, CA, United States, [3] Department of Psychiatry, University of California, San Diego, La Jolla, CA, United States

OPEN ACCESS

Edited by:
Pankaj Seth,
National Brain Research Centre (NBRC), India

Reviewed by:
Tory P. Johnson,
Johns Hopkins University, United States
Sourish Ghosh,
National Institutes of Health (NIH), United States
Jonathan David Geiger,
University of North Dakota, United States

***Correspondence:**
Jerel Adam Fields
jafields@health.ucsd.edu

Specialty section:
This article was submitted to Neuroinfectious Diseases, a section of the journal Frontiers in Neurology

Received: 02 February 2021
Accepted: 21 May 2021
Published: 15 June 2021

Citation:
Han MM, Frizzi KE, Ellis RJ, Calcutt NA and Fields JA (2021) Prevention of HIV-1 TAT Protein-Induced Peripheral Neuropathy and Mitochondrial Disruption by the Antimuscarinic Pirenzepine. Front. Neurol. 12:663373. doi: 10.3389/fneur.2021.663373

HIV-associated distal sensory polyneuropathy (HIV-DSP) affects about one third of people with HIV and is characterized by distal degeneration of axons. The pathogenesis of HIV-DSP is not known and there is currently no FDA-approved treatment. HIV trans-activator of transcription (TAT) is associated with mitochondrial dysfunction and neurotoxicity in the brain and may play a role in the pathogenesis of HIV-DSP. In the present study, we measured indices of peripheral neuropathy in the doxycycline (DOX)-inducible HIV-TAT (iTAT) transgenic mouse and investigated the therapeutic efficacy of a selective muscarinic subtype-1 receptor (M_1R) antagonist, pirenzepine (PZ). PZ was selected as we have previously shown that it prevents and/or reverses indices of peripheral neuropathy in multiple disease models. DOX alone induced weight loss, tactile allodynia and paw thermal hypoalgesia in normal C57Bl/6J mice. Conduction velocity of large motor fibers, density of small sensory nerve fibers in the cornea and expression of mitochondria-associated proteins in sciatic nerve were unaffected by DOX in normal mice, whereas these parameters were disrupted when DOX was given to iTAT mice to induce TAT expression. Daily injection of PZ (10 mg/kg s.c.) prevented all of the disorders associated with TAT expression. These studies demonstrate that TAT expression disrupts mitochondria and induces indices of sensory and motor peripheral neuropathy and that M_1R antagonism may be a viable treatment for HIV-DSP. However, some indices of neuropathy in the DOX-inducible TAT transgenic mouse model can be ascribed to DOX treatment rather than TAT expression and data obtained from animal models in which gene expression is modified by DOX should be accompanied by appropriate controls and treated with due caution.

Keywords: HIV, tat, neuropathy, mitochondrial dysfunction, sciatic nerve, pirenzepine

INTRODUCTION

HIV has infected over 37 million people worldwide. The introduction of combined antiretroviral therapy (cART) has been successful in suppressing viral load, prolonging lifespan and improving quality of life of HIV-infected individuals. However, extending life span with cART has been accompanied by an increased prevalence of HIV-associated distal sensory polyneuropathy (HIV-DSP), which now affects over one third of patients with HIV (1). HIV-DSP is initially perceived in the feet and may progress proximally to the legs and hands, with patients experiencing a range of symptoms including loss of sensation to touch, heat or vibration, numbness, tingling and burning pain and allodynia (2). HIV-DSP is characterized by distal degeneration of sensory axons in a dying-back pattern (1, 3) and there is loss of small unmyelinated intraepidermal nerve fibers (IENF) in skin biopsies from distal legs of patients with HIV-DSP (4). The pathogenesis of HIV-DSP has been associated with neurotoxicity of both HIV-associated proteins (3, 5, 6) and cART (7–10). There is no FDA-approved treatment for HIV-DSP and patients exhibiting pain are frequently treated with agents used for other neuropathic pain conditions such as gabapentin, lidocaine gel, capsaicin cream and opioids (2, 11).

One of the HIV viral proteins implicated in HIV-DSP is HIV trans-activator of transcription (TAT). This protein is essential for efficient HIV viral replication and is secreted by HIV-infected microglia, macrophages and astrocytes (6, 12–14). TAT is detectable in the cerebrospinal fluid and peripheral blood samples of HIV-patients (15, 16). The pathogenic role of TAT has been investigated using doxycycline-inducible TAT (iTAT) transgenic mouse models (6). The two predominant models in the field differ only by the number of TAT gene insertions into the genome, with mice having either multiple (6) or single copies (17). With doxycycline (DOX) treatment, the iTAT-tg mouse models express TAT under the glial fibrillary acidic protein (GFAP) promoter in astrocytes at a concentration comparable to that detected in HIV patients on cART (6, 18). These iTAT mice develop cognitive deficits and CNS neuropathologies similar to those seen in HIV patients such as astrogliosis, loss of dendritic spines, neuronal apoptosis and increased infiltration of activated monocytes and T-lymphocytes (6, 19, 20). The pathogenic mechanism of TAT-induced neuropathology has been linked to disruption of mitochondria (14), including increased fission (21, 22).

RNA transcripts for Tat have been detected in the peripheral nervous system of the iTAT tg models, probably transcribed by the GFAP-expressing satellite and Schwann cells (17, 23). However, despite extensive studies on how TAT affects the CNS, few studies have examined the consequence of TAT in the PNS. It has been argued that mitochondrial energy deficits in distal terminals of sensory neurons lead to degeneration or retraction of these regions (24). Mitochondrial dysfunction has been implicated in the pathogenesis of neuropathic pain including mechanical allodynia seen in HIV patients (25, 26) and contributes to a variety of peripheral neuropathies (25), including those associated with diabetes (27–29), chemotherapy (30) and HIV (31). Thus, ameliorating mitochondrial dysfunction may offer an approach to treating both the degenerative and painful aspects of HIV-DSP.

We have previously shown that adult sensory neurons are under metabolic constraint mediated by activation of the muscarinic subtype-1 receptor (M_1R) (32). Pharmacologically inhibiting M_1R with the selective antagonist pirenzepine (PZ) activates the AMPK/PGC-1α pathway, enhances mitochondrial function and promotes neurite outgrowth *in vitro.* PZ treatment also prevented and/or reversed multiple indices of diabetic and chemotherapy-induced peripheral neuropathies in rodent models of these conditions (7, 33, 34). Most pertinent to our present studies, topical administration of the specific M_1R antagonist MT7 to the eye both prevented and reversed corneal sensory nerve loss caused by topical delivery of the neurotoxic HIV envelope protein gp120 (32). We have therefore extended investigation of the therapeutic potential of M_1R antagonism against HIV-DSP by determining efficacy of systemic PZ against functional and structural disorders of peripheral nerve caused by TAT expression using the iTAT-tg mouse model.

METHODS

Animals

All animal procedures were approved by the Institutional Animal Care and Use Committee at the University of California San Diego. Animals were housed in an AALAC-accredited vivarium in groups of 3–5 per cage on TEK-Fresh bedding (7099, Envigo) under a 12-hour light:dark cycle with free access to food (5001 diet, Purina, USA) and water. Studies were performed in adult male and female 7–8-month-old mice. The iTAT transgenic mouse model requires treatment with the antibiotic DOX to induce TAT protein expression. However, DOX is known to have anti-inflammatory effects (35) and could potentially serve as an independent variable. Thus, two studies were performed—one to assess potential neurotoxic effects of DOX in normal mice and the second to measure neuropathy in DOX-induced TAT expressing mice and the impact of PZ therapy. The first study consisted of male and female C57BL/6J mice treated with vehicle ($n = 9$) or DOX ($n = 8$). DOX was administered daily at 80 mg/kg i.p. for 2 weeks, as behavioral deficits arising from transgene expression in TAT-expressing mice occur within 7 days of DOX treatment (6). We previously showed that 2 weeks of DOX treatment of the iTAT tg mice induces strong expression of the TAT gene from the GFAP promoter, which is expressed in the peripheral nervous system by Schwann cells (36).

The second study used DOX-inducible TAT transgenic mice treated with vehicle (5 males and 3 females, abbreviated as

Abbreviations: HIV, human immunodeficiency virus; tg, transgenic; CNS, central nervous system; PNS, peripheral nervous system; HIV-DSP, HIV-associated distal sensory polyneuropathy; TAT, trans-activator of transcription; PZ, pirenzepine; M_1R, muscarinic subtype-1 receptor; iTAT, doxycycline-inducible HIV-TAT; cART, combined antiretroviral therapy; IENF, intraepidermal nerve fibers; DOX, doxycycline; GFAP, glial fibrillary acidic protein; CCM, corneal confocal microscopy; RPM, rotations per minute; MNCV, motor nerve conduction velocity; SNCV, sensory nerve conduction velocity; EMG, electromyogram; $M_{achilles}$ wave, M wave at the Achilles tendon; M_{notch} wave, M wave at the sciatic notch; PBST, phosphate-buffered saline-tween 20; TFAM, transcription factor A.

iTAT), DOX (4 males and 3 females, abbreviated as iTAT+DOX) or DOX and PZ (3 males and 3 females, abbreviated as iTAT+DOX+PZ). The iTAT transgenic mice were produced by crossbreeding Teton-GFAP mice and TRE-Tat86 mice (6) and the DOX-induced expression of TAT in the nervous system of this model has been validated (36). TAT was induced by i.p. DOX administration at 80 mg/kg once daily, five times per week for 2 weeks. For the iTAT+DOX+PZ group, PZ was administered at 10 mg/kg *via* subcutaneous injection once daily five times per week. PZ treatment was initiated on the same day as DOX to assess potential neuroprotective effects. For vehicle treatment, 0.9% saline was administered via subcutaneous and intraperitoneal injection.

After 2 weeks of treatment, rotarod performance, electrophysiological function and hind-paw withdrawal threshold to von Frey filaments and heat were measured (week 3 of the study), followed by corneal confocal microscopy (CCM) to quantify corneal sensory innervation (week 4 of the study). Upon completion of CCM, the mice were euthanized and hind-paw foot skin was collected for assessment of intraepidermal nerve fiber density and sciatic nerves for immunoblot analyses.

Behavioral Tests

Response to Heat Stimulation

The function of small sensory fibers in hind-paw skin was measured by recording latency of hind-paw withdrawal to a heat stimulus using a thermal nociception test device (UARD) as described in technical detail elsewhere (37). The temperature of the device glass surface was stabilized at 30°C and the heating rate was 1°C/sec, with a 20 s cut-off. Measurements were made on both hind paws and repeated four times. The median of the four measurements for each hind paw was calculated and thermal response latency of the mouse calculated by averaging the median measurements of left and right hind paws.

Response to Von Frey Filaments

The function of large myelinated sensory fibers in hind-paw skin was measured by recording sensitivity to light touch using manual von Frey filaments (range of 0.16 to 6.0 grams of force, Kom Kare, Inc.) as described in detail elsewhere (37). The testing filament sequence was used to calculate the 50% paw withdrawal threshold (in grams of force) for each hind paw exactly as described elsewhere (38).

Rotarod

Impaired motor function can disrupt behavioral responses upon sensory stimuli. To ensure that behavioral responses were not due to impaired motor function, motor coordination of the animals was measured using a 1.25 inch diameter rotarod (Stoelting Co.) as described previously (37) with the rate of rotation increased from the starting speed of four rotations per minute (RPM) to a maximum of 40 RPM within 120 s. After 120 s, rods consistently rotated at 40 RPM for another 180 s. One acclimation run was performed before the test run.

Electrophysiology

To evaluate the function of large myelinated motor nerve fibers, motor nerve conduction velocity (MNCV) was measured as described previously (37). Each mouse was anesthetized with 4% isoflurane in oxygen and the nerve and body temperatures stabilized at 37°C. The grounding platinum-tipped sub-dermal needle electrode (Grass Technologies) was inserted into skin at the back of the neck. Two recording electrodes were inserted into the interosseous muscle between the second and third, and third and fourth toes. The sciatic nerve was stimulated with a PowerLab stimulator set to deliver a 200-mV, 50-μs-duration square-wave stimulus every 2 s. The stimulating electrode was inserted into the ankle at the Achilles tendon and the sciatic notch to record the resulting electromyogram (EMG) containing the M wave at the Achilles tendon ($M_{achilles}$ wave) and at the notch (M_{notch} wave). This process was repeated three times. MNCV was obtained by calculating the difference between $M_{achilles}$ and M_{notch} for three repeats and dividing the median by the distance between the Achilles tendon and the sciatic notch.

Nerve Structure

Intraepidermal Nerve Fiber Density

Analysis of small sensory fibers in the epidermis (intraepidermal nerve fibers, IENF) was performed as described in detail previously (37). Briefly, hind-paw skin was fixed in 4% buffered paraformaldehyde overnight at 4°C then stored in 0.1M sodium phosphate buffer at 4°C before embedding in paraffin blocks. 6 μm sections were cut using a rotary microtome (Leitz, model 1512) and mounted onto glass slides. Mounted tissues were immunostained with antibody against protein gene product (PGP) 9.5 (1:1,000; cat. #7863-0504, AbD Serotec). Quantification of IENF was done using bright field light microscopy at 40× magnification. All nerve fragments in the epidermis were counted for detection of early IENF terminal loss prior to retraction as far as the dermis (39). The length of the paw skin was traced under a light microscope using Scion Image software and a tracing pad. IENF density was reported as IENF profiles/mm.

Corneal Nerves

To visualize sensory innervation of the cornea, each mouse was anesthetized with 4% isoflurane in oxygen before transfer to the platform of a corneal confocal microscope (Heidelberg Retina Tomograph 3 with Rostock Cornea Module). Eye gel (GenTeal^{TM}, Novartis) was applied to both eyes to prevent drying and to connect the eyes to the microscope lens. The microscope objective was positioned close to the center of the apex of cornea and the depth adjusted to the beginning of the sub-basal nerve plexus. Using the Rostock Imaging Software, 40 sequential images, with 2 μm spacing, were collected encompassing the corneal epithelium, sub-basal nerve plexus and stroma. After identifying the sub-basal nerve plexus:stromal junction, five consecutive images of the sub-basal nerve layer moving outwards toward the epidermis and the first 10 images of the stromal layer were quantified. Corneal nerves in each image were traced using a digitizing tablet connected to a computer running Image J

software (Image Processing Analysis in Java, National Institutes of Health). Corneal nerve density in each image was reported as number of pixels per area.

ImmunoBlot

Sciatic nerves from all groups in both studies were homogenized in a buffer containing protease inhibitor cocktails (Calbiochem, cat. no. 524624 and 539131) plus 1.0 mmol/L HEPES (Gibco, cat. no. 15630-080), 5.0 mmol/L benzamidine, 2.0 mmol/L 2-mercaptoethanol (Gibco, cat. no. 21985), 3.0 mmol/L EDTA (Omni pur, cat. no. 4005), 0.5 mmol/L magnesium sulfate, 0.05% sodium azide; final pH 8.8 as previously described (7). Samples were pre-cleared by centrifugation at 5,000 × g for 5 min at room temperature. Supernatants were retained as whole lysate and stored at −80°F until use.

After determination of protein content by bicinchoninic acid assay (Thermo Fisher Scientific, cat. no. 23225), lysates were loaded (20 μg total protein/lane) on 4–12% Bis-Tris gels (Invitrogen, cat. no. WG1402BX10) and electrophoresed in 5% HEPES running buffer and transferred onto PVDF membrane with iBlot transfer stacks (Invitrogen, cat. no. IB24001) using NuPage transfer buffer (ThermoFisher Scientific, cat. no NP0006). The membranes were blocked in 5% BSA in phosphate-buffered saline-tween 20 (PBST) for 1 h. Membranes were incubated overnight at 4°C with primary antibodies (TFAM, ThermoFisher Scientific, cat# PA5-23776; Total OxPhos Complex Kit, ThermoFisher Scientific, cat# 458099; DNM1L Santa Cruz Biotechnology; sc-32989). Following visualization, blots were stripped and probed with a mouse monoclonal antibody against β-actin (ACTB; Sigma Aldrich, cat. no. A5441) in blocking buffer as a loading control. All blots were washed in PBST then incubated with species-specific IgG conjugated to HRP (American Qualex, cat. no. A102P5) diluted 1:5,000 in PBST and visualized with SuperSignal West Femto Maximum Sensitivity Substrate (ThermoFisher Scientific, cat. no. 34096). Images of protein bands were analyzed by semi-quantitative analysis using the VersaDoc gel imaging system and Quantity One software (Bio-Rad). The densitometry of TFAM, OXPhos, and DNM1L bands were normalized to densitometry of ACTB.

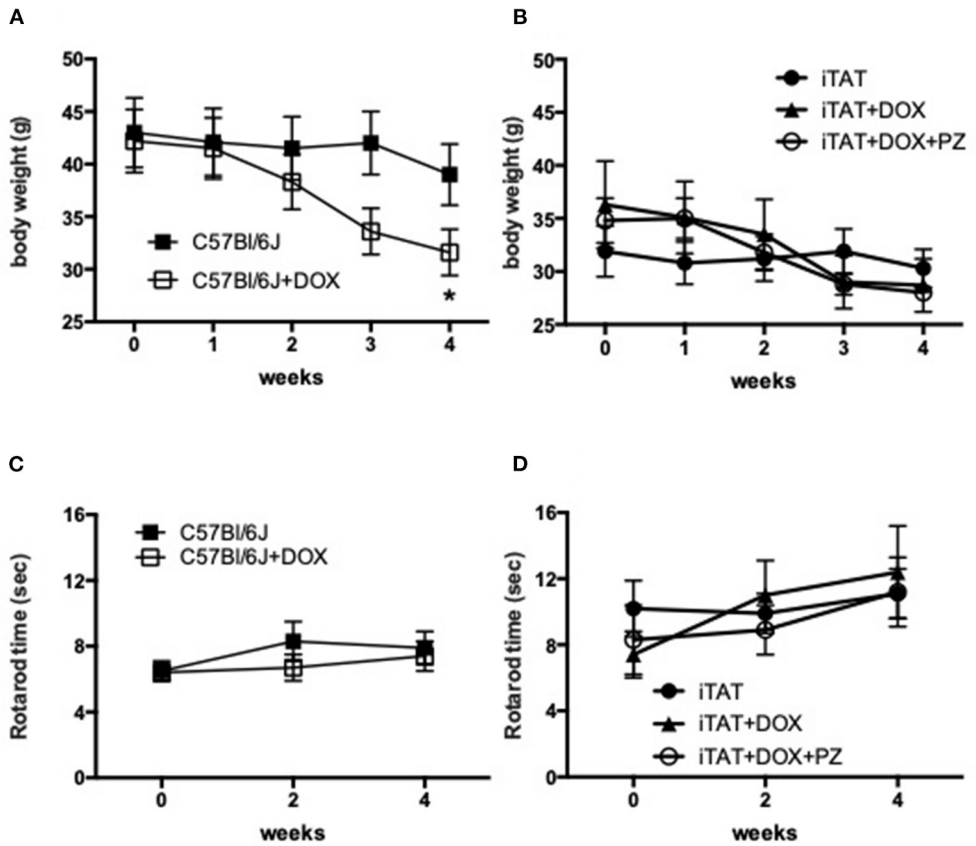

FIGURE 1 | Body weight and sensorimotor function. **(A)** Body weight in C57Bl6/J mice treated with vehicle (filled squares) or DOX (open squares). **(B)** Body weight in TAT transgenic mice treated with vehicle (filled circles), DOX (filled triangles) or DOX and PZ (open circles). **(C)** Rotarod performance in C57Bl6/J mice treated with vehicle (filled squares) or DOX (open squares). **(D)** Rotarod performance in TAT transgenic mice treated with vehicle (filled circles), DOX (filled triangles) or DOX and PZ (open circles). Data are group mean of $N = 6$–9/group ± SEM. Statistical comparisons by two way repeat measures ANOVA followed by Dunnett's *post-hoc* test. *$p < 0.05$ vs. within group time 0.

Statistical Analysis

All studies, assays and measurements were performed on coded animals and tissues by observers unaware of the codes. Within group comparisons over time were made by one-way ANOVA or two-way ANOVA with repeat measures followed by Dunnett's *post hoc* test. Between group comparisons were made by unpaired *t* test or one-way ANOVA with Tukey's or Dunnett's *post hoc* test, as indicated.

RESULTS

Body Weight and Sensorimotor Function

Body weight and rotarod performance were assessed before and after DOX treatment to determine any potential systemic effects of DOX. In normal C57Bl/6J mice, DOX treatment decreased body weight over time so that by study end mice were significantly ($p < 0.05$) lighter than before onset of treatment (onset = 42.2±8.6 vs. final = 31.6 ± 6.2 g; mean ± SD; **Figure 1A**). Vehicle treatment did not change body weight in iTAT mice over time (onset = 31.9 ± 6.7 vs. final =30.3 ± 5.1 g; mean ± SD; **Figure 1B**), whereas DOX treatment caused a trend to loss of body weight over time (onset = 36.3 ± 10.9 vs. final = 28.7 ± 6.5 g; mean ± SD; **Figure 1B**) that was not prevented by PZ treatment (onset = 34.8 ± 5.2 vs. final = 28.0 ± 1.6; mean ± SD; **Figure 1B**). Sensorimotor coordination in normal C57Bl/6J mice, as assessed by the rotarod test, did not change following daily DOX treatment for 2 weeks (**Figure 1C**). Similarly, there was no change in rotarod performance over time in iTAT mice, whether treated with vehicle, DOX or DOX+PZ (**Figure 1D**). Therefore, despite a DOX-induced loss of weight, sensorimotor function of DOX-treated mice remained intact, allowing valid measures of behavioral responses in subsequent sensory assays.

Stimulus-Evoked Behavior and Nerve Electrophysiology

In normal C57Bl/6J mice, DOX treatment significantly ($p < 0.01$) decreased 50% paw response threshold (C57 = 1.01 ± 0.34 vs. C57 + DOX = 0.44 ± 0.21g; mean ± SD; **Figure 2A**, left sub-panel) and significantly ($p < 0.01$) increased paw response to heat (C57 = 36.9±0.7 vs. C57+DOX = 38.5±1.3°C; mean ± SD; **Figure 2B**, left sub-panel) whereas MNCV was unaffected by DOX treatment (C57 = 46.9 ± 3.1 vs. C57 + DOX = 47.9 ± 2.9 m/s; mean ± SD; **Figure 2C**, left sub-panel). DOX treatment of iTAT mice also induced significant ($p < 0.001$) tactile allodynia (iTAT = 0.84 ± 0.23 vs. iTAT+DOX = 0.25 ± 0.16 g; mean ± SD) and heat hypoalgesia (iTAT = 37.2 ± 1.7 vs. 39.2±1.9°C; mean ± SD) when compared to vehicle treated iTAT mice (**Figures 2A,B**, right sub-panels). This data showed that the DOX treatment regime used impacted sensory nerve function, thereby precluding determination as to whether tactile allodynia and heat hypoalgesia observed in DOX treated iTAT mice were due to TAT expression or DOX. In contrast to C57 mice, iTAT mice treated with DOX developed significant ($p < 0.05$) MNCV slowing when compared to vehicle-treated iTAT mice (iTAT = 47.1 ± 3.5 vs. iTAT + DOX = 41.3 ± 6.1 m/s; mean ± SD; **Figure 2C**, right sub-panel), suggesting that MNCV slowing was

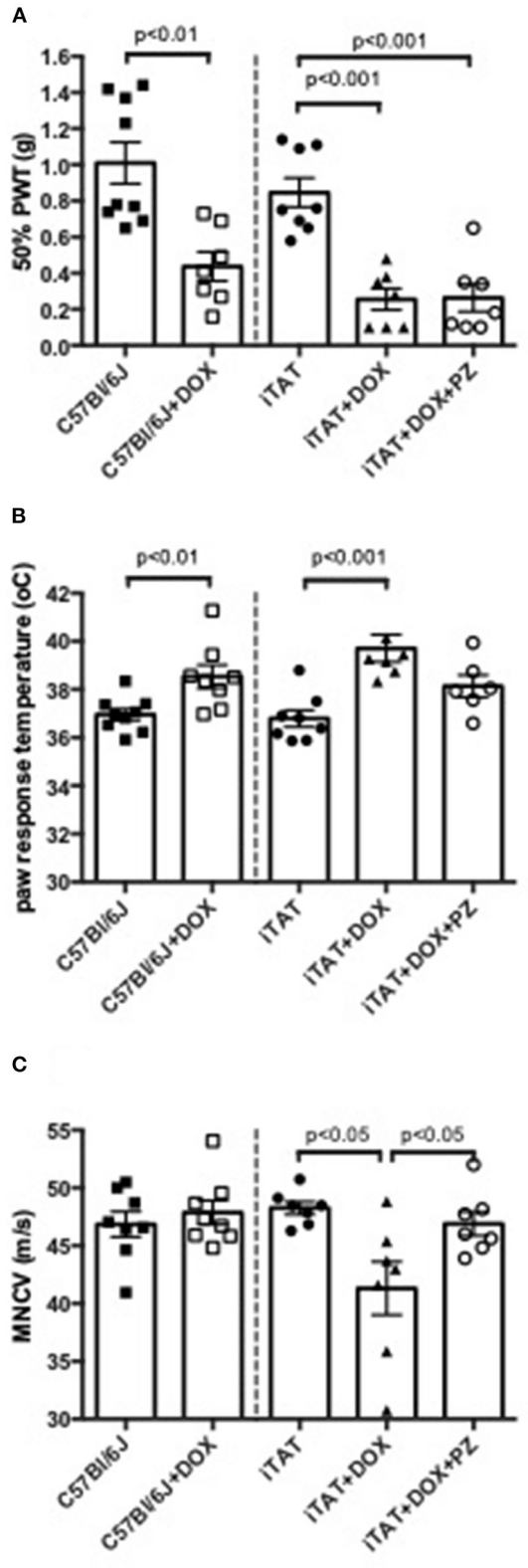

FIGURE 2 | Stimulus-evoked behavior and nerve electrophysiology. **(A)** Paw response to von Frey filaments, **(B)** temperature of paw withdrawal to

(Continued)

FIGURE 2 | escalating heat and **(C)** motor nerve conduction velocity in C57Bl6/J mice treated with vehicle or DOX and iTAT transgenic mice treated with vehicle, DOX or DOX and PZ Data are group mean of $N = 6$–9/group ± SEM. Statistical comparisons by unpaired *t* test (left sub-panel) or one-way ANOVA followed by Tukey's *post-hoc* test (right sub-panel).

likely due to TAT expression and not the DOX regime *per se*. Concurrent treatment of iTAT mice with DOX and PZ did not alter tactile allodynia (0.29 ± 0.21 g), whereas it returned paw heat response (37.9 ± 1.3; mean ± SD) and MNCV (46.9 ± 2.7 m/s; mean ± SD) to values that were not significantly different from vehicle-treated iTAT mice (**Figures 2A–C**, right sub-panel).

Sensory Nerve Structure

Representative images of corneal sub-basal nerves and the dermal and intra-epidermal nerve fibers (IENF) present in hind-paw plantar skin are shown in **Figures 3A,B**, respectively. In normal C57Bl/6J mice, DOX treatment was without effect on corneal sub-basal nerve density (**Figure 3C**, left sub-panel) or paw skin IENF density (**Figure 3D**, left sub-panel) indicating that DOX is not toxic to small fiber structure. DOX-treated iTAT mice had significantly ($p < 0.05$) reduced nerve density in the corneal sub-basal plexus (3,396 ± 359 pixels/image; mean ± SD) compared to vehicle-treated iTAT mice (3,935 ± 425 pixels/image; mean ± SD) and this was prevented by concurrent treatment with PZ (4,106 ± 422 pixels/image; mean ± SD; **Figure 3C**). Thus, it appears that PZ prevents corneal nerve loss associated with induction of TAT expression. In contrast, neither DOX treatment alone, or in combination with PZ, caused a significant effect on paw skin IENF density of iTAT mice when compared to vehicle-treated iTAT mice (**Figure 3D**).

Mitochondrial Proteins in Sciatic Nerve

In light of the DOX-induced physiological changes between C57 and iTAT mice the limited amounts of sciatic were used for exploratory biochemical studies of mitochondrial markers. Sciatic nerve protein lysates were assayed by immunoblot for proteins associated with mitochondrial transcription (TFAM), mitochondrial oxidative phosphorylation at complex III (UQCRC2), complex IV (MTCO1) and complex V (ATP5) and with mitochondrial fission (DNM1L) relative to the housekeeping gene β-actin (ACTB) (**Figure 4A**) in order to explore the potential role of mitochondrial dysfunction in TAT-induced neuropathy and establish any effects of the PZ intervention on mitochondrial proteins. In C57Bl/6J mice DOX treatment had no effect on any of these mitochondrial-associated proteins (**Figures 4A–D**, left sub-panels) suggesting that DOX alone is not disruptive of mitochondria. DOX treatment was also without impact on TFAM (**Figures 4A,B**, right sub-panel), CIII-UQCRC2 or CV-ATP5 protein (**Figure 4A**: quantification not shown). However, in iTAT mice, DOX treatment caused a significant ($p < 0.05$) reduction in CIV-MTCO1 protein (1.11 ± 0.07 AU; mean ± SD) compared to vehicle-treated iTAT mice (1.23 ± 0.06 AU; mean ± SD) and iTAT mice treated with DOX and PZ (1.28 ± 0.02 AU; mean ± SD; **Figures 4A,C**). DOX treatment of iTAT mice also caused a significant ($p < 0.05$) increase in levels of DNM1L (0.68 ± 0.06 AU; mean ± SD) compared to vehicle-treated iTAT mice (0.58±0.03 AU; mean ± SD) that was also absent in mice treated with PZ (0.60 ± 0.01 AU; mean ± SD; **Figures 4A,D**). These findings suggested that PZ prevented both the TAT-induced reduced expression of proteins associated with oxidative phosphorylation complex IV and a corresponding in mitochondrial fission.

DISCUSSION

We investigated the pathogenic role of TAT protein in HIV-DSP using a well-characterized iTAT–tg mouse model and demonstrated that induction of TAT leads to functional and structural indices of motor and sensory neuropathy, accompanied by reduced expression of proteins of the electron transport chain and increased expression of a protein involved in mitochondrial fission. Concurrent treatment with the M_1R antagonist PZ prevented all indices of mitochondrial dysfunction and peripheral neuropathy. While MNCV, corneal nerves and mitochondrial protein expression co-vary with both TAT expression and PZ therapy, we cannot yet ascribe a causal relationship linking TAT expression, mitochondrial dysfunction and peripheral neuropathy and further mechanistic studies are required to address this possibility.

The trans-activator of transcription (HIV-TAT) protein is an important regulatory protein that allows HIV to replicate efficiently (13). Low levels of TAT protein and viral replication persist in HIV patients on cART despite suppression of the viral load (40, 41). Expression of TAT in the iTAT-tg mouse model has been associated with neuronal dysfunction and damage in the CNS (6, 19, 20) that resembles disorders seen in HIV patients. A recent study conducted with a similar DOX-inducible TAT expressing transgenic mouse model also reported peripheral neuropathy, as indicated by tactile allodynia and reduction of paw IENF density, with no changes in paw thermal withdrawal threshold (17). In our present study we replicated the report of tactile allodynia, but this was accompanied by paw thermal hypoalgesia and normal IENF density. There are a number of differences in the design and analysis of the two studies that could contribute to these discrepancies. Firstly, we provided DOX by daily ip injection for 2 weeks whereas the prior report provided DOX in the diet for 9 weeks. Our more aggressive DOX regimen induced weight loss but not impairment of sensorimotor coordination as measured by rotarod performance, so that sensory assays relying on limb withdrawal responses remain valid. Our study design also allowed us to identify any DOX-associated impact on the PNS independent of TAT induction and demonstrated that both tactile allodynia and paw thermal hypoalgesia in DOX-treated iTAT-tg mice also occurred in DOX-treated non-tg mice and are thus likely attributable to the DOX regimen rather than TAT expression. The prior study limited their comparison to normal mice treated with DOX vs. iTAT-tg mice treated with DOX and thus could not resolve any impact of the DOX regimen *per se*. Further, loss of IENF was detected after 6 weeks of DOX exposure in iTAT-tg mice, but not 8 days

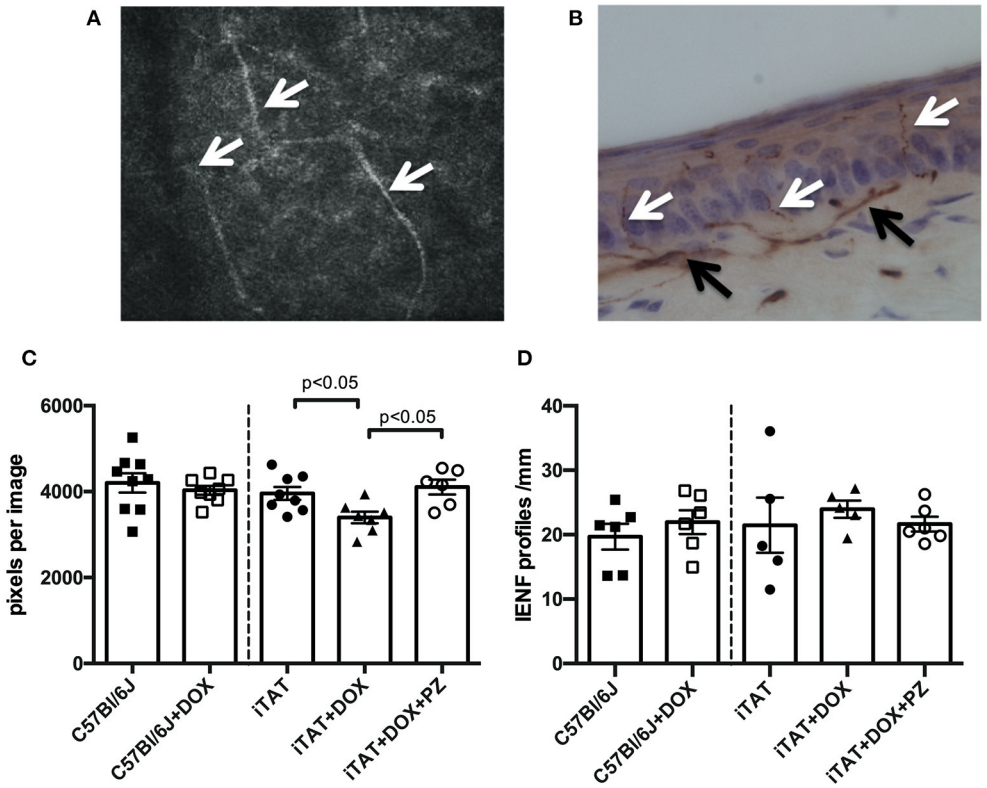

FIGURE 3 | Sensory nerve structure. **(A)** Representative image of mouse corneal sub-basal nerves (white arrowheads). **(B)** Representative image of mouse paw skin dermal (black arrowheads) and intra-epidermal (white arrowheads) PGP9.5+ve nerves. **(C)** Corneal nerve density in C57Bl6/J mice treated with vehicle or DOX and in TAT transgenic mice treated with vehicle, DOX or DOX and PZ. **(D)** Intra-epidermal nerve fiber density of C57Bl6/J mice treated with vehicle or DOX and of TAT transgenic mice treated with vehicle, DOX or DOX and PZ. Data are group mean of $N = 5$–9/group ± SEM. Statistical comparisons by unpaired *t* test (left sub-panel) or one-way ANOVA followed by Tukey's *post-hoc* test (right sub-panel).

(17). Our failure to detect this disorder could reflect the shorter duration of DOX exposure and TAT induction (2 weeks) or withdrawal of DOX for 2 weeks prior to tissue collection that could allow IENF time to regenerate. Finally, there is also a report of sex-dependent effects of TAT on responses to inflammatory or neuropathic insults (42) and while the prior report was limited to female mice, we included both sexes. However, in *post-hoc* exploratory analyses we identified no differences in PNS function or structure between sexes.

Despite the above caveats, large fiber MNCV slowing is likely due to TAT expression, as DOX did not affect this parameter in normal mice. To the best of our knowledge, this is the first study to quantify function of large myelinated motor fibers in the iTAT-tg mouse model, although nerve conduction studies have been used for diagnosing peripheral neuropathy in HIV patients (43–46). Similarly, our novel finding of reduced corneal sensory nerve density is not a consequence of DOX exposure *per se* and is consistent with recent reports of reduced corneal nerve density in patients with HIV neuropathy (47, 48). In a previous study we demonstrated that topical delivery of the HIV envelope protein gp120 to the eye of normal mice also leads to loss of corneal sensory nerves (32), so that two HIV-associated proteins linked with neuropathy independently impact corneal nerves. In both cases, PZ was effective at preventing and/or reversing reduced corneal nerve density, which is consistent with its capacity to provide neuroprotection and promote neurite growth in sensory nerves (32). At present we cannot determine whether the efficacy of PZ was via prevention of corneal nerve degeneration, collateral sprouting from surviving neurons or some combination of both and future intervention treatment studies will be required to address this issue. Our findings also indicate that, at least in the DOX-induced iTAT model, MNCV slowing and corneal nerve depletion precede IENF loss. Electrophysiological testing, a widely used neurological diagnostic technique, and non-invasive corneal confocal microscopy therefore have potential as early biomarkers of large and small fiber peripheral neuropathy in HIV patients.

In neuronal cell cultures, TAT damages neurons by inducing mitochondrial depolarization and increasing mitochondrial fission leading to rapid release of reactive oxygen species and smaller mitochondrial size (14). Mitochondrial fission is controlled by a dynamin like protein 1 (DNM1L), which has been shown to be dysregulated in the brains of people with HIV-associated neurocognitive disorders (21, 22). Similar

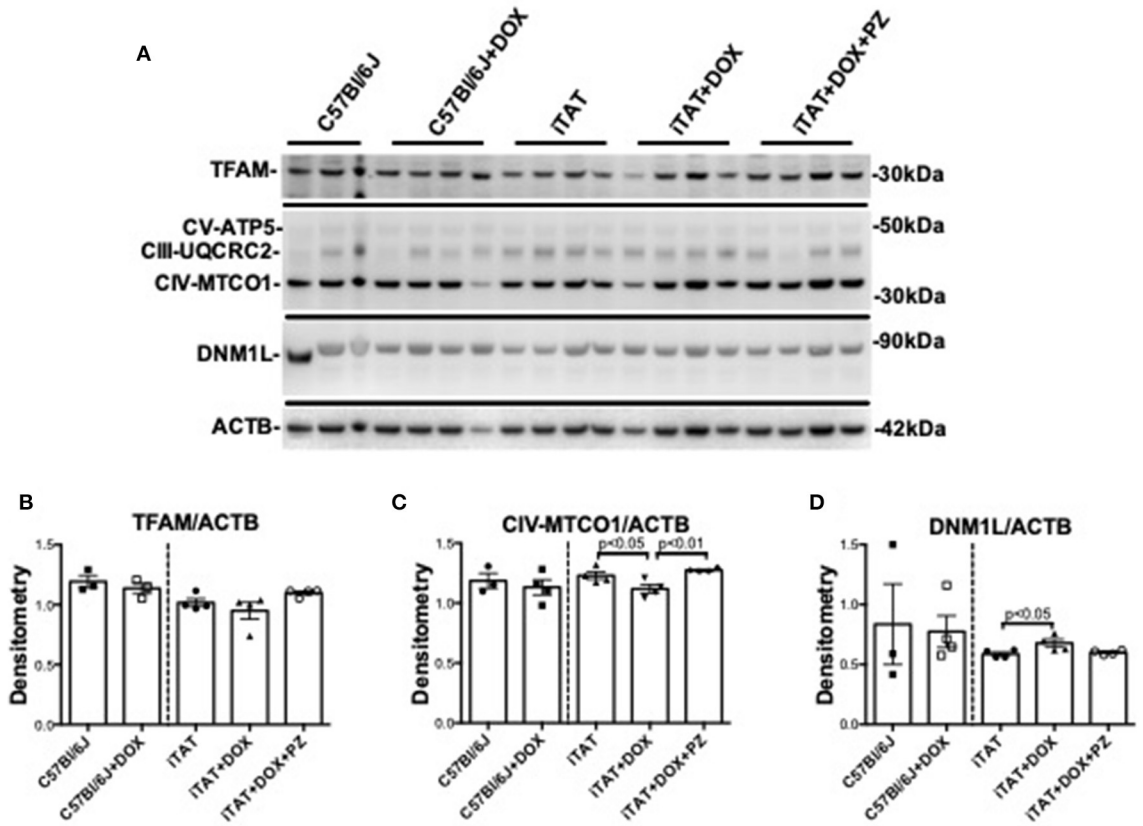

FIGURE 4 | Mitochondrial proteins in mouse sciatic nerve. **(A)** Representative immunoblot for TFAM, proteins of oxidative phosphorylation complexes III, IV, and V, DNM1L and ACTB. **(B)** Densitometric analysis of TFAM normalized to ACTB. **(C)** Densitometric analysis of complex IV(MTC01 sub-unit) protein normalized to ACTB. **(D)** Densitometric analyses of DNM1L protein normalized to ACTB. Data are mean + SEM of $N = 3$ for C57Bl/6J group and $N = 4$/group for remaining groups. Statistical analyses by unpaired test or one-way ANOVA with Tukey's *post-hoc* test.

mitochondrial functional and morphological abnormalities have been observed in postmortem brains of iTAT-tg mice (14). Our current findings in sciatic nerves are consistent with recent studies showing that TAT disrupts oxidative phosphorylation and mitochondrial dynamics in multiple cellular models (49, 50). Reversal of TAT-induced mitochondrial alterations after PZ administration may reflect the capacity of PZ to activate ERK/CREB signaling to promote neurite outgrowth in sensory neurons via regulation of microtubule polymerization and mitochondrial trafficking (51). Interestingly, this signaling pathway is also inhibited by TAT protein leading to subsequent neurite retraction (52). Thus, the therapeutic efficacy of PZ against indices of TAT associated HIV-DSP is consistent with its general mitochondrial enhancing and nerve growth-promoting properties.

Our study is limited to the use of a mouse model that expresses only one HIV-associated protein and the use of DOX to induce TAT expression. Although the iTAT-tg mouse model does not illustrate the complex interaction between HIV and HIV proteins that may impact development of HIV-DSP in humans, it does focus attention on one specific protein and its role in clinical features of HIV-DSP such as nerve conduction slowing and reduction of corneal sensory nerve density (2, 47, 48). Appropriate controls in our study also allowed us to segregate the impact of DOX on sensory nerve function. This study is also limited to descriptive analyses of DSP-related symptoms in the iTAT-tg mouse and how PZ affects these symptoms. While the covariance of mitochondrial associated proteins with neuropathy following TAT expression and PZ treatment offers potential pathogenic and therapeutic mechanisms further studies are needed to better understand the physiological and molecular mechanisms involved and establish any causal links.

In summary, TAT expression in DOX-induced TAT transgenic mice produced indices of large and small fiber neuropathy that replicate those seen in clinical HIV-DSP. These deficits were prevented by treatment with the selective M_1R antagonist, PZ, as were changes in expression of proteins of mitochondrial respiration and fission. It was notable that our DOX regimen independently impacted sensitivity to touch and heat in normal mice suggesting a need for caution and appropriate controls when using this DOX regime to induce expression of proteins of interest.

DATA AVAILABILITY STATEMENT

The raw data supporting the conclusions of this article will be made available by the authors, without undue reservation.

ETHICS STATEMENT

The animal study was reviewed and approved by Institutional Animal Care and Use Committee at the University of California San Diego.

AUTHOR CONTRIBUTIONS

JF, RE, and NC conceived, designed, coordinated the study, and edited the manuscript. MH performed the experiments, analyzed data and wrote the manuscript. KF performed the experiments and analyzed the data. All authors contributed to the article and approved the submitted version.

FUNDING

This work was supported by NIH STTR award NS105177 (JF) and MH115819 (JF).

REFERENCES

1. Schutz SG, Robinson-Papp J. HIV-related neuropathy: current perspectives. *HIV AIDS.* (2013) 5:243–51. doi: 10.2147/HIV.S36674
2. Aziz-Donnelly A, Harrison TB. Update of HIV-associated sensory neuropathies. *Curr Treat Options Neurol.* (2017) 19:36. doi: 10.1007/s11940-017-0472-3
3. Melli G, Jack C, Lambrinos GL, Ringkamp M, Hoke A. Erythropoietin protects sensory axons against paclitaxel-induced distal degeneration. *Neurobiol Dis.* (2006) 24:525–30. doi: 10.1016/j.nbd.2006.08.014
4. Holland NR, Stocks A, Hauer P, Cornblath DR, Griffin JW, McArthur JC. Intraepidermal nerve fiber density in patients with painful sensory neuropathy. *Neurology.* (1997) 48:708–11. doi: 10.1212/WNL.48.3.708
5. Keswani SC, Polley M, Pardo CA, Griffin JW, McArthur JC, Hoke A. Schwann cell chemokine receptors mediate HIV-1 gp120 toxicity to sensory neurons. *Ann Neurol.* (2003) 54:287–96. doi: 10.1002/ana.10645
6. Kim BO, Liu Y, Ruan Y, Xu ZC, Schantz L, He JJ. Neuropathologies in transgenic mice expressing human immunodeficiency virus type 1 Tat protein under the regulation of the astrocyte-specific glial fibrillary acidic protein promoter and doxycycline. *Am J Pathol.* (2003) 162:1693–707. doi: 10.1016/S0002-9440(10)64304-0
7. Fields JA, Swinton MK, Carson A, Soontornniyomkij B, Lindsay C, Han MM, et al. Tenofovir disoproxil fumarate induces peripheral neuropathy and alters inflammation and mitochondrial biogenesis in the brains of mice. *Sci Rep.* (2019) 9:17158. doi: 10.1038/s41598-019-53466-x
8. Pettersen JA, Jones G, Worthington C, Krentz HB, Keppler OT, Hoke A, et al. Sensory neuropathy in human immunodeficiency virus/acquired immunodeficiency syndrome patients: protease inhibitor-mediated neurotoxicity. *Ann Neurol.* (2006) 59:816–24. doi: 10.1002/ana.20816
9. Zhu Y, Antony JM, Martinez JA, Glerum DM, Brussee V, Hoke A, et al. Didanosine causes sensory neuropathy in an HIV/AIDS animal model: impaired mitochondrial and neurotrophic factor gene expression. *Brain.* (2007) 130:2011–23. doi: 10.1093/brain/awm148
10. Huang W, Calvo M, Karu K, Olausen HR, Bathgate G, Okuse K, et al. A clinically relevant rodent model of the HIV antiretroviral drug stavudine induced painful peripheral neuropathy. *Pain.* (2013) 154:560–75. doi: 10.1016/j.pain.2012.12.023
11. Finnerup NB, Attal N, Haroutounian S, McNicol E, Baron R, Dworkin RH, et al. Pharmacotherapy for neuropathic pain in adults: a systematic review and meta-analysis. *Lancet Neurol.* (2015) 14:162–73. doi: 10.1016/S1474-4422(14)70251-0
12. Maragos WF, Tillman P, Jones M, Bruce-Keller AJ, Roth S, Bell JE, et al. Neuronal injury in hippocampus with human immunodeficiency virus transactivating protein, Tat. *Neuroscience.* (2003) 117:43–53. doi: 10.1016/S0306-4522(02)00713-3
13. Mousseau G, Mediouni S, Valente ST. Targeting HIV transcription: the quest for a functional cure. *Curr Top Microbiol Immunol.* (2015) 389:121–45. doi: 10.1007/82_2015_435
14. Rozzi SJ, Avdoshina V, Fields JA, Mocchetti I. Human immunodeficiency virus Tat impairs mitochondrial fission in neurons. *Cell Death Discov.* (2018) 4:8. doi: 10.1038/s41420-017-0013-6
15. Bachani M, Sacktor N, McArthur JC, Nath A, Rumbaugh J. Detection of anti-tat antibodies in CSF of individuals with HIV-associated neurocognitive disorders. *J Neurovirol.* (2013) 19:82–8. doi: 10.1007/s13365-012-0144-8
16. Bellino S, Tripiciano A, Picconi O, Francavilla V, Longo O, Sgadari C, et al. The presence of anti-Tat antibodies in HIV-infected individuals is associated with containment of CD4+ T-cell decay and viral load, and with delay of disease progression: results of a 3-year cohort study. *Retrovirology.* (2014) 11:49. doi: 10.1186/1742-4690-11-49
17. Wodarski R, Bagdas D, Paris JJ, Pheby T, Toma W, Xu R, et al. Reduced intraepidermal nerve fibre density, glial activation, and sensory changes in HIV type-1 Tat-expressing female mice: involvement of Tat during early stages of HIV-associated painful sensory neuropathy. *Pain Rep.* (2018) 3:e654. doi: 10.1097/PR9.0000000000000654
18. Johnson TP, Patel K, Johnson KR, Maric D, Calabresi PA, Hasbun R, et al. Induction of IL-17 and nonclassical T-cell activation by HIV-Tat protein. *Proc Natl Acad Sci USA.* (2013) 110:13588–93. doi: 10.1073/pnas.1308673110
19. Carey AN, Sypek EI, Singh HD, Kaufman MJ, McLaughlin JP. Expression of HIV-Tat protein is associated with learning and memory deficits in the mouse. *Behav Brain Res.* (2012) 229:48–56. doi: 10.1016/j.bbr.2011.12.019
20. Carey AN, Liu X, Mintzopoulos D, Paris JJ, Muschamp JW, McLaughlin JP, et al. Conditional Tat protein expression in the GT-tg bigenic mouse brain induces gray matter density reductions. *Prog Neuropsychopharmacol Biol Psychiatry.* (2013) 43:49–54. doi: 10.1016/j.pnpbp.2012.12.018
21. Fields JA, Serger E, Campos S, Divakaruni AS, Kim C, Smith K, et al. HIV alters neuronal mitochondrial fission/fusion in the brain during HIV-associated neurocognitive disorders. *Neurobiol Dis.* (2015) 86:154–69. doi: 10.1016/j.nbd.2015.11.015
22. Avdoshina V, Fields JA, Castellano P, Dedoni S, Palchik G, Trejo M, et al. The HIV protein gp120 alters mitochondrial dynamics in neurons. *Neurotox Res.* (2016) 29:583–93. doi: 10.1007/s12640-016-9608-6
23. Ngwainmbi J, De DD, Smith TH, El-Hage N, Fitting S, Kang M, et al. Effects of HIV-1 Tat on enteric neuropathogenesis. *J Neurosci.* (2014) 34:14243–51. doi: 10.1523/JNEUROSCI.2283-14.2014
24. Cashman CR, Hoke A. Mechanisms of distal axonal degeneration in peripheral neuropathies. *Neurosci Lett.* (2015) 596:33–50. doi: 10.1016/j.neulet.2015.01.048
25. Bennett GJ, Doyle T, Salvemini D. Mitotoxicity in distal symmetrical sensory peripheral neuropathies. *Nat Rev Neurol.* (2014) 10:326–36. doi: 10.1038/nrneurol.2014.77
26. Hao S, The Molecular and pharmacological mechanisms of HIV-related neuropathic pain. *Curr Neuropharmacol.* (2013) 11:499–512. doi: 10.2174/1570159X11311050005
27. Chandrasekaran K, Anjaneyulu M, Choi J, Kumar P, Salimian M, Ho CY, et al. Role of mitochondria in diabetic peripheral neuropathy: influencing the NAD(+)-dependent SIRT1-PGC-1alpha-TFAM pathway. *Int Rev Neurobiol.* (2019) 145:177–209. doi: 10.1016/bs.irn.2019.04.002
28. Fernyhough P, Roy Chowdhury SK, Schmidt RE. Mitochondrial stress and the pathogenesis of diabetic neuropathy. *Expert Rev Endocrinol Metab.* (2010) 5:39–49. doi: 10.1586/eem.09.55
29. Rumora AE, LoGrasso G, Haidar JA, Dolkowski JJ, Lentz SI, Feldman EL. Chain length of saturated fatty acids regulates mitochondrial

trafficking and function in sensory neurons. *J Lipid Res.* (2019) 60:58–70. doi: 10.1194/jlr.M086843
30. Trecarichi A, Flatters SJL. Mitochondrial dysfunction in the pathogenesis of chemotherapy-induced peripheral neuropathy. *Int Rev Neurobiol.* (2019) 145:83–126. doi: 10.1016/bs.irn.2019.05.001
31. Roda RH, Hoke A. Mitochondrial dysfunction in HIV-induced peripheral neuropathy. Int *Rev Neurobiol.* (2019) 145:67–82. doi: 10.1016/bs.irn.2019.04.001
32. Calcutt NA, Smith DR, Frizzi K, Sabbir MG, Chowdhury SK, Mixcoatl-Zecuatl T, et al. Selective antagonism of muscarinic receptors is neuroprotective in peripheral neuropathy. *J Clin Invest.* (2017) 127:608–22. doi: 10.1172/JCI88321
33. Jolivalt CG, Frizzi KE, Han MM, Mota AJ, Guernsey LS, Kotra LP, et al. Topical delivery of muscarinic receptor antagonists prevents and reverses peripheral neuropathy in female diabetic mice. *J Pharmacol Exp Ther.* (2020) 374:44–51. doi: 10.1124/jpet.120.265447
34. Saleh A, Sabbir MG, Aghanoori MR, Smith DR, Roy Chowdhury SK, Tessler L, et al. Muscarinic Toxin 7 Signals Via Ca(2+)/calmodulin-dependent protein kinase kinase beta to augment mitochondrial function and prevent neurodegeneration. *Mol Neurobiol.* (2020) 57:2521–38. doi: 10.1007/s12035-020-01900-x
35. Krakauer T, Buckley M. Doxycycline is anti-inflammatory and inhibits staphylococcal exotoxin-induced cytokines and chemokines. *Antimicrob Agents Chemother.* (2003) 47:3630–3. doi: 10.1128/AAC.47.11.3630-3633.2003
36. Fields J, Dumaop W, Elueteri S, Campos S, Serger E, Trejo M, et al. HIV-1 Tat alters neuronal autophagy by modulating autophagosome fusion to the lysosome: implications for HIV-associated neurocognitive disorders. *J Neurosci.* (2015) 35:1921–38. doi: 10.1523/JNEUROSCI.3207-14.2015
37. Jolivalt CG, Frizzi KE, Guernsey L, Marquez A, Ochoa J, Rodriguez M, et al. Peripheral neuropathy in mouse models of diabetes. *Curr Protoc Mouse Biol.* (2016) 6:223–55. doi: 10.1002/cpmo.11
38. Chaplan SR, Bach FW, Pogrel JW, Chung JM, Yaksh TL. Quantitative assessment of tactile allodynia in the rat paw. *J Neurosci Methods.* (1994) 53:55–63. doi: 10.1016/0165-0270(94)90144-9
39. Beiswenger KK, Calcutt NA, Mizisin AP. Epidermal nerve fiber quantification in the assessment of diabetic neuropathy. *Acta Histochem.* (2008) 110:351–62. doi: 10.1016/j.acthis.2007.12.004
40. Fletcher CV, Staskus K, Wietgrefe SW, Rothenberger M, Reilly C, Chipman JG, et al. Persistent HIV-1 replication is associated with lower antiretroviral drug concentrations in lymphatic tissues. *Proc Natl Acad Sci USA.* (2014) 111:2307–12. doi: 10.1073/pnas.1318249111
41. Palmer R, Use of complementary therapies to treat patients with HIV/AIDS. *Nurs Stand.* (2008) 22:35–41. doi: 10.7748/ns2008.08.22.50.35.c6641
42. Bagdas D, Paris JJ, Carper M, Wodarski R, Rice ASC, Knapp PE, et al. Conditional expression of HIV-1 tat in the mouse alters the onset and progression of tonic, inflammatory and neuropathic hypersensitivity in a sex-dependent manner. *Eur J Pain.* (2020) 24:1609–23. doi: 10.1002/ejp.1618
43. Fuller GN, Jacobs JM, Guiloff RJ. Thalidomide, peripheral neuropathy and AIDS. *Int J STD AIDS.* (1991) 2:369–70. doi: 10.1177/095646249100200514
44. Leger JM, Bouche P, Bolgert F, Chaunu MP, Rosenheim M, Cathala HP, et al. The spectrum of polyneuropathies in patients infected with HIV. *J Neurol Neurosurg Psychiatry.* (1989) 52:1369–74. doi: 10.1136/jnnp.52.12.1369
45. Ronchi O, Grippo A, Ghidini P, Lolli F, Lorenzo M, Di Pietro M, et al. Electrophysiologic study of HIV-1 + patients without signs of peripheral neuropathy. *J Neurol Sci.* (1992) 113:209–13. doi: 10.1016/0022-510X(92)90248-J
46. Tagliati M, Grinnell J, Godbold J, Simpson DM. Peripheral nerve function in HIV infection: clinical, electrophysiologic, laboratory findings. *Arch Neurol.* (1999) 56:84–9. doi: 10.1001/archneur.56.1.84
47. Kemp HI, Petropoulos IN, Rice ASC, Vollert J, Maier C, Strum D, et al. Use of corneal confocal microscopy to evaluate small nerve fibers in patients with human immunodeficiency virus. *JAMA Ophthalmol.* (2017) 135:795–800. doi: 10.1001/jamaophthalmol.2017.1703
48. Petropoulos IN, Al-Mohammedi A, Chen X, Ferdousi M, Ponirakis G, Kemp H, et al. The utility of corneal nerve fractal dimension analysis in peripheral neuropathies of different etiology. *Transl Vis Sci Technol.* (2020) 9:43. doi: 10.1167/tvst.9.9.43
49. Thangaraj A, Periyasamy P, Liao K, Bendi VS, Callen S, Pendyala G, et al. HIV-1 TAT-mediated microglial activation: role of mitochondrial dysfunction and defective mitophagy. *Autophagy.* (2018) 14:1596–619. doi: 10.1080/15548627.2018.1476810
50. Teodorof-Diedrich C, Spector SA. Human immunodeficiency virus type 1 gp120 and tat induce mitochondrial fragmentation and incomplete mitophagy in human neurons. *J Virol.* (2018) 92:e00993–18. doi: 10.1128/JVI.00993-18
51. Sabbir MG, Calcutt NA, Fernyhough P. Muscarinic acetylcholine type 1 receptor activity constrains neurite outgrowth by inhibiting microtubule polymerization and mitochondrial trafficking in adult sensory neurons. *Front Neurosci.* (2018) 12:402. doi: 10.3389/fnins.2018.00402
52. Santerre M, Bagashev A, Gorecki L, Lysek KZ, Wang Y, Shrestha J, et al. HIV-1 Tat protein promotes neuronal dysregulation by inhibiting E2F transcription factor 3 (E2F3). *J Biol Chem.* (2019) 294:3618–33. doi: 10.1074/jbc.RA118.003744

Conflict of Interest: NIH STTR award NS105177 is held by JF and WinSanTor Inc. NC is a scientific founder of WinSanTor Inc. and has an equity interest on the company while KF is an employee of WinSanTor Inc. The terms of this arrangement have been reviewed, approved and managed by the University of California San Diego in accordance with its conflict of interest policies.

The remaining authors declare that the research was conducted in the absence of any commercial or financial relationships that could be construed as a potential conflict of interest.

frontiers in Neurology

REVIEW
published: 22 June 2021
doi: 10.3389/fneur.2021.593605

Role of Brain Arterial Remodeling in HIV-Associated Cerebrovascular Outcomes

*Antonio Spagnolo-Allende and Jose Gutierrez**

Department of Neurology, Columbia University Irving Medical Center, New York, NY, United States

As the life expectancy of people living with HIV (PLWH) on combination antiretroviral therapy (cART) increases, so does morbidity from cerebrovascular disease and neurocognitive disorders. Brain arterial remodeling stands out as a novel investigational target to understand the role of HIV in cerebrovascular and neurocognitive outcomes. We therefore conducted a review of publications in PubMed, EMBASE, Web of Science and Wiley Online Library, from inception to April 2021. We included search terms such as HIV, cART, brain, neuroimmunity, arterial remodeling, cerebrovascular disease, and neurocognitive disorders. The literature shows that, in the post-cART era, PLWH continue to experience an increased risk of stroke and neurocognitive disorders (albeit milder forms) compared to uninfected populations. PLWH who are immunosuppressed have a higher proportion of hemorrhagic strokes and strokes caused by opportunistic infection and HIV vasculopathy, while PLWH on long-term cART have higher rates of ischemic strokes, compared to HIV-seronegative controls. Brain large artery atherosclerosis in PLWH is associated with lower CD4 nadir and higher CD4 count during the stroke event. HIV vasculopathy, a form of non-atherosclerotic outward remodeling, on the other hand, is associated with protracted immunosuppression. HIV vasculopathy was also linked to a thinner media layer and increased adventitial macrophages, suggestive of non-atherosclerotic degeneration of the brain arterial wall in the setting of chronic central nervous system inflammation. Cerebrovascular architecture seems to be differentially affected by HIV infection in successfully treated versus immunosuppressed PLWH. Brain large artery atherosclerosis is prevalent even with long-term immune reconstitution post-cART. HIV-associated changes in brain arterial walls may also relate to higher rates of HIV-associated neurocognitive disorders, although milder forms are more prevalent in the post-cART era. The underlying mechanisms of HIV-associated pathological arterial remodeling remain poorly understood, but a role has been proposed for chronic HIV-associated inflammation with increased burden on the vasculature. Neuroimaging may come to play a role in assessing brain arterial remodeling and stratifying cerebrovascular risk, but the data remains inconclusive. An improved understanding of the different phenotypes of brain arterial remodeling associated with HIV may reveal opportunities to reduce rates of cerebrovascular disease in the aging population of PLWH on cART.

Keywords: HIV, brain, arterial remodeling, cerebrovascular disease, HIV-associated neurocognitive impairment

OPEN ACCESS

Edited by:
Kelly Stauch,
University of Nebraska Medical Center, United States

Reviewed by:
Ronald J. Ellis,
University of California, San Diego, United States
Allison M. Andrews,
Temple University, United States

****Correspondence:***
Jose Gutierrez
jg3233@cumc.columbia.edu

Specialty section:
This article was submitted to Neuroinfectious Diseases, a section of the journal Frontiers in Neurology

Received: *11 August 2020*
Accepted: *07 May 2021*
Published: *22 June 2021*

Citation:
Spagnolo-Allende A and Gutierrez J (2021) Role of Brain Arterial Remodeling in HIV-Associated Cerebrovascular Outcomes. Front. Neurol. 12:593605. doi: 10.3389/fneur.2021.593605

INTRODUCTION

Despite the effectiveness of modern combination antiretroviral therapy (cART), HIV infection continues to be frequently accompanied by cerebrovascular disease and cognitive decline (1–3). Arterial remodeling is emerging as a possible link between HIV infection and cerebrovascular disease and, possibly, cognitive disorders (4–6). However, our understanding of the pathogenic role of HIV in arterial remodeling, especially among the increasing population of people living with HIV (PLWH) in long-term cART, remains limited. In this review, we will discuss potential mechanisms underlying HIV-associated arterial remodeling. We will also summarize our current understanding of the potential role that HIV-associated arterial remodeling plays in cerebrovascular disease and cognitive disorders among PLWH, especially among those aging with HIV and in cART. To that end, we conducted a review of publications in PubMed, EMBASE, Web of Science, and Wiley Online Library, from inception to April 2021. We included search terms such as HIV, cART, brain, neuroimmunity, arterial remodeling, cerebrovascular disease, stroke, and neurocognitive disorders.

HIV AND CEREBROVASCULAR DISEASE IN THE cART ERA

The life expectancy of PLWH is now generally approaching that of the general HIV-seronegative population, thanks to the advent of cART in the mid-1990s (7–9). Although fewer PLWH are dying of AIDS-related diseases, the prevalence of comorbidities in PLWH that are not caused by AIDS, such as cardiovascular disease, remains high compared with HIV-seronegative controls. Cardiovascular disease is the second leading, non-AIDS cause of death among PLWH in the United States, and third in Europe (10). This includes cerebrovascular disease, which remains prevalent among PLWH even after the widespread adoption of cART (11–13). For instance, while the seminal Strategic Timing of Antiretroviral Therapy (START) study demonstrated a 40% reduction in AIDS-related diseases with early cART administration (14), early cART and lower AIDS rates did not preclude increased cerebrovascular risk in PLWH (15).

Studies conducted in high-income countries have established that PLWH in the post-cART era have a 1 to 5% population burden of stroke, while 4 to 34% show ischemic brain lesions on autopsy (16–19). In the United States (US), the total number of primary stroke diagnoses made in PLWH rose by 67% between 1997 and 2006, according to a population study of hospital stroke diagnoses (13). The timing of this increase, quite notably, coincided with the propagating adoption of cART and the simultaneous decrease, by 7%, of stroke admissions in the general population. The authors remarked that the case increase was mostly caused by a rise in ischemic rather than hemorrhagic stroke hospitalizations among PLWH. They also reported that the proportion of PLWH hospitalized for ischemic stroke had more than doubled in the studied period. In a 2019 analysis of a large US healthcare claims database (20), stroke rates in PLWH were shown to be nearly triple that of HIV-seronegative controls, adjusting for sex and age. In 2015, men living with HIV enrolled in the US-based Veterans Aging Cohort Study were still shown to have an increased risk of ischemic stroke compared to HIV-seronegative controls (21). Hemorrhagic stroke, on the other hand, was more frequently seen in the immunosuppressed than those on stable cART (22, 23). In Europe, a Danish population-based cohort study showed the incidence of cerebrovascular events in PLWH was 1.6 times that of HIV-seronegative controls, adjusting for traditional vascular risk factors (24). This rate, it should be noted, may indeed be higher. Since both HIV and cART are independently associated with traditional cardiovascular risk factors, adjusting for them may have negatively biased those results (25–28). Stroke burden among PLWH in low-to-middle-income countries is less well-defined, but a higher burden of HIV and AIDS, along with increasing prevalence of traditional risk factors, makes these populations even more vulnerable to cardiovascular events (29, 30). In Malawi, for instance, the second most common cause of stroke in 2017 was HIV (29) and in 2010, a reference hospital in Tanzania reported that 20% of stroke cases co-occurred with HIV infection (31).

The post-cART rise in HIV-associated stroke events, some researchers originally suspected, could be caused by the overall increase in HIV infections, possible side effects of new cART drugs, improved survival on cART, or even just better recognition of stroke symptoms among PLWH (2). The exact causes, however, remain difficult to pin down even today. Studies trying to determine stroke rates in HIV-positive populations often rely on incomplete data regarding cardiovascular risk factors and on standardized disease codes that may not appropriately capture cerebrovascular events among PLWH (12). Nonetheless, the literature strongly supports the existence of cerebrovascular risk in HIV infection beyond what would be explained by traditional risk factors. Compared to HIV-seronegative controls, PLWH with cerebrovascular disease may be younger and less likely to have the rates of high blood pressure and elevated cholesterol typically seen in stroke patients (11, 32, 33). Surveys of PLWH have shown a premature occurrence of stroke events compared to their HIV-seronegative counterparts, especially in low-to-middle-income countries (34).

Interestingly, a cohort of elite controllers (PLWH who maintain undetectable viral load without cART) still showed increased coronary atherosclerosis and biomarkers of immune activation compared to HIV-seronegative controls (35). This points to reasons other than high viremia and cART side effects to explain HIV-associated atherosclerosis. The SMART study also showed that interrupting cART in immunocompetent PLWH led to increase in cardiovascular events, compared to those whose cART continued after immune reconstitution, providing further support for the role of cART in prevention, rather than promotion, of cardiovascular disease in PLWH (36). A separate cohort of elite controllers showed higher median carotid intima-media thickness than seronegative controls, adjusting for traditional cardiovascular risk factors (37). Moreover, autopsy studies have found altered vascular caliber in the brain of PLWH who experienced long-term viral suppression before death (1, 5, 38–40).

A multicenter cohort study in the US also showed that the Framingham Stroke Risk Score underestimated long-term risk of stroke among men living with HIV (41). In fact, standard cardiovascular risk prediction functions that were developed for use in the general population tend to systematically underestimate risk in PLWH (26). This exposes the limitations in our current understanding of the pathophysiology of cerebrovascular disease among PLWH, which may differ from that of people who are HIV-seronegative. Even in the absence of AIDS, the inflammatory effects of HIV may be contributing to vascular disease in the brain, with varying effects depending on immunological and cART status (42). Inflammation-mediated vascular remodeling may therefore be playing a key role in HIV-associated cerebrovascular disease, beyond the isolated effects of chronically high viremia, which is much less commonly seen post-cART. Furthermore, the effects of cerebrovascular changes in HIV infection may not be limited to stroke: they may also have a role to play in the HIV-associated neurocognitive disorders, still prevalent in the post-cART era (43–46).

HIV-ASSOCIATED ENDOTHELIAL DYSFUNCTION

Arterial remodeling is the process in which arteries undergo structural and functional changes as a response to biological stimuli. A response that results in increase in arterial size is defined as outward remodeling (e.g., dolichoectasia, aneurysm), whereas a decrease in size or caliber is defined as inward remodeling (e.g., atherosclerosis) (47). Arterial remodeling can also be described as hypertrophic (thickening of the vascular wall), eutrophic (constant wall thickness) or hypotrophic (thinning of the wall) (48). When the endothelium is functionally intact, it senses stimuli such as blood flow and shear stress to modulate arterial remodeling (49, 50). A dysfunctional endothelium could alter the production or passage of vasoconstricting and vasodilating signals, thereby altering the natural course of arterial remodeling. Studies have shown that in PLWH, even after long-term cART, HIV-associated endothelial dysfunction can be present and flow-mediated dilation of arteries impaired (51–53). Endothelial dysfunction leads to abnormal clotting and increased nitric oxide production, altering vessel tone, permeability and chemokine expression. This leads to leukocyte transendothelial migration (2, 36, 54–56). The ultimate consequence of these changes is wall remodeling, plaque formation and/or increased presence of inflammatory cells in the vessel wall. As a consequence of HIV-induced arterial remodeling, both thrombus formation (cause of ischemic strokes) and possibly rupture (cause of hemorrhagic strokes) may be precipitated (2, 57).

While HIV-associated endothelial dysfunction (and its compromise of brain vasculature) is becoming a clearer independent entity in the literature, the mechanisms through which it may lead to arterial remodeling and adverse cerebrovascular outcomes remains unclear. HIV-1 is not understood to be directly vasculotropic. Endothelial cells do, however, express the receptors needed for viral entry (CD4 and CXCR5) (58). While viral replication does not take place in these cells, endothelial function may nonetheless be altered in ways that could initiate and propagate atherogenesis (2). Circulating HIV-infected immune cells, freely circulating HIV, HIV proteins (released by host cell lysis or actively secreted), and HIV-induced proinflammatory cytokines; all have the potential to activate the endothelium (59, 60). A 2011 biomarker study of 44 PLWH and 29 seronegative controls proposed soluble CD163 (sCD163), a monocyte- and macrophage-specific molecule, as a marker of HIV activity (61). In that study, in PLWH who initiated cART in early HIV infection ($\leq$1 year), sCD163 decreased to levels comparable to HIV-seronegative individuals. In those who initiated cART later (>1 year after infection), however, sCD163 remained chronically elevated. The same study also found plasma soluble CD14 levels elevated in individuals with chronic HIV infection, before and after cART initiation, compared with HIV-seronegative controls. Both molecules, sCD14 and sCD16, have been found to play a role in atherogenesis in PLWH (62).

Continuous, cumulative exposure to noxious viral particles and inflammatory signals over time, which happens even while in cART, may damage the endothelium, increasing its permeability and promoting leucocyte invasion into the vessel wall. A chronic inflammatory state may then set the stage for arterial wall remodeling. Circulating HIV protein Tat, for example, has been found to cause coronary endothelial dysfunction and non-compliance, oxidative stress and disruption of brain microvascular endothelial function, in animal models and in humans (63, 64). In a macaque model, Simian Immunodeficiency Virus protein Nef was associated with a range of pathological vascular phenotypes, from medial hypertrophy to thrombosis (65, 66). In a porcine model, HIV protein Nef was shown to decrease endothelium-dependent vasorelaxation in pulmonary arteries (66). Both Nef and Tat have been associated with increases in endothelial apoptosis, angiogenesis, inflammatory cytokines and cell adhesion molecules (67). During initial infection, before viremia can be suppressed by cART, increased circulation of viral proteins and active inflammation may lead to a more rapid and dramatic remodeling of vascular architecture (68).

Viral protein Gp120, in both soluble and surface-bound forms, has also been shown able to alter function of bystander cells that are not directly infected with HIV, including endothelial cells. It has been associated with endothelial cell apoptosis, adhesion molecule expression, production of inflammatory cytokines, increased expression of matrix metalloproteinases, and increased permeability (69–73). A study found Gp120 to promote endothelial cell senescence in humans; a phenotype that promotes inflammation, vasoconstriction, and thrombus formation (74, 75). The chronic effects of HIV proteins on the endothelium may be intertwined with (and confounded by) the effects of concomitant cART. cART-induced endothelial damage has been shown to play a role in the mechanism of endothelial dysfunction and cerebrovascular risk. However, the deleterious effects of cART are mostly thought to occur through metabolic abnormalities, not direct endothelial damage (2, 55, 76). While some specific ART classes (e.g., protease inhibitors)

and individual drugs (e.g., abacavir) have been associated with increased cerebrovascular risk, current cART regimes are largely believed to reduce the risk overall, not increase it (42, 76). There is also variability in the ability of different antiretrovirals to reach therapeutic concentrations in cerebrospinal fluid (CSF): under suboptimal drug pressure, continuous replication of HIV in the central nervous system (CNS) is possible (77). This is evidenced by CSF viral escape, in which HIV RNA can be detected in CSF when it is undetectable in plasma. CSF viral escape occurs in 4 to 20% of PLWH, has been associated with cART regimes of protease inhibitors and nucleoside reverse transcriptase inhibitors, and with CNS inflammation (78, 79). This exposes the cerebrovascular endothelium to higher concentrations of viral particles and proteins, despite systemic viral suppression. It is possible that HIV-coded proteins interact with traditional risk factors, chronic inflammation, and cART, to ultimately cause endothelial dysfunction. This, in turn, may lead to pathological phenotypes of arterial remodeling and ultimately cerebrovascular disease, as represented in **Figure 1** (67). Such interactions are sure to be complex, however, and much remains to be discovered about them.

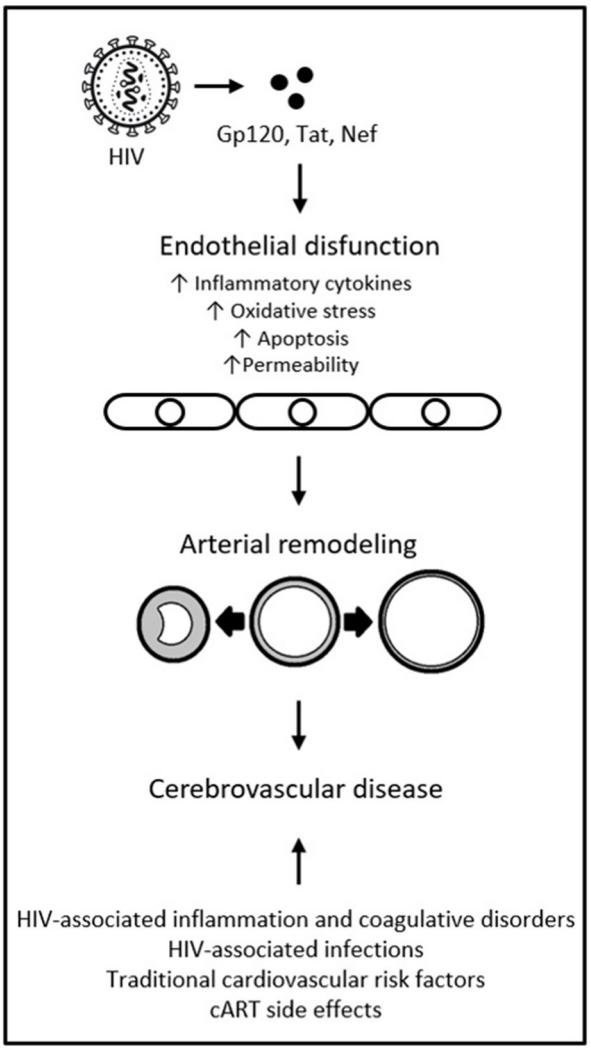

FIGURE 1 | HIV-coded proteins as a cause of endothelial dysfunction and arterial remodeling. Adapted from "HIV proteins and endothelial dysfunction: implications in cardiovascular disease," by A. R. Anand, G. Rachel and D. Parthasarathy, 2018, *Frontiers in cardiovascular medicine*, 5, p. 185 (https://www.frontiersin.org/articles/10.3389/fcvm.2018.00185/full). CC BY.

HIV-ASSOCIATED INWARD ARTERIAL REMODELING

Compared to HIV-seronegative controls, PLWH in long-term cART continue to show increased rates of atherosclerosis, an extreme phenotype of inward remodeling, with associated increase in risk of acute ischemic events (80, 81). The current body of knowledge of HIV-associated atherogenesis has been gained mostly through clinical studies, with very few experimental studies to help explain the mechanisms for this association, although it is well-accepted that HIV infection promotes accelerated atherosclerosis in extra and intracranial arteries (57, 82). A 2015 US-based brain bank study described a direct association between HIV status and inward remodeling of intracranial arteries (57). They observed that, compared with HIV-seronegative controls, PLWH had a predisposition for inward remodeling of brain large arteries, with thicker media, thicker arterial walls, and smaller lumen-to-wall ratio. These associations were found after adjusting for vascular risk factors, with no statistical difference in stenosis or calcification. With a sample of 142 HIV-positive and 142 HIV-seronegative brain donors, half of all brain infarcts among the PLWH in that study were attributed to one of two arterial remodeling extremes: atherosclerosis or dolichoectasia. Atherosclerosis accounted for a quarter of brain infarcts in the study's PLWH sample. Intracranial atherosclerosis was significantly associated with a lower CD4 nadir and a higher antemortem CD4 count. This, the authors noted, was a novel finding, and one which agreed with HIV-associated changes that had been reported in extracranial arteries by other studies (83, 84). It suggested a role for the immune system in the development of atherosclerosis, one in which a bigger difference between CD4 count before and after successful cART results in greater vascular inflammation. Successfully treated HIV infection with immune reconstitution could therefore be associated with higher rates of inward remodeling of intracranial arteries, compared to immunocompromised PLWH (who would present a different remodeling phenotype) and to HIV-seronegative controls. The exact mechanisms linking inward remodeling and ultimately atherosclerosis with HIV, however, remain unexplained.

In a another brain bank study, from 2018 (85), it was observed that intimal lymphocytic inflammation was involved in brain arterial remodeling, possibly contributing to the cerebrovascular pathological findings in that PLWH sample. The authors analyzed large brain arteries from 84 PLWH and 78 HIV-seronegative controls. In brain samples of PLWH with antemortem CD4 count over 200, and of HIV-seronegative

controls, a higher number of CD3 T cells infiltrating the intima was associated with histological markers of hypertrophic inward remodeling. In samples from PLWH with CD4 counts less than 200, however, the presence of CD3 T cells in the intima was associated with hypertrophic outward remodeling instead. The researchers hypothesized that "a sufficient" CD3 T cell count may be needed to generate an inflammatory response that leads to inward remodeling in HIV, with subsequent luminal and blood flow reductions. The authors also reported that adventitial CD3 T cells were decreased among PLWH compared to HIV-seronegative controls. The decrease was more pronounced in samples belonging to immunosuppressed PLWH. The CD3 T cell numbers in the intima, however, did not differ by HIV status, as they did in the adventitia, and adventitial CD3 T cells were not associated with atherosclerosis. The authors of that study could not elucidate the exact role of CD3 T cells in brain arterial remodeling, as that marker comprises a variety of cell subpopulations with different functions. Their results, however, pre-suppose that inflammatory cells in the brain of PLWH may affect distinct arterial layers differently, and immune cell quality and quantity in each layer may be associated with immune status and disease history. It is possible that CD3 T cells are involved in brain inflammatory changes such as HIV-associated vasculitis, arterial dilatation and inflammation limited to the CSF (86, 87). The use of a semi-quantitative measurement of CD3 T cells, and the fact that all HIV-positive brain samples proceeded from the same site, were limitations to this study. Its results nonetheless point to the existence of differential markers of inflammation in, and differential remodeling of, brain arteries in immunocompromised PLWH when compared to immunocompetent PLWH and to HIV-seronegative individuals.

Biomarker studies indicate that there may also be a role for monocyte-macrophage activation in HIV-associated atherosclerosis. A study using a transgenic mouse model (88) showed that, in mice with an $ApoE^{-/-}$ phenotype who also expressed HIV-1, HIV expression was enough to accelerate atherosclerosis, with increased caspase-1 pathway activation in inflammatory monocytes. The same study also analyzed *in vivo* samples from PLWH and postmortem samples from an HIV-positive human tissue bank. The authors documented that *in vivo* plasma IL-18 was higher in PLWH compared with HIV-seronegative controls. Higher IL-18 levels were associated with markers of monocyte-macrophage activation and non-calcified, inflammatory coronary plaques. In the postmortem tissue sample of PLWH, aortic plaques were associated with caspase-1-positive cells and CD 163-positive macrophages. This study demonstrated that exposure to HIV may independently accelerate atherogenesis in humans. It also highlighted the possible role of the caspase-1 pathway and of monocyte-macrophage activation in HIV-associated atherogenesis.

Cerebrovascular disease mechanisms in PLWH may also vary according to CD4 count. In a retrospective study of PLWH (89) it was seen that, among 115 stroke cases, most (22%) were due to large artery atherosclerosis (17%, due to small artery disease; 16%, infectious; 8%, cardioembolic; 21%, cryptogenic; and 16%, other causes). They found that large artery atherosclerosis was significantly associated with longer HIV infection and CD4 nadir less than 200. In the same sample, stroke due to large artery atherosclerosis was associated with higher CD4 count in the year prior to stroke, independent of CD4 nadir. They concluded that large artery atherosclerosis was the most frequent stroke mechanism in PLWH whose nadir CD4 count was less than 200 (which suggests cART start later in infection history) and whose CD4 count near the time of the stroke was higher (which suggests successful cART). These *in vivo* results support those of the brain bank study described above (85), where hypertrophic inward remodeling, of which atherosclerosis constitutes an extreme, was most frequently seen in brain arteries of PLWH with higher antemortem CD4 count.

Detecting HIV-associated brain arterial remodeling in PLWH, *in vivo*, however, remains a challenge. Imaging has a limited diagnostic or prognostic role in HIV-associated arterial remodeling. But this role may be expanded in the future, with the advent of more advanced or specific imaging procedures. Black-blood MRI (BBMRI), for example, is an advanced technique that allows better visualization of the vascular wall thickness by nulling the signal from the vascular lumen. In current practice, it is mostly used to assess visual markers of cardiovascular and cerebrovascular risk from eccentric lipid-rich plaques (90). But in PLWH it could be used to measure the vessel wall thickness (91, 92), as seen in the example presented in **Figure 2**, abstracted from the 2019 study "Subclinical Atherosclerosis Imaging in People Living with HIV" (93). In an imaging study with subjects with low traditional cardiovascular risk, HIV-status was significantly associated with increased vascular thickening, after adjusting for age (92). In another study, PLWH on cART also showed increased carotid artery wall thickness on MR imaging compared to HIV-seronegative controls with similar cardiovascular risk (94). In sum, the full potential of MRI techniques to measure arterial remodeling in PLWH in a way that could be clinically relevant remains undefined, but promising.

HIV-ASSOCIATED OUTWARD ARTERIAL REMODELING

While inward remodeling leads to vessel stenosis and atherosclerosis, outward remodeling is usually accompanied by media thinning and vessel dilation (4, 95). In the same US-based 2015 brain pathology study described above (57), the researchers found that outward remodeling was the "defining arterial phenotype" among PLWH that experienced prolonged immunosuppression prior to death. They correlated dolichoectasia (an extreme outward remodeling phenotype) with media thinning and higher viral load at the time death. Furthermore, higher lumen-to-wall ratio was the only arterial remodeling variable associated with cryptogenic brain infarcts in their PLWH sample. This somewhat confounded their other finding that inward remodeling was linked to HIV, albeit in HIV-positive cases with higher antemortem CD4 counts. The authors posited that immune reconstitution (with increased

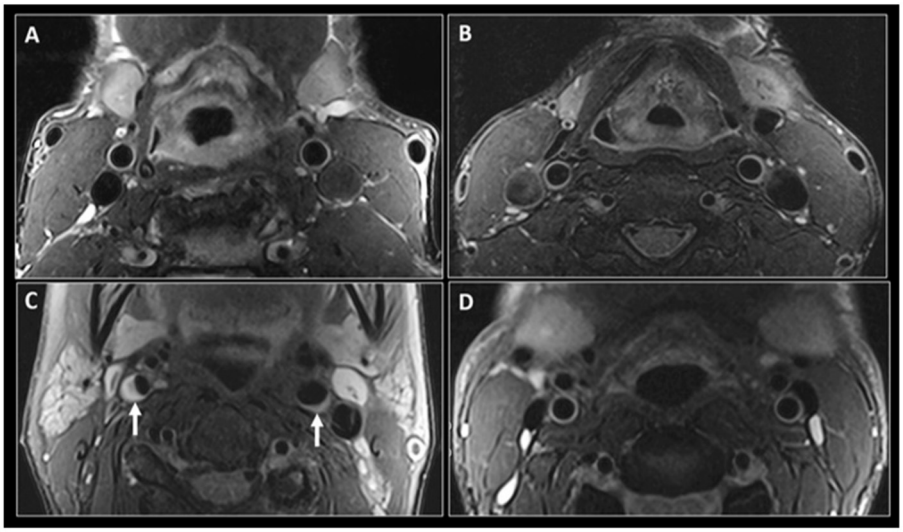

FIGURE 2 | Black-blood MR imaging of the carotid arteries. Adapted from "Subclinical atherosclerosis imaging in people living with HIV," by I. C. Schoepf, R. R. Buechel, H. Kovari, D. A. Hammoud and P. E. Tarr, 2019, *Journal of clinical medicine*, 8(8), p. 1125 (https://www.mdpi.com/2077-0383/8/8/1125). CC BY. Fat saturated T2-weighted black-blood MR images at the level of the common carotid arteries in a 56-year-old HIV-positive man **(A)** and a 47-year-old HIV-negative man **(B)**. Similar imaging technique at the level of the internal carotid arteries in a 56-year-old HIV-positive woman **(C)** shows narrowing of the vascular lumen bilaterally by a plaque (small arrows), more significant on the right side. **(D)** shows similar imaging at the level of internal carotid arteries in a 47-year-old HIV-negative man with no evidence of atherosclerosis.

numbers of CD3 T cells) would generate a different and more robust inflammatory response, leading to a different remodeling phenotype, than what is seen in the immunosuppressed. This hypothesis, however, is yet to been tested.

In the other US-based brain bank study, from 2018 (85), the authors found that intimal lymphocytic inflammation with hypertrophic outward remodeling was associated with adventitial macrophages and increased elastolysis activity. They described similar findings in a separate study of the same cohort (96). This association has also been documented in extracranial arteries, such as in aortic and coronary aneurysmal dilatations (97–99). The authors of the 2018 brain bank study (85) proposed that an interaction between immunosuppression and intimal CD3 T cells may potentiate arterial dilatation, rather than constriction. Adventitial CD3 T cell expression was not associated with intracranial large artery atherosclerosis in their sample. Consequently, they proposed that inflammatory cells "may affect the intima differently than the adventitia of brain arteries." The exact role of adventitial CD3 T cells in arterial inflammation or remodeling is yet to be described, but it is certainly possible that these cells are involved in other inflammation-induced vascular changes. Indeed, separate studies have associated the presence of CD3 T cells with HIV-associated vasculopathy and arterial dilatation (86, 87). These inflammatory cells could contribute to adventitial inflammation in PLWH while having a different role in the intimal inflammatory process that leads to stenosis or atherosclerosis.

Evidence is accumulating in support of an independent role for HIV in the pathogenesis of vasculopathy. In the current literature, HIV-associated vasculopathy conventionally refers to abnormalities of blood vessels that are a direct or indirect consequence of HIV infection, with no alternative etiological explanation (42). This diagnosis is usually reserved for PLWH who present with clinical or radiological features of vasculopathy and in whom other causes have been ruled out (2). In past clinical case series, 13 to 28% of ischemic strokes in PLWH had been attributed to HIV-associated arterial vasculopathy. Most of these studies, however, did not rule out vasculopathy attributable to opportunistic infection (3, 100, 101). Evidence of vasculopathy has also been found in postmortem brain samples of PLWH, even in subjects with long-term successful viral suppression before death (102, 103). Animal models have directly linked HIV infection to vasculopathy, independently from other causes. For example, a study of the murine AIDS model in mice suggested that retroviral infection can cause endothelial dysregulation and vasculopathy. Similar experimental findings have been corroborated in humans (104–106). Outward remodeling with thinning of the arterial media layer has been reported as a possible pre-clinical stage for HIV vasculopathy (38). HIV infection could be initiating vascular injury in the brain, or perhaps contribute to further injury to vasculature already damaged by atherosclerosis, pre-disposing PLWH to stroke. The exact mechanism of arterial wall damage in the context HIV remains poorly understood, especially among subjects on long-term cART. But pathological data suggests that, among people who died with HIV, antemortem low CD4 counts and low CD4 nadir were associated with intracranial arterial outward remodeling involving wall thinning and arterial dilatation (57).

In vivo imaging may also be an important tool in assessing outward remodeling phenotypes in brain arteries associated with HIV infection. A 2019 MRI study (68) using T2-weighted imagining sequences, found that the vascular caliber of the anterior cerebral artery, A1 segment, was higher in PLWH compared to HIV-seronegative controls, matched for sex and race. Meaningfully, higher CD4 T cell count and longer duration of infection were associated with decrease in A1 caliber of PLWH. The findings of this study were in agreement with postmortem observations in brains of PLWH (5, 38, 40). It is therefore possible that the observed MRI changes in lumen caliber would reflect HIV-associated vessel wall thinning and/or loss of compliance with protracted infection. A brain bank study recognized an association between HIV infection and thinning of medial arterial layers, which may be a pre-clinical stage in HIV-related vasculopathy (38). Other studies have established adventitial inflammation in the context of HIV infection is associated with a thinner media, and outward remodeling of the arterial wall that would ultimately lead to dolichoectasia (40, 107). Chronic HIV-induced damage to the inner endothelial layer could affect vascular compliance, which could at least partially explain the arterial luminal changes observed in brain MRI studies of PLWH (59, 68, 108).

CEREBROVASCULAR REMODELING AND HIV-ASSOCIATED NEUROCOGNITIVE DISORDERS IN THE cART ERA

HIV-associated neurocognitive disorders (HAND) refer to a wide range of neuropsychological impairments in the context of HIV infection. While the cellular and physiological mechanisms that lead to HAND remain poorly understood, they likely involve chronic neuroinflammation and have the potential to alter cerebrovascular architecture (109–111). HIV encephalitis and widespread neuronal loss, previously thought to have pivotal roles in the development of HAND, are no longer typically seen in PLWH on long-term, stable cART who present with neurocognitive impairments (112). While a recent study of histopathological phenotypes associated with HAND showed that pre-synaptic degeneration may precede somatodendritic degeneration and lead to neurocognitive impairment (113), the study cohort was composed of individuals with more advanced illness and high frequency of HIV encephalitis, which may not be reflective of the growing PLWH population who remain in long-term cART (114). The introduction of cART, in fact, reduced the overall frequency of HIV encephalitis from 54% to less than 15% (115, 116). However, markers of HIV-induced inflammation in the CNS are still present after viral replication has been suppressed by cART (117, 118). The post-cART pathology of HAND seems to have shifted to subtler, chronic neurodegeneration, affecting more cortical regions (119).

The effects of aging, chronic HIV infection and chronic cART may interact and cause neurodegeneration. These mechanisms include neuroinflammation, oxidative stress, DNA damage, cell senescence and defective proteostasis (proteasome, proteolysis and autophagy disfunctions) (120). These common alterations may be synergistic and lead to abnormal accumulation of proteins typically involved in neuronal damage and dementia (Amyloid β, Tau, α-synuclein). Dementia cases associated with HIV in the post-cART era usually also show diffuse astrogliosis, microglial nodules, white matter alterations and vascular changes with peri-vascular lymphocytic infiltration (121). Due to the several common and overlapping molecular markers involved, trying to differentiate HAND from the mechanisms of normal aging, Alzheimer's disease, vascular and other forms of dementia continues to be a source of controversy and debate (122). Vascular disease of the brain, however, is almost universally thought to play a role in post-cART HAND (6, 114, 123, 124).

Neuroinflammation associated with HIV infection has the potential to compromise normal cerebrovascular function. While HIV-induced intracranial large artery atherosclerosis would restrict blood flow, the infection may also cause cerebral small vessel disease (CSVD), further affecting cerebral perfusion (15, 125–130). While CSVD in the general population is largely associated with hypertension, diabetes, and aging (131), PLWH on cART seem to be at even higher risk, unexplained by those exposures alone. A French study, for instance, revealed that PLWH with well-controlled infection had twice the prevalence of silent CSVD as uninfected controls (129). The authors put forward HIV infection as an independent risk factor for CSVD. An American study, on the other hand, suggested that HIV infection and CSVD are independent, additive processes that together cause brain atrophy and cognitive impairment (132). The direct effects of HIV on cerebral vessels are also difficult to separate from the potential toxic effects of long-term cART. A US-based cross-sectional study, for instance, showed an association between CSVD and cART regimes that include protease inhibitors (133), after adjusting for diabetes. Mild CSVD itself, the same study showed, was associated with HAND.

Irrespective of the specific mechanisms, post-cART HIV infection increasingly seems associated with cerebrovascular dysregulation and, ultimately, vascular remodeling leading to neurocognitive dysfunction, especially in aging PLWH (116, 134). Small and large intracranial vessel remodeling, particularly atherosclerosis for those on long-term cART, could be contributing factors to cognitive impairment in older PLWH (124). In a 2014 US-based cohort study, PLWH who were over 50 years of age were twice as likely as younger PLWH to have HAND, even after adjusting for dementia risk factors (135, 136). A similar risk disparity has been observed in South African aging cohorts (137, 138). HAND risk increases seen with age, however, remain confounded by the increasing prevalence of cerebrovascular risk factors in aging PLWH (139, 140). A 2010 US cohort study of 1,555 adult PLWH, for instance, found that older age, elevated blood pressure, BMI, high cholesterol, and a prior diagnosis of AIDS were all associated with worse neuropsychological performance (141).

A 2016 American cohort study of 197 PLWH showed that only 10% had a measurable improvement of HAND after cART introduction, with 77% remaining more or less neurocognitively stable and 13% deteriorating to more severe HAND while on cART (142). The START trial, on the other hand, failed to confirm major improvement of HAND brought on by early cART (14,

140). HAND, for the most part, does not seem to progress in most PLWH on stable cART after immune reconstitution. Still, for patients diagnosed with HAND who initiate cART, HAND rarely resolves completely. Some alterations in brain function induced by HIV infection may therefore be structural, longer lasting and/or unpreventable even by stable cART. In a US-based 2019 brain bank study that included 94 PLWH, researchers performed antemortem measures of motor functioning, processing speed, working memory, verbal fluency, and executive functioning (143). They reported an association between brain arterial wall thickening and poorer global cognitive score, processing speed and verbal fluency. Associations were independent of traditional vascular risk factors, CD4 count, viral load, or cART use. Intracranial arterial wall thickening was also associated with both incident and, more strongly, with worsening HAND at the time of death. The effects that classic vascular risk factors have on cognitive performance appear greater in studies of cohorts with higher CD4 counts (143, 144). The association between classical vascular risk factors and cognitive performance may therefore be outweighed by the effects of persistent immunosuppression.

Even accounting for limitations in sample size and biases inherent to autopsy series, the 2019 brain bank study mentioned above (143) signals a potential role for arterial remodeling in HIV-associated neurocognitive decline. This role was studied *in vivo* in a 2018 US-based cross-sectional analysis of 72 PLWH and 36 HIV-seronegative controls, all over 50 years of age (111). The authors found an association between markers of vascular remodeling (specifically, lower Tie-2, and higher VEGF) and worse neurocognitive function only in PLWH, suggesting that HIV infection moderates this association. Variables other than HIV itself linking arterial remodeling with HAND, however, cannot been ruled out. Brain arterial wall thickening is, after all, naturally associated with aging, Alzheimer's disease and other forms of dementia (145). Moreover, while atherosclerosis is a frequent phenotype of arterial inward remodeling, it is not the only one (146, 147). Compensatory intimal thickening with no atheroma may result from the normal aging process, resulting in wall thickening and arterial stiffness (145, 148). Diabetes, also associated with HAND, could likewise confound the association between arterial remodeling and cognitive scores (149, 150). In the same 2019 brain bank study from above (143), possible mechanisms linking viral suppression, lumen preservation, and cognition remained undetermined. That viral suppression and cART use were both associated with larger luminal diameters and better cognition was, nonetheless, highly suggestive (143, 151). It is also possible that HIV-associated inflammation may act as an effect modifier in the association between intracranial arterial wall thickness and cognition, as opposed to having an individual causal effect. Further studies measuring systemic inflammation and cerebrovascular pathology would be necessary to test if this is the case. Still, there is accumulating evidence of a possible role for HIV-induced vascular remodeling in the development and progression of HAND post-cART initiation, a role that should be further explored.

While more severe forms of HAND have become rare post-cART (43), there is evidence for widespread vascular cognitive impairment (VCI) in aging PLWH, albeit in milder and subclinical forms (129, 143, 152, 153). VCI refers to all types of cognitive disorder associated with cerebrovascular disease, regardless of specific mechanisms (154). It comprises cognitive deficits ranging from mild cognitive impairment to dementia. While the neuropsychological and neuroimaging phenotypes of VCI and HAND are largely overlapping and may even represent aspects of the same neuropathological entity for PLWH, the literature mostly describes them independently (43). In PLWH on long-term cART, mild forms of both HAND and VCI are associated with persistent subclinical or clinical cerebrovascular disease, with HIV acting as a vascular risk factor (34, 155, 156). Further studies have posited that HIV-induced chronic immune activation, immune senescence, viral reservoir activity, microbial translocation, and reactivation of its commonly associated pathogens (such as CMV and herpes simplex) are also involved in mild HAND and VCI (112, 114, 157, 158).

Although the exact causes remain unknown (and are sure to be multifactorial and complex), both VCI and HAND are thought to be, at least partially, generated and/or worsened by HIV-induced cerebrovascular disease (110, 159). HIV-induced intracranial arterial remodeling may therefore play a pathogenic role in both entities. Some researchers have put forward a new hypothesis proposing that the neurovasculature may actually be a primary target for chronic HIV injury (112, 160). Endothelial cell surfaces, they propose (and we have discussed), are chronically perturbed in PLWH who are successfully treated and virally suppressed. This, they posit, leads to chronic alteration of the neurovascular unit, altering the brain's arteries, microvasculature and, subsequently, blood perfusion. Results from the National NeuroAIDS Tissue Consortium brain gene array study may back up this theory (160). The authors of that study found that HAND (without HIV encephalopathy) is characterized by abnormal regulation of gene transcription in brain endothelial cells (161). This chronic alteration of neurovascular biology may be a prevalent process in virally suppressed PLWH. Neurovascular unit damage-associated forms of VCI and HAND could indeed be the more prevalent forms in the post-cART. This would help explain the milder clinical profile of cognitive impairment in cohorts of PLWH on long-term, successful cART, in whom acute inflammatory infiltrates of the brain are rarely seen, while low-grade chronic immune activation is much more prevalent (6, 123, 162–165). In the patients who remain immunocompromised, however, acute inflammation would continue to be the more prevalent mechanism of injury to brain vasculature (112, 160).

CONSIDERATIONS REGARDING SARS-COV-2 AND HIV COINFECTION

The coronavirus disease 2019 (COVID-19) pandemic is caused by the severe acute respiratory syndrome coronavirus 2 (SARS-CoV-2). This virus binds to the angiotensin-converting enzyme 2 (ACE2) to infect cells (166, 167). This enzyme is expressed in the lungs, small intestine and brain (168). The expression of ACE2 in cortical neurons and glia makes them susceptible to SARS-CoV-2, which may explain the high incidence of anosmia

and other neurological deficits seen in COVID-19 (169). In the brain, however, ACE2 is also expressed in endothelial and smooth muscle cells. ACE2 normally counteracts the effects of ACE1 and angiotensin II. Overexpression of ACE2 in neuronal cells and endothelial progenitor cells, in fact, has a protective effect from ischemic stroke (170, 171). As SARS-CoV-2 invades cells it depletes ACE2 through receptor endocytosis, leaving ACE1 unopposed. Resulting angiotensin II excess impairs endothelial function, leading to a proinflammatory state with organ-damaging effects seen in the lungs, heart and brain (172). SARS-CoV-2 proliferation in vascular endothelial cells also leads to endothelialitis (173). SARS-CoV-2 antigens can activate the complement system, macrophages, and neutrophils, further damaging endothelial cells. This injury may compound the loss ACE2's vasoprotective effects (174). This is particularly concerning given that even limited injury to the endothelium of cerebral vessels can initiate *in situ* thrombosis and lead to strokes (175, 176).

Recent retrospective studies of PLWH hospitalized due to COVID-19 conducted in the US, however, found no significant differences in clinical outcomes of PLWH compared to HIV-seronegative controls (177, 178). Cohort studies conducted in Spain similarly reported a lack of significant differences in COVID-19 hospitalization outcomes for the two groups (179, 180). One of those studies further noted that PLWH receiving cART regimes that included tenofovir disoproxil fumarate with emtricitabine had indeed lower risk of COVID-19 infections and hospitalizations, compared to PLWH receiving other cART regimes (180). But these results remain in need of confirmation in other populations. While possible interactions of SARS-CoV-2 and HIV are actively being researched, the possible long-term effects remain unknown, especially as it relates to PLWH on long-term cART. It is possible that SARS-CoV-2 may compound endothelial damage brought on by chronic HIV infection in the brain vasculature, with certain cART regimes offering more protection from these effects. Nevertheless, the research on SARS-CoV-2 infection in PLWH is still too nascent to offer any conclusions.

DISCUSSION

The vast majority of PLWH reside in low-to-middle-income countries, where overall stroke incidence has more than doubled in the last 40 years (181, 182). It is thus expected that global stroke incidence in PLWH will continue to increase (183). In high-income countries, on the other hand, the absolute numbers of stroke in PLWH on cART are comparatively low (42). Nonetheless, the relative rise in HIV-associated ischemic stroke post-cART introduction is still a public health concern. Therefore, developing the capacity to prevent cerebrovascular morbidity and mortality in an aging PLWH population constitutes an increasingly urgent public health priority, for both low-to-middle- and high-income countries.

The literature reveals that PLWH on cART still suffer higher rates of cerebrovascular disease than the general population (10–13). Stroke in PLWH occurs pre-maturely and is less associated with traditional risks factors compared to HIV-seronegative controls (11, 12, 32, 33). Ischemic stroke is the type most often associated with HIV in the post-cART era, with hemorrhagic stroke remaining the more frequent form in immunocompromised PLWH (3, 22, 23, 184). But significant gaps in the literature remain regarding the specific pathophysiology of cerebrovascular disease in PLWH. These gaps may preclude health providers and researchers from more accurately assessing and preventing cerebrovascular risk in PLWH, compared to HIV-seronegative populations. Still, considering the available data, emphasizing cardiovascular risk reduction interventions to optimize cardiovascular health is essential for maintaining brain health in an aging PLWH population. Such interventions may mitigate the effects of HIV-associated pathological cerebrovascular remodeling, when combined with appropriate and sustained cART (132).

Increasing evidence shows that vascular endothelium is affected by circulating HIV products in the context of long-term cART, even with low or undetectable viremia and no discernible direct interaction between endothelial cells and the virus (51–53). HIV-induced endothelial dysfunction is a likely precursor to arterial remodeling. The endothelium may initiate and propagate atherogenesis while also inducing thrombus formation, predisposing PLWH to ischemic stroke (2, 57). In order to minimize the effects of HIV in brain vascular endothelium, cART regimes that are more likely to reach and maintain therapeutic concentrations in the CNS should be favored. Still, the complex interactions between HIV-infection, circulating HIV particles, cART, and traditional cerebrovascular risk factors leading to arterial remodeling remain poorly understood. Additionally, endothelial damage induced by of SARS-CoV-2 and HIV coinfection, in the context of the COVID-19 pandemic, is a possibility. This and other possible long-term effects of the COVID-19 pandemic on PLWH on cART, however, remain to be seen.

HIV infection is associated with inward remodeling in general, and atherosclerosis in particular, of intracranial arteries (57, 82). Because lower CD4 nadir is associated with intracranial large artery atherosclerosis, even after prolonged immune reconstitution brought on by cART (89), proper population screening leading to early HIV diagnosis is essential. Early diagnosis would allow for the start and maintenance of cART before an accentuated drop in CD4 occurs, which could potentially help prevent brain atherosclerosis associated with a lower CD4 nadir.

Arterial remodeling may also play a role in HAND, especially in the milder forms which patients on stable cART more often express (116, 134). Both small and large vessel atherosclerosis have been linked to cognitive impairment in older PLWH (124). Long-term cART and viral suppression, on the other hand, were associated with larger intracranial arterial vessel diameters and better cognition (143, 151). The current literature shows that treated HIV infection is associated with premature aging, which affects the brain (128). However, the extent of the overlap between HIV-induced changes in the brain of PLWH, non-HIV types of dementia, and normal aging, remains a matter of debate. While the exact

mechanisms through which PLWH on cART develop VCI and HAND are unknown, they are at least partially originated or worsened by intracranial cerebrovascular remodeling (110, 159). Interventions aimed at preventing pathological brain vascular remodeling may, therefore, have some positive effects on the overlapping forms of HIV-associated cognitive decline post-cART. Such interventions and their effects are also targets for future research.

Neuroimaging may have a role to play in the future of cerebrovascular risk assessment and prevention in HIV infection. MRI techniques have been able to detect the arterial wall thickening and atherosclerosis associated with treated HIV infection (91, 92). MRI also showed some promise in measuring HIV-associated vasculopathy *in vivo*. A recent imaging study, for instance, showed that anterior cerebral artery caliber was higher in PLWH compared to controls, but higher CD4 T cell count and longer-treated HIV infection were associated with decreases in that same caliber (68). MR imaging may therefore be used in the future to assist in elucidating the natural history of arterial remodeling in successfully treated HIV infection, but the current literature on this subject remains limited and inconclusive. The clinical and screening applications of imaging these for the benefit of PLWH cerebrovascular health remains to be tested.

No pharmacological interventions were found in the literature that would significantly reverse HIV-associated pathological brain arterial remodeling. For the general population, statin therapy has shown some effect on improving pathological remodeling phenotypes and atheroma composition, leading to modest improvement of microvascular function in coronary artery disease (185). Statins have also shown some protective effects against stroke and other embolic events in patients with aortic atherosclerotic plaques (186). Therapeutics that would reverse pathological arterial remodeling in the brain of PLWH, however, have not been studied. Therefore, it is recommendable that effective HIV long-term care continues to be accompanied by standard cardiovascular risk prevention, which has the potential to impede the progression of pathological vessel remodeling. More research leading to an improved understanding of brain arterial remodeling phenotypes associated with HIV may reveal further therapeutic targets. These targets would present opportunities to reduce the burden of cerebrovascular disease and cognitive impairment in the aging population of PLWH on cART.

AUTHOR CONTRIBUTIONS

AS-A reviewed the literature and co-wrote the manuscript. JG co-wrote the manuscript.

FUNDING

Research reported in this publication was supported by the National Institute on Aging (NIA) of the National Institutes of Health (NIH), under award numbers R01AG066162-01 and R01AG057709-02.

REFERENCES

1. Deeks SG. Immune dysfunction, inflammation, and accelerated aging in patients on antiretroviral therapy. *Top HIV Med.* (2009) 17: 118–23.
2. Benjamin LA, Bryer A, Emsley HC, Khoo S, Solomon T, Connor MD. HIV infection and stroke: current perspectives and future directions. *Lancet Neurol.* (2012) 11:878–90. doi: 10.1016/S1474-4422(12)70205-3
3. Tipping B, de Villiers L, Wainwright H, Candy S, Bryer A. Stroke in patients with human immunodeficiency virus infection. *J Neurol Neurosurg Psychiatry.* (2007) 78:1320–4. doi: 10.1136/jnnp.2007.116103
4. Qiao Y, Anwar Z, Intrapiromkul J, Liu L, Zeiler SR, Leigh R, et al. Patterns and implications of intracranial arterial remodeling in stroke patients. *Stroke.* (2016) 47:434–40. doi: 10.1161/STROKEAHA.115.009955
5. Gutierrez J, Elkind MS, Petito C, Chung DY, Dwork AJ, Marshall RS. The contribution of HIV infection to intracranial arterial remodeling: a pilot study. *Neuropathology.* (2013) 33:256–63. doi: 10.1111/j.1440-1789.2012.01358.x
6. Brew BJ. Has HIV-associated neurocognitive disorders now transformed into vascular cognitive impairment? *AIDS.* (2016) 30:2379–80. doi: 10.1097/QAD.0000000000001225
7. Sabin CA. Do people with HIV infection have a normal life expectancy in the era of combination antiretroviral therapy? *BMC Med.* (2013) 11:251. doi: 10.1186/1741-7015-11-251
8. Teeraananchai S, Kerr SJ, Amin J, Ruxrungtham K, Law MG. Life expectancy of HIV-positive people after starting combination antiretroviral therapy: a meta-analysis. *HIV Med.* (2017) 18:256–66. doi: 10.1111/hiv.12421
9. Sabin C. Review of life expectancy in people with HIV in settings with optimal ART access: what we know and what we don't. *J Int AIDS Soc.* (2012) 15:18076. doi: 10.7448/IAS.15.6.18076
10. Smith CJ, Ryom L, Weber R, Morlat P, Pradier C, Reiss P, et al. Trends in underlying causes of death in people with HIV from 1999 to 2011 (D:A:D): a multicohort collaboration. *Lancet.* (2014) 384:241–8. doi: 10.1016/S0140-6736(14)60604-8
11. Quiros-Roldan E, Raffetti E, Foca E, Brianese N, Ferraresi A, Paraninfo G, et al. Incidence of cardiovascular events in HIV-positive patients compared to general population over the last decade: a population-based study from 2000 to 2012. *AIDS Care.* (2016) 28:1551–8. doi: 10.1080/09540121.2016.1198750
12. Chow FC. HIV infection, vascular disease, and stroke. *Semin Neurol.* (2014) 34:35–46. doi: 10.1055/s-0034-1372341
13. Ovbiagele B, Nath A. Increasing incidence of ischemic stroke in patients with HIV infection. *Neurology.* (2011) 76:444–50. doi: 10.1212/WNL.0b013e31820a0cfc
14. INSIGHT START Study Group, Lundgren JD, Babiker AG, Gordin F, Emery S, Grund B, et al. Initiation of antiretroviral therapy in early asymptomatic HIV infection. *N Engl J Med.* (2015) 373:795–807. doi: 10.1056/NEJMoa1506816
15. Kearns A, Gordon J, Burdo TH, Qin X. HIV-1–associated atherosclerosis: unraveling the missing link. *J Am Colle Cardiol.* (2017) 69:3084–98. doi: 10.1016/j.jacc.2017.05.012
16. Kieburtz KD, Eskin TA, Ketonen L, Tuite MJ. Opportunistic cerebral vasculopathy and stroke in patients with the acquired immunodeficiency syndrome. *Arch Neurol.* (1993) 50:430–2. doi: 10.1001/archneur.1993.00540040082019
17. Berger JR, Harris JO, Gregorios J, Norenberg M. Cerebrovascular disease in AIDS: a case-control study. *AIDS.* (1990) 4:239–44. doi: 10.1097/00002030-199003000-00010
18. Connor MD, Lammie GA, Bell JE, Warlow CP, Simmonds P, Brettle RD. Cerebral infarction in adult AIDS patients: observations from the Edinburgh HIV autopsy cohort. *Stroke.* (2000) 31:2117–26. doi: 10.1161/01.STR.31.9.2117

19. Pinto AN. AIDS/HIV infection and cerebrovascular disease. In: *Seminars in Cerebrovascular Diseases and Stroke.* Vol. 5. WB Saunders (2005). p. 40–6. doi: 10.1053/j.scds.2005.04.015
20. Alonso A, Barnes AE, Guest JL, Shah A, Shao IY, Marconi V. HIV infection and incidence of cardiovascular diseases: an analysis of a large healthcare database. *J Am Heart Assoc.* (2019) 8:e012241. doi: 10.1161/JAHA.119.012241
21. Sico JJ, Chang C-CH, So-Armah K, Justice AC, Hylek E, Skanderson M, et al. HIV status and the risk of ischemic stroke among men. *Neurology.* (2015) 84:1933–40. doi: 10.1212/WNL.0000000000001560
22. Durand M, Sheehy O, Baril JG, LeLorier J, Tremblay CL. Risk of spontaneous intracranial hemorrhage in HIV-infected individuals: a population-based cohort study. *J Stroke Cerebrovasc Dis.* (2013) 22:e34–41. doi: 10.1016/j.jstrokecerebrovasdis.2012.03.014
23. Chow FC, He W, Bacchetti P, Regan S, Feske SK, Meigs JB, et al. Elevated rates of intracerebral hemorrhage in individuals from a US clinical care HIV cohort. *Neurology.* (2014) 83:1705–11. doi: 10.1212/WNL.0000000000000958
24. Rasmussen LD, Engsig FN, Christensen H, Gerstoft J, Kronborg G, Obel NJA. Risk of cerebrovascular events in persons with and without HIV: a Danish nationwide population-based cohort study. *AIDS.* (2011) 25:1637–46. doi: 10.1097/QAD.0b013e3283493fb0
25. Fedele F, Bruno N, Mancone M. Cardiovascular risk factors and HIV disease. *AIDS Rev.* (2011) 13:119–29.
26. Triant VA, Perez J, Regan S, Massaro JM, Meigs JB, Grinspoon SK, et al. Cardiovascular risk prediction functions underestimate risk in HIV infection. *Circulation.* (2018) 137:2203–14. doi: 10.1161/CIRCULATIONAHA.117.028975
27. Deeks SG, Phillips AN. HIV infection, antiretroviral treatment, ageing, and non-AIDS related morbidity. *BMJ.* (2009) 338:a3172. doi: 10.1136/bmj.a3172
28. Friis-Møller N, Sabin CA, Weber R, d'Arminio Monforte A, El-Sadr WM, Reiss P, et al. Combination antiretroviral therapy and the risk of myocardial infarction. *N Engl J Med.* (2003) 349:1993–2003. doi: 10.1056/NEJMoa030218
29. Benjamin LA, Allain TJ, Mzinganjira H, Connor MD, Smith C, Lucas S, et al. The role of human immunodeficiency virus–associated vasculopathy in the etiology of stroke. *J Infect Dis.* (2017) 216:545–53. doi: 10.1093/infdis/jix340
30. Feinstein MJ, Bogorodskaya M, Bloomfield GS, Vedanthan R, Siedner MJ, Kwan GF, et al. Cardiovascular complications of HIV in endemic countries. *Curr Cardiol Rep.* (2016) 18:113. doi: 10.1007/s11886-016-0794-x
31. Mlay M, Bakari M. The prevalence of HIV among patients admitted with stroke at the Muhimbili national hospital, dar es salaam, Tanzania. *Tanzan J Health Res.* (2010) 12:105–13. doi: 10.4314/thrb.v12i2.56397
32. Grinspoon S, Carr A. Cardiovascular risk and body-fat abnormalities in HIV-infected adults. *N Engl J Med.* (2005) 352:48–62. doi: 10.1056/NEJMra041811
33. Chow FC, Regan S, Feske S, Meigs JB, Grinspoon SK, Triant VA. Comparison of ischemic stroke incidence in HIV-infected and non-HIV-infected patients in a US health care system. *J Acquir Immune Defic Syndr.* (2012) 60:351–8. doi: 10.1097/QAI.0b013e31825c7f24
34. Barnes RP, Lacson JC, Bahrami H. hiv infection and risk of cardiovascular diseases beyond coronary artery disease. *Curr Atheroscler Rep.* (2017) 19:20. doi: 10.1007/s11883-017-0652-3
35. Pereyra F, Lo J, Triant VA, Wei J, Buzon MJ, Fitch KV, et al. Increased coronary atherosclerosis and immune activation in HIV-1 elite controllers. *AIDS.* (2012) 26:2409–12. doi: 10.1097/QAD.0b013e32835a9950
36. Phillips AN, Carr A, Neuhaus J, Visnegarwala F, Prineas R, Burman WJ, et al. Interruption of antiretroviral therapy and risk of cardiovascular disease in persons with HIV-1 infection: exploratory analyses from the SMART trial. *Antivir Ther.* (2008) 13:177–87.
37. Hsue PY, Hunt PW, Schnell A, Kalapus SC, Hoh R, Ganz P, et al. Role of viral replication, antiretroviral therapy, and immunodeficiency in HIV-associated atherosclerosis. *AIDS.* (2009) 23:1059–67. doi: 10.1097/QAD.0b013e32832b514b
38. Gutierrez J, Glenn M, Isaacson RS, Marr AD, Mash D, Petito CJS. Thinning of the arterial media layer as a possible preclinical stage in HIV vasculopathy: a pilot study. *Stroke.* (2012) 43:1156–8. doi: 10.1161/STROKEAHA.111.643387
39. Gutierrez J, Rosoklija G, Murray J, Chon C, Elkind MS, Goldman JE, et al. A quantitative perspective to the study of brain arterial remodeling of donors with and without HIV in the brain arterial remodeling study (BARS). *Front Physiol.* (2014) 5:56. doi: 10.3389/fphys.2014.00056
40. Gutierrez J, Menshawy K, Gonzalez M, Goldman J, Elkind MS, Marshall R, et al. Brain large artery inflammation associated with HIV and large artery remodeling. *AIDS.* (2016) 30:415–23. doi: 10.1097/QAD.0000000000000927
41. Mateen FJ, Post WS, Sacktor N, Abraham AG, Becker JT, Smith BR, et al. Long-term predictive value of the Framingham risk score for stroke in HIV-positive vs HIV-negative men. *Neurology.* (2013) 81:2094–102. doi: 10.1212/01.wnl.0000437296.97946.73
42. Benjamin L, Khoo S. HIV infection and stroke. *Handb Clin Neurol.* (2018) 152:187–200. doi: 10.1016/B978-0-444-63849-6.00015-3
43. Cysique LA, Brew BJ. Vascular cognitive impairment and HIV-associated neurocognitive disorder: a new paradigm. *J Neurovirol.* (2019) 25:710–21. doi: 10.1007/s13365-018-0706-5
44. Chow FC, Wilson MR, Kunling W, Ellis RJ, Bosch RJ, Linas BPJA. Stroke incidence is highest in women and non-hispanic blacks living with HIV in the ALLRT cohort. *AIDS.* (2018) 32:1125. doi: 10.1097/QAD.0000000000001799
45. Chow FC, Lyass A, Mahoney TF, Massaro JM, Triant VA, Wu K, et al. Baseline 10-year cardiovascular risk scores predict cognitive function in older persons, and particularly women, living with human immunodeficiency virus infection. *Clin Infect Dis.* (2020) 71:3079–85. doi: 10.1093/cid/ciz1214
46. Montoya JL, Iudicello J, Oppenheim HA, Fazeli PL, Potter M, Ma Q, et al. Coagulation imbalance and neurocognitive functioning in older HIV-positive adults on suppressive antiretroviral therapy. *AIDS.* (2017) 31:787–95. doi: 10.1097/QAD.0000000000001404
47. Hollestelle SC, de Vries MR, van Keulen JK, Schoneveld AH, Vink A, Strijder CF, et al. Toll-like receptor 4 is involved in outward arterial remodeling. *Circulation.* (2004) 109:393–8. doi: 10.1161/01.CIR.0000109140.51366.72
48. Mulvany MJ, Baumbach GL, Aalkjaer C, Heagerty AM, Korsgaard N, Schiffrin EL, et al. Vascular remodeling. *Hypertension.* (1996) 28:505–6.
49. Taylor AJ, Burke AP, Farb A, Yousefi P, Malcom GT, Smialek J, et al. Arterial remodeling in the left coronary system: the role of high-density lipoprotein cholesterol. *J Am Coll Cardiol.* (1999) 34:760–7. doi: 10.1016/S0735-1097(99)00275-2
50. Schoenhagen P, Ziada KM, Vince DG, Nissen SE, Tuzcu EM. Arterial remodeling and coronary artery disease: the concept of "dilated" versus "obstructive" coronary atherosclerosis. *J Am Coll Cardiol.* (2001) 38:297–306. doi: 10.1016/S0735-1097(01)01374-2
51. Stein JH, Klein MA, Bellehumeur JL, McBride PE, Wiebe DA, Otvos JD, et al. Use of human immunodeficiency virus-1 protease inhibitors is associated with atherogenic lipoprotein changes and endothelial dysfunction. *Circulation.* (2001) 104:257–62. doi: 10.1161/01.CIR.104.3.257
52. Bonnet D, Aggoun Y, Szezepanski I, Bellal N, Blanche S. Arterial stiffness and endothelial dysfunction in HIV-infected children. *AIDS.* (2004) 18:1037–41. doi: 10.1097/00002030-200404300-00012
53. Dube MP, Lipshultz SE, Fichtenbaum CJ, Greenberg R, Schecter AD, Fisher SD, et al. Effects of HIV infection and antiretroviral therapy on the heart and vasculature. *Circulation.* (2008) 118:e36–40. doi: 10.1161/CIRCULATIONAHA.107.189625
54. Vos AG, Idris NS, Barth RE, Klipstein-Grobusch K, Grobbee DE. Pro-Inflammatory markers in relation to cardiovascular disease in HIV Infection. A systematic review. *PLoS ONE.* (2016) 11:e0147484. doi: 10.1371/journal.pone.0147484
55. Nou E, Lo J, Grinspoon SK. Inflammation, immune activation, and cardiovascular disease in HIV. *AIDS.* (2016) 30:1495–509. doi: 10.1097/QAD.0000000000001109
56. Zungsontiporn N, Tello RR, Zhang G, Mitchell BI, Budoff M, Kallianpur KJ, et al. Non-classical monocytes and monocyte chemoattractant protein-1 (MCP-1) correlate with coronary artery calcium progression in chronically hiv-1 infected adults on stable antiretroviral therapy. *PLoS ONE.* (2016) 11:e0149143. doi: 10.1371/journal.pone.0149143
57. Gutierrez J, Goldman J, Dwork AJ, Elkind MS, Marshall RS, Morgello S. Brain arterial remodeling contribution to nonembolic brain infarcts in patients

with HIV. *Neurology.* (2015) 85:1139–45. doi: 10.1212/WNL.0000000000001976
58. Re MC, Furlini G, Cenacchi G, Preda P, La Placa M. Human immunodeficiency virus type 1 infection of endothelial cells *in vitro*. *Microbiologica.* (1991) 14:149–52.
59. Chi D, Henry J, Kelley J, Thorpe R, Smith JK, Krishnaswamy G. The effects of HIV infection on endothelial function. *Endothelium.* (2000) 7:223–42. doi: 10.3109/10623320009072210
60. Kuller LH, Tracy R, Belloso W, De Wit S, Drummond F, Lane HC, et al. Inflammatory and coagulation biomarkers and mortality in patients with HIV infection. *PLoS Med.* (2008) 5:e203. doi: 10.1371/journal.pmed.0050203
61. Burdo TH, Lentz MR, Autissier P, Krishnan A, Halpern E, Letendre S, et al. Soluble CD163 made by monocyte/macrophages is a novel marker of HIV activity in early and chronic infection prior to and after anti-retroviral therapy. *J Infect Dis.* (2011) 204:154–63. doi: 10.1093/infdis/jir214
62. Hanna DB, Lin J, Post WS, Hodis HN, Xue X, Anastos K, et al. Association of macrophage inflammation biomarkers with progression of subclinical carotid artery atherosclerosis in HIV-infected women and men. *J Infect Dis.* (2017) 215:1352–61. doi: 10.1093/infdis/jix082
63. Paladugu R, Fu W, Conklin BS, Lin PH, Lumsden AB, Yao Q, et al. Hiv tat protein causes endothelial dysfunction in porcine coronary arteries. *J Vasc Surg.* (2003) 38:549–55; discussion 55–6. doi: 10.1016/S0741-5214(03)00770-5
64. Kim TA, Avraham HK, Koh YH, Jiang S, Park IW, Avraham S. HIV-1 Tat-mediated apoptosis in human brain microvascular endothelial cells. *J Immunol.* (2003) 170:2629–37. doi: 10.4049/jimmunol.170.5.2629
65. Marecki J, Cool C, Voelkel N, Luciw P, Flores S. Evidence for vascular remodeling in the lungs of macaques infected with simian immunodeficiency virus/HIV NEF recombinant virus. *Chest.* (2005) 128 (6 Suppl):621S−2S. doi: 10.1378/chest.128.6_suppl.621S
66. Duffy P, Wang X, Lin PH, Yao Q, Chen C. HIV Nef protein causes endothelial dysfunction in porcine pulmonary arteries and human pulmonary artery endothelial cells. *J Surg Res.* (2009) 156:257–64. doi: 10.1016/j.jss.2009.02.005
67. Anand AR, Rachel G, Parthasarathy D. HIV proteins and endothelial dysfunction: implications in cardiovascular disease. *Front Cardiovasc Med.* (2018) 5:185. doi: 10.3389/fcvm.2018.00185
68. De Alwis PM, Smith B, Wu T, Artrip C, Steinbach S, Morse C, et al. *In-vivo* MRI reveals changes to intracerebral vasculature caliber in HIV infection. *Front Neurol.* (2019) 10:687. doi: 10.3389/fneur.2019.00687
69. Anand AR, Ganju RK. HIV-1 gp120-mediated apoptosis of T cells is regulated by the membrane tyrosine phosphatase CD45. *J Biol Chem.* (2006) 281:12289–99. doi: 10.1074/jbc.M511786200
70. Anand AR, Prasad A, Bradley RR, Deol YS, Nagaraja T, Ren X, et al. HIV-1 gp120-induced migration of dendritic cells is regulated by a novel kinase cascade involving Pyk2, p38 MAP kinase, and LSP1. *Blood.* (2009) 114:3588–600. doi: 10.1182/blood-2009-02-206342
71. Munshi N, Balasubramanian A, Koziel M, Ganju RK, Groopman JE. Hepatitis C and human immunodeficiency virus envelope proteins cooperatively induce hepatocytic apoptosis via an innocent bystander mechanism. *J Infect Dis.* (2003) 188:1192–204. doi: 10.1086/378643
72. Freedman BD, Liu QH, Del Corno M, Collman RG. HIV-1 gp120 chemokine receptor-mediated signaling in human macrophages. *Immunol Res.* (2003) 27:261–76. doi: 10.1385/IR:27:2-3:261
73. Banda NK, Bernier J, Kurahara DK, Kurrle R, Haigwood N, Sekaly RP, et al. Crosslinking CD4 by human immunodeficiency virus gp120 primes T cells for activation-induced apoptosis. *J Exp Med.* (1992) 176:1099–106. doi: 10.1084/jem.176.4.1099
74. Hijmans JG, Stockleman K, Reiakvam W, Levy MaV, Brewster LM, Bammert TD, et al. Effects of HIV-1 gp120 and tat on endothelial cell sensescence and senescence-associated micro RNA s. *Physiol Rep.* (2018) 6:e13647. doi: 10.14814/phy2.13647
75. Katsuumi G, Shimizu I, Yoshida Y, Minamino T. Vascular senescence in cardiovascular and metabolic diseases. *Front Cardiovasc Med.* (2018) 5:18. doi: 10.3389/fcvm.2018.00018
76. Bavinger C, Bendavid E, Niehaus K, Olshen RA, Olkin I, Sundaram V, et al. Risk of cardiovascular disease from antiretroviral therapy for HIV: a systematic review. *PLoS One.* (2013) 8:e59551. doi: 10.1371/journal.pone.0059551
77. Ene L, Duiculescu D, Ruta SM. How much do antiretroviral drugs penetrate into the central nervous system? *J Med Life.* (2011) 4:432–9.
78. Mukerji SS, Misra V, Lorenz DR, Uno H, Morgello S, Franklin D, et al. Impact of antiretroviral regimens on cerebrospinal fluid viral escape in a prospective multicohort study of antiretroviral therapy-experienced human immunodeficiency virus-1–infected adults in the United States. *Clin Infect Dis.* (2018) 67:1182–90. doi: 10.1093/cid/ciy267
79. Pérez-Valero I, Ellis R, Heaton R, Deutsch R, Franklin D, Clifford DB, et al. Cerebrospinal fluid viral escape in aviremic HIV-infected patients receiving antiretroviral therapy: prevalence, risk factors and neurocognitive effects. *AIDS.* (2019) 33:475–81. doi: 10.1097/QAD.0000000000002074
80. Warriner AH, Burkholder GA, Overton ET. HIV-related metabolic comorbidities in the current ART era. *Infect Dis Clin North Am.* (2014) 28:457–76. doi: 10.1016/j.idc.2014.05.003
81. Islam F, Wu J, Jansson J, Wilson DP. Relative risk of cardiovascular disease among people living with HIV: a systematic review and meta-analysis. *HIV Med.* (2012) 13:453–68. doi: 10.1111/j.1468-1293.2012.00996.x
82. Hanna DB, Post WS, Deal JA, Hodis HN, Jacobson LP, Mack WJ, et al. HIV infection is associated with progression of subclinical carotid atherosclerosis. *Clin Infect Dis.* (2015) 61:640–50. doi: 10.1093/cid/civ325
83. Hsue PY, Lo JC, Franklin A, Bolger AF, Martin JN, Deeks SG, et al. Progression of atherosclerosis as assessed by carotid intima-media thickness in patients with HIV infection. *Circulation.* (2004) 109:1603–8. doi: 10.1161/01.CIR.0000124480.32233.8A
84. Patel K, Wang J, Jacobson DL, Lipshultz SE, Landy DC, Geffner ME, et al. Aggregate risk of cardiovascular disease among adolescents perinatally infected with the human immunodeficiency virus. *Circulation.* (2014) 129:1204–12. doi: 10.1161/CIRCULATIONAHA.113.001978
85. Shenoy A, Dwork A, Elkind MSV, Marshall R, Morgello S, Gutierrez J. Brain large artery lymphocytic inflammation and human immunodeficiency virus-related brain arterial remodeling. *J Virol.* (2018) 92e0081–18. doi: 10.1128/JVI.00081-18
86. Gherardi R, Belec L, Mhiri C, Gray F, Lescs MC, Sobel A, et al. The spectrum of vasculitis in human immunodeficiency virus–infected patients. A clinicopathologic evaluation. *Arthritis Rheum.* (1993) 36:1164–74. doi: 10.1002/art.1780360818
87. Chetty R. Vasculitides associated with HIV infection. *J Clin Pathol.* (2001) 54:275–8. doi: 10.1136/jcp.54.4.275
88. Kearns AC, Liu F, Dai S, Robinson JA, Kiernan E, Tesfaye Cheru L, et al. Caspase-1 activation is related with HIV-associated atherosclerosis in an HIV transgenic mouse model and HIV patient cohort. *Arterioscler Thromb Vasc Biol.* (2019) 39:1762–75. doi: 10.1161/ATVBAHA.119.312603
89. Gutierrez J, Hatleberg CI, Evans H, Yin MT. Role of pre-stroke immunity in ischemic stroke mechanism among patients with HIV. *AIDS Care.* (2019) 31:270–4. doi: 10.1080/09540121.2018.1510096
90. Wasserman BA. Advanced contrast-enhanced MRI for looking beyond the lumen to predict stroke: building a risk profile for carotid plaque. *Stroke.* (2010) 41 (10 Suppl):S12–6. doi: 10.1161/STROKEAHA.110.596288
91. Mee TC, Aepfelbacher J, Krakora R, Chairez C, Kvaratskhelia N, Smith B, et al. Carotid magnetic resonance imaging in persons living with HIV and 10-year atherosclerotic cardiovascular disease risk score. *Antivir Ther.* (2018) 23:695–8. doi: 10.3851/IMP3258
92. Rose KA, Vera JH, Drivas P, Banya W, Keenan N, Pennell DJ, et al. Atherosclerosis is evident in treated HIV-infected subjects with low cardiovascular risk by carotid cardiovascular magnetic resonance. *J Acquir Immune Defic Syndr.* (2016) 71:514–21. doi: 10.1097/QAI.0000000000000900
93. Schoepf IC, Buechel RR, Kovari H, Hammoud DA, Tarr PE. Subclinical atherosclerosis imaging in people living with HIV. *J Clin Med.* (2019) 8:1125. doi: 10.3390/jcm8081125
94. LaBounty TM, Hardy WD, Fan Z, Yumul R, Li D, Dharmakumar R, et al. Carotid artery thickness is associated with chronic use of highly active antiretroviral therapy in patients infected with human immunodeficiency virus: a 3.0 Tesla magnetic resonance imaging study. *HIV Med.* (2016) 17:516–23. doi: 10.1111/hiv.12351
95. Ward MR, Pasterkamp G, Yeung AC, Borst C. Arterial remodeling. Mechanisms and clinical implications. *Circulation.* (2000) 102:1186–91. doi: 10.1161/01.CIR.102.10.1186

96. Gutierrez J, Menshawy K, Goldman J, Dwork AJ, Elkind MS, Marshall RS, et al. Metalloproteinases and brain arterial remodeling among individuals with and those without HIV infection. *J Infect Dis.* (2016) 214:1329–35. doi: 10.1093/infdis/jiw385
97. He R, Guo DC, Estrera AL, Safi HJ, Huynh TT, Yin Z, et al. Characterization of the inflammatory and apoptotic cells in the aortas of patients with ascending thoracic aortic aneurysms and dissections. *J Thorac Cardiovasc Surg.* (2006) 131:671–8. doi: 10.1016/j.jtcvs.2005.09.018
98. Newman KM, Jean-Claude J, Li H, Scholes JV, Ogata Y, Nagase H, et al. Cellular localization of matrix metalloproteinases in the abdominal aortic aneurysm wall. *J Vasc Surg.* (1994) 20:814–20. doi: 10.1016/S0741-5214(94)70169-5
99. Dogan A, Tuzun N, Turker Y, Akcay S, Kaya S, Ozaydin M. Matrix metalloproteinases and inflammatory markers in coronary artery ectasia: their relationship to severity of coronary artery ectasia. *Coron Artery Dis.* (2008) 19:559–63. doi: 10.1097/MCA.0b013e3283109079
100. Ortiz G, Koch S, Romano JG, Forteza AM, Rabinstein AA. Mechanisms of ischemic stroke in HIV-infected patients. *Neurology.* (2007) 68:1257–61. doi: 10.1212/01.wnl.0000259515.45579.1e
101. Mochan A, Modi M, Modi G. Stroke in black South African HIV-positive patients: a prospective analysis. *Stroke.* (2003) 34:10–5. doi: 10.1161/01.STR.0000043821.35051.FA
102. Guedes BF, Gomes HR, Lucato LT, Puglia P Jr, Nitrini R, Castro LH. Human immunodeficiency virus-associated vasculopathy with CNS compartmentalization of HIV-1. *J Neurovirol.* (2015) 21:101–4. doi: 10.1007/s13365-014-0307-x
103. Lantos PL, McLaughlin JE, Schoitz CL, Berry CL, Tighe JR. Neuropathology of the brain in HIV infection. *Lancet.* (1989) 1:309–11. doi: 10.1016/S0140-6736(89)91316-0
104. Oliviero U, Bonadies G, Apuzzi V, Foggia M, Bosso G, Nappa S, et al. Human immunodeficiency virus per se exerts atherogenic effects. *Atherosclerosis.* (2009) 204:586–9. doi: 10.1016/j.atherosclerosis.2008.10.012
105. Solages A, Vita JA, Thornton DJ, Murray J, Heeren T, Craven DE, et al. Endothelial function in HIV-infected persons. *Clin Infect Dis.* (2006) 42:1325–32. doi: 10.1086/503261
106. Seaberg EC, Benning L, Sharrett AR, Lazar JM, Hodis HN, Mack WJ, et al. Association between human immunodeficiency virus infection and stiffness of the common carotid artery. *Stroke.* (2010) 41:2163–70. doi: 10.1161/STROKEAHA.110.583856
107. Burke AP, Kolodgie FD, Farb A, Weber D, Virmani R. Morphological predictors of arterial remodeling in coronary atherosclerosis. *Circulation.* (2002) 105:297–303. doi: 10.1161/hc0302.102610
108. Anderson TJ. Arterial stiffness or endothelial dysfunction as a surrogate marker of vascular risk. *Can J Cardiol.* (2006) 22:72B—80B. doi: 10.1016/S0828-282X(06)70990-4
109. Saylor D, Dickens AM, Sacktor N, Haughey N, Slusher B, Pletnikov M, et al. HIV-associated neurocognitive disorder—pathogenesis and prospects for treatment. *Nat Rev Neurol.* (2016) 12:234–48. doi: 10.1038/nrneurol.2016.27
110. Gannon P, Khan MZ, Kolson DL. Current understanding of HIV-associated neurocognitive disorders pathogenesis. *Curr Opin Neurol.* (2011) 24:275–83. doi: 10.1097/WCO.0b013e32834695fb
111. Montoya JL, Iudicello J, Fazeli PL, Hong S, Potter M, Ellis RJ, et al. Elevated markers of vascular remodeling and arterial stiffness are associated with neurocognitive function in older HIV+ adults on suppressive antiretroviral therapy. *J Acquir Immune Defic Syndr.* (2017) 74:134–41. doi: 10.1097/QAI.0000000000001230
112. Gelman BB. Neuropathology of HAND with suppressive antiretroviral therapy: encephalitis and neurodegeneration reconsidered. *Curr HIV/AIDS Rep.* (2015) 12:272–9. doi: 10.1007/s11904-015-0266-8
113. Levine AJ, Soontornniyomkij V, Masliah E, Sinsheimer JS, Ji SS, Horvath S, et al. A candidate gene study of intermediate histopathological phenotypes in HIV-associated neurocognitive disorders. *J Neurovirol.* (2020) 26:509–10. doi: 10.1007/s13365-020-00871-y
114. Clifford DB, Ances BM. HIV-associated neurocognitive disorder. *Lancet Infect Dis.* (2013) 13:976–86. doi: 10.1016/S1473-3099(13)70269-X
115. Vago L, Bonetto S, Nebuloni M, Duca P, Carsana L, Zerbi P, et al. Pathological findings in the central nervous system of AIDS patients on assumed antiretroviral therapeutic regimens: retrospective study of 1597 autopsies. *AIDS.* (2002) 16:1925–8. doi: 10.1097/00002030-200209270-00009
116. Bandera A, Taramasso L, Bozzi G, Muscatello A, Robinson JA, Burdo TH, et al. HIV-associated neurocognitive impairment in the modern ART era: are we close to discovering reliable biomarkers in the setting of virological suppression? *Front Aging Neurosci.* (2019) 11:187. doi: 10.3389/fnagi.2019.00187
117. Peluso MJ, Meyerhoff DJ, Price RW, Peterson J, Lee E, Young AC, et al. Cerebrospinal fluid and neuroimaging biomarker abnormalities suggest early neurological injury in a subset of individuals during primary HIV infection. *J Infect Dis.* (2013) 207:1703–12. doi: 10.1093/infdis/jit088
118. Nguyen TP, Soukup VM, Gelman BB. Persistent hijacking of brain proteasomes in HIV-associated dementia. *Am J Pathol.* (2010) 176:893–902. doi: 10.2353/ajpath.2010.090390
119. Everall IP, Hansen LA, Masliah E. The shifting patterns of HIV encephalitis neuropathology. *Neurotox Res.* (2005) 8:51–61. doi: 10.1007/BF03033819
120. Mackiewicz MM, Overk C, Achim CL, Masliah E. Pathogenesis of age-related HIV neurodegeneration. *J Neurovirol.* (2019) 25:622–33. doi: 10.1007/s13365-019-00728-z
121. Fields J, Dumaop W, Langford TD, Rockenstein E, Masliah E. Role of neurotrophic factor alterations in the neurodegenerative process in HIV associated neurocognitive disorders. *J Neuroimmune Pharmacol.* (2014) 9:102–16. doi: 10.1007/s11481-013-9520-2
122. Milanini B, Valcour V. Differentiating HIV-associated neurocognitive disorders from Alzheimer's disease: an emerging issue in geriatric NeuroHIV. *Curr HIV/AIDS Rep.* (2017) 14:123–32. doi: 10.1007/s11904-017-0361-0
123. Smail RC, Brew BJ. HIV-associated neurocognitive disorder. *Handb Clin Neurol.* (2018) 152:75–97. doi: 10.1016/B978-0-444-63849-6.00007-4
124. Heaton R, Franklin D, Letendre S, Ellis R, Fennema-Notestine C, Vaida F, et al. Aging amplifies HIV neurocognitive impairment: the effects may be related to vascular and metabolic factors. *J Neurovirol.* (2012) 18:S46.
125. Peterson TE, Huppler Hullsiek K, Wyman Engen N, Kumarasamy N, Lebech AM, Liappis A, et al. Inflammation associates with impaired small arterial elasticity early in HIV disease. *Open Forum Infect Dis.* (2018) 5:ofy117. doi: 10.1093/ofid/ofy117
126. Subramanian S, Tawakol A, Burdo TH, Abbara S, Wei J, Vijayakumar J, et al. Arterial inflammation in patients with HIV. *JAMA.* (2012) 308:379–86. doi: 10.1001/jama.2012.6698
127. Longenecker CT, Jiang Y, Yun CH, Debanne S, Funderburg NT, Lederman MM, et al. Perivascular fat, inflammation, and cardiovascular risk in HIV-infected patients on antiretroviral therapy. *Int J Cardiol.* (2013) 168:4039–45. doi: 10.1016/j.ijcard.2013.06.059
128. Benjamin LA, Bryer A, Lucas S, Stanley A, Allain TJ, Joekes E, et al. Arterial ischemic stroke in HIV: defining and classifying etiology for research studies. *Neurol Neuroimmunol Neuroinflamm.* (2016) 3:e254. doi: 10.1212/NXI.0000000000000254
129. Moulignier A, Savatovsky J, Assoumou L, Lescure FX, Lamirel C, Godin O, et al. Silent cerebral small-vessel disease is twice as prevalent in middle-aged individuals with well-controlled, combination antiretroviral therapy–treated human immunodeficiency virus (HIV) than in HIV-uninfected individuals. *Clin Infect Dis.* (2018) 66:1762–9. doi: 10.1093/cid/cix1075
130. Lui G, Ma RC, Chook P, Wong CK, Tam CH, Chan MH, et al. Brief report: progression of atherosclerosis in HIV-infected individuals—prospective data from an asian cohort. *JAIDS.* (2017) 75:198–202. doi: 10.1097/QAI.0000000000001358
131. Pantoni L. Cerebral small vessel disease: from pathogenesis and clinical characteristics to therapeutic challenges. *Lancet Neurol.* (2010) 9:689–701. doi: 10.1016/S1474-4422(10)70104-6
132. Sanford R, Strain J, Dadar M, Maranzano J, Bonnet A, Mayo NE, et al. HIV infection and cerebral small vessel disease are independently associated with brain atrophy and cognitive impairment. *AIDS.* (2019) 33:1197–205. doi: 10.1097/QAD.0000000000002193
133. Soontornniyomkij V, Umlauf A, Chung SA, Cochran ML, Soontornniyomkij B, Gouaux B, et al. HIV protease inhibitor exposure predicts cerebral small vessel disease. *AIDS.* (2014) 28:1297–306. doi: 10.1097/QAD.0000000000000262

134. Bertrand L, Meroth F, Tournebize M, Leda AR, Sun E, Toborek M. Targeting the HIV-infected brain to improve ischemic stroke outcome. *Nat Commun.* (2019) 10:2009. doi: 10.1038/s41467-019-10046-x
135. Fazeli PL, Crowe M, Ross LA, Wadley V, Ball K, Vance DE. Cognitive functioning in adults aging with HIV: a cross-sectional analysis of cognitive subtypes and influential factors. *J Clin Res HIV AIDS Prev.* (2014) 1:155–69. doi: 10.14302/issn.2324-7339.jcrhap-13-191
136. Valcour V, Shikuma C, Shiramizu B, Watters M, Poff P, Selnes O, et al. Higher frequency of dementia in older HIV-1 individuals: the hawaii aging with HIV-1 cohort. *Neurology.* (2004) 63:822–7. doi: 10.1212/01.WNL.0000134665.58343.8D
137. Joska JA, Westgarth-Taylor J, Myer L, Hoare J, Thomas KG, Combrinck M, et al. Characterization of HIV-associated neurocognitive disorders among individuals starting antiretroviral therapy in South Africa. *AIDS Behav.* (2011) 15:1197–203. doi: 10.1007/s10461-010-9744-6
138. Joska JA, Westgarth-Taylor J, Hoare J, Thomas KG, Paul R, Myer L, et al. Neuropsychological outcomes in adults commencing highly active antiretroviral treatment in South Africa: a prospective study. *BMC Infect Dis.* (2012) 12:39. doi: 10.1186/1471-2334-12-39
139. Marquine MJ, Umlauf A, Rooney A, Fazeli PL, Gouaux B, Woods SP, et al. The veterans aging cohort study (VACS) Index is associated with concurrent risk for neurocognitive impairment. *J Acquir Immune Defic Syndr.* (2014) 65:190–7. doi: 10.1097/QAI.0000000000000008
140. Wright EJ, Grund B, Cysique LA, Robertson K, Brew BJ, Collins G, et al. Factors associated with neurocognitive test performance at baseline: a substudy of the INSIGHT strategic timing of antiretroviral treatment (START) trial. *HIV Med.* (2015) 16:97–108. doi: 10.1111/hiv.12238
141. Heaton RK, Clifford DB, Franklin DR Jr, Woods SP, Ake C, Vaida F, et al. HIV-associated neurocognitive disorders persist in the era of potent antiretroviral therapy: CHARTER study. *Neurology.* (2010) 75:2087–96. doi: 10.1212/WNL.0b013e318200d727
142. Sacktor N, Skolasky RL, Seaberg E, Munro C, Becker JT, Martin E, et al. Prevalence of HIV-associated neurocognitive disorders in the multicenter AIDS cohort study. *Neurology.* (2016) 86:334–40. doi: 10.1212/WNL.0000000000002277
143. Gutierrez J, Byrd D, Yin MT, Morgello S. Relationship between brain arterial pathology and neurocognitive performance among individuals with human immunodeficiency virus. *Clin Infect Dis.* (2019) 68:490–7. doi: 10.1093/cid/ciy501
144. Wright EJ, Grund B, Robertson K, Brew BJ, Roediger M, Bain MP, et al. Cardiovascular risk factors associated with lower baseline cognitive performance in HIV-positive persons. *Neurology.* (2010) 75:864–73. doi: 10.1212/WNL.0b013e3181f11bd8
145. Gutierrez J, Honig L, Elkind MS, Mohr JP, Goldman J, Dwork AJ, et al. Brain arterial aging and its relationship to alzheimer dementia. *Neurology.* (2016) 86:1507–15. doi: 10.1212/WNL.0000000000002590
146. Rincon F, Sacco RL, Kranwinkel G, Xu Q, Paik MC, Boden-Albala B, et al. Incidence and risk factors of intracranial atherosclerotic stroke: the Northern Manhattan stroke study. *Cerebrovasc Dis.* (2009) 28:65–71. doi: 10.1159/000219299
147. Ohira T, Shahar E, Chambless LE, Rosamond WD, Mosley TH Jr, Folsom AR, et al. Risk factors for ischemic stroke subtypes: the atherosclerosis risk in communities study. *Stroke.* (2006) 37:2493–8. doi: 10.1161/01.STR.0000239694.19359.88
148. Gutierrez J, Elkind MS, Virmani R, Goldman J, Honig L, Morgello S, et al. A pathological perspective on the natural history of cerebral atherosclerosis. *Int J Stroke.* (2015) 10:1074–80. doi: 10.1111/ijs.12496
149. Valcour VG, Shikuma CM, Shiramizu BT, Williams AE, Watters MR, Poff PW, et al. Diabetes, insulin resistance, and dementia among HIV-1–infected patients. *J Acquir Immune Defic Syndr.* (2005) 38:31. doi: 10.1097/00126334-200501010-00006
150. McCutchan JA, Marquie-Beck JA, Fitzsimons CA, Letendre SL, Ellis RJ, Heaton RK, et al. Role of obesity, metabolic variables, and diabetes in HIV-associated neurocognitive disorder. *Neurology.* (2012) 78:485–92. doi: 10.1212/WNL.0b013e3182478d64
151. Kamat A, Lyons JL, Misra V, Uno H, Morgello S, Singer EJ, et al. Monocyte activation markers in cerebrospinal fluid associated with impaired neurocognitive testing in advanced HIV infection. *J Acquir Immune Defic Syndr.* (2012) 60:234–43. doi: 10.1097/QAI.0b013e318256f3bc
152. Blokhuis C, Mutsaerts H, Cohen S, Scherpbier HJ, Caan MWA, Majoie C, et al. Higher subcortical and white matter cerebral blood flow in perinatally HIV-infected children. *Medicine.* (2017) 96:e5891. doi: 10.1097/MD.0000000000005891
153. Su T, Mutsaerts HJ, Caan MW, Wit FW, Schouten J, Geurtsen GJ, et al. Cerebral blood flow and cognitive function in HIV-infected men with sustained suppressed viremia on combination antiretroviral therapy. *AIDS.* (2017) 31:847–56. doi: 10.1097/QAD.0000000000001414
154. O'Brien JT, Erkinjuntti T, Reisberg B, Roman G, Sawada T, Pantoni L, et al. Vascular cognitive impairment. *Lancet Neurol.* (2003) 2:89–98. doi: 10.1016/S1474-4422(03)00305-3
155. Gutierrez J, Albuquerque ALA, Falzon L. HIV infection as vascular risk: a systematic review of the literature and meta-analysis. HIV infection as vascular risk: a systematic review of the literature and meta-analysis. *PloS ONE.* (2017) 12:e0176686. doi: 10.1371/journal.pone.0176686
156. Lacson JC, Barnes RP, Bahrami H. Coronary artery disease in HIV-infected patients: downside of living longer. *Curr Atheroscler Rep.* (2017) 19:18. doi: 10.1007/s11883-017-0651-4
157. Holloway CJ, Boccara F. HIV-related cardiovascular disease: closing the gap in mortality. *Curr Opin HIV AIDS.* (2017) 12:509–12. doi: 10.1097/COH.0000000000000420
158. Hsue PY, Deeks SG, Hunt PW. Immunologic basis of cardiovascular disease in HIV-infected adults. *J Infect Dis.* (2012) 205 (Suppl. 3):S375–82. doi: 10.1093/infdis/jis200
159. Elicer IM, Byrd D, Clark US, Morgello S, Robinson-Papp J. Motor function declines over time in human immunodeficiency virus and is associated with cerebrovascular disease, while HIV-associated neurocognitive disorder remains stable. *J Neurovirol.* (2018). 24:514–22. doi: 10.1007/s13365-018-0640-6
160. Gelman BB, Chen T, Lisinicchia JG, Soukup VM, Carmical JR, Starkey JM, et al. The national NeuroAIDS tissue consortium brain gene array: two types of HIV-associated neurocognitive impairment. *PLoS ONE.* (2012) 7:e46178. doi: 10.1371/journal.pone.0046178
161. Kallianpur AR, Gittleman H, Letendre S, Ellis R, Barnholtz-Sloan JS, Bush WS, et al. Cerebrospinal fluid ceruloplasmin, haptoglobin, and vascular endothelial growth factor are associated with neurocognitive impairment in adults with HIV infection. *Mol Neurobiol.* (2019) 56:3808–18. doi: 10.1007/s12035-018-1329-9
162. Cysique LA, Moffat K, Moore DM, Lane TA, Davies NW, Carr A, et al. HIV, vascular and aging injuries in the brain of clinically stable HIV-infected adults: a (1)H MRS study. *PLoS ONE.* (2013) 8:e61738. doi: 10.1371/journal.pone.0061738
163. Harezlak J, Buchthal S, Taylor M, Schifitto G, Zhong J, Daar E, et al. Persistence of HIV-associated cognitive impairment, inflammation, and neuronal injury in era of highly active antiretroviral treatment. *AIDS.* (2011) 25:625–33. doi: 10.1097/QAD.0b013e3283427da7
164. Ulfhammer G, Edén A, Mellgren Å, Fuchs D, Zetterberg H, Hagberg L, et al. Persistent central nervous system immune activation following more than 10 years of effective HIV antiretroviral treatment. *AIDS.* (2018) 32:2171–8. doi: 10.1097/QAD.0000000000001950
165. Saloner R, Cysique LA. HIV-Associated neurocognitive disorders: a global perspective. *J Int Neuropsychol Soc.* (2017) 23:860–9. doi: 10.1017/S1355617717001102
166. Zhou P, Yang XL, Wang XG, Hu B, Zhang L, Zhang W, et al. A pneumonia outbreak associated with a new coronavirus of probable bat origin. *Nature.* (2020) 579:270–3. doi: 10.1038/s41586-020-2012-7
167. Hoffmann M, Kleine-Weber H, Schroeder S, Krüger N, Herrler T, Erichsen S, et al. SARS-CoV-2 cell entry depends on ACE2 and TMPRSS2 and is blocked by a clinically proven protease inhibitor. *Cell.* (2020) 181:271–80.e8. doi: 10.1016/j.cell.2020.02.052
168. Doobay MF, Talman LS, Obr TD, Tian X, Davisson RL, Lazartigues E. Differential expression of neuronal ACE2 in transgenic mice with overexpression of the brain renin-angiotensin system. *Am J Physiol Regul Integr Comp Physiol.* (2007) 292:R373–81. doi: 10.1152/ajpregu.00292.2006
169. Baig AM. Neurological manifestations in COVID-19 caused by SARS-CoV-2. *CNS Neurosci Ther.* (2020) 26:499–501. doi: 10.1111/cns.13372

170. Chen J, Xiao X, Chen S, Zhang C, Chen J, Yi D, et al. Angiotensin-converting enzyme 2 priming enhances the function of endothelial progenitor cells and their therapeutic efficacy. *Hypertension.* (2013) 61:681–9. doi: 10.1161/HYPERTENSIONAHA.111.00202
171. Chen J, Zhao Y, Chen S, Wang J, Xiao X, Ma X, et al. Neuronal over-expression of ACE2 protects brain from ischemia-induced damage. *Neuropharmacology.* (2014) 79:550–8. doi: 10.1016/j.neuropharm.2014.01.004
172. Hess DC, Eldahshan W, Rutkowski E. COVID-19-Related stroke. *Transl Stroke Res.* (2020) 11:322–5. doi: 10.1007/s12975-020-00818-9
173. Pugin D, Vargas MI, Thieffry C, Schibler M, Grosgurin O, Pugin J, et al. COVID-19–related encephalopathy responsive to high-dose glucocorticoids. *Neurology.* (2020) 95:543–6. doi: 10.1212/WNL.0000000000010354
174. Kuba K, Imai Y, Penninger JM. Multiple functions of angiotensin-converting enzyme 2 and its relevance in cardiovascular diseases. *Circ J.* (2013) 77:301–8. doi: 10.1253/circj.CJ-12-1544
175. Dubois C, Panicot-Dubois L, Gainor JF, Furie BC, Furie B. Thrombin-initiated platelet activation *in vivo* is vWF independent during thrombus formation in a laser injury model. *J Clin Invest.* (2007) 117:953–60. doi: 10.1172/JCI30537
176. Atkinson BT, Jasuja R, Chen VM, Nandivada P, Furie B, Furie BC. Laser-induced endothelial cell activation supports fibrin formation. *Blood.* (2010) 116:4675–83. doi: 10.1182/blood-2010-05-283986
177. Sigel K, Swartz T, Golden E, Paranjpe I, Somani S, Richter F, et al. Coronavirus 2019 and people living with human immunodeficiency virus: outcomes for hospitalized patients in New York City. *Clin Infect Dis.* (2020) 71:2933–8. doi: 10.1093/cid/ciaa880
178. Karmen-Tuohy S, Carlucci PM, Zervou FN, Zacharioudakis IM, Rebick G, Klein E, et al. Outcomes among HIV-positive patients hospitalized with COVID-19. *J Acquir Immune Defic Syndr.* (2020) 85:6–10. doi: 10.1101/2020.05.07.20094797
179. Vizcarra P, Perez-Elias MJ, Quereda C, Moreno A, Vivancos MJ, Dronda F, et al. Description of COVID-19 in HIV-infected individuals: a single-centre, prospective cohort. *Lancet HIV*. (2020) 7:e554–64. doi: 10.1016/S2352-3018(20)30164-8
180. del Amo J, Polo R, Moreno S, Diaz A, Martinez E. Incidence and severity of COVID-19 in HIV-positive persons receiving antiretroviral therapy. *Ann Intern Med.* (2020) 173:536–41. doi: 10.7326/M20-3689
181. Johnson W, Onuma O, Owolabi M, Sachdev S. Stroke: a global response is needed. *Bull World Health Organ.* (2016) 94:634. doi: 10.2471/BLT.16.181636
182. Ortblad KF, Lozano R, Murray CJ. The burden of HIV: insights from the global burden of disease study 2010. *AIDS.* (2013) 27:2003–17. doi: 10.1097/QAD.0b013e328362ba67
183. Abdallah A, Chang JL, O'Carroll CB, Musubire A, Chow FC, Wilson AL, et al. Stroke in human immunodeficiency virus-infected individuals in Sub-Saharan Africa (SSA): a systematic review. *J Stroke Cerebrovasc Dis.* (2018) 27:1828–36. doi: 10.1016/j.jstrokecerebrovasdis.2018.02.016
184. Benjamin LA, Corbett EL, Connor MD, Mzinganjira H, Kampondeni S, Choko A, et al. HIV, antiretroviral treatment, hypertension, and stroke in Malawian adults: a case-control study. *Neurology.* (2016) 86:324–33. doi: 10.1212/WNL.0000000000002278
185. Eshtehardi P, McDaniel MC, Dhawan SS, Binongo JN, Krishnan SK, Golub L, et al. Effect of intensive atorvastatin therapy on coronary atherosclerosis progression, composition, arterial remodeling, and microvascular function. *J Invasive Cardiol.* (2012) 24:522–9.
186. Tunick PA, Nayar AC, Goodkin GM, Mirchandani S, Francescone S, Rosenzweig BP, et al. Effect of treatment on the incidence of stroke and other emboli in 519 patients with severe thoracic aortic plaque. *Am J Cardiol.* (2002) 90:1320–5. doi: 10.1016/S0002-9149(02)02870-9

Conflict of Interest: The authors declare that the research was conducted in the absence of any commercial or financial relationships that could be construed as a potential conflict of interest.

frontiers in Neurology

ORIGINAL RESEARCH
published: 22 July 2021
doi: 10.3389/fneur.2021.663793

Alprazolam Prompts HIV-1 Transcriptional Reactivation and Enhances CTL Response Through RUNX1 Inhibition and STAT5 Activation

Angel Lin[1,2], *Weam Othman Elbezanti*[1,3], *Alexis Schirling*[1,4], *Adel Ahmed*[5], *Rachel Van Duyne*[2], *Simon Cocklin*[5] *and Zachary Klase*[2,6]*

[1] Department of Biological Sciences, University of the Sciences, Philadelphia, PA, United States, [2] Department of Pharmacology and Physiology, Drexel University College of Medicine, Philadelphia, PA, United States, [3] Center for Cellular Immunotherapies, University of Pennsylvania, Philadelphia, PA, United States, [4] HIV-1 Dynamics and Replication Program, National Cancer Institute, Frederick, MD, United States, [5] Department of Biochemistry and Molecular Biology, Drexel University College of Medicine, Philadelphia, PA, United States, [6] Center for Neuroimmunology and CNS Therapeutics, Institute of Molecular Medicine and Infectious Diseases, Drexel University College of Medicine, Philadelphia, PA, United States

OPEN ACCESS

Edited by:
Dianne T. Langford, Temple University, United States

Reviewed by:
Tricia H. Burdo, Temple University, United States
Rafal Kaminski, Temple University, United States

***Correspondence:**
Zachary Klase
zk76@drexel.edu

Specialty section:
This article was submitted to Neuroinfectious Diseases, a section of the journal Frontiers in Neurology

Received: *03 February 2021*
Accepted: *17 June 2021*
Published: *22 July 2021*

Citation:
Lin A, Elbezanti WO, Schirling A, Ahmed A, Van Duyne R, Cocklin S and Klase Z (2021) Alprazolam Prompts HIV-1 Transcriptional Reactivation and Enhances CTL Response Through RUNX1 Inhibition and STAT5 Activation. Front. Neurol. 12:663793. doi: 10.3389/fneur.2021.663793

The HIV-1 pandemic is a significant challenge to the field of medicine. Despite advancements in antiretroviral (ART) development, 38 million people worldwide still live with this disease without a cure. A significant barrier to the eradication of HIV-1 lies in the persistently latent pool that establishes early in the infection. The "shock and kill" strategy relies on the discovery of a latency-reversing agent (LRA) that can robustly reactivate the latent pool and not limit immune clearance. We have found that a benzodiazepine (BDZ), that is commonly prescribed for panic and anxiety disorder, to be an ideal candidate for latency reversal. The BDZ Alprazolam functions as an inhibitor of the transcription factor RUNX1, which negatively regulates HIV-1 transcription. In addition to the displacement of RUNX1 from the HIV-1 5′LTR, Alprazolam potentiates the activation of STAT5 and its recruitment to the viral promoter. The activation of STAT5 in cytotoxic T cells may enable immune activation which is independent of the IL-2 receptor. These findings have significance for the potential use of Alprazolam in a curative strategy and to addressing the neuroinflammation associated with neuroHIV-1.

Keywords: HIV-1, latency, alprazolam, stat5, latency reversing agent, runx1

INTRODUCTION

HIV-1, the causative agent of AIDS, is a retrovirus that has infected ∼38 million people worldwide (1). While the advent of ART therapy has transformed the pandemic from a severe and acute condition to a chronic and manageable one, there is currently no cure for the disease due to the persistence of an HIV-1 latent reservoir (2). Integration of the HIV-1 viral DNA into host chromatin is an irreversible step in the HIV-1 life cycle, after which the activity of HIV-1 transcription is dependent on both viral and host transcription factors (3). One of the main targets of HIV-1 is CD4+ T cells.

After infection, the vast majority of these target cells support replication of the virus. During this productive infection, the 5'long terminal repeat (LTR) of the HIV-1 genome acts as an inducible promoter within the host chromatin to drive viral transcription (4, 5). In a small portion of infected cells, HIV-1 remains non-productive and transcriptionally silent, therefore the viral genome persists stably in the host chromatin, and latent transcription allows the infected cell to dodge immune surveillance and its cytopathic fate (4, 6–8).

However, the condition of latency is reversible. With the correct stimulation, latent HIV-1 can be reactivated. A strategy termed "Shock and Kill" aims to purge the latent reservoir by reactivating non replicating viral genomes and resubmit the infected cells to immune clearance (9–11). One of the main obstacles in this strategy is to find chemical stimuli that not only reactivate latent virus efficiently but also promote immune clearance. While many latency reversal agents (LRAs) from different classes have been tested in laboratory settings and clinical trials, they fall short of reducing the size of the latent reservoir due to deficiencies in reactivating potential and prompting proper immune response (11–14). One example is the widely tested FDA-approved drug- Vorinostat (SAHA). Originally developed for cancer treatment as a histone deacetylase (HDAC) inhibitor, it was found to reactive latent HIV-1 transcription. However, studies suggest that HDAC inhibitors negatively impact CTL response (15–17). In short, new stimuli for latency reversal are needed and the purpose of this study is to explore a promising host candidate, RUNX1, as a target to switch viral transcription back on. The Runt related transcription factor 1 (RUNX1) is a critical host factor required for permanent silencing of CD4 in maturing CD8+ T cells (18, 19). The RUNX1 protein contains a DNA binding domain, forms a heterodimer with binding partner CBF-β to efficiently bind to DNA and regulates transcription by recruiting additional transcription factors (20). RUNX1 functions as a platform to recruit other transcription factors that have an effect on transcription. Therefore, it can serve as both an activating and a repressing factor (21–23). RUNX1 binding to the consensus sites within the CD4 silencer region is crucial for T cell differentiation through the recruitment and binding of many additional transcription factors such as HDACs and histone methyltransferase (HMT) (24, 25). RUNX1 has also been shown to bind to positive transcription elongation factor (p-TEFb), which allows RUNX1 to contribute to CD4 silencing and may facilitate HIV-1 transcriptional silencing (26–28).

The HIV-1 LTR contains a RUNX1 binding site and the binding of RUNX1 to the HIV-1 LTR suppresses HIV-1 transcription (29, 30). Using Ro5-3335, a benzodiazepine (BDZ) compound known to interfere with RUNX1 and CBF-β function, HIV-1 transcription can be moderately reactivated (29, 30). However, since Ro5-3335 in addition to inhibiting RUNX binding also inhibits Tat (31), an important viral protein that drives transcription, it is not an ideal candidate for the shock and kills strategy to reverse HIV-1 latency. The search for an ideal RUNX1 inhibitor and LRA led to the use of another BDZ compound, Alprazolam. Alprazolam was found to robustly reactivate latent HIV-1 transcription without negatively impact Tat function (29, 30). We speculated that Alprazolam might interact with RUNX1 in a similar fashion as Ro5-3335, however, the detailed mechanism was unknown.

Benzodiazepines (BDZs) such as diazepam (Valium) and Alprazolam (Xanax), are effective anxiolytic (anti-anxiety) agents approved by the FDA for the treatment of panic and anxiety disorders. This effect is the result of the ability of BDZs to positively allosterically regulate the gamma-aminobutyric acid (GABA)-A receptor in the central nervous system (CNS) (32). BDZs have well-described pharmacokinetics and penetrate the blood-brain barrier (32, 33), making them an attractive therapy to address issues in the CNS. Persistent HIV-1 infection of CNS reservoirs drives a spectrum of neuropathologic, behavioral, and cognitive effects (34–43). Even with effective ART therapy, these neuropathologies are apparent in HIV-1 infected individuals (44, 45). The adverse neurologic outcomes associated with HIV-1 infection are thought to be primarily driven by chronic neuroinflammation (46–48). Understanding the mechanisms by which BDZs affect HIV-1 transcription and any associated effect on immune function may allow us to design therapies to address the latent reservoir and immune dysfunction in both the periphery and the CNS.

This study presents evidence that Alprazolam is working as a *bona fide* RUNX1 inhibitor and drives Signal Transducer and activator 5 (STAT5) recruitment to the HIV-1 LTR driving latency reactivation. In the CNS, STAT5 is expressed in the hypothalamic arcuate nucleus (ARC), dopaminergic and somatostatin neurons (49–51) and preferentially activated by granulocyte-macrophage colony-stimulating factor (GM-CSF). It has been shown that HIV-1 infection negatively impacts the activation level of both STAT5 and GM-CSF and therefore may impair macrophage function (52). GM-CSF has been tested as an adjuvant of ART in clinical studies and demonstrated to improve host defense and immune outcomes such as increased CD4+ T cell count and decreased plasma HIV-1 RNA detected in HIV-1 patients. The mechanism behind such effect is unclear but may be associated with STAT5 activation (53, 54).

The cytotoxic T cells (CD8+ T cells) are essential in the recognition of virally infected cells and foreign antigens. IL-2 is responsible for CD8+ T cell activation and the differentiation into potent effector cells to elicit rapid expansion and eradicate infections (55). STAT5 is activated by a wide variety of cytokines and growth factors, including IL-2 and GM-CSF, through phosphorylation. STAT5 is a 90kDA protein encoded by two closely related genes (STAT5a and STAT5b), located on human chromosome 17 (56). The activation by phosphorylation is targeted to the tyrosine residue 694 and 699 on STAT5A and STAT5B, respectively, by the receptor-associated Janus family tyrosine kinase (Jak) (57). Activated STAT5 then dimerize as a STAT5A/B heterodimer, translocate to the nucleus, and induce gene transcription that is crucial to T cell survival, proliferation, and cytokine production (56, 58, 59). The STAT5a/b heterodimer commonly binds to the consensus sequence TTC (T/C) N (G/A) GAA which is the interferon gamma-activated sequence (GAS) motif (60). STAT5 binding site was also found on the HIV-1 promoter (61) and we show that the activation of STAT5 via Alprazolam may potentiate IFNγ production in CD8 T cells. This

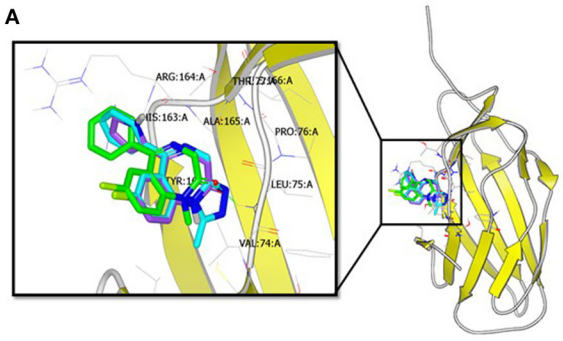

Compound	Number of Autodock4 clusters	Predicted Autodock4 ΔG binding (Kcal/mol)	Pose validated (Posit)	Posit probability
Alprazolam	1	-6.51	Yes	0.99
Clonazepam	1	-6.21	Fail	0
Diazepam	2, the lowest energy cluster is not the highest populated	-5.75	Yes	0.42
R05-3335	1	-5.97	Yes	0.72

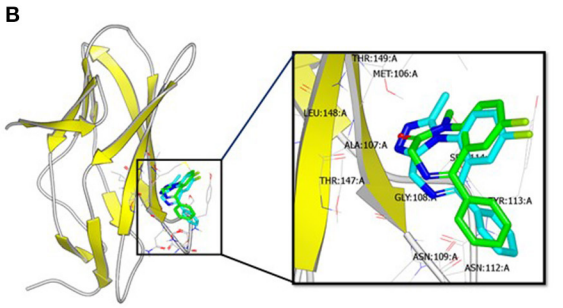

Compound	Number of Autodock4 clusters	Predicted Autodock4 ΔG binding (Kcal/mol)	Pose validated (Posit)	Posit probability
Alprazolam	1	-5.74	Yes	0.99
Clonazepam	4, the highest populated cluster hasthe lowest energy	-5.69	Failed	0
Diazepam	1	-5.64	Yes	0.5
R05-3335	2, the highest populated cluster has the lowest energy	-5.53	Failed	0

FIGURE 1 | Binding modes of benzodiazepines to RUNX1. **(A)** Alprazolam (cyan), diazepam (green), and R05-355 (purple) were predicted to bind at the bound pocket. Alprazolam has the highest POSIT probability (0.99 vs. 0.42 for diazepam and 0.72 for R05-355). **(B)** Only alprazolam (cyan) and diazepam (green) were predicted to bind at the unbound-RUNX1 pocket. Alprazolam has the highest POSIT probability (0.99 for alprazolam vs. 0.5 for diazepam).

study shows evidence to demonstrate that Alprazolam acts as a RUNX1 inhibitor and potential LRA that may positively impact immune response toward HIV-1 infected cells.

RESULTS

BDZs That Alter RUNX1 Activity May Directly Interact With RUNX1

Our recent publication provided evidence that BDZs alter the epigenetics of the integrated HIV-1 LTR and activate viral transcription (30). The structural similarities of clinically relevant BDZs such as Alprazolam, Diazepam, and Clonazepam to the RUNX1 inhibitor Ro5-3335 suggests that these compounds also interact with RUNX1 to affect its function. Although studies have shown interactions between Ro5-3335 and RUNX1, no information is currently available on how these two molecules interact.

To investigate whether the structural similarities between BDZs and Ro5-3335 translates into being able to interact with RUNX1, docking studies were performed. We evaluated the potential interaction of Ro5-3335, Alprazolam, Clonazepam, and Diazepam using the docking programs Gold and Autodock. We chose to also investigate whether these compounds may prefer the liganded or unliganded forms of RUNX1. The unbound (PDB:1EAN) (**Figure 1A**) and the bound (PDB: 3WTS) (**Figure 1B**) structures of RUNX1 share an overall backbone structure but differ in the orientation of several side chains. Druggable sites were found on each structure through quick blind docking of the ligands using the two docking software to the entire protein. Subsequently, these pockets were selected for further in-depth analysis using the cluster analysis function of Autodock4 (62, 63). Only alprazolam and diazepam were predicted to bind to the unbound form (**Figure 1A**), while alprazolam, diazepam and Ro5-3335 were predicted to bind to the bound form (**Figure 1B**).

This analysis suggests that these BDZs could interact with RUNX1 and that their potential binding sites are on a face distinct from the known interaction regions for DNA and CBFβ. Additionally, these analyses suggest a second binding pocket on RUNX1 that may be engaged only by Alprazolam and diazepam, but not Ro5-3335 and clonazepam. The differential binding modes suggest that Alprazolam and diazepam may mediate other effects on RUNX1 function beyond that seen with Ro5-3335.

Alprazolam Alters the Expression of RUNX Responsive Genes in PBMCs

To determine if Alprazolam functions as a RUNX1 inhibitor we examined the expression of several RUNX responsive genes in PBMCs in response to Ro5-3335 and Alprazolam treatments (**Figure 2**). PBMCs from three HIV-1 patients were treated with alprazolam or Ro5-3335 for 48 h. RNA was harvested using Trizol and cDNA was synthesized by reverse transcription. qPCR was performed using primers for five

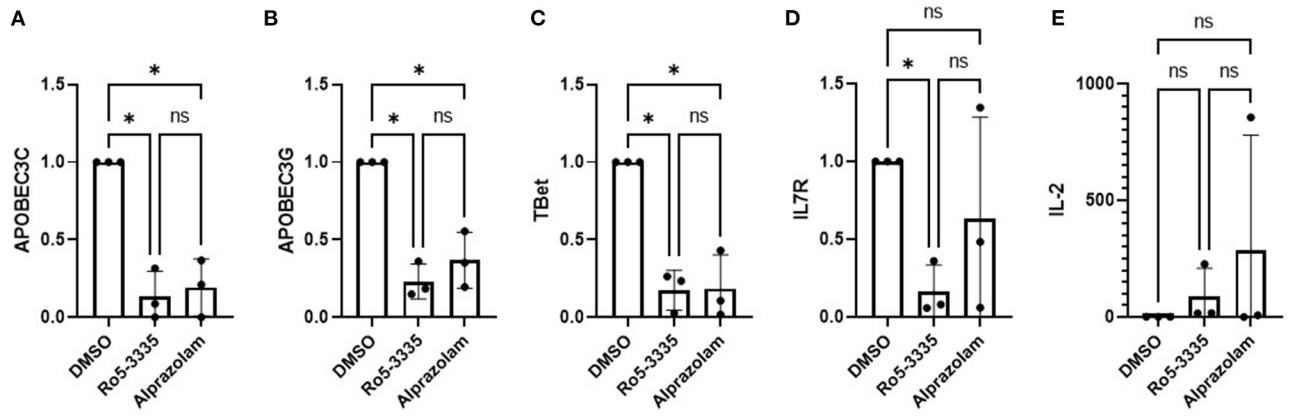

FIGURE 2 | Effect of alprazolam *ex vivo* on RUNX1 responsive genes. Peripheral blood mononuclear cells (PBMC) from three HIV-1-1 positive individuals were treated with 10μM Alprazolam or Ro5-3335 for 48 h. RNA was harvested using Trizol and cDNA was synthesized by RT reaction. qPCR was performed for five known RUNX responsive genes: **(A)** APOBEC3C, **(B)** APOBEC3G, **(C)** Tbet, **(D)** IL-7R and **(E)** IL-2. Expression levels are plotted as GAPDH normalized expression with the levels in the control for each individual. Dots represent each individual data point and graphs show the average. ANOVA was used to determine statistical differences. $*p < 0.05$.

known RUNX1 responsive genes: APOBEC3C, APOBEC3G, T-bet, IL7R, and IL-2 (64–70). As expected, as a RUNX1 inhibitor, Ro5-3335 significantly suppressed the expression of all the selected RUNX responsive genes except IL-2. Similarly, Alprazolam treatment resulted in a statistically significant decrease in APOBEC3C, APOBEC3G, and T-bet expression. IL-2 has been reported to be negatively regulated by RUNX1. In this assay, treatment of cells with Ro5-3335 and Alprazolam resulted in no statistically significant change in IL-2 expression. The suppression of APOBEC3C, APOBEC3G and T-bet mRNA in a manner similar to the known RUNX1 inhibitor Ro5-3335 suggests that Alprazolam inhibits RUNX1.

Effect of Ro5-3335 and Alprazolam on IL17 Promoter-Reporter

We next sought to determine if Alprazolam could suppress RUNX1 mediated transcription in a reporter assay. RUNX1 is known to form a complex with RORϒt, the orphan nuclear receptor, and bind to IL17 enhancer and promoter to up-regulate IL17 expression (71, 72). We tested the ability of Ro5-3335 and Alprazolam to alter the expression of luciferase under the control of the IL17 promoter. We hypothesized that a RUNX inhibitor should be able to suppress the activity of the IL17 promoter. 293T cells were transfected with an IL17 promoter luciferase reporter plasmid and treated with Ro5-3335 and Alprazolam (**Figure 3**). As expected, Ro5-3335 inhibited IL17 promoter activity in a dose-dependent fashion with a maximal decrease in activity of 95.56% observed at 100 nM. Alprazolam also induced a dose-dependent decrease in luciferase activity with the greatest inhibition noted at 1μM (76% inhibition). These experiments demonstrate that alprazolam has an effect on the expression from IL17 promoter, but at higher concentrations than Ro5-3335 with IC 50 at 43.25 nM and 1.53 nM, respectively (**Supplementary Figure 1**).

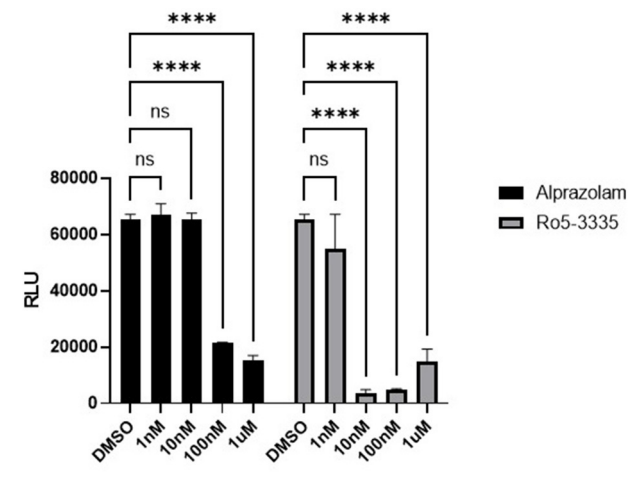

FIGURE 3 | Effect of alprazolam on IL17. 293T cells were transfected with IL17-luciferase reporter plasmid and treated with Ro5-3335 or alprazolam. Luciferase activity was measured using a luciferase assay kit. Luciferase light units after treatment with RO5-3335 or alprazolam with overexpression of RUNX1. $****P \leq 0.0001$, ns = not significant.

Benzodiazepine Activation of the LTR Is Associated With Recruitment of STAT5 and CBP/P300

Considering that Ro5-3335 reactivates HIV-1 transcription through RUNX1 inhibition, we hypothesize that Alprazolam may produce the same effect. To evaluate the latency reactivation

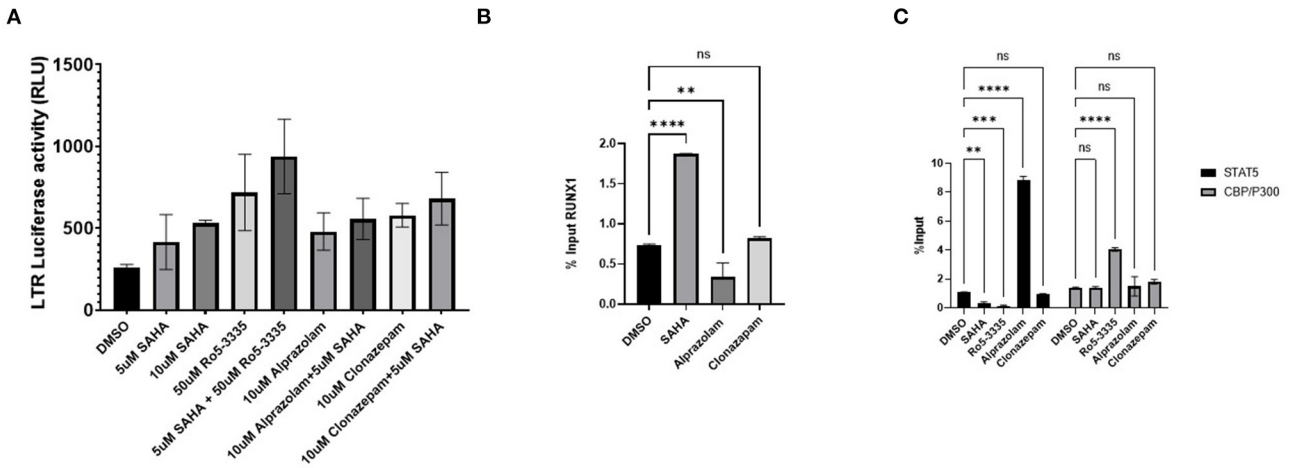

FIGURE 4 | Recruitment of STAT5 and CBP/P300 to the LTR by benzodiazepines in TZMBL Cells. TZMBL cells were treated with Benzodiazepines: RO5-3335, Alprazolam and Clonazepam with or without HDACi SAHA for 48 hrs at the indicated concentrations. **(A)** Cells were lysed and LTR driven luciferase was determined. **(B)** ChIP analysis was performed to determine RUNX1 binding to the HIV-1 LTR. **(C)** ChIP analysis was performed to determine STAT5 and CBP/P300 binding to the HIV-1 LTR. $^{**}P \leq 0.01$, $^{***}P \leq 0.001$, $^{****}P \leq 0.0001$, ns = not significant.

potential of Alprazolam, TZMbl cells, a Hela derived cell line with HIV-1 LTR- driven luciferase reporter was used to measure transcriptional activation. TZMbl cells were treated with Alprazolam, or two additional BDZs: Ro5-3335 and Clonazepam at 10μM, with or without 5μM SAHA for 48 h. After which, cells were lysed and luminescence was measured. As expected, SAHA as an HDAC inhibitor increased the amount of LTR activation. All BDZs tested, including Alprazolam, Clonazepam and Ro5-3335 also activated the LTR and displayed a moderate additive effect when combined with SAHA (**Figure 4A**). To understand the mechanism of the BDZ-driven activation, ChIP analysis was performed. STAT5 is an important signal transactivator induced by cytokines and interleukins, and a coactivator of CBP/P300 which plays an important role in transcriptional activation. Previous studies have revealed a role for RUNX1 in suppressing STAT5 activity due to a >50% chance of sharing a binding motif (73, 74). ChIP revealed as RUNX1 is dislodged from the HIV-1 LTR by Alprazolam (**Figure 4B**), a significant increase in the amount of STAT5 and CBP/P300 recruited to the HIV-1 LTR when HIV-1 LTR transcription was reactivated by Alprazolam and Ro5-3335, respectively. While the treatment with Clonazepam does not affect STAT5 nor CBP/P300 recruitment, SAHA and Ro5-3335 treatment negatively impacted STAT5 recruitment (**Figure 4C**). This is in agreement with our recently published findings that show recruitment of STAT5 and CBP/P300 to the HIV-1 LTR in the presence of alprazolam, but not clonazepam nor Ro5-3335 (30).

The Loss of RUNX1 Binding to the HIV-1 LTR Also Increases the Recruitment of STAT5 and CBP/P300

We next sought to determine if elimination of the RUNX1 binding site in the HIV-1 LTR would similarly increase STAT5 recruitment. To study the effect of RUNX1 binding on HIV-1 replication, an HIV-1 molecular clone that has a mutation in the RUNX1 binding site was constructed using site-directed mutagenesis. Our lab has shown that RUNX1 binds to U3 of the HIV-1 LTR (29). A point mutation in the first and second residues in the RUNX1 binding site, 55-60bp downstream of the beginning of the HIV-1 LTR (from ACCACA to CACACA), was performed as mutation of these nucleotides abrogates RUNX binding and eliminates RUNX1 effect on an HIV-1 LTR driven reporter (29). Mutations were generated in the 3′LTR of pNL4-3, as the U3 region from the 3' LTR is propagated during reverse transcription. Moreover, because the *nef* gene overlaps with the RUNX1 binding site at the 3′ LTR and nef is dispensable in the cell culture, mutations were generated in a nef-minus (Δnef) virus. The resulting proviral plasmid was designated pNL4-3 Δnef mutRUNX BS (ΔRUNX). We transfected the Δnef and ΔRUNX molecular clones into J-LTR-GFP cells and observed viral replication as measured by the accumulation of GFP+ cells over time. We observed faster replication kinetics in cells infected with the ΔRUNX compared to wildtype (WT) and ΔNef viruses, which is consistent with an increase in LTR activity upon inhibiting RUNX1 (**Figure 5A**). Similar results were seen when we infected Jurkat cells with Δnef or ΔRUNX virus and measured virus production in the supernatant over time (**Figure 5B**). To understand the effect that mutating the RUNX1 binding site has on HIV-1 viral fitness we performed a competition assay over multiple rounds of infection. J-LTR-GFP cells were infected with ΔNef and ΔRUNX viruses at a 1:1 ratio of infectious units. Cells were washed after 24 h and GFP expression was measured for 14 days. Supernatant from the peak of infection was used to infect the next round. After three rounds RNA was extracted from supernatant from the peak of each infection and RT-PCR was performed against the LTR to generate fragments for

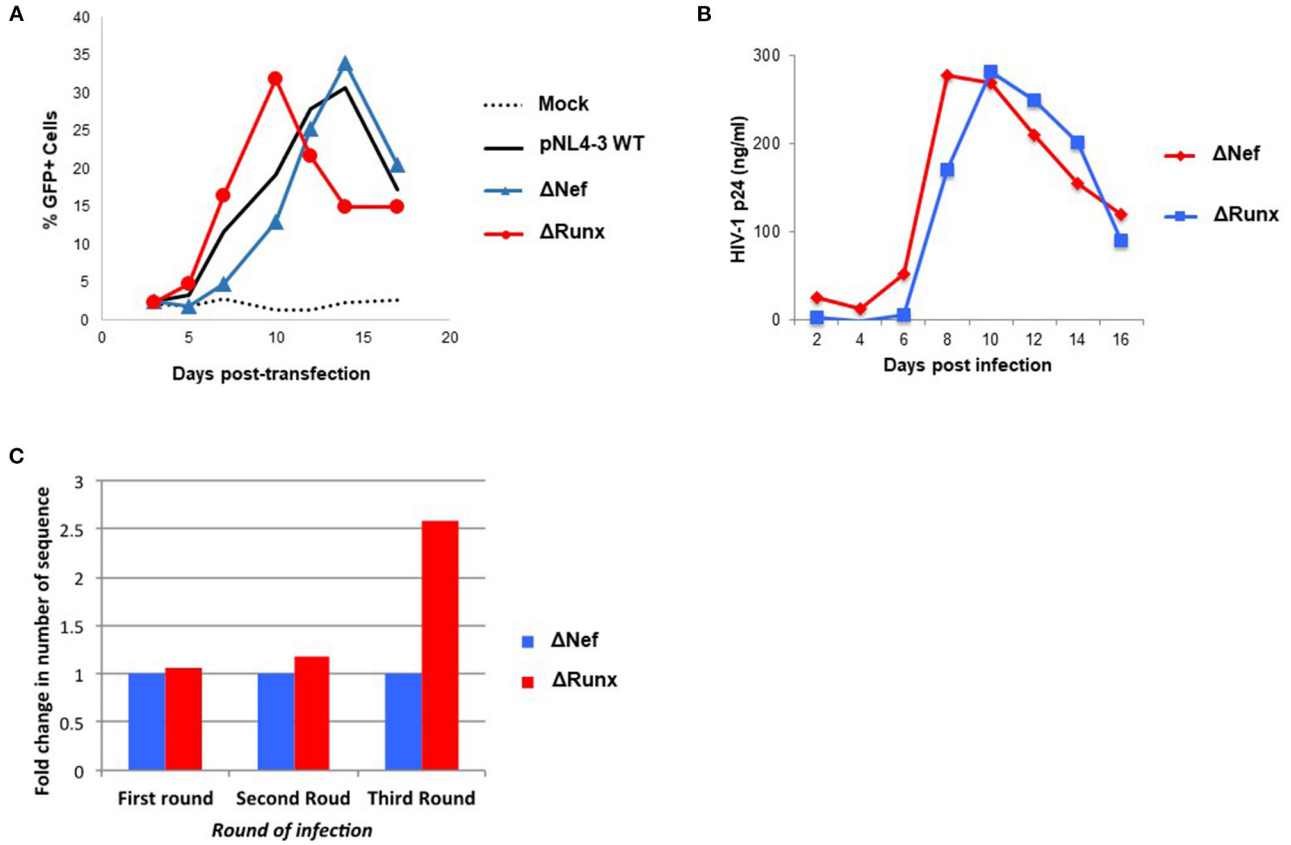

FIGURE 5 | Deletion of the RUNX1 binding site from the HIV-1 LTR enhances replication kinetics relative to WT. **(A)** J-LTR-GFP cells were transfected with pNL4-3 WT, ΔNef, ΔRUNX molecular clones and replication was monitored by measuring the percentage of GFP positive cells in the culture every 2-3 days post-transfection. **(B)** Jurkat cells were infected with equal nanogram quantities of viral stocks for ΔNef or ΔRUNX and replication was followed over time by p24 ELISA. **(C)** A competition assay was performed where J-LTR-GFP were infected with equal infectious units of the two viruses and supernatant from the peak of infection was used to infect a new round of cells. Extracellular RNA isolated from the peak of each round of infection was amplified using primers against the LTR and sequenced to be able to determine the relative abundance of each virus in each round of infection.

TA cloning and subsequent sequencing. The relative abundance of each virus (Δnef or ΔRUNX) was determined for each round (**Figure 5C**). An increase in the abundance of ΔRUNX was observed in each round (1.06-fold, 1.17-fold, and 2.5-fold). Taken together this data indicates that the ΔRUNX virus has better fitness than the Δnef control virus.

Treatment of cells containing an integrated HIV-1 LTR with RUNX1 inhibitors Ro5-3335 or alprazolam showed an increase in LTR associated STAT5 and associated transcription (**Figure 4**). To verify the effect of decreased RUNX1 binding on primary cells, PBMC from healthy donors were infected with Δnef or ΔRUNX (**Figure 6A**). Infected PBMCs at 48 h post-infection were fixed for ChIP-qPCR analysis. ChIP for RUNX1 confirmed that mutating the RUNX1 binding site results in loss of RUNX1 at the integrated HIV-1 LTR in primary cells infected de novo (**Figure 6B**). Elimination of the RUNX1 binding site increased the presence of STAT5 and subsequently CBP/P300 on the LTR (**Figures 6C,D**).

Alprazolam Increases the Global Phosphorylation and Activation of STAT5

Alprazolam induces the recruitment of the transactivator STAT5 to the HIV-1 LTR (**Figure 4C**). However, it was unclear whether this effect is specific to the HIV-1 LTR or due to broad activation of STAT5 due to RUNX1 inhibition. To examine this, Phospho-Tag Gel was used to further retard the movement of phosphorylated proteins in the gel and western blotting was performed to visual STAT5 specifically. TZMbl cells were treated with Alprazolam at the concentration of 0uM, 0.1um, 1uM, and 10uM. The increase of phosphorylation on STAT5 is dose-dependent when TZMbl cells were treated with 1uM and 10uM of Alprazolam (**Figure 7A**). To verify phosphorylation on STAT5, TZMbl (**Figure 7B**), HEK293T (**Figure 7C**) and U87MG (**Figure 7D**) cells were treated with BDZs for 48 h followed by whole-cell protein extraction and western blot for STAT5 protein. It was discovered that Alprazolam does not increase the expression of unmodified STAT5, yet it does increase the amount

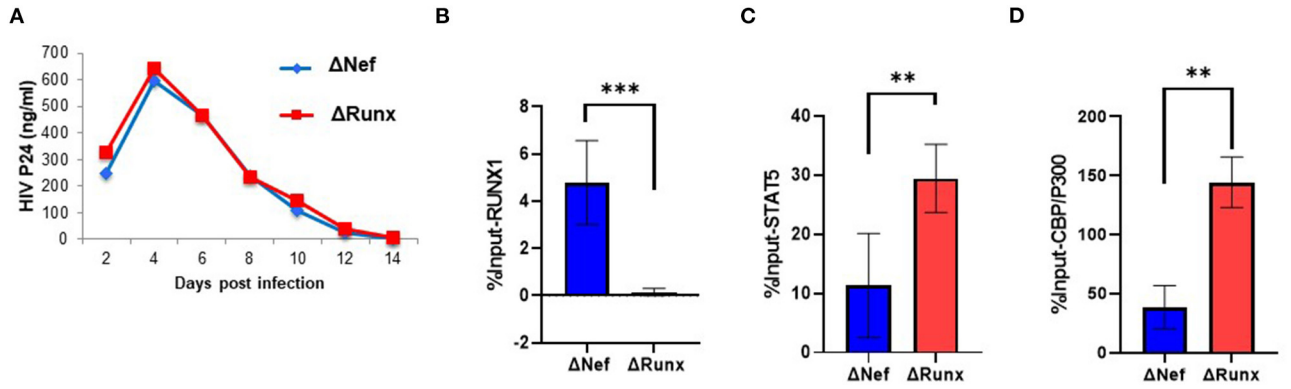

FIGURE 6 | Recruitment of STAT5 and CBP/P300 to the LTR in Primary Cells with RUNX1 binding inhibition. PBMC blasts from healthy donors were infected with ΔNef or ΔRUNX. **(A)** Viral replication was followed over time by p24 ELISA. After 48 h infection, PBMC cells were fixed and prepped for CHIP analysis with IP targeting **(B)** RUNX1 **(C)** STAT5 and **(D)** CBP/P300. $^{**}P \leq 0.01$, $^{***}P \leq 0.001$.

of Y694 phosphorylated or activated STAT5. Ro5-3335 and Clonazepam, compounds that did not induce STAT5 recruitment in our ChIP assays [**Figure 4** and (30)] did not induce STAT5 phosphorylation. Densitometry analysis reveals an elevation in the ratio of activated STAT5 to global STAT5 is induced by Alprazolam treatment (**Figure 7E**).

Tyrosine phosphorylation of STAT5 proteins enables nuclear translocation and enhances transcriptional activity. We demonstrated that Alprazolam reactivates HIV-1 transcription specifically through the recruitment of STAT5 and elevation of STAT5 phosphorylation (**Figure 7**). To confirm whether Alprazolam also upregulates STAT5 mediated transcriptional activity, we utilized the HEK-BLUE IL-2 reporter cell line, a HEK293 derived cell line that contains the IL-2 receptor, signaling cascade through the tyrosine kinases of the Janus family (Jak1/Jak3) and the STAT5-inducible gene- secreted embryonic alkaline phosphatase (SEAP). HEK-BLUE IL-2 cells were seeded in a 96 well plate and treated with Alprazolam ranging from 1μM to 5μM, 50μM Ro5-3,335 or the positive and negative controls IL-2 and TGF-ß, respectively, for 24 h. SEAP protein was then harvested from the cell suspension, stained using QUANTI-BLUE, and measured using the absorbance read at 650 nm. Alprazolam was shown to robustly enhance STAT5 mediated activation in a dose-dependent manner (**Figure 8A**). This is consistent with the ChIP data that demonstrates that although both compounds function as RUNX1 inhibitors, only Alprazolam enables the recruitment of STAT5 to the HIV-1 promoter. Western blot analysis also shows an elevation of phosphorylated STAT5 on Y694 when HEK-Blue IL-2 is treated with Alprazolam but not Ro5-3335 nor Clonazepam (**Figure 8B**).

Alprazolam Positively Affects Intracellular Production of IFNγ and TNFα in HIV-1 Gag Responsive CD8+ T-Cells From People Living With HIV-1

Evidence shows that ART treatment, while effective in reducing viral load in a patient, also negatively impacts their CD8+ T cell response (75). The induction (or "shock") of viral transcription is supposed to be followed by extermination of the reactivated cells by the crucial effector CTLs (76). Unfortunately, some LRA such as the HDAC inhibitors have been shown to suppress CTLs (77). STAT5 activation is critical in multiple immune functions, including T-cell response. We hypothesized that Alprazolam's ability to potentiate STAT5 activity might result in an improved response in CTLs. To test this, PBMCs from three HIV-1-infected subjects whose viral load had been suppressed on ART for >6 months were used to evaluate cytokine expression response to HIV-1 Gag peptides in the presence of 0.5 μM SAHA, 0.1 μM Alprazolam, the two in combination, or 0.1 μM Ro5-3335. In brief, PBMCs were treated overnight in RPMI supplemented with FBS and Glutamine. After treatment, cells were exposed to pooled HIV-1 Gag peptide and Golgi Stop (BD Biosciences), to prevent the export of cytokines, for 6 h before intracellular cytokine stating for IFNγ, IL-2, and TNFα was performed (**Figure 9**, **Supplementary Figure 2**). The addition of either SAHA, alprazolam or Ro5-3335 before Gag peptide treatment allowed us to examine changes in Gag induced cytokine expression in response to these drugs. Although SAHA treatment decreased the percentage of cells expressing IFNγ and TNFα in cytotoxic T cells in response to Gag in four of five subjects; the changes were not statistically significant. Alprazolam treatment caused more IFNγ and TNFα production than either SAHA, SAHA and Alprazolam combined, or Ro5-3335 treatment (**Figures 9A,B**). None of the treatments affected the number of cells expressing IL-2 in response to Gag (**Figure 9C**). Alprazolam has no effect on any of the three cytokine production in $CD4^+$ T cells (**Supplementary Figure 3**).

DISCUSSION

CD8+ T cells are an important part of the immune response toward viral infection (78). CD8+ T cells rely on direct (cell to cell interaction) or indirect (cytokine) stimulation mediated by CD4 T cells to differentiate into effector cells (79). Despite the

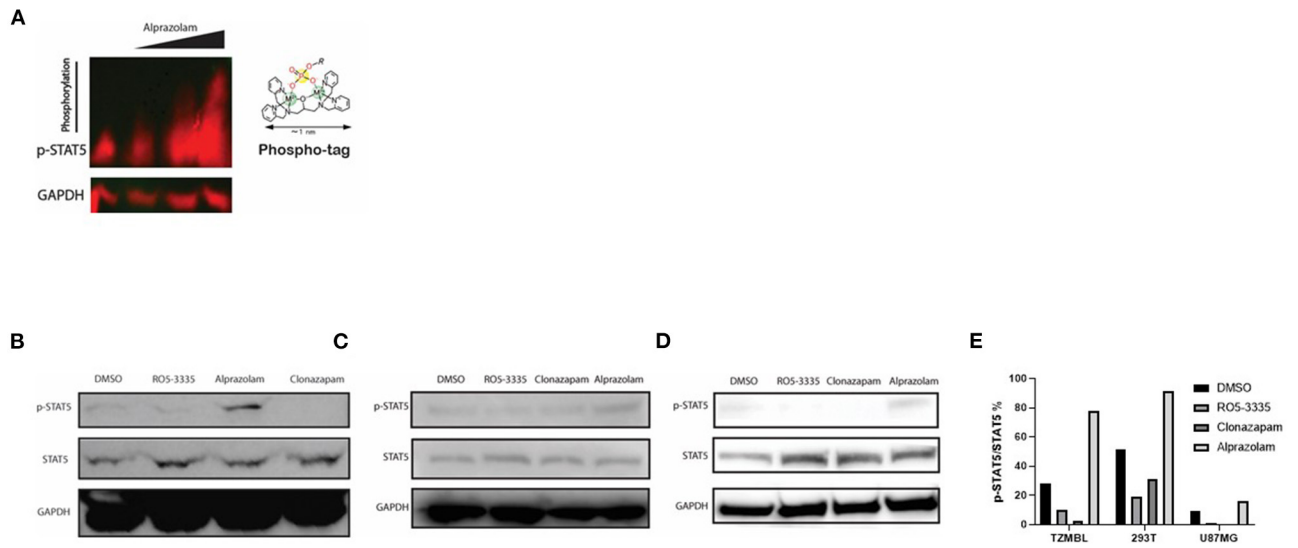

FIGURE 7 | Expression of Activated STAT5 was increased when TZMBL cells were treated with Alprazolam. TZMBl **(A, B)**, HEK293T **(C)** and U87MG **(D)** cells were treated with Benzodiazepines: 50 μM RO5-3335, 10μM Alprazolam, or 10μM Clonazepam for 48 h. Cells were lysed and whole cell lysate was collected and loaded onto an SDS-PAGE Gel **(A)** Phospho-Tag SDS-PAGE was performed to evaluate the dose effect of alprazolam on STAT5 phosphorylation. From left to right, TZMBL cells were treated with DMSO, 0.1μM, 1μM and 10μM of Alprazolam. **(B–D)** Western Blot was performed to evaluate the effect of Benzodiazepines on STAT5 expression and phosphorylation **(E)** Densitometry was performed and the ratio of activated STAT5 over global STAT5 was graphed.

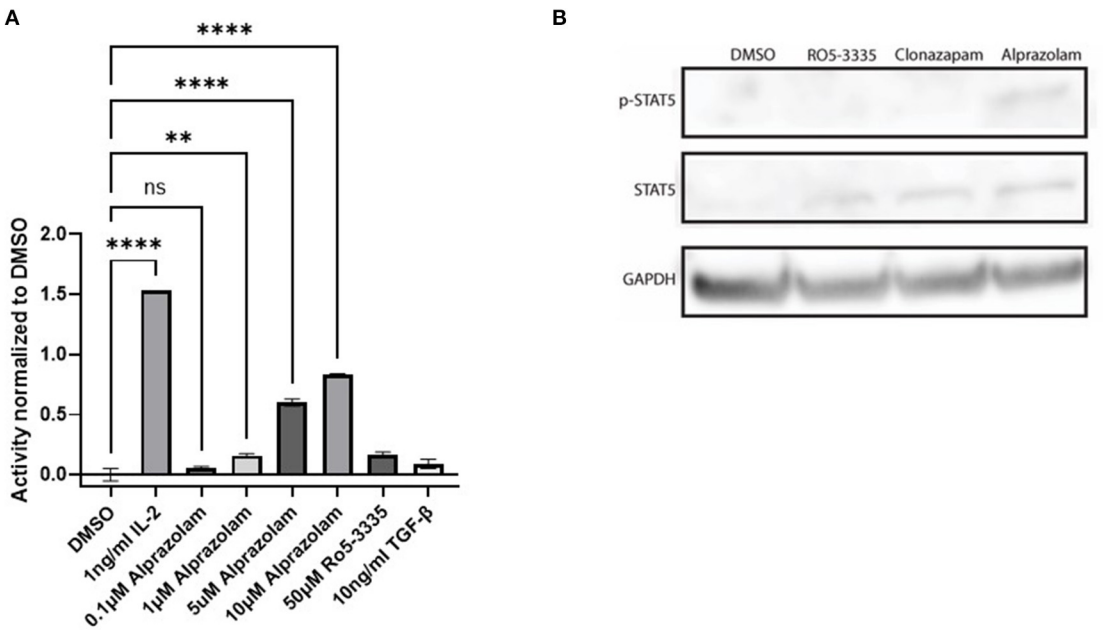

FIGURE 8 | Alprazolam activates a STAT5 sensitive reporter. HEK-Blue-IL2 cells were treated with indicated doses of IL-2, alprazolam or Ro5-3335 and incubated for 48 h at 37C 5% CO2. **(A)** Extracellular alkaline phosphatase activity was then measured by colorimetric assay. Results show the average absorbance of three replicates. $^{**}P \leq 0.01$, $^{****}P \leq 0.0001$, ns = not significant **(B)** Western blot was performed to evaluate the effect of Benzodiazepines on STAT5 expression and phosphorylation.

effectiveness of ART, HIV-1 infection has been associated with defects in cytokine production and while SAHA, a promising LRA, demonstrates reactivating potential for latent transcription, the negative impact HDACi impose on the CTL response does not align with the objective of eradicating the HIV-1 reservoir (15–17). Alprazolam has been shown to robustly reactivate

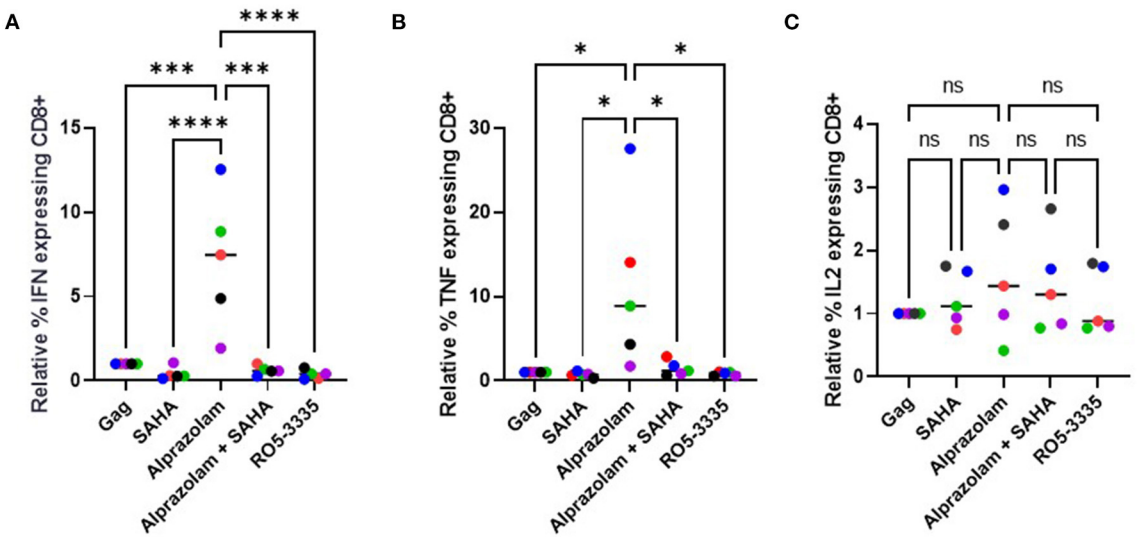

FIGURE 9 | The effect of alprazolam and SAHA on Gag specific CTL response. PBMCs from 5 HIV-1 positive individuals suppressed on therapy were treated with vehicle control, 500 nM SAHA, 100 nM alprazolam, SAHA plus alprazolam or 100nM Ro5-3335 overnight and then exposed to a set overlapping Gag peptides in the presence of Brefaldin A for 6 h. Cells were stained for live/dead marker, CD3, CD4, CD8 and cytokines of interest. The number of **(A)** IFNγ, **(B)** TNFα **(C)** IL-2 expressing CD8+ T-cells for each condition is shown normalized to untreated control. $^{*}P \leq 0.05$, $^{***}P \leq 0.001$, $^{****}P \leq 0.0001$, ns = not significant.

latent transcription (30). Our data suggest that Alprazolam may have additional utility due to the activation and recruitment of STAT5 to the HIV-1 LTR while SAHA negatively impacts the recruitment of STAT5. STAT5 binding to the HIV-1 promoter is directly associated with transcriptional activation of the HIV-1 genome. Interestingly, Alprazolam can also activate STAT5 in non-HIV-1 infected cells, therefore, despite CD8+ T cells being a non-target to HIV-1 infection, the activation of STAT5 in CD8 cells may have allowed increased biding of STAT5 on the IFNγ promoter and jump-start cytokine production. The ability to activate CD8 T cells without increased cytokine production from CD4+ T cells is beneficial from a therapeutic standpoint since CD4 T cell's immunoregulatory function is often dysregulated and HIV-1 disease progression is associated with the loss of CD4 T cells (**Supplementary Figure 3**) A study has demonstrated that a subset of ART-naive patients was unable to functionally activate STAT5 in response to IL-2 stimulation on their CD8+ T cells *ex vivo* (48). The use of Alprazolam as an alternative method to activate STAT5 may potentially help with patients who are resistant to the therapy.

STAT5 activation can occur in multiple parts of the HIV-1 life cycle. Interaction between the HIV-1 viral envelope gp120 and the CD4 receptor can induce STAT5 activation and DNA binding (57). HIV-1 Nef also indirectly activates STATs (60). During viral infection, interferons (IFNs) induce transcription of interferon-stimulated genes (ISG) through the activation of STATs (80). Though STATs are crucial for antiviral and inflammatory responses, HIV-1 may have evolved to limit STAT5 activation to evade immune clearance, since it has been shown that HIV-1 infected cells do not induce high interferon levels (81) and STAT5 expression is reduced in HIV-1 patients (49). Impaired production of cytokines can be a predictor of the morality of HIV-1 patients. patients with more robust cytokine production are associated with longevity as STAT5 activation in CD8+ T Cells promotes its effector and memory development (82, 83).

It has been shown that SAHA and other HDACs impair CTL function by inhibiting IFNγ production (80). The literature suggests that Alprazolam enhances immune function (84). It has been shown that when BDZs are taken at physiological levels, they have immunoprotective effects. BDZs have also been shown to enhance the antibody response through stimulating helper T cell functions in restraint-stressed mice (85). Furthermore, Alprazolam and midazolam can decrease the adverse effect of surgical stress on the thymus and spleen in mice and maintain their cellularity (86, 87). In addition, Alprazolam protected and enhanced the immune system by increasing the activity of natural killer cells and enhancing the proliferation of lymphocytes in mice (88). Diazepam has been reported to negatively impact phagocytic activity in polymorphonuclear cells (PMN) and monocytes, triazolobenzoldiazepines like alprazolam and triazolam was shown to enhance T cell function and antibacterial activity (89). These seemingly conflicting results may be due to the ability of only a certain subclass of BDZs to bind to the second potential target site on RUNX1 (**Figure 1**) a prediction that correlates with modulation of STAT5 activity both on the LTR and in the whole cell.

In addition to viral transcriptional reactivation and CTL response enhancement, to achieve the goal of viral eradication, it may be important to target immune checkpoints as well. T cell exhaustion due to chronic inflammation can reduce the polyfunctionality of CD8+ T cells. It has been shown that elevated STAT5 activation in CD8+ T cells is associated with the decreased immune-suppressive capability of PD-1 (90).

Therefore, the usage of Alprazolam may have improved immune response also by inhibiting the suppressive impact of exhaustion markers. Combining Alprazolam with other exhaustion marker inhibitors may further benefit the cause of reducing the size of HIV-1 latency reservoir.

Chronic inflammation caused by HIV-1 infection affects the CNS as well. Neuroinflammation is a major factor of several neurodegenerative disorders including neuroHIV-1 (91–95). Neuroinflammation can contribute to neuronal and immune damage through the chronic activation of microglia and perivascular macrophages of the CNS (15, 35–38). Myeloid cells are long-lived and resistant to cell death caused by infection (35, 37), making them a platform to drive neuroinflammatory events in subjects on suppressive ART therapy. Due to the prolonged life span for patients on ART the prevalence of neurologic issues has increased. Engagement of benzodiazepine receptors, such as those found on microglia and astrocytes, is associated with decreased cytotoxicity (96). Modulation of STAT5 activity secondary to RUNX1 inhibition by Alprazolam was shown in U87MG, an astrocyte cell line, and may be a strategy for addressing this chronic neuroinflammatory state. HIV-1 infected individuals are more likely to be prescribed BDZs than the general population (97, 98), BDZ use is associated with the risk of HIV-1-1 infection (99, 100) and BDZs are a commonly abused substance (101). Given the overlap of substance use and HIV-1 infection, combined with BDZ prescribing practices, it is critical to understand how these drugs may be altering both epigenetics and immune cell function.

METHOD

Ligand Docking

Compounds were built and energy-minimized using the MM2 force field (ChemBio3D Ultra 13.0) with RMS gradient of 0.01 and number of alterations of 104. The minimized structures were then saved as pdb files for the docking simulations. Autodock tools graphical interface was then used to prepare the ligands for docking (102, 103).

The protein structures (RUNX1 unbound, pdb: 1EAN and liganded RUNX1, pdb: 3WTS) (62) were downloaded from the protein data bank then prepared by Autodock tools graphical interface (MGtools 1.5.6rc3) where nonpolar hydrogens were merged, Kollman charges were added, and Gasteiger charges were calculated. The grid box for the docking search was set to include the whole protein structure for the docking search.

AutoGrid 4.2 algorithm (102, 103) was used to evaluate the binding energies between the ligands and the protein and to generate the energy maps for the docking run. For high accuracy mode, the maximum number of evaluations (25 × 106) were used. hundred runs were generated for each ligand by using Autodock 4.2 Lamarckian genetic algorithm for the searches. Cluster analysis was performed on docked results, with a root-mean-square tolerance of 0.5 Å. And the lowest energy conformer from the highest populated cluster was selected as a binding pose for each ligand. The fitting of each pose was independently corrected and validated using POSIT (OpenEye Scientific Software, Santa Fe, NM. http://www.eyesopen.com).

Cell Culture, Treatments, and Transfections

J-LTR-GFP (Jurkat LTR-GFP) and Jurkat cells were propagated in Roswell Memorial Park Institute (RPMI) media supplemented with 10% Fetal Bovine Serum (FBS), 100 U/mL penicillin, 100 ug/mL streptomycin, and 0.3 mg/mL L-glutamine. J-LTR-GFP cells are Jurkat T-cell based reporter cells that contain an integrated HIV-1 LTR driven GFP and were obtained through the NIH AIDS Reagent Program, Division of AIDS, NIAID, NIH (#11587) from Dr. Olaf Kutsch.

TZM-bl cells (NIH-AIDS Reagent Program, catalog number 8129, NIH, Bethesda, MD) and 293T cells (ATCC) were maintained in Dulbecco's modified Eagle's medium (DMEM; HyClone, GE Healthcare Life Sciences, Chicago, IL) supplemented with 10% FBS, 100 units ml−1 penicillin,100 μg ml−1 streptomycin and 0.3 mg ml−1 L-glutamine (PSG, Gibco, Thermo Fisher Scientific

To transfect 293T with IL17-luciferase reporter, Lipofectamine LTX (Invitrogen) was used according to the manufacturer's instructions.

All cells were grown at 37°C with 5% CO2.

FDA approved BDZs were obtained from (Sigma-Aldrich): Alprazolam (A0357000), clonazepam (C1277. SAHA (SML0061).

Luciferase Assay

For the determination of HIV-1 LTR reactivation in 293T cells cultures were treated with BDZs or SAHA for 48 hours. Following treatment, cell lysates were prepared using GloLysis buffer (Promega) and luciferase activity was determined using BrightGlo Luciferase Reagent (Promega) and read on a spectrophotometer following manufacturer's instructions. For the determination of IL17 promoter activity, 15,000 293T cells were seeded in each well of a 96 well-plate and transfected 24 h later with a plasmid containing the IL17 promoter controlling the expression of firefly luciferase. Twenty-four h post-transfection cells were treated with BDZs and SAHA. Twenty-four h post-treatment cell lysates were prepared using GloLysis buffer (Promega) and luciferase activity was determined using BrightGlo Luciferase Reagent (Promega) and read on a spectrophotometer following manufacturer's instructions: Dual-Glo Luciferase Assay System (Promega, E2920).

Measurement of RUNX responsive genes. PBMCs from three HIV-1-1 patients who had been suppressed on therapy for <6 months were generously provided by Dr. Frank Maldarelli from the NIH. 10 × 106 PBMCs were divided between three conditions: DMSO control, 50μM Ro5-3335, and 10 μM Alprazolam. PBMCs were cultured in RPMI with 10% FBS and the indicated drugs for 24 h. RNA was extracted from the cells and used for RT-qPCR to detect HIV-1 Gag mRNA. RNA was extracted using Trizol reagent (Invitrogen) following the manufacturer's protocol. Following reverse transcription, the samples were diluted 1:50, and 2.5 microliters were used for quantitative PCR in a BioRad CFX384 qPCR machine. All mRNA analyses were normalized to GAPDH. Nucleic acid amplification was tracked by the SYBR Green method.

The following primer pairs were used for detection:

T-bet 5′GGTTGGAGGACACCGACTAA, 5′ATCCTTCT TGAGCCCCACTT,

IL-2 5′AAACTCACCAGGATGCTCAC, 5′GTCCCTGGGTCTTAAGTGAAAG,

APOBEC3G 5′CCGAGGACCCGAAGGTTAC, 5′TCCAACAGTGCTGAAATTCG,

APOBEC3C 5′AGCGCTTCAGAAAAGAGTGG, 5′AAGTTTCGTTCCGATCGTTG,

IL-7R 5′CCCTCGTGGAGGTAAAGTGC, 5′CCTTCCCGATAGACGACACTC,

GAPDH 5′GCTCACTGGCATGGCCTTCCGTGT, 5′TGGAGGAGTGGGTGTCGCTGTTGA.

Replication Assay

JLTRG cells were transfected with 1ug of the indicated pNL4-3 molecular clones per 1 × 106 cells. Briefly, cells were incubated with DNA in 0.7ug/ml DEAE-Dextran for 15min at 37C. 1 × STBS was added and cell pellets were resuspended in RPMI-10 in a 24-well plate. Cells were collected every 2 to 3 days, fixed in 1% formaldehyde, and analyzed for %GFP positive cells by flow cytometry.

Generation of RUNX1 binding site mutant virus. A plasmid that contains HIV-1 LTR with mutation in nef gene that does not express nef protein (p398.6) was used as a shuttle vector (104, 105). Site-directed mutagenesis was performed to alter the sequence of the promoter at the 3′ U3 region on the Shuttle vector to obtain mutated binding site for RUNX1. The mutated plasmid was transformed into *E. coli* and selected clones were sent for sequencing. Positive clones were defined as p398.6 mutant RUNX1 binding site (p398.6 mutRUNX BS). Then, to clone the mutant promoter back into pNL4-3 (the entire proviral HIV-1 plasmid), restriction enzymes (NcoI and BamHI) were used to cut the altered sequence from the shuttle vector and pNL4-3 was also cut with the same restriction enzymes. Both plasmid fragments were gel extracted and ligated back into the pNL4-3 vector with T4 ligase. The mutant plasmid was transformed into E. coli and selected colonies were verified by sequencing. A new RUNX1 mutant binding site proviral plasmid (HIV-1Δnef mutRUNX BS) was successfully constructed.

Primers for site-directed mutagenesis:

RUNXMut Fwd 5′atccttgatctgtggatctcacacacacaaggctacttcc

RUNXMut Rev 5′ggaagtagccttgtgtgtgtgagatccacagatcaaggat.

Competition Assay

ΔRUNX and Δnef control was used to infect J-LTR-GFP with an equal ratio of infectious particles. Viral stocks were generated by transfection of HEK 293T cells with the pNL4-3 mutants described above. Forty-eight h post-transfection supernatant was harvested and filtered through a 0.2μM filter. Viral stocks were quantified by p24 ELISA and TZMbl beta-galactosidase assay to determine the Gag concentration and infectious units/ml of stock, respectively. The virus was were washed from cells after 24 h and viral growth was tested over 14 days. The peak day is assessed by measuring GFP percentage every other day. At the peak day, the sample taken from the supernatant was used to extract RNA from using Trizol, and 1ml of the supernatant containing virus was used to infect non-infected JLTR-G cells to start the second round of infection. The second round of infection is also assessed for 14 days. Then at the peak day, a sample is taken from the supernatant for RNA extraction and 1ml from the supernatant is used to infect non-infected JLTR-G to start the third round of infection. The peak day is also assessed at the third round of infection to take a sample for RNA extraction. Reverse transcription (RT) reaction was done for each round of infection and then PCR was performed using primers that were designed to amplify the region that flanks the RUNX1 binding site. After extracting the PCR product, TA cloning was performed by inserting the PCR product in a TA vector. Then after bacterial transformation, white clones (which were not stained with X-gal substrate) were chosen to send to sequencing At least 75 clones from each round of infection were sent to be sequenced. Sequence results were analyzed using Clustal W multiple alignments to quantify and compare clones having ΔRUNX vs. Δnef control.

Primers for sequencing of

For 5′TTCAGCTACCACCGCTTGAG

Rev 5′ GTACTCCGGATGCAGCTCTC.

ChIP

For ChIP analysis, TZM-bl or PBMC were treated with different treatments and fixed for chip according to manufacturer's protocol: PierceTM Agarose ChIP kit (ThermoFisher, catalog number 26156). All antibodies used were diluted 1:100. Histone H3 (acetyl K9) antibody [AH3-120]-ChIP Grade (Abcam, ab12179). Pierce p300/CBP (CREB-Binding Protein) antibody (NM11) (Thermo scientific, MA5-13634). Human/Mouse STAT5a/b Pan Specific Antibody (R&D Systems, AF2168).

Primers against HIV-1 U3 LTR were used for qPCR:

F 5′CTAGCATTTCGTCACATGGCCCGAGA3′

R 5′GTGGGTTCCCTAGTTAGCCAGAG 3′.

P24 ELISA

P24 ELISA was performed using the ZeptoMetrix HIV-1 P24 Antigen Elisa Kit using the vendor suggested protocol.

HEK-BLUE IL-2 Assay

HEK-BLUE IL-2 cells were acquired from Invitrogen (HKB-iL2). Growth Media: DMEM, 4.5 g/l glucose, 2 mM L-glutamine, 10% (v/v) fetal bovine serum (FBS), 100 U/ml penicillin, 100 mg/ml streptomycin,100 mg/ml Normocin. HEK-BLUE IL-2 cells were generated by transfecting HEK293 cells with the human IL-2Rα, IL-2Rβ, and IL-2Rγ genes, along with the human JAK3 and STAT5 genes to obtain a fully active IL-2 signaling pathway as well as a reporter gene expressing a secreted embryonic alkaline phosphatase (SEAP) under the control of the IFN-b minimal promoter fused to four STAT5 binding sites. HEK BLUE IL-2 Cells were maintained in growth media and detached from the culture flask through gentle washes using PBS. Cells were seeded in 96 well-plates and treated with appropriate drugs and then incubated in a 37C incubator for 24 or 48 h before cell suspension is harvested for SEAP quantification using QUANTI-BLUE, which is a solution that changes the cell suspension color from pink to blue in the presence of alkaline phosphatase.

Intracellular cytokine staining. PBMCs from HIV-1 positive individuals suppressed on therapy for >6 months were thawed, resuspended in 1 × 106 per ml in RPMI/IL2 (RPMI + 10% FBS, Penn/Strep, L-glutamine, 30 IU/ml IL-2), had 1 ml of

cell suspension placed in a 12 × 75 mm falcon tube per condition and allowed to rest overnight at 37C with 5% CO2. SAHA, Alprazolam, or vehicle control were added to the tubes as appropriate and incubated for 4 h. After incubation with drugs, anti-CD29 and anti-49d co-stimulatory antibodies (BD Biosciences) were added along with pooled HIV-1-1 B Gag peptides (AIDS Reagent) at 2ug/ml final concentration per peptide. One h after the addition of peptides BD Golgi Stop was added and PBMCs were incubated overnight at 37C with 5% CO2. PBMCs were then stained for CD3, CD4, CD8, and viability (Zombie Yellow, BioLegend) before being permeabilized with BD Cytofix/Cytoperm reagent. Permeabilized cells were stained for IL-2 and IFNγ before being fixed and analyzed by flow cytometry.

ETHICAL STATEMENT

PBMCs for intracellular cytokine staining were obtained from venous blood draw of HIV-1 positive individuals approved under the University of the Sciences' protocol (IRB protocol 900702-3 and 797649-3). Blood draws were performed at the Smith Center for Urban Health and Infectious Disease, East Orange, NJ, and written informed consent was obtained for the collection of blood donations from participating subjects.

PBMCs for the analysis of RUNX1 responsive genes were obtained from Dr. Frank Maldarelli and the NIH Clinical Center. The human sample collection protocol was approved by the NIH Clinical Center Institutional Review Board as part of a separate ongoing study. Written informed consent was obtained in all cases and all applicable protections of patient rights and privacy applied. For this study, specific samples were requested from the sample bank based on the given criteria.

DATA AVAILABILITY STATEMENT

The original contributions presented in the study are included in the article/**Supplementary Material**, further inquiries can be directed to the corresponding authors.

ETHICS STATEMENT

The studies involving human participants were reviewed and approved by University of the Sciences Review Board (IRB protocol 900702-3 and 467 797649-3). The patients/participants provided their written informed consent to participate in this study.

AUTHOR CONTRIBUTIONS

AL, WE, and AA performed experiments, analyzed data, and designed experiments. AS and RV aided in experiments. AL and ZK wrote the manuscript. SC oversaw and designed the docking experiments and aided in writing the manuscript. ZK oversaw and aided in the design of the experiments and performed analysis. RV aided in experimental design and manuscript writing. All authors contributed to the article and approved the submitted version.

FUNDING

This work was supported by an NIDA/NIH grant (DP2 DA044550-01) to ZK, Drexel University College of Medicine internal funds to ZK, and NIAID/NIH grant (R01 AI150491) to SC.

ACKNOWLEDGMENTS

The authors would like to thank Dr. Frank Maldarelli and the NIH Clinical Center for providing human blood sample.

SUPPLEMENTARY MATERIAL

The Supplementary Material for this article can be found online at: https://www.frontiersin.org/articles/10.3389/fneur.2021.663793/full#supplementary-material

REFERENCES

1. *Global HIV-1 & AIDS Statistics — 2020 Fact Sheet*. Geneva: UNAIDS (2020).
2. Hammer SM, Squires KE, Hughes MD, Grimes JM, Demeter LM, Currier JS, et al. A controlled trial of two nucleoside analogues plus indinavir in persons with human immunodeficiency virus infection and CD4 cell counts of 200 per cubic millimeter or less. *New Eng J Med.* (1997) 337:725–33. doi: 10.1056/NEJM199709113371101
3. Mbonye U, Karn J. Transcriptional control of HIV-1 latency: cellular signaling pathways, epigenetics, happenstance and the hope for a cure. *Virology.* (2014) 454–455:328–39. doi: 10.1016/j.virol.2014.02.008
4. Karn J. The molecular biology of HIV-1 latency: breaking and restoring the Tat-dependent transcriptional circuit. *Curr Opin HIV AIDS.* (2011) 4:11. doi: 10.1097/COH.0b013e328340ffbb
5. Pierson T, McArthur J, Siliciano RF. Reservoirs for HIV-1-1: mechanisms for viral persistence in the presence of antiviral immune responses and antiretroviral therapy. *Ann Rev Immunol.* (2000) 18:665–708. doi: 10.1146/annurev.immunol.18.1.665
6. Finzi D, Blankson J, Siliciano JD, Margolick JB, Chadwick K, Pierson T, et al. Latent infection of CD4+ T cells provides a mechanism for lifelong persistence of HIV-1-1, even in patients on effective combination therapy. *Nat Med.* (1999) 5:512–7. doi: 10.1038/8394
7. Shukla A, Ramirez NP, D'Orso I. HIV-1-1 proviral transcription and latency in the new era. *Viruses.* (2020) 12:555. doi: 10.3390/v12050555. [Epub ahead of print].s
8. Dufour C, Gantner P, Fromentin R, Chomont N. The multifaceted nature of HIV-1 latency. *J Clin Invest.* (2020) 130:3381–90. doi: 10.1172/JCI136227
9. Margolis DM, Garcia JV, Hazuda DJ, Haynes BF. Latency reversal and viral clearance to cure HIV-1-1. *Science.* (2016) 353: aaf6517. doi: 10.1126/science.aaf6517
10. Archin NM, Sung JM, Garrido C, Soriano-Sarabia N, Margolis DM. Eradicating HIV-1-1 infection: seeking to clear a persistent pathogen. *Nat Rev Microbiol.* (2014) 12:750–64. doi: 10.1038/nrmicro3352
11. Margolis DM, Archin NM, Cohen MS, Eron JJ, Ferrari G, Garcia JV, et al. Curing HIV-1: seeking to target and clear persistent infection. *Cell.* (2020) 181:189–206. doi: 10.1016/j.cell.2020.03.005
12. Spivak AM, Planelles V. HIV-1-1 eradication: early trials (and tribulations). *Trend Mol Med.* (2016) 22:10–27. doi: 10.1016/j.molmed.2015.11.004

13. Rasmussen TA, Sogaard OS. Clinical interventions in HIV-1 cure research. *Adv Exp Med Biol.* (2018) 1075:285–318. doi: 10.1007/978-981-13-0484-2_12
14. Ait-Ammar A, Kula A, Darcis G, Verdikt R, De Wit S, Gautier V, et al. Current status of latency reversing agents facing the heterogeneity of HIV-1-1 cellular and tissue reservoirs. *Front Microbiol.* (2019) 10:3060. doi: 10.3389/fmicb.2019.03060
15. Jones RB, O'Connor R, Mueller S, Foley M, Szeto GL, Karel D, et al. Histone deacetylase inhibitors impair the elimination of HIV-1-infected cells by cytotoxic T-Lymphocytes. *PLoS Pathog.* (2014) 10:e1004287. doi: 10.1371/journal.ppat.1004287
16. Kleinman AJ, Xu C, Cottrell ML, Sivanandham R, Brocca-Cofano E, Dunsmore T, et al. Pharmacokinetics and immunological effects of romidepsin in rhesus macaques. *Front Immunol.* (2020) 11:579158. doi: 10.3389/fimmu.2020.579158
17. Rosas-Umbert M, Ruiz-Riol M, Fernandez MA, Marszalek M, Coll P, Manzardo C, et al. *In vivo* effects of romidepsin on T-Cell activation, apoptosis and function in the BCN02 HIV-1-1 Kick&Kill clinical trial. *Front Immunol.* (2020) 11:418. doi: 10.3389/fimmu.2020.00418
18. Coffman J. Runx transcription factors and the developmental balance between cell proliferation and differentiation. *Cell Biol Int.* (2003) 27:315–24. doi: 10.1016/S1065-6995(03)00018-0
19. Mevel R, Draper JE, Lie ALM, Kouskoff V, Lacaud G. RUNX transcription factors: orchestrators of development. *Development.* (2019) 146:dev148296. doi: 10.1242/dev.148296
20. Watanabe T, Yoshida N, Satake M. Biological implications of filamin A-bound PEBP2beta/CBFbeta retention in the cytoplasm. *Crit Rev Eukaryot Gene Expr.* (2005) 15:197–206. doi: 10.1615/CritRevEukarGeneExpr.v15.i3.20
21. Hoogenkamp M, Lichtinger M, Krysinska H, Lancrin C, Clarke D, Williamson A, et al. Early chromatin unfolding by RUNX1: a molecular explanation for differential requirements during specification versus maintenance of the hematopoietic gene expression program. *Blood.* (2009) 114:299–309. doi: 10.1182/blood-2008-11-191890
22. Huang G, Zhang P, Hirai H, Elf S, Yan X, Chen Z, et al. PU.1 is a major downstream target of AML1 (RUNX1) in adult mouse hematopoiesis. *Nat Genet.* (2008) 40:51–60. doi: 10.1038/ng.2007.7
23. Lichtinger M, Ingram R, Hannah R, Muller D, Clarke D, Assi SA, et al. RUNX1 reshapes the epigenetic landscape at the onset of haematopoiesis. *EMBO J.* (2012) 31:4318–33. doi: 10.1038/emboj.2012.275
24. Guo H, Friedman AD. Phosphorylation of RUNX1 by cyclin-dependent kinase reduces direct interaction with HDAC1 and HDAC3. *J Biol Chem.* (2011) 286:208–15. doi: 10.1074/jbc.M110.149013
25. Reed-Inderbitzin E, Moreno-Miralles I, Vanden-Eynden SK, Xie J, Lutterbach B, Durst-Goodwin KL, et al. RUNX1 associates with histone deacetylases and SUV39H1 to repress transcription. *Oncogene.* (2006) 25:5777–86. doi: 10.1038/sj.onc.1209591
26. Jiang H, Zhang F, Kurosu T, Peterlin BM. Runx1 binds positive transcription elongation factor b and represses transcriptional elongation by RNA polymerase II: possible mechanism of CD4 silencing. *Mol Cell Biol.* (2005) 25:10675–83. doi: 10.1128/MCB.25.24.10675-10683.2005
27. Goldfarb AN. Megakaryocytic programming by a transcriptional regulatory loop: a circle connecting RUNX1, GATA-1, and P-TEFb. *J Cell Biochem.* (2009) 107:377–82. doi: 10.1002/jcb.22142
28. Jiang H, Peterlin BM. Differential chromatin looping regulates CD4 expression in immature thymocytes. *Mol Cell Biol.* (2008) 28:907–12. doi: 10.1128/MCB.00909-07
29. Klase Z, Yedavalli VS, Houzet L, Perkins M, Maldarelli F, Brenchley J, et al. Activation of HIV-1-1 from latent infection via synergy of RUNX1 inhibitor Ro5-3335 and SAHA. *PLoS Pathog.* (2014) 10:e1003997. doi: 10.1371/journal.ppat.1003997
30. Elbezanti W, Lin A, Schirling A, Jackson A, Marshall M, Duyne RV, et al. Benzodiazepines drive alteration of chromatin at the integrated HIV-1-1 LTViruses R. (2020) 12:191. doi: 10.3390/v12020191
31. Hsu MC, Schutt AD, Holly M, Slice LW, Sherman MI, Richman DD, et al. Inhibition of HIV-1 replication in acute and chronic infections in vitro by a Tat antagonist. *Science.* (1991) 254:1799–802. doi: 10.1126/science.1763331
32. Griffin CE, 3rd, Kaye AM, Bueno FR, Kaye AD. Benzodiazepine pharmacology and central nervous system-mediated effects. *Ochsner J.* (2013) 13:214–23.
33. Alavijeh MS, Chishty M, Qaiser MZ, Palmer AM. Drug metabolism and pharmacokinetics, the blood-brain barrier, and central nervous system drug discovery. *NeuroRx.* (2005) 2:554–71. doi: 10.1602/neurorx.2.4.554
34. Avalos CR, Abreu CM, Queen SE, Li M, Price S, Shirk EN, et al. Brain macrophages in simian immunodeficiency virus-infected, antiretroviral-suppressed macaques: a functional latent reservoir. *Mbio.* (2017) 8:e01186-17. doi: 10.1128/mBio.01186-17
35. Mallard J, Williams K. An SIV macaque model of SIV and HAND: the need for adjunctive therapies in HIV-1 that target activated monocytes and macrophages. *J Neurovirol.* (2018) 24:213–9. doi: 10.1007/s13365-018-0616-6
36. Rappaport J, Volsky DJ. Role of the macrophage in HIV-1-associated neurocognitive disorders and other comorbidities in patients on effective antiretroviral treatment. *J Neurovirol.* (2015) 21:235–41. doi: 10.1007/s13365-015-0346-y
37. Navia BA, Cho ES, Petito CK, Price RW. The AIDS dementia complex: II. Neuropathology. *Ann Neurol.* (1986) 19:525–35. doi: 10.1002/ana.410190603
38. Clayton KL, Garcia JV, Clements JE, Walker BD. HIV-1 infection of macrophages: implications for pathogenesis and cure. *Pathog Immun.* (2017) 2:179–92. doi: 10.20411/pai.v2i2.204
39. Yadav A, Collman RG. CNS inflammation and macrophage/microglial biology associated with HIV-1-1 infection. *J Neuroimmune Pharmacol.* (2009) 4:430–47. doi: 10.1007/s11481-009-9174-2
40. Minagar A, Shapshak P, Fujimura R, Ownby R, Heyes M, Eisdorfer C. The role of macrophage/microglia and astrocytes in the pathogenesis of three neurologic disorders: HIV-1-associated dementia, Alzheimer disease, multiple sclerosis. *J Neurol Sci.* (2002) 202:13–23. doi: 10.1016/S0022-510X(02)00207-1
41. Williams DW, Calderon TM, Lopez L, Carvallo-Torres L, Gaskill PJ, Eugenin EA, et al. Mechanisms of HIV-1 entry into the CNS: increased sensitivity of HIV-1 infected CD14(+)CD16(+) monocytes to CCL2 and key roles of CCR2, JAM-A, and ALCAM in Diapedesis. *PLoS ONE.* (2013) 8:e69270. doi: 10.1371/journal.pone.0069270
42. Crowe S, Zhu T, Muller WA. The contribution of monocyte infection and trafficking to viral persistence, and maintenance of the viral reservoir in HIV-1 infection. *J Leukoc Biol.* (2003) 74:635–41. doi: 10.1189/jlb.0503204
43. Joseph SB, Arrildt KT, Sturdevant CB, Swanstrom R. HIV-1-1 target cells in the CNS. *J Neurovirol.* (2015) 21:276–89. doi: 10.1007/s13365-014-0287-x
44. Saylor D, Dickens AM, Sacktor N, Haughey N, Slusher B, Pletnikov M, et al. HIV-1-associated neurocognitive disorder - pathogenesis and prospects for treatment. *Nat Rev Neurol.* (2016) 12:309. doi: 10.1038/nrneurol.2016.27
45. Thakur KT, Boubour A, Saylor D, Das M, Bearden DR, Birbeck GL. Global HIV-1 neurology: a comprehensive review. *AIDS.* (2019) 33:163–184. doi: 10.1097/QAD.0000000000001796
46. Walsh JG, Reinke SN, Mamik MK, McKenzie BA, Maingat F, Branton WG, et al. Rapid inflammasome activation in microglia contributes to brain disease in HIV-1/AID. *Retrovirology.* (2014) 11:35. doi: 10.1186/1742-4690-11-35
47. Rubin LH, Sacktor N, Creighton J, Du Y, Endres CJ, Pomper MG, et al. Microglial activation is inversely associated with cognition in individuals living with HIV-1 on effective antiretroviral therapy. *AIDS.* (2018) 32:1661–7. doi: 10.1097/QAD.0000000000001858
48. Ulfhammer G, Eden A, Mellgren A, Fuchs D, Zetterberg H, Hagberg L, et al. Persistent central nervous system immune activation following more than 10 years of effective HIV-1 antiretroviral treatment. *AIDS.* (2018) 32:2171–8. doi: 10.1097/QAD.0000000000001950
49. Cave BJ, Norman M, Flynn A, Townsend J, Wakerley JB, Tortonese JD. Prolactin-induced activation of STAT5 within the hypothalamic arcuate nucleus. *Neuroreport.* (2005) 16:1423–6. doi: 10.1097/01.wnr.0000176516.19347.6f
50. Ma FY, Anderson GM, Gunn TD, Goffin V, Grattan DR, Bunn JS. Prolactin specifically activates signal transducer and activator of transcription 5b in neuroendocrine dopaminergic neurons. *Endocrinology.* (2005) 146:5112–9. doi: 10.1210/en.2005-0770

51. Bennett E, Mcguinness L, Gevers EF, Thomas GB, Robinson CAF I, Davey HW, et al. Hypothalamic STAT proteins: regulation of somatostatin neurones by growth hormone via STAT5b. *J Neuroendocrinol.* (2005) 17:186–94. doi: 10.1111/j.1365-2826.2005.01296.x
52. Pericle F, Pinto LA, Hicks S, Kirken RA, Sconocchia G, Rusnak J, et al. HIV-1-1 infection induces a selective reduction in STAT5 protein expression. *J Immunol.* (1998) 160:28–31.
53. Angel JB, High K, Rhame F, Brand D, Whitmore JB, Agosti JM, et al. Phase III study of granulocyte-macrophage colony-stimulating factor in advanced HIV-1 disease: effect on infections, CD4 cell counts and HIV-1 suppression. Leukine/HIV-1 Study Group. *AIDS.* (2000) 14:387–95. doi: 10.1097/00002030-200003100-00012
54. Kahn JO. Evaluation of HIV-1-1 immunogen, an immunologic modifier, administered to patients infected with HIV-1 having 300 to 549 × 10(6)/L CD4 cell counts: A randomized controlled trial. *JAMA.* (2000) 284:2193. doi: 10.1001/jama.284.17.2193
55. Smith KA. Interleukin-2: inception, impact, and implications. *Science.* (1988) 240:1169–76. doi: 10.1126/science.3131876
56. Levy DE, Darnell JE Jr. Stats: transcriptional control and biological impact. *Nat Rev Mol Cell Biol.* (2002) 3:651–62. doi: 10.1038/nrm909
57. Cicala C, Arthos J, Selig SM, Dennis G, Hosack DA, Van Ryk D, et al. HIV-1 envelope induces a cascade of cell signals in non-proliferating target cells that favor virus replication. *Proc Nat Acad Sci USA.* (2002) 99:9380–85. doi: 10.1073/pnas.142287999
58. Leonard WJ, O'Shea JJ. JAKS AND STATS: biological implications. *Ann Rev Immunol.* (1998) 16:293–322. doi: 10.1146/annurev.immunol.16.1.293
59. Horvath CM, Darnell EJ. The state of the STATs: recent developments in the study of signal transduction to the nucleus. *Curr Opin Cell Biol.* (1997) 9:233–9. doi: 10.1016/S0955-0674(97)80067-1
60. Federico M, Percario Z, Olivetta E, Fiorucci G, Muratori C, Micheli A, et al. HIV-1-1 Nef activates STAT1 in human monocytes/macrophages through the release of soluble factors. *Blood.* (2001) 98:2752–61. doi: 10.1182/blood.V98.9.2752
61. Crotti A, Lusic M, Lupo R, Lievens PMJ, Liboi E, Chiara GD, et al. Naturally occurring C-terminally truncated STAT5 is a negative regulator of HIV-1-1 expression. *Blood.* (2007) 109:5380–9. doi: 10.1182/blood-2006-08-042556
62. Shiina M, Hamada K, Inoue-Bungo T, Shimamura M, Uchiyama A, Baba S, et al. A novel allosteric mechanism on protein-DNA interactions underlying the phosphorylation-dependent regulation of Ets1 target gene expressions. *J Mol Biol.* (2015) 427:1655–69. doi: 10.1016/j.jmb.2014.07.020
63. Backstrom S, Wolf-Watz M, Grundstrom C, Hard T, Grundstrom T, Sauer HU. The RUNX1 runt domain at 1.25A resolution: a structural switch and specifically bound chloride ions modulate DNA binding. *J Mol Biol.* (2002) 322:259–72. doi: 10.1016/S0022-2836(02)00702-7
64. Kim D, Kwon E, Hartley PD, Crosby DC, Mann S, Krogan NJ, et al. CBFβ stabilizes HIV-1 Vif to counteract APOBEC3 at the expense of RUNX1 target gene expression. *Molecular Cell.* (2013) 49:632–44. doi: 10.1016/j.molcel.2012.12.012
65. Anderson BD, Harris SR. Transcriptional regulation of APOBEC3 antiviral immunity through the CBF-β/RUNX axis. *Sci Adv.* (2015) 1:e1500296. doi: 10.1126/sciadv.1500296
66. Tanaka T, Kurokawa M, Ueki K, Tanaka K, Imai Y, Mitani K, et al. The extracellular signal-regulated kinase pathway phosphorylates AML1, an acute myeloid leukemia gene product, and potentially regulates its transactivation ability. *Mol Cell Biol.* (1996) 16:3967–79. doi: 10.1128/MCB.16.7.3967
67. Djuretic IM, Levanon D, Negreanu V, Groner Y, Rao A, Ansel MK. Transcription factors T-bet and Runx3 cooperate to activate Ifng and silence Il4 in T helper type 1 cells. *Nat Immunol.* (2007) 8:145–53. doi: 10.1038/ni1424
68. Ono M, Yaguchi H, Ohkura N, Kitabayashi I, Nagamura Y, Nomura T, et al. Foxp3 controls regulatory T-cell function by interacting with AML1/Runx1. *Nature.* (2007) 446:685–9. doi: 10.1038/nature05673
69. Wang H, Zang C, Taing L, Arnett KL, Wong YJ, Pear WS, et al. NOTCH1-RBPJ complexes drive target gene expression through dynamic interactions with superenhancers. *Proc Nat Acad Sci USA.* (2014) 111:705–10. doi: 10.1073/pnas.1315023111
70. Wong WF, Kurokawa M, Satake M, Kohu K. Down-regulation of Runx1 expression by TCR signal involves an autoregulatory mechanism and contributes to IL-2 production. *J Biol Chem.* (2011) 286:11110–18. doi: 10.1074/jbc.M110.166694
71. Zhang F, Meng G, Strober W. Interactions among the transcription factors Runx1, RORγt and Foxp3 regulate the differentiation of interleukin 17–producing T cells. *Nat Immunol.* (2008) 9:1297–306. doi: 10.1038/ni.1663
72. Wong WF, Kohu K, Chiba T, Sato T, Satake M. Interplay of transcription factors in T-cell differentiation and function: the role of Runx. *Immunology.* (2011) 132:157–64. doi: 10.1111/j.1365-2567.2010.03381.x
73. Ogawa S, Satake M, Ikuta K. Physical and functional interactions between STAT5 and Runx transcription factors. *J Biochem.* (2008) 143:695–709. doi: 10.1093/jb/mvn022
74. Ribeiro D, Melão A, Van Boxtel R, Santos CI, Silva A, Silva MC, et al. STAT5 is essential for IL-7–mediated viability, growth, and proliferation of T-cell acute lymphoblastic leukemia cells. *Blood Adv.* (2018) 2:2199–213. doi: 10.1182/bloodadvances.2018021063
75. Ogg GS, Jin X, Bonhoeffer S, Moss P, Nowak MA, Monard S, et al. Decay kinetics of human immunodeficiency virus-specific effector cytotoxic T lymphocytes after combination antiretroviral therapy. *J Virol.* (1999) 73:797–800. doi: 10.1128/JVI.73.1.797-800.1999
76. Siliciano JD, Siliciano FR. HIV-1-1 eradication strategies: design and assessment. *Curr Opin HIV-1 AIDS.* (2013) 8:318–25. doi: 10.1097/COH.0b013e328361eaca
77. Walker-Sperling VE, Pohlmeyer CW, Tarwater PM, Blankson NJ. The effect of latency reversal agents on primary CD8+ T cells: implications for shock and kill strategies for human immunodeficiency virus eradication. *EBio Med.* (2016) 8:217–29. doi: 10.1016/j.ebiom.2016.04.019
78. Zhang N, Bevan J. Michael: CD8+ T cells: foot soldiers of the immune system. *Immunity.* (2011) 35:161–8. doi: 10.1016/j.immuni.2011.07.010
79. Yang OO, Kalams SA, Trocha A, Cao H, Luster A, Johnson RP, et al. Suppression of human immunodeficiency virus type 1 replication by CD8+ cells: evidence for HLA class I-restricted triggering of cytolytic and noncytolytic mechanisms. *J Virol.* (1997) 71:3120–8. doi: 10.1128/jvi.71.4.3120-3128.1997
80. Garcia-Sastre A. Type 1 interferons and the virus-host relationship: a lesson in detente. *Science.* (2006) 312:879–82. doi: 10.1126/science.1125676
81. Kryworuchko M, Pasquier V, Keller H, David D, Goujard C, Gilquin J, et al. Defective interleukin-2-dependent STAT5 signalling in CD8 T lymphocytes from HIV-1-positive patients: restoration by antiretroviral therapy. *AIDS.* (2004) 18:421–6. doi: 10.1097/00002030-200402200-00007
82. Hand TW, Cui W, Jung YW, Sefik E, Joshi NS, Chandele A, et al. Differential effects of STAT5 and PI3K/AKT signaling on effector and memory CD8 T-cell survival. *Proc Nat Acad Sci USA.* (2010) 107:16601–6. doi: 10.1073/pnas.1003457107
83. Ostrowski SR, Gerstoft J, Pedersen BK, Ullum H. Impaired production of cytokines is an independent predictor of mortality in HIV-1-1-infected patients. *AIDS.* (2003) 17:521–30. doi: 10.1097/00002030-200303070-00007
84. Fride E, Skolnick P, Arora KP. Immunoenhancing effects of alprazolam in mice. *Life Sci.* (1990) 47:2409–20. doi: 10.1016/0024-3205(90)90485-A
85. Okimura T, Nagata I. Effect of benzodiazepine derivatives: I. Augmentation of T cell-dependent antibody response by diazepam in mouse spleen cells. *J Immunopharmacol.* (1986) 8:327–46. doi: 10.3109/08923978609026493
86. Freire-Garabal M, Belmonte A, Balboa JL, Nunez JM. Effects of midazolam on T-cell immunosuppressive response to surgical stress in mice. *Pharmacol Biochem Behav.* (1992) 43:85–9. doi: 10.1016/0091-3057(92)90642-S
87. Freire-Garabal M, Belmonte A, Orallo F, Couceiro J, Nunez JM. Effects of alprazolam on T-cell immunosuppressive response to surgical stress in mice. *Cancer Lett.* (1991) 58:183–7. doi: 10.1016/0304-3835(91)90098-3
88. Hosmalin A, Lebon P. Type I interferon production in HIV-1-infected patients. *J Leuk Biol.* (2006) 80:984–93. doi: 10.1189/jlb.0306154
89. Covelli V, Maffione AB, Greco B, Cannuscio B, Calvello R, Jirillo E. In vivo effects of alprazolam and lorazepam on the immune response in patients with migraine without aura. *Immunopharmacol Immunotoxicol.* (1993) 15:415–28. doi: 10.3109/08923979309035237
90. Buferne M, Chasson L, Grange M, Mas A, Arnoux F, Bertuzzi M, et al. IFNgamma producing CD8(+) T cells modified to resist major immune checkpoints induce regression of MHC class I-deficient melanomas.

Oncoimmunology. (2015) 4:e974959. doi: 10.4161/2162402X.2014.974959
91. Giordano G, Pugliese F, Bilotta F. Neuroinflammation, neuronal damage or cognitive impairment associated with mechanical ventilation: a systematic review of evidence from animal studies. *J Crit Care*. (2020) 62:246–55. doi: 10.1016/j.jcrc.2020.12.017
92. Lian L, Zhang Y, Liu L, Yang L, Cai Y, Zhang J, et al. Neuroinflammation in ischemic stroke: focus on MicroRNA-mediated polarization of microglia. *Front Mol Neurosci*. (2020) 13:612439. doi: 10.3389/fnmol.2020.612439
93. Paul BD, Snyder SH, Bohr AV. Signaling by cGAS-STING in neurodegeneration, neuroinflammation, and aging. *Trends Neurosci*. (2021) 44:83–96. doi: 10.1016/j.tins.2020.10.008
94. Sil S, Niu F, CHIV-1ero ET, Singh S, Periyasamy P, Buch S. Role of inflammasomes in HIV-1-1 and drug abuse mediated neuroinflammaging. *Cells*. (2020) 9:1857. doi: 10.3390/cells9081857
95. Wang J, Liang J, Deng J, Liang X, Wang K, Wang H, et al. Emerging role of microglia-mediated neuroinflammation in epilepsy after subarachnoid hemorrhage. *Mol Neurobiol*. (2021) 58:2780–91. doi: 10.1007/s12035-021-02288-y
96. Venneti S, Lopresti BJ, Wiley AC. The peripheral benzodiazepine receptor (Translocator protein 18kDa) in microglia: from pathology to imaging. *Prog Neurobiol*. (2006) 80:308–22. doi: 10.1016/j.pneurobio.2006.10.002
97. Wei HT, Chen MH, Wong WW, Chou YH, Liou YJ, Su TP, et al. Benzodiazepines and Z-drug use among HIV-1-infected patients in Taiwan: a 13-year nationwide cohort study. *Biomed Res Int*. (2015) 2015:465726. doi: 10.1155/2015/465726
98. Wixson SE, Brouwer SE. Sex differences in benzodiazepine use in the HIV-1-infected population. *AIDS Care*. (2014) 26:1218–22. doi: 10.1080/09540121.2014.894615
99. Drake S, Swift W, Hall W, Ross M. Drug use, HIV-1 risk-taking and psychosocial correlates of benzodiazepine use among methadone maintenance clients. *Drug Alcohol Depend*. (1993) 34:67–70. doi: 10.1016/0376-8716(93)90047-T
100. Ickowicz S, Hayashi K, Dong H, Milloy MJ, Kerr T, Montaner JS, et al. Benzodiazepine use as an independent risk factor for HIV-1 infection in a Canadian setting. *Drug Alcohol Depend*. (2015) 155:190–4. doi: 10.1016/j.drugalcdep.2015.07.017
101. Schmitz A. Benzodiazepine use, misuse, and abuse: a review. *Ment Health Clin*. (2016) 6:120–6. doi: 10.9740/mhc.2016.05.120
102. Morris GM, Goodsell DS, Huey R, Olson JA. Distributed automated docking of flexible ligands to proteins: parallel applications of AutoDock 2.4. *J Comput Aided Mol Des*. (1996) 10:293–304. doi: 10.1007/BF00124499
103. Morris GM, Huey R, Olson JA. Using AutoDock for ligand-receptor docking. *Curr Protoc Bioinformatics*. (2008) 24:8.14.1–40. doi: 10.1002/0471250953.bi0814s24
104. Ammosova T, Yedavalli VR, Niu X, Jerebtsova M, Van Eynde A, Beullens M, et al. Expression of a protein phosphatase 1 inhibitor, cdNIPP1, increases CDK9 threonine 186 phosphorylation and inhibits HIV-1-1 transcription. *J Biol Chem*. (2011) 286:3798–804. doi: 10.1074/jbc.M110.196493
105. Verhoef K, Sanders RW, Fontaine V, Kitajima S, Berkhout B. Evolution of the human immunodeficiency virus type 1 long terminal repeat promoter by conversion of an NF-kappaB enhancer element into a GABP binding site. *J Virol*. (1999) 73:1331–40. doi: 10.1128/JVI.73.2.1331-1340.1999

Conflict of Interest: The authors declare that the research was conducted in the absence of any commercial or financial relationships that could be construed as a potential conflict of interest.

frontiers in Neurology

ORIGINAL RESEARCH
published: 16 August 2021
doi: 10.3389/fneur.2021.651272

Monoacylglycerol Lipase Inhibitor MJN110 Reduces Neuronal Hyperexcitability, Restores Dendritic Arborization Complexity, and Regulates Reward-Related Behavior in Presence of HIV-1 Tat

Alexis F. League[1], Benjamin L. Gorman[1], Douglas J. Hermes[1], Clare T. Johnson[1], Ian R. Jacobs[1], Barkha J. Yadav-Samudrala[1], Justin L. Poklis[2], Micah J. Niphakis[3], Benjamin F. Cravatt[3], Aron H. Lichtman[2], Bogna M. Ignatowska-Jankowska[4] and Sylvia Fitting[1]**

[1] Department of Psychology and Neuroscience, University of North Carolina Chapel Hill, Chapel Hill, NC, United States, [2] Department of Pharmacology and Toxicology, Virginia Commonwealth University, Richmond, VA, United States, [3] Department of Chemistry, Scripps Research Institute, La Jolla, CA, United States, [4] Okinawa Institute of Science and Technology, Neuronal Rhythms in Movement Unit, Okinawa, Japan

While current therapeutic strategies for people living with human immunodeficiency virus type 1 (HIV-1) suppress virus replication peripherally, viral proteins such as transactivator of transcription (Tat) enter the central nervous system early upon infection and contribute to chronic inflammatory conditions even alongside antiretroviral treatment. As demand grows for supplemental strategies to combat virus-associated pathology presenting frequently as HIV-associated neurocognitive disorders (HAND), the present study aimed to characterize the potential utility of inhibiting monoacylglycerol lipase (MAGL) activity to increase inhibitory activity at cannabinoid receptor-type 1 receptors through upregulation of 2-arachidonoylglycerol (2-AG) and downregulation of its degradation into proinflammatory metabolite arachidonic acid (AA). The MAGL inhibitor MJN110 significantly reduced intracellular calcium and increased dendritic branching complexity in Tat-treated primary frontal cortex neuron cultures. Chronic MJN110 administration *in vivo* increased 2-AG levels in the prefrontal cortex (PFC) and striatum across Tat(+) and Tat(–) groups and restored PFC N-arachidonoylethanolamine (AEA) levels in Tat(+) subjects. While Tat expression significantly increased rate of reward-related behavioral task acquisition in a novel discriminative stimulus learning and cognitive flexibility assay, MJN110 altered reversal acquisition specifically in Tat(+) mice to rates indistinguishable from Tat(–) controls. Collectively, our results suggest a neuroprotective role of MAGL inhibition in reducing neuronal hyperexcitability, restoring dendritic arborization complexity, and mitigating neurocognitive alterations driven by viral proteins associated with latent HIV-1 infection.

Keywords: endocannabinoids, excitotoxicity, HIV, Tat, monoacylglycerol lipase, MJN110, 2-arachidonoyl glycerol

OPEN ACCESS

Edited by:
Kelly Stauch, University of Nebraska Medical Center, United States

Reviewed by:
Manish Malviya, Memorial Sloan Kettering Cancer Center, United States
Michael R. Nonnemacher, Drexel University, United States

****Correspondence:***
Alexis F. League
aleague@live.unc.edu
Sylvia Fitting
sfitting@email.unc.edu

Specialty section:
This article was submitted to Multiple Sclerosis and Neuroimmunology, a section of the journal Frontiers in Neurology

Received: *09 January 2021*
Accepted: *12 July 2021*
Published: *16 August 2021*

Citation:
League AF, Gorman BL, Hermes DJ, Johnson CT, Jacobs IR, Yadav-Samudrala BJ, Poklis JL, Niphakis MJ, Cravatt BF, Lichtman AH, Ignatowska-Jankowska BM and Fitting S (2021) Monoacylglycerol Lipase Inhibitor MJN110 Reduces Neuronal Hyperexcitability, Restores Dendritic Arborization Complexity, and Regulates Reward-Related Behavior in Presence of HIV-1 Tat. Front. Neurol. 12:651272. doi: 10.3389/fneur.2021.651272

INTRODUCTION

With the advent of combination antiretroviral therapy (cART), mortality rates among human immunodeficiency virus type-1 (HIV-1)-infected individuals have decreased by more than 50% (1). The consequent growth in the population of people with latent HIV-1 (PWH) has introduced a new demand for supplemental treatments, as cART itself is neurotoxic with prolonged exposure (2, 3) and leads to greater susceptibility to issues driven by synaptic dysfunction including HIV-associated neurocognitive disorders [HAND, (4)], which occurs in up to 50% of infected individuals (5). Further, cART is largely unable to deplete expression of residual HIV-1 proteins in the tissues of the central nervous system [CNS; (6–9)]. One such viral protein, transactivator of transcription (Tat) enters the host genome early after infection (10), and has been shown to induce synaptodendritic injury and cognitive deficits in murine models of HIV-1 (11–14) by altering the cellular environment through proinflammatory processes which contribute significantly to the pathogenesis of HAND (7, 15, 16).

Previous work has demonstrated *in vitro* Tat excitotoxicity (17–19) which is downregulated in frontal cortex primary neuron cultures with direct application of endogenous ligands N-arachidonoylethanolamine (AEA) and 2-arachidonoylglycerol (2-AG) via cannabinoid receptors type-1 [CB_1R; (20)]. Blocking enzymatic degradation of 2-AG and/or AEA likely has greater translational value, as activity of endogenous ligands and associated downstream products provides an extended therapeutic window due to longer half-life and greater conferred selectivity at target receptors relative to many currently available phytocannabinoid-based treatments (21–23). Additionally, therapeutic enhancement of cannabinoid signaling by enzyme inhibitors appears to be localized to sites of injury in contrast to direct agonists, which more widely affect cannabinoid signaling across the brain and are more likely to drive off-target effects (24–27).

The endocannabinoid system is a promising avenue for development of therapeutic strategies in disease, as existing literature shows anti-inflammatory and neuro-regulatory properties of agonists at CB_1R (28–30) and cannabinoid receptors type-2 [CB_2R; (31, 32)]. Potential neuroprotective effects of the endocannabinoid system in the context of neuroHIV have been reviewed previously (33, 34). Activation of CB_1R and CB_2R may downregulate the proinflammatory cytokine levels associated with synaptodendritic injury (35, 36), behavioral disturbances observed in PWH and HIV-1 transgenic rats (36, 37), and peripheral neuropathy (38–40). Nevertheless, therapeutic use of the CB_1R agonists are limited due to associated pervasive psychoactive side effects including sensorimotor, affective, and cognitive disturbances (41). Thus, research efforts have focused on development of drugs targeting components of the endogenous cannabinoid system, including enzymes regulating the biosynthesis and degradation of the endogenous cannabinoids AEA and 2-AG to enhance tonic endocannabinoid activity (42–44).

Of particular interest is the effect of monoacylglycerol lipase (MAGL), which contributes to about 85% of total 2-AG hydrolysis in the CNS (45, 46). In addition to promoting activity at CB_1R, inhibition of MAGL has recently been shown to downregulate inflammation in central (47) and peripheral (48) nervous system models by reducing breakdown of endogenous ligands into inflammatory metabolites such as arachidonic acid [AA; (49)] and downstream products like prostaglandins (47, 50). As increased prostaglandin activity drives inflammatory responses, reduction of AA production may reduce neuroinflammation caused by CNS insult. Indeed, MAGL inhibitor MJN110 has demonstrated neuroprotective effects in models of neuropsychiatric and neurodegenerative diseases (51) and ischemic stroke (52).

The aims for this project were 4-fold: first, to characterize neuroprotective effects of MJN110 treatment against Tat-associated excitotoxicity in frontal cortex neuron cultures via live calcium imaging; second, to assess Tat- and MJN110-induced alterations to neuronal morphology via immunocytochemistry *in vitro*; third, to assess the effects of Tat and MJN110 treatment *in vivo* using a HIV-1 Tat transgenic mouse model (13, 53) of behavioral flexibility as an indicator of MJN110 efficacy in restoring prefrontal cortex function (54–56); and fourth, to characterize brain region-specific alterations to endocannabinoid-related protein expression as a function of Tat and MJN110 treatment via ultrahigh performance liquid chromatography tandem mass spectrometry.

MATERIALS AND METHODS

Experiments were conducted in accordance with the NIH *Guide for the Care and Use of Laboratory Animals*. All procedures were approved by the University of North Carolina at Chapel Hill Institutional Animal Care and Use Committee.

Primary Neuron Cultures

Primary neuron cultures were derived from embryonic day 17 (E17) C57BL/6J mouse (Charles River, Raleigh, NC) frontal cortex and incubated as previously described (32). Briefly, brains were collected and frontal cortex tissue was dissected and minced. Neurons were isolated with 30-min incubation (37°C) in neurobasal medium (ThermoFisher Scientific, #21103049, USA) with 2.5 mg/mL trypsin, 0.015 mg/mL DNAse, 2% B27 (50X; ThermoFisher Scientific, #17504044, USA), 0.5 mM L-glutamine (ThermoFisher Scientific, #25030081, USA), 25 mM glutamate (Sigma-Aldrich, #604968, USA), and 1% penicillin-streptomycin (ThermoFisher Scientific, #15140122, USA). Tissue was triturated and filtered twice through 70 μm pore nylon mesh before dissociated cells were plated on poly-L-lysine-coated (Sigma-Aldrich, #P2636) 35 mm glass-bottom dishes (MatTek, #P35G-0-10-C, USA; 1 * 10^5 cells per dish) or cover slips (Fisherbrand 22 mm microscope cover slips, Cat No. 12-547, USA; 2 * 10^5 cells per slip) for calcium imaging or immunocytochemistry, respectively. Neurons were maintained in a humidified incubator with 5% CO_2 at 37 °C (Eppendorf, Hauppauge, NY) in neurobasal medium supplemented with 25 μM glutamate, 2% B27, 0.5 mM L-glutamine, and 1%

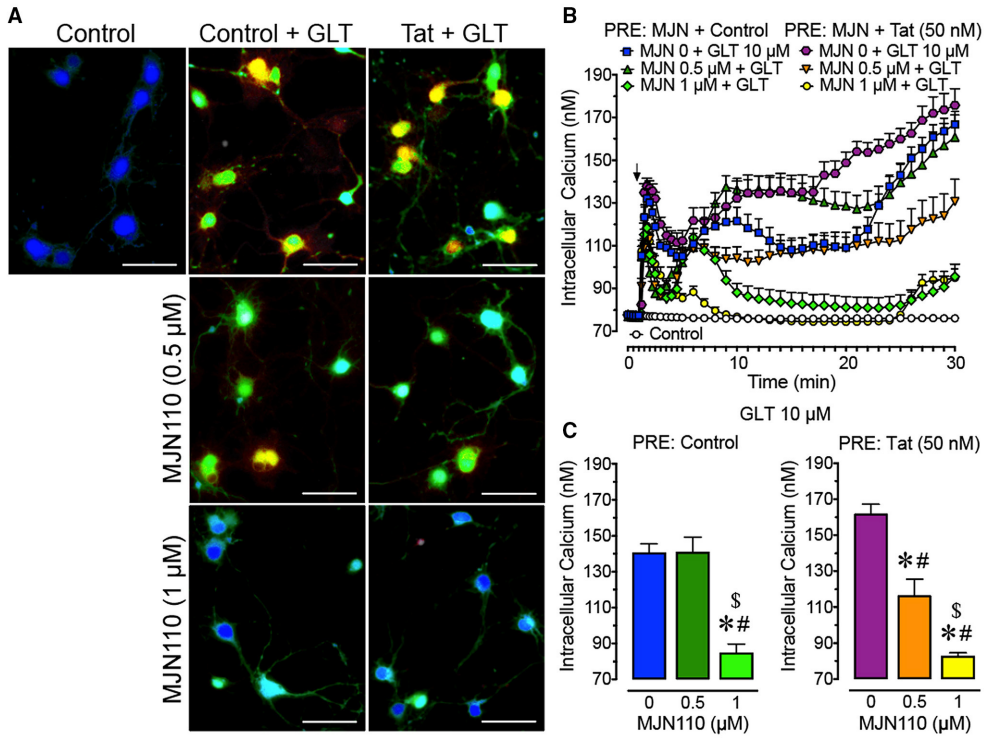

FIGURE 1 | Primary frontal cortex neuron cultures (DIV 7-11) were untreated or pre-incubated with different concentrations of MJN110 (0–1 μM) and/or a subthreshold concentration of Tat 50 nM before Ca^{2+} imaging began (1 h and 30 min prior, respectively). **(A)** Pseudocolor images of neuronal ratiometric calcium imaging taken 30 min after a glutamate (GLT) 10 μM challenge (except for the control condition) with comparing frontal cortex neurons pre-incubated with vehicle solution or different concentrations of MJN110 (0.5–1 μM) and/or a subthreshold concentration of Tat 50 nM. **(B)** $[Ca^{2+}]_i$ levels were plotted over a 30-min time period with GLT 10 μM being applied at the 1-min mark (arrow). Application of GLT 10 μM onto neurons caused significant increases in $[Ca^{2+}]_i$ levels in the presence and absence of Tat and this effect was inhibited with MJN110 pretreatment in a concentration dependent manner. **(C)** The $[Ca^{2+}]_i$ levels are summarized for the last 10 min of calcium assessment and indicate that the lower concentration of MJN110 (0.5 μM) is more inhibitory in the presence of Tat compared to the control condition. Data are mean ± SEM. Statistical significance was determined using ANOVA and Bonferroni correction where applicable. An alpha level of $p < 0.05$ was considered significant for all statistical tests. $^{*}p < 0.05$ vs. GLT 10 μM (PRE: Control); $^{\#}p < 0.05$ vs. GLT 10 μM (PRE: Tat 50 nM); $^{\$}p < 0.05$ vs. MJN110 0.5 μM + GLT 10 μM (PRE: Control). GLT, glutamate; PRE, pretreatment.

penicillin-streptomycin. Supplemented medium was 50% exchanged every 48 h. On day *in vitro* 10, cells were prepared for imaging.

Treatments *in vitro*

Primary frontal cortex neuron cultures were treated with HIV-1 Tat_{1-86} (50–100 nM; ImmunoDx, IIIB, #1002, USA), glutamate (0.1–10 μM; Sigma-Aldrich, #604968, USA), and/or MJN110 (0.5–1 μM; 50), which were diluted in Hanks Balanced Salt Solution (HBSS; ThermoFisher Scientific, #14025092, USA) supplemented with 10 mM HEPES (ThermoFisher Scientific, #15630080, USA). Tat_{1-86} concentrations in the 50–100 nM range were chosen for the present study as they recapitulate cellular deficits observed in PWH (57–60). For experiments using glutamate to induce excitation, a subthreshold concentration of Tat_{1-86} [50 nM; i.e., concentration insufficient to elicit excitatory response when bath-applied to neurons; established by (32) was used to drive neurons into a disease state prior application of glutamate during imaging. Concentrations of glutamate and MJN110 were chosen based on preliminary experiments (**Supplementary Figure 1**) and previous studies (61) which assessed activity elicited *in vitro* by this neurotransmitter and drug, respectively.

Live-Cell Fluorescence Imaging

Neurons were incubated for 30 min in fluorescent intracellular calcium indicator fura-2 AM (2 μL/mL; ThermoFisher Scientific, #F1221, USA) diluted in HBSS (with Ca^{2+}, ThermoFisher Scientific, #14025076, USA) supplemented with HEPES (10 mM; ThermoFisher Scientific, #15630080, USA) according to manufacturer instructions. Half of the neurons were then exposed to 50 nM Tat (**Figure 1**) and/or MJN110 (500 nM or 1 μM; **Figure 2**) for an additional 1 h or 30 min prior to imaging (**Figures 1**, **2**, respectively). Relative fluorescence ratio images were recorded for 30 min with a computer-controlled stage encoder with environmental control (37 °C, 95% humidity, 5% CO_2) using a Zeiss Axio Observer Z.1 inverted microscope (Zeiss, Thornwood, NY, USA) with a 20x objective at 340/380 nm and 510 nm excitation and emission wavelengths, respectively. Following 1 min baseline imaging, 10 μM glutamate (**Figure 1**)

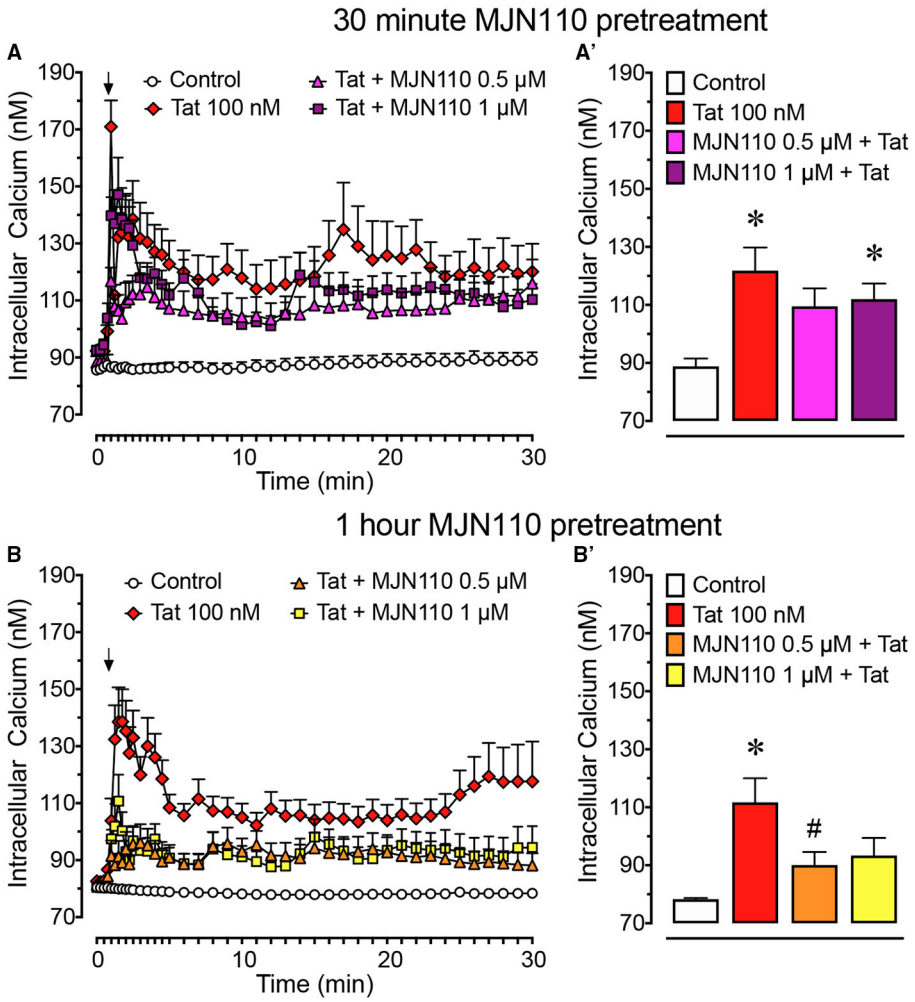

FIGURE 2 | Primary frontal cortex neuron cultures (DIV 7-11) were untreated or pre-incubated for **(A)** 30 min or **(B)** 1 h with different concentrations of MJN110 before $[Ca^{2+}]_i$ imaging began. $[Ca^{2+}]_i$ levels were plotted over a 30-min time period with Tat 100 nM being applied at the 1-min mark (arrow). **(A)** Pre-incubation of MJN110 for 30 min prior to Tat application was not able to inhibit significant increases in $[Ca^{2+}]_i$ induced by Tat when observed across a 30-min time period. **(A')** The $[Ca^{2+}]_i$ levels are summarized for the last 10 min of calcium assessment and indicate that none of the MJN110 concentrations is able to inhibit Tat-induced increases in $[Ca^{2+}]_i$ levels. **(B)** Pre-incubation of MJN110 for 1 h prior to Tat application inhibited Tat-associated $[Ca^{2+}]_i$ upregulation over a 30-min time period. **(B')** The $[Ca^{2+}]_i$ levels are summarized for the last 10 min of calcium assessment and indicate that MJN110 0.5 μM was able to significantly inhibit Tat-induced $[Ca^{2+}]_i$ increases. Data are mean ± SEM. Statistical significance was determined using ANOVA and Bonferroni correction where applicable. An alpha level of $p < 0.05$ was considered significant for all statistical tests. $^*p < 0.05$ vs. Control; $^{\#}p < 0.05$ vs. Tat 100 nM.

or 100 nM Tat (**Figure 2**) was bath-applied to cultures. Excitation patterns were assessed for the remaining 29 min. Fifteen neurons were randomly selected from each culture and somas from each were tagged as regions of interest. Relative fluorescence ratios were used to quantify fluctuations in intracellular calcium ion ($[Ca^{2+}]_i$) activity across the experimental timeframe (62). At least three independent experiments were run for each treatment group.

Immunocytochemistry

Neurons were fixed for 10 min with 4% paraformaldehyde in phosphate-buffered saline (ThermoFisher Scientific, #J61899-AP, USA) and stained as previously described (32). In brief, neurons were immunolabeled using primary antibodies against MAP2ab (Millipore, MAB378, USA; 1:500) with secondary antibodies conjugated to goat-anti-mouse Alexa 488 (ThermoFisher Scientific, #O-6380, USA; 1:1,000) diluted in PBS (ThermoFisher Scientific, #20012043). Nuclei of cells were stained using Hoechst 33342 (3 min; ThermoFisher Scientific, #H3570, USA) and coverslips were mounted using Prolong Gold (ThermoFisher Scientific, #P36930, USA). Z-stack images were obtained using ZEN 2010 Blue Edition software (Zeiss, Thornwood, NY, USA) with a Zeiss LSM 700 laser scanning confocal microscope using a 63x immersion objective (Zeiss, Thornwood, NY, USA). Dendritic branching complexity (e.g., maximum process length and distance from soma with maximal branching) and soma area were assessed with orthogonal projections from Z-stack images using the

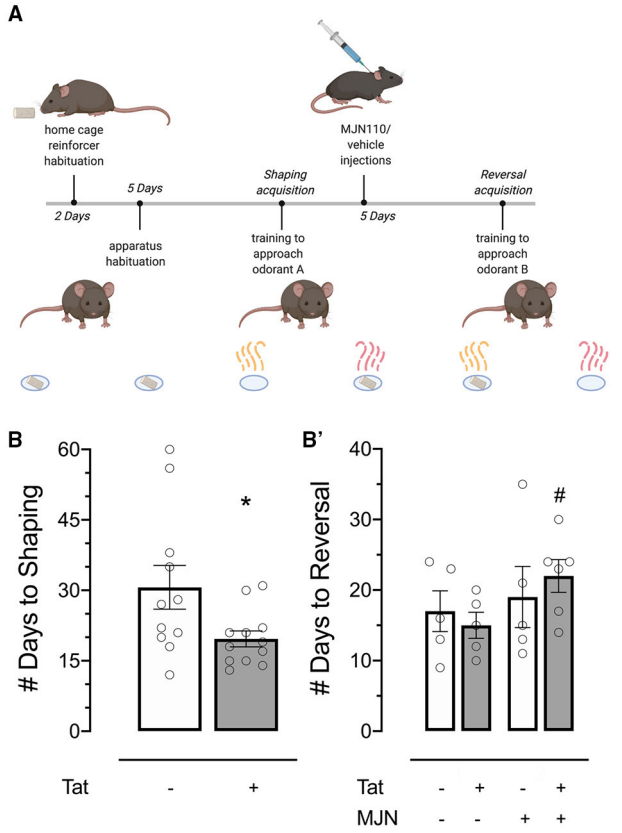

FIGURE 3 | (A) Behavioral timeline schematic for the two-choice Odor Discrimination Flexibility (ODF) task. **(B)** Tat(+) subjects acquired the shaping task significantly faster than Tat(–) controls. **(B')** MJN110-treated Tat(+) subjects acquired the reversal task significantly slower than vehicle-treated Tat(+) subjects. Data are mean ± SEM. Statistical significance was determined using ANOVA and Bonferroni correction where applicable. An alpha level of $p < 0.05$ was considered significant for all statistical tests. $^{*}p < 0.05$ vs. Tat(–); $^{\#}p < 0.05$ vs. Tat(+)/vehicle.

Sholl analysis tool within ImageJ software [Version 2.1.0; (63)].

Animals

Brain-restricted, doxycycline-inducible HIV-1 IIIB Tat_{1-86} transgenic mice were developed on a hybrid C57BL/6J background as previously described (53, 64) using a tetracycline "on" system. Mice expressing Tat under the tetracycline-responsive element were crossed with mice expressing glial fibrillary acidic protein (GFAP) promoter-driven reverse tetracycline transactivator. Expression was induced with 6 mg/g doxycycline (DOX) administration through chow diet (product TD.09282; Envigo, Indianapolis, IN, USA). Genotyping by PCR was performed at 4 weeks of age to determine which mice were Tat(+) (i.e., expressing both GFAP-rTA and TRE-tat genes) and which were Tat(–) (i.e., expressing only the GFAP-rtTA gene).

Twenty-four female transgenic mice [12 Tat(+)] 3–4 months of age were held on *ad libitum* DOX chow diet (6,000 ppm, TD.09282, Envigo, NJ, USA) for 3 months prior to and throughout behavioral testing to induce and maintain Tat expression. All tests took place in the colony room during the dark phase of the 12-h light cycle.

Treatments *in vivo*

For behavioral experiments, 1 mg/kg MJN110 (61) dissolved in saline-based vehicle [1:1:18; ethanol, Kolliphor (Sigma-Aldrich, #C5135, USA), and 0.9% NaCl saline, respectively; (25)] or vehicle alone was injected subcutaneously (10 μL/g body mass) for 5 days preceding, then throughout reversal trials (**Figure 3**). All injections were performed approximately 2 h before behavioral testing.

Odor Discrimination Flexibility Task

Behavioral Assay

Mice were habituated to reinforcers (sweetened yogurt chips; Bio-Serv, Flemington, NJ, USA) and the test environment (3 min/day) for 7 and 5 days, respectively, preceding shaping trials (**Figure 3A**). Following habituation, two cups scented individually with 100 μL peanut oil (Amazon, #B00QGWM57M, USA) and 2-phenylethanol (2-PE; Sigma-Aldrich, #77861, USA) were placed at east and west ends of the test arena (**Supplementary Figure 2**, courtesy of G.F. League Co., Inc., Greenville, SC, USA), in recessed areas where reinforcers (quartered to reduce satiation) remained out of sight until a nose poke response was made. One reinforcer was available per trial.

Mice were trained 5 days per week in the two-choice operant paradigm wherein one olfactory stimulus was paired with the reinforcer (**Figure 3A**). Odorants were used at response sites to aid in stimulus discrimination (65) and mask any odor which may be present in reinforcers, which could otherwise bias response learning (66). Reward-paired scent was randomly assigned and counterbalanced across subjects, and target location was randomized between trials to preclude location-based learning. Experimenters were blind to subject genotype throughout behavioral testing and data analysis.

Shaping Trials

Subjects were placed into a holding chamber at the south end of the test arena. To signal a trial, the holding area was briefly (2 s) illuminated from above with a mildly aversive white LED light before the partition was lifted to cue access to the darker test arena, illuminated with red light. The white trial signal light remained on until subjects entered the test area or for 1 min of no entry, after which point subjects were manually directed to the arena from the holding chamber. Upon subject entry, the partition was closed and latency to interact with reward-paired odor location was recorded. Trials began when the subject body crossed into the testing area, and terminated upon reward consumption. All sessions were video-recorded (GoPro Hero6 Black; GoPro Smart Remote; Vanguard ESPOD CX1OS tripod) and analyzed by two experimenters to assess response latency and correctness (97.92% inter-rater agreement; Cohen's $k = 0.79$).

Drug Administration

After consistent discriminative choice for the cup paired with reward was established (i.e., a nose poke into the positive

predictor cup and no interaction with the negative predictor cup across 8 out of 10 consecutive trials; 12–60 days), subjects were injected subcutaneously as described above. Shaping trials were continued during drug habituation to maintain learned responses, and reversal training began on injection day 6 (**Figure 3A**).

Reversal Training

The reversal paradigm was identical to that of shaping, except the opposite scent predicted reward. Injections were administered daily throughout reversal training. After consistent discriminative choice for the opposite cup was established (using the same criteria for the acquisition phase; 9–35 days), the experiment was terminated and subjects advanced to protein quantification analysis with mass spectrometry. Within-trial response latency was recorded to assess potential locomotor deficits/cannabimimetic effects presenting as slower approach to a reward-predictive cue.

Reinforcer Consumption Test

Tat has previously been shown to induce reward deficits and increase sensitivity to reinforcer-induced reward enhancement, contributing to depressive and addictive phenotypes, respectively (67). To measure anhedonic response and assess whether genotype influences reward salience of the reinforcer used in the ODF task, a consumption test and olfactory sensitivity test was conducted with a separate cohort of mice in home cages. After 5 days habituation to reinforcers, subjects were given access to a large amount of reinforcer (1.35 g) for 5 min and total volume consumed was quantified by measuring change in reinforcer weight.

Olfactory Sensitivity Test

Olfaction abilities were probed to ensure genotype-dependent differences in acquisition latency were not due to greater sensitivity of one group in detecting reinforcer odor in the ODF task. In this task, a reinforcer was buried in the center of home cages 0.5 cm beneath the bedding surface (68). Subjects were placed inside the south end of the cage, and latency to locate and consume the reinforcer was recorded. Trials terminated upon reinforcer consumption or after 5 min, whichever occurred first.

Ultraperformance Liquid Chromatography/Tandem Mass Spectrometry (UPLC-MS/MS)

Subjects were sacrificed by rapid decapitation following isoflurane-induced anesthesia and brains were collected, dissected, and snap-frozen in liquid nitrogen. Calibration curves were prepared at the following concentrations: 0.028 pmol to 2.8 pmol for N-arachidonoylethanolamine (anandamide; AEA), 2.6 pmol to 260 pmol for 2-arachidonoylglycerol (2-AG), 0 and 0.033 nmol to 3.3 nmol for AA along with negative and blank controls. Samples were stored at −80 °C until the day of analysis. The internal standard (ISTD) was added to each calibrator, control, and sample except the blank control at concentrations of 0.28 pmol AEA-d8, 26 pmol 2-AG-d8, 0 and 0.33 nmol AA-d8. The calibrator, control and samples were analyzed as previously described (69). In brief, samples were homogenized in 100 μL ethanol and then 900 μL water was added. Sample cleanup was performed using UCT Clean Up® C18 solid phase extraction column (United Chemical Technologies, Inc., Bristol, PA, USA) conditioned with methanol followed by water. Samples were added and the columns were then washed with deionized water. Lipids were eluted with methanol, evaporated under nitrogen, and reconstituted in mobile phase. A Shimadzu UPLC system (Kyoto, Japan) attached to a Sciex 6500 QTRAP system with an IonDrive Turbo V source for TurbolonSpray® (Sciex, Ontario, Canada) controlled by Analyst software (Sciex, Ontario, Canada) was used for the analysis of AEA, 2-AG, and AA.

Chromatographic separation of AEA, 2-AG, and AA was performed on a Discovery® HS C18 Column 15 cm × 2.1 mm, 3 μm (Supelco: Bellefonte, PA, USA) kept at 25°C. The mobile phase consisted of A: acetonitrile and B: water with 1 g/L ammonium acetate and 0.1% formic acid. The following gradient was used: 0.0–2.4 min at 40% A, 2.5–6.0 min at 40% A, hold for 2.1 min at 40% A, then 8.1–9 min 100% A, hold at 100% A for 3.1 min and return to 40% A at 12.1 min with a flow rate of 1.0 mL/min. The source temperature was 600°C with ionspray voltage of 5,000 V. The curtain gas and source gases 1 and 2 had flow rates of 30, 60, and 50 mL/min, respectively. The mass spectrometer was operated in multiple reaction monitoring (MRM) positive ionization mode for AEA, 2-AG, and negative ionization mode for AA. The following transition ions (m/z) with their corresponding collection energies (eV) in parentheses were measured as follows: AEA: 348>62 (13) and 348>91 (60); AEA-d8: 356>63 (13); 2-AG: 379>287 (26) and 379>296 (28); 2-AG-d8: 384>287 (26); AA: 303>259 (-25) and 303>59 (-60); AA-d8: 311>267 (-25). The total run time for the analytical method was 14 min. Calibration curves were analyzed with each analytical batch for each analyte. A linear regression of the ratio of the peak area counts of analyte and corresponding deuterated ISTD vs. concentration was used to construct calibration curves.

Data Analysis

Mean $[Ca^{2+}]_i$ change time course data from *in vitro* experiments were analyzed using analysis of variance (ANOVA) when appropriate. Violations of compound symmetry in repeated-measures ANOVAs for the within-subjects factors (i.e., comparing time points) were addressed by using the Greenhouse-Geisser degrees (p_{GG}) of freedom correction factor (70). Separate ANOVAs followed by Bonferroni *post-hoc* analysis were conducted for the final 10 min of the experimental time course to assess differences in sustained excitation between treatment groups.

Behavioral data for the shaping phase are plotted as latency (days) required to meet advancement criteria, and were analyzed as survival curves using the logrank test. Behavioral data for the reversal phase are plotted as latency (days) to meet completion criteria and latency (seconds) to meet criteria within trials, and were analyzed using Cox regression and two-way ANOVAs with genotype [2 levels: Tat(−) mice, Tat(+) mice] and MJN110 treatment (2 levels: vehicle, MJN110 1 mg/kg) as between-subjects factors where appropriate followed by Bonferroni *post-hoc* tests.

Brain region-specific endocannabinoid levels were analyzed by two-way ANOVAs with genotype [2 levels: Tat(−) mice, Tat(+) mice] and MJN110 treatment (2 levels: vehicle, MJN110 1 mg/kg) as between-subjects factors followed by Bonferroni *post-hoc* tests and correlated with mean within-trial response latency for the reversal phase.

All data are presented as mean ± SEM. Alpha values of <0.05 were considered significant for all statistical tests. All experiments and data analyses were carried out by experimenters blind to treatment conditions.

RESULTS

Live-Cell Fluorescence Imaging

Glutamate-Induced Intracellular $[Ca^{2+}]_i$ Increase Was Dysregulated by Tat Pretreatment and Downregulated by MJN110 in a Concentration-Dependent Manner

To understand the role of MAGL inhibition and Tat in mediating neurotoxicity after a glutamate challenge, $[Ca^{2+}]_i$ responses of frontal cortex neuron cultures pretreated with Tat (50 nM) and MJN110 (0–1 μM) and then challenged with glutamate (10 μM) during imaging (**Figure 1**) were investigated. For excitation, various glutamate concentrations were tested (0.1–10 μM) to induce a sustained $[Ca^{2+}]_i$ response for 30 min in frontal cortex neurons (**Supplementary Figure 1**). A three-way mixed ANOVA was conducted with Tat application [2 levels: control, Tat 50 nM], MJN110 treatment (3 levels: vehicle, 0.5 μM, 1 μM) as between-subjects factors and time as a within-subjects factor. Results demonstrated a significant main effect for time [$F_{(40,12,400)} = 61.6$, $p_{GG} < 0.001$] and MJN110 [$F_{(2,\ 310)} = 34.9$, $p < 0.001$]. Further significant interactions were noted for time x MJN110 [$F_{(80,\ 12,400)} = 16.6$, $p_{GG} < 0.001$], time x Tat x drug [$F_{(80,\ 12,400)} = 4.7$, $p_{GG} < 0.001$], and Tat x MJN110 [$F_{(2,\ 310)} = 7.2$, $p = 0.001$] **(Figure 1B)**. A two-way ANOVA with Tat and MJN110 treatments as between-subjects factors was conducted on the last 10 min of the experimental time course and revealed a significant MJN110 effect [$F_{(2,310)} = 29.0$, $p < 0.001$] and Tat x MJN110 interaction [$F_{(2,\ 310)} = 4.6$, $p = 0.010$] with MJN110 significantly downregulating $[Ca^{2+}]_i$ levels in a concentration dependent manner. Only in the presence of Tat, MJN110 0.5 μM elicited a significant attenuation of the glutamate-induced $[Ca^{2+}]_i$ activity compared to MJN110-free vehicle application ($p < 0.001$). MJN110 0.5 μM did not significantly downregulate $[Ca^{2+}]_i$ levels compared to vehicle for control conditions when Tat was absent (**Figure 1C**).

Tat-Induced Dysregulation of $[Ca^{2+}]_i$ Increase Was Mitigated by Pretreatment With MJN110 in a Time- and Concentration-Dependent Manner

To understand the role of MAGL inhibition in Tat-mediated neurotoxicity, $[Ca^{2+}]_i$ responses of frontal cortex neuron cultures to Tat 100 nM when pretreated with vehicle or MJN110 (0.5–1 μM) 30 min or 1-h prior imaging (**Figure 2**) was investigated. Two-way mixed ANOVAs were conducted with treatment (4 levels: control, Tat 100 nM, MJN110 0.5 μM +Tat, MJN110 1 μM + Tat) as a between-subjects factor and time as a within-subjects factor. When MJN110 was applied to neuron cultures 30 min prior Tat 100 nM, results demonstrated a significant main effect for time [$F_{(40,\ 11,760)} = 9.3$, $p_{GG} < 0.001$], a main effect of treatment [$F_{(3,\ 294)} = 10.6$, $p < 0.001$], and a time x treatment interaction [$F_{(120,\ 11,760)} = 2.4$, $p = 0.001$] (**Figure 2A**). A one-way ANOVA conducted on the last 10 min revealed a significant treatment effect [$F_{(3,\ 294)} = 5.5$, $p = 0.001$], with Tat 100 nM treatment and pretreatment of MJN110 1 μM + Tat showing significantly higher $[Ca^{2+}]_i$ levels compared to the control condition ($p = 0.001$ and $p = 0.036$, respectively; **Figure 2A'**). The MJN110 0.5 μM + Tat condition was not significantly different from control, nor did it differ from the Tat and MJN110 1 μM + Tat groups; thus indicating 30-min pretreatment with MJN110 prior Tat 100 nM excitation is not sufficient to inhibit $[Ca^{2+}]_i$ levels in frontal cortex neuron cultures.

When MJN110 was pretreated 1 h prior Tat 100 nM exposure, a two-way mixed ANOVA demonstrated a significant main effect for time [$F_{(40,\ 11,840)} = 6.4$, $p_{GG} < 0.001$], a main effect of treatment [$F_{(3,\ 296)} = 17.0$, $p < 0.001$], and a time x treatment interaction [$F_{(120,\ 11,840)} = 2.7$, $p < 0.001$] (**Figure 2B**). A one-way ANOVA conducted on the last 10 min of the experimental time course revealed a significant treatment effect [$F_{(3,\ 296)} = 6.0$, $p = 0.001$], with only Tat 100 nM treatment displaying significantly higher $[Ca^{2+}]_i$ levels compared to the control condition ($p < 0.001$) and significantly differing from the MJN110 0.5 μM + Tat condition ($p = 0.044$; **Figure 2B'**). No other effect was noted to be significant. Thus, results suggest that MJN110 pretreatment for 1 h prior to Tat 100 nM excitation is able to inhibit $[Ca^{2+}]_i$ activity in frontal cortex neuron cultures.

Immunocytochemistry

Dendritic Branching Complexity Was Increased in Tat-Exposed Frontal Cortex Neurons Treated With MJN110

Soma area (μm^2), maximum process length (μm), and distance from soma with maximal branching (defined by radial distance from the center of the soma with maximum number of intersections) were analyzed to assess changes to neuronal morphology driven by Tat (100 nM) and/or MJN110 (1 μM, **Table 1**). A two-way ANOVA with Tat and MJN110 treatment as between-subjects factors for soma area displayed no significant effect and/or interaction for Tat or MJN110 treatment. Maximum process length was also not significantly altered by MJN110, but trended toward decreased length in neurons treated with Tat ($p = 0.070$, **Table 1**). Distance from soma with maximal branching was significantly increased with MJN110 treatment and displayed a significant Tat x MJN110 treatment interaction such that Tat-untreated neurons showed no significant branch pattern differences with MJN110 treatment ($p = 0.810$), but Tat-treated neurons displayed significant increases in branching complexity with MJN110 treatment ($p = 0.002$, **Table 1**).

Odor Discrimination Flexibility Task

Rate of Shaping Acquisition Was Faster in Tat(+) Subjects

Behavioral acquisition in the shaping phase of the ODF task was analyzed to assess whether genotype affected

TABLE 1 | Effects of Tat (100 nM) and MJN110 (1 μM) on neuronal morphology from frontal cortex neuron cultures [a].

Measure	Tat	Vehicle	MJN110 (1 μM)	Tat effect		MJN110 effect		Tat x MJN110	
		Mean ± SEM	Mean ± SEM	$F_{1,32}$	*p*	$F_{1,32}$	*p*	$F_{1,32}$	*p*
Soma area (μm^2)	Control	174.6 ± 20.37	174.5 ± 13.86	<1.0	0.77	<1.0	0.93	<1.0	0.93
	Tat	179.8 ± 41.10	184.7 ± 21.00						
Maximum process length (μm)	Control	67.8 ± 2.55	72.3 ± 5.01	3.5	0.07	1.8	0.19	<1.0	0.81
	Tat	59.0 ± 4.72	65.6 ± 3.74						
Distance from soma with maximal branching	Control	26.1 ± 2.32	28.9 ± 2.32	<1.0	0.38	**11.6**	**<0.01**	**4.6**	**0.04**
	Tat	19.4 ± 1.94	31.7 ± 2.21						

[a] *Sholl analysis of neuronal morphology in frontal cortex neuron cultures in vehicle- or MJN110-treated control or Tat-treated neurons expressed as the mean ± SEM. The parameters measured by Sholl analysis are indicated in the first column. One-way ANOVAs for each dependent measure were conducted with Tat and MJN110 treatment as between-subjects factors. F-values and p-values are presented from ANOVA results. Bolded values denote significant differences at α = 0.05; mean ± SEM, n = 9 cells per group.*

TABLE 2 | Effects of genotype and MJN110 treatment on latency (days) to acquire the reversal phase of the ODF task [b].

Variables in the equation	B	SE	Wald	df	Sig.	Exp(B)	95% CI for Exp(B)	
							Lower	Upper
Genotype	−0.624	0.598	1.088	1	0.297	0.536	0.166	1.731
Treatment	0.428	0.612	0.489	1	0.485	1.534	0.462	5.092
Genotype*Treatment	−1.328	0.949	1.959	1	0.162	0.265	0.041	1.702

[b] *Cox regression with genotype and treatment as factors. While omnibus tests found a significant effect of genotype in reversal learning, this effect loses significance when treatment and its interaction with Tat are factored into the model.*

the rate of task learning. Shaping acquisition was significantly faster in Tat(+) relative to Tat(−) subjects [**Figure 3B**; $X^2_{(1,N=23)} = 6.422$, $p = 0.011$].

Faster Reversal Acquisition in Tat(+) Subjects Was Slowed to Rates Comparable to Tat(–) Controls With MJN110 Treatment

Reversal acquisition latency was separately assessed to determine the effects of genotype and MJN110 treatment specifically on cognitive flexibility. While the effect of genotype demonstrated significance in omnibus tests of behavioral acquisition in the reversal phase [$X^2_{(3,N=21)} = 7.983$, $p = 0.046$], it was found to be statistically insignificant when treatment and its interaction with genotype were taken into account (**Table 2**). Specifically, within Tat(+) subjects, MJN110 treatment significantly increased the number of trials required to acquire the reversal learning task (**Figure 3B'**; 22.00 ± 2.32 vs. 15.00 ± 1.84 for MJN110- and saline-treated subjects, respectively; $p = 0.048$) presenting as latencies more similar to Tat(−) subjects.

Neither Genotype Nor MJN110 Treatment Significantly Affected Within-Trial Response Latency

Response latency within trials was also assessed to determine whether genotype or drug treatment affected the speed with which subjects approached the reward-predictive cue. No significant effects of Tat or MJN110 on within-trial response latency were observed (**Figure 4A**; $p = 0.337$ and 0.368, respectively), indicating locomotor deficits/cannabimimetic effects were not likely factors driving observed differences.

Tat Expression Did Not Influence Reinforcer Consumption Volume

No significant differences were observed between Tat(−) and Tat(+) subjects in total volume consumed in the test session (**Figure 4B**), indicating the observed effect was not dependent upon appetite differences between groups.

Tat Expression Did Not Influence Olfactory Sensitivity

While previous work has demonstrated increased odor detection thresholds in HIV-positive relative to HIV-negative individuals (71), no differences in latency were observed between genotypes (**Figure 4C**), indicating the effect captured in the ODF task was not driven by genotype-associated differential sensitivity to odor.

UPLC-MS/MS

2-AG and AEA Were Differentially Expressed Across Examined Brain Regions Between Tat and MJN110 Conditions

2-AG, AEA, and AA levels were quantified in the prefrontal cortex (PFC), hippocampus, and striatum to characterize the effects of genotype and MJN110 treatment on brain region-specific endocannabinoid levels. In vehicle-treated subjects, 2-AG levels across brain regions were not significantly affected by Tat (**Figures 5A–A"**; PFC $p = 0.501$, hippocampus $p = 0.063$, and striatum $p = 0.155$). However, MJN110 treatment significantly upregulated 2-AG in the PFC [**Figure 5A**; $F_{(1,\ 18)} = 4.8$, $p = 0.042$] and striatum [**Figure 5A"**; $F_{(1,\ 18)} = 34.1$, $p < 0.0001$]. While Tat(+) subjects had significantly lower PFC AEA levels relative to Tat(−) controls [$F_{(1,\ 18)} = 11.0$, $p =$

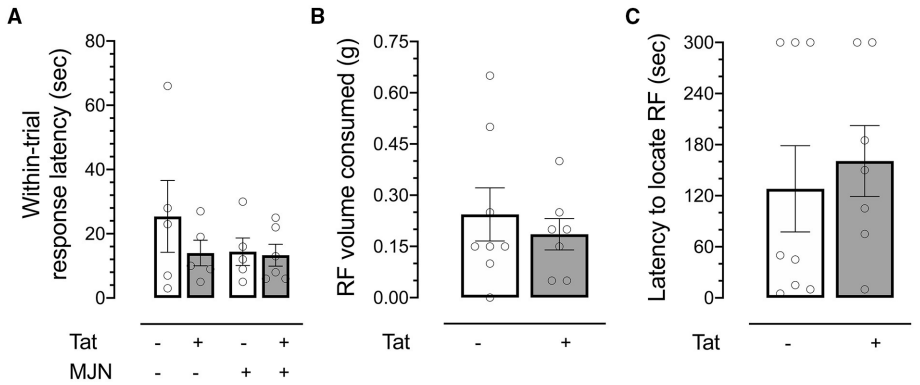

FIGURE 4 | (A) No significant differences were observed between groups in response latency within reversal trials. **(B)** No significant differences in volume of reinforcer consumed were observed between genotypes. **(C)** No significant differences were observed between Tat(+) and Tat(–) subjects in latency to locate a hidden reinforcer. Data are mean ± SEM. Statistical significance was determined using ANOVA and Bonferroni correction where applicable. An alpha level of $p < 0.05$ was considered significant for all statistical tests. RF, reinforcer.

0.004], MJN110 significantly upregulated AEA in this region [**Figure 5B**; $F_{(1, 18)} = 8.1$, $p = 0.011$]. Neither hippocampal nor striatal AEA levels were significantly altered by MJN110 or Tat (**Figures 5B',B"**, respectively). No significant Tat- or MJN110-associated differences in AA levels were observed in any brain region assessed (**Figures 5C–C"**), though Tat(+) subjects trended toward lower hippocampal levels across treatments (**Figure 5C'**; $p = 0.067$).

PFC AA and Striatal AEA Levels Positively Correlated With Within-Trial Response Latency in Tat(+) and MJN110-Treated Subjects, Respectively

While neither genotype nor MJN110 treatment significantly affected PFC AA levels ($p = 0.418$ and $p = 0.104$, respectively), these measures were found to be positively correlated with response latency within behavior trials in Tat(+) subjects ($R^2 = 0.55, p = 0.014$). A significant positive relationship was also found between striatal AEA levels and within-trial response latency across groups ($R^2 = 0.232$, $p = 0.031$). This effect appears to be driven by MJN110, as drug-treated subjects displayed a stronger relationship than vehicle-treated controls (MJN110 $R^2 = 0.40$, $p = 0.050$; vehicle $R^2 = 0.26$, $p = 0.136$).

DISCUSSION

MJN110 treatment restored intracellular $[Ca^{2+}]_i$ response and dendritic branching complexity in Tat-treated neurons to that of vehicle-treated controls *in vitro*, and shifted reversal task acquisition latency among Tat(+) subjects to within the statistical range of Tat(-) controls *in vivo*. Given that the behavioral effect corresponded with significant Tat-induced and MJN110-induced increases in hippocampal, prefrontal cortex, and striatal 2-AG levels, the observed latency shift could be linked to treatment-dependent alteration of perceived reward salience.

Tat has been shown to induce neurotoxicity and synaptic damage across murine models of HIV, presenting as N-methyl-D-aspartate (NMDA) receptor phosphorylation, cytokine secretion, expression of apoptotic proteins, reduction of neurite length, and reduced appearance of puncta along neuronal processes (57, 72–75). Increasing 2-AG and AEA have previously been found to rescue effects of Tat in PFC neurons presenting as downregulation of high intracellular calcium levels and increased neuronal survival (20); further, 2-AG has a larger therapeutic window relative to AEA due to its higher physiological expression (76). Both 2-AG and MAGL are implicated in immune activation response control in macrophages and microglia, where 2-AG prevents proinflammatory cytokine production (77) and downregulates hippocampal inflammation-induced cyclooxegenase (COX)-2 expression in response to excitotoxic stimuli (78). MJN110-induced reduction of Tat-driven excitability is likely mediated by inhibitory effects of CB_1R agonism *in vitro* as well as interactions with eicosanoid signaling pathways *in vivo* (79), though a CB_1R knockout mouse model or co-administration of a CB_1R antagonist such as rimonabant would be required to specifically delineate this potential mechanism.

While MJN110 and similar drugs have shown therapeutic potential in models of inflammation-associated neural dysfunction (32, 80), motivation regulation (81), stress (82), and neuropathic pain (83), beneficial aspects of these treatments may not generalize across test conditions. Elevation of 2-AG may regulate neural activity in subjects susceptible to excitotoxicity, but in a normal physiological context, the upregulation may result paradoxically in proinflammatory effects due to 2-AG hydrolysis into AA. AA metabolizes into other proinflammatory prostaglandins and eicosanoids (84) reported previously to be increased in women living with HIV (85). An interaction might exist between Tat(–) and Tat(+) subjects such that MJN110 treatment may shift activity of Tat(+) subjects closer to the level of Tat(–) untreated controls. MJN110 may have no additional beneficial effect in physiological systems wherein inhibitory correction is not needed. Alternative strategies may thus target upstream diacylglycerol lipase, responsible for biosynthesis of 2-AG (86). As MJN110 appears to drive different patterns of behavioral and neuronal activity and structure across physiological and pathological conditions, it could be explored

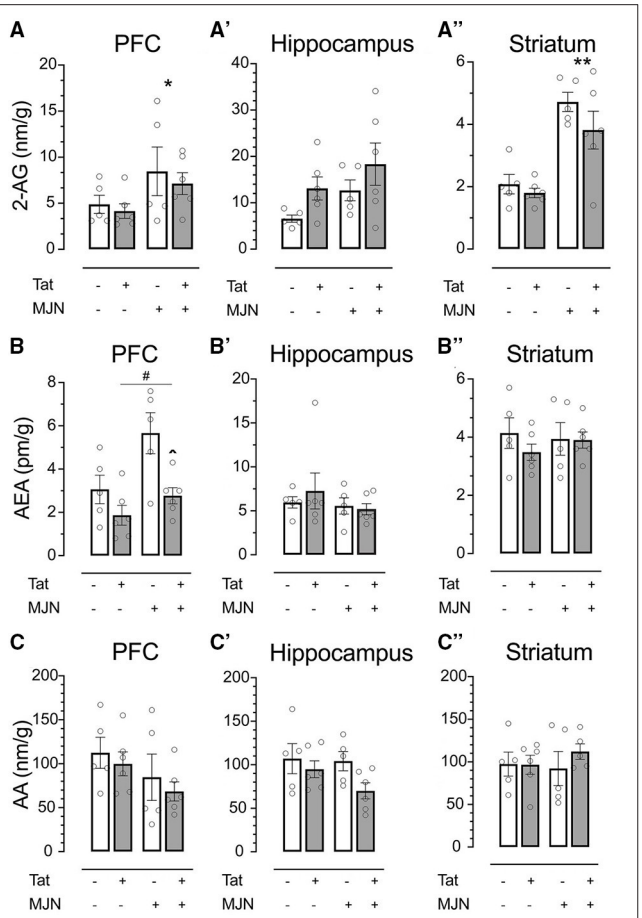

FIGURE 5 | (A) MJN110 treatment significantly increased PFC 2-AG levels across genotypes. **(A')** Neither Tat nor MJN110 significantly affected hippocampal 2-AG levels. **(A")** MJN110 significantly increased striatal 2-AG levels across genotypes. **(B)** Tat(+) subjects across treatment groups had significantly lower PFC AEA levels relative to Tat(–) controls. MJN110 significantly increased PFC AEA in Tat(+) subjects. No significant differences in hippocampal **(B')** or striatal AEA **(B")** were observed between groups. No significant differences in PFC **(C)**, hippocampal **(C')**, or striatal AA **(C")** were observed between groups. Data are mean ± SEM. Statistical significance was determined using ANOVA and Bonferroni correction where applicable. An alpha level of $p < 0.05$ was considered significant for all statistical tests. *$p <$ 0.05 vs. vehicle treatment; **$p < 0.0001$ vs. vehicle treatment; ^$p < 0.05$ vs. vehicle-treated Tat(+) subjects; #$p < 0.01$ vs. Tat(–) subjects.

whether depletion of 2-AG upstream might have greater neuroprotective potential as proinflammatory metabolites are further reduced and potential adverse effects of excessive 2-AG upregulation are functionally precluded (87, 88).

The finding that MJN110 (1 mg/kg) significantly upregulated AEA levels in the PFC of Tat(+) mice warrants further exploration. FAAH inhibition has shown to have brainregion-dependent effects on 2-AG levels (89), but the reverse effect for AEA with MAGL inhibition is less commonly found. While earlier-generation MAGL inhibitors such as JZL184 have some known cross-reactivity with FAAH, more selective MAGL inhibitors including MJN110 (25, 61) or KML29 (24, 90) show negligible cross-reactivity with FAAH and do not elevate AEA levels in the whole brain (24, 25, 61, 90). Similarly, we have not seen any AEA elevation in control, Tat(–) mice following repeated treatment with MJN110 at 1 mg/kg. It is likely Tat expression alone modifies endocannabinoid system function in such a way that MAGL blockade results in AEA elevation not observed in control animals, and the mechanism remains to be elucidated. It has been shown previously that Tat reduces the potency of 2-AG-induced inhibition on excitation (30).

HIV-1 has been shown to exert damage to dopaminergic cells and cause synaptic connectivity loss in dopaminergic projection pathways (91), presenting frequently in infected individuals as apathy and motivation dysregulation (92, 93). These behavioral sequelae of HAND are accompanied by increased markers of inflammation in the striatum (94). HIV-1 infection and substance abuse disorders are frequently comorbid (95, 96), and previous work has shown that neurons in regions implicated in reward seeking, such as the medial PFC, are hyperexcitable in the presence of HIV, particularly in models of salient reward self-administration (97, 98). As Tat binds and produces conformational changes to dopamine transporters (99, 100), rewarding effects of reinforcers are also influenced by direct Tat-induced inhibition of dopamine uptake in the striatum (101, 102). Specifically, Tat has been demonstrated to inhibit dopamine transporter (DAT) reuptake function by interacting (i.e., forming hydrogen bonds) with the DAT residues Tyr88 and His547 (103–106). Further, the resulting dopaminergic alterations can drive inflammation and immune dysfunction in PWH (107, 108) and increase susceptibility of these individuals to behavioral dysregulation presenting as greater addiction severity and HAND (109). Given the highly significant effect of MJN110 treatment on striatal 2-AG levels observed presently, subsequent investigations will shift focus to the effect of Tat and MJN110 on reward-seeking behavior as a proxy for motivation.

To better elucidate the effect of MJN110 on potential Tat-induced addiction-like behaviors (110), a progressive fixed ratio reinforcement schedule will be employed in an operant-conditioning task to assess reward-related motivation differences between genotypes and treatment groups. If data are consistent with Kesby et al. (67) and the effect of Tat is altered by MJN110 treatment, it is likely that the most influenced behavioral effect of the drug relies upon its action in cortico- and mesolimbic circuitry.

CONCLUSION

As efforts continue to address shortcomings of currently available therapeutics in HIV-1 treatment, the present study aimed to characterize a potentially viable neuroprotective drug which has been shown to attenuate inflammatory responses across numerous models of CNS insult. Analyzing MAGL inhibition effects on Tat-induced behavioral, neuronal, and endocannabinoid level changes served as a proxy for understanding functional outcomes of chronic endocannabinoid signaling modulation, and whether targeting 2-AG at the stage of hydrolysis may be restorative in models of HAND. While the mechanistic actions and biological outcomes of novel cannabinoid drugs continue to be investigated, characterization

of these compounds in disease states (particularly those which currently remain only partially suppressed) serves to broaden our understanding of their utility across models of inflammatory nervous system insult.

DATA AVAILABILITY STATEMENT

The raw data supporting the conclusions of this article will be made available by the authors, without undue reservation.

ETHICS STATEMENT

The animal study was reviewed and approved by University of North Carolina at Chapel Hill Institutional Animal Care and Use Committee.

AUTHOR CONTRIBUTIONS

AFL, BLG, and SF wrote the manuscript. AFL, BLG, DJH, CTJ, BJY-S, JLP, and SF contributed to data collection and analysis. AFL, DJH, IRJ, BLG, JLP, MJN, BFC, AHL, BMI-J, and SF provided contributions to study design. All authors contributed to the article and approved the submitted version.

FUNDING

This work was supported by the National Institute on Drug Abuse (NIDA), R01 DA045596 (SF), R21 DA041903 (SF), T32 DA007244 (AFL, DJH, and IRJ), R01 DA039942 (AHL), and P30 DA033934 (AHL and JLP). Bogna M. Ignatowska-Jankowska was supported by the fellowship from the Japan Society for Promotion of Science (JSPS). Renderings of behavioral assay were created using BioRender.com.

SUPPLEMENTARY MATERIAL

The Supplementary Material for this article can be found online at: https://www.frontiersin.org/articles/10.3389/fneur.2021.651272/full#supplementary-material

REFERENCES

1. UNAIDS. *Latest Global and Regional Statistics on the Status of the AIDS Epidemic [Fact sheet]*. (2021). Available online at: https://www.unaids.org/en/resources/documents/2021/UNAIDS_FactSheet
2. Ellis RJ, Rosarto D, Clifford DB, MacArthur JC, Simpson D, Alexander T, et al. continued high prevalence and adverse clinical impact of human immunodeficiency virus associated sensory neuropathy in the era of combination antiretroviral therapy. *Arch Neurol.* (2010) 67:552. doi: 10.1001/archneurol.2010.76
3. Akay C, Cooper M, Odeleye A, Jensen BK, White MG, Vassoler F, et al. Antiretroviral drugs induce oxidative stress and neuronal damage in the central nervous system. *J Neurovirol.* (2014) 20:39–53. doi: 10.1007/s13365-013-0227-1
4. Ellis R, Langford D, Masliah E. HIV and antiretroviral therapy in the brain: neuronal injury and repair. *Nat Rev Neurosci.* (2007) 8:33–44. doi: 10.1038/nrn2040
5. Alakkas A, Ellis RJ, Watson CW, Umlauf A, Heaton RK, Letendre S, et al. White matter damage, neuroinflammation, and neuronal integrity in HAND. *J Neurovirol.* (2019) 25:32–41. doi: 10.1007/s13365-018-0682-9
6. Hudson L, Liu J, Nath A, Jones M, Raghavan R, Narayan O, et al. Detection of the human immunodeficiency virus regulatory protein tat in CNS tissues. *J Neurovirol.* (2000) 6:145–55. doi: 10.3109/13550280009013158
7. Mediouni S, Jablonski J, Paris J, Clementz C, Thenin-Houssier S, McLaughlin J, et al. Didehydro-Cortistatin A Inhibits HIV-1 Tat Mediated Neuroinflammation and Prevents Potentiation of Cocaine Reward in Tat Transgenic Mice. *Curr HIV Res.* (2015) 13:64–79. doi: 10.2174/1570162X13666150121111548
8. Zayyad Z, Spudich S. Neuropathogenesis of HIV: from initial neuroinvasion to HIV-associated neurocognitive disorder (HAND). *Curr HIV AIDS Rep.* (2015) 12:16–24. doi: 10.1007/s11904-014-0255-3
9. Henderson LJ, Johnson TP, Smith BR, Reoma LB, Santamaria UA, Bachani M, et al. Presence of Tat and transactivation response element in spinal fluid despite antiretroviral therapy. *AIDS.* (2019) 33:S145–57. doi: 10.1097/QAD.0000000000002268
10. Nath A, Steiner J. Synaptodendritic injury with HIV-Tat protein: What is the therapeutic target? *Exp Neurol.* (2014) 251:112–4. doi: 10.1016/j.expneurol.2013.11.004
11. Carey AN, Sypek EI, Singh HD, Kaufman MJ, McLaughlin JP. Expression of HIV-Tat protein is associated with learning and memory deficits in the mouse. *Behav Brain Res.* (2012) 229:48–56. doi: 10.1016/j.bbr.2011.12.019
12. Bertrand SJ, Aksenova MV, Mactutus CF, Booze RM. HIV-1 Tat protein variants: critical role for the cysteine region in synaptodendritic injury. *Exp Neurol.* (2013) 248:228–35. doi: 10.1016/j.expneurol.2013.06.020
13. Fitting S, Ignatowska-Jankowska BM, Bull C, Skoff RP, Lichtman AH, Wise LE, et al. Synaptic dysfunction in the hippocampus accompanies learning and memory deficits in human immunodeficiency virus type-1 Tat transgenic mice. *Biol Psychiatry.* (2013) 73:443–53. doi: 10.1016/j.biopsych.2012.09.026
14. Marks WD, Paris JJ, Barbour AJ, Moon J, Carpenter VJ, Mclane VD, et al. HIV-1 Tat and morphine differentially disrupt pyramidal cell structure and function and spatial learning in hippocampal area CA1: continuous versus interrupted morphine exposure. *Eneuro.* (2021) 8:ENEURO.0547–20. doi: 10.1523/ENEURO.0547-20.2021
15. Hauser KF, Knapp PE. Interactions of HIV and drugs of abuse. *Int Rev Neurobiol.* (2014) 118:231–313. doi: 10.1016/b978-0-12-801284-0.00009-9
16. Ozturk T, Kollhoff A, Anderson AM, Howell JC, Loring DW, Waldrop-Valverde D, et al. Linked CSF reduction of phosphorylated tau and IL-8 in HIV associated neurocognitive disorder. *Sci Rep.* (2019) 9:1–10. doi: 10.1038/s41598-019-45418-2
17. Hauser KF, Fitting S, Dever SM, Podhaizer EM, Knapp PE. Opiate Drug Use and the Pathophysiology of NeuroAIDS. *Curr HIV Res.* (2012) 10:435–52. doi: 10.2174/157016212802138779
18. Shin AH, Thayer SA. Human immunodeficiency virus-1 protein Tat induces excitotoxic loss of presynaptic terminals in hippocampal cultures. *Mol Cell Neurosci.* (2013) 54:22–9. doi: 10.1016/j.mcn.2012.12.005
19. Fitting S, Knapp PE, Zou S, Marks WD, Bowers MS, Akbarali HI, et al. Interactive HIV-1 Tat and morphine-induced synaptodendritic injury is triggered through focal disruptions in Na+ influx, mitochondrial instability, and Ca2+ overload. *J Neurosci.* (2014) 34:12850–64. doi: 10.1523/JNEUROSCI.5351-13.2014
20. Xu C, Hermes DJ, Nwanguma B, Jacobs IR, Mackie K, Mukhopadhyay S, et al. Endocannabinoids exert CB 1 receptor-mediated neuroprotective effects in models of neuronal damage induced by HIV-1 Tat protein. *Mol Cell Neurosci.* (2017) 83:92–102. doi: 10.1016/j.mcn.2017.07.003
21. Uhelski ML, Khasabova IA, Simone DA. Inhibition of anandamide hydrolysis attenuates nociceptor sensitization in a murine model of chemotherapy-induced peripheral neuropathy. *J Neurophysiol.* (2015) 113:1501–10. doi: 10.1152/jn.00692.2014
22. Parker LA, Limebeer CL, Rock EM, Sticht MA, Ward J, Turvey G, et al. A comparison of novel, selective fatty acid amide hydrolase (FAAH),

monoacyglycerol lipase (MAGL) or dual FAAH/MAGL inhibitors to suppress acute and anticipatory nausea in rat models. *Psychopharmacology (Berl).* (2016) 233:2265–75. doi: 10.1007/s00213-016-4277-y
23. Wang Y, Zhang X. FAAH inhibition produces antidepressant-like efforts of mice to acute stress via synaptic long-term depression. *Behav Brain Res.* (2017) 324:138–45. doi: 10.1016/j.bbr.2017.01.054
24. Ignatowska-Jankowska BM, Ghosh S, Crowe MS, Kinsey SG, Niphakis MJ, Abdullah RA, et al. In vivo characterization of the highly selective monoacylglycerol lipase inhibitor KML29: antinociceptive activity without cannabimimetic side effects. *Br J Pharmacol.* (2014) 171:1392–407. doi: 10.1111/bph.12298
25. Ignatowska-Jankowska BM, Wilkerson JL, Mustafa M, Abdullah R, Niphakis MJ, Wiley JL, et al. Selective monoacylglycerol lipase inhibitors: antinociceptive versus cannabimimetic effects in mice. *J Pharmacol Exp Ther.* (2015) 353:424–32. doi: 10.1124/jpet.114.222315
26. Pertwee RG. Elevating endocannabinoid levels: pharmacological strategies and potential therapeutic applications. *Proc Nutr Soc.* (2014) 73:96–105. doi: 10.1017/S0029665113003649
27. Di Marzo V, Piscitelli F. The Endocannabinoid System and its Modulation by Phytocannabinoids. *Neurotherapeutics.* (2015) 12:692–8. doi: 10.1007/s13311-015-0374-6
28. Howlett AC. Cannabinoid receptor signaling. *Cannabinoids.* (2005) 53–79. doi: 10.1007/3-540-26573-2_2
29. Compagnucci C, Di Siena S, Bustamante MB, Di Giacomo D, Di Tommaso M, Maccarrone M, et al. Type-1 (CB 1) cannabinoid receptor promotes neuronal differentiation and maturation of neural stem cells. *PLoS ONE.* (2013) 8:e54271. doi: 10.1371/journal.pone.0054271
30. Wu MM, Thayer SA. HIV Tat protein selectively impairs CB1 receptor-mediated presynaptic inhibition at excitatory but not inhibitory synapses. *Eneuro.* (2020) 7:ENEURO.0119–0120. doi: 10.1523/ENEURO.0119-20.2020
31. Li X, Han D, Tian Z, Gao B, Fan M, Li C, et al. Activation of cannabinoid receptor type II by AM1241 ameliorates myocardial fibrosis via Nrf2-mediated inhibition of TGF-β1/Smad3 pathway in myocardial infarction mice. *Cell Physiol Biochem.* (2016) 39:1521–36. doi: 10.1159/000447855
32. Hermes DJ, Xu C, Poklis JL, Niphakis MJ, Cravatt BF, Mackie K, et al. Neuroprotective effects of fatty acid amide hydrolase catabolic enzyme inhibition in a HIV-1 Tat model of neuroAIDS. *Neuropharmacology.* (2018) 141:55–65. doi: 10.1016/j.neuropharm.2018.08.013
33. Wu MM, Zhang X, Asher MJ, Thayer SA. Druggable Targets of the endocannabinoid system: implications for the treatment of Hiv-associated neurocognitive disorder. *Brain Res.* (2019) 1724:146467. doi: 10.1016/j.brainres.2019.146467
34. Yadav-Samudrala BJ, Fitting S. Mini-review: The Therapeutic Role of Cannabinoids in Neurohiv. *Neurosci Lett.* (2021) 750:135717. doi: 10.1016/j.neulet.2021.135717
35. Guha D, Wagner MCE, Ayyavoo V. Human immunodeficiency virus type 1 (HIV-1)-mediated neuroinflammation dysregulates neurogranin and induces synaptodendritic injury. *J Neuroinflammation.* (2018) 15:126. doi: 10.1186/s12974-018-1160-2
36. McLaurin KA, Cook AK, Li H, League AF, Mactutus CF, Booze RM. Synaptic connectivity in medium spiny neurons of the nucleus accumbens: a sex-dependent mechanism underlying apathy in the HIV-1 transgenic rat. *Front Behav Neurosci.* (2018) 12:285. doi: 10.3389/fnbeh.2018.00285
37. Makhathini KB, Abboussi O, Mabandla MV, Daniels WMU. The effects of repetitive stress on tat protein-induced pro-inflammatory cytokine release and steroid receptor expression in the hippocampus of rats. *Metab Brain Dis.* (2018) 33:1743–53. doi: 10.1007/s11011-018-0283-6
38. Starowicz K, Przewlocka B. Modulation of neuropathic-pain-related behaviour by the spinal endocannabinoid/endovanilloid system. *Philos Trans R Soc B Biol Sci.* (2012) 367:3286–99. doi: 10.1098/rstb.2011.0392
39. Yi Z, Xie L, Zhou C, Yuan H, Ouyang S, Fang Z, et al. P2Y 12 receptor upregulation in satellite glial cells is involved in neuropathic pain induced by HIV glycoprotein 120 and 2′, 3′-dideoxycytidine. *Purinergic Signal.* (2018) 14:47–58. doi: 10.1007/s11302-017-9594-z
40. Bagdas D, Paris JJ, Carper M, Wodarski R, Rice ASC, Knapp PE, et al. Conditional expression of HIV-1 tat in the mouse alters the onset and progression of tonic, inflammatory and neuropathic hypersensitivity in a sex-dependent manner. *Eur J Pain.* (2020) 24:1609–23. doi: 10.1002/ejp.1618
41. Di Marzo V. Targeting the endocannabinoid system: to enhance or reduce? *Nat Rev Drug Discov.* (2008) 7:438–55. doi: 10.1038/nrd2553
42. Ahn K, McKinney MK, Cravatt BF. Enzymatic pathways that regulate endocannabinoid signaling in the nervous system. *Chem Rev.* (2008) 108:1687–707. doi: 10.1021/cr0782067
43. Lichtman AH, Blankman JL, Cravatt BF. Endocannabinoid overload. *Mol Pharmacol.* (2010) 78:993–5. doi: 10.1124/mol.110.069427
44. Petrosino S, Di Marzo V. FAAH and MAGL inhibitors: therapeutic opportunities from regulating endocannabinoid levels. *Curr Opin Invest Drugs.* (2010) 11:51–62.
45. Dinh TP, Carpenter, D.l, Leslie FM, Freund TF, Katona I, Sensi SL, Kathuria S, et al. Brain monoglyceride lipase participating in endocannabinoid inactivation. *Proc Natl Acad Sci USA.* (2002) 99:10819–24. doi: 10.1073/pnas.152334899
46. Blankman JL, Simon GM, Cravatt BF. A Comprehensive Profile of Brain Enzymes that Hydrolyze the Endocannabinoid 2-Arachidonoylglycerol. *Chemistry and Biology.* (2007) 14:1347–56. doi: 10.1016/j.chembiol.2007.11.006
47. Rahmani MR, Shamsizadeh A, Moghadam-Ahmadi A, Bazmandegan G, Allahtavakoli M. JZL184, as a monoacylglycerol lipase inhibitor, down-regulates inflammation in a cannabinoid pathway dependent manner. *Biomed Pharmacother.* (2018) 103:1720–6. doi: 10.1016/j.biopha.2018.05.001
48. Sakin YS, Dogrul A, Ilkaya F, Seyrek M, Ulas UH, Gulsen M, et al. The effect of FAAH, MAGL, and Dual FAAH/MAGL inhibition on inflammatory and colorectal distension-induced visceral pain models in Rodents. *Neurogastroenterol Motility.* (2015) 27:936–44. doi: 10.1111/nmo.12563
49. Muldoon PP, Akinola LS, Schlosburg JE, Lichtman AH, Sim-Selley LJ, Mahadevan A, et al. Inhibition of monoacylglycerol lipase reduces nicotine reward in the conditioned place preference test in male mice. *Neuropharmacology.* (2020) 176:108170. doi: 10.1016/j.neuropharm.2020.108170
50. Zhang X, Thayer SA. Monoacylglycerol lipase inhibitor JZL184 prevents HIV-1 gp120-induced synapse loss by altering endocannabinoid signaling. *Neuropharmacology.* (2018) 128:269–81. doi: 10.1016/j.neuropharm.2017.10.023
51. Ren SY, Wang ZZ, Zhang Y, Chen NH. Potential application of endocannabinoid system agents in neuropsychiatric and neurodegenerative diseases—focusing on FAAH/MAGL inhibitors. *Acta Pharmacol Sin.* (2020) 41:1263–71. doi: 10.1038/s41401-020-0385-7
52. Choi SH, Arai AL, Mou Y, Kang B, Yen CCC, Hallenbeck J, et al. Neuroprotective effects of MAGL (Monoacylglycerol Lipase) inhibitors in experimental ischemic stroke. *Stroke.* (2018) 49:718–26. doi: 10.1161/STROKEAHA.117.019664
53. Bruce-Keller AJ, Turchan-Cholewo J, Smart EJ, Geurin T, Chauhan A, Reid R, et al. Morphine causes rapid increases in glial activation and neuronal injury in the striatum of inducible HIV-1 tat transgenic mice. *Glia.* (2008) 56:1414–27. doi: 10.1002/glia.20708
54. Fellows LK. Ventromedial frontal cortex mediates affective shifting in humans: evidence from a reversal learning paradigm. *Brain.* (2003) 126:1830–7. doi: 10.1093/brain/awg180
55. O'Doherty JP. Reward representations and reward-related learning in the human brain: insights from neuroimaging. *Curr Opin Neurobiol.* (2004) 14:769–76. doi: 10.1016/j.conb.2004.10.016
56. Ridderinkhof KR. The Role of the Medial Frontal Cortex in Cognitive Control. *Science.* (2004) 306:443–7. doi: 10.1126/science.1100301
57. Kruman II, Nath A, Mattson MP. HIV-1 protein tat induces apoptosis of hippocampal neurons by a mechanism involving caspase activation, calcium overload, and oxidative stress. *Exp Neurol.* (1998) 154:276–88. doi: 10.1006/exnr.1998.6958
58. El-Hage N, Bruce-Keller AJ, Yakovleva T, Bazov I, Bakalkin G, Knapp PE, et al. Morphine Exacerbates HIV-1 Tat-Induced Cytokine Production in Astrocytes through Convergent Effects on [Ca2+]i, NF-κB Trafficking and Transcription. *PLoS ONE.* (2008) 3:e4093. doi: 10.1371/journal.pone.0004093
59. El-Hage N, Podhaizer EM, Sturgill J, Hauser KF. Toll-like receptor expression and activation in astroglia: differential regulation by HIV-1 Tat, gp120, and Morphine. *Immunol Invest.* (2011) 40:498–522. doi: 10.3109/08820139.2011.561904

60. Perry SW, Barbieri J, Tong N, Polesskaya O, Pudasaini S, Stout A, et al. Human immunodeficiency Virus-1 Tat activates calpain proteases via the ryanodine receptor to enhance surface dopamine transporter levels and increase transporter-specific uptake and vmax. *J Neurosci.* (2010) 30:14153–64. doi: 10.1523/JNEUROSCI.1042-10.2010
61. Niphakis MJ, Cognetta AB, Chang JW, Buczynski MW, Parsons LH, Byrne F, et al. Evaluation of NHS Carbamates as a Potent and Selective Class of Endocannabinoid Hydrolase Inhibitors. *ACS Chem Neurosci.* (2013) 4:1322–32. doi: 10.1021/cn400116z
62. Grynkiewicz G, Poenie M, Tsien RY. A new generation of Ca^{2+} indicators with greatly improved fluorescence properties. *J Biol Chem.* (1985) 260:3440–50. doi: 10.1016/S0021-9258(19)83641-4
63. Kumamoto N, Gu Y, Wang J, Janoschka S, Takemaru KI, Levine J, et al. A role for primary cilia in glutamatergic synaptic integration of adult-born neurons. *Nat Neurosci.* (2012) 15:399–405. doi: 10.1038/nn.3042
64. Chauhan A, Turchan J, Pocernich C, Bruce-Keller A, Roth SD, Butterfield A, et al. Intracellular human immunodeficiency virus Tat expression in astrocytes promotes astrocyte survival but induces potent neurotoxicity at distant sites via axonal transport. *J Biol Chem.* (2003) 278:13512–9. doi: 10.1074/jbc.M209381200
65. Liu G, Patel JM, Tepe B, McClard CK, Swanson J, Quast KB, et al. An objective and reproducible test of olfactory learning and discrimination in mice. *J Vis Exp.* (2018) 133:e57142. doi: 10.3791/57142
66. Rokni D, Hemmelder V, Kapoor V, Murthy VN. An olfactory cocktail party: figure-ground segregation of odorants in rodents. *Nat Neurosci.* (2014) 17:1225–32. doi: 10.1038/nn.3775
67. Kesby JP, Markou A, Semenova S. The effects of HIV-1 regulatory TAT protein expression on brain reward function, response to psychostimulants and delay-dependent memory in mice. *Neuropharmacology.* (2016) 109:205–15. doi: 10.1016/j.neuropharm.2016.06.011
68. Yang M, Crawley JN. Simple behavioral assessment of mouse olfaction. *Curr Prot Neurosci.* (2009) 48:Unit 8.24. doi: 10.1002/0471142301.ns0824s48
69. Dempsey SK, Gesseck AM, Ahmad A, Daneva Z, Ritter JK, Poklis JL. Formation of HETE-EAs and dihydroxy derivatives in mouse kidney tissue and analysis by high-performance liquid chromatography tandem mass spectrometry. *J Chromatogr B.* (2019) 1126–1127:121748. doi: 10.1016/j.jchromb.2019.121748
70. Greenhouse SW, Geisser S. On methods in the analysis of profile data. *Psychometrika.* (1959) 24:95–112. doi: 10.1007/BF02289823
71. Mueller C, Temmel AFP, Quint C, Rieger A, Hummel T. Olfactory Function in HIV-positive Subjects. *Acta Otolaryngol.* (2002) 122:67–71. doi: 10.1080/00016480252775760
72. Bonavia R, Bajetto A, Barbero S, Albini A, Noonan DM, Schettini G. HIV-1 Tat causes apoptotic death and calcium homeostasis alterations in rat *Neurons*. (2001)288:301–8. doi: 10.1006/bbrc.2001.5743
73. Hategan A, Bianchet MA, Steiner J, Karnaukhova E, Masliah E, Fields A, et al. HIV Tat protein and amyloid-β peptide form multifibrillar structures that cause neurotoxicity. *Nat Struct Mol Biol.* (2017) 24:379–86. doi: 10.1038/nsmb.3379
74. Nass SR, Hahn YK, Mclane VD, Varshneya NB, Damaj MI, Knapp PE, et al. Chronic HIV-1 Tat exposure alters anterior cingulate cortico-basal ganglia-thalamocortical synaptic circuitry, associated behavioral control, and immune regulation in male mice. *Brain Behav Immun Health.* (2020) 5:100077. doi: 10.1016/j.bbih.2020.100077
75. Tang X, Lu H, Ramratnam B. Neurotoxicity of HIV-1 Tat is attributed to its penetrating property. *Sci Rep.* (2020) 10:14002. doi: 10.1038/s41598-020-70950-x
76. Gil-Ordóñez A, Martín-Fontecha M, Ortega-Gutiérrez S, López-Rodríguez ML. Monoacylglycerol lipase (MAGL) as a promising therapeutic target. *Biochem Pharmacol.* (2018) 157:18–32. doi: 10.1016/j.bcp.2018.07.036
77. Krishnan G, Chatterjee N. Endocannabinoids alleviate proinflammatory conditions by modulating innate immune response in muller glia during inflammation. *Glia.* (2012) 60:1629–45. doi: 10.1002/glia.22380
78. Zhang J, Chen C. Endocannabinoid 2-Arachidonoylglycerol Protects Neurons by Limiting COX-2 Elevation. *J Biol Chem.* (2008) 283:22601–11. doi: 10.1074/jbc.M800524200
79. Kohnz RA, Nomura DK. Chemical approaches to therapeutically target the metabolism and signaling of the endocannabinoid 2-AG and eicosanoids. *Chem Soc Rev.* (2014) 43:6859–69. doi: 10.1039/C4CS00047A
80. Hermes DJ, Yadav-Samudrala BJ, Xu C, Paniccia JE, Meeker RB, Armstrong ML, et al. GPR18 Drives FAAH Inhibition-induced Neuroprotection Against HIV-1 Tat-induced Neurodegeneration. *Exp Neurol.* (2021) 341:113699. doi: 10.1016/j.expneurol.2021.113699
81. Feja M, Leigh MPK, Baindur AN, McGraw JJ, Wakabayashi KT, Cravatt BF, et al. The novel MAGL inhibitor MJN110 enhances responding to reward-predictive incentive cues by activation of CB1 receptors. *Neuropharmacology.* (2020) 162:107814. doi: 10.1016/j.neuropharm.2019.107814
82. Grabner GF, Zimmermann R, Schicho R, Taschler U. Monoglyceride lipase as a drug target: At the crossroads of arachidonic acid metabolism and endocannabinoid signaling. *Pharmacol Ther.* (2017) 175:35–46. doi: 10.1016/j.pharmthera.2017.02.033
83. Wilkerson JL, Niphakis MJ, Grim TW, Mustafa MA, Abdullah RA, Poklis JL, et al. The Selective Monoacylglycerol Lipase Inhibitor MJN110 Produces Opioid-Sparing Effects in a Mouse Neuropathic Pain Model. *Journal of Pharmacol Exp Ther.* (2016) 357:145–56. doi: 10.1124/jpet.115.229971
84. Grabner GF, Eichmann TO, Wagner B, Gao Y, Farzi A, Taschler U, et al. Deletion of monoglyceride lipase in astrocytes attenuates lipopolysaccharide-induced neuroinflammation. *J Biol Chem.* (2016) 291:913–23. doi: 10.1074/jbc.m115.683615
85. Weinberg A, Huo Y, Kacanek D, Patel K, Watts DH, Wara D, et al. Brief report. *J Acquir Immune Defic Syndr.* (2019) 82:181–7. doi: 10.1097/QAI.0000000000002111
86. Ueda N, Tsuboi K, Uyama T, Ohnishi T. Biosynthesis and degradation of the endocannabinoid 2-arachidonoylglycerol. *Biofactors.* (2011) 37:1–7. doi: 10.1002/biof.131
87. Valdeolivas S, Pazos MR, Bisogno T, Piscitelli F, Iannotti FA, Allara M, et al. The inhibition of 2-arachidonoyl-glycerol (2-AG) biosynthesis, rather than enhancing striatal damage, protects striatal neurons from malonate-induced death: a potential role of cyclooxygenase-2-dependent metabolism of 2-AG. *Cell Death Dis.* (2013) 4:e862. doi: 10.1038/cddis.2013.387
88. Wilkerson JL, Donvito G, Grim TW, Abdullah RA, Ogasawara D, Cravatt BF, et al. Investigation of diacylglycerol lipase alpha inhibition in the mouse lipopolysaccharide inflammatory pain model. *J Pharmacol Exp Ther.* (2017) 363:394–401. doi: 10.1124/jpet.117.243808
89. Di Marzo V, Maccarrone M. FAAH and anandamide: is 2-AG really the odd one out? *Trends Pharmacol Sci.* (2008) 29:229–33. doi: 10.1016/j.tips.2008.03.001
90. Chang JW, Niphakis MJ, Lum KM, Cognetta AB, Wang C, Matthews ML, et al. Highly selective inhibitors of monoacylglycerol lipase bearing a reactive group that is bioisosteric with endocannabinoid substrates. *Chem Biol.* (2012) 19:579–88. doi: 10.1016/j.chembiol.2012.03.009
91. Gelman BB, Chen T, Lisinicchia JG, Soukup VM, Carmical JR, Starkey JM, et al. The National NeuroAIDS tissue consortium brain gene array: two types of HIV-associated neurocognitive impairment. *PLoS ONE.* (2012) 7:e46178. doi: 10.1371/journal.pone.0046178
92. Bryant VE, Whitehead NE, Burrell LE, Dotson VM, Cook RL, Kathryn Devlin K, et al. Depression and apathy among people living with HIV: implications for treatment of HIV associated neurocognitive disorders. *AIDS Behav.* (2015) 19:1430–7. doi: 10.1007/s10461-014-0970-1
93. Nickoloff-Bybel EA, Calderon TM, Gaskill PJ, Berman JW. HIV Neuropathogenesis in the presence of a disrupted dopamine system. *J Neuroimmune Pharmacol.* (2020) 15:729–42. doi: 10.1007/s11481-020-09927-6
94. Bade AN, Gorantla S, Dash PK, Makarov E, Sajja BR, Poluektova LY, et al. Manganese-enhanced magnetic resonance imaging reflects brain pathology during progressive HIV-1 infection of humanized mice. *Mol Neurobiol.* (2016) 53:3286–97. doi: 10.1007/s12035-015-9258-3
95. Cook JA, Burke-Miller JK, Steigman PJ, Schwartz RM, Hessol NA, Milam J, et al. Prevalence, comorbidity, and correlates of psychiatric and substance use disorders and associations with HIV risk behaviors in a multisite cohort of women living with HIV. *AIDS Behav.* (2018) 22:3141–54. doi: 10.1007/s10461-018-2051-3

96. Illenberger JM, Harrod SB, Mactutus CF, Mclaurin KA, Kallianpur A, Booze RM. HIV infection and neurocognitive disorders in the context of chronic drug abuse: evidence for divergent findings dependent upon prior drug history. *J Neuroimmune Pharmacol.* (2020) 15:715–28. doi: 10.1007/s11481-020-09928-5
97. Ferris MJ, Mactutus CF, Booze RM. Neurotoxic profiles of HIV, psychostimulant drugs of abuse, and their concerted effect on the brain: current status of dopamine system vulnerability in NeuroAIDS. *Neurosci Biobehav Rev.* (2008) 32:883–909. doi: 10.1016/j.neubiorev.2008.01.004
98. Wayman WN, Chen L, Hu XT, Napier TC. HIV-1 Transgenic rat prefrontal cortex hyper-excitability is enhanced by cocaine self-administration. *Neuropsychopharmacology.* (2016) 41:1965–73. doi: 10.1038/npp.2015.366
99. Zhu J, Ananthan S, Mactutus CF, Booze RM. Recombinant human immunodeficiency virus-1 transactivator of transcription1-86 allosterically modulates dopamine transporter activity. *Synapse.* (2011) 65:1251–4. doi: 10.1002/syn.20949
100. Yuan Y, Huang X, Midde NM, Quizon PM, Sun WL, Zhu J, et al. Molecular Mechanism of HIV-1 Tat Interacting with Human Dopamine Transporter. *ACS Chem Neurosci.* (2015) 6:658–65. doi: 10.1021/acschemneuro.5b00001
101. Paris JJ, Carey AN, Shay CF, Gomes SM, He JJ, McLaughlin JP. Effects of conditional central expression of HIV-1 Tat protein to potentiate cocaine-mediated psychostimulation and reward among male mice. *Neuropsychopharmacology*. (2017) 39:380–8. doi: 10.1038/npp.2013.201
102. Javadi-Paydar M, Roscoe RF, Denton AR, Mactutus CF, Booze RM. HIV-1 and cocaine disrupt dopamine reuptake and medium spiny neurons in female rat striatum. *PLoS ONE.* (2017) 12:e0188404. doi: 10.1371/journal.pone.0188404
103. Quizon PM, Yuan Y, Zhu Y, Zhou Y, Strauss MJ, Sun W-L, et al. Mutations of human dopaminetransporter at tyrosine88, aspartic Acid206, and histidine547 influence basal and HIV-1 tat-inhibited dopamine transport. *J Neuroimmune Pharmacol*. (2021). doi: 10.1007/s11481-021-09984-5
104. Midde NM, Yuan Y, Quizon PM, Sun WL, Huang X, Zhan CG, et al. Mutations at tyrosine 88, lysine 92 and tyrosine 470 of human dopamine transporter result in an attenuation of HIV-1 Tat-Induced Inhibition of dopamine transport. *Neuroimmune Pharmacol*. (2015) 10:122–35. doi: 10.1007/s11481-015-9583-3
105. Quizon PM, Sun WL, Yuan Y, Midde NM, Zhan CG, Zhu J. (2016). Molecular mechanism: the human dopamine transporter histidine 547 regulates basal and HIV-1 Tat protein-inhibited dopamine transport. *Sci. Rep.*(2016) 6:39048. doi: 10.1038/srep39048
106. Sun WL, Quizon PM, Yuan Y, Strauss MJ, McCain R, Zhan CG, et al. Mutational effects of human dopamine transporter at tyrosine88, lysine92, and histidine547 on basal and HIV-1 Tat-inhibited dopamine transport. *Sci Rep.* (2019) 9:3843. doi: 10.1038/s41598-019-39872-1
107. Matt SM, Gaskill PJ. Dopaminergic impact of cART and anti-depressants on HIV neuropathogenesis in older adults. *Brain Res.* (2019) 1723:146398–146398. doi: 10.1016/j.brainres.2019.146398
108. Nolan RA, Muir R, Runner K, Haddad EK, Gaskill PJ. Role of macrophage dopamine receptors in mediating cytokine production: implications for neuroinflammation in the context of Hiv-associated neurocognitive disorders. *J Neuroimmune Pharmacol.* (2019) 14:134–56. doi: 10.1007/s11481-018-9825-2
109. Saylor D, Dickens AM, Sacktor N, Haughey N, Slusher B, Pletnikov M, et al. HIV-associated neurocognitive disorder — pathogenesis and prospects for treatment. *Nat Rev Neurol.* (2016) 12:234–48. doi: 10.1038/nrneurol.2016.27
110. Panee J, Pang X, Munsaka S, Berry MJ, Chang L. Independent and Co-morbid HIV infection and meth use disorders on oxidative stress markers in the cerebrospinal fluid and depressive symptoms. *J Neuroimmune Pharmacol*. (2015) 10:111–21. doi: 10.1007/s11481-014-9581-x

Conflict of Interest: The authors declare that the research was conducted in the absence of any commercial or financial relationships that could be construed as a potential conflict of interest.

Publisher's Note: All claims expressed in this article are solely those of the authors and do not necessarily represent those of their affiliated organizations, or those of the publisher, the editors and the reviewers. Any product that may be evaluated in this article, or claim that may be made by its manufacturer, is not guaranteed or endorsed by the publisher.

Advantages of publishing in Frontiers

OPEN ACCESS
Articles are free to read for greatest visibility and readership

FAST PUBLICATION
Around 90 days from submission to decision

HIGH QUALITY PEER-REVIEW
Rigorous, collaborative, and constructive peer-review

TRANSPARENT PEER-REVIEW
Editors and reviewers acknowledged by name on published articles

Frontiers
Avenue du Tribunal-Fédéral 34
1005 Lausanne | Switzerland

Visit us: www.frontiersin.org
Contact us: frontiersin.org/about/contact

REPRODUCIBILITY OF RESEARCH
Support open data and methods to enhance research reproducibility

DIGITAL PUBLISHING
Articles designed for optimal readership across devices

FOLLOW US
@frontiersin

IMPACT METRICS
Advanced article metrics track visibility across digital media

EXTENSIVE PROMOTION
Marketing and promotion of impactful research

LOOP RESEARCH NETWORK
Our network increases your article's readership